AD NUMBER	
AD350590	
CLASSIFICATION CHANGES	
TO:	**UNCLASSIFIED**
FROM:	**SECRET//RESTRICTED DATA**
LIMITATION CHANGES	
TO: **Approved for public release; distribution is unlimited.**	
FROM: **Distribution authorized to U.S. Gov't. agencies and their contractors; Administrative/Operational Use; FEB 1963. Other requests shall be referred to Aeronautical Systems Division, ATTN: Propulsion Laboratory, Wright-Patterson AFB, OH 45433. Restricted Data.**	
AUTHORITY	
OSD/WHS memo dtd 17 Mar 2016; OSD/WHS memo dtd 17 Mar 2016	

DEPARTMENT OF DEFENSE
WASHINGTON HEADQUARTERS SERVICES
1155 DEFENSE PENTAGON
WASHINGTON, DC 20301-1155

MAR 1 7 2016

MEMORANDUM FOR DEFENSE TECHNICAL INFORMATION CENTER
(ATTN: DTIC-OQ INFORMATION SECURITY)
8725 JOHN J. KINGMAN ROAD, SUITE 0944
FORT BELVOIR, VA 22060-6218

SUBJECT: OSD MDR Case 13-M-3701

We have reviewed the attached document in consultation with the Department of Energy, Department of the Navy, and Department of the Air Force and have declassified it in full. If you have any questions please contact Mr. John D. Smith by phone at 571-372-0482 or by email at john.d.smith887.civ@mail.mil, john.d.smith887.civ@mail.smil.mil, or john.smith@osdj.ic.gov.

George R. Sturgis
Deputy Chief, Records and Declassification Division

Attachments:
1. MDR request w/ document list
2. Document 2

~~SECRET~~
~~RESTRICTED DATA~~

AD 350590

DEFENSE DOCUMENTATION CENTER

FOR

SCIENTIFIC AND TECHNICAL INFORMATION

CAMERON STATION, ALEXANDRIA, VIRGINIA

Office of the Secretary of Defense 5 USC 552
Chief, RDD, ESD, WHS +
Date: 02 Oct 2015 Authority: EO 13526
Declassify: X Deny in Full: _____
Declassify in Part: _____
Reason: _____
MDR: 13 -M- 3701

Department of the Navy
DON/AA DRMD
Date: 10 Oct 2014 Authority: EO 13526
Declassify: X Deny in Full: ____
Declassify in Part: ____
Reason: _____
MDR 2015 -M- 0001

DECLASSIFIED IN FULL
Authority: EO 13526
Chief, Records & Declass Div, WHS
Date: OCT 0 2 2015

DEPARTMENT OF ENERGY DECLASSIFICATION REVIEW	
1st Review Date: 10/17/13 Authority: ☐ DC ☒ DD Name: R.L. Shankle 2nd Review Date: 10/30/2013 Authority: DD Name: S. Fivozinsky	DETERMINATION (CIRCLE NUMBER(S)) 1. CLASSIFICATION RETAINED 2. CLASSIFICATION CHANGED TO: NSI 3. CONTAINS NO DOE CLASSIFIED INFO 4. COORDINATE WITH: _____ 5. CLASSIFICATION CANCELED 6. CLASSIFIED INFO BRACKETED 7. OTHER (SPECIFY): _____

~~RESTRICTED DATA~~
~~SECRET~~

R1

13-M-3701

~~SECRET RESTRICTED DATA~~
~~ATOMIC ENERGY ACT OF 1954~~

ASD-TDR-63-277
Volume IV

(UNCLASSIFIED TITLE)
NUCLEAR RAMJET PROPULSION SYSTEM
APPLIED RESEARCH AND ADVANCED TECHNOLOGY
(PROJECT PLUTO)

VOLUME IV
PROPULSION SYSTEM DESIGN AND STRUCTURAL ANALYSIS

TECHNICAL DOCUMENTARY REPORT ASD-TDR-63-277, VOLUME V

15 February 1963

Directorate of Aeromechanics
Propulsion Laboratory
Aeronautical Systems Division
Air Force Systems Command
Wright-Patterson Air Force Base, Ohio

Project No. 655A, Tasks Nos. 1 and 5

(Prepared under Contract AF 33(657)-8123
by The Marquardt Corporation, Van Nuys, California
Author: R. D. Grossman)

~~EXCLUDED FROM AUTOMATIC REGRADING; DOD DIR 5200.10 DOES NOT APPLY~~

~~SECRET RESTRICTED DATA~~
~~ATOMIC ENERGY ACT OF 1954~~

63 ASRM-36

NOTICES

~~RESTRICTED DATA~~

~~This document contains~~ restricted data as defined in the Atomic Energy Act of 1954. Its transmittal or the disclosure of its contents in any manner to an unsuthorized person is prohibited by law.

When US Government drawings, specifications, or other data are used for any purpose other than a definitely related government procurement operation, the government thereby incurs no responsibility nor any obligation whatsoever; and the fact that the government may have formulated, furnished, or in any way supplied the said drawings, specifications, or other data is not to be regarded by implication or otherwise, as in any manner licensing the holder or any other person or corporation, or conveying any rights or permission to manufacture, use, or sell any patented invention that may in any way be related thereto.

Copies of this report should not be returned to the Aeronautical Systems Division unless return is required by security considerations, contractural obligation, or notice on a specific document.

FOREWORD

This report was prepared by The Marquardt Corpor ion, Van Nuys, California, on Air Force Contract AF 33(657)-8123, under Task o. 1 and No. 5 of Project No. 655A, "Nuclear Ramjet Propulsion Systems Resea n and Technology". The work was administered under the direction of the P pulsion Laboratory (Directorate of Aeromechanics), Aeronautical Systems Di sion. R. F. Latham was Project Engineer for the Laboratory.

The studies presented here were performed during e contract period 1 January-31 December 1962. The Marquardt Corporation act vities were under the direction of A. O. Mooneyham, Senior Project Engineer. Chief contributors were J. G. Bendot, Aerothermodynamics; R. D. Grossman, I sign and Development; R. K. Nuno, Controls.

This report is the final technical summary report and concludes the work on Contract AF 33(657)-8123. The contractor's report number is Marquardt Report 6003. The volumes of this report are as foll ws:

Volume I:	Summary
Volume II:	Propulsion System Performance and A othermodynamics
Volume III:	Propulsion System Controls
Volume IV:	Propulsion System Design and Structu al Analysis
Volume V:	Propulsion System Test Planning and ound Test Facility Studies
Volume VI:	Structural Materials Investigations

This report is ~~classified Secret-Restricted Data~~ n conformance with requirements contained in AF-provided security guidance (orm 151) and OC DOC 75.

ABSTRACT

(This abstract is ~~classified CONFIDENTIAL~~)

This volume contains the results of design, structures and materials studies and structures component testing of a nuclear propulsion system in support of the Pluto reactor program. These studies include design concepts, structural analysis of steady state and dynamic loads, material evaluation, and recommended dynamic and structural test programs. The methods of analysis used have been outlined in each case for reference.

SUMMARY

The mechanical and structural design effort during his contract period (1 January 1962 through 31 December 1962) has been direc d towards the design of a flight type propulsion system, designated the MA50- B, which incorporates a reactor reflecting Tory IIC reactor technology. E ort has also been expended in design and fabrication of development test har are for component testing.

Design layouts have been completed for the MA50-XC Propulsion System in addition to the major components that make up the entire system; namely, the inlet and diffuser duct, ejector exhaust nozzle, reactor co rol rods support system, reactor lateral and axial support structure, inlet pike translation and bypass door mechanism and exhaust nozzle attachment.

Design and fabrication have been completed for the direct-connect and free jet aerodynamic coupling test hardware, engine airfram lateral attachment test hardware, and reactor lateral support spring test har are.

Test outlines and test results for the aerodynamic coupling tests are reported in Volume II of this report.

CONTENTS

CONTENTS (Continued)

CONTENTS (Continued)

ILLUSTRATIONS

ILLUSTRATIONS (Continued)

ILLUSTRATIONS (Continued)

ILLUSTRATIONS (Continued)

ILLUSTRATIONS (Continued)

ILLUSTRATIONS (Continued)

ILLUSTRATIONS (Continued)

TABLES

TABLES (Continued)

1.0 INTRODUCTION

The model MA50-XCB nuclear ramjet propulsion syst as shown in Figures 1 and 2 consists of a variable geometry supersonic inl with a modified isentropic spike, a subsonic diffuser incorporating a var ble area bypass, a nuclear reactor similar in construction to the Tory IIC reac r with integrated control system, and a convergent-divergent ejector type ex ost nozzle.

The inlet, which is an underslung, axisymmetric, ternal-internal compression type, has a translating centerbody spike with a ma num travel of seven inches. The spike actuation mechanism is housed within e centerbody structure and is air-operated. Air is supplied to the actuato through a slot located in the centerbody structure. The bypass doors are loc ed in the vicinity of the aft centerbody structure and are an integral part o the supersonic inlet structure.

The subsonic diffuser duct, from aft of the super nic inlet to the front face of the reactor, is an integral part of the missile rframe structure.

The nuclear reactor is composed of a series of in ridual ceramic elements that make up the fueled core and front rear and radial reflectors. The reactor is maintained in the form of a right circular cylinder a series of spring-loaded expansion shell pads. A series of axial tie tub (which pass through the reactor) collect all aft directional loads through ear bearing plates and transfer them to a front support structure. All ax t loads imposed upon the reactor are transferred to the airframe through a she ring located in the vicinity of the front support structure.

The reactor control rod translating mechanisms are mounted forward of the front support structure and housed within the inlet duct Control rod actuators are mounted in the annulus between the diffuser duct d the missile airframe.

The exhaust nozzle, is a convergent-divergent ejec or type with fixed primary and secondary nozzle flow areas. This design em ys a convergent-divergent outer shell with an inner shell in the convergent section only. The annulus between the inner and outer shell is sized such th the engine cooling air (secondary flow) cools the convergent portion of the n le by forced convection. The divergent portion of the nozzle is then film- led by the air issuing from the annular passage just aft of the throat.

The weights and centers of gravity for the MA50-X and its components are shown in Table I. Margins of safety are presented in ble II.

Manuscript released by The Marquardt Corporation on 15 February 963 for publication as an ASD Technical Documentary Report.

2.0 PROPULSION SYSTEM DESIGN CRITERIA

2.1 General Discussion

Particular emphasis for efficient operation of any pr ulsion system designed for high speed flight must be placed on lightweight a reliable structure, which will provide the necessary performance. Structur design will determine the shape and size of individual structural members to o ain the minimum weight of these structures. Design criteria are concerned wi the data associated with the operational life, the associated loads, tempera ures, and times at load and temperature. Also included will be nomenclature nd design factors for use in analysis together with the physical properties the materials used in fabrication. Such data are presented in the pages fo owing.

2.2 Mission Parameters

2.2.1 Contractual Requirements

The following typical mission parameters are pecified in Reference 1, Paragraph 1.1, to be used as a basis for propulsion s tem design:

Minimum range	11,000 nautical miles
Maximum payload	10,000 pounds

2.2.2 Flight Capability

High altitude cruise at 35,000 feet at Mach 3 5 to 4.0:

Minimum time	4.0 hours
Maximum time	7.0 hours

Penetration at 500 to 1000 feet at Mach 2.8 t 3.0:

Minimum time	2.0 hours
Maximum time	3.0 hours

Component design lifetime to be adequate for gh reliability in performing above maximum requirements.

The Pluto propulsion system is designated the Marquardt Model MA50-XCA Nuclear Ramjet Engine. Operating envelopes for this engine are presented in Reference 2. The envelope limits are associated with ntrol and actuator requirements and structural limitations of materials. Due o the establishment of temperature and pressure limitations (inlet air tota tempera-ture of 1070°F and diffuser exit pressure of 420 psia), the system uld operate at Mach 3.2, Sea Level, on an ICAO Standard Day. This point pl es the system in the most severe steady state operating condition (exceeding e requirements stated above) and should be taken as the structural design po t.

2.3 Typical Mission Profiles

Vehicle total mission flight profiles used by Marquardt ...r ICAO Standard and ANA 421 Hot and Cold Days, and presented in Figures 3, 4 and 5, are reproduced for reference from Ling-Temco-Vought data presented in Reference 3, and again in Reference 4. Critical Mach number vs. altitude combinations from these curves are as follows:

Day Condition	Operational Phase	Altitude (feet)	Mach No
ANA 421	High Altitude Cruise	32,000	3.55
Hot Day	Low Altitude Cruise	1,000	2.92
ANA 421	High Altitude Cruise	35,000	4.0
Cold Day	Low Altitude Cruise	1,000	3.1
ICAO	High Altitude Cruise	35,000	3.8
Std Day	Low Altitude Cruise	1,000	3.1

A typical regime represents a flight of 11,000 nautical miles in approximately 310 minutes. These regimes consist of launch and rocket boost to high altitude, steady state cruise at high altitude for approximately 5-2/3 hours, letdown to low altitude in approximately 2.0 minutes, and steady state cruise to target for the balance of flight, approximately 1-1/3 hours. During cruise phases intermittent maneuver and gust loadings will occur.

Contractual requirements of Section 2.2.0 specify a more critical design life of 10 hours. The flight envelope (Figure 6) for ICAO Standard Day specifies a more severe low altitude cruise combination of Mach 3.2 at Sea Level.

2.4 Flight Envelopes

The preliminary Pluto propulsion system operating envelopes for the Model MA50-XCB Nuclear Ramjet for ICAO Standard and ANA 421 Hot and Cold days were presented in Reference 2 and are reproduced in Figures 6, 7, and 8. A typical boost trajectory is shown in Figure 9. Limits for these envelopes are as follows:

1. Mach 2.0 lower limit is established by operation requirements on pneumatic components.

2. Upper altitude limit is established as the line of constant diffuser exit pressure of 45 psia (assures required to 1 pneumatic pressure ratio) up to 50,000 feet.

3. Mach number and altitude requirement is set either by ram air total temperature of 1070°F or a diffuser duct total pressure of 420 psia.

2.5 Nomenclature

2.5.1 Operational Phases

As an aid to systematic analyses, propose typical missile mission profiles are divided into a series of operational ases. These phases which are studied separately for individual maximum loac gs and collectively for lifetime loading effects, are the following:

1. Ground handling
2. Boost
   a. Burnout (launch to burnout)
   b. Separation (booster separation tc igh altitude cruise)
3. High altitude cruise
4. Letdown
5. Low altitude (penetration) cruise
6. Weapons delivery (ejection of multipl stores during final phase of low altitude flight)

2.5.2 Reference Axes

The following reference axes notations we used in the analyses: (1) loads, linear accelerations, and dimensions posit e when acting aft, up, and to the left (viewed from aft); (2) moments, angule accelerations, and angular velocities about references axes follow the "left h d" rule:

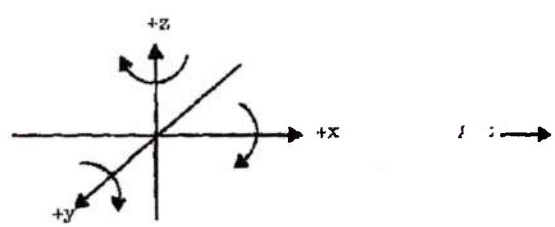

2.6 Basic Operational Factors

2.6.1 Inertial Load Factors

2.6.1.1 Flight Maneuver Factors at Missile Center of (avity

The inertial load factors presented in Table I represent the translational acceleration at the vehicle center of gravity and are reproduced from data presented by Ling-Temco-Vought in Reference 3. Rotational accelerations $\dot{W}_y$ and $\dot{W}_z$ are referenced to the vehicle center of gravity.

Dynamic load shears and moments for ejection multiple warheads must be added to the static rigid body shears and moments derived from these load factors.

2.6.1.2 Flight Maneuver Translational Inertial Load Factors at Centers of Gravity of Individual Components

The component inertial loads shown in Table IV were calculated from data presented in Reference 3 (Figure 18).

2.6.1.3 Design Limit Load Factors for Reactor

The following inertial factors (Figure 19 of Reference 3) represent the combined inertial effects of both translational and rotational acceleration acting at the reactor center of gravity at vehicle Fuselage Station 842.48. The vertical load factors for the case of weapons ejection are presented in Table V for the reactor end stations.

2.6.1.4 Design Limit Ground Handling Inertial Factors

The following factors (Table VI) are in terms translational acceleration at the missile center of gravity (refer to Reference 3, Figure 20).

2.6.2 Vibration Environment

1.	Launch-Boost	Average 3.0g RMS in all directions (180db)	5 to 2000 cps
2.	Cruise (Boundary Layer Noise)	Average 2.25 g in all directions(164db)	5 to 2000 cps

2.7 Analytical Factors

2.7.1 Design Factors and Factors of Safety

Multiplying numerical factors used in the structural analysis design of structural components are classed as "Design Factor and "Factors of Safety" (Table VII).

2.7.1.1 Design Factors

Structural deformations alter propulsion stem performance and, if excessive, may result in functional failure. Desi factors are utilized to provide greater assurance against deformations that re difficult to predict with confidence.

2.7.1.2 Factors of Safety

Factors of Safety are utilized to reduce e possibility of catastrophic structural failure, such as buckling or rupture

2.7.1.3 Limit Loads

A limit load is defined as the maximum va e of the load to which a structural member will be subjected during a critica design condition.

2.7.1.4 Design Load

A design load is a limit load increased b a specified Design Factor of Factor of Safety.

2.7.1.5 Use of Factors

To avoid confusion, the limit values of l ds and/or stresses shall be utilized in all calculations and design facto or factors of safety applied only in the calculation of margins of safety.

2.8 Margins of Safety

Calculated values of limit stresses increased by t appropriate multiplying design or safety factor are compared to the pertine allowable mechanical strength properties and margins of safety derived as ollows:

$$\text{Margin of Safety} = \left(\frac{\text{Allowable Stresses}}{\text{Limit Stresses X factor}}\right) - .00$$

2.9 Limits of Structural Deformation

Material strain within the elastic action range ra ly affects end product function, but additional progressive deformation associ ed with time and temperature will progressively alter propulsion system perf mance and may result in system malfunction.

For a given functional design the object of struct al design, then, is to determine the amounts of deformation that can be tolerate without excessive functional loss and then to provide the minimum weight str ture that will accomplish these requirements.

Deformation limits vary between individual structural components, depending upon their function in the system and the interaction between components.

Allowable limits of deformation are specified in the separate analyses of individual components presented in later sections of this report.

2.10 Materials and Material Properties

2.10.1 Choice of Material

A study of available materials suitable for high temperature operation indicates that nickel base alloys are the most suitable for the current load, time, and environment operational requirements of the Luto propulsion system.

Rene' 41, a precipitation-hardened type of nickel base alloy, the strength of which is developed by various solution and aging heat treatments, appears to be more attractive for use in the present thermal environment. However, if the thermal environment should become less severe, then 15-7PH may be considered.

2.10.2 Over Aging and Cyclic Loading

Long life at temperatures approaching the precipitation heat treatment range may result in excessive overaging and lower stress rupture life. In addition, the low cycle-high stress level fatigue life decreases rapidly at temperatures near the precipitation treatment range.

Since the operational temperatures of the inlet structures are in the 1000°F range, the chosen material should be investigated for cyclic loading.

2.11 Design Parameters

Engine design parameters are shown in Figures 10, 11, and 12 presenting net flow areas, Mach numbers, temperatures, pressures, and auxiliary air requirements.

3.0 INLET

3.1 Design

3.1.1 Discussion

Design layouts have been completed for th basic inlet. Basic lines are shown in Figures 13 and 14, and structural fram g, the spike translation mechanism, and the bypass door actuation mechanism e shown in Figures 15, 16, and 17, respectively.

The inlet is a complete, self-contained s embly starting at Engine Station 49.348 (at tip of spike) and terminating Engine Station 286.936. The inlet assembly is attached to the underside the vehicle by bolts through oversized holes for vertical loads only and by shear pin connection for forward and aft loads. Side loads are resisted by couple between the shear pin connection and six shear pins equally spaced arou the structural ring at Engine Station 286.936.

3.1.2 Boundary Layer Air Bleed

Provision for efficiently discharging inl boundary layer bleed air is made by ducting the air through the two lower s uts into the annulus between the inner and outer shells of the inlet diffuse such that the boundary layer bleed exits axially downstream through a stepped utlet.

3.1.3 Bypass Doors

Bypass doors are used to control the airf w to the reactor. Due to the control package, the doors are located in the bsonic section of the supersonic inlet diffuser where the nuclear heat generat n rates are low and space restriction for the actuator mechanism is less se re. The doors are of the vertically hinged, counterbalanced shutter type, mou d on both sides of the inlet on the inlet horizontal centerline. The doc are designed to operate at a maximum pressure differential of 420 psi at des n point, and are capable of opening and reclosing within three seconds when is required that the inlet restart during low altitude cruise. The doors a rotated by means of a top crank operated from a single pneumatic actuator, hereby insuring synchronization.

3.1.4 Spike Translation

The inlet must be capable of start, reste , and shock positioning at Mach numbers below and above design point. The ike must move forward to start or restart the inlet and must retract for oper ion at higher Mach number. At reduced Mach numbers the intersection point of he two compression shocks moves forward, and it is necessary to extend the sp e forward to keep these shocks positioned properly on the centerbody and bou ary layer bleed forward of this intersection point. The translating spike is d igned to retract 1.00 inch and extend 6.00 inches forward from the design positi as determined by critical operation at Mach 2.8. Also, the spike is designed o translate, under normal operation, at one inch per second with the capabil y of translating 7.00 inches in three seconds.

The spike translation mechanism is designed to operate against a maximum spike load of 58,000 pounds. A modified pneumatic gear motor with servo valve (input speed: 1200 rpm; output speed: 8.2 rpm) drives a cone drive worm gear (30:1 reduction), which drives a 19-tooth pinion, which drives two racks (3 1/2 diametral pitch teeth with effective face width of four inches) that are attached to the inlet spike, thereby providing for spike translation.

The centerbody spike is mounted to a guide system, which consists of four one-inch rods (equally spaced circumferentially about and radially located 5.25 inches from the inlet horizontal centerline) and roller guide bushings affixed to the internal centerbody structure. Axial loads are resisted by the actuation mechanism, and the side loads are resisted by the guide system.

3.1.5 Weights and Centers of Gravity

Weights and centers of gravity for the inlet are listed in Table VIII.

3.2 Structural Analysis

3.2.1 Discussion

The following preliminary structural analysis of the inlet is concerned primarily with major structural items, (Figures 18 and 19). It has been found that in most cases the inertia forces counteract the primary air loads and are small in magnitude. It has therefore been considered sufficiently accurate to omit them from this analysis.

It has been assumed that the structure has been subjected to three possible conditions:

1. A steady state, long time (10 hours) flight regime near sea level with air entering the inlet at 1.0° pitch angle.

2. A short time flight regime (3 minutes) near sea level with air entering the inlet at 6.0° pitch angle and 3.6° yaw angle; this regime represents a "pull-up" condition.

3. A short time flight regime similar to (2) but with shock outside the cowl producing abnormal axial loads on the spike itself.

The following nomenclature is used in the structural analysis:

F = Stress, psi

Δp = Pressure differential, psi

I = Moment of inertia, in^4

b = Width of section, in.

t = Thickness, in.

F_{cr} = Allowable crippling stress, psi

M.S. = Margin-of-safety

3.2.2 Cowl Lip

The pressures for a condition of Mach 3.0 . 1000 feet from data given in Figure 20 are combined as follows to determin cowl stresses and deflections, as these were the only data available at the ti of this analysis.

Pressures on inside and outside lip surfac for an axial length of 4.8 inches are shown in Figure 21 (Sketch A).

Pressures on inside and outside cowl surfa c for an additional axial length of 8.4 inches are shown in Figure 21 (Sket B).

These pressures are averaged as follows to ind the average pressure on the whole 13.2 inches of axial length and a to l loading per inch of circumference as shown in Figure 21 (Sketch C).

ΔP (psi)	Length (inches)	Loading Per Inch of Circumference (lb/inch)	
-37	(4.8)	- 177.5	Sketch
-96	(8.4)	- 806.0	Sketch
-74.5	(13.2)	- 983.5	

The foregoing loading of Figure 21 (Sketch) is now broken into three portions to represent unsymmetrical loading co itions that could result from pitch or yaw angles of attack at the same alti de and speed.

It is assumed in this analysis that the ou ard loading on the windward side drops to one-half its original value, that e outward loading on the leeward side could increase to twice its original alue and that the loadings on the neutral sides would remain unchanged. The t ee loadings which will be superimposed one on another for analysis of the st cture then appear in Figure 22.

Stresses due to hoop tension and bending a combined at the 0° and the 90° locations. Section properties and locations which stresses are calculated are shown in Table IX and Figure 23. Moments e from Table X.

3.2.2.1 Circumferential Location 0°

$$f\ (\text{"e", "g", or "n"}) = F_{H.T.} + \frac{M\bar{d}}{I} = + \frac{984 \times 20}{3.94} + \frac{-13,250(-0.56)}{0.631}$$

$$= 5000 + 11,000 = 16,000 \text{ psi}$$

$$f(\text{"s"}) = + \frac{984 \times 20}{3.94} + \frac{-13,250(0.50)}{0.631} = 5000 - 10,500 = -5500 \text{ psi}$$

$$f(\text{"a"}) = + \frac{984 \times 20}{3.94} + \frac{-13,250(0.147)}{0.631} = 5000 - 3080 = +1920 \text{ psi}$$

$$f(\text{"l"}) = + \frac{984 \times 20}{3.94} + \frac{-13,250(1.067)}{0.631} = 5000 - 22,400 = -17,400 \text{ psi}$$

3.2.2.2 Circumferential Location 90°

$$f(\text{"e", "g", or "n"}) = F_{H.T.} + \frac{M\bar{d}}{I} = + \frac{984 \times 20}{3.94} + \frac{14,500(-0.522)}{0.631}$$

$$= +5000 - 12,000 = -7000 \text{ psi}$$

$$f(\text{"s"}) = + \frac{984 \times 20}{3.94} + \frac{14,500(0.50)}{0.631} = +5000 + 11,500 = +16,500 \text{ psi}$$

$$f(\text{"a"}) = + \frac{984 \times 20}{3.94} + \frac{14,500(0.147)}{0.631} = +5000 + 3370 = +8370 \text{ psi}$$

$$f(\text{"l"}) = + \frac{984 \times 20}{3.94} + \frac{14,500(1.067)}{0.631} = +5000 + 24,500 = +29,500 \text{ psi}$$

3.2.2.3 Longitudinal Lip Bending at Station 6.92 (Hollow Section)

Bending Moment: 1989 inch-pounds

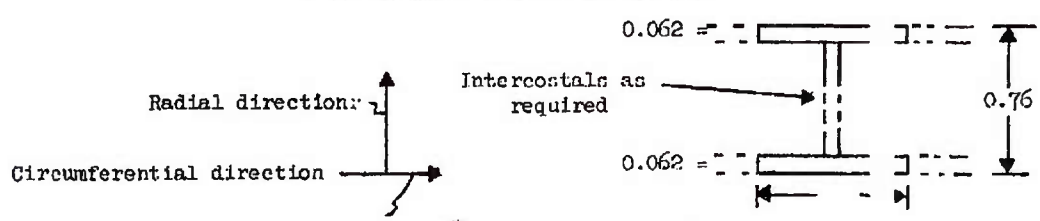

$$I = (0.062 \times 1.0 \times 0.349^2)2 = 0.01[illegible] \text{ in}^4$$

$$f_b = \frac{M\bar{d}}{I} = \frac{1989 \times 0.349}{0.01512} = 45{,}800 \text{ ps[illegible]}$$ (longitudinal tension [illegible] inside surface and longi[illegible]dinal compression on [illegible]side surface)

3.2.2.4 Longitudinal Lip Bending at Station 5.[illegible] (Solid Section)

Depth is 0.40 inch. Take circumferenti[illegible] dimension as 1.00 inch, moment as 925 inch-pounds:

$$f_b = \frac{M\bar{d}}{I} = \frac{925 \times 6}{1.0 \times 040^2} = 34{,}700 \text{ psi}$$

3.2.2.5 Margins of Safety

The stresses of Para. 3.2.2.1, 3.2.2.2, [illegible]nd 3.2.2.3 are all considered as "short time" stresses occurring during a ma[illegible]uver and/or gust. For the purpose of design conservatism, the above stre[illegible]es are raised by the factor of 1.25 and compared with material yield stress[illegible] for short times. At local points where buckling is not a problem, the operatin[illegible] stresses are raised by the factor of 1.10 and compared with the material y[illegible]ld stresses--short time.

3.2.2.6 Circumferential Bending and Tension, Lo[illegible]tion 0°

Temperature taken as 1100°F; material F[illegible]e' 41:

Tension on outside: $MS = \frac{+105{,}000}{+16{,}000 \times 1.2} - 1 = 4.25$

Tension at splice: $MS = \frac{+105{,}000 \times 0.[illegible]}{+16{,}000 \times 1.[illegible]} - 1 = 4.06$

Compression on inside: $MS = \frac{-105{,}000}{-17{,}400 \times 1.[illegible]5} - 1 = 3.82$

Compression on leading edge (tangential direct n):

Take b = 2.00 in., take $t_{effective}$ as 0.057 + 143 (0.25-0.057) = 0.0846 in.

$$b/t = \frac{200}{0.0846} = 23.6$$

$$F_{cr} = 0.452\ \bar{E}\ \left(\frac{t}{b}\right)^2 = 0.452 \times 22.7 \times 10^6 \left(\frac{1}{23.6}\right)^2 = 8{,}400 \text{ psi}$$

(Reference 6, Table B 5.2)

$$MS = \frac{-18{,}400}{-1.25 \times 5500} - 1 = 1.67$$

3.2.2.7 Circumferential Bending and Tension, Location °

Temperature taken as 1100°F; material Rene' 41

Tension on inside surface: $MS = \frac{+105{,}000}{+1.25 \times 29{,}500} 1 = 1.85$

Tension at splice: $MS = \frac{+105{,}000 \times 0.8}{+ 1.10 \times 29{,}50} -1 = 1.75$

3.2.2.8 Longitudinal Bending Stress at Location 0°

Temperature taken as 1100°F; material Rene' 41

Compression on outside surface from Para. 3.2.: 3

There is a weld splice, so efficiency of joint aken as 0.85:

$$MS = \frac{105{,}000 \times 0.85}{45{,}800 \times 1.25} - 1 = +0.56$$

3.2.2.9 Summary Note

Since the above calculations were made there h been a slight modification of skin gages; however, it is believed that chan s in gages will not appreciably affect the above analysis.

3.2.3 Diffuser Skin

3.2.3.1 Bursting Effects

This applies to the inner of double skin

R = 17.88 inches; design pressure inside 400 psi
(maximum which would occur locally betwe frames)

Pressure outside = 15 psi; P = 3 psi

By conventional formula for bursting of cylinder,

$$f_{HT} = \frac{P \times R}{t} = \frac{385 \times 17.88}{0.10} = 68,750$$

Material: Renc' 41

Joint Allowable:

10 hours, 0.2% creep = 0.85 x 92,000 = 78 100 psi

$$MS = \frac{78,100}{1.1 \times 68,750} - 1 = +0.03$$

3.2.4 Load Paths of Unsymmetrical Airloads

3.2.4.1 Loads Normal to Centerline of Spike

The spike geometry and loads normal to t center are shown in Figure 24.

The relation of cone length to diameter

$$f_n = \frac{l}{d} = \frac{46.1}{30.48} = 1.51$$

Although data are not available for valu of f_n down to 1.51 (Reference 7, Tables I and II), it is conservative to use e shortest cone $f_n = 3.0$, to arrive at normal force derivatives and centers of essure. The value of f_a, the ratio of length to diameter for the cylinder mstream of the cone, is conservatively assumed to be zero.

From Reference 7 (Table I), with $f_n = 3.0$ and f = 0, the change in normal force coefficient, C_n, with angle of attack, α using the second order expansion method, is

$$\frac{dC_n}{d\alpha} = 1.83 \text{ rad}^{-1}$$

From Table II, $f_n = 3.0$, $f_a = 0$, $X_{cp}/d = 2.00$ (cond order expansion method). This places Center of Pressure at 2/3 the d tance from the tip to the base of the $f_n = 3.0$ cone.

At sea level and Mach 3 conditions, the dynamic ressure, q, is

$$q = \frac{\gamma}{2} P_o M_o^2 = \frac{1.41}{2} \times 14.7 \times 3.0^2 = 93.4 \text{ p}$$

The normal force on the cone = $C_n\, q\, S\, \alpha$, wher S is the cross-sectional area of the cone base, and α is the angle of attack radians.

$$\text{Take } S = (\pi)\,(30.48^2)/\,4 = 731 \text{ in.}^2$$

Using the coefficient C_n of the preceding page ltiplied by 1.25 to cover discrepancies that may exist between the theoretical one and the actual spike, the normal force per degree angle of attack is esti ted to be:

$$F_N = 1.25 \times 1.83 \times 93.4 \times 731 \times \frac{1}{57.3°/\text{rad}} = 2730 \text{ lbs/deg e}$$

The fore and aft center-of-pressure location fc this load will be taken at 60 percent of the distance from the tip to the base compared to the 67 percent for an $f_n = 3.0$ cone.

3.2.4.2 Cowl and Innerbody Unsymmetrical Loadings

The loads of Figure 25 appear in plan view in F ure 26 along with moment load calculations.

Design conditions selected (see Figure 27) are r 6° pitch angle of attack for the inlet relative to entering air and 3.6° ngle of yaw for the inlet relative to entering air.

$$R_{EE} = \frac{37{,}600\ (127.86 + 32.60 + 39.06 - 10.4) - 10{,}840\ (127.86 + 32.60) - 87{,}200}{127.86}$$

$$= (7{,}500{,}000 - 1{,}740{,}000 - 87{,}200) \quad 127.86 = 44{,}400 \text{ lbs.}$$

Shears, moments, and torques from Y direction components only are shown in Figure 28.

The torques are considered as reacted by the body in proportion to the distance from the centerline to the fitting squared at any one station. Such reaction distributions are tabulated in Table XI.

Shears, moments, and torques from Z direction components only are calculated below, and the results are shown in Figure 29.

Distance from (A-A) to centroid of group is

$$\frac{\Sigma x}{6} = \frac{464.22}{6} = -77.3 \text{ inches} = \text{centroid P of vertical reactions}$$

Loads of Figure 29 are transposed to the centroid and the moment distributed out to the various reaction points as

$$p_z = \frac{mx'}{\Sigma (x')^2}$$ where minus below indicates compression at joint

$$\Sigma \text{ (vertical load)} = 62{,}800 - 18{,}080 = 44{,}720 \text{ lbs}$$

$$\Sigma \text{ (moment about P)} = 62{,}800\ (199.52 - 77.3 - 10.4) - 145{,}200 - 18{,}080\ (199.52 - 77.3 - 39.06)$$

$$\Sigma M_p = + 7{,}020{,}000 - 145{,}200 - 1{,}502{,}000 = 5{,}372{,}200 \text{ in-lbs}$$

Load at any station (from moment) is then

$$p = \frac{5{,}372{,}200\ x'}{18{,}867} = 285\ x'$$

The calculation for this load is summarized in Table XII.

The vertical load is divided equally among : e six stations.

$$\frac{44,720}{6} = 7452 \text{ lbs/each}$$

To determine fore and aft loads, the structu e is broken into segments and the radii and pressures of Figure 30 are applie The pressures given in Figure 30 represent the symmetrical portion of the asymmetrical load system used for analysis of the cowl lip.

The inside pressure of the innerbody is take as 62 instead of 110 to obtain conservative panel pressures. The pressure calculations appear in Table XIII.

Loads of Table XIII are now summarized (a p: s load is one acting aft):

Spike less skirt:

+7540 + 2400 - 3350 - 6580 = +10 lbs

Spike including skirt attached to it:

+10 - 4370 = -4360 lbs

Fixed part of innerbody complete:

-3500 - 28,100 - 56,600 - 56,300 = 144, 00 lbs

Complete innerbody, including spike:

-144,400 - 4360 = 148,760 lbs

There will also be a drag on the wedge struc ure between the inlet and the vehicle. The half angle is 8°, and the average eight is 5.0 inches. The base width at Section A-A of Figure 18 is 50 inches.

From Reference 8, the pressure ratio across two-dimensional shock at Mach 3.0 for a half angle of 8° is $p/p_o = 1.80$, so that at sea level conditions the pressure behind the shock is 1.80 x 14.7 = 26 psia. This pressure is considered constant from the entering edge back to Sec on A-A (Figure 18). The inside pressure will be considered as ambient, 14.7 sia, for the present such that total drag for the wedge structure aft to Sectio A-A becomes

(50 in. x 5 in.) (26.5 - 14.7) = (250) (11.8 = 2950 lbs

$$\left[q \text{ (ref. only)} = \frac{\alpha}{2} P_o M_o^2 = \frac{1.41}{2} \times 14.7 \times 3.0 = 93.4 \text{ psi}\right]$$

Axial load from the inlet and wedge struc ıre is then:

$$- 148,760 + 2950 = - 145,810 \text{ lbs (ac ng forward)}$$

The effect of inlet forward load on the v tical fitting at the inlet vehicle joint is now considered. The analysis is milar to that presented in Figure 29. However, in this case, the couple whic is reacted vertically at the six fittings, results from axial loading on the ag fitting at the vertical centerline of Section E-E.

Figure 31 shows the fitting. Calculatior are presented below.

The couple resulting from forward load on hc inlet is:

$$145,810 \times 25.08 = 3,660,000 \text{ in./lbs}$$

Point P is the centroid of the vertical r ctions (Figure 29 and Table XII) that must resist this moment.

The load at any station due to the applie moment is then

$$p = \frac{3,660,000\ x'}{18.867} = 194.0\ x'$$

This example is evaluated in Table XIV.

3.2.4.3 Summary Tables of Attachment Reactions

Following the nomenclature of Figure 18, e reactions from airloads of the unsymmetrical condition are listed in Tabl XV.

Loads marked with an asterisk would act o the aft portion of the split frame at Section (A-A), rather than directly fitting points (k) and (l).

3.2.5 Strut

The forward load is 148,760 lbs from the nerbody to the diffuser double wall for a normal cruising condition (Page

There are three struts to carry this shea load, so the load on each is:

$$\frac{148,760}{3} = 49,500 \text{ lbs}$$

Radial reactions induced at spar stations (E-) and (F-F) are:

$$\frac{49,500 \times 6.6}{32.6} = 10,020 \text{ lbs total in radi direction}$$

These reactions are apportioned between inne and outer support rings in inverse proportion to the ring radii cubed for pre iminary design purposes (see Figure 32). NOTE: Short time maneuver loads f a the innerbody could produce loads of

$$\frac{-204,400}{-148,760}$$

or 1.38 times the above values (see Para. 3.2.5.2).

3.2.5.1 Struts (Normal Symmetrical Loads Alone)

Load on struts from supporting rings are sho in Figure 33.

3.2.5.2 Special Load Conditions Wherein Shock Has Mo Forward From Its Normal Location

With the shock moved well forward, the aft l s on the spike is at 40,000 lbs. Using the normal cruising pressures for th fixed portion of the innerbody, the minimum forward load of the entire inne dy is now estimated as follows:

Minimum Forward Load = -148,760 + 4360 + 40,000 = -1 000 lbs
(Reference Page

With the shock moved well aft, the spike forw d load has been estimated at 60,000 lbs. Using the normal cruising pressures r the fixed portion of the innerbody, the maximum forward load of the innerbody e estimated as follows:

Maximum Forward Load = -148,760 + 4360 - 60,000 = -204 00 lbs

The above may be compared with the normal cru e condition forward load:

Normal Forward Load = -144,400 - 4360 = -148,760 lbs (ge

3.2.5.3 Loads on Strut Spars from Unsymmetrical Loads ormal to the Centerline

The total loads from the spike and the fixed rtion of the innerbody, as shown on Figure 26, are the resultant loads on a ane rotated 30° 58' from a vertical plane.

X - Direction Reaction "R" + "S" = $600{,}000 \times \frac{2}{3} + \frac{564{,}000}{11.82} - \frac{18{,}100\ (\ldots .06)}{11.\ldots}$

$= 40{,}000 + 47{,}700 - 59{,}8\ldots = +27{,}9\ldots$ lbs

Load "R" = Load on "S" = $\frac{27{,}900}{2}$ = 13,950 lbs Tension on Joint

3.2.6 Innerbody Ring at Section (F-F)

The innerbody rings, the diffuser ring, and the struts form a redundant system of load paths. However, a simplified and conservative set of loads on the innerbody ring of Section (F-F) has been employed to find the maximum bending moment. The ring is subjected to both transient short time and steady state long time loads.

3.2.6.1 Steady State Long Time Loads

The innerbody forward load is taken as -148,76... lbs (Figures 32 and 33). The loads normal to the centerline of the innerbody are considered the same as those for the 1° angle of attack condition which is one sixth of those in Figure 36.

Steady State Flight Condition Ring Moments are calculated in Tabels XVI and XVII.

For the unsymmetrical portion of moments, PR is ,760 x 10.79 = 40,500 (see Figure 37). Moments for symmetrical portion of loads are carried over from preceding page.

3.2.6.2 Short Time Maneuver Loads

The innerbody forward load is taken as -204,000 lbs, which is 1.38 times normal thrust (see Figure 32 and Paragraph 3.2.5.2). T loadings then appear as shown in Figure 38.

The unsymmetrical load is taken as 7/6 times th vertical load shown in Figure 36.

Ring moments from short time maneuver loads are calculated in Table XVIII, and ring section properties are calculated in Figure .

3.2.6.3 Stresses and Margins

Using the ring section properties and the two b ic loading condition ring moments determined in the previous pages, the marg s of safety of this ring are calculated as follows (Material is Rene' 41):

Steady State - Long Time Loading:

Free Flange $f_{b_i} = \frac{Mc}{I} = \frac{-27,100 \times 1.84}{3.27} = -15,250$ psi (C pression)

I.B. Skin near Flange $f_{b_o} = \frac{-27,110\ (-1.45)}{3.27} = +12,000$ i (Tension)

It is proposed to maintain a 10 percent fety factor to material yield and a 25 percent safety factor to structural fa ure. The yield allowable is taken as the stress level to force a yield of 0.2 ercent with 25-hour exposure at 1100°F. The ultimate allowable is taken as t short time 0.2 percent yield stress at 1100°F.

MS on Yield $= \frac{-92,000}{1.10\ (-15,250)} - 1 =$ mple

MS on Failure $= \frac{-105,000}{1.25\ (-15,250)} - 1 =$ Ample

Short Time Maneuver Loading:

Free Flange $f_{b_i} = \frac{Mc}{I} = \frac{-92,060 \times 1.84}{3.27} = 51,800$ psi (Co ression)

I.B. Skin near Flange $f_{b_o} = \frac{-92,060\ (-1.45)}{3.27} = +40,800$ i (Tension)

It is proposed to maintain a 10 percent fety factor to material yield and a 25 percent safety factor to structural fa ure. Short time yield is employed here for the allowable, because buckling cou occur when yielding commences.

MS on Yield $= \frac{-105,000}{1.10\ (51,800)} - 1 =$ .85

MS Against Failure $= \frac{-105,000}{1.25\ (51,800)} - 1$ +0.62

3.2.7 Innerbody Skin

At Section (F-F) of Figure 26, the following re the loads across the section:

Shear forward of section: 21,090 lbs (transv se)

Moment at section: 169,400 in.-lbs

Shear aft of section: 169,400/32.6 = 5,200 l (transverse)

Normal shear flow to each longeron from inne ody thrust is 49,500/32.6 = 1520 lbs/in. (see Figure 32).

Normal shear flow to each longeron from shor time thrust with shock in abnormal position on the spike is 1.38 x 1520 = 2100 bs/in. (see Figure 37).

Shear buckling forward of Section (F-F):

Panel width, 5.00 inches; radius, 12.5 inche t, 0.125 in.

Maximum shear on side

$$\frac{V}{\pi Rt} = \frac{21,090}{\pi \times 12.5 \times 0.125} = 4300 \text{ psi}$$

To estimate critical shear buckling, see Ref ence 10.

$$T_o = \left\{(0.10\, E\frac{t}{R}) + 5\, E\, (\frac{t}{d})^2 \left[1 + 0.8\, (\frac{d}{h})^2\right]\right\} 0.75$$

$$= \left\{(0.10 \times 22.5 \times 10^6 \times \frac{0.125}{12.5}) + 5 \times 22 \times 10^6\, (\frac{0.125}{21})^2 \left[1 + 0 \quad (\frac{21}{5})^2\right]\right\} 0.75$$

$$= \left\{(22,500) + 3980 \quad \left[15.1\right]\right\} 0.75 = 62,000 \text{ psi}$$

The margin of safety against shear buckling adequate.

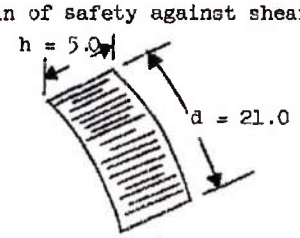

3.2.7.1 Collapse of Skin between Frame Supports st. Forward of Section (F-F)

Normal pressures are 311 psi outside and 2 psi inside (Figure 30). However, to account for possible higher values o pressure introduced by angles of attack and yaw, a maximum outside pressure 400 psia with 62 psia inside will be employed here. Therefore, $\Delta P = 338$ i (see Reference 11, Page 306, Table XVI, Cond. Q, Support 31):

p' = pressure of collapse from external essure

$$= 0.807 \frac{Et}{lr} \left[\left(\frac{1}{1 - \nu^2}\right)^3 \frac{t^2}{r^2} \right]^{1/4} = 48 \text{ psia}$$

It is proposed to maintain a safety fact of 10 percent on the peak short time operating pressure:

$$MS = \frac{485}{1.10 \times 338} - 1 = +0.30$$

3.2.7.2 Shear Buclking of Skins between Sections -F) and (E-E)

Loading (short time maximum) from Paragr n 3.2.7 is 2100 lb/in. to allow for uneven distributions plus shear from nsverse shear (skin shear to each side of strut is taken at 75 percent, or 0 5 x 2100 = 1575 lb/in. To estimate critical shear buckling stress as in ragraph 3.2.7 (except frame spacing is 7.7 and R is 11.50 in.):

$$T_o = \left\{ \left(0.10\, E \frac{t}{R}\right) + 5E \left(\frac{t}{d}\right)^2 \left[1 + 0.8 \left(\frac{d}{h}\right.\right.\right\} 0.75$$

$$= 39{,}000 \text{ psi}$$

Since it is proposed to maintain a safet factor of 10 percent for this short time buckling shear stress, the margin safety is:

$$MS = \frac{37{,}000}{1.10 \times \left(\frac{1575}{0.125}\right)} - 1 = \frac{37{,}000}{12{,}860} - 1 = \text{ple}$$

3.2.7.3 Collapse of Skin Between Frame Supports Aft of Section (F-F)

Design pressure, with some allowance for asymmetry at angles of attack, is taken as

$$1.15 \times 311 = 358$$

$$\Delta P = 358 - 62 = 296 \text{ psi}$$

$$p'^{*} = 0.807 \times \frac{22.5 \times 10^6 \times 0.125^2}{7.7 \times 11.5} \left[\left(\frac{1}{1 - 0.3^2}\right)^3 \frac{0.125^2}{11.5^2} \right]^{1/2} = 341 \text{ psi}$$

Proposed extra margin between operating load and buckling failure is 10 percent.

$$MS = \frac{341}{1.10 \times 296} - 1 = + 0.05$$

3.2.7.4 Innerbody Intermediate Frames

Aft of Section (F-F) of Figure 19, the panel spacing is 7.7 inches. Maximum differential pressure is 358 - 62 = 296 psi. Loading on one ring per inch of its circumference is 296 x 7.7 = 2280 lbs per inch. The elastic stability capacity of the ring is computed following Reference 11, Page 295, Table XV, Case 12. The section properties appear in Figure 40.

$$p' = \frac{3\,EI}{R^3} = \frac{3 \times 22.5 \times 10^6 \times 0.0817}{11.28^3} = 3810 \text{ lbs per in}$$

It is proposed to keep a 25 percent extra factor against such a collapse; therefore,

$$MS = \frac{3810}{1.25 \times 2280} - 1 = + 0.34$$

- - - - - - - - - - -

*Reference 5, Page 306, Table XVI, Cond. Q, Support 31

3.2.8 Thrust Fitting

The critical loads (Figure 41) on this pi occur at the maximum forward load condition of the innerbody--Paragraph 3.2. 2 (-204,400 lbs) and the lateral load of the yaw condition--Figure 27 (44,4 lbs). There will also be a wedge drag of 2950 lbs.

Total load = -204,400 + 2950 = -201,450 l

At Section (A-A) through the pin there wi be both bending and shear.

Bending is

206,000 lbs x 0.70 inches = 144,000 -lbs

Section (A-A) Moment of Inertia is

$$\frac{\pi D^4}{64} = \frac{\pi \times 2.75^4}{64} = 2.82^4 \text{ inches}$$

$$f_b = \frac{Mc}{I} = \frac{144,000 \times 1.375}{2.82} = 70,200 \text{ p}$$

$$f_{s(av)} = \frac{S}{A} = \frac{206,000 \times 4}{\pi \times 2.75^2} = 34,700 \text{ p}$$

Material: Rene' 41

Short time 0.2 percent yield at 1100°F is

105,000 psi

Short time ultimate stress at 1100°F is

152,000 psi

Long time (10 hours) 0.2 percent yield at 1100 F is 92,000 psi

$$\text{MS (short time yield)} = \frac{105,000}{1.10 \times 70,200} - 1 = +0.36$$

$$\text{MS (short time ultimate)} = \frac{152,000}{1.25 \times 70,200} - 1 = +0.74$$

$$\text{MS (long time yield)} = \frac{92,000}{1.10 \times 70,200 \times \left(\frac{145,800}{206,000}\right)^{*}} - 1 = +\ 68$$

$^{*}\left(\frac{145,800}{206,000}\right)$ = Ratio $\frac{\text{Normal Operating Load}}{\text{Maximum Short Time Load}}$ (See Page)

4.0 SUBSONIC DIFFUSER AND REACTOR CONTRC SUPPORT STRUCTURE

4.1 Design

4.1.1 Discussion

For purposes of this report, the subsonic iffuser is defined as that part of the propulsion system between Fuselage St ion 660 (Figures 1 and 2) and the front face of the reactor. The reactor contrc support structure is defined as the components within the subsonic diffuser at make up the mechanical linkage between the reactor control rods and the act tor as well as the structure needed to support this linkage and the rods.

Design of the subsonic diffuser, which (f m the point of view of the propulsion system) is a pressure duct, is limited t defining aerodynamic lines. These lines are defined to permit optimum perfc ance of the propulsion system with the smallest possible duct size. Mechar al and structural design of the duct is the responsibility of the airframe nufacturer, inasmuch as the duct is an integral part of the airframe.

The design of the reactor control rod act tors, associated linkage, and support structure is a more complex problem f the engine manufacturer than is the subsonic diffuser. For the former, it s necessary to obtain requirements from the reactor company, geometric and env onmental limitations from the airframe company, and inputs from the propulsi system controls group, and to integrate all these into a well-designed st ctural system.

Listed below are the factors that have be considered in this design:

1. Stroke: approximately 40 inches
2. Temperature: 1070°-1200°F
3. Rate of travel: Full stroke in 0.75 conds
4. Minimum passage blockage
5. Maximum axial g load: 25 g
6. Maximum radial g load: 4.5-0.25g
7. Accessibility
8. Friction load between control rods a reactor tubes
9. Air drag loads in rods
10. Air drag loads in the support mechan m

11. Limiting deflections of supports, rods, d duct

12. Vibration of supports and control rods 0 36 inches D.A. Frequency, 0-3000 cps

13. Reliability

14. Number, types, and position of control r s: 12 shim and 2 vernier

In designing this portion of the system sever approaches have been studied. The design as shown in Figure 2 has been consid cd most promising from the point of view that it presents the smallest bloc ge in the diffuser and provides the best accessibility to the actuator.

In the matter of mechanical and structural fu tions, the air motor, gear box, and control valve are positioned on the outsid periphery of the duct to afford greater accessibility for maintenance and to duce flow blockage in the duct.

A rack and pinion type drive unit is located the main support strut. The unit is driven by the motor through a shaft tha is located inside the strut. The rack is attached to a spider fitting, which cks up four control rods from the reactor, at the downstream end of the ra . The attachment of the control rod to the spider fitting may be either fix or a quick-disconnect type with manual or remote handling features. Mov ent of the rack translates the spider fitting along a guide shaft that is supp ted between the main support and the aft support. The guide shaft also a as a housing for the feedback transducer, which is geared down and opera s off the main rack. When moving upstream, the rack is housed and guided in tube that is supported between the main support and the forward support.

Figure 2 does not reflect any method of attac ent between the supports and the duct. Because of differential thermal c ansion, these points will, of necessity, be a slip-fit type of connection.

A detailed design study and subsequent structu al analysis of this area must be accomplished before a final decision can b made as to the best system. However, before this study can be accomplished an verall control system study must be made that will more accrurately define the equirements of this structure.

4.1.2 Weights and Centers of Gravity

Weights and centers of gravity for the reacto control rod support structure and actuation mechanism are shown in Table XI

4.2 Preliminary Analysis of Control Rod Support Structure

4.2.1 Loads

Weight of control rod = 5.7 lbs

Weight of rack (estimated) = 1 in.^{2} x 50 n. long x 0.3 density = 15 lbs

Weight of spider fitting (estimated) = 1 6 in.^{2} blockage

Estimated average thickness = 3 inches

Weight ≅ 13.6 x 3 x 0.3 = 12.25 lbs

4.2.1.1 Aerodynamic Drag Load Per Strut = 422 lb

Total load per strut (inertia) = (4) (5. + 15 + 12.25 = 50 lbs

4.2.1.2 Strut Design Load

Load at the 6g boost condition = (6) (5) 422 = 722 lbs

The twelve coarse control rods are actua d in groups of four and are reacted by three struts as shown in Figure 42. T allow for ther- mal expansion, the struts are fixed at the center and have a s ding support at the duct wall.

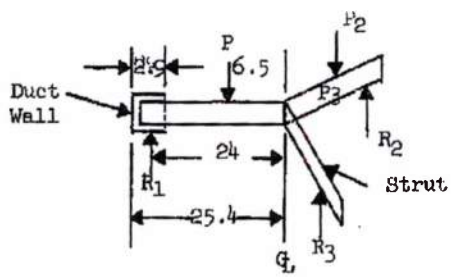

$P_1 = P_2 = P_3$

$R_1 = R_2 = R_3$

Assume struts fixed a centerline.

Assume only shear loa carried thru R_1, R_2, R_3 at the duc wall

$P_1 = R_1$ etc

$P_1 = 722$ lbs

Moment = 722 (24 - 65) = 12,620 in-lbs (max)

According to Reference 5 and Figure 43:

$$I_{xx} = ctL^3$$

$$C_1 = f\left(\frac{L_1}{D_1}\right)$$

$$D_1 = 1.50 - 0.05 = 1.45$$

$$\frac{L_1}{D_1} = \frac{5.20}{1.45} = 3.58$$

$C_1 = 0.20$

$Y_1 = 49.09\% \; L_1$

$I = (0.2)\,(0.05)\,(5.20)^3 = 1.408$ in.

$Y_1 = (0.4909)\,(5.20) = 2.55$

$C = 2.55 + 0.025 = 2.58$

$f_{bc} = (12{,}620)(2.58)/1.408 = 23{,}200$ ps compression

$f_{bT} = (12{,}620)(2.67)/1.408 = 24{,}000$ ps tension

Using 19-9 DX material and assuming that buc ing is not critical, then:

$F_{TY} = 37{,}000$ psi at 1200°F

$F_{Tu} = 75{,}000$ psi at 1200°F

$E = 22 \times 10^6$ at 1200°F

MS = (37,000/24,000) -1 = + 0.54 tensi

4.2.2 Deflection Check of Strut

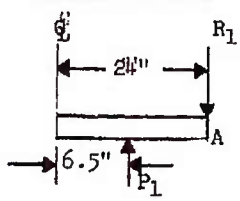

$R_1 = P_1 = 722$ lbs

$\ell = 24$

$a = 6.5$

$I = 1.408$

$E = 22 \times 10^6$

4.2.2.1 Deflection at PT A Duc to R

$$y_1 = \frac{PL^3}{3EI}$$

4.2.2.2 Deflection at PT A Due to P_1

$$y_1 = \frac{P}{6EI}\,(3\,a^2\ell - a^3)$$

4.2.2.3 Total Deflection at PT A = $y_1 - y_2$

$$y_1 - y_2 = \frac{P}{6EI}\left(2\ell^3 - 3a^2\ell + a^3\right)$$

$$= \frac{722}{(6)(22)(10)^6\ 1.408}\quad (2)(24)^3 - (3)(6.5)^2\ (24)\quad (6.5)^3$$

$y_1 - y_2 = 0.097$ in. = Max Deflection

5.0 REACTOR SUPPORT SYSTEM

5.1 Side Support System Design

During FY 1962 attention has been centered on the minim ation of the lateral support annulus dime sion in the interest of increasing e aerodynamic perfo mance of the overall Pluto system.

The analytic optimization of the latere l support annulu is based on an assumed dynamic model (see Section 5.2.2) and consists of the timization tion of both the radial spring rate and the support spring configura on. The spring rate is optimized to give a minimum required energy storage i the system for the specified design criteria. The spring configuration was elected to achieve a maximum of strain energy storage in the spring for a mi mum volume of spring material. A detailed description of this work may be foun in Section 5.2.3.

The nuclear reactor core and its reflectors consist of assembly of approximately 450,000 hexagonal ceramic tubes measuring 0.297 inc s across the flats and 2.0 to 4.0 inches in length. The tubes are stacked en to end to form continuous tubes approximately 62.0 inches in length, and these turn are assembled side to side to form a right circular cylinder 53.25 inche in diameter. The reactor cylinder is aligned axially in the airframe duct.

The core assembly is clamped into the desired cylindric shape and is supported to the airframe by the lateral support system. The resent design concept consists of a series of close fitting, curved pressur pads, which form an expandable shell around the core. They are compressed gainst the core by radially orientated springs, which in turn bear against monolithic cylindrical shell that encloses the entire core, pressure pad, an spring assembly.

The pressure pads are supported in radial planes by the prings and in tangential and meridional directions by radially oriented pin- nd-socket connections to the pressure shell.

The pressure shell, in turn is supported tangentially b means of a longitudinal tongue and groove rail system, which allows radial gr th of the shell with relation to the airframe.

The reactor tube matrix and spring support system are es entially a spring mass system, which is sensitive to vibration loading. The s ring system must be so designed that response of the reactor to vibration los s from the airframe will not be excessive.

Weights and centers of gravity are shown in Table XX.

5.1.1 Side Support System Function

The reactor lateral support structure must be c pable of (1) insuring an adequate clamping pressure on the reactor matrix, (2) accommodating severe relative thermal expansion between the matrix and the c taining

shell, (3) limiting the transverse deflection of the core from inert: and vibration loads, and (4) permitting the reactor to be handled as a com; ete assembly.

A compressive force must be exerted on the tub: matrix at all times to prevent excessive distortion of the tube bundle or gros: separation of tubes. The necessity for this compressive force arises from oth structural and aerodynamic considerations. Separation induces adverse lo paths in the support system; and tube misalignment, with resulting flow block: e, could be caused by both distortion and separation.

A severe differential thermal expansion exists etween the reactor and the surrounding structure; i.e., the reactor, at 250(F, thermally expands into its supporting shell, which is at approximately 1: 0°F.

The side support system must furnish adequate pport to the reactor when it is subjected to lateral inertia loads. The reac: r and the support springs, being essentially a spring-mass system, are sensiti to vibration loads. The support system must prevent the occurrence of exces: ve reactor response from this type of loads input.

The system should be designed in a way that pe: its the handling of the reactor as an entity. Such a design will ease groun handling and reactor-vehicle assembly problems.

The above requirements must be met while maint ning the structural integrity of the ceramic tubes. In addition, the structu: of the side support system should be contained in as small an annulus as po ible, thereby assuring as high a degree of performance as possible for the ngine-vehicle system.

5.1.2 Side Support Annulus Thickness to Vehicle Drag omparison

Since the drag of the vehicle is approximately roportional to the cross sectional area, a 1/8-inch reduction in radius will ieve a 1 percent reduction in drag; i.e., reducing the side support annulus rom 1.5 to 1.0 inches will result in a 4 percent reduction in vehicle drag. nus, considering the low thrust-to-drag margins associated with nuclear ramj e (approximately 10 percent), it is extremely important to minimize the side pport annulus dimension.

5.1.3 Reduction in Annulus Width

Considerable effort was expended in 1962 to mi nize this annulus width, pointing toward a target of 1.0 inches. The results e illustrated in Figure 44, which depicts the reduction in annulus width vs time for the years 1961 and 1962. The reduction was achieved through optimiz ion of the spring rate and the spring used in the side support system. Sec on 5.2 contains a detailed description of this work.

5.1.4 Design Side Support System

The resulting side support system is show in Section (C-C), Figure 45. The system consists of four main components: sp g pressure pad, (expansion pad) radial spring, pressure shell, and the sup rt rails.

The spring pressure pad transmits radial ads between the reactor and the spring system. It aids in distributing the oncentrated spring loads into the radial reflector. It also carries tangen al shear loads due to friction between the pad and reactor, into the support r ls.

The spring provides a compressive load du g ground handling and flight, contains reactor thermal and inertial movemen , and transfers resulting loads to the spring pressure shell.

The spring pressure shell reacts the ther l expansion loads and shears the reactor inertia loads to the support rails. This shell also helps isolate reactor axial movements from those of the ai rame. This isolation is accomplished by slicing the shell into short axial ections so that a minimum of the friction load resulting from reactor move t will be transferred to the airframe structure. The support rails trans reactor inertia loads from the spring pressure shell to the structure of t airframe.

5.1.5 Operating and Installation Requirements

Assumed criteria are outlined for the sid upport system using either tangentially or radially oriented springs. Fi es 46 and 47 show temperatures assumed for structural analysis. Table XXI p ents the relative differential thermal expansion that occurs during the sys lifetime. Table XXII summarizes the thermal and inertial conditions used i design analysis. In addition to the above, the following general criteria st also be met.

1. Maximum permitted reactor lateral de ction = 0.100 inches. This requirement arise from considerations of tie rod-to-core inter ence.

2. No finite separation between the reac r and the support system is permitted for a design condition; i.e., the support system n t remain in contact with the reflector at ll times.

5.1.5.1 Assumptions

1. The structural shell surrounding the actor remains circular.

2. The tube matrix behaves as a rigid cy nder.

3. The side support structure can be int grated into a single elastic constant or spring r e.

4. Only the translational mode of the reactor s of interest.

5. Only friction-induced slip damping is pres t.

6. The dynamic input is a sinusoidal, undampe motion with a frequency of 9.5 cps and a p k load of 7g (see Note 1).

7. Average coefficient of friction on the ref ctor-support system interface is equal to 0.30.

Note 1. The major vibration loads input to the upport system occur as a result of fuselage response, during the low altitud cruise phase of flight to free flight conditions. These conditions are terr n avoidance, atmospheric gusts, and stores ejection. Fuselage response to t rain avoidance is an approximate sinusoidal low frequency motion. That du to stores ejection is sinusoidal but highly damped (5-second duration), while t gust input is random. These three fuselage responses combine into a 7g peak oad at a discrete frequency. The input used in analysis is conservatively ass ed to be a 7g peak, sinusoidal, steady state vibration, occurring at the 9.5-c fuselage frequency.

5.2 Side Support System Analysis

5.2.1 Nomenclature

A = Amplification factor (dynamic deflectio static deflection)

P_o = Magnitude of driving load (lbs/in$_a$

n = Inertia load factor (g)

W = Reactor weight (185 lbs/in$_a$)

V_z = Apparent load on springs (lbs/in$_a$)

F = Friction damping load (lbs/in$_a$)

μ = Reflector--support system interface fri ion coefficient

R = Outer radius of reflector (in.)

p_o = Reactor preload pressure (psi)

Δp_T = Change in reactor pressure due to diffe ntial thermal expansion (psi)

Δp_I = Change in reactor maximum pressure due inertia load (psi)

p_s = Static reactor pressure after diff ential thermal expansion (psi)

$\Delta\delta_T$ = Differential thermal expansion (in

$\Delta\delta_I$ = Reactor deflection from inertia lo (in_r)

p_m = Reactor dynamic and static pressur (psi)

f = Driving frequency (cps)

f_n = Resonant frequency of reactor spri -mass system (cps)

g = Gravity constant (386.4 in/sec^2)

K_z = Support system integrated spring r e ($lbs/in_a/in_r$)

k_r = Support system radial spring rate si/in_r)

E = Spring material elastic moduli (ps

T_m = Maximum tensile load in tangential pring systems (lbs/in_{r_a})

k_c = Circumferential spring rate (lbs/i /in_c)

V_o = Volume of spring element (in^3)

l = Spring element length (in)

β = Ratio of distance from end of spri to load point to spring length

n_p = Number of springs in parallel

n_s = Number of springs in series

η = Surface efficiency of the spring

σ = Allowable stress of the spring mat ial (psi)

b = Ratio of end thickness to center t kness of the spring

ψ = Structural efficiency of the sprin

Subscripts

r = Radial

z = Transverse

a = Axial

o = initial or preload conditions

c = circumferential direction

Superscripts

c = low altitude cruise conditions

b = boost-transition conditions

5.2.2 Dynamics Model and Optimum Spring Rate

5.2.2.1 Dynamics Model

A dynamic analysis of the reactor and support s tem, based on an idealized fluid cylinder vibrating in an elastic medium, ference 4, has shown that appreciable excitation of distortional modes of the ube matrix is unlikely in the frequency range of interest (5-30 cps). Howe r, a low frequency resonance could exist corresponding to the rigid-body trans tion mode of the matrix. This mode occurs at the system fundamental frequ cy, which is determined by the mass of the reactor and the spring constant of t side support structure.

The result of the above dynamic analysis and co ideration of the inertia load inputs suggests a simple dynamics model on which e prelim-inary dynamic analysis of various lateral support structure configura ons will be based. The model is a single-degree-of-freedom, slip-damped syste

The radial and tangential configurations are sh n sche-matically in Figure 48. Figure 49 shows the idealized dynamics model ith ex-planatory details.

Load on the reactor mass is

$$V_z = A\,n\,W \tag{1}$$

The solution to the amplification factor, A, is ell known. Reference 12, page 437 gives

$$A = \frac{\sqrt{1 - \left(\frac{4}{\pi}\frac{F}{P_o}\right)^2}}{1 - f^2/f_n^{\,2}} \tag{2}$$

where

$$f_n = \frac{1}{2\pi}\sqrt{\frac{K_z}{M}} \tag{3}$$

The above equation for amplification facto represents an approximate solution of the model. A plot of the exact solutio of A vs. f/f_n with F/P_o as a parameter, may be found on page 438 of Reference .

The assumption that the tube matrix reflec as a rigid cylinder permits the solution of the reactor pressure distributi from a static balance of the load. A deflection of the cylindrical matrix amount $\Delta\delta_I$ (see Figure 50) results in a distribution of deflection given by

$$\Delta\delta_\theta = \Delta\delta_I \cos\theta \tag{4}$$

So

$$\Delta p_\theta = \Delta p_I \cos\theta \tag{5}$$

where

$$\Delta p_I = k_r \, \Delta\delta_I \tag{6}$$

$\Delta\delta_I$ defined in Figure 50

The differential force dV_z along the axis c displacement is given by

$$dV_z = \Delta p_I \, R \cos^2\theta \, d\theta \tag{7}$$

Summing this force over the periphery gives

$$V_z = \int_0^{2\pi} \Delta p_I \, R \cos^2\theta \, d\theta = \pi R \, \Delta p_I \tag{8}$$

or

$$\Delta p_I = \frac{V_z}{\pi R} \tag{9}$$

The integrated spring rate, K_z, follows from this

$$K_z = \frac{V_z}{\Delta \delta_I} = \pi R k_r \tag{10}$$

The friction force is derived in a similar manner The incremental friction force opposing the inertia force is

$$dF = \mu p_s \sin^2 \theta \, d\theta \tag{11}$$

Integration over the periphery gives

$$F = \int_0^{2\pi} \mu p_s R \sin^2 \theta \, d\theta = 4 \mu R p_s \tag{12}$$

5.2.2.2 Optimum Spring Rate

For the spring configurations suitable for the la ral support structure the volume of material required is directly proportic l to the maximum value of elastic strain energy that the springs must absorb For a spring with the following characteristic

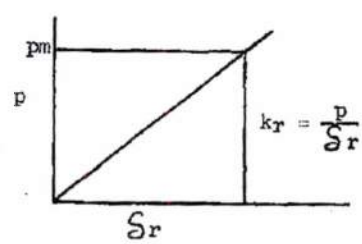

the energy stored is

$$W_e^2 - 1/2 \, p_m \delta_r = 1/2 \, p_m^2/k_r \tag{13}$$

Thus, the volume of spring material required is p portional to the parameter p_m^2/k_r. Since the springs constitute an apprec ble portion of the side support structure, and since the volume of the rema ing structural material is approximately proportional to the maximum spring ond,

the least maximum value of p_m^2/k_r will also result in very n rly the minimum size of the entire support structure. The design procedure c scribed below is based on this criterion.

The objective of the design is to limi the value of the reactor inertial deflection ($\Delta \delta_T$) to a given magnitude by l lection of the parameters that will result in the least value of p_m^2/k_r. Th s means that with a given spring rate the static pressure ps, which is

$$p_s = p_o + \Delta p_T \tag{14}$$

is adjusted so that the friction damping force is of sufficie t value to limit reactor deflection to 0.10 inches. By following the above p cedure for different spring rates (k_r), a minimum value of p_m^2/k_r is found. T e spring rate associated with reactors may be used for design. The result of such a minimization procedure, for the design criteria used, are presente in Figure 51. This indicates that the optimum spring rates are 181 psi/in., for radial systems) and 140,000 lbs/in.$_a$/in.$_c$* (for tangential systems). T ese rates correspond to criteria based on the boost-transition design con cion. The linear portion of each curve results from the satisfaction of the se aration requirement (Paragraph 5.1.5.3) at initial boost condition.

5.2.3 Structural

5.2.3.1 Spring Material Optimization

In the previous section, the spring rat was fixed, resulting in a minimum radial dimension for the side support st ucture. The spring that furnishes this rate must be as efficient as possi le so that additional dimensional losses are minimized.

The strain energy capability of the spr ng can be expressed by

$$W_e = \frac{1}{2} \int_V \sigma \theta \, d V = \frac{\sigma_m^2}{2E} \int_V \left(\frac{\sigma}{\sigma_m}\right)^2 d V \tag{15}$$

where

σ = bending stress

σ_m = maximum allowable stress

* This spring rate corresponds to 197 psi/inch in terms of an equivalent radial spring rate.

This may also be expressed by

$$W_e = \frac{\psi \sigma_m^2}{2E} \tag{16}$$

where

$$\psi = \frac{1}{V_o} \int_V \left(\frac{\sigma}{\sigma_m}\right)^2 dV \tag{17}$$

in which ψ is called the structural efficiency of the spring. It may be seen that if σ is equal to σ_m throughout the spring material, then 100 percent efficiency is realized. For bending beams, which have good spatial efficiency, the maximum efficiency is realized when the stress distribution over the length of the beam is constant. This stress distribution is approximately realized by a two-point loaded beam with tapered ends:

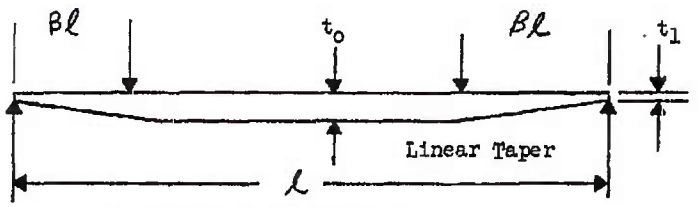

The moment distribution is

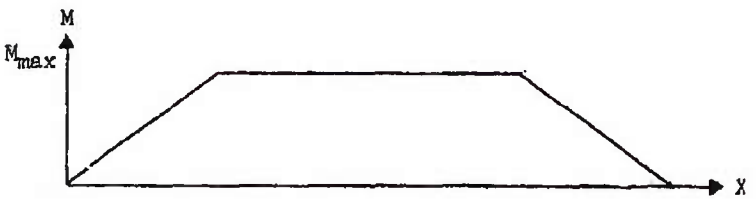

with the resulting stress distribution as

The thickness variation, which results the constant stress case, is actually parabolic. However, a parabolic tap is difficult to achieve practically in thin sheet, so a linear taper is used an approximation. Using Equation 16, the volume of the spring material may be e rossed as

$$V_o = \frac{E\,\ell}{\eta\,\psi\,\sigma_m^2}\; p_m^2/k_r \tag{18}$$

since W is proportional to p_m^2/k_r. The parameter η is the s face efficiency of the spring; i.e., the spring reacts a load of $\ell p/\eta$. Th volume of the spring is

$$V_o = \beta\ell\,(t_o + t_1) + t_o\,\ell(1 - 2\beta \tag{19}$$

The structural efficiency is evaluated from the integral in E ation 17 and is

$$\psi = \frac{1}{3}\;\frac{1 - 2\beta(1 - D)}{1 - \beta\,(1 - b)} \tag{20}$$

where

$$D = \frac{1}{(1 - b)^3}\left[-\ell n\, b - \frac{1}{2}(1-b \quad (3-b)\right] \tag{21}$$

With Equations 18, 19, and 20, the required total spring thic ess is

$$t = \frac{E}{\eta\,\sigma_m^2}\,\frac{p_m^2}{k_r}\;\frac{1}{\psi\left[1 - \beta(1 - \quad \right]} \tag{22}$$

The spring length, ℓ , may be determined from the spring rate equired and the spring beam dimensions, and is

$$\ell = \frac{t}{n_p\;n_s}\left(\frac{\eta\, n_p\,\sigma_m}{3\beta\, p_m}\right)^{1/2} \tag{23}$$

Thus, for given values of the parameters the minimum thickness of material required and its associated length can b determined from Equations 22 and 23.

The above design procedure was carried , and resulted in the spring presented in Figure 45. The spring has the foll ing specifications:

Radial free height = 0.857 inches

Radial installed height = 0.807 inches

Spring length = 4.450 inches

Distance to load point = 1.556 inches

Element maximum thickness = 0.092 inches

End thickness (linear taper) = 0.046 inches

Spring rate = 188 psi/in.$_r$ (cold)

Spring rate = 181 psi/in.$_r$ (380°)

Spring rate = 150 psi/in.$_r$ (1400°)

Maximum stress = 109 ksi (boost-transition)

Steady state stress = 37.3 ksi (cruise)

Maximum reactor pressure = 70.7 psi (boost-transition)

Steady state reactor pressure = 25.8 psi (cruise)

Preload reactor pressure = 9.4 psi (cold)

Preload spring deflection = 0.050 inches

5.2.3.2 Component Analysis

5.2.3.2.1 Spring Pressure Shell

Although it is desirable to hold this shell to the minimum thickness possible, the redundancy of the shell geometry makes this difficult to achieve analytically. The following analysis conservatively assumes that each circumferential web and a portion of the shell-in combination act as a ring (see Figure 52). If the web-shell combination is sufficiently stiff, the equivalent ring will be loaded in hoop tension.

Shell loads are critical at boost-transition condition:

Maximum pressure	=	70.7 psi
Shell temperature	=	400°F
Shell material	=	Rene' 41
Material allowable	=	120 Ksi

Shell point loads:

$$P = 1/4 \frac{22.5}{57.3} 27.4 (70.7) = 190 \text{ lbs/in}$$

Moment of inertia of Section (A-A):

$$I_{AA} = 0.00610 \text{ in}^4$$

Assume ring loaded at 32 equidistant points and determine deflection from Reference 5 (Case 9, page 158):

$$\delta_{max} = 0.0094 \text{ inches}$$

Deflection is small.

Hoop tension analysis:

Diameter = 55.19 in.

Reflector diameter = 53.25 in.

Equivalent ring pressure:

$$p_{EQ} = \frac{53.25}{55.19} 70.7 = 68.2 \text{ psi}$$

$$\text{Hoop Stress} = \frac{68.2 \times 27.50}{1.25} = 15 \text{ Ks}$$

$$\text{MS (Hoop Tension)} = \frac{120}{1.1 \times 15} - 1 = \underline{\underline{[illegible]}}$$

$$\text{Length between rails} = \frac{\pi 55.19}{16} = 10.6 \text{ in.}$$

Rail width = 1.25 in.

Beam length = 10.6 - 1.25 = 9.35 in.

Load/section = 68.2 x 10.6 = 724 lbs/in$_a$

Load on web = 68.2 x 9.35 = 638 lbs/in$_a$

The difference is carried as a shear in the all web

$$724 - 638 = 86 \text{ lbs/in}_a$$

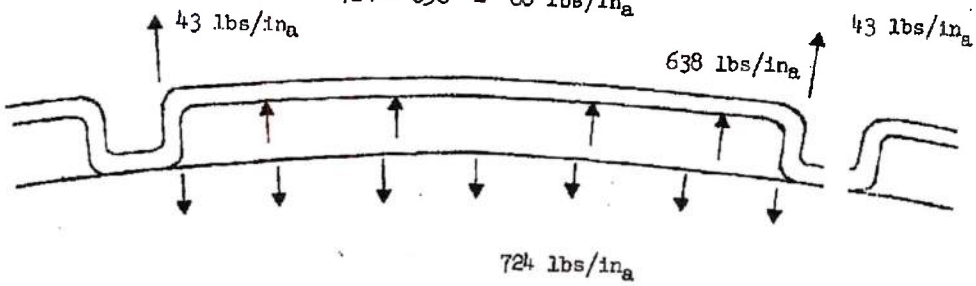

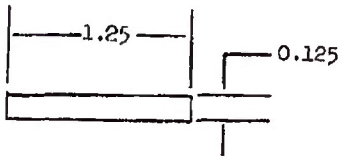

$$M = \frac{Wl^2}{8} = \frac{68.2\ (1.25)^2}{8} = 13.3 \text{ in-lb/}_a$$

Assume a stress concentration factor of 4:

$$f_b = 4\,\frac{6M}{t^2} = \frac{24 \times 13.3}{(0.125)^2} = 20.4 \text{ Ksi}$$

$$f_t = \frac{4pr}{t} = \frac{4 \times 68.2 \times 27.59}{0.125} = 60.2 \text{ Ksi}$$

$$f_{total} = 20.4 + 60.2 = 80.6 \text{ Ksi}$$

$$\text{MS (Bending + Tension)} = \frac{120}{1.1 \times 80.6} - 1 = +0.35$$

5.2.3.2.2 Spring Pressure Pad

5.2.3.2.2.1 Pad Lug Bending

Conservatively analyze the pad as a p ssure loaded beam:

Maximum Pressure = 70.7 psi

Pad Temperature = 1400°F

Pad Material = Rene' 41

Allowable = 120 Ksi

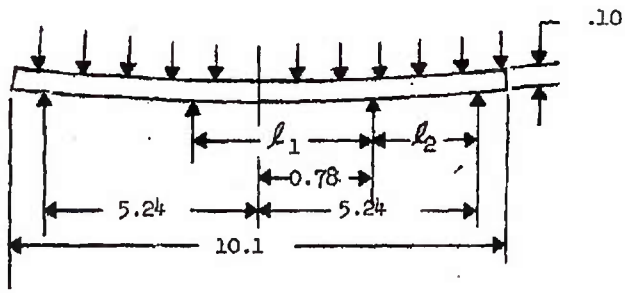

$$M_{Max} = \frac{W}{12}\left(\frac{l_2^3 - l_1^3}{l_2 - l_1}\right) = 164 \text{ in-lbs. } n_a$$

$$\sigma = \frac{6M}{t^2} = \frac{6 \times 164}{(0.10)^2} = 98.5 \text{ Ksi}$$

$$MS \text{ (Bend)} = \frac{120}{1.1 \times 98.5} - 1 = +0.$$

The pad lugs react the friction load at is produced by reactor movements and is a maximum on the side pads.

Pad lug bending is critical at the st e ejection condition.

Pressure = 23.6 psi

Lug Temperature = 1500°F (Assumed)

Allowable = 95 Ksi

Lugs are 3.3 inches on center

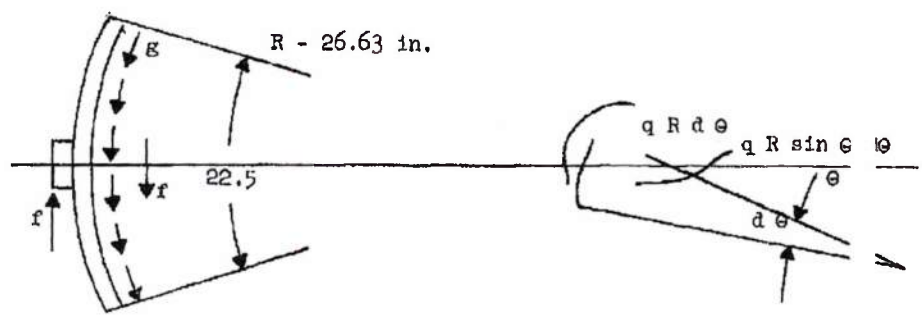

$$f = \int_{\theta_1}^{\theta_2} q\, R \sin\theta\, d\theta$$

$$q = \mu\, p \sin\theta$$

So:

$$f = \int_{\theta_1}^{\theta_2} \mu\, p\, R \sin^2\theta\, d\theta$$

$$= (0.3)(23.6)(26.62) \int_{28.8^\circ}^{101.3^\circ} \sin^2\theta\, d\theta$$

$$= 189 \times 0.393 = 74.1 \text{ lbs/in}_n$$

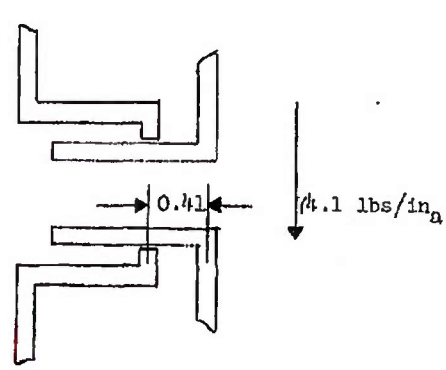

$$M = 0.41 \times 74.1 = 30.4 \text{ in-lbs/in}_a$$

$$M = 30.4 \text{ in-lbs/in}_a \times 3.3 \text{ in}_a\text{/lug} = 1 \quad \text{in-lbs/lug}$$

$$z = \frac{\pi}{64 \times 0.313}\left[(0.625)^4 - (0.375)^4\right] \quad 0.0208 \text{ in.}^3$$

$$f_b = \frac{M}{Z} = \frac{100}{0.0208} = 4.8 \text{ Ksi}$$

$$MS\ (\text{Bend}) = \frac{95}{1.1 \times 4.8} - 1 = \text{High}$$

5.3 Front Support Structural Criteria

5.3.1 Discussion of Axial Support System

Axially directed air and inertial forces . ting aftward upon the assembly of hexagonal ceramic tubes comprising the rea or core are reacted by bearing on metal base plates that bear against flanges n metal tie tubes extending through the core. These tubes are attached to . structural grid located forward of the core and act as tension ties. The grid connected to the airframe at its periphery.

This axial support system provides for a (fferential thermal expansion between the ceramic core and the metal structure l means of sp. . springs located on the tubes between the core and the grid.

During assembly, tube lengths are adjuste nechanically to clamp the core against the springs and the springs against the , id. The resulting spring deflection preload compresses the core against the a: face plates and prevents forward movement.

Forward growth of the core due to differe: ial expansion further deflects the springs and increases the spring aft-direc i preload. Elastic and plastic stress-induced elongations of the tie tubes artially relieve the spring deflection.

The net force exerted by the springs upon ie core must exceed forward-directed core loads if core forward motion is to b prevented.

Forward-directed loading on the reactor c e may occur momentarily during several flight phases.

Immediately after rocket booster burnout, ı inertia factor of -0.32 g is attained. The net force, however, is less tl ı that of the aft-directed air drag (Refer to Figure 53).

During unstart-restart conditions, the air drag on the reactor core becomes negligible while that on the airframe is unai ected. Inertia of the core will force it forward against the springs.

5.3.1.2 Discussion of Axial Dynamic Loading Conditions

To obtain insight into the expected dynamic loa on a full scale reactor, a one-third scale engine was tested during Octobe 1962. Data from the tests were extrapolated to the full scale system at con tions of Mach 3, an altitude of 1,000 feet, and ANA Hot Day temperature.

Time response was corrected for full scale diff ences and temperature differences. Since the full scale diffuser is three mes long-er, the time for a pressure disturbance originating at the inlet to r ch the reactor is three times as great and, hence, pressure response data ob ined with the one-third scale system should be reduced by a factor of one-third However, since the test reactor was full length, the time for propagation of p ssure disturbances through the reactor remains the same between the one-thi scale and neglecting the effects of the nozzle. Both the fore and aft pres re re-sponse times were also corrected for sonic velocity differences betwe the full scale condition T_{T_o} of 1570°R and test data temperature of 900°R. Th net re-sult of the scale and temperature corrections was an expanding of the ime scale of both front and rear response curves by a factor of:

$$\frac{\text{Full Scale}}{1/3 \text{ Scale}} \times \sqrt{\frac{T_{T_o} - 1/3 \text{ Scale}}{T_{T_o} - \text{Full Scale}}} = 2.3$$

but maintaining the relative lag through the core.

Equivalent full scale pressure levels were obta ed by ratioing steady state values recorded for one-third scale system test. just prior to inlet unstart to those given in Reference 13 for Mach 3.0, A Hot Day, and 1,000 feet. The pressure ratios from one-third scale to full sca were assumed to remain constant throughout the transient.

Typical one-third scale data corrected to full ale con-ditions are presented in Figure 54. The corrected data are also pres ted in Figure 55 in terms of Δ P across the full scale core during unstart ambient. The effect of such a Δ P change on reactor drag load was evaluated assuming the steady state Δ P was equivalent to the full scale steady state d g (Figure 56) and that drag remained proportional to ΔP throughout the transie .

Based on these assumptions, Figure 57 was prepa d and was considered representative of the change in full scale reactor drag lo s through-out the unstart transient. The curve is presented as a series of str ght lines as used to simplify the mathematical analysis. The effects of a hot re on pressure response were not considered, and friction in the side suppo system was neglected. The loads of this curve were then incorporated into t differen-tial equation of motion for the reactor to determine their effects. ction 5.3.2 presents the derivation of the equations used in this analysis, ogether with sample calculations. Figures 58 and 59 present the calculated d placements and velocities of the reactor over the time period of the unstart tra ient.

This analysis indicates that the reactor e:eives forward loads and then abrupt reloads during the unstart transient. F the load change shown in Figure 57 for ground test operation, the forward load are marginally sufficient to cause separation from the base block in that ela ic energy stored in the tie rods returns the reactor slightly past zero deflect n (Figure 58).

In flight, however, an unstarted inlet i reases vehicle drag sharply. Therefore, upon inlet unstart in flight, the re tor becomes subject not only to forward forces arising from abrupt changes in ass flow through the propulsion system, but also, since the reactor motion is u estricted in the forward direction, to the relative deceleration of the vehicle ith respect to the reactor. Figure 53 presents the estimated reactor drag lo variation during an unstart transient that is accompanied by additive 3g ve cle deceleration. A deceleration of 3g was selected as representative of a sever inflight drag condition. In the preparation of Figure 53 it was assumed tha the 3g additive forward load was applied prior to time = 0 and displaced the t e = 0 drag level from that of Figure 57. The 3g load remained constant over th unloading portion of the unstart transient (to t = 0.045) and did not affec the rate, but dissipated as reload (and restart) occurred. The deceleration oad decrease was assumed to occur linearly over the flat portion at the bottom the 0g drag curve (time = 0.045 to time = 0.057). Offsetting the reload s rt time (from that of Figure 57) was accomplished to compensate for pressure ulse travel time through the diffuser. The amount of offset and the rate of de leration load decrease were arbitrarily selected to simplify the straight li construction of the drag load curve.

In relation to the 0g drag load curve (F ure 57), Figure 53 is, therefore, lowered by a factor of 3 times the reactor m s from t = 0 to t = 0.045 seconds but with the same slope, and shows immediate eload with no stay time at minimum load. From time = 0.057 seconds on, Figu s 57 and 53 are identical, since all deceleration loads are assumed to have di ipated and vehicle reacceleration loads were not considered.

A mathematical analysis similar to that nducted for the ground test (0g) condition was conducted for the flight condit n. Section 5.3.2 presents sample calculations of reactor motion under the oad variation of Figure 53. Figures 60 and 61 present the calculated result t displacements and velocities of the reactor. As shown by these figures, the severity of the displacement and velocities increases considerably over that ol ained under ground test conditions. A maximum separation from the base bl k of 0.127 inches followed by rapid oscillatory separation at high velocities is dicated. Although these motion characteristics do not appear to overstres the tie rods, it appears probable that ceramic damage would result from such im t load cycling.

It should be noted that the forward reac r springs were not considered in this analysis due to their relatively low sp ng constant (45 lbs/in./in. (Reference 13). Redesign of the forward spring sy em could probably overcome the predicted forward deflection. It is recomme d that such redesign be investigated.

5.3.2 Dynamic Analysis

5.3.2.1 Derivation of Equations for Reactor Dynamic Load Analysis

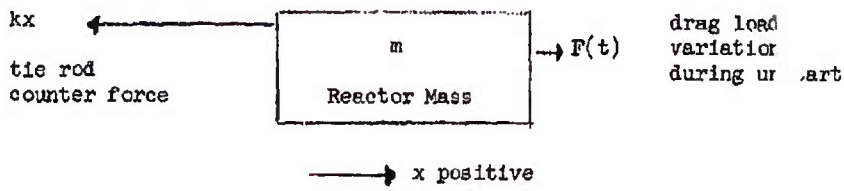

For the above system

$$m \frac{dx^2}{dt^2} = F(t) - kx \tag{24}$$

or

$$\frac{d^2x}{dt^2} + \frac{k}{m} x = \frac{1}{m} F(t) \tag{25}$$

To solve per Reference 14 let

$$\frac{d^2x}{dt^2} + \frac{k}{m} x = 0 \tag{26}$$

Assume

$$x = e^{Rt} = x_1$$

then

$$\frac{dx}{dt} = R e^{Rt}$$

and

$$\frac{d^2x}{dt^2} = R^2 e^{Rt}$$

Substituting in Equation (26)

$$R^2 e^{Rt} + \frac{k}{m} e^{Rt} = 0$$

$$\therefore R = \pm \left(-\frac{k}{m}\right)^{1/2}$$

and x_1, becomes

$$x_1 = c_1 e^{\left(\frac{k}{m}\right)^{1/2} i t} + c_2 e^{-\left(\frac{k}{m}\right)^{1/2} i t} \qquad (27)$$

Assume $1/m\ F(t)$ can be expressed as $a + bt$

and let

$$x = A + Bt = x_2$$

then

$$\frac{dx}{dt} = B \qquad \frac{dx^2}{dt^2} = 0$$

Then Equation (25) can be expressed as

$$\frac{k}{m} A + \frac{k}{m} Bt = a + bt$$

$$\therefore A = a/k/m \qquad B = b/k/m$$

and

$$x = x_1 + x_2$$

$$x = c_1 e^{\left(\frac{k}{m}\right)^{1/2} i t} + c_2 e^{-\left(\frac{k}{m}\right)^{1/2} i t} + \frac{a}{k/m} + \frac{b}{k/m} t \qquad (28)$$

which can also be expressed as

$$x = (c_1 + c_2) \cos \left(\frac{k}{m}\right)^{1/2} t + (c_1 + c_2) i \sin \left(\frac{k}{m}\right)^{1/2} t + \frac{a}{k/m} + \frac{b}{k/m} t \qquad (29)$$

Differentiating Equation (28)

$$\frac{dx}{dt} = c_1 \, i \left(\frac{k}{m}\right)^{1/2} e^{\left(\frac{k}{m}\right)^{1/2} i t} - c_2 \, i \left(\frac{k}{m}\right)^{1/2} e^{-\left(\frac{k}{m}\right)^{1/2} i t} + \frac{b}{k/m} \qquad (30)$$

or

$$\frac{dx}{dt} = c_1 \, i \left(\frac{k}{m}\right)^{1/2} \left[\cos \left(\frac{k}{m}\right)^{1/2} t + i \sin \left(\frac{k}{m}\right)^{1/2} t\right]$$

$$- c_2 \, i \left(\frac{k}{m}\right)^{1/2} \left[\cos \left(\frac{k}{m}\right)^{1/2} t - i \sin \left(\frac{k}{m}\right)^{1/2} t\right] + \frac{b}{k/m} \qquad (31)$$

Equations (29) and (30) define the displacement nd velocity of the reactor during an unstart transient. c_1 and c_2 can be aluated from known conditions at time = 0; however, x must be positive at t = . Values of a and b can be determined from test data by defining the unstart t nsient in terms of successive straight lines (Figure 57).

The value of m was taken as 11,400 lbs from Ref ence 13, and the steady state load, at Mach 3, 1000-foot altitude, ANA Hot Day, rom Figure 56.

The tie rod strain under this load was computed rom an effective area and weighted modulus of elasticity for the 81 Rene' 41 nd 40 R235 tie rods. A tie rod temperature of 1300°F was assumed (Referenc 1). Rod length was taken as 80 inches. The initial steady state deflection w there-fore:

$$x = \frac{\ell F}{EA \text{ (no. of rods)}} = \frac{80 \, (263{,}000)}{24.5 \times 10^6 \, (0.095) \, (121)} = 0.075 \text{ i}$$

The tie rod spring constant, k, was therefore

$$k = \frac{F}{x} = \frac{263{,}000}{0.075} = 3.5 \times 10^6 \text{ lbs/in.}$$

5.3.2.2 Sample Calculations of Reactor Displacement and elocity Changes During Unstart-Ground Test

For conditions at t = 0 (Figure 57)

$$x = 0.075 \qquad \frac{dx}{dt} = 0$$

the first straight line segment can be expressed as

$$\frac{a + bt}{m} = \frac{1}{m} F(t)$$

therefore,

$$a = 8{,}900 \qquad b = -190{,}000$$

also,

$$\frac{k}{m} = 118{,}500$$

$$\left(\frac{k}{m}\right)^{1/2} = 344$$

at t = 0, Equation (28) and (30) become

$$x = c_1 + c_2 + \frac{a}{k/m}$$

$$\frac{dx}{dt} = c_1 i \left(\frac{k}{m}\right)^{1/2} - c_2 i \left(\frac{k}{m}\right)^{1/2} + \frac{b}{k/m}$$

Solving for c_1 and c_2 and substituting

$$c_1 = \frac{1.61}{6.88i} \qquad c_2 = \frac{1.61}{6.88i}$$

Since all constants are now known, x and dx/dt can now be determined for times up to 0.045 seconds:

$$c_1 + c_2 = 0 \qquad (c_1 - c_2)\, i = 0.0047$$

$$x = 0.0047 \sin 344\, t + 0.075 - 1.61\, t$$

$$\frac{dx}{dt} = \frac{1.61}{6.88\, i}(344\, i)\, e^{344\, i\, t} - \frac{1.61}{688\, i}(344\, i)\, e^{-344\, i\, t} - 1.61$$

Solving at t = 0.045,

$$x = 0.003 \text{ inches}$$

and

$$\frac{dx}{dt} = -3.20 \text{ inches/sec}$$

Thus, the tie rods have relaxed from 0.075 to 0.003 and the reactor is moving forward at 3.2 inches/sec. Each straight line segment of Figure 57 is treated similarly, and a, b, c_1, and c_2 are reevaluated each time. For those line segments where the velocity reverses direction, the time of zero velocity is determined and the maximum (or minimum) displacement is determined.

5.3.2.3 Sample Calculations for Reactor Displacement and Velocity Changes During Unstart-Flight Operation

It was assumed that the application of the 5g load prior to time = 0 (Figure 53) did not change the reactor motion characteristics at time = 0 from the characteristics under ground test conditions (i.e., x = 0.075 and dx/dt = 0). This assumption was made to simplify the analysis and was justified because the change in initial drag load was relatively small, and its effect on initial displacement and velocity would also be relatively small.

Therefore, at t = 0,

$$x = 0.075$$

and

$$\frac{dx}{dt} = 0$$

Solving for the constants a, b, c_1, and c_2 as in Paragraph 5.3.2.2,

$$a = 7770$$

$$b = -190{,}000$$

$$c_1 = \frac{1.61 + 3.26\,i}{688\,i}$$

$$c_2 = \frac{-1.61 + 3.26\,i}{688\,i}$$

Solving Equations (29) and (31) with the known constants at t = .045,

$$x = -0.016 \text{ inches}$$

and

$$\frac{dx}{dt} = -3.76 \text{ inches/sec}$$

Thus, the reactor has separated from the base plate and has f ard momentum. To evaluate reactor motion over the next straight line segment new equations must be derived since the constants can not be evaluated for negative. Under a negative x, k = 0 and the equations are invalid. For x = n tive at t = 0, Equation (25) becomes

$$\frac{d^2x}{dt^2} = \frac{1}{m} F(t)$$

Expressing 1/m F (t) as a + bt,

$$\frac{d^2x}{dt^2} = a + bt$$

Integrating for dx/dt and x,

$$\frac{dx}{dt} = at + \frac{b}{2} t^2 + c_1 \qquad (32)$$

$$x = \frac{a}{2} t^2 + \frac{b}{6} t^3 + c_1 t + c_2 \qquad (33)$$

At t = 0,

$$\frac{dx}{dt} = c_1 = -3.76$$

$$x = c_2 = -0.016$$

From Figure 52,

$$a = -834$$

$$c = 96{,}000$$

Equation (33) is solved for the time at which x returns to ze Equations (32) and (33) are only valid up to this time after which Equations ( ) through (31) must be used, since k is again the factor.

Setting Equation (33) equal to 0 and sol ng for t,

$$0 = -417\, t^2 + 16{,}000\, t^3 - 3.76\, t - 0.016$$

$$t = 0.033$$

Therefore, after time 0.045 + 0.033 = 0.078 of gure 53 Equations(32) and (33) no longer apply for the straight line segment om t = 0.045 to t = 0.090. The segment from t = 0.078 to t = 0.090 is evalu ed as before using Equations (28) through (31).

The remaining line segments of Figure 53 are ev uated similarly. Equations (32) and (33) are applied whenever x is negativ at the start of a line segment. For all line segments times of maximum and nimum velocity are determined to define completely the behavior over the unst t transient.

5.3.3 Structural Summary

According to Reference 13 (page III-29), data f the standard tie rod springs are as follows:

Material Inconel X	Inconel X
Number of springs	103
Outside Diameter, inches	1.75
Inside Diameter, inches	1.32
Spring constant, lbs/in. at 1100°F	45
Free length, inches	4.4
Bottom-out length, inches	2.9
Assembly pre-load, lbs	55.97

There are 121 tie rods, and the total reactor w ght supported is approximately 11,500 lbs. Assuming the tubes are equally l ded, $\frac{11,500}{121}$ = 95 lbs/tube dead weight loading (1.0g).

Thus, a 1.0g forward inertia load would exceed e 55.97-lb preload by 39.03 lbs and would deflect the spring 0.87 inches. Su movement cannot be tolerated.

If loaded after the core and support structure ve reached stabilized temperature levels and all differential expansion has occu ed, the additional preload due to the core expansion spring deflection will b available. Total spring travel can be only 4.4 - 2.9 = 1.5 inches and spring loa is then 1.5 x 45 = 67.5 lbs. Since this value is less than the 95 lbs/tube l d, forward movement would still occur.

The present spring system appears unsatisfactor for the unstart condition. Since the present load data are of a preliminary ture, spring redesign should be delayed until final load studies are availa e.

5.3.4 Conclusions and Recommendations

1. Reactor damage due to forward loadin may occur dur-
ing ground testing of a full scale Pluto engine if inlet unsta occurs. Full
scale engine dynamic evaluations should be conducted with a du y reactor prior
to any hot core testing.

2. Definite forward loadings are predic d to accompany
inlet unstart in flight due to the additional forward loads re lting from thrust
loss and drag increase. Modifications to the existing Tory II front support
system are indicated.

3. Additional dynamic load evaluation s uld be accomp-
lished with the finalized one-third scale inlet configuration ascertain the
effects of inlet "hard start" (restart with bypass doors close and to deter-
mine possible change in the load characteristics with increasc inlet contrac-
tion. These tests should be performed at dcsign and off-desig Mach numbers.

5.4 Side Support System Test

5.4.1 Discussion

An extensive spring evaluation test prog m for the Pluto
reactor side support system was continued during 1962. Seven ring configura-
tions (Reference 15) were to be investigated to support earlie preliminary de-
sign studies:

1. Split cylindrical tube
2. Solid cylindrical tube
3. Modified Belleville
4. Buggy (elliptical)
5. Torsion bar
6. Corrugated
7. Plate

Test programs for evaluating the perform ce of Belleville
corrugated and flat ribbed plate springs (all fabricated from ne' 41 alloy ma-
terial) were conducted in the past (Reference 16). Because in arly 1962 the
Belleville spring exhibited the most desirable high temperatur characteristics
from the standpoints of load-deflection and permanent set, ini al 1962 spring
tests were directed toward the evaluation of Belleville spring incorporating
modifications intended to reduce initial permanent set and to crease load car-
rying capacity. Belleville springs of R-235 alloy material we on hand lending
emphasis to this work. Subsequently, concerted analytical ana sis of the other
spring forms listed above indicated their potential was inferi to the Belle-
ville spring regarding functional requirements.

Concurrent with the above work, analysis was b un on a new type of spring, embodying the aspects of a tapered curved beam a . designed specifically to minimize the lateral support annulus dimension. A d ailed test program was formulated to evaluate the mechanical performance of thi spring type under expected operating conditions.

5.4.2 High Temperature Springs

5.4.2.1 Belleville Spring

A theoretical analysis of the stress profile o a Belleville spring (Reference 17) shows that very high stress concentratio occur at the inner diameter edges, the higher stress being at the convex e e. Consequently, the actual stresses occurring at both inner diameter edge usually exceed the allowable yield stress of the spring material and are res nsible for the permanent set (local edge material plastic yield) during ini al load-deflection operation.

It was assumed that, if the rather sharp inner iameter edges were modified, high stresses would be decreased resulting in r uced permanent set and a more uniform stress distribution across the spri . Particular attention was given to the alleviation of stress concentrati s by employing full edge radii.

The test items were conventional form Bellevil springs of R-235 material with an optimum solution heat treatment. Nominal mensions were 0.100-inch material, 2.000-inch O.D., 0.875-inch I.D., and 0.05 inch coned height. These springs were designed with a linear load rate t approximately 85 percent of the spring deflection capability, and a load li t (flat position) of 1800 pounds (Reference 18). Several springs were modif d by rounding the inside edges. Full edge radii of 1/64, 1/32, and 1/16 an inch were used on either or both edges. Figure 62 shows some typica springs that were tested. A spring containing 1/16-inch full radii on both ner diameter edges is presented in Figure 63.

The spring research effort entailed compressiv static load-deflection tests, which were conducted in a Baldwin Universal T t Machine at ambient and elevated temperatures. Appropriate spring holding fi ures, CHAL thermocouples, and Brown temperature recording equipment were use

Single spring specimens of each of the convent nal and modified configurations were tested with and without strain gages at mbient temperature. A nonstrain gaged single spring setup is shown in Figu 64. The loading method shown in the figure is referred to as flat plate load. g. The nonstrain gaged springs were first preset by deflection to the flat sition, and then subjected to a load-deflection test to 85% of the maximum flection for three cycles to establish the spring rate.

In order to determine the spring stress profil one modified spring and one conventional spring (springs identical in physic dimension except inner diameter edge modification) were instrumented with train gages and tested. SR-4 type A-19 gages were installed on both outsi and in-

side spring surfaces at mirror view locations equally spaced (ngle) in spiral fashion as shown in Figure 65. The spiral method of gage plac ment permitted average radial-wise strain coverage and also facilitiated att ment of electrical leads. The actual test setup for these tests is shown Figure 66, and details of the "house-of-cards" type of test arrangement are own in Figure 67. A cone pointed ram was used to prevent damage to gages (as op sed to a flat plate) and yet produce effective flat plate loading. In gene t, the test load-deflection procedure for gaged springs duplicated the above p edure for non-gaged springs.

In addition to the single spring tests, mpressive tests with 10-spring series stacks of conventional springs were con ted. Spring stack load-deflection rate was determined at ambient temperat and constant deflection-load relaxation characteristics at 85 percent of t stack deflection capability were evaluated at 1400°F. Setups of spring st ks for the ambient and elevated temperature tests are shown in Figures 68 1 69, respectively.

The average permanent set of a single c entional spring at initial deflection to flat position was approximately 32 p ent of the original coned height (nominal, 0.050 inches). No differences permanent set were observed between the conventional and any modified spring s shown in Figure 70.

The spring rate for the conventional fo spring is linear up to 85 percent of deflection capability, and the load li t is approximately 1845 pounds as noted in Figure 71. These data verify t spring design (Reference 18).

For comparative purposes, one conventio R-235 alloy spring was tested at the same conditions as had been applied t a conventional Rene' 41 alloy spring of near identical physical dimensions (t ted in 1961). Figure 72 indicates that the Rene' 41 spring underwent a perm nt set of only 42 percent of the R-235 spring set at the comparable deflectio points. In Figure 73 the Rene' 41 spring exhibits approximately 12 perce greater load carrying capacity at 85 percent of the spring deflection capab ity.

An increase in load carrying capability s exhibited by springs tested with a radius on the outer I.D. edge (Figure 74 The spring that had the greatest increase was the one with a 1/16 inch ra us. In the figure, a spring with the above outer edge conditions shows a increase of 12 percent in load capacity over that of the conventional spring the 85 percent level of deflection capability. The increase in load ca ity was predicted from the formulae in Reference 17 and is the result of e edge radius permitting a shorter couple moment arm around the spring cent d as depicted schematically in Figure 75. Corresponding load-deflection dat in the same figure verified this mechanical phenomenon. Also it will be n ed in Figure 74 that no significant performance effects resulted from springs th a radius on only the inner I.D. edge as compared with the conventional sprin data. In addition to increasing spring load capacity, rounded I.D. edges sh ld also increase spring performance and integrity under a high temperat vibrational load environment.

Strain gages were installed on two nearly ide ical springs, on one conventional spring (No. 29), and on one modified s ing (No. 25) having 1/16-inch full radius on both I.D. edges (Figure 65). A gages were positioned to record strains in the tangential direction. Ide ical loading point for both springs was accomplished by a cone pointed ram (gure 67). Strain results were obtained for presetting and preset spring condi ons during deflection to the flat position. These strain results were con rted to stress values and are plotted in Figure 76.

In general, the rather consistent strain data dicate that high local compressive stress at the conventional spring outer .D. edge was considerably reduced with a full rounded edge. The penalty for e edge stress improvement was manifested in an increase of the remaining s ing stress profile as compared to that of the conventional spring. Trend of t modified spring stress data here suggests that a "tear drop" form of edge ro ling may reduce the developed stresses in the outer portion of the profile. E periment-al stresses, although slightly lower, are in good agreement with the retical stresses calculated from the formulae in Reference 17.

The load-deflection rate for a preset 10-spri series stack of conventional form springs was found to be in close agreeme with the rate of a single spring when tested at both ambient and elevated te erature; i.e., the deflection capability is ten times that of a single spring for the same load. At 1400°F the stack load is a maximum of 83 percent of t e corres-ponding load at ambient temperature as shown in Figure 77. The rate change was predicted and is attributable to the reduction of material modul of elasticity at elevated temperature.

Load loss of a preset 10-spring series stack d to con-stant deflection at 85 percent of the stack deflection capability at 400°F is presented in Figure 78. The test data show an approximate linea load loss rate of 3 percent per hour.

5.4.2.1.1 Conclusions

1. Of the modified Belleville springs teste the one with a 1/16-inch radius on the outer I.D. edge was found to have the greatest increase in load-carrying capability.

2. Creep test results indicate that a const t relax-ation rate of approximately 3 percent per hour was obtained. Extra ating this to 10 hours will give a total lifetime reduction of 30 percent, which is excessive. The results indicate that redesign of the Belleville spr g is re-quired to reduce the lifetime relaxation rate.

3. No future testing is contemplated for t Belle-ville spring at Marquardt. The curved plate spring appears more att ctive from the standpoint of reducing the lateral support annulus.

5.4.2.2 Tapered Curved Plate Springs

The springs presently under development Marquardt for lateral side support of the Pluto reactor are linear rate, tap ed, curved plate spring stacks consisting of two sets of parallel spring aves stacked in series. Single 1.0 inch wide spring leaves and an assemble stack are shown in Figure 79. The spring material is Rene' 41 with an optimum olution heat treatment.

The spring leaf is normally 4.450 inches n length with widths of 1 inch, 2 inches, and 4 inches. The nominal height a spring stack of any width is 0.750 inches. Each spring stack had a n inal 0.375-inch deflection capability, with a rated load of 366 pounds pe inch of spring width.

Spring tests at ambient temperature were un on a Baldwin Universal Tester as shown in Figure 80. A dial gage was used r recording spring deflection, and the readouts of multiple SR4 type A-18 rain gages on a spring leaf were monitored by an SR-4 strain indicator. Rep sentative strain gage locations are shown schematically in Figure 81.

The setup used for high temperature test in an Elevated Temperature Test Machine is shown in Figure 82. This setup in lved a special spring stack holding apparatus, 12-inch Hevi-Duty split tube f nace, CH-AL thermocouples, Brown temperature recorder, Baldwin load cell, ring deflectom-eter, and automatic load programming equipment.

Spring stack load rate was established f the various width stacks under conditions of static compressive load-deflc ion at both ambient and 1400°F. The magnitudes and effects of transverse rains were determined for single spring leaves of each width. Dynamic perf mance was investigated under a cyclic load traverse over a simulated Pluto light trajectory at 1400°F for a period in excess of 10 hours. A diagram the cyclic load schedule is presented in Figure 83.

5.4.2.3 High Temperature Spring Test Results

Significant results of the spring tests e as follows:

1. Ambient temperature load-deflection tes for spring stacks 1 inch and 2 inches in width indicate an average data s ead of 10 percent as shown in Figure 84. These spring stacks, in addition a 4-inch stack, exhibited an average of 24 percent greater spring rate an the predicted rate based on nominal spring dimensions. Stack permanent s averaged 4 percent of stack initial deflection capability. Strain gage d a indicated that permanent sets were caused by stress concentrations near e mid-span load points. The test spring rate of a 1-inch stack was 3.4 p cent greater than the calculated spring rate of the subject stack based on tual dimensions.

2. Longitudinal material strains of single s cing leaves verified the existence of stress concentrations around the r l-span load points as shown in Figures 85 and 86. Comparison of transver strain data presented in Figures 87 and 88 shows that spring edge area st in increas- es with increased spring width (tendency of spring edge to turn in ward spring side containing longitudinal tension strain).

3. Evaluation of spring rate for 1-inch and -inch spring stacks at 1400°F (Figure 84) produced data consistent with t e de- creased material modulus of elasticity for the test temperature.

4. Spring stacks, 2 inches in width tested a 1400°F for 10 hours under cyclic load-deflection conditions (Figure 83) ex bited the following uniformly increasing material creep:

	Sector			
	A (in.)	B (in.)	C	Total Creep (in.)
Stack S/N 2	0.022	0.006	0	0.028
Stack S/N 4	0.024	0.011	0	0.035

These material deformations are attributed primarily to stress conc trations.

5. Ambient temperature recalibrations of spr g stacks tested at elevated temperatures produced rates nearly identical to e initi- al ambient rates for respective stacks.

Conclusions from the significant test results listed above are as follows:

1. Tests indicate that springs can be desigr with a 22 percent confidence in the predicted spring rate, based on nomina spring dimensions. This percentage should improve as spring tolerances ar reduced.

2. Maximum deviation in the predicted vs. ex rimental strains was 25 percent. This deviation is probably due to the stre concen- tration caused by the spring loading bosss.

3. Cyclic, 10-hour creep testing indicated a otal re- laxation of 0.035 inches in spring-free height. This means a relax ion of 4.1 percent based on a nominal spring-free height of 0.857 inches. his value although based on only two spring tests, should be well within Plut lateral support design requirements.

4. Future spring tests should be pointed tow d increas- ing confidence in the total relaxation that the spring will undergo hen sub- jected to the Pluto flight loads environment.

5.4.3 Engine-Airframe Lateral Attachment Test: -Phases I and II

5.4.3.1 Discussion

During the second quarter of 1962, expe mental vibratory tests were conducted to evaluate the characteristics of a pro sed engine-airframe lateral support system. The history and results of ese tests are contained in Reference 19.

The objective of the tests was to evalu e the assembly integrity, the response modes, and the spring system characte stics of a 360° cross section of the engine-side support system in a vibratio loads and elevated temperature environment.

The full scale side support specimen te ed consisted of a tangential (to core) corrugated spring array coupled to a t ck-rail system suspending a simulated core within an outer ring (see Figure).

Results of the above test were compared ith the predicted dynamic responses as derived from a model analysis compiled i Reference 4. Inconclusive correlation was evident due to (1) the inflexibili of the core-side support assembly and (2) only one possible core preload prings) magnitude. In addition, many difficulties occurred with the major y of dynamic instrumentation at elevated temperature. Analysis indicated the eed for evaluation of a generalized test specimen at ambient temperature.

A second full scale engine-side support onfiguration, somewhat similar to the basic geometry of the first item, was esigned and tested during the last quarter of 1962. The primary test obj tives here were to bracket the dynamic test conditions used in the first test nd to evaluate the basic dynamic response of the core matrix with variable s e spring preloads.

The results of the second test are repo ed in Reference 20.

5.4.3.2 Phase I Test

The test item consisted of a full scale 60° cross section of the side support system linking a simulated reactor c and outer ring. The core outside diameter was 53.25 inches, the outer ng inner diameter was 61.50 inches, and the thickness of the assembled unit was 10 inches.

The principal components of the side su ort system were expansion shells and tracks, curved linear rate corrugated sp ngs, spring retainer shells, and rails (as shown in Figure 90). All support components were fabricated from Rene' 41 alloy. On assembly, the nominal spri g compressive load was approximately 900 pounds per spring, resulting in an verage core pressure of 16 psi.

5. Core resonant conditions in the ran of 20 to 26 cps for two horizontal in-line accelerometers are indicated by th data plots in Figures 98 and 99, which are typical of all the data listed i Table XXIII. Apparently, these resonant data are in good agreement with th 21-cps resonant frequency determined from calculations (Reference 4) consider g a rigid body made for the core. Corresponding sine wave acceleration data for Figures 98 and 99) indicating core and outer ring dynamic responses are sted in Tables XXIV and XXV.

6. No change in amplification factor w indicated between ambient and 1300°F testing.

7. Phase angle and g level relationshi between horizontal in-line accelerometers (Figure 98) indicated a core disto ional mode (as opposed to rigid body mode) in the order of 0.02 inches for t 10 to 40 cps frequency band.

8. Flat random excitation data paralle l the sine wave data in that discrete resonant frequencies were not eminent a either ambient or high temperatures.

9. Post-test load-deflection calibrati of springs showed no change from the pre-test calibrations.

10. Structural integrity of the side su ort system was maintained throughout the test.

Conclusions that may be drawn from the sults are summarized as follows:

1. Apparently, binding of the rail-tra assemblies was primarily responsible for erratic dynamic response of the cor relative to the ring (static tests provided an indication of irregular core p ipheral friction distributions).

2. Results of the static g level tests ndicate that, as predicted, a sinusoidal core pressure distribution was exhibi l by the core matrix when the inertial loading exceeded the core friction.

3. Vertical response of the bottom of t e core (Figure 98) compared with horizontal dynamic input indicates distorti al "breathing" of the core.

5.4.3.3 Phase II Test

5.4.3.3.1 Test Hardware Design and Description

Test hardware was designed and fabric d for the reaction airframe lateral support dynamic response test (slice te . The major components of this hardware are the reactor core matrix, supp ring, and spring support assemblies. The configuration as shown in Fig 100 is 10 inches wide and simulates a section through the reactor airfr structure. The

reactor core matrix consists of approximately 78,000 hexagonal steati e tubes (0.3005 inches across flats), 36 peripheral shims, 107 tie rod tubes, and 14 control rod tubes. The outside diameter of the assembled core matri is 53.250 inches. The core matrix is compressed radially by a series of 18 pad segments that form a cylindrical shell around the periphery. There is no phys cal connection between these pad segments; however, the compressive force is produced in the core matrix, through the pad segments, by a series of preloade spring assemblies. Radially outward, the spring loads are reacted by a rigi support ring that simulates the airframe structure. A track and rail type co nection is provided between each pad segment and the support ring to react th shear loads. Seventy-two spring assemblies are used for the entire test fi ure, furnishing a spring rate of 150 psi/in. Four spring assemblies are m nted between each pad segment and the support ring. The spring assembly con sts of a 3.00-inch O.D. primary coil spring, a 1.00-inch O.D. coil spring de pener, and a spring guide. Provisions are made for adjustment of the spring loads during various test setups. All metal parts are fabricated from mild steel except the ceramic hexagonal tubes and the springs, which are chorme-va idium.

The assembled test item is presented in Figure 101. Total weight of his test item was approximately 3400 pounds.

5.4.3.3.2 Dynamic Tests

Ambient temperature dynamic tests were conduc d on a 28,000 force-pound MB Electrodynamic Shaker Model C210 at a facility tside Marquardt. Desired vertical vibration (Figure 102) was obtained in a dition to imposed g loads on the test item at the expected flight magnitude pproximately 8g). The C210 control system is similar to that of the C100.

A typical instrumentation setup is shown in a ematic form in Figure 103. SR-4 Type A-7 strain gages on spring coils were ilized as prime instrumentation regarding core dynamic displacement. Accele meters and linear motion transducers served as backup instrumentation to the train gages.

All tests were performed at ambient temperatu . Dynamic conditions for nine scheduled runs entailed sine wave sweeps of con- trolled discrete frequencies through the range of 5 to 300 to 5 cps a 0.5 to 8g. Three core preload pressures of 5, 15, and 30 psi were utilized th g inputs as follows:

Preload (psi)	g Input
5	0.5, 2,3
15	2, 4, 6
30	3, 6, 8

Results of the static and dynamic tests are s marized as follows:

1. Information on dynamic responses of a sim ated core matrix to vibration loads was obtained during the subject test p gram.

2. Displacement data indicated that the core atrix responded dynamically as a right-circular cylinder at the first reson t frequency. Examples of core displacements for several runs are shown in igure 104.

3. At the second resonant frequency, the cor respond-ed dynamically in elliptical form. Core modes at the first and secon resonant frequencies for Run 4 are presented in Figure 105.

4. These core mode shapes are in good agreem t with theory as presented in Reference 4.

5. The frequencies at which the first and se nd modes occurred were higher than predicted by a factor of 2. This is thought to be due to an increase in the theoretical integrated spring rate caused b mechan-ical binding at the reactor periphery.

6. Maximum core displacements relative to th outer ring frame occurred at the 6g input force level and 15-psi core prelo . The displacements were approximately 0.100 inches around the bottom verti l cen-terline and approximately 0.030 inches around each end of the horizont l cen-terline for the first and second mode conditions, respectively.

7. Apparent core separations observed during he 5 psi core preload and 3g input run were not reflected in the core displace nt data.

8. The first resonant frequency of the core i creases and displacement decreases with an increase in core preload pressure shown in Figure 106.

9. Steatite hexagonal tube damage was slight nd in-significant. No other apparent structural damage to the test item occ rred during the test program.

Conclusions that may be drawn from the results re sum-marized as follows:

1. The analysis for the theoretical dynamic m les of core deformation as presented in Reference 4 were substantiated to a h gh de-gree by test results for first and second resonant frequencies.

2. At input frequencies above approximately 1) cps, core responses were negligible for all conditions tested.

3. Core separation can be prevented with prop - val-ues of core pressures during high g load inputs.

4. For any core preload, core displacement creases approximately in proportion to increases in input force levels.

5. Steatite tube damage was not detrimental o the operation aspects of the test item.

6.0 EXIT NOZZLE

6.1 Design

6.1.1 Discussion

The exit nozzle is a convergent-divergent ejec or type that extends from Engine Station 565.470 to Engine Station 668.070, s shown in Figure 107. The nozzle is cantilevered from and attached to the irframe near the aft face of the reactor. The nozzle-to-vehicle attach joir is a quick-disconnect type, which consists of the vehicle ring, exit nozz e ring, locking ring, and split ring retainer. The exit nozzle attach ring nd locking ring are full-threaded, American Standard stub 29° Acme screw thread , with 2- inch lead and 1-inch pitch. The split ring retainer is assembled tc the locking ring with a series of 3/8-inch diameter bolts. When fully assem led, a labryrinth type seal is made between the airframe ring and the exit ozzle attach ring. This joint design has the advantages of uniform distri ited mass around the circumference to minimize thermal stress, thin sections t reduce gamma heat generation, uniform circumferential load distribution the increases joint structural efficiency, and a single joining member (lock ring) hat has optimum quick-disconnect potential.

The nozzle is designed to provide for radial a l axial thermal expansion between the nozzle outer shell, nozzle liner, and eactor expansion pads. The aft face of the aft series of reactor circumfer itial expansion pads is flanged to nest into a radial slip joint in a supp t ring, thereby allowing radial thermal expansion of the reactor. The nozzl liner forms a slip joint with the inside diameter of the support ring that llows the liner to expand axially. The liner is attached to the nozzle ou r shell at the throat area by eight pylons, equally spaced about its circumf ence.

The exit area between the nozzle outer shell a l the exit nozzle shroud is designed to provide a constant annular area in orde that boattail drag may be minimized. The exit nozzle is designed to inco orate Rene' 41 material throughout.

6.1.2 Weights and Centers of Gravity

Weights and centers of gravity for the ejector exhaust nozzle are shown in Table XXVI.

6.1.3 Design Data

6.1.3.1 Operational Data

Critical operational phases for the exit nozzl system occur during high altitude cruise and low altitude cruise. Critical p ssure loading and temperature environments occur during the following flight o rations:

High Altitude Cruise: Mach 3.9 at 35,000 eet
on an ICAO Standar Day

Low Altitude Cruise: Mach 3.22 at 1000 eet on an ICAO Standard y

Pressure and temperature profiles for these erational regimes are presented in Figures 108 to 113.

6.1.3.2 Configuration

Radial and axial coordinates defining the co iguration of the various components comprising the exit nozzle system are pr ented in Figures 114 and 115.

6.2 Structural Analysis

6.2.1 Nozzle Forward Cylinder and Convergent Cone rimary Shell)

6.2.1.1 Discussion

The ring assembly by which the nozzle is att hed to the airframe extends aft to Nozzle Station 11.7 (E.S. 577.170) and is sentially a right circular cylinder. The cylindrical shell portion of the e t extends to Nozzle Station 13.7 (E.S. 579.170) where a 3 1/2-inch radius tr sition knuckle joins the cylinder to a convergent circular cone. This co is in turn connected to the small end of a diverging cone by a double cu e transition section which forms the nozzle throat.

From the nozzle forward station to approxima ly 10.0 inches aft of the minimum diameter section of the throat the net p ssure differential between the nozzle inner and outer surfaces is internal, cting outward radially. This bursting pressure decreases with distance fro the forward end.

Because hoop tension varies directly with bo pressure and cylinder radius, the requirement for wall thickness also decre es with distance from the forward end.

Further, because joints are required at inte ections of the cylinders, cones, and transition knuckles, a saving in stru ural weight may be achieved by progressively reducing gages at these points. ial stresses are small compared to hoop stresses.

6.2.1.2 Operating Condition

Critical operation occurs during low altitud cruise at Mach 3.22 and 1000 feet on an ICAO Standard Day. Pressure and tem rature profiles for this phase of operation are presented in Figures 108 and 12.

The shell temperature is nearly constant, va ing from a high of 1225°F to a low of 1215°F.

6.2.1.3 Material Properties

The nozzle material is Rene' 41 sheet, solutic heat-treated at 1975°F for 30 minutes, water quenched, aged at 1650°F for 4 hours, and air cooled.

At 1225°F:

$F_{t_y} \cong 106{,}000$ psi (Yield Stress)

$F_{t_u} \cong 160{,}000$ psi (Ultimate Stress)

Stress Rupture: 1 hr > 100,000; 10 hrs > 100,000; 100 hrs = 100,000 psi

6.2.1.4 Analytical Factors

Design Factor = 1.15

Factor of Safety = 1.25

Weld Efficiency = 85 percent

6.2.1.5 Analysis for Hoop Tension Loading

$$f = \frac{p\,R}{1.0 \times t} \quad \text{and} \quad t = \frac{p\,R}{f}$$

$$t \text{ required} = \frac{p\,R}{F_t}$$

Since the operating temperature is relatively low for this material creep and stress, rupture for the life involved is not critical. The design will be based upon yield stress which will be modified by a 1.15 design factor and an 85 percent weld efficiency factor.

$$F_{t_y} = 106{,}000 \text{ psi}$$

$$\text{Design Stress} = \frac{106{,}000 \times 0.85}{1.15} = 78{,}500$$

$$t_{req.} = \frac{p\,R}{78{,}500}$$

Required material thicknesses are shown in Table XXVII.

Minimum Margin of Safety (see Figure 116):

At Station 24, t rqd = 0.0765 and t specified = 0.08

$$MS = \frac{0.08}{0.0765} - 1 = +0.05$$

6.2.1.6 Analysis for Transverse and Axial Loading

6.2.1.6.1 Discussion

Axial stresses resulting from axial drag and from transverse bending are rarely critical for an exit nozzle structure. Hoop tension or compression loading producing circumferential and radial stresses govern the gage requirements and are not additive to axial stresses.

6.2.1.6.2 Axial Drag Force

Critical loading occurs at Mach 3.22 and 10[illegible] feet on an ICAO Standard Day. P = 367,438-lb limit (Reference: Figure 111)

6.2.1.6.3 Inertia Factors

Referring to design criteria inertia factors specified in Table IV for weapons ejection in low altitude cruise,

$$g_z = \begin{matrix} +8.50 \\ -1.17 \end{matrix}$$

and

$$g_x = \begin{matrix} +0.3 \\ -0 \end{matrix}$$

6.2.1.6.4 Weight and Center of Gravity

The total weight of the nozzle and shroud assembly is 1054 lb and the center of gravity is at Nozzle Station 28.75 (E.S. 4.22)

6.2.1.6.5 Axial and Shear Stresses

Critical loadings are:

$$P_{axial} = 367{,}438 + 1100 \times 0.3 = 367{,}768$$

$$M_y = +8.5 \times 1100 \times 30 = 280{,}500$$

$$V_z = 8.5 \times 1100 = 9350 \text{ lb}$$

Assume these loads act on the 0.093 [illegible]age shell.

R_i = 28.06 in.

$R_m = 28.06 + \frac{0.093}{2} = 28.1065$ in.

$f_b = \frac{M}{\pi r^2 t}$ $f_t = \frac{P_{axial}}{A}$

$f_s = \frac{V}{\pi r t}$

$f_b = \frac{280,500}{\pi \times 28.1065^2 \times 0.093} = 1220$ psia

$f_s = \frac{9350}{\pi \times 28.1065 \times 0.093} = 1142$ psi

$f_t = \frac{367,768}{\pi \times 2 \times 28.1065 \times 0.093} = 22,250$ psi

Combined axial stress = 22,250 + 1220 = 23,470 psi

Shear = 1142 psi

6.2.1.6.6 Analysis Factors

Design = 1.15

Factor of safety = 1.25

Weld factor = 0.85

MS (Combined Bending and Axial)

$MS = \frac{106,000 \times 0.85}{23,470 \times 1.15} = +2.33$

MS (Ultimate Shear)

$F_{s_u} = F_{t_u} \times 0.6 = 0.6 \times 160,000 = 96,000$ psi

$MS = \frac{96,000 \times 0.85}{1142 \times 1.25} - 1 =$ High

6.2.2 Cone-Cylinder and Cone-Cone Intersections

6.2.2.1 General Discussion

The change of slope in the shell membranes at a c e-cylinder intersection produces large localized stresses.

The required thickness of the transition sections ay be determined from Formula 3 of Para. UA-4(d), Page 111 of Reference 21:

$$t = \frac{PLM}{2\,SE - 0.2P}$$

or

$$P = \frac{2\,SE\,t}{LM + 0.2t}$$

where

M = 1/4 (3 + L/r)

P = Internal pressure, psi (use 100 psi as conservative average)

t = Material thickness

S = Maximum allowable working stress, psi

E = Lowest efficiency of joint: 80% (Refer to Para. UW-12, Reference 21)

L = Inside spherical or crown radius, inches (16.485 in.)

r = Inside knuckle radius, inches (21.48 in.)

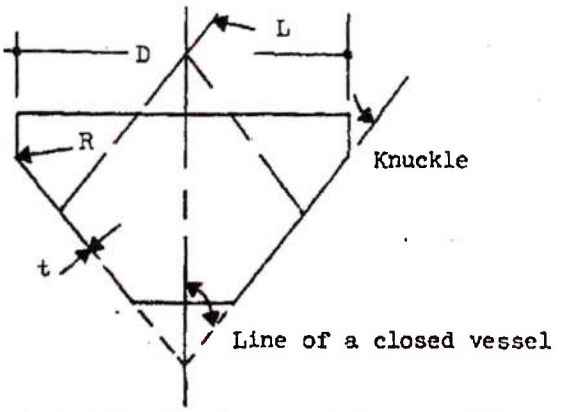

(Reference: Figure UA-4 (3), Page 110 of Reference 21)

The actual exit shape is as follows:

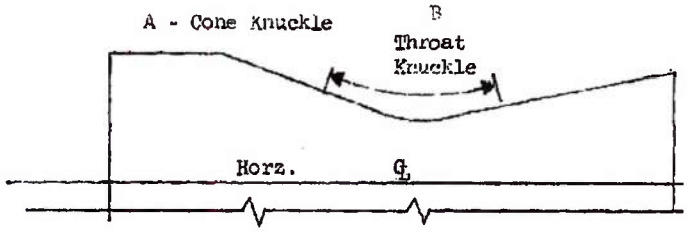

Section A conforms to code shape, but Sec on B is reversed in that the section representing the head is smaller rat r than larger than the cone. The theory still applies, however, since the cc angle is small and the transition fairly flat.

6.2.2.2 Nozzle Throat

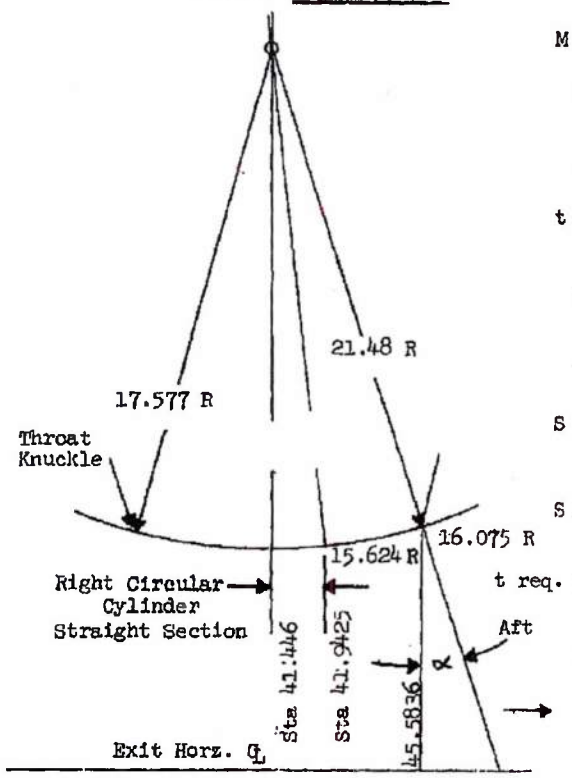

$$M = 1/4\left(3 + \sqrt{\frac{L}{r}}\right)$$

$$= 1/4\left(3 + \sqrt{\frac{16.4}{21.4}}\right)$$

$$= 1/4\,(3 + 0.875) \quad 0.97$$

$$t = \frac{PLM}{2\,S\,E + P\,(M - \quad 2)}$$

$$= \frac{100 \times 16.4 \quad \times 0.97}{(2\,S \times 0.80)\ 10 \quad (0.97 - 0.2)}$$

$$= \frac{1598}{1.6\,S + 77}$$

S = 106,000 psi and design factor of 1.15

$$S = \frac{106{,}000}{1.15} = 92, \quad 0$$

$$t\ \text{req.} = \frac{1598}{1.6 \times 92{,}000 + \quad}$$

$$= \frac{1598}{147{,}377} = 0.010 \quad \text{in.}$$

The gage chosen for the convergent cone and the throat is 0.[illegible] inches. The divergent aft cone is 0.063 inches.

By proportion, $\frac{0.0108}{0.063} \times 147{,}372 = 25{,}200$ psi. At the throat where R_i = 16.1 inches, the bending moment is approximately 225 lb x 8.5 gs x 32 in. = 61,200 in/lb (assume acting at joint with aft cone)

$$f_b = \frac{M}{\pi r^2 t} = \frac{61{,}200}{\pi \times (16.1)^2 \times 0.063} = 1{,}195 \text{ psi}$$

The axial drag is 33,650 lb.

$$\Sigma f_t = \frac{33{,}650}{2 \times 16.1 \times 0.063} = 16{,}600 \text{ psi}$$

$$\Sigma f_b + f_t = 17{,}800 \text{ psi}$$

Transition stress + f_b + f_t = 25,200 + 17,800 = 43,000 psi

F_{t_y} = 106,000 psi and $\frac{106{,}000 \times 0.8}{1.15} = 73{,}700$ psi

$$MS = \frac{73{,}700}{43{,}000} - 1 = +0.71$$

Notes: 1. This analysis is conservative; the uniform pressure of 100 psi is greater than the actual average pressure, and the axial load effect was included in the original solution for t reqd.

2. For an analysis of bursting hoop stress refer to Para. 6.2.1.

6.2.2.3 Convergent Cone

The required thickness of the conical portion is determined by Formula 4 in Section UG-32-g of Reference 21:

$$t = \frac{PD_1}{2 \cos \alpha \, (S E - 0.6 P)}$$

α = 30°, $\cos \alpha$ = 0.866 and 2 cos = 1.732

E = 0.80

P = 200 psi (assumed

D_1 = 18.0 inches

$$S = 106{,}000 / 1.15 = 92{,}000$$

$$t_{req.} = \frac{200 \times 18}{1.732\ (92{,}000 \times 0.8 - 0.6 \times 200)} = \frac{3600}{1.732 \times 73{,}480}$$

$$= 0.0284$$

$$MS = \frac{0.08}{0.0284} - 1 = +1.82$$

6.2.2.4 Forward Cylinder - Convergent Cone Intersection

Refer to Reference 21, Section UA-4-d, Equation 3.

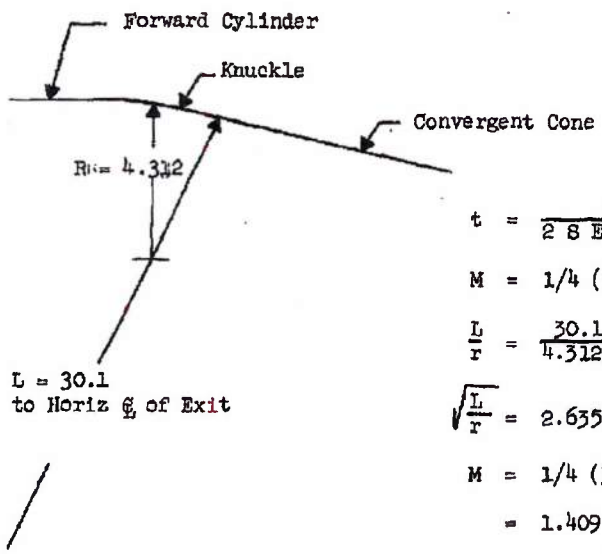

$$t = \frac{PLM}{2\ S\ E - 0.\ \ P}$$

$$M = 1/4\ (3 + \sqrt{L/r})$$

$$\frac{L}{r} = \frac{30.1}{4.3125} = 6.975$$

$$\sqrt{\frac{L}{r}} = 2.635$$

$$M = 1/4\ (3 + 2.635)$$

$$= 1.409$$

$$P \cong 200 \text{ psi}$$

$$E = 0.8$$

$$S = 106{,}000/1.15 = 92{,}000$$

$$t = \frac{200 \times 30.1 \times 1.409}{(2 \times 92{,}000 \times 0.8) - (0.2 \times 200)} = \frac{8500}{147{,}000 - 40} = \frac{8500}{146{,}960} = 0.0578$$

$$MS = \frac{0.08}{0.0578} - 1 = +0.38$$

6.2.3 Divergent Exit Cone

6.2.3.1 General Discussion

The exit internal pressure decreases rapidl aft of the forward cylinder, and approximately 10 inches aft of the nozzle t oat becomes less than that of the annulus. Most of the divergent cone sectio is subjected to collapsing pressure.

6.2.3.2 Design of Cone

The weight of a cylinder subjected to an ex rnal collapsing pressure may be minimized by stiffening a thin shell with xternal rings that hold the shell essentially round. The flexural rigidi of the combination must equal that of the minimum momolithic shell that ll support the required pressure.

As the shell thickness decreases, the requi d weight of the rings increases. The optimum combination for minimum weig must be determined by trial. Preliminary calculations indicate that a 0. 3 gage approaches the optimum requirement.

In the following analyses a 0.063 gage of R e' 41 will be analyzed without stiffeners to determine the strength of the s ll alone.

The material to be used is Rene' 41 sheet, lution heat-treated at the mill and solution heat-treated by Marquardt at 197 F (30 minutes), water-quenched, aged at 1650°F (4 hours), and then air coo d.

6.2.3.3 Pressure and Temperature Data

Operation in low altitude cruise phase at M h 3.22 and 1000 feet on an ICAO Standard Day produces critical pressure temp ature loading (see Figures 108 and 112). Pressure and temperature data fol w:

	Engine Station							
	613.412	623.416	633.416	643.416	653.416	662	[	668.070
Annulus Pressure (psia)	60.22	60.22	60.22	60.22	60.22	59	)	14.00
Nozzle Internal Pressure (psia)	109.00	60.22	37.75	28.50	23.50	20	)	19.75
Nozzle Δp (psi)	+48.75	0	-22.49	-31.72	-36.72	-38	)	+5.75
Nozzle Internal Radius (in.)	15.656	17.80	20.41	22.75	24.46	26	ı	27.259
Nozzle Temperature (°F)	1220	1225	1230	1245	1280	135		1450

The shell axial length is 39.05 inches.

6.2.3.4 Analysis of Ring-Stiffened Cone for Exte al Pressure

The methods employed in Reference 22 for etermining the collapsing pressure of thin-walled cylinders with ring stiffer s will be employed to determine the size and location of rings required.

The shell is assumed to be divided into series of short shells whose lengths are the distance between rings. This ass ption applies well and is conservative for a conical shell.

6.2.3.4.1 Ring at Station 660.320

The height of the ring to be used must e limited or the ring will interfere with the cooling annulus airflow.

Shell inner radius = 26.18 inches

Differential pressure for Mach 3.22 at .000 feet on ICAO Standard Day = -39.22 psi

Shell temperature = 1325°F

E of Rene' 41 $\cong$ 24.3 x 10^6

The height of a stiffening ring is lim ed to 1.0 inches by the annulus airflow requirements.

6.2.3.4.1.1 Ring Section Properties

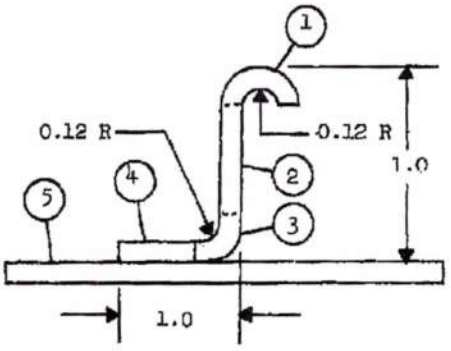

Assume effective shell width acting with ring as 30 t = 1.89 inches.

Item	Area	y_1	AY_1	AY_1^2	I_{ox}
1	0.0572	0.9426	0.0538	0.0507	0.0003
2	0.0422	0.532	0.02145	0.01142	0.000982
3	0.02106	0.10653	0.00224	0.0002385	0.00006
4	0.0636	0.103	0.00656	0.000676	0.000034
5	0.1190	0.0315	0.00376	0.0001182	0.0000396
	0.30306		0.08781	0.0631527	0.0014156

$$\bar{y} = 0.08781/0.30306 = 0.29 \text{ in.}$$

$$I = 0.0631527 + 0.0014156 - 0.29 \times 0.08781$$

$$0.0392 \text{ in}^4$$

6.2.3.4.1.2 Required Flexural Rigidity

For the case of a ring-stiffened cylinder, re er to Section IV, Page 36, of Reference 23. The shell is assumed divided int a series of short shells whose lengths are the distances between rings. he flexural rigidity, EI_s, of the combined ring stiffener and shell requir l to prevent collapsing from an external pressure is:

$$EI_s = \frac{W_s D^3 L_s}{24}$$

where

I_s = Required moment of inertia of stiffener and effective width of shell

E = Modulus of elasticity of material = 24.3×10^6

D = Cylinder outer diameter = 52.486 in.

L_s = Ring spacing

W_s = Maximum allowable unit pressure = 39.22 psi

For Station 660.320, the ring is placed close o the thickened throat section. The adjoining ring forward on the shell is s ced 6.0 inches away.

T_3 = 1350°F and E = 24.3×10^6

D^3 = 144,000

$$I_s = \frac{39.22 \times 144{,}000\ L_s}{24 \times 24.3 \times 10^6} = 0.0392$$

$L_{s_{req.}}$ = 4.05 in.

Since the shell width between the n[illegible]le and the ring is small, the stiffening effect on the shell is greater t[illegible]n if an equal spacing were used on both sides. A ring spacing of six inche[illegible]s therefore utilized to the next forward ring.

Spacing to thickened aft section = [illegible]2.47 - 660.320

= [illegible]5

Spacing to forward ring = 6.00

Average spacing = 4.05 in.

Since a high margin of safety was ob[illegible]ined on the thickened aft section, the shell is fully effective over the [illegible]ce to the ring at Station 660.320, and the section is sufficient.

6.2.3.4.2 Ring at Shell Station 651.320

Shell I.R. = 25.20 in.

O.R. = 25.263 in.

O.D. = 50.526 in.

Δp = 60.22 - 23.5 = 36.72 psi

T = 1285°F (Use 1300°F)

E = 25×10^6

L_s = 6.0

$$I_{s_{req.}} = \frac{36.72 \times \overline{50.526}^3 \times 6.0}{24 \times 25 \times 10^6} = 0.0475 \text{ in.}^4$$

A ring section similar to that used at [illegible]tation 660.320 will be utilized with an over-all height of 1.5 inches and mat[illegible]rial gage of 0.063. An effective shell skin width of 2.5 inches is assumed

Item	Area	y_1	Ay_1	Ay_2	I_{ox}
1	0.0433	1.5469	0.0670	0.1033	0.0002
2	0.0668	0.7505	0.05025	0.0377	0.0062
3	0.01579	0.14967	0.00236	0.000354	0.0000
4	0.0512	0.0945	0.00483	0.000456	0.0000
5	0.1575	0.0315	0.00496	0.0001562	0.0000
	0.33459		0.12940	0.1419666	0.0066

$\bar{y}$ = 0.1294/0.33459 = 0.3875 in.

I_x = 0.1419666 + 0.00661915 - (0.3875 x 0.1 4)
= 0.11849 in.^{4}

I_x = 0.1185 > 0.0475 required for 6.0 in. s ing; therefore, space 3rd ring at 8.0 inche from this (second) ring.

$$MS = \frac{0.1185}{0.0475 \times 1.25} - 1 = +0.99$$

6.2.3.4.3 Ring at Shell Station 646.320

T = 1252°F

Inner radius = 23.69; outer = 23.75; O.D. = 7.50

Exit pressure = + 27 psia

Annulus pressure = - 60.22

Δp = - 33.22 psi

E of Rene' 41 = 25.5 x 10^6 at 1250°F

I = 0.1185 in.^{4}

$$L_{s_{req}} = \frac{0.1185 \times 24 \times 25.5 \times 10^6}{33.22 \times 47.5^3} = 20.4$$

For L_s = 8.0 in.

$$I_{s_{req}} = \frac{33.22 \times 47.5^3 \times 8}{24 \times 25.5 \times 10^6} = 0.0463 < 0.1184$$

$$MS = \frac{0.1184}{0.0463 \times 1.25} - 1 = +1.0$$

Space next ring at 10 inches.

6.2.3.4.4 Ring at Shell Station 636.320

Exit pressure = + 34 psia

Annulus Pressure = - 60.22 psia

Δp = - 26.22

Inner radius = 21.32; outer = 21.383; D. = 42.766

T = 1235°F (Use 1250)

E = 25.5 x 10^6

$$I_{e_{req}} = \frac{26.22 \times \overline{42.77}^3 \times 10}{24 \times 25.5 \times 10^6} = 0.0335 \text{ i}^4$$

Section properties of 1 1/8 inch ring 0.063 gage:

I = 0.0453 in.^{4} with 2.35 in. effect e shell

I = 0.0453 > 0.0335 req.

$$MS = \frac{0.0453}{0.0335 \times 1.25} - 1 = + 0.085$$

6.2.3.4.5 Shell Stations 623.416 to 636.320

At Station 623.416 10 inches aft of th throat, the annulus and exit pressures balance and the cylinder is subject to zero radial pressure.

At Station 633.416, 10 inches further t a Δp of 23.22 psi exists. A ring is located at Station 636.320. The averag shell pressure is $\frac{0 + 23.33}{2}$ = 12.61 psi. The average radius is $\frac{16.096 + 20.6}{2}$ = 18.35 in. The length is 10 inches.

By the method of Reference 22,

$$\frac{D}{t} = \frac{2\,(18.35 + 0.063)}{0.063} = \frac{36.826}{0.063} = 5$$

$$\frac{L}{R} = \frac{10}{18.143} = 0.55$$

K > 200

$$W_c = 25.5 \times 10^5 \times 200 \times \left(\frac{0.063}{36.823}\right)^3 = .5 \text{ psi} > 12.61$$

23.33 psi

No rings are required in this area.

$$MS = \frac{25.5}{12.61 \times 1.25} - 1 = + 0.61$$

6.2.3.5 Stiffening Angles--Stiffening Crippling Stress

Analysis by the methods given in Reference 23. Refer to Figure 11, page 228 of Reference 23 for equivalent sections.

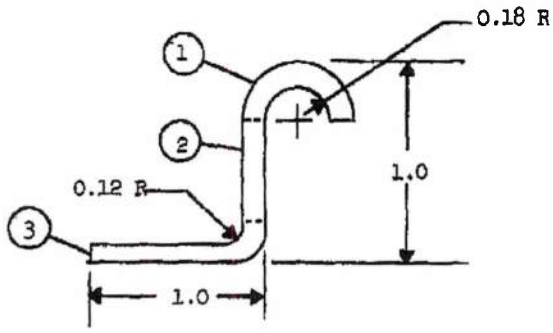

Material is Rene' 41 sheet of 0.08 gage; temperature is 1400°F; $E = 24.8 \times 10^6$.

Material treatment is solution heat treat at 1[illegible]5°F for 30 minutes, water quench, age at 1650°F for 4 hours AC.

$$F_{c_y} = 118{,}000 \text{ psi}$$

$$F_{c_c} = \frac{\sqrt{F_{c_y} E}}{(b'/t)^{0.75}}$$ for individual angle sect[illegible]ns Equation 15, page 229 of [illegible]f-erence 23.

where

F_{c_y} = Compressive yield stress

E = Young's modulus in compression

b'/t = Equivalent $b/t = \frac{a+b}{2t}$

C_e = Edge support coefficient

C_e = 0.316 for 2 edges free

= 0.342 for 1 edge free

= 0.366 for no edge free

The weighted crippling stress for stiffer s consisting of several equivalent angle sections is:

$$F_{c_c} = \frac{\Sigma\,(\text{crippling loads of angles})}{\Sigma\,(\text{areas of angles})}$$ Reference 23, page 229

$$\sqrt{F_{c_y} E} = \sqrt{118{,}000 \times 24.8 \times 10^6}$$

$$= \sqrt{2{,}820{,}000{,}000} = 530{,}000$$

Item 1 $F_{c_c} = \dfrac{0.316 \times 530{,}000}{(2.83)^{0.75}} = \dfrac{167{,}000}{2.18} = 76{,}700$ psi

Item 2 $F_{c_c} = \dfrac{0.366 \times 530{,}000}{(4.55)^{0.75}} = \dfrac{194{,}000}{3.6} = 54{,}000$ psi

Item 3 $F_{c_c} = \dfrac{194{,}000}{6.9^{0.75}} = \dfrac{194{,}000}{4.5} = 43{,}000$ psi

$$F_{c_c}\text{ combined} = \frac{(76{,}700 \times 0.454) + (54{,}000 \times 0.727) + (43{,}0\;\;) \times 1.105)}{(0.454 + 0.727 + 1.105)}$$

$$= \frac{34{,}800 + 39{,}300 + 47{,}500}{2.286} = \frac{121{,}600}{2.286}$$

$$= 53{,}000 \text{ psi}$$

Area of ring and skin at Station 660.320 0.303 in.^{2}

$p = -39.22$ psi

Ring spacing = 6.0 in.

$p = p\,RS = 39.22 \times 26.18 \times 6 = 6130$ l

$P/A = \dfrac{6130}{0.303} = 20{,}200$ psi

$MS = \dfrac{53{,}000}{20{,}200 \times 1.25} - 1 = +1.09$

Rings at other stations are of smaller di eter and are less heavily loaded; they are, therefore, satisfactory by compa son.

6.2.3.6 Exit Nozzle Divergent Cone--Transverse and Ax .l Loading

The cone is loaded transversely and axially b inertia forces and axially by pressure forces. Since the cone acts as a va able section cantilever beam with the reduced area forward, the critical se ion occurs at the forward end station where the shell gage changes from 0.08 t 0.063 (Station 623.416).

6.2.3.6.1 Axial Air Load

Maximum axial air load occurs in low altitu cruise at Mach 3.22 and 1000 feet on an ICAO Standard Day. The total aft axi load - 33,650 pounds.

6.2.3.6.2 Dead Weight and Center of Gravity

The weight of the divergent cone aft of the ozzle throat minimum diameter area at Engine Station 613.417 is $\approx$223.6 l (total assembly weight). The assembly center of gravity is located 32.6 i hes aft of the throat. The weight of the 0.08-inch section is $\approx$38.1 lbs, an its CG is 5.8 inches aft of the throat.

6.2.3.6.3 Weight and CG of 0.063-in. Section Aft of S tion 623.416

$$W = 223.6 - 38.1 = 185.5 \text{ lbs}$$

$$CG = \frac{(223.6 \times 32.6) - (38.1 \times 5.8)}{185.5} = \frac{7680 -}{185.} \quad 21$$

$$= 40.2 \text{ i}$$

Arm to Station 520.412 = 40.2 - 10 = 30.2 i

M = 185.5 x 30.2 = 5600 in.-lbs (dead weig)

V = 185.5 lbs

612.3.6.4 Inertia Load Factors

The critical combined y-z load factor actin at the missile center of gravity is $\approx$5.0 g. A conservative value of 10 acting on the exit nozzle is assumed for this analysis.

6.2.3.6.5 Transverse Shear and Bending at Station 623 16

The bending stress at a section in a right rcular cylinder is:

$$f_b = \frac{M}{\pi r^2 t}$$

For a truncated cone, $f_{b_1} = f_b \text{ Sec } \beta$ where β is the angle between the axial center line and meridional lines in t shell. Assuming a straight surface between throat and exit,

$$\beta = 10°55'.$$

$$\text{Sec } \beta = \frac{1}{\text{Cos } \beta} = \frac{1}{0.98190} = 1.02$$

R at Station 623.416 $\approx$ 17.5 inches

$$f_b = \frac{M}{\pi \times 35^2 \times 0.063} = \frac{M}{242}$$

$$f_{b_1} = 0.00422 \text{ M}$$

For a 1.0 g inertia f_{b_1} = 0.00422 x 5 0 = 23.6 psi

10 g = 236 psi

The transverse shear stress at Statio 623.416 is:

$$f_{s_1} = \frac{V_1}{\pi rt}$$

where

$$V_1 = V - \frac{M \tan \beta}{r}$$

for 1 g

$$V_1 = 185.5 - \frac{5600 \times 0.19287}{17.5} = 185.5 - 61.7 = 123.8 \text{ lbs}$$

$$f_s = \frac{123.8}{\pi \times 17.5 \times 0.063} = 35.7 \text{ psi for 1.0 g}$$

$$= 357 \text{ psi for 10 g}$$

6.2.3.6.6 Axial Air Load Stress

Total air load at throat - 33,650 lbs Since the section is obviously over strength, assume the same load at Stat n 623.416.

Section area = $(2 \times 17.563)\pi \times 0.063$ 7.05 in.^{2}

$$P/A = \frac{33,650}{7.05} - 4780 \text{ psi}$$

6.2.3.6.7 Combined Axial Stress

Conservatively utilizing an inertia load facto of 10.0 g, the full cone drag load, and a design factor of 1.15, the design li t stress is:

$$f_t = (236 + 4780)(1.15) = 5770 \text{ psi}$$

6.2.3.6.8 Material Properties

The temperature at Shell Station 623.416 is 12 °F, and the F_{t_y} of Rene' 41 sheet is 107,500 psi.

Assuming a weld joint efficiency of 85 percent

$$F_{tu} = 150{,}000 \text{ psi}$$

Assuming

$$F_{su} = 0.5\, F_{tu},$$

$$F_{su} = 75{,}000 \text{ psi}$$

6.2.3.6.9 Margins of Safety

$$\text{MS Combined Tension Yield} = \frac{107{,}500 \times 0.85}{5770} - 1 \quad \text{High}$$

$$\text{MS Combined Tension Ultimate} = \frac{150{,}000 \times 0.85}{5016 \times 1.25} - 1 \quad \text{High}$$

$$\text{MS Ultimate Shear} = \frac{75{,}000 \times 0.85}{357 \times 1.25} - 1 + \text{High}$$

Note: Loads utilized in this analysis of comb ed axial-transverse, while not the true values, were obviously conservative, and in view of the high margins obtained are deemed sufficient.

6.2.3.7 Exit End Doubler Ring

6.2.3.7.1 Discussion

From Exit Station 662.470 to the aft end at St ion 668.070, a 1/4-inch thick plate ring is utilized to stiffen the unsupp ted open end of the 0.063 gage conical shell (Figure 117). A similar ring s provided on the airframe shell that encloses the nozzle.

The annulus formed between these shells is uti zed as a cooling air duct. The shells converge toward the open end, and by t ering the end portions of the stiffening rings a convergent-divergent cooling air exhaust nozzle is formed.

6.2.3.7.2 Pressure Loading

The divergent cone is subjected to a ıet external collapsing pressure differential. The critical pressure-temper ıure combination occurs during low altitude cruise on an ICAO Standard Day at Mach 3.22 and 1000 feet. Pressure profiles for the operation are presented in .gure 110. The following are data from these curves:

	Exit Station			
	662.470	665.470	666.97	668.070
Annulus pressure, psia	-59.0	-54.7	-48.5	-14.00
Nozzle pressure, psia	+20.2	+20.0	+20.0	+19.75
Δp on nozzle	-38.8	-34.7	-28.5	+ 5.75

The axial forces acting on this smal section are negligible.

6.2.3.7.3 Temperature

The temperature through the shell th kness is assumed uniform. The temperature profile for Mach 3.22 at 1000 feet n an ICAO Standard Day is presented as Figure 112. Values for the ring are s follows:

	Exit Station			
	662.470	665.470	666.97	668.070
Temperature, °F	1350	1392	1425	1450

6.2.3.7.4 Material

The material is Rene' 41 plate, mill nnealed and process-treated as follows:

Solution heat-treat at 1975°F (30 mi tes); water quench; age at 1650°F (4 hours); air ool.

6.2.3.7.5 Analysis by Method of Reference 24

In this report Donnel's equation for he equilibrium of cylindrical shells in torsion is applied to find the critica stresses under other loading conditions for cylinders with simply supported dges.

6.2.3.7.6 Critical Buckling Stress for Uniform External essure

Pressure applied to entire outer surface radis y; ends open; edges simply supported.

Solve for nondimensional buckling parameter,

$$z = \frac{L^2}{rt}\sqrt{1-\mu^2}$$

Obtain buckling constant,

$$k_y = f_y\left(\frac{t\,L^2}{D\,\pi^2}\right)$$

Solve for f_y = critical compressive hoop stres

Values apply where n = 1 < 2

D = plate flexural stiffness/unit length = $\frac{t^3}{12 \quad - \quad ^2)}$

Assums

μ = 0.3

t = 0.25 in.

L = 6.0 in.

r = 26.9 in. (average)

E = at 1375°F (average) = 24.3×10^6

$$D = \frac{24.3 \times 10^6 \times (0.25)^3}{12\,(1-0.3^2)} = 34{,}700$$

$$z = \frac{(6^2)}{(26.9)\,(0.25)}\sqrt{(1-0.3^2)} = 5.09$$

$$r/t\sqrt{1-\mu^2} = \frac{26.9}{0.25} \times 0.951 = 102.2$$

From Figure 1 of Reference 24:

k_y = 4.7

$$f_{y_{cr}} = \left[\frac{k_y}{\left(\frac{t\,L^2}{D\,\pi^2}\right)}\right] = \frac{4.7}{\left(\frac{0.25 \times 6^2}{34{,}700 \times \pi^2}\right)} = \frac{4.7 \times 34\ 00\,\pi^2}{0.25 \times 6}$$

= 178,000 psi

For f_c (hoop compression), assume aver e pressure of 35 psi over ring width.

$$f_c = \frac{35 \times 26.9}{0.25} = 3770 \text{ psi}$$

Design factor = 1.15

Factor of safety = 1.25

$$MS(\text{Ultimate}) = \frac{178,000}{3770 \times 1.25} - 1 = \text{Hig}$$

6.2.3.7.7 Analysis by Method of Reference 5

Refer to Reference 5, page 270, Case 1 Table XIII. This theory applies to a more concentrated loading than the ac al case involved. A conservative assumption will be used in which the entire pre ure acting on the ring is concentrated at the end.

Then:

$$\text{Max } s_2 = \frac{-2 V_o}{t} \lambda R$$

V_o = transverse shear normal to wall lbs/in.)

$$\lambda = \sqrt[4]{\frac{3(1-\mu^2)}{R_2^2 t^2}}$$

R_2 = R = mean radius of shell

μ = Poisson's ratio = 0.3

t = 0.25 in.

s_2 = hoop stress

$$\lambda = \sqrt[4]{\frac{3(1-0.3^2)}{26.9^2 \times 0.25^2}}$$

$$= \left(\frac{2.71}{4.52}\right)^{1/4} = (0.6)^{1/4}$$

$$= 0.88$$

V_o = p (assume 35 psi average for 1.(inch width)

$$s_2 = \frac{-2 \times 35}{0.25} \times 0.88 \times 26.9 = 6620 \text{ ps}$$

Station 662.470 to 668.070 = 5.6 inche

If it is assumed that the entire load is ncentrated at the end:

$V_o = 5.6 \times 35 \times s_2 = 5.6 \times 6620 = 37{,}000$ i

F_{t_y} of Rene' 41 at 1450°F = 127,000 psi (r stock)

Design factor = 1.15

$$MS\ (Yield) = \frac{127{,}000}{37{,}000 \times 1.15} - 1 = +1.98$$

6.2.4 Ejector Shroud (Nozzle Inner Liner)

6.2.4.1 Discussion

The inner liner acts as a second nozzle and xtends aft to the exit nozzle throat. It serves as a heat shield between th exhaust flow and the primary nozzle. Airflow from the lateral support annulus s ducted between these exit nozzle shells and used for nozzle cooling.

Exit nozzle exhaust flow pressure is less t n that in the cooling annulus. The shroud is subjected to a collapsing pre ure.

Radial components of pressure loadings are acted within the shroud. Axial components are transferred to the exit nozz at the throat by means of radially oriented pin and socket supports. Ax l inertial forces are reacted similarly. The shroud acts as a simply suppor d beam to transfer radial inertia loads to the exit throat and the airframe t the reactor aft end.

6.2.4.1.1 Method of Analysis

Analysis of the cylindrical and conical s lls is based on the methods of Reference 22 previously utilized in Section 6.2 for the divergent cone aft section of the exit nozzle.

6.2.4.1.2 Operational Regimes, Pressure and Tempera re

Critical pressure and temperature regimes ccur during low altitude cruise operation at Mach 3.22 and 1,000 feet on an I O Standard Day.

Data related to this operational phase of he regime are presented in Figure 108 and in Table XXVII.

6.2.4.1.3 Materials

The material used is Rene' 41 sheet stock process- solution heat treated at 1975°F for 30 minutes, water quenched, a d at 1650°F for 4 hours, and air cooled. The following strength values apply

Temperature (°F)	$F_{t_y} \times 10^{-3}$	$E \times 10^{-6}$
1350	104.8	25
1400	102	24.3
1450	99	23
1500	96	21.5
1550	93	19.5

Assume

$$F_{c_y} = F_{t_y}$$

$$F_{s_u} = 0.6\, F_{t_u}$$

6.2.4.2 Analysis of Forward Cylinder

The forward 22.25 inches of the liner is a right circular cylinder with an I.D. of 53.5 inches. The open end is stiffer l by a heavy doubler ring and is simply supported in the radial direction l the flange of the support ring attached to the airframe. The liner ring sli es inside this ring and is unrestrained in the axial direction.

Critical operation occurs in low altitud cruise at Mach 3.22 and 1,000 feet on an ICAO Standard Day. The net differer al pressure between the inner and outer shell surfaces is compressive and va es from 66 psi at the forward end to 26 psi at the aft end.

Utilizing the methods of Reference 22:

$L = 22.25$ in.

$R = 26.75$ in.

$L/R = \frac{22.25}{26.75} = 0.833$

$D = 53.50$ in.

The average shell temperature is 1350°F d E is 25 x 10^6 psi.

t	D/t	K	t/D	$(t/D)^3$	W_c (psi)
0.063	850	220	0.001178	1.63^{-9}	8.95
0.080	667	190	0.001493	3.34^{-9}	15.85
0.093	576	175	0.001735	5.23^{-9}	22.95
0.109	490	160	0.00204	9.45^{-9}	37.80
0.125	428	140	0.00234	1.285^{-8}	45.10
0.156	343	135	0.00292	2.5^{-8}	84.2
0.1875	285	130	0.00351	4.32^{-8}	140.5

The forward edge of the shell aft to Station 8.47 is 0.1875 gage material. Ring grooves are machined in this area to pr ide a pressure seal, but the majority of the section is full thickness.

Maximum p = 66.0 psi at the forward end

$$MS\ (t = 0.1875) = \frac{140.5}{66 \times 1.25} - 1 = 0.70$$

The shell is spin-formed and is assumed taper in thickness from 0.1875 at Station 568.47 to 0.125 at Station 580.47, here p = 31 psi and W_c = 45.10 psi

$$MS\ (t = 0.125) = \frac{45.10}{31 \times 1.25} - 1 = +0.16$$

6.2.4.3 Analysis of Aft Cone (Convergent)

Analysis methods are those utilized in the st y of the exit shell (Refer to Paragraphs 6.2.1 and 6.2.3).

L = 18.0 inches

R fwd = 27.5 inches; r aft = 18.25 inches; erage r = 23.0 inches

Average temperature = 1450°F

E of Rene' 41 = 23×10^6 psi

$$L/R = \frac{18}{23} = 0.782$$

t	D/t	K	t/D	$(t/D)^3$	W_c (psi
0.063	730	225	0.00137	2.58^{-9}	13.4
0.080	575	200	0.00173	5.17^{-9}	23.8
0.093	495	185	0.00202	8.22^{-9}	35.0
0.109	422	175	0.00237	1.33^{-8}	53.5
0.125	378	160	0.00272	2.01^{-8}	74

At the forward end, p = 27 psi and R = .75 inches.

At the aft end, p = 44.3 and R = 18.27 ches.

For a 23-inch average R, W_c = 74 psi fo a 1/8-inch gage.

W_c for R = 27.75 on the forward cylinde = 45.10 psi.

$$MS \text{ (forward end)} = \frac{45.10}{27 \times 1.25} - 1 = + \; 333$$

At the aft end the radius of 18.25 will rovide a higher W_c than the 74.0 psi for the average R = 23.0 inches. The W_c alue for R = 16.0 inches in the throat area is greater than 100 psi. The 0.125 age, therefore, is deemed satisfactory.

$$MS = \frac{74}{44.3 \times 1.25} - 1 = + 0.33$$

6.2.4.4 Analysis of Throat (Aft End)

The axial length from the point of tang cy with the convergent conical shell to the open aft end is approximately 10 nches. The variation in shell radius is small, and the average radius is 16.(inches. The maximum collapsing pressure is 140 psi at the throat mid-point a decreases to zero at the open end (see Figure 118).

Utilizing the method of Reference 22,

$$L/R = \frac{10}{16} = 0.625$$

Assume t = 0.109 in.,

$$D/t = \frac{32}{1109} = 293, \quad K \cong 225$$

t = 1550°F maximum and E = 19.5×10^6 si minimum

$$\left(\frac{t}{D}\right)^3 = \left(\frac{0.109}{0.32}\right)^3 = 3.97 \times 10^{-8}$$

$$W_c = 225 \times 18.5 \times 10^6 \times 3.97 \times 10^{-8} = 51.5 \text{ psi} > 140 \text{ psi}$$

Using t = 0.125,

$$D/t = \frac{32.0}{0.125} = 256, \quad K \cong 210$$

$$t/D^3 = 5.93 \times 10^{-8}$$

$$W_c = 210 \times 19.5 \times 10^6 \times 5.93 \times 10^{-8} = 243 \text{ p}$$

$$MS = \frac{243}{140 \times 1.25} - 1 = +0.39$$

6.2.5 Analysis of Exit Nozzle Attach Joint

6.2.5.1 General Discussion

The exit nozzle is cantilevered from the airfr e at the aft face of the reactor where it is attached by a quick disconnectin ring joint consisting of an airframe ring, an exit nozzle ring, a locking ing, and a split ring retainer (see Figure 107).

The exit nozzle and locking ring are threaded. The retainer ring is fastened to the locking ring with 3/8-inch diameter s ar bolts.

The attach ring is subjected to (1) the axial r load and inertia forces acting on the exit nozzle assembly, (2) a differe ial air pressure between its circumferential surfaces, and (3) the transvers shear and bending moments of the inertial loads on the nozzle.

6.2.5.1.1 Design Loads

Critical pressures and temperatures occur du ng low altitude cruise operation at Mach 3.22 and 1000 feet on an ICAO Stan rd Day.

The net axial drag force acting on the nozzl assembly, nozzle and liner, at the attach joint is 367,438 pounds (limit).

The nozzle assembly weight is 1054 pounds, a the inertial load factors are $g_x = 0$, $g_z = 8.5$, $g_y - 1.0$.

The airframe annulus pressure is 60.22 psia, nd the exit-liner annulus pressure is 320 psia at Station 565.47 and 305 psi at the joint of center line station. For analysis, a uniform differential 250 psi and net axial load of 375,000 pounds are conservatively assumed.

6.2.5.1.2 Temperatures

A uniform temperature of 1400°F is assumed f the entire attach structure with no variation throughout the length or radi l thickness.

6.2.5.1.3 Material

The material is Rene' 41 fabrication, h it-treated at 1975°F for 1/2 hour, water quenched, aged at 1650°F for 4 hours and air cooled. The rings are machined from forged rings.

For 1400°F, the material properties are as follows:

F_{t_u} = 130,000 psi

F_{t_y} = 100,000 psi

E = 24 x 10^6

0.2% plastic creep in 10 hrs = 68,000 p .

1% creep, 10 hrs = 85,000 psi

6.2.5.2 Analysis of Vehicle Coupling

The open end cylinder with its integral f nge is subjected to a uniformly distributed axial load, applied in bearing to he flange, and to a uniform internal (bursting) pressure. The assumed couplin geometry is illustrated in Figure 119. A method for analyzing such a structu is presented in Reference 5, Case 16, Table XIII, page 263, and is applied i the calculations which follow:

V_o = transverse shear normal to wall, l linear in.

M_o = bending moment, uniform along circ ference, in.-lb/linear in.

p = unit pressure, psi (250 psi)

t = wall thickness, in. (0.375 in.)

a = median diameter of vessel, in. (58 25 in.)

b = median diameter of flange, in. (59 75 in.)

h = flange thickness, in. (0.75 in.)

P = tensile force, lb. (375,000 lb.)

f = $\sqrt{at}$, (4.688 in.)

d = flange outer diameter, in. (59.50 .)

s_1 = meridional membrane stress

s_1 = meridional bending stress

s_2 = hoop membrane stress

s_2^1 = hoop bending stress

$$T_1 = \frac{t^3 (3a^2 + 5d^2)}{h^3 (d^2 - a^2)} = 33.864 \text{ lb/in.}$$

$$T_2 = \frac{3.58\, t^3}{h^3 (d^2 - a^2)} \frac{d}{3} \log_e \frac{b}{a} + 0.1 (b^2 - a^2) = 0.1033 \quad \text{/in.}$$

$$V_o = \frac{(f^2 - \frac{h^3}{2t} t_1)(t + 0.2325\, ft)\, p - 2T_2 (h + 0.5377\, f)\, P}{1.86\, ft + T_1 L^2 (2 + 0.116 \frac{f}{t} t_1) + 1.6103\, fh + 0.866\, f^2} = -12.31 \text{ lb/in.}$$

$$M_o = \frac{(h^2 T_1 + 1.86\, ft)\, V_o + ht_2 P - 0.5\, tp\, (f^2 - \frac{h^3}{2t} t_1}{1.5\, T\, h - 3.464\, t} = 710.93 \quad \text{in-lb/in.}$$

The maximum axial stress in the cylinder is:

$$S \text{ (cylinder)} = \frac{6M_o}{t^2} + \frac{P}{\pi at} = 84{,}500 \text{ psi}$$

$$MS \text{ (cylinder)} = \frac{100{,}000}{1.15 \times 84{,}500} - 1 = + \underline{0.03}$$

The maximum radial stress in the flange is:

$$S_R \text{ (flange)} = \frac{6}{h^2} (M_o - 1/2\, V_{oh}) + \frac{V_o}{h} + p = 816 \text{ psi}$$

The maximum tangential stress in the flange is

$$S_t \text{ (flange)} = \frac{6}{h^2} (M_o - \frac{1}{2} V_{oh}) + \frac{0.8}{h^2(d^2 - a^2)} d^2 (-15\, M + 7.5\, hV_o + 1.2\, P \log_e$$

$$\frac{b}{a} + 0.447\, tP\, (b^2 - a^2) + \frac{h^2}{4t^3} T_1 (V_o + hp) = 11{,}840 \text{ psi}$$

$$MS \text{ (flange)} = \frac{100{,}000}{1.15 \times 11{,}840} - 1 = \underline{\text{High}}$$

6.2.5.3 Retaining Ring and Bolts

The retaining ring is segmented and is bo ed to the lock ring by 140 3/8-inch stud bolts. Retaining ring geometry is sh n in Figure 120.

Total nozzle assembly axial load = 375,00 lbs

Load/bolt = 375,000/140 = 2680 lbs/lmt.

6.2.5.3.1 Bolt Shear

$A = 0.7854\ (0.375)^2 = 0.1102\ \text{in.}^2$

$f_s = 2680/0.1102 = 24{,}300\ \text{psi}$

$F_{s_u} = 0.6 \times 130{,}000 = 78{,}000\ \text{psi}$

$$MS\ (\text{shear}) = \frac{7800}{24{,}300 \times 1.25} - 1 = +1.56$$

6.2.5.3.2 Bolt Bearing on Retainer

$A = 0.15 \times 0.375 = 0.0563\ \text{in.}^2$

$f_{br} = 2680/0.0563 = 47{,}600\ \text{psi}$

$F_{br_u} = F_{t_u}$ (conservative) $= 130{,}000$ psi

$$MS = \frac{130{,}000}{47{,}600 \times 1.25} - 1 = +1.18$$

6.2.5.3.3 Bolt Coupling Loading

The axial load transfers from the lock ng to the bolt, and thence through the retainer ring to the vehicle fitti shell (Figure 121). The moment occasioned by load transfer in the retain ring is assumed to be reacted by a couple acting between the bolt cente ine and the bearing of the retainer on the lock ring.

Moment Arm = 0.25 inches

Load/bolt = 2680 lbs; moment = 2680 x 0 5 = 670 lbs;

$$\text{Couple} = \frac{670}{0.50} = 1340\ \text{in.-lbs}$$

Bolt inner dia. = 0.3179; A = 0.079 in.²

$F_t = 1340/0.079 = 17{,}000\ \text{psi}$

$$MS = \frac{100{,}000}{17{,}000 \times 1.15} - 1 = \text{High}$$

6.2.5.3.4 Bending of Retainer Ring

O.D. of lock ring = 60.9 in.; circumference = 193.5 in.; 140 bolts are specified.

Perimeter of retainer ring at mid height = 186 in.; $\frac{186}{140}$ = 1.33 in./bolt.

Assuming a cross sectional area 1.01 inches wide to act as a beam in simple bending,

$$f = \frac{6M}{bd^2} = \frac{6 \times 2680 \times 0.251}{1.0 \times (0.4)^2} = 25{,}300 \text{ psi}$$

$$MS = \frac{100{,}000}{25{,}300 \times 1.15} - 1 = +2.44$$

6.2.5.3.5 Ring Shear-Out

Area = 0.31 x 0.4/2 = 0.124 in.^{2}

P/A = 2680/0.124 = 21,620 psi

F_{s_u} = 78,000 psi

$$MS = \frac{78{,}000}{21{,}620 \times 1.25} - 1 = +1.9$$

6.2.5.4 Analysis of Lock Ring (Figure 122)

Assume each thread reacts one half of the 375,000-pound limit axial load. The load per inch of thread at the pitch diameter is:

$$P = \frac{375{,}000}{\pi \times 59.6475 \times 2} = 1000 \text{ lb/in.}$$

At Section A-A, assuming a 1.0-inch circumferential width of shell and thread acting as a beam,

$$M = 1000 \times 0.4375 = 437.5 \text{ in.-lb}$$

$$I = \frac{1 \times (0.415)^3}{12} = 0.00595 \text{ in.}^4$$

$$f_b = \frac{437.5 \times 0.2075}{0.00595} = 15{,}250 \text{ psi}$$

$$\text{Axial stress} = \frac{2 \times 1000}{1 \times 0.415} = 4820 \text{ psi}$$

$$\text{Total stress} = 15{,}250 + 4820 = 20{,}070 \text{ psi}$$

$$\text{MS (yield)} = \frac{100{,}000}{20{,}070 \times 1.15} - 1 = +3.33$$

$$\text{MS (10-hr creep of 1\%)} = \frac{85{,}000}{20{,}070 \times 1.15} - 1 = 2.67$$

6.2.5.4.1 Thread Shear at Pitch Diameter

$$\text{Area} = 0.50 \text{ in.}^2$$

$$F_{s_u} = 0.6\, F_{t_u} = 78{,}000 \text{ psi}$$

$$P = 1000 \text{ lbs};\ F_s = \frac{1000}{0.5} = 2000 \text{ psi}$$

$$\text{MS} = \frac{78{,}000}{1.25 \times 2000} - 1 = \text{High}$$

6.2.5.4.2 Analysis of Lock Ring as a Cylinder

Due to the high margins obtained in a similar analysis of the airframe portion of the attach assembly and the margins obtained in the preceding analyses of the lock ring, no further investigation is deemed necessary.

6.2.5.4.3 Bending on Lock Ring--Section B-B

Assuming 1/140 x circumference-wide strip as a beam,

$$M = 0.54 \times 2680 = 1450 \text{ in.-lbs}$$

$$I = \frac{0.970 \times (0.55)^2}{12} = 0.0135 \text{ in.}^4$$

$$f = \frac{1450 \times 0.275}{0.0135} = 29{,}600 \text{ psi}$$

$$\text{Axial stress} = \frac{2680}{0.97 \times 0.55} = 5020 \text{ psi}$$

$$f_b + f_t = 29{,}600 + 5020 = 34{,}620 \text{ psi}$$

$$\text{MS (Yield)} = \frac{100{,}000}{34{,}620 \times 1.15} - 1 = +1.5$$

$$\text{MS (10-hr. creep of 1.0\%)} = \frac{85{,}000}{34{,}620 \times 1.15} - 1 = +1.14$$

6.2.5.4.4 Analysis--Exit Nozzle Attach Ring

A section of this ring is shown in Figure 3.

6.2.5.4.5 Stress at Section A-A

Load per inch on each thread is:

$$P = \frac{375,000}{(3.14)\ (59.647)\ (2)} = 995 \text{ lbs/in.}$$

$$M = (0.458)\ (995) = 450 \text{ in.-lbs/in.}$$

$$I = \frac{1.0\ (0.437)^3}{12} = 0.00697 \text{ in.}^4 \text{ (assuming 1.0-in. wide section)}$$

$$f(\text{total}) = \frac{(450)\ (0.2185)}{0.00697} + \frac{375,000}{(3.14)\ (58.77)\ 0.437} = 1\ 720 \text{ psi}$$

$$MS = \frac{100,000}{1.15 \times 18,720} - 1 = \text{High}$$

7.0 MODELS

7.1 Direct-Connect Aerodynamic Coupling

7.1.1 Design

The direct-connect aerodynamic coupling hardware for this contract period is a modification of the test hardware used in the 1961 aerodynamic coupling tests (see Figures 124-128).

To evaluate simulated reactor airflow distribution, a control rod and actuator assembly and front support assembly were designed to simulate geometrically the flight engine hardware and to create as nearly as possible the blockage and airflow distribution anticipated in the flight engine. A transition plate and exit plate were designed with approximately 50 total and static pressure pickups for use at the aft reactor face during testing. Test results are reported in Volume II.

7.2 One-Third Scale Free Jet Model

7.2.1 Design

The 1/3 scale free jet model shown in Figure 129 utilizes the basic hardware from the direct-connect aerodynamic coupling test hardware; i.e., the reactor section, exit nozzle, exit nozzle spacers, and certain instrumentation sections.

Figures 130 to 142 show engine components in various stages of fabrication. The new hardware that was designed and fabricated included a free jet inlet with translating centerbody spike and by-pass doors, subsonic diffuser section and translating exit nozzle plug. The geometric lines of the inlet nozzle and centerbody are reduced from the flight engine by a scaling factor of 0.3625, which produces an inlet cowl diameter of 4 inches. The inlet spike is translated by means of a hydraulic actuator that is mounted inside the centerbody structure. This actuator operates on 1000 psi supply pressure and is capable of translating the spike 2.5 inches at the rate of 0.25 inches per second working against a load of 3000 pounds.

Two by-pass doors are located on the external wall of the inlet structure near the aft end of the centerbody, one door on each side of the horizontal centerline. Each door has an open area of 18.8 square inches. A hydraulic actuator for each door is mounted externally and is capable of positioning the doors from full open to full closed within two seconds.

The exit nozzle plug is positioned at the center of the exit nozzle throat and is contoured for a linear area variation during translation. The plug is translated by means of a hydraulic actuator, which is capable of translating the plug 18 inches against a 2500-pound load at the rate of one inch per second.

The reactor section was modified to allow fo: :hermal expansion of the reactor core when tested with 450°F inlet air. A: :l thermal expansion was contained by use of a spring-loaded ring mounted at t : forward face of the reactor. Radial thermal expansion was contained by use :f spring-loaded straps around the periphery of the core matrix. All the bas : compon-ents for this engine were fabricated from mild steel and 4130 steel Test results are reported in Volume II.

8.0 REFERENCES

1. "Letter Contract between Department of the Air Force and ' ; Marquardt Corporation", Contract AF 33(657)-8123, 16 April 1962, ~~SECRET RESTRICTED DATA,~~ Reg. 10,201.

2. "Performance Bulletin No. 5 for the Marquardt Nuclear Ram, t Engine", The Marquardt Corporation, 1 June 1962, Marquardt 5893, ~~SECRET RESTRICTED DATA,~~ Reg. 22,593.

3. "Aerothermodynamics for Pluto", Part II, Volume 5, "Struc ral Design and Materials", Ling-Temco-Vought, April 1962, ASD-TDR-62-395, ~~SECRET RESTRICTED DATA,~~ Reg. 22,718.

4. "Preliminary Analysis of Lateral Vibrations of the Pluto 1 actor", The Marquardt Corporation, 15 December 1961, Marquardt Report 373, ~~SECRET RESTRICTED DATA,~~ Reg. 22,350.

5. "Formulas for Stress and Strain", R. J. Roark, 1954, McGr -Hill, New York.

6. "Analysis and Design of Aircraft Structures", E. F. Bruhn, 1949, Tri-State Offset Co., Cincinnati.

7. "A Second-Order Shock-Expansion Method Applicable to Bodi of Revolution Near Zero Lift", C. A. Syvertson and T. H. Dennis, Nation Advisory Committee for Aeronautics, 1957, NACA Technical Report 1328.

8. "Computation Curves for Compressible Fluid Problems", C. I Dailey and F. C. Wood, 1949, John Wiley & Sons, New York.

9. "Statics of Circular-Ring Stiffeners for Monocoque Fuselag ", W. Stieda, National Advisory Committee for Aeronautics, February 194 NACA Technical Memorandum 1004.

10. "Loads Imposed upon Intermediate Frames of Stiffened Shell ", Paul Kuhn, National Aeronautics and Space Administration, NASA Techni l Note 687.

11. "Strength of Metal Aircraft Elements", Air Force, Navy, Co erce Departments, March 1955, ANC-5 Bulletin.

12. "Mechanical Vibrations", Den Hartog, 1947, McGraw-Hill, Ne York.

13. "Tory IIC Data Book", 16 October 1962, University of Calif nia, Lawrence Radiation Laboratory, ~~SECRET RESTRICTED DATA,~~ Reg. 22,107.

14. "Elements of the Differential and Integral Calculus", Gran lle, Smith, and Longley, Ginn & Co.

15. "Nuclear Ramjet Propulsion System Research and Development or 1962", The Marquardt Corporation, 5 January 1962, Marquardt Propo l 3067A (Vol. I), ~~SECRET RESTRICTED DATA,~~ Reg. 22,400.

16. "Annual Report for 1961, Nuclear Ramjet Propulsion System, P .to Project," The Marquardt Corporation, 30 January 1962, Marquardt Report 876, ~~SECRET RESTRICTED DATA~~, Reg. 22,395

17. "The Uniform-Section Disk Spring", American Society of Mecha cal Engineers 1936. ASME, New York, Vol. 58, No. 6.

18. "Handbook of Mechanical Spring Design", Associated Spring Cc oration, Bristol, Conn., 1951.

19. "Test Report, Reactor Side Support System", The Marquardt Cc oration, 1 June 1962, Marquardt Report S-276, ~~SECRET RESTRICTED DATA~~, eg. 22,625.

20. "Engine-Airframe Lateral Attachment Test (Phase II)," The Ma uardt Corporation, 31 January 1962, Marquardt Report 5960, ~~CONFIDENTI RESTRICTED DATA~~, Reg. 23,066.

21. "Rules for Construction of Unfired Pressure Vessels", Americ Society of Mechanical Engineers, 1959, ASME Boiler and Pressure Vessel de Section VIII.

22. "A Study of the Collapsing Pressures of Thin-Walled Cylinder , R. Sturm, Illinois Institute of Technology, Bulletin 329.

23. "The Ultimate Strength of Aluminum-Alloy Formed Structural S pes in Compression", Robert A. Needham, Journal of Aeronautical Scienc 4-54, Vol. 21, No. 4, p. 217.

24. "A Simplified Method of Elastic-Stability Analysis for Thin lindrical Shells", S. B. Batdorf, National Advisory Committee for Aerc utics, 1947, NACA Technical Report 874.

TABLE I

TABLE OF WEIGHTS AND CENTERS OF GRAVITY FOR MA50-XCB PROPULSION SYSTEM

Item	Weight (lb)	Engine Station C.G.
MA50-XCB Propulsion System	16,456	477
Inlet	2,717	170
Diffuser Duct*	919	405
Reactor Control Rod Support Mechanism	297	441
Reactor and Support System	11,468	533
Exhaust Nozzle	1,054	594

* To be furnished by manufacturer

TABLE II

MARGINS OF SAFETY

Item	Type of Stress	argin
Cowl		
Inside skin	Tension	1.75
Outside skin	Tension	4.06
Inside skin	Compression	3.82
Leading edge	Compression	1.67
Skin (near leading edge)	Bending	0.56
Diffuser Skin		
Long time "limit" load	Hoop tension	0.03
Short time "ultimate" load	Hoop tension	0.26
Innerbody Support Ring		
Long time "limit" load	Compression	nple
Long time "ultimate" load	Compression	nple
Short time "limit" load	Compression	0.85
Short time "ultimate" load	Compression	0.62
Innerbody Skin		
Short time "limit" load	Compression	0.30
Short time "limit" load	Shear	nple
Long time "ultimate" load	Compression	0.05
Thrust Fitting (Pin)		
Short time "limit" load	Bending	0.36
Long time "limit" load	Bending	0.68
Short time "ultimate" load	Bending	0.74
Reactor Support		
Pressure shell	Hoop tension	.gh
Shell web	Bending	0.35
Pressure pad	Bending	0.11
Pressure pad lug	Bending	.gh

TABLE II (Continued)

Item	Type of Stress	Margin
Exit Nozzle		
Forward cylinder	Hoop tension	M imum = + 0.05
Forward cylinder	Combined bending and axial	+ 2.33
Forward cylinder	Shear	High
Throat	Combined bending and axial	+ 1.32
Forward cone	Combined bending and axial	+ 1.82
Cone-Cylinder Intersection	Combined bending and axial	+ 0.38
Aft Cone		
Station 636.32	Collapsing	+ 0.085
Station 623.41 to 636.32	Collapsing	+ 0.61
	Bending and Axial	High
	Shear	High
Aft Doubler	Collapsing	High
Shroud		
Forward cylinder	Collapsing	+ 0.70
Station 15	Collapsing	+ 0.16
Cone	Collapsing	+ 0.33
Throat	Collapsing	+ 0.39

TABLE III

INERTIAL LOAD FACTORS

Parameter	Launch Conditions		Low Level Maximum Cruise		War Head Ejection	High Altitude Cruise
	At Burnout	At Separation				
Altitude	12,500	21,500	1000	1000	10,000	30,000
Mach Number	2.25	2.95	2.90	3.0	2.9	3.5
Day Condition	Hot	Hot	Hot	Cold	Hot	Cold
g_x	+ 6.0 - 0	+ 0 - 0.32	+ 0 - 0.3	+ 0 - 0.3	+ 0 - 0.3	+ 0.10 -
g_y	± 1.0	± 1.0	± 1.0	± 1.0	± 0.25	± 1.0
g_z	0	0	+ 4.25 - 2.25	+ 4.25 - 2.25	+ 2.8 - 0.8	+ 1.5 - 0
$\dot{w}_y$	± 0.12	0	± 0.50	± 0.50	± 0.50	± 0.50
$\dot{w}_z$	± 0.25	± 0.25	± 0.50	± 0.25	0	± 0.50

TABLE IV

INERTIA LOAD FACTORS FLIGHT MANEUVER CONDITIONS

(Translational Accelerations (g-1/2) at Centers of Gravity of Propulsion System Items)

Flight Phase	Inlet			Duct			Reactor Controls			Reactor			Exit		
	g_x	g_y	g_z	g_x	g_y	g_z	g_x	g_y	g_x	g_x	g_y	g_z	g_x	g_y	g_z
Boost at	+6.015	+1.144	+0	+6.0	+1.0	+0.005	+6.0	+1.038	+0.031	+6.0	+1.09	+0.042	+6.0	+1.06	+0.103
Burnout	-0	-0.856	-0.0672	-0	-1.0	-0.005		-1.038	-0.031		-1.09	-0	-0	-1.06	-0.103
Rocket	+0	+1.091	+0	+0	+1.06	+0	+0	+1.09	+0	+0	+1.14	+0	+0	+1.18	+0
Rejection	-0.32	-1.091	-0	-0.32	-1.06	-0	-0.32	-1.09	-0	-0.32	-1.14	-0	-0.32	-1.18	-0
High Altitude	+0.164	+1.182	+1.690	+0.10	+1.12	+1.62	+0.10	+1.17	+1.67	+0.10	+1.28	+1.78	+0.10	+1.37	+1.87
Cruise	-0.164	-1.182	-0.190	-0.10	-1.12	-0.12	-0.10	-1.17	-0.17	-0.10	-1.28	-0.28	-0.10	-1.37	-0.37
Low Altitude	+0.364	+1.182	+4.44	+0.3	+1.12	+4.37	+0.3	+1.17	+4.44	+0.3	+1.5	+4.53	+0.3	+1.37	+4.62
Cruise	-0.064	-1.182	-2.44	-0	-1.12	-2.37	-0	-1.17	-2.44	-0	-1.5	-2.53	-0	-1.37	-2.62
Weapons	+0.364	+0.25	+5.50	+0.3	+0.25	+4.50	+0.3	+0.25	+5.0	+0.3	+1.5	*	+0.3	+0.25	+8.50
Ejection	-0.064	-0.25	-0.99	-0.0	-0.25	-0.92	-0.0	-0.25	-0.97	-0	-1.5	-1.08	-0	-0.25	-1.17

* +5.77 g at reactor forward end, Fuselage Station 882.4
+6.68 g at reactor aft end, Fuselage Station 938.5

TABLE V

VERTICAL LOAD FACTORS

Parameters	Low Level Maximum Maneuver	Low Level Warhead Ejection
Altitude	1000	1000
Mach Number	2.9	2.9
Day Conditions	Hot	Hot
g_x	+ 0.3	+ 0.3
g_y	± 1.5	± 1.5
g_z	+ 4.5 - 2.5	*

* Values of g_z for weapons ejection at the reactor ends are as follows:

Forward End	Aft End
F.S. 882.4	F.S. 938.5
g_z = + 5.77	g_z = + 6.68

TABLE VI

GROUND HANDLING LOAD FACTORS

Parameter	Hoist	Transport	Erection
g_x	± 0.25	± 5.0	± 1.0
g_y	± 0.25	± 0.05	± 0
g_z	+ 2.67 - 0	+ 2.0 - 1.0	+ 2.0 - 1.0

TABLE VII

ANALYTICAL DESIGN FACTORS AND FACTORS OF SAFETY

Type of Limit Stress	Material Mechanical Strength Property	Multiplying Factor	
		Design	Safety
A. For temperature regimes in which time and material creep are negligible factors			
Single (uniaxial) (tension, compression, etc.)	Yield or proportional limit	1.10	--
Combined stresses biaxial, or triaxial	Yield or proportional limit	1.15	--
Single or combined	Short time ultimate	--	1.25
B. For temperature regimes in which time is a major factor			
Single	Uniaxial steady state creep	1.10	--
Combined	Uniaxial steady state creep for type of stress involved	1.15	--
Single or combined	Creep rupture for type of stress involved	--	1.25
Single or combined	Fatigue for type of stress and load-temperature pattern involved	--	1.25

TABLE VIII

WEIGHTS AND CENTERS OF GRAVITY FOR AXISYMMETRIC LET

	Weight (lbs)	Center of avity Engine St ion
Inlet Assembly	2717.1	169.9
Nose Cone (Movable parts)	145.9	88.7
Innerbody - Rings	132.8	130.6
Innerbody - Skins	219.4	137.0
Outer Structure - Rings	333.7	192.1
Outer Structure - Skins	920.0	194.8
Longerons	251.1	146.4
Attach Struts	369.2	221.0
Actuating Mechanism	345.0	111.6

TABLE IX

SECTION PROPERTIES AND LOCATIONS FOR CALCULATION OF STRESS

Item	Thickness h (av)	w	Area h · w	d from * ref line	Ad	$\bar{d}$	$A\bar{d}$	$A\bar{d}^2$	I_o
a	0.228	3.28	0.74900	0.700	0.52400	+0.147	+0.10980	0.016120	0.000582
b	0.400	1.762	0.70500	0.480	0.33800	-0.073	-0.05150	0.003760	0.009400
c	0.600	1.920	1.15300	0.370	0.42700	-0.183	-0.21100	0.038600	0.020000 approx.
d	0.062	0.90	0.05570	0.800	0.04450	+0.247	+0.01375	0.003400	--
e	0.062	0.90	0.05570	0.031	0.00173	-0.522	-0.02905	0.015190	--
f	0.062	2.30	0.14250	1.250	0.17800	+0.697	+0.09940	0.069400	--
g	0.062	2.30	0.14250	0.031	0.00441	-0.522	-0.07450	0.038900	--
h	0.090	1.26	0.11320	1.120	0.12720	+0.567	+0.06430	0.036500	--
j	0.090	1.26	0.11320	0.107	0.01212	-0.446	-0.05050	0.022520	--
k	1.000	0.09	0.09000	0.600	0.05400	+0.047	+0.00423	0.000199	0.007500
l	0.062	2.30	0.14280	1.620	0.23150	+1.067	+0.15220	0.162500	--
m	0.090	1.26	0.11320	1.520	0.17200	+0.967	+0.10940	0.105800	--
n	0.062	2.30	0.14280	0.031	0.00442	-0.522	-0.07460	0.039000	--
o	0.090	1.26	0.11320	0.107	0.01212	-0.446	-0.05050	0.022550	--
p	1.200	0.09	0.10800	0.800	0.08650	+0.247	+0.02670	0.006600	0.012930
			3.93980	0.553	2.21750		+0.57958 -0.54165 +0.03793	0.581039 0.631451 in.^{4}	0.050412

* Reference line is at 20.188 inch radius.

R to N.A. = 20.188-0.553 = 19.635 inch

TABLE X

MOMENTS FROM AIR LOAD

1	2	3	4	5	6
x Location (degrees)	Moment from Loading I	Moment from Loading II	Combined Moment of I and II	sin	+20 sin x-M
Centerline					
0	+ 13250	- 26500	- 13250	0	0
10	+ 12650	- 25400	- 12750	0.17	- 44500
20	+ 10500	- 21000	- 10500	0.34	- 72000
30	+ 7350	- 14650	- 7300	0.50	- 73000
40	+ 2820	- 5610	- 2790	0.64	- 35900
50	- 1910	+ 3810	+ 1900	0.76	+ 29100
60	- 6650	+ 13320	+ 6580	0.86	+114000
70	- 10850	+ 21600	+ 10750	0.94	+202000
80	- 13640	+ 27200	+ 13560	0.98	+276000
Side					
90	- 14500	+ 29000	+ 14500	1.00	+290000
100	- 13640	+ 27200	+ 13560	0.98	+276000
110	- 10850	+ 21600	+ 10750	0.94	+202000
120	- 6650	+ 13320	+ 6580	0.86	+114000
130	- 1910	+ 3810	+ 1900	0.76	+ 29100
140	- 2820	- 5610	- 2790	0.64	- 35900
150	+ 7350	- 14650	- 7300	0.50	- 73000
160	+ 10500	- 21000	- 10500	0.34	- 72000
170	+ 12650	- 25400	- 12750	0.17	- 44500
Centerline					
180	+ 13250	- 26500	- 13250	0	0
					Σ 1,900,000 Units

Notes:

Columns 2 and 3 derived from Reference 5 (Case 27 data with = $\pi/2$).

Column 2 based on + 492 lbs/in. maximum (inward)
Column 3 based on - 984 lbs/in. maximum (outward)

(+) moments place compression on outside of ring.

Columns 2 and 3 integrate to transverse loads of 30,900 lbs, 5,450 lbs or a total transverse load of 46,350. Radial deflection, Δ, of point at x = 0 relative to a line joining points at x = 90° and x = 270° is:

$$\Delta = \frac{1,900,000}{E\,I} = \frac{1,900,000}{22.7 \times 10^6 \times 0.631} = 0.132 \text{ in.}$$

TABLE XI

TORQUE LOADS AT VARIOUS SECTIONS

Section	Distance from Centerline to fitting y	y^2	Ratio $y^2/1534$	Torque (in.-lbs)	Σ Torq	
A-A	22.5	506	0.330	370,000	370	00
B-B	21.76	472	0.308	345,000	715	00
C-C	18.24	333	0.217	243,000	958	00
D-D	12.40	154	0.100	112,000	1,070	00
E-E	8.30	69	0.045	50,000	1,120	00
		1534	1.000	1,120,000	See N	e

Note: These values utilized for plot (Figure 27) of torques be sustained by inlet itself.

TABLE XII

SHEARS, MOMENTS, AND TORQUES FROM Z DIRECTION COMPON TS

1	2	3	4		
Location	x to Section A-A	x' from Centroid to Section	$(x')^2$	Load a	Joint
A-A	0	+ 77.30	5,980	22,	0
B-B	- 26.90	+ 50.40	2,540	14,	0
C-C	- 53.50	+ 23.80	566	6,	0
D-D	- 95.50	- 18.20	331	- 5,	0
E-E	-127.86	- 50.56	2,550	- 14,	0
F-F	-160.46	- 83.16	6,900	- 23,	0
	-464.22	(+) is aft centroid	18,867	(+) t	s.

TABLE XIII

PRESSURE CALCULATIONS

Segment Station Location	Large Area (in.^{2})	Small Area (in.^{2})	Average Δ P (psi)	Forward Load (lb)	Aftward Load (lb)	Description
-37.7 to -15	124	0	35-62 = -27	3,350		pike
-15 to 0	453	124	42-62 = -20	6,580		ithout
0 to 5	610	453	110-62 = +48		7,540	kirt
5 to 8.4	660	610	110-62 = +48		2,400	
8.4 to 18.7 Outer	730	639	110-62 = +48	4,370		pike
8.4 to 18.7 Inner	730	639	62-62 = 0		0	kirt
18.7 to 22.4	639	566	110-62 = +48	3,500		
22.4 to 39.06	566	453	311-62 = 249	28,100		ixed Part
39.06 to 71.66	453	226	311-62 = 249	56,500		of
71.66 to 89.96	226	0	311-62 = 249	56,300		nner Body
0 to 5.0	1210	1150	110-62 = 48	2,880		
5 to 13.2	1210	1112	110-62 = 48		4,700	nner Skin
13.2 to 22.4	1112	1010	110-62 = 48		4,900	of
22.4 to 39.06	1010	966	311-62 = 249		10,940	ouble Wall
39.06 to 71.66	966	880	311-62 = 249		21,400	owling
71.66 to 89.96	880	855	311-62 = 249		6,220	
0 to 5.0	1278	1150	31-62 = -31	3,970		uter Surface of ouble Wall

NOTE: These symmetrical loads are base loads on which the loads 25 to 29 and Tables XI and XII are superposed to obtain an rical load pattern. Figures neymmet-

TABLE XIV

JOINT LOADS

1	2	3	4		5
Location	Section A-A	x' from Centroid to Section	$(x')^2$	Lo	p at Joint
A-A	0	+77.30	5,980		15,000
B-B	-26.90	+50.40	2,540		9,790
C-C	-53.50	+23.80	566		4,610
D-D	-95.50	-18.20	331		3,530
E-E	-127.86	-50.56	2,550		9,800
F-F	-160.46	-83.16	6,900		16,120
	-464.22	(+) is aft of centroid	18,867	(	tension

$$\frac{\Sigma x}{6} = \frac{-464.22}{6} = -77.3 \text{ inches}$$

TABLE XV

ATTACHMENT REACTIONS FROM AIRLOADS FOR THE UNSYMMETRICAL CONDITION

Fitting Point	Description and References	X	Y	Z
a Center	Figure 29 Z = -31,153 Figure 31 Z = -16,120	0	0	- 47,273
b Left	Figure 29 Z = 0.5 (-21,853) = - 10,926 Figure 28 Z = 50,000 ÷ 16.6 = + 3010 Figure 31 Z = 0.05 (-9800) = - 4900	0 0	0 0	- 12,816
c Right	Figure 29 Z = 0.5 (-21,853) = - 10, 926 Figure 28 Z = -(50,000 ÷ 16.6) = - 3010 Figure 31 Z = 0.5 (-9800) = - 4900	0	0	- 18,836
d Left	Figure 29 Z = 0.5 (-12,643) = - 6321 Figure 28 Z = 112,000 ÷ 24.8 = + 4520 Figure 31 Z = 0.5 (-3530) = - 1765	0	0	- 3,566
e Right	Figure 29 Z = 0.5 (-12,643) = - 6321 Figure 28 Z = -(112,000 ÷ 24.8) = - 4520 Figure 31 Z = 0.5 (-3530) = - 1765	0	0	- 16,606
f Left	Figure 29 Z = 0.5 (-673) = - 336 Figure 28 Z = 243,000 ÷ 36.48 = + 6670 Figure 31 Z = 0.5 (4610) = + 2305	0	0	+ 8,639
g Right	Figure 29 Z = 0.5 (-673) = - 336 Figure 28 Z = -(243,000 ÷ 36.48) = - 6670 Figure 31 Z = 0.5 (4610) = + 2305	0	0	- 4,701
h Left	Figure 29 Z = 0.5 (+6,927) = + 3464 Figure 28 Z = 345,000 ÷ 43.52 = + 7920 Figure 31 Z = 0.5 (+9790) = + 4895	0	0	+ 16,279

TABLE XV (Continued)

Fitting Point	Description and References	X	Y	Z
j Right	Figure 29 Z = 0.5 (+6,927) = + 3464 Figure 28 Z = -(345,000 ÷ 43.52) = - 7920 Figure 31 Z = 0.5 (+9790) = + 4895			+ 439
k Left	Figure 29 Y = 0.5 (+17,640) = 8820 (Aft of Section A-A joint) Figure 29 Z = 0.5 (+14,547) = + 7,278 Figure 31 Z = 0.5(15,000) = 75,000 Figure 28 Z = 370,000 ÷ 45 = + 8,220	0	* + 8,820	+ 22,998
l Right	Figure 27 Y = 0.5 (+17,640) = 8820 (Aft of Section A-A Joint) Figure 29 Z = 0.5 (+14,547) = + 7,278 Figure 31 Z = 0.5 (15,000) = + 7,500 Figure 28 Z = 370,000 ÷ 45 = - 8,220	0	* + 8,820	+ 6,558
t Center	Figure 27 Y = -44,400 Figure 31 X = +145,800	** +145,800	-44,400	0

** For a short time, this load could rise to 204,400 lbs (See Paragraph 3.2.5)

TABLE XVI

SYMMETRICAL LOAD PORTION OF STEADY STATE FLIGHT CONDITION RING MOMENTS

θ	Symmetrical Load Portion				
	C_1 P at 0°	C_1 P at 120°	C_1 P at 240°	Total	MF C_1 (in-s)
0	- 0.24	- 0.025	- 0.025	- 0.190	- 17 00
15	- 0.12	0.065	- 0.015	- 0.070	- 6 10
30	- 0.02	0.090	- 0.050	+ 0.020	
45	0.05	0.100	- 0.072	+ 0.078	
60	0.088	0.088	- 0.075	+ 0.101	+ 9 50
75	0.10	0.050	- 0.072	+ 0.078	
80	0.090	- 0.020	- 0.050	+ 0.020	
105	0.005	- 0.120	- 0.015	- 0.070	
120	0.025	- 0.240	+ 0.025	- 0.190	- 17 00
125	- 0.015	- 0.120	+ 0.065	- 0.070	
160	- 0.050	- 0.020	+ 0.090	+ 0.020	
165	- 0.072	0.050	+ 0.100	+ 0.078	
180	- 0.075	0.088	+ 0.088	+ 0.101	+ 9 50
195	- 0.072	0.100	+ 0.050	+ 0.078	
210	- 0.050	0.090	- 0.020	+ 0.020	
225	- 0.015	0.065	- 0.120	- 0.070	
240	0.025	0.025	- 0.24	- 0.190	- 17 00
255	0.065	- 0.015	- 0.12	- 0.070	
270	0.090	- 0.050	- 0.02	+ 0.020	
285	0.100	- 0.072	0.05	+ 0.078	
300	0.088	- 0.075	0.088	+ 0.101	+ 9 50
315	0.050	- 0.072	0.100	+ 0.078	
330	- 0.020	- 0.050	0.090	+ 0.020	
345	- 0.120	- 0.015	0.065	- 0.070	- 6 10
360	- 0.240	0.025	0.025	- 0.190	- 17 00

Notes:

Coefficient C_1 is from Reference 9; (+) moment is compres on on outside; PR = 8500 x 10.79 = 91,600 (from Table XI)

TABLE XVII

STEADY STATE FLIGHT CONDITION RING MOMENTS

	Unsymmetrical		Symmetrical	mbined
ϕ	C_1 P at 0°	$M_P = C_1PR$ (in-lbs)	M_P (in-lbs)	M_P n-lbs)
0	- 0.24	- 9,710	- 17,400	27,110
15	- 0.12	- 4,860	- 6,410	11,270
30	- 0.02			
45	0.05			
60	0.088	+ 3,560	+ 9,250	12,810
75	0.100			
90	0.090			
105	0.065			
120	0.025	+ 1,012	- 17,400	16,388
135	- 0.015			
150	- 0.050			
165	- 0.072			
180	- 0.075	- 3,040	+ 9,250	6,210
195	- 0.072			
210	- 0.050			
225	- 0.015			
240	0.025	+ 1,012	- 17,400	16,388
255	0.065			
270	0.090			
285	0.100			
300	0.088	+ 3,560	+ 9,250	12,810
315	0.050			
330	- 0.020			
345	- 0.120	- 4,860	- 6,410	11,270
360	- 0.240	- 9,710	- 17,400	27,110

Notes: Coefficient C_1 is from Reference 9; (+) mo ent is compression on outside. For unsymmetrical portion of moments, PR is 3,760 x 10.79 = 40,500 (ee Figure 37). Moments for symmetrical portion of ads are carried over from Table XVI.

TABLE XVIII

RING MOMENTS FROM SHORT TIME MANEUVER LOADS

ø	Symmetrical		Unsymmetrical		Combi ed
	Total Cl	Moment (in-lbs)	Total Cl	Moment (in-lbs)	Mome (in-l s)
0	- 0.190	- 23,960	- 0.24	- 68,100	- 92, 60
15	- 0.070	- 8,810	- 0.12	- 34,050	- 42, 60
30	+ 0.020		- 0.02		
45	+ 0.078		0.05		
60	+ 0.101	+ 12,700	0.088	+ 25,000	+ 37, 00
75	+ 0.078		0.100		
80	+ 0.020		0.090		
105	- 0.070		0.065		
120	- 0.190	- 23,960	0.025	+ 7,100	- 16, 0
125	- 0.070		- 0.015		
160	+ 0.020		- 0.050		
165	+ 0 078		- 0.072		
180	+ 0.101	+ 12,700	- 0.075	- 21,300	- 8, 0
195	+ 0.078		- 0.072		
210	+ 0.020		- 0.050		
225	- 0.070		- 0.015		
240	- 0.190	- 23,960	0.025	+ 7,100	- 16, 0
255	- 0.070		0.065		
270	+ 0.020		0.090		
285	+ 0.078		0.100		
300	+ 0.101	+ 12,700	0.088	+ 25,000	+ 37, 0
315	+ 0.078		0.050		
330	+ 0.020		- 0.020		
345	- 0.070	+ 8,810	- 0.120	- 34,050	- 42, 0
360	- 0.190	- 23,960	- 0.240	- 68,100	- 92, 0

Notes: Data are from Table XVI; (+) moment is compressio on outside for symmetrical portion PR = 11,698 x 10. = 126,000; for unsymmetrical portion PR = 26,320 x .79 = 284,000.

TABLE XIX

WEIGHT AND CENTERS OF GRAVITY FOR CONTROL ROD SUPPORT STRUCTU
AND ACTUATION MECHANISM

Item	Weight	Engine Station C	.
Assembly Total	297.7	422.4 Hot* 441.:	Cold
(a) Front Support	9.7	393.4	
(b) Main Support Assembly	28.0	419.8	
(c) Vernier Rod Strut Assemblies	9.4	419 8	
(d) Motors and Servo Valves	90.0	419.8	
(e) Linear Transducers + Housing	10.0	419.8	
(f) Torque Drive Shaft + Gears	3.2	419.8	
(g) Rack Guide Tubes	24.0	422.6	
(h) Aft Support Structure	11.5	466.6	
(j) Drive Racks	75.0	396.6 Hot 436.6	old
(k) Spider Fittings	36.9	423.6 Hot 463.6	old

* "Hot refers to an operating power reactor condition; "Cold" refers to a zero power reactor condition.

TABLE XX

WEIGHTS AND CENTERS OF GRAVITY FOR REACTOR AND SUPPORT SY EM

Item	Weight (lbs)	Engine Station C .
Reactor and Support System	11,468	533.940
Core and Reflector	7,569	537.046
Tie Rods	402	531.203
Retainer Assembly	228	509.563
Base Blocks	520	565.408
Grid	900	501.186
Lateral Support Structure	1,593	536.870
Axial Support Structure	256	501.186

TABLE XXI

THERMAL EXPANSION OF TANGENTIALLY AND RADIALLY ORIENTED RINGS

Expansion (radial)
R (Core) = 23.625 in.
R (Reflector) = 26.625 in.
R (Pressure Shell) = 28.125 in

Reactor Component	Material	End of Boost (60 sec)			Steady Stat	Cruise (300 sec)		
		Temp. °F	Coef/Exp.	Δ R	Temp. °F	Co	/Exp	Δ R
Core	Fueled BeO	2570	5.65×10^{-6}	0.3345	2570	5.	$\times 10^{-6}$	0.3345
Zone 1	Unfueled BeO	*		0.0046	1890	5.	$\times 10^{-6}$	0.0046
Zone 2	Unfueled BeO			0.0066	1490	4.	$\times 10^{-6}$	0.0066
Zone 3	Unfueled BeO			0.0091	1390	4.	$\times 10^{-6}$	0.0091
TOTAL				0.3548				0.3548
Tangential System								
Exp. Shell	Rene' 41	360	6.8×10^{-6}	0.0525	1500	8.	$\times 10^{-6}$	0.322
Radial Diff.	Rene' 41	360	6.8×10^{-6}	0.302	1500	8.	$\times 10^{-6}$	0.033
Diam. Diff	Rene' 41	360	6.8×10^{-6}	0.604	1500	8.	$\times 10^{-6}$	0.066
Circ. Diff.	Rene' 41	360	6.8×10^{-6}	1.895	1500	8.	$\times 10^{-6}$	0.207
Radial System								
Pressure Shell	Rene' 41	300	6.8×10^{-6}	0.0439	1200	7.	$\times 10^{-6}$	0.248
Radial Diff.				0.311				0.107

* Reflector expansion assumed the same as cruise.

TABLE XXII

SUMMARY OF CRITERIA

(Inertia Load Factors Taken from Section 2.0)

Condition	Spring Temperature (°F)	Relative Thermal Expansion		Inertia Load Factor (g)	Type of I d
		Radial System (in.)	Tangential System (in.)		
Ground Handling	70	0	0	3.75	Static *
Boost	70	0	0	3.00 (RMS)	Random vi ation
Boost Transition	380	0.311	0.302	3.00 (RMS) 2.23	Random vi ation Static*
High Altitude Cruise	1400	0.107	0.033	2.25 (RMS) 4.16	Random vi ation Static*
Low Altitude Cruise	1400	0.107	0.033	2.25 (RMS) 5.95 7.0 (Peak)	Random vi ation Static* Sinusoida vibra- tion at 9 cps

* Conservatively assumed static.

TABLE XXIII

TABLE OF DYNAMIC TEST RUNS "NOMINAL CONDITIONS"

Run No.	Temperature (°F)	Type of Test	Frequency Range	"g" Load	Duration of Run (min)	Comments
1	Ambient	Sine wave sweep	5-500	0.5 RMS	10	Check out } A-C noise interference
2	Ambient	Sine wave sweep	5-500	0.75 RMS	10	Check out } A-C noise interference
3	Ambient	Sine wave sweep	5-2000	1 RMS	15	Low response
4	Ambient	Sine wave sweep	5-500	2 RMS	11	
5	Ambient	Sine wave sweep	5-500	3 RMS	11	
6	Ambient	Sine wave sweep	500-13	4 RMS	9	Broke shaker head support brace - repaired
7	Ambient	Flat random	20-500	3 RMS overall	10	
8	400-1130	Sine wave sweep	500-5	3 RMS	15	Lost 3 of 8 high temperature accelerometers
9	400-1130	Flat random	20-500	3 RMS overall	10	
10	1100-1380	Sine wave sweep	500-5	3 RMS	10	
11	1100-1380	Flat random	20-500	3 RMS overall	10	

TABLE XXIV

ACCELEROMETER RESPONSE
(Run No. 4)

Input Frequency (cps)	Input g_{RMS}	Response g_{RMS}							
	A-10	A-3	A-4	A-5	A-6	A-7	A-8	A-9	A-11
12	0.55*	1.70*	0*	--	1.5*	--	0.3	0.8	0.8
15	0.65*	2.1	0.3*	0.26*	1.85*	--	0.9	1.1	1.8
20	0.75*	2.3	0.85*	0.60*	2.0*	--	1.6	1.1	1.3
25	0.85*	2.30*	0.85*	0.44*	2.0*	--	0.88	1.2	1.3
30	1.0*	2.05*	0.65*	0.52*	1.9*	--	1.0	1.6	1.2
35	1.20*	1.75*	0.40*	--	1.70*	--	1.0	1.2	2.0
40	1.25*	1.65*	0.30*	--	1.70*	--	0.75	1.0	1.2
80	1.5	2.0	1.2	1.5	2.0	1.6	1.0	2.0	2.0
140	1.7	3.0	0	1.8	2.5	2.4	2.0	2.0	2.5
200	2.5	3.2	4.0	2.0	3.5	3.0	--	3.8	2.5
250	2.3	4.0	3.6	2.0	3.0	3.5	--	3.5	--
320	2.2	3.8	1.2	2.0	2.5	2.5	--	2.4	1.0
400	2.2	2.5	0.80	1.0	1.0	0.80	2.5	1.0	0.50
440	1.7	3.0	0.80	0.70	1.2	0.50	1.0	1.0	0.60
500	1.5	2.6	1.8	0.60	1.0	0.70	0.50	2.0	[illegible]

* Frequency analyzed.

TABLE XXV

ACCELEROMETER RESPONSE
(Run No. 10)

Input Frequency (cps)	Input g_{RMS}	Response g_{RMS}				
	A-10	A-3	A-4	A-5	A-8	9
12	~0.95*	2.2*	--	--	--	
15	1.0*	2.45*	0.5	0.2	0.8	6
20	1.0*	2.65*	--	--	--	
25	1.0*	2.75*	2.0	0.8	0.5	4
30	1.1*	2.70*	2.2	2.0	1.0	8
35	1.2*	2.65*	--	--	--	
40	1.5*	2.50*	2.5	1.0	1.0	0
80	3.0	--	3.0	1.0	1.5	0
140	3.0	--	3.0	2.5	2.5	0
200	3.1	5.5	3.0	2.5	--	7
250	2.9	--	2.5	1.7	--	0
320	2.7	--	3.0	1.0	0.5	5
400	2.0	--	3.0	0.8	1.0	5
440	1.7	--	1.0	1.0	1.0	5
500	2.0	4.5	1.5	1.5	1.0	0

* Frequency analyzed.

TABLE XXVI

WEIGHTS AND CENTERS OF GRAVITY FOR EJECTOR EXHAUST NOZZ

Item	Weight (lb)	Engine Stat n
Exhaust Nozzle Assembly	1054	594.2
Primary Shell	370.9	618.9
Secondary Shell	239.5	587.7
Lock Ring	178.4	568.1
Attach Ring	162.1	571.0
Ring Assembly - Expansion	41.0	565.8
Stiffener Ring - Aft	9.1	660.3
Stiffener Ring - Forward	8.4	654.3
Stiffener Ring - Intermediate	7.9	646.3
Stiffener Ring - Intermediate	6.1	636.3
Drag Brace (12 required)	8.7	573.9
Pylon (8 required)	9.0	613.3
Support Doubler (8 required)	11.8	613.9
Fitting - Inner (8 required)	1.1	663.4

TABLE XXVII

REQUIRED MATERIAL THICKNESS

Exit Station	Internal Radius (in.)	Nozzle Interior* (psia)	Δp (psi)	t reqd $\frac{(\Delta p)(}{78,00}$ (in.)
0	28.06	320	260	0.093
5	28.06	300	240	0.086
10	28.06	292	232	0.083
15	28.06	288	228	0.081
20	28.06	286	226	0.080
22	27.80	284	224	0.079
24	26.70	283	223	0.076
26	25.50	282	222	0.075
28	24.40	280	220	0.068
30	23.20	279	219	0.064
32	22.10	277	217	0.061
34	21.00	275	215	0.057
36	19.90	273	213	0.054
38	18.70	270	210	0.050
40	17.70	266	206	0.046
42	16.90	262	202	0.043
44	16.40	258	198	0.041
46	16.20	254	194	0.040
48	16.10	248	188	0.038
52	16.40	77	17	0.003

* Airframe cooling annulus pressure profile assume uniform at 60 psia (Figure 110).

TABLE XXVIII

SHROUD PRESSURE AND TEMPERATURE DATA

(Low Altitude Cruise at Mach 3.22 and 1,000 ft, ICAO Standard D

Engine Station	Inner Surface	Outer Surface	Pressure (psia)	Temperature (°F)
0	320	254	66	1350
570.470	300	254	46	1350
575.470	296	254	38	1350
585.470	286	258	28	1355
587.24	284	258	26	1360
590.470	283	256	27	1380
595.470	279	252	27	1420
600.470	274	241	33	1465
605.037	267	216	51	1520
611.289	254	126	128	1550
613.413	249	109	140	1550
615.87	160	90	70	1490
616.969	81	81	0	--

1

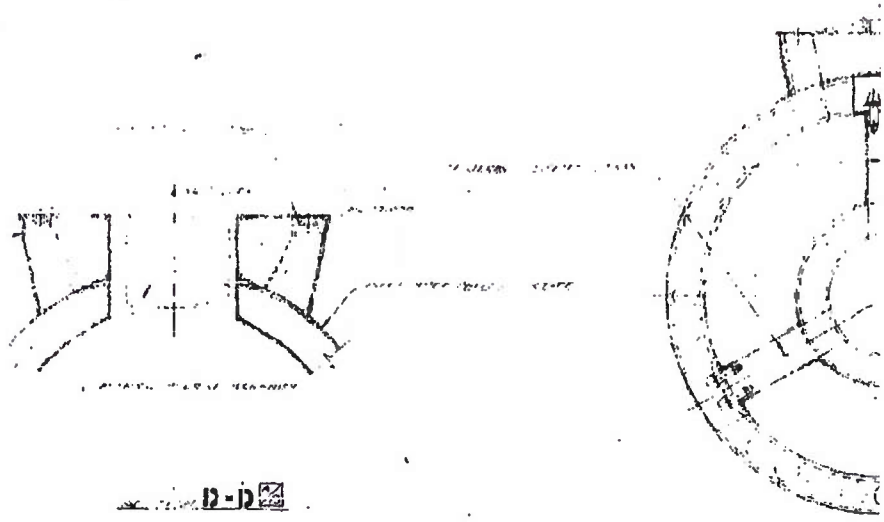

[redacted] [redacted]

2

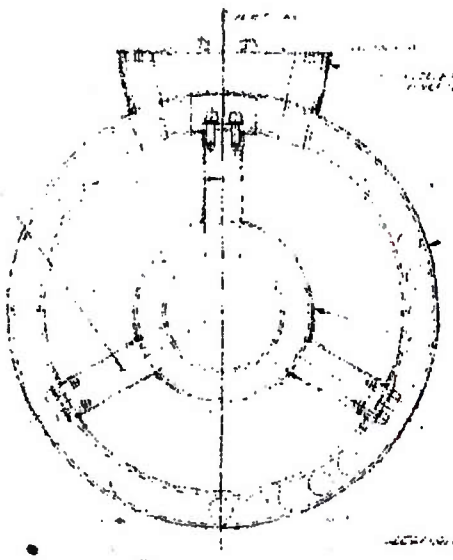

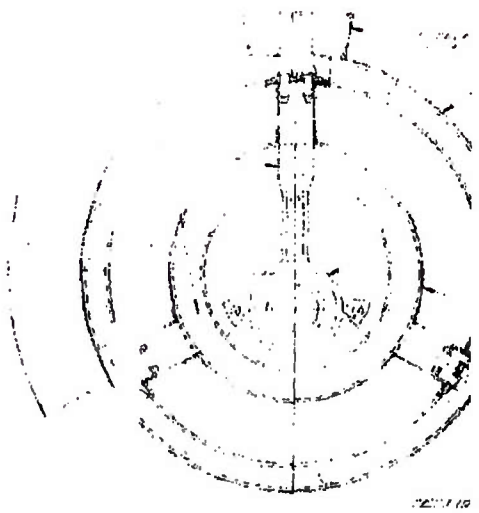

G-G

X81420

21 20 19

[redacted] [redacted]

3

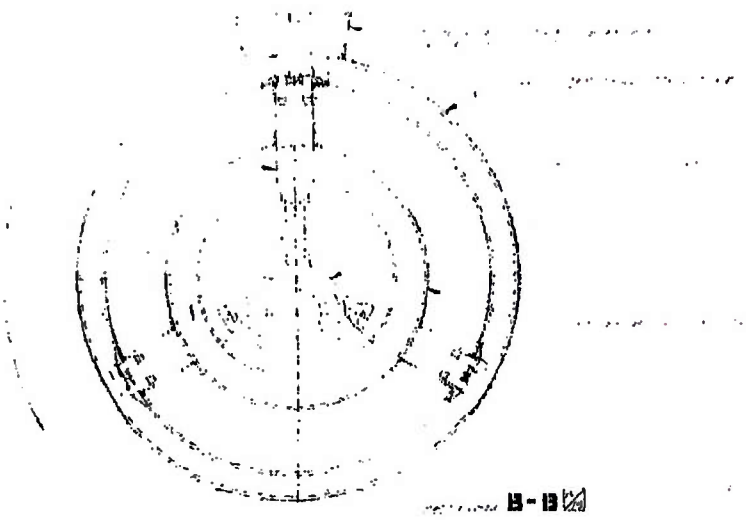

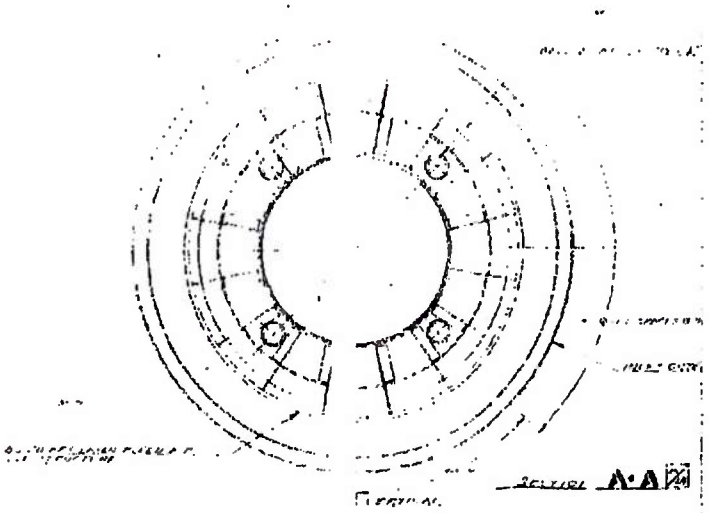

19 18 17

4

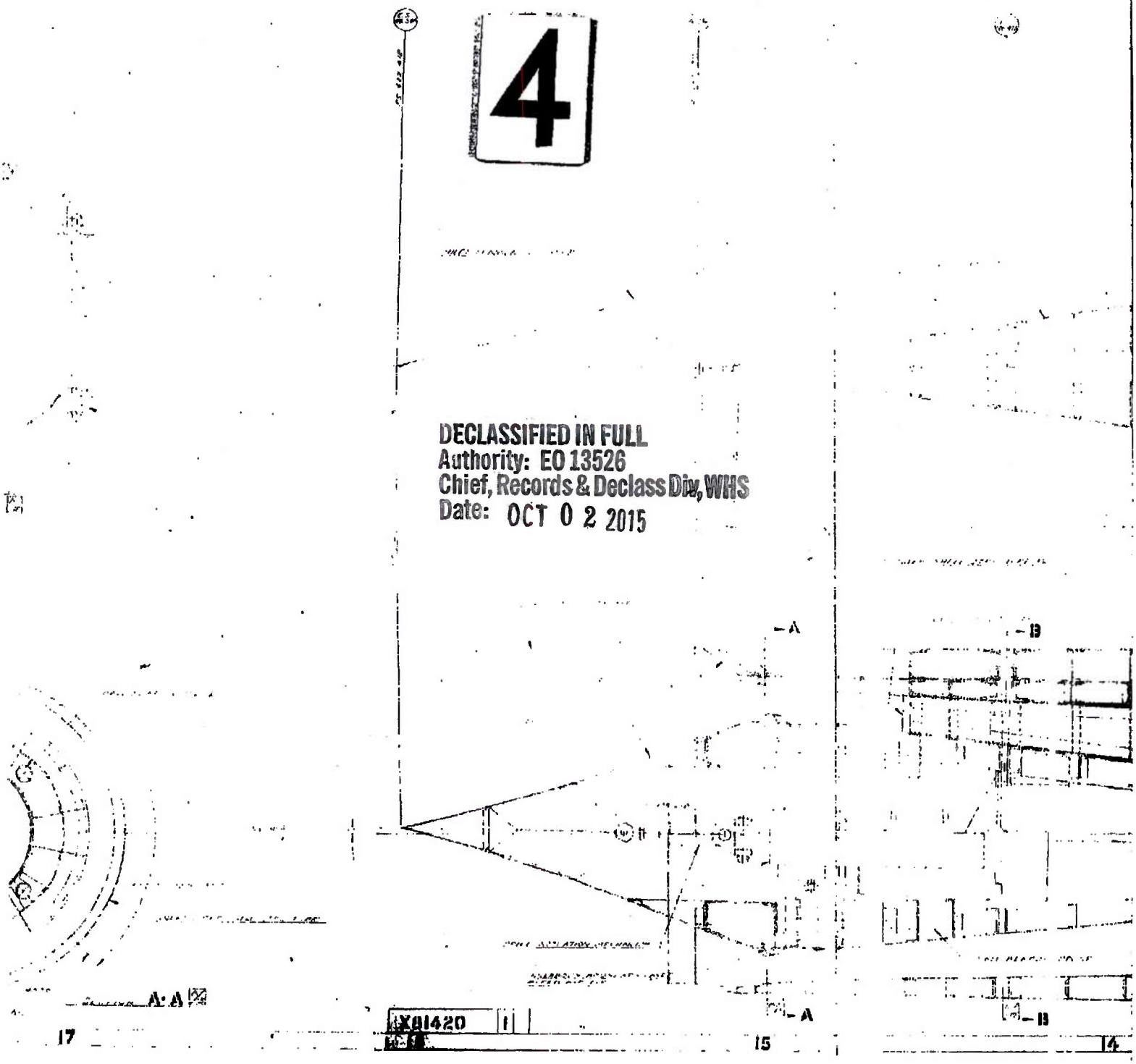

5

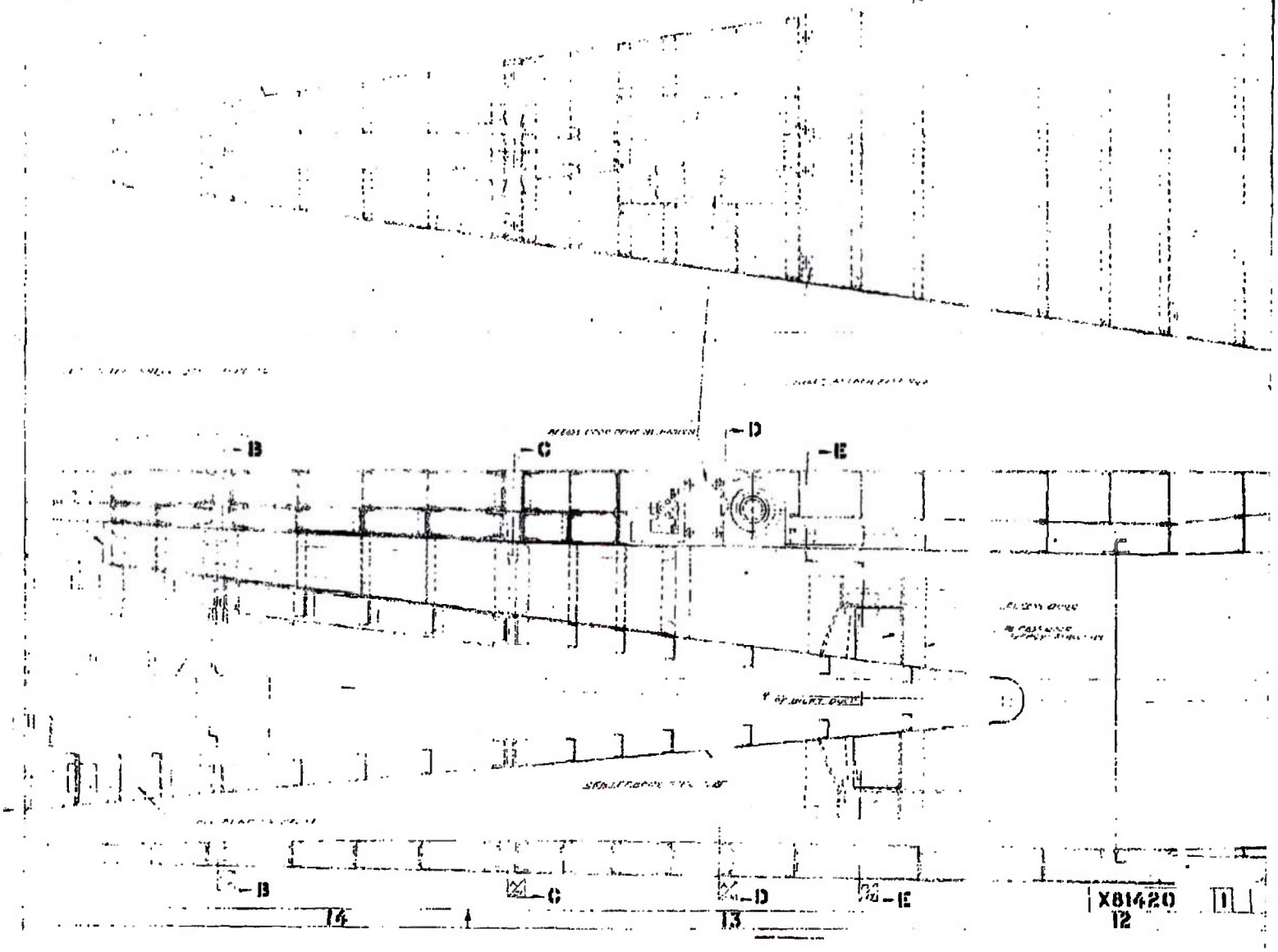

[redacted]

6

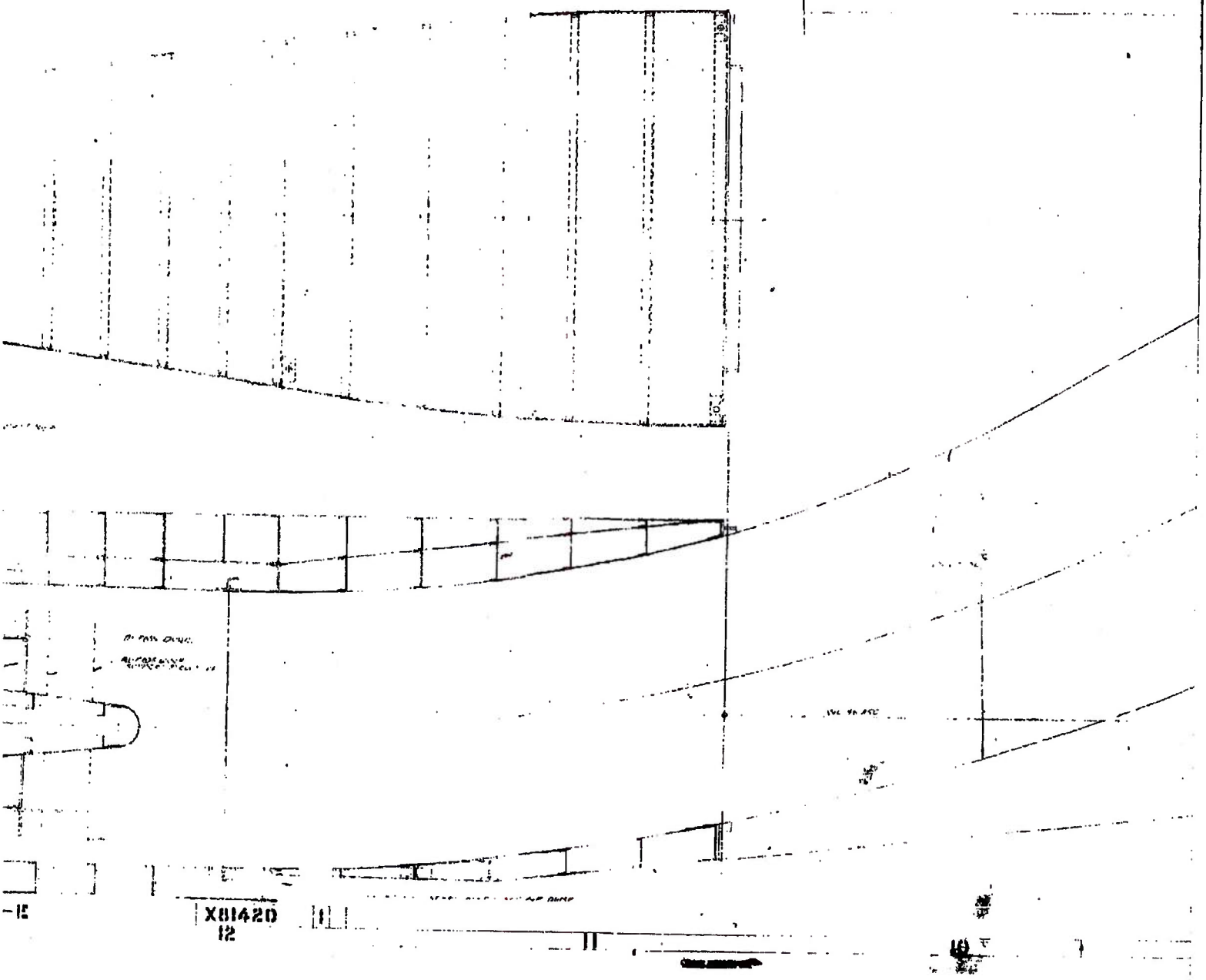

[redacted]

7

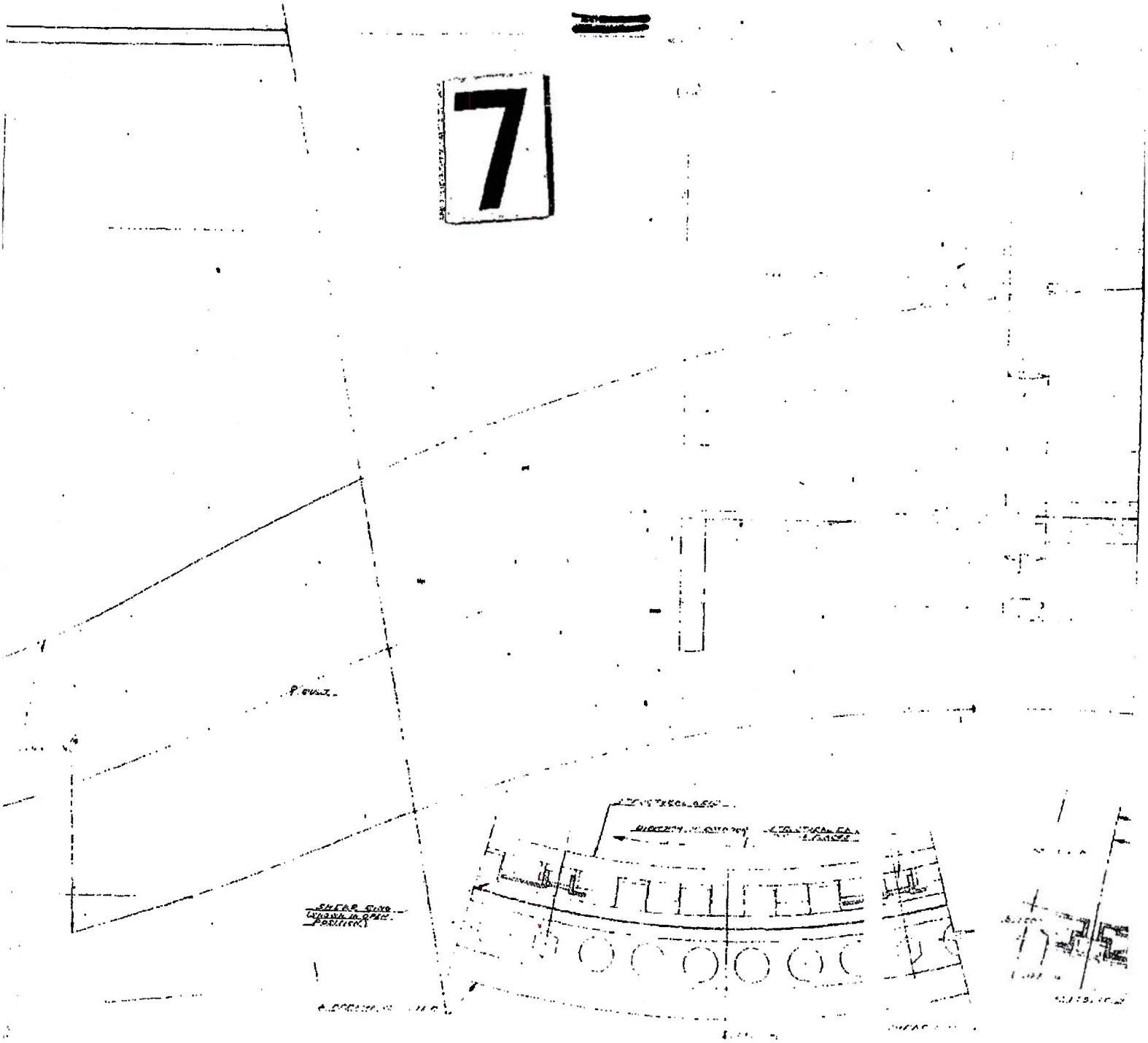

X81420

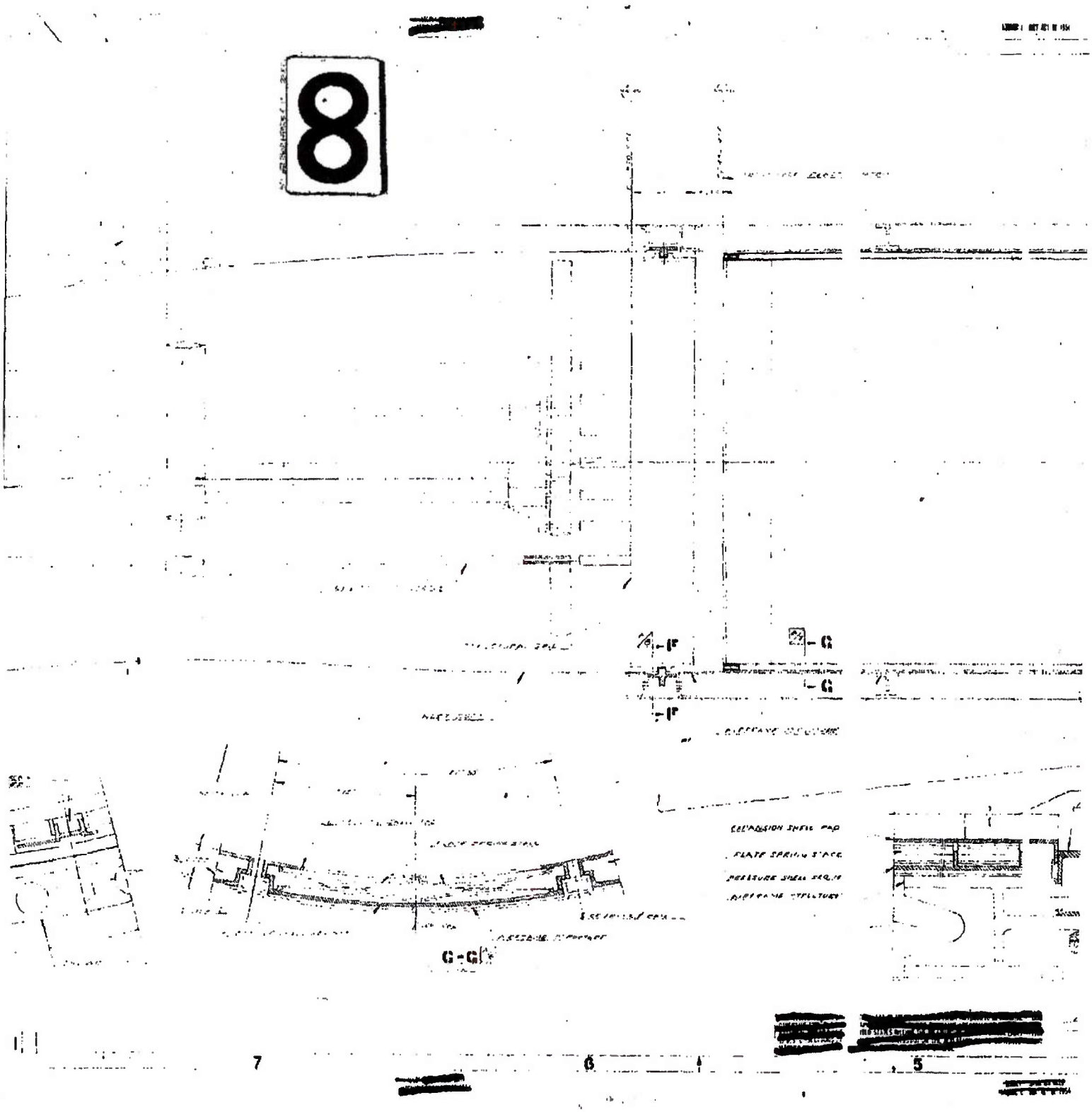

[redacted]

9

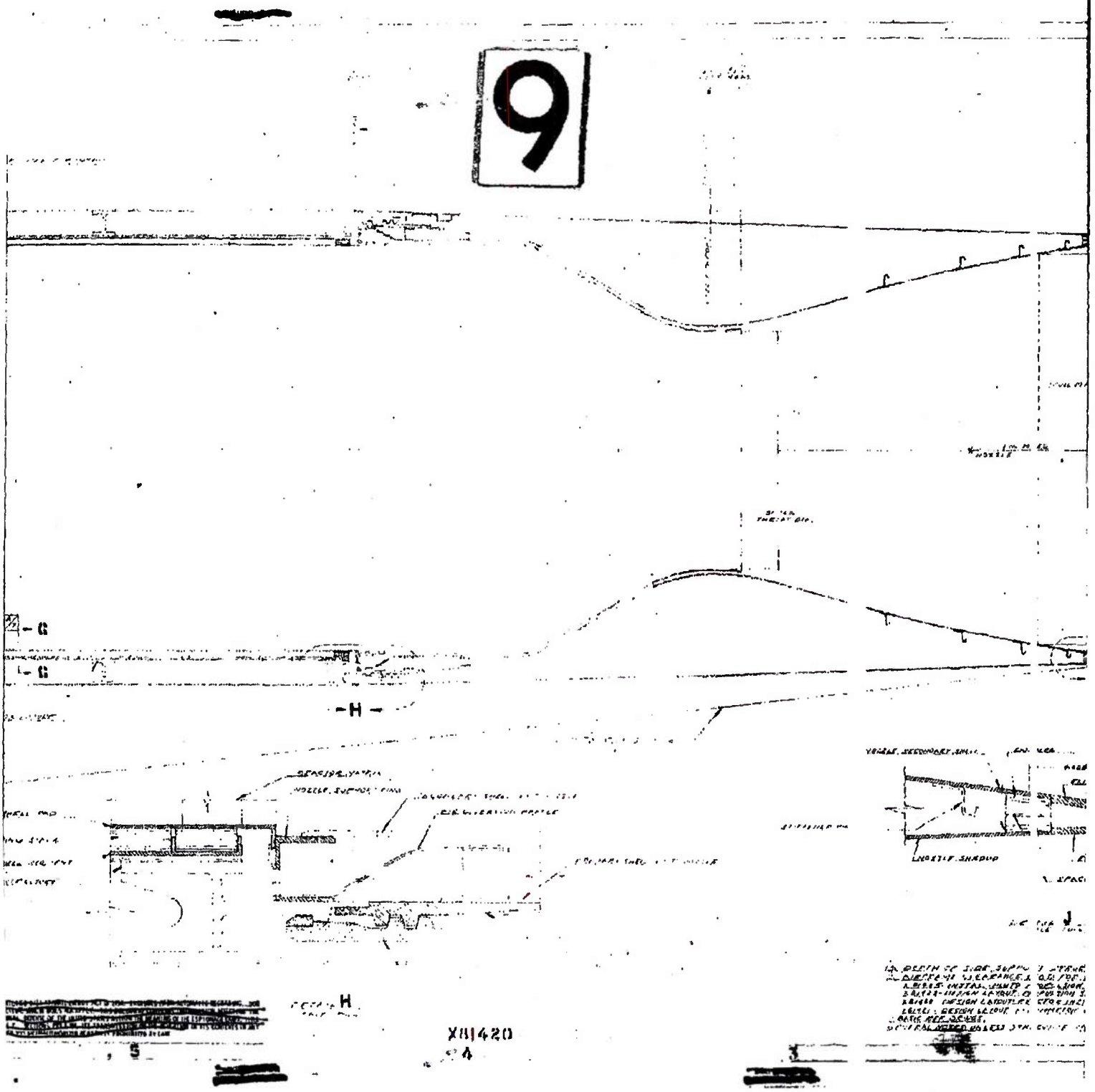

[redacted]

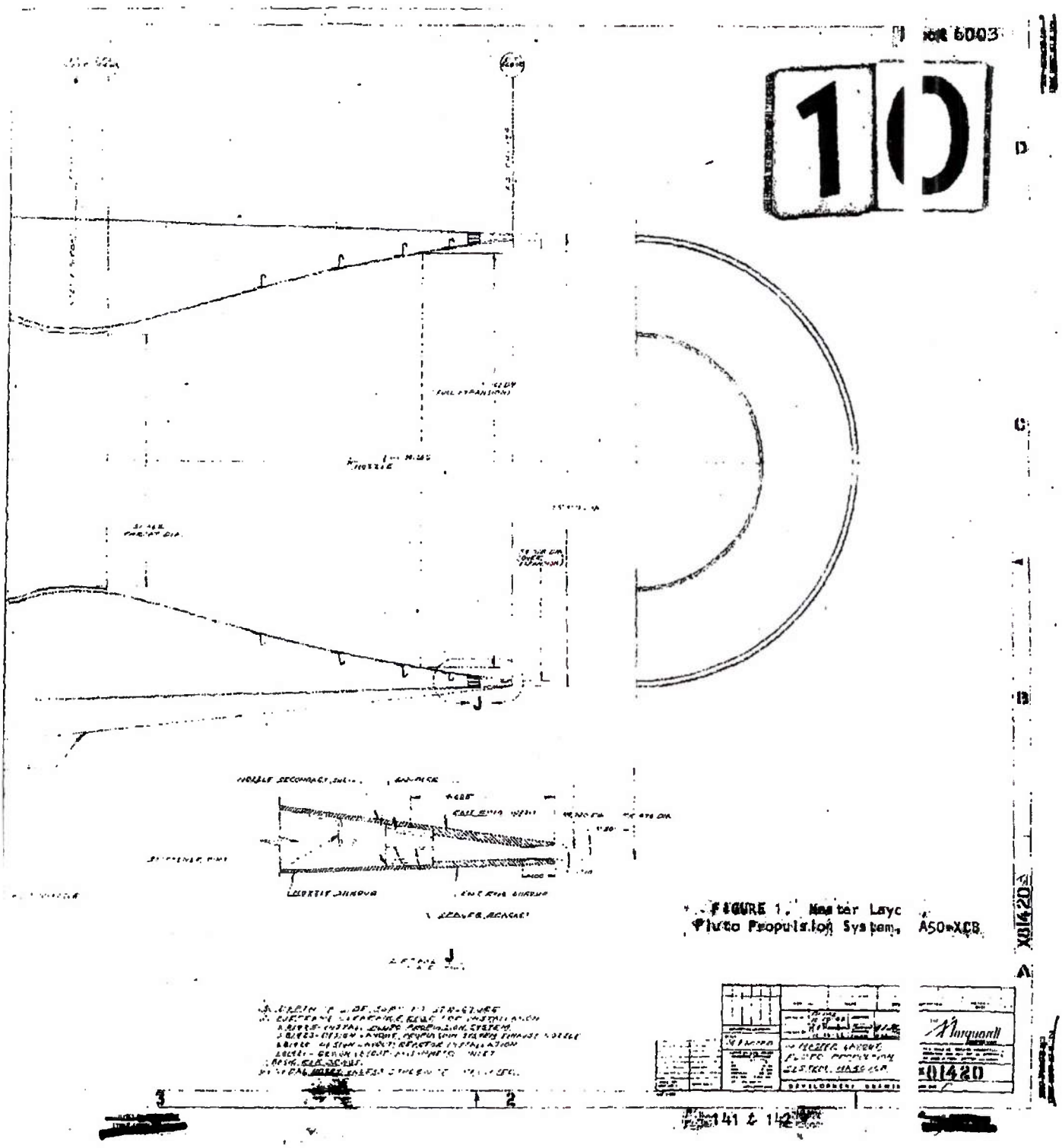

FIGURE 1. Master Layo
Pluto Propulsion System, ASO-XCB

[redacted]

ASD-TDR-63-277, Vol. IV

[redacted]

~~SECRET RESTRICTED DATA~~
~~ATOMIC ENERGY ACT OF 1954~~

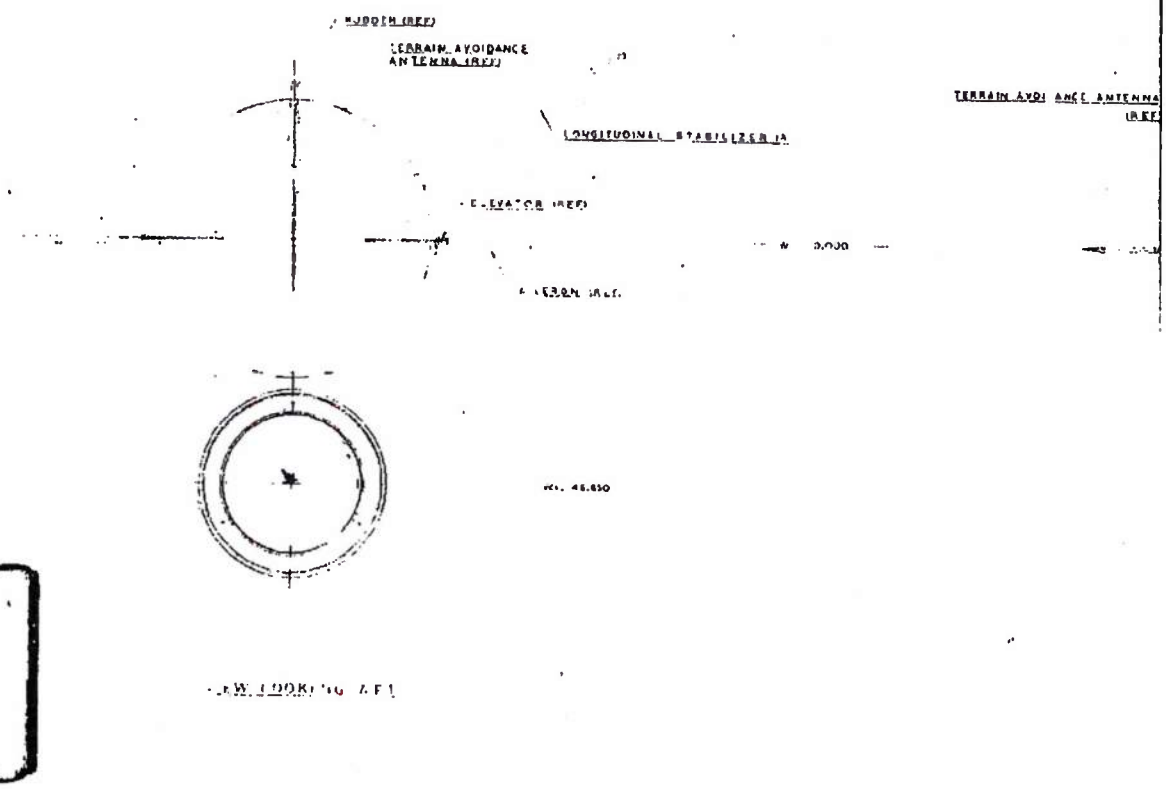

1

~~SECRET RESTRICTED DATA~~
~~ATOMIC ENERGY ACT OF 1954~~

[redacted]

[redacted]

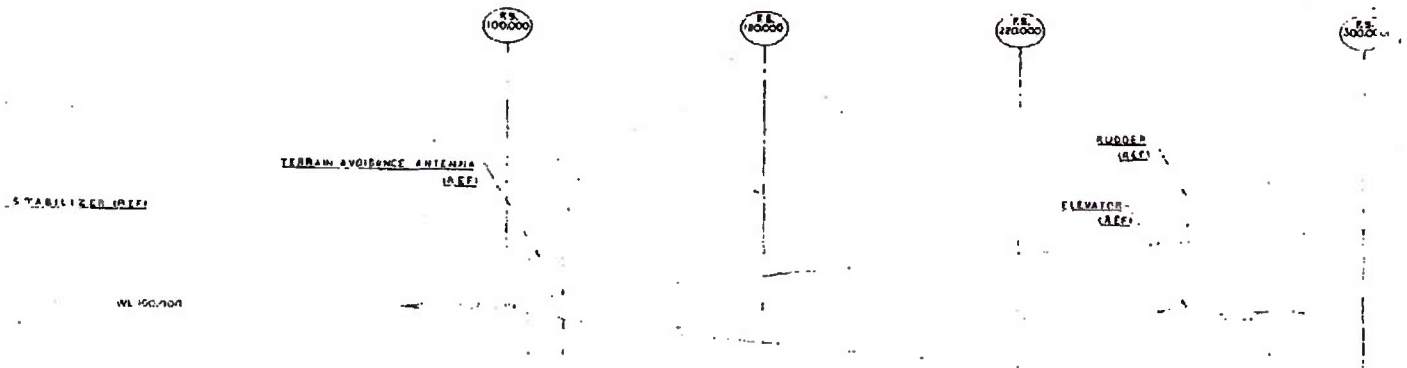

2

[redacted] X81425 [redacted]

13 12 11

[redacted]

[redacted]

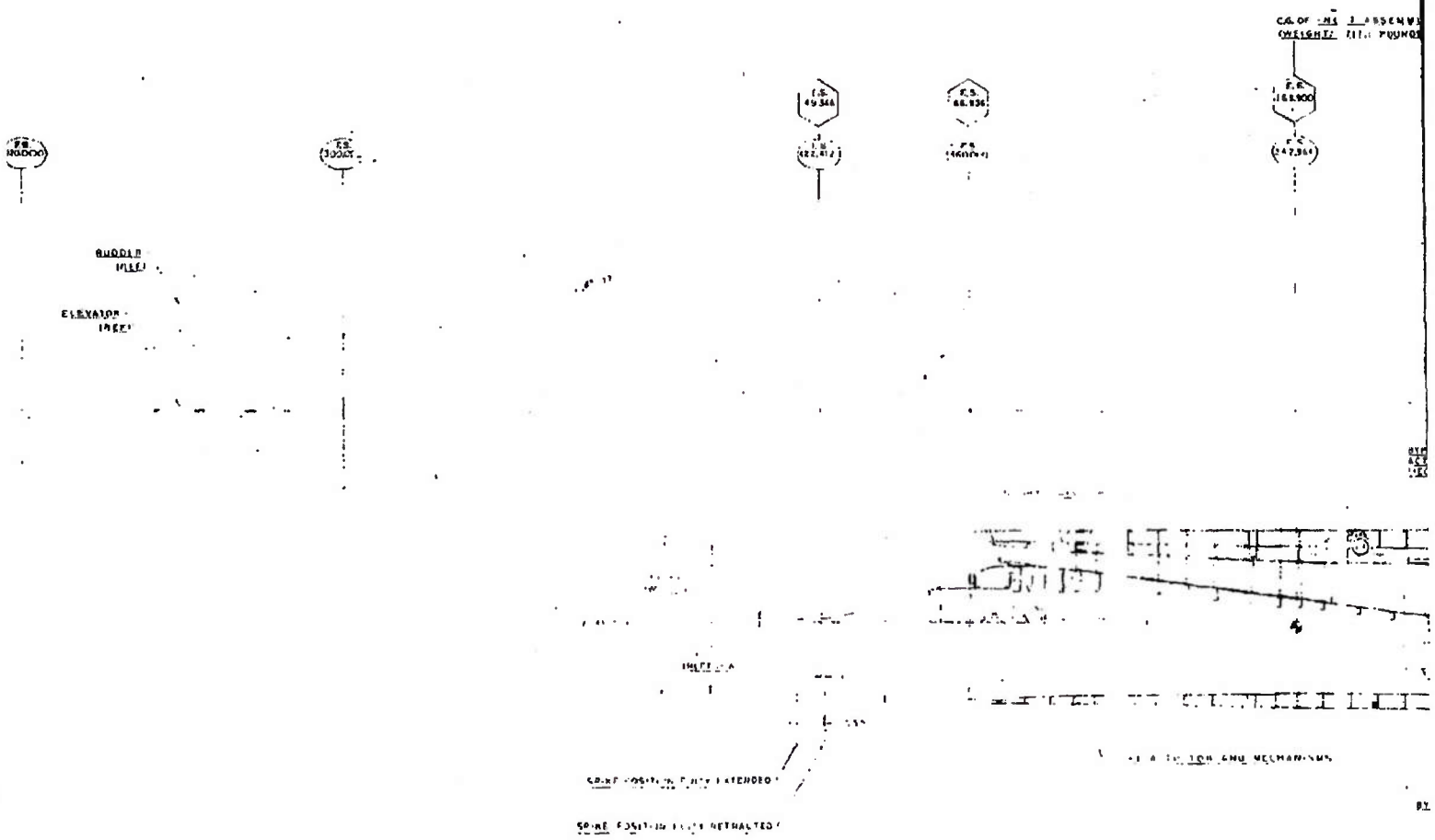

3

[redacted]

[redacted]

C.G. OF INLET ASSEMBLY
(WEIGHT: 7737.1 POUNDS)

C.G. OF CONTROL SUPPORT STRUCTURE
(WEIGHT: 2057 POUNDS)

AIRFRAME, OUTER W

REACTOR CONT AND MECHANIS

BOUNDARY LAYER BLEED REMOVAL

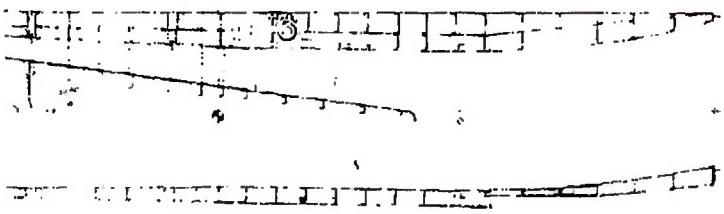

DECLASSIFIED IN FULL
Authority: EO 13526
Chief, Records & Declass Div, WHS
Date: OCT 0 2 2015

X81425 [redacted]

[redacted]

[redacted]

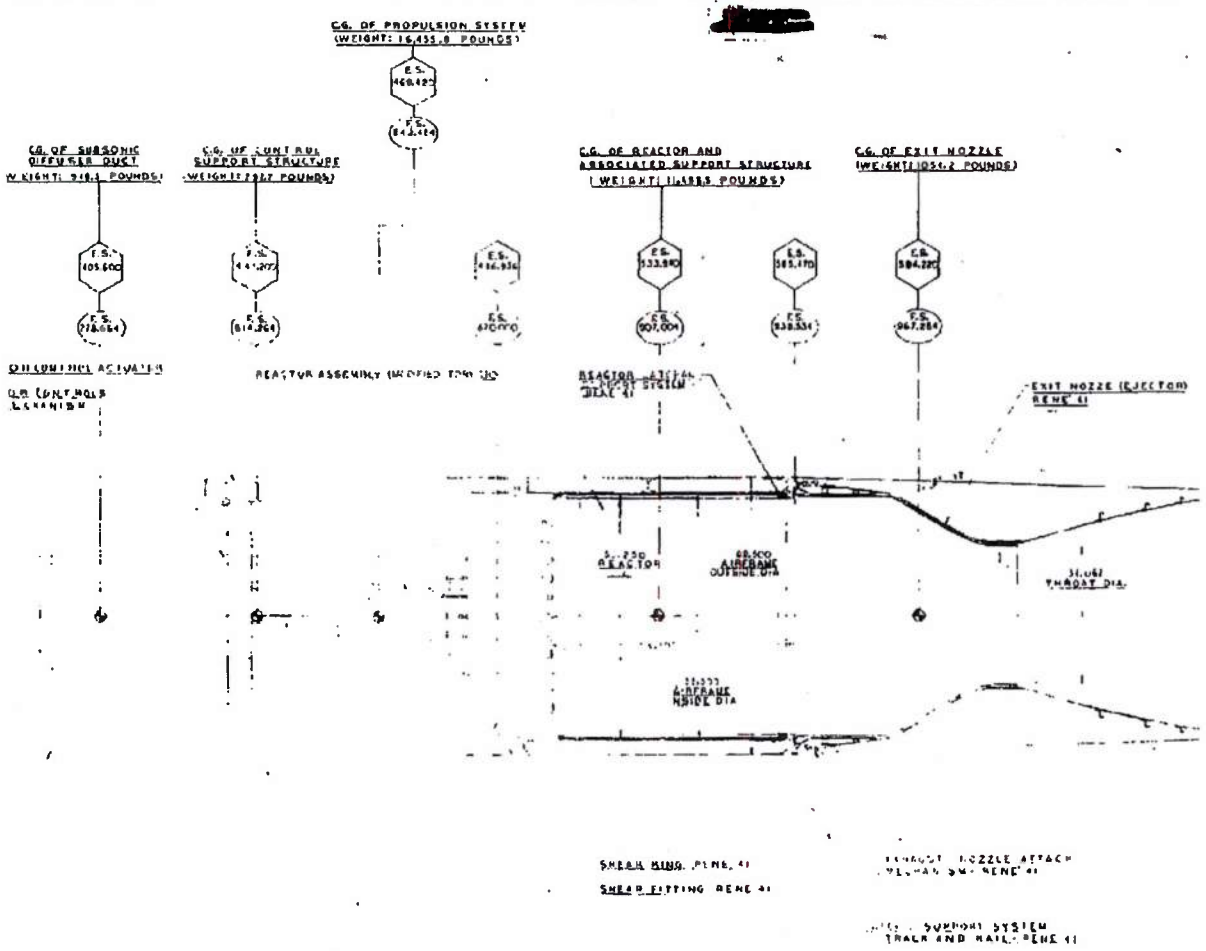

5

[redacted]

X81425

[redacted]

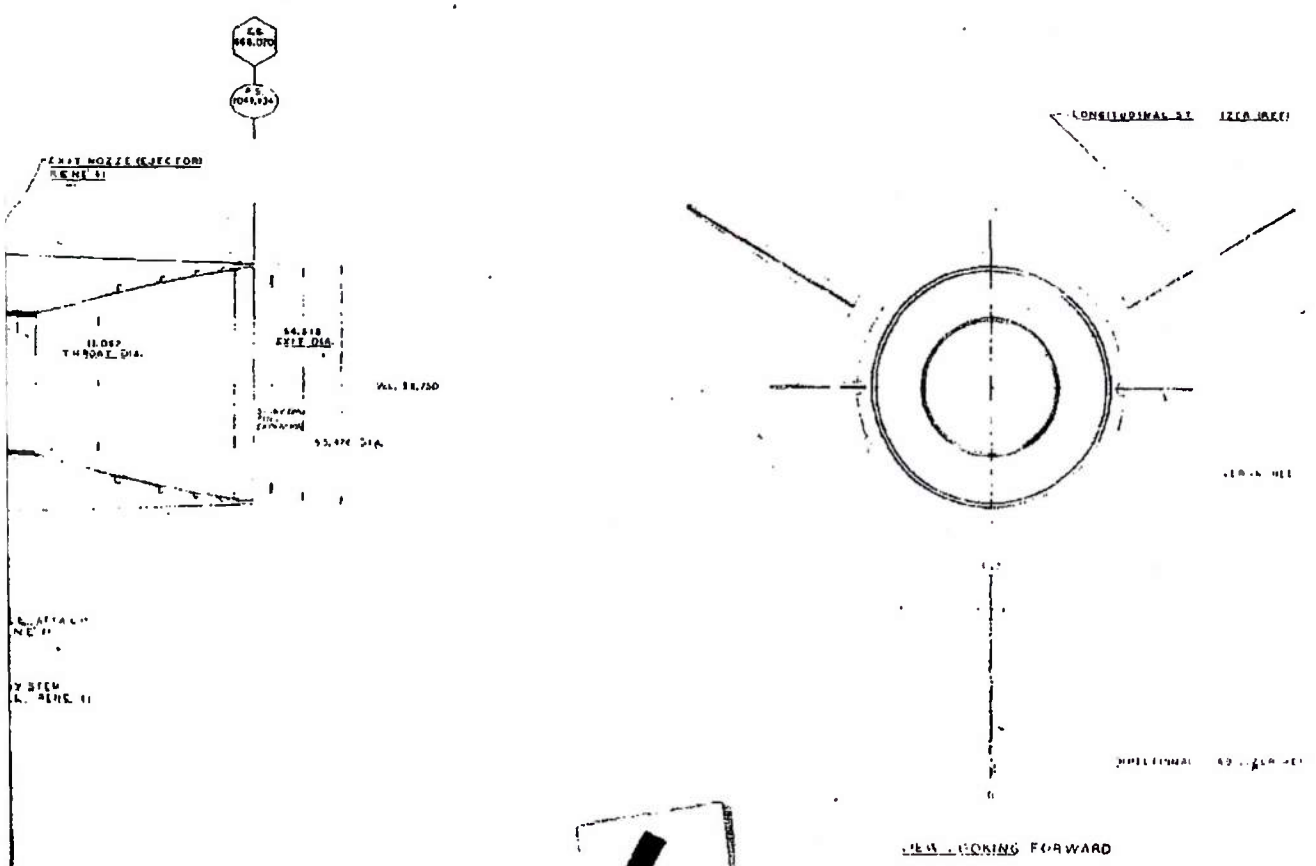

6

Pluto

X81425

[redacted]

4 3 2

[redacted]

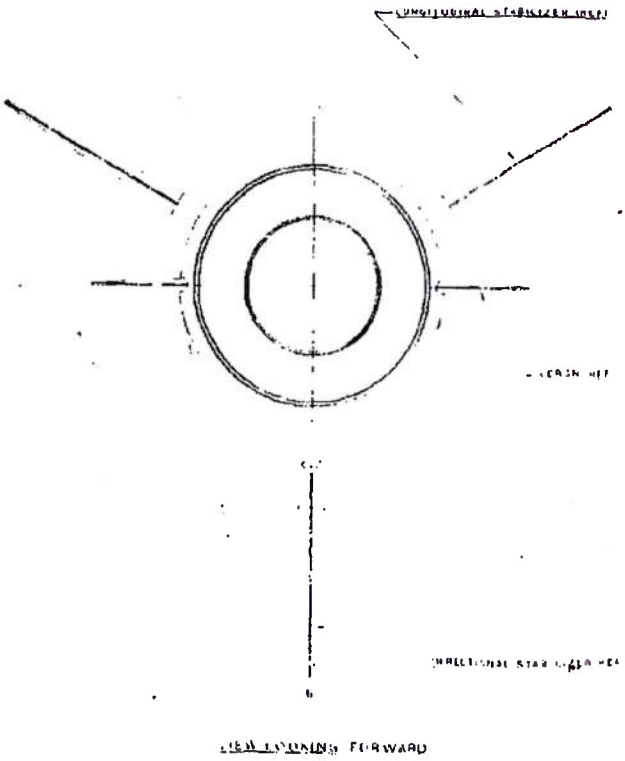

7

FIGURE 2. Installation
Pluto Propulsion System, MA50-XCB

X81425

[redacted]

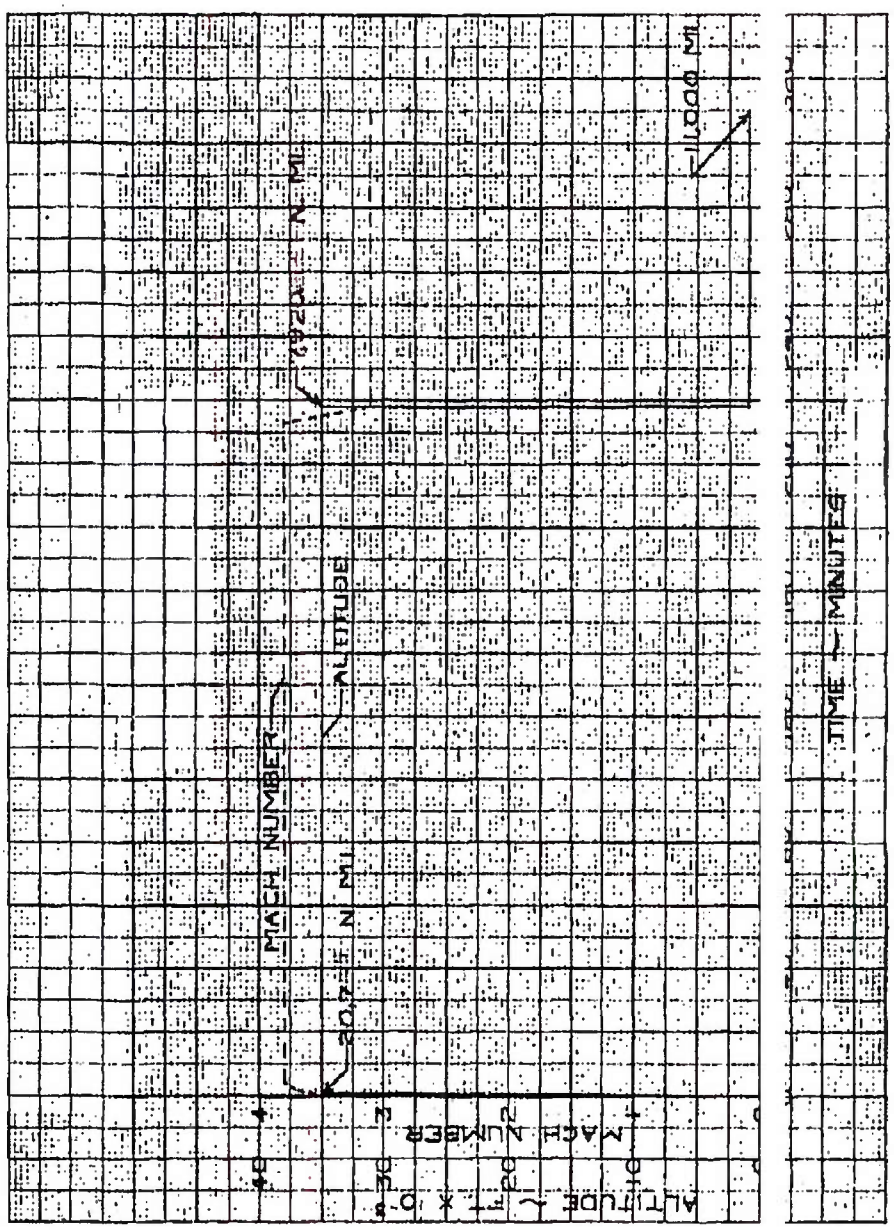

FIGURE 3. Typical Mission Profile for 11,000 Nautical Miles (ICAO Standard Day)

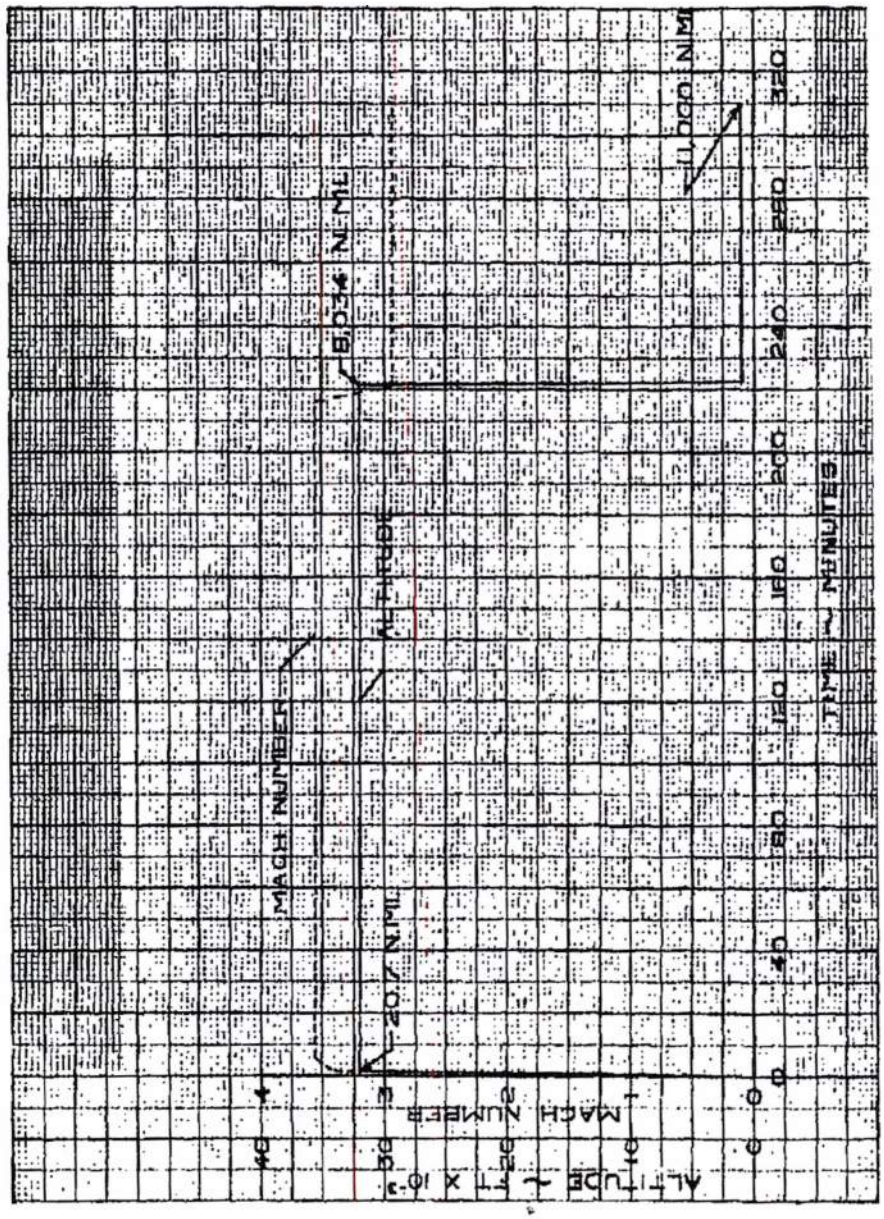

FIGURE 4. Typical Mission Profile for 11,000 Nautical Miles (ANA Hot Day)

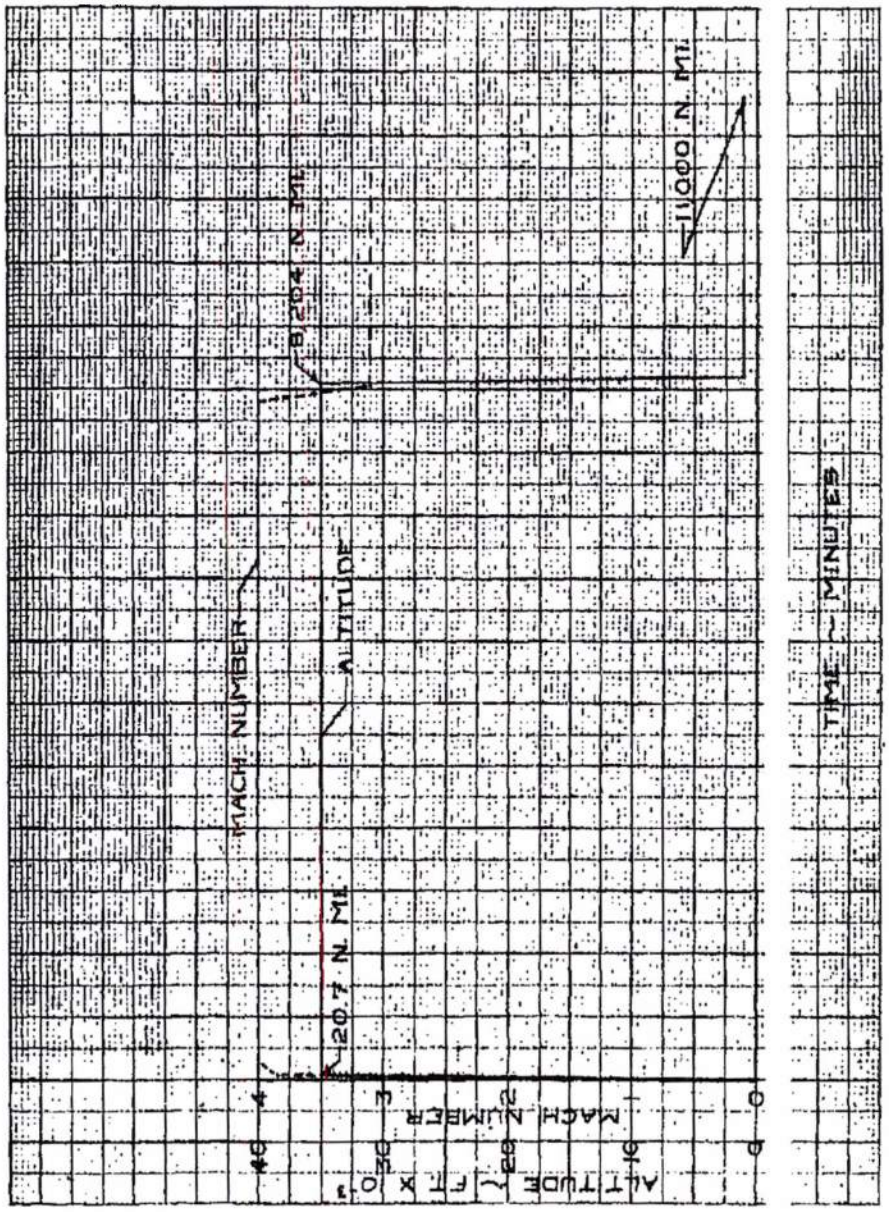

FIGURE 5. Typical Mission Profile for 11,000 Nautical Miles (AWA Cold Day)

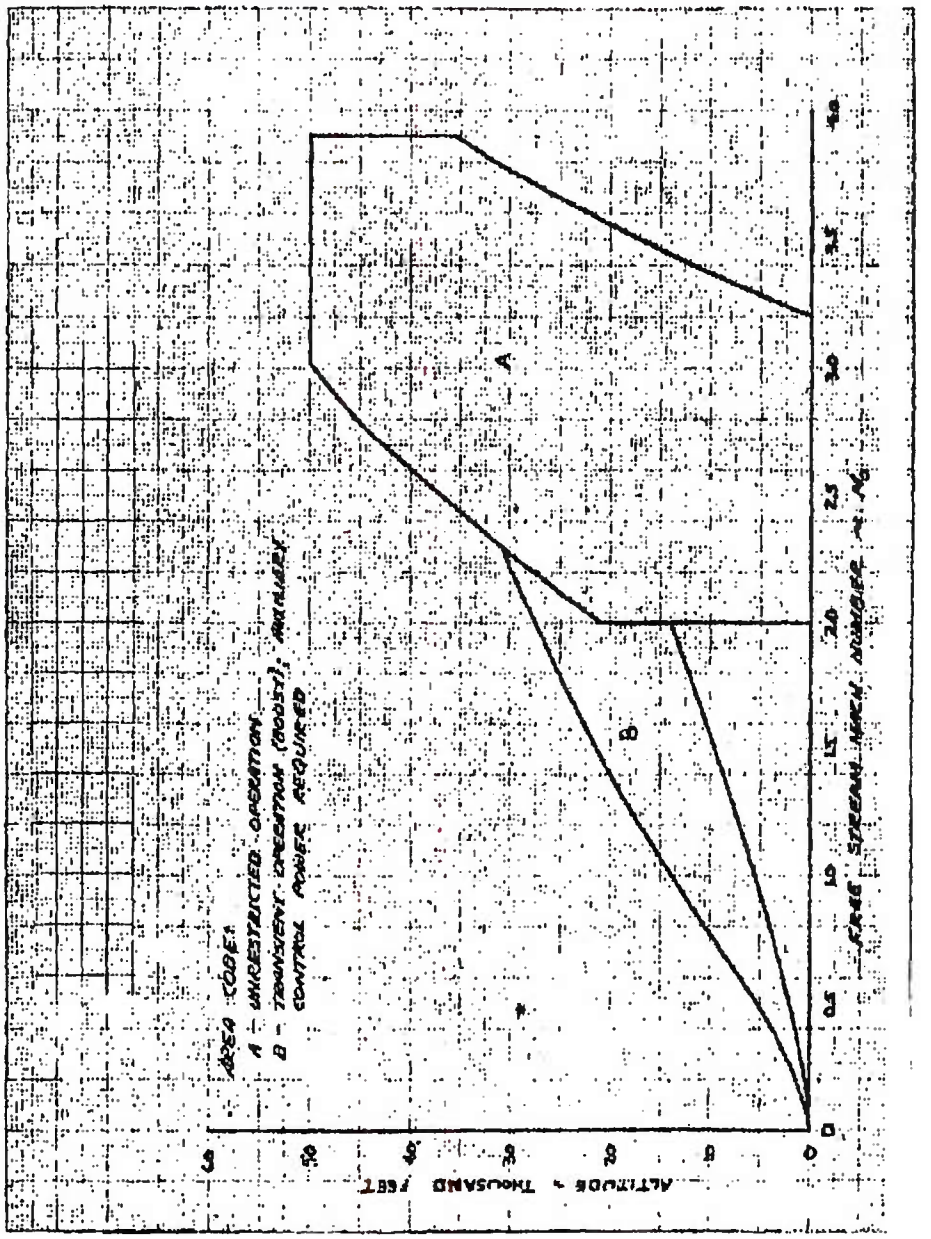

FIGURE 6. Estimated Operating Envelope for Marquardt Model MA50-XCB Ramjet (ICAO Standard Day)

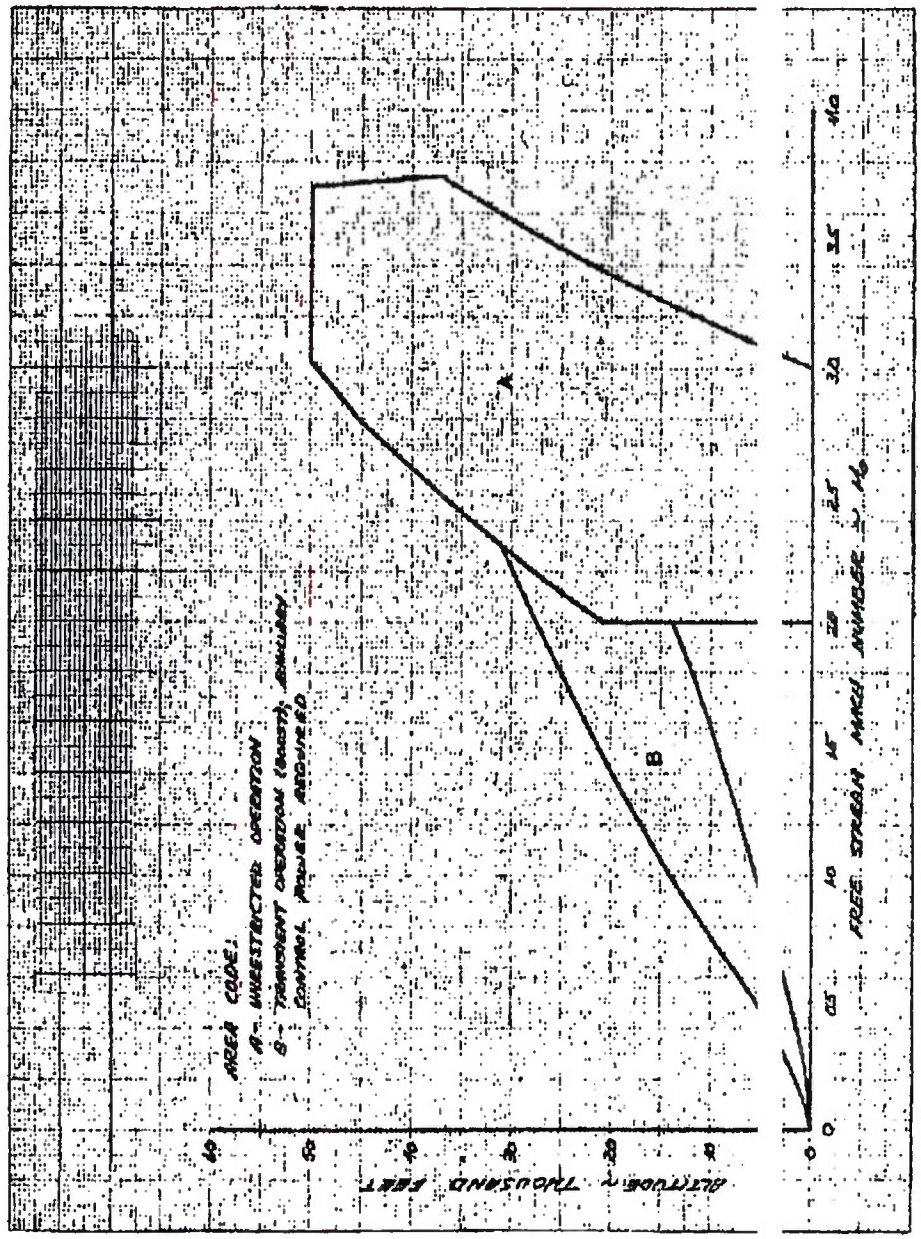

FIGURE 7. Estimated Operating Envelope for Marquardt Model MA5C-XCB Ramjet (ANA Hot Day)

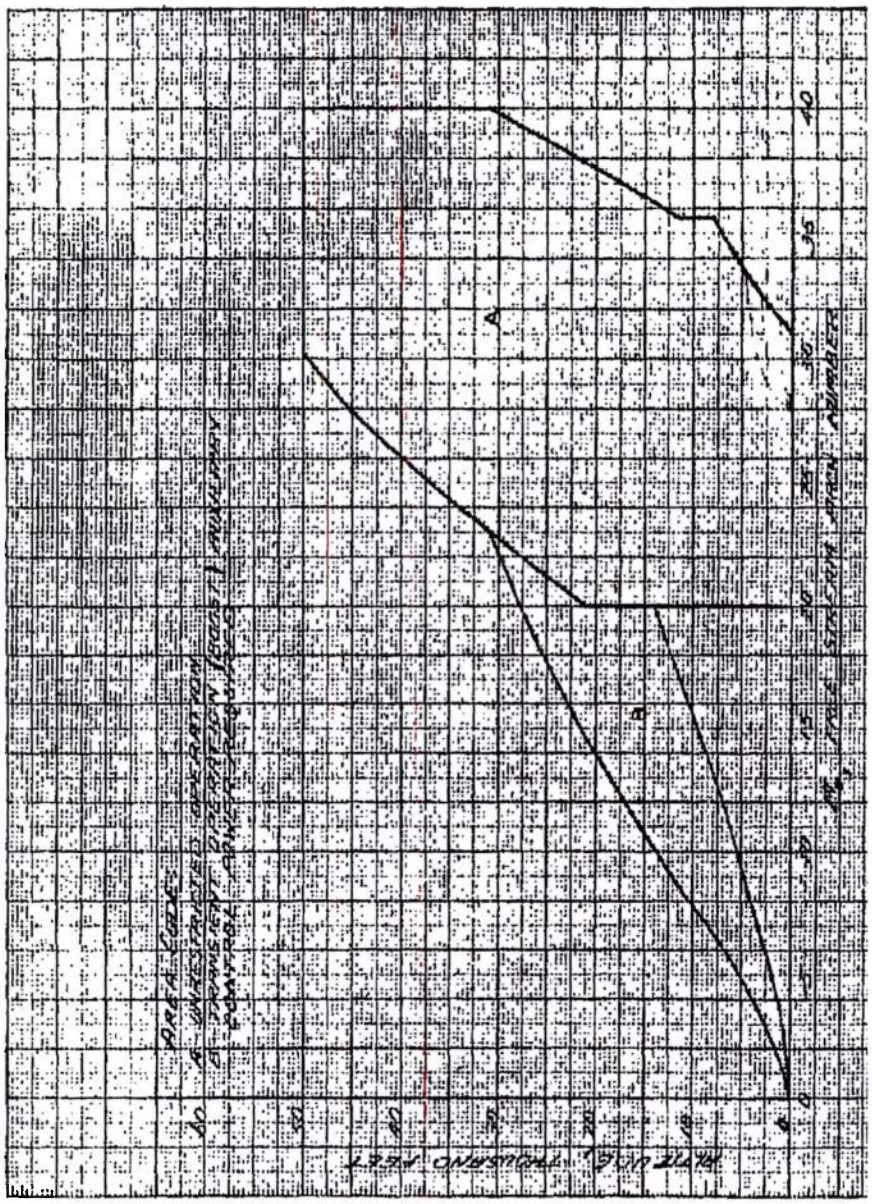

FIGURE 8. Estimated Operating Envelope for Marquardt Model MA50-XCB Ramjet (ANA Cold Day)

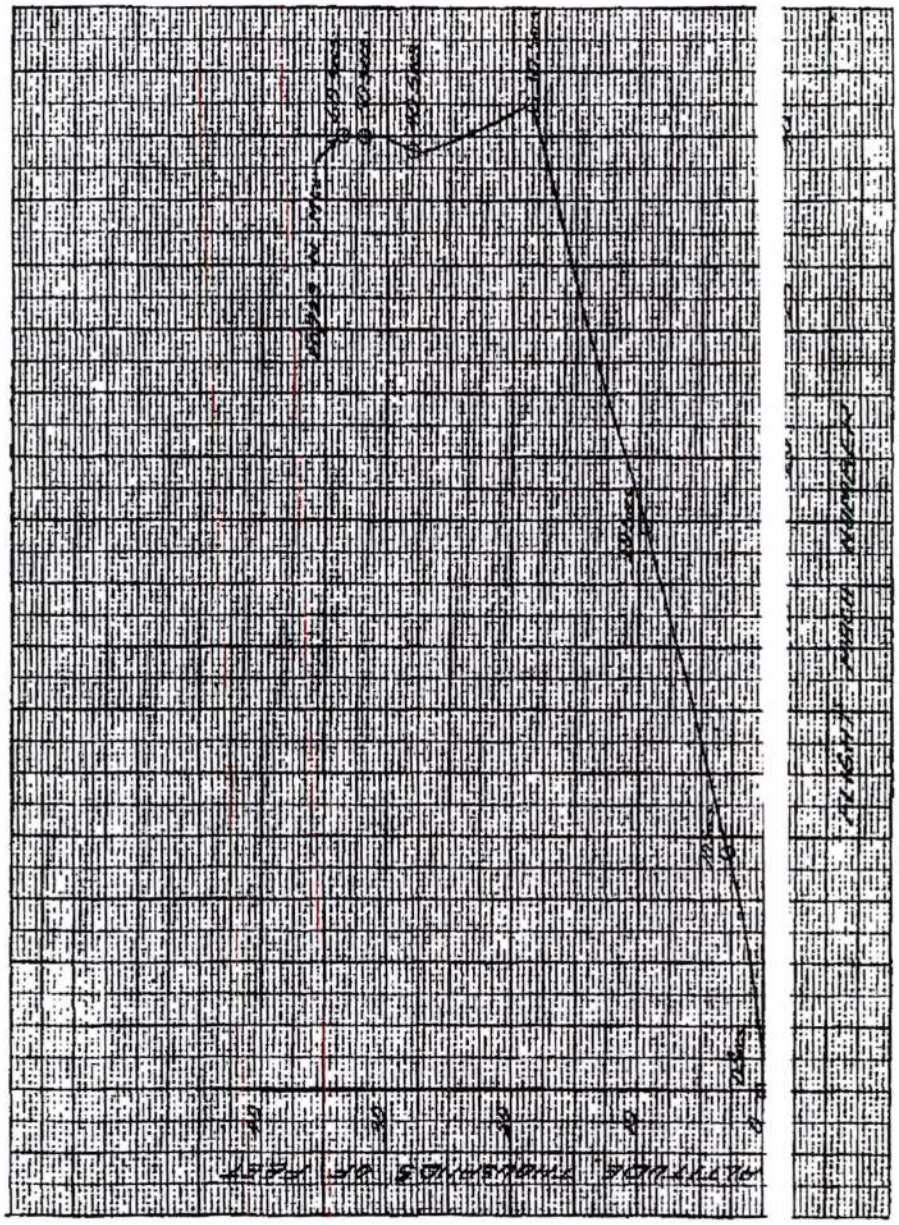

FIGURE 9. Typical Pluto Boost Trajectory

~~SECRET RESTRICTED DATA~~
~~ATOMIC ENERGY ACT OF 1954~~

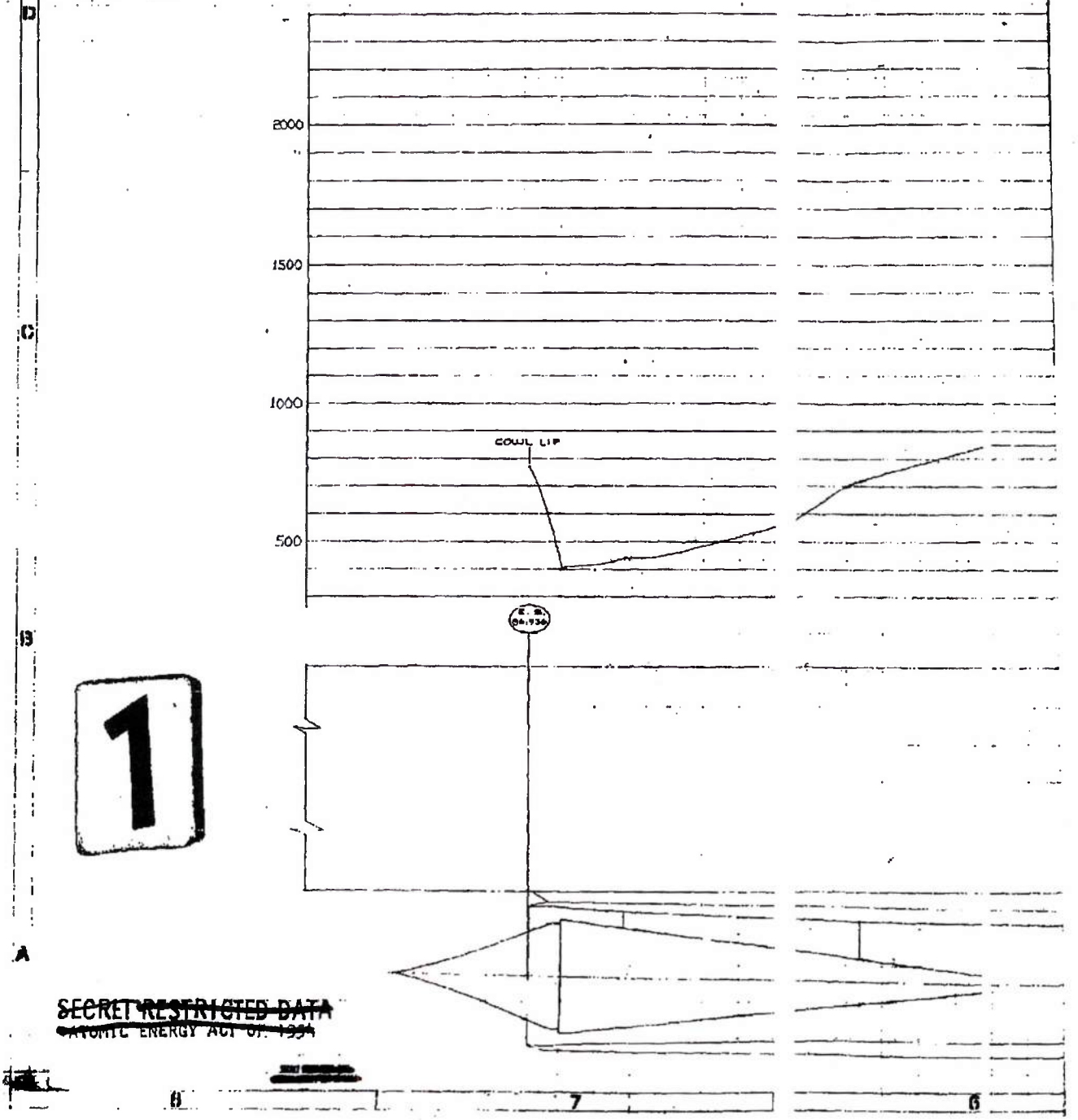

~~SECRET RESTRICTED DATA~~
~~ATOMIC ENERGY ACT OF 1954~~

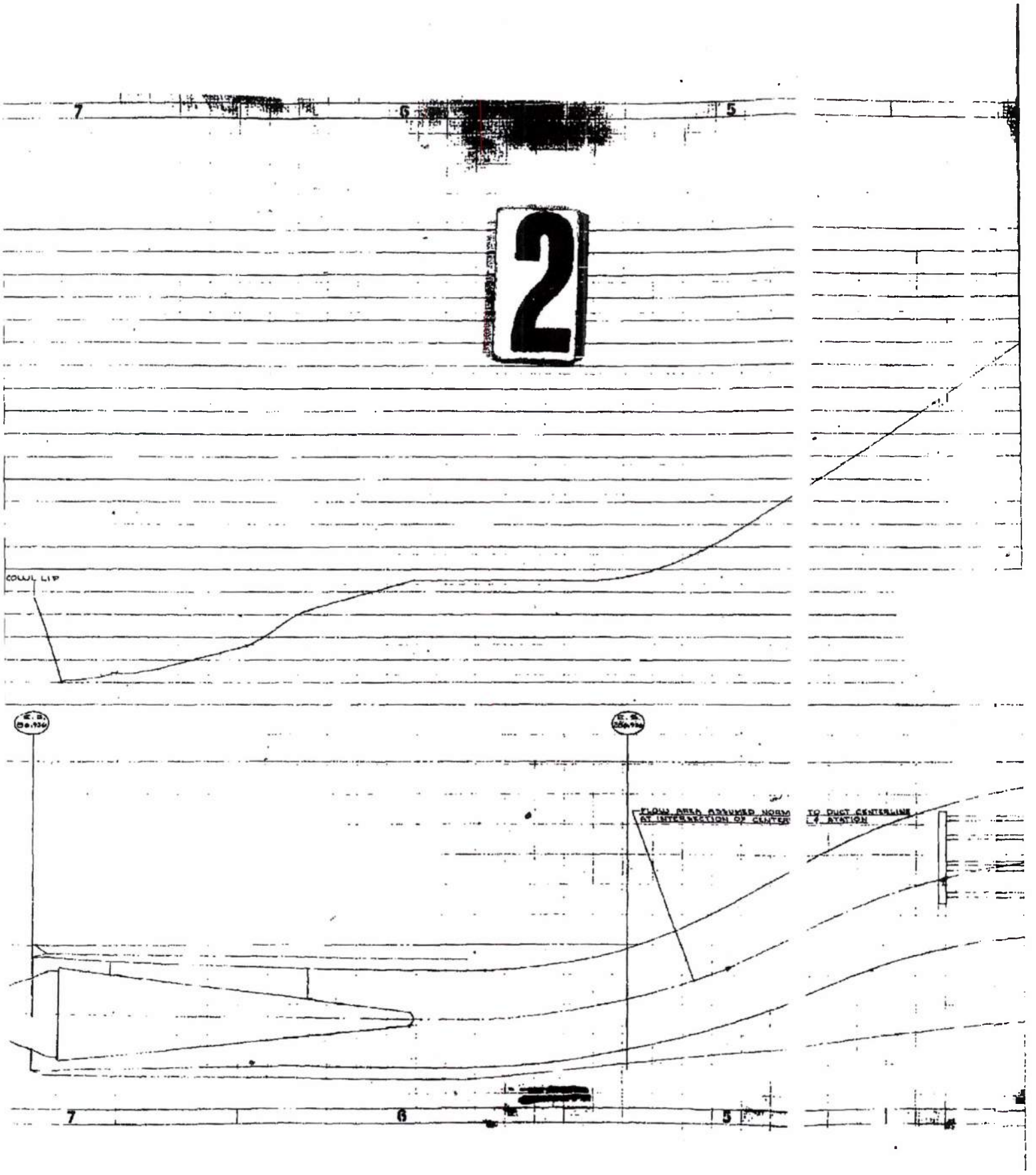

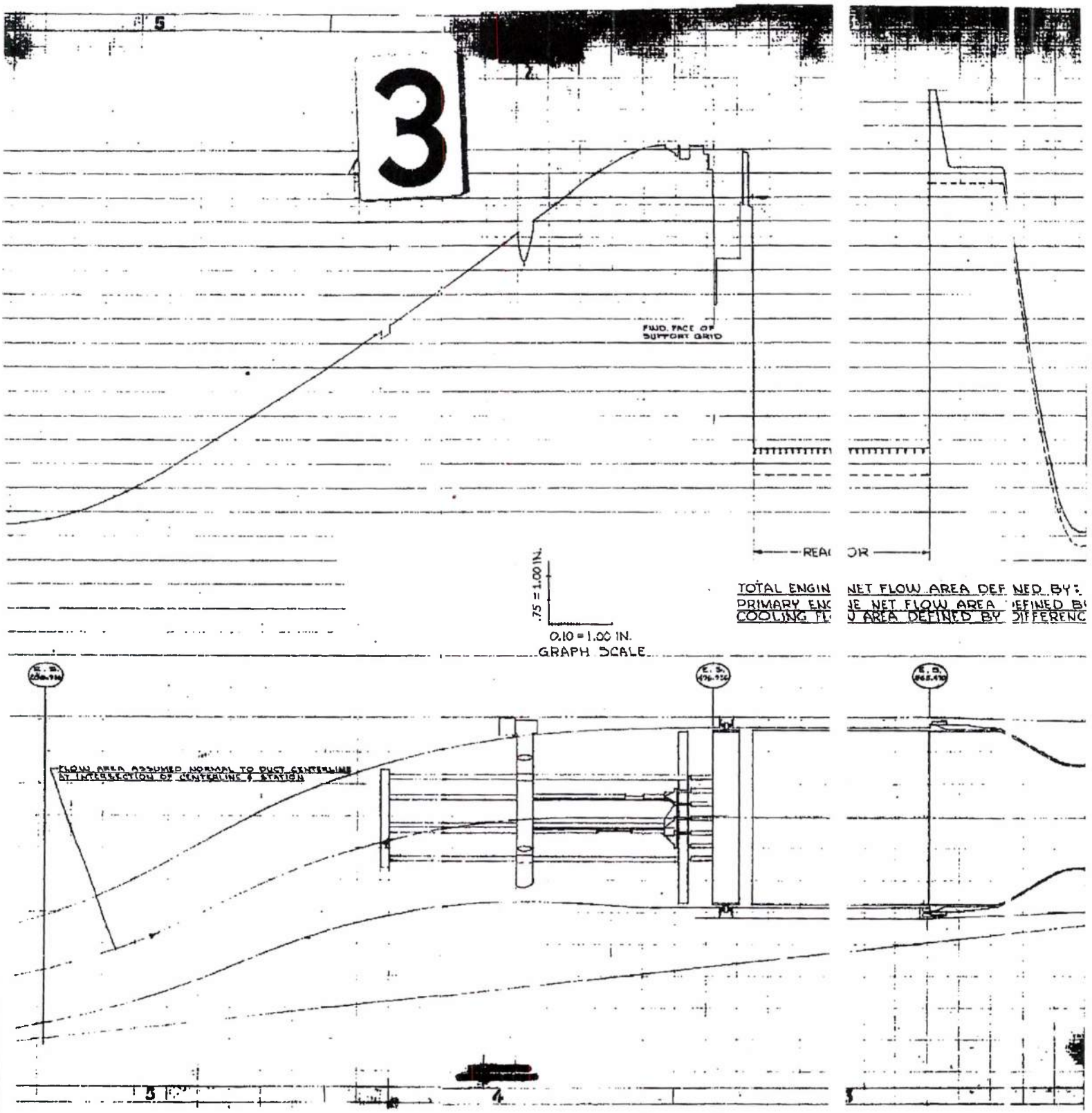

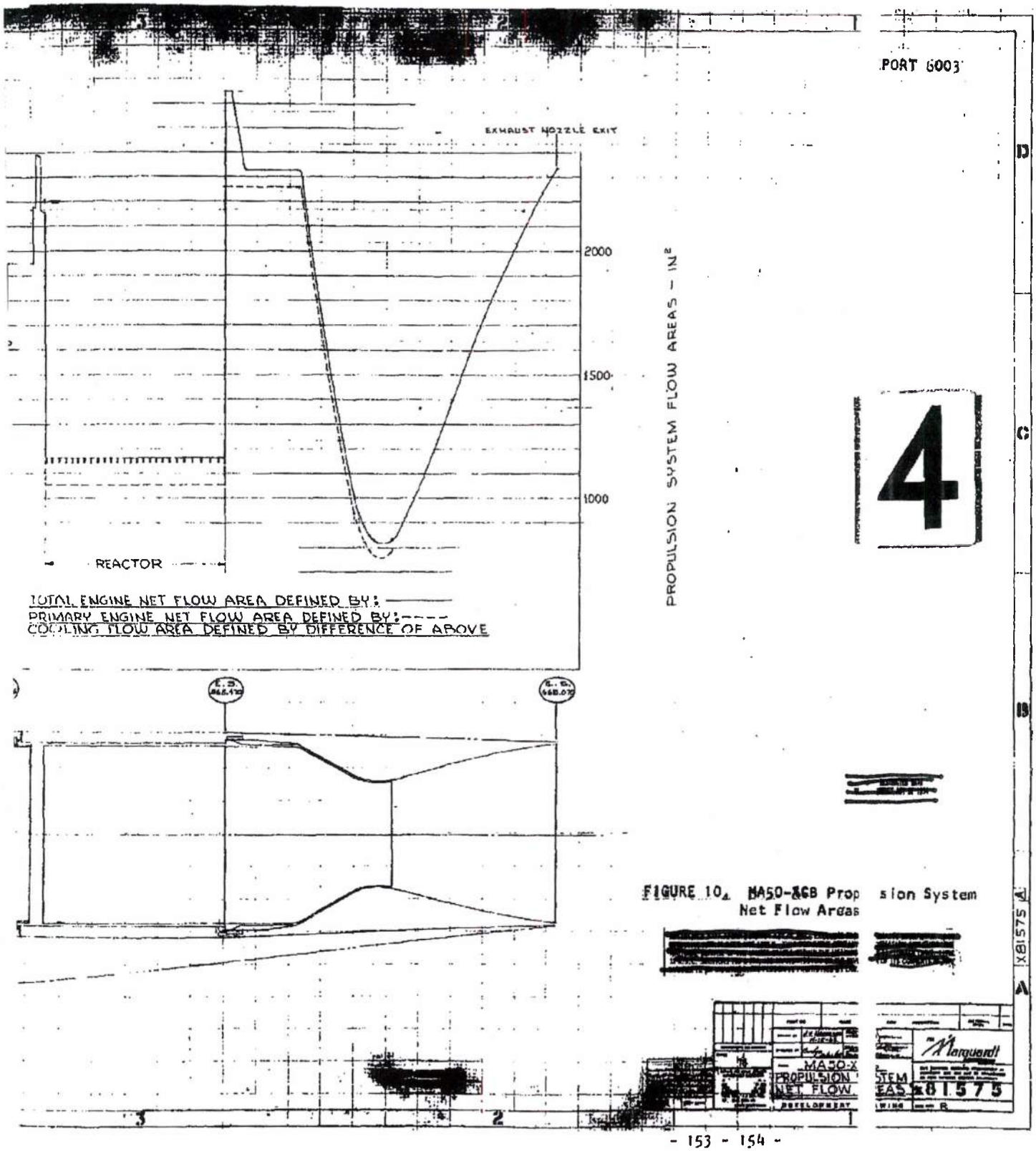

FIGURE 10. MA50-X6B Propulsion System Net Flow Areas

[redacted]

[redacted]

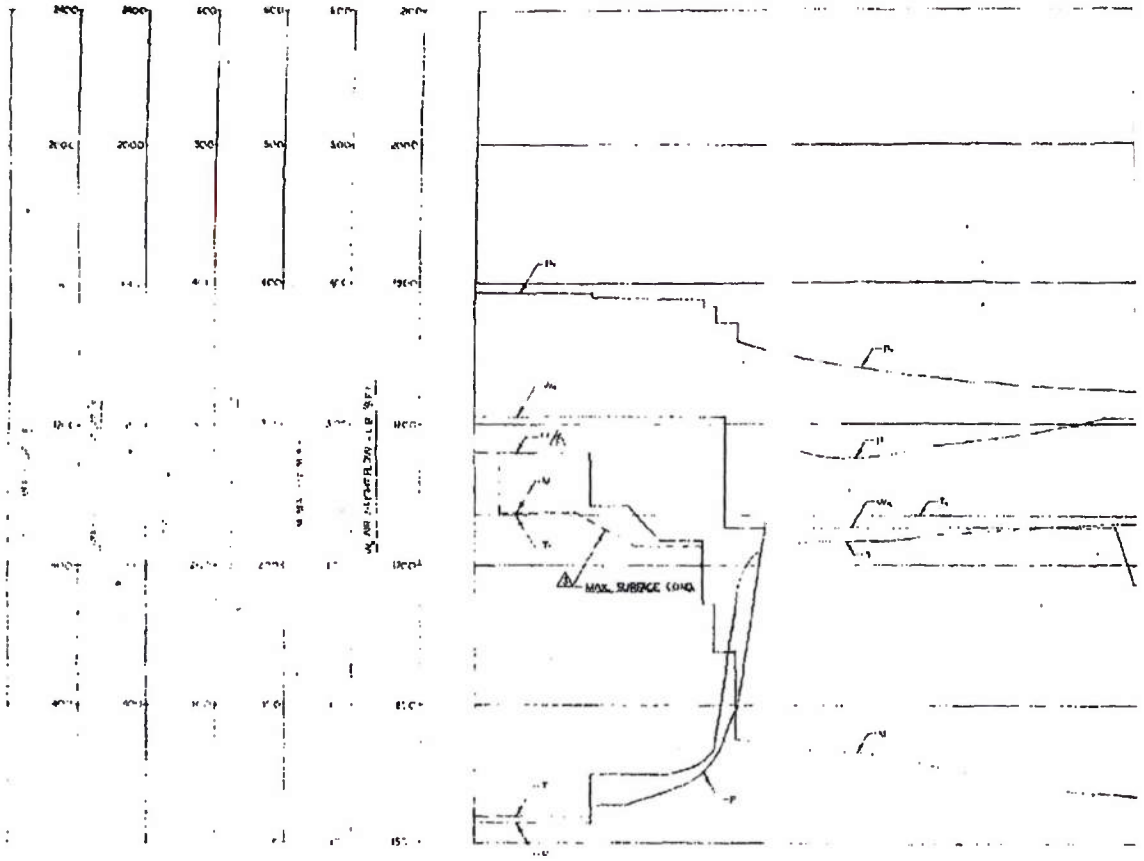

1

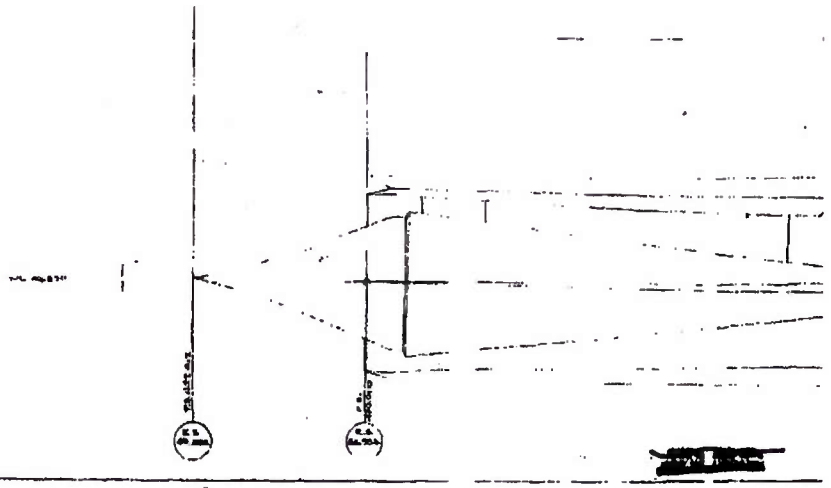

[redacted]

[redacted]

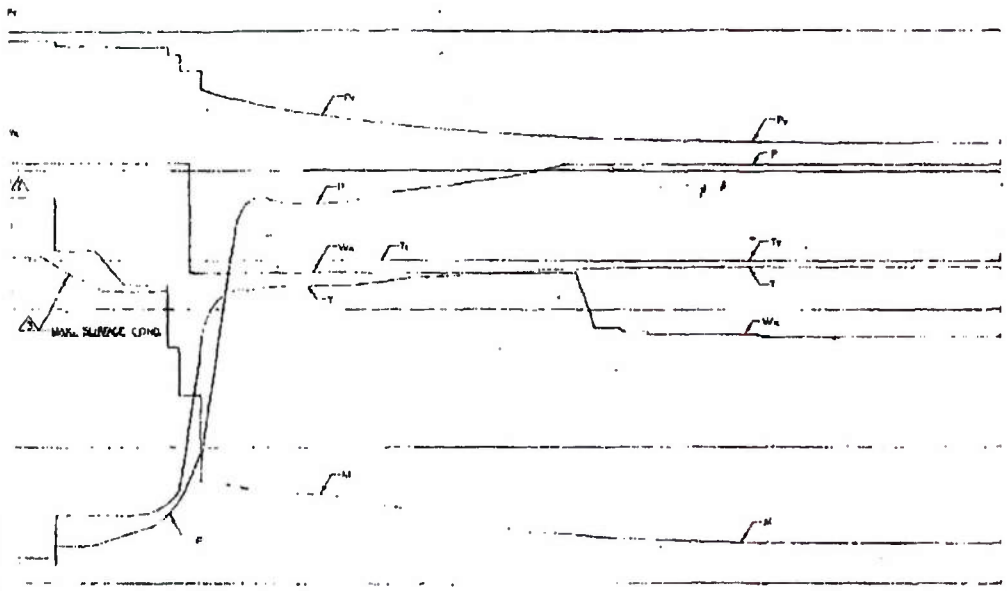

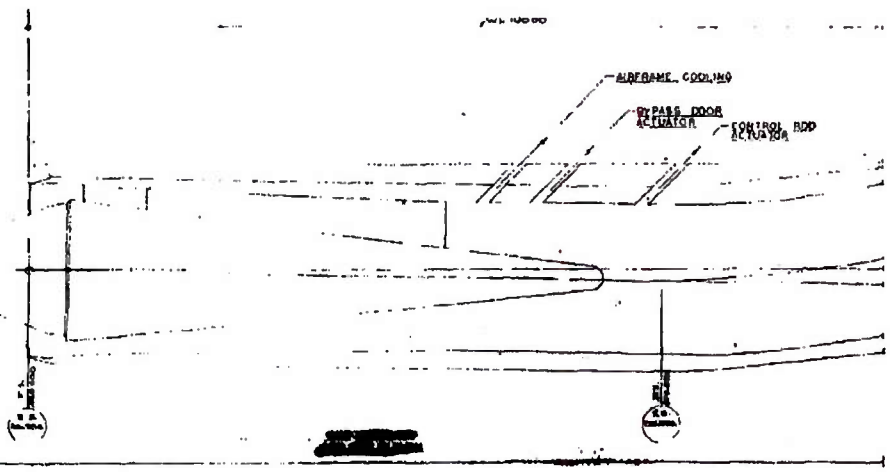

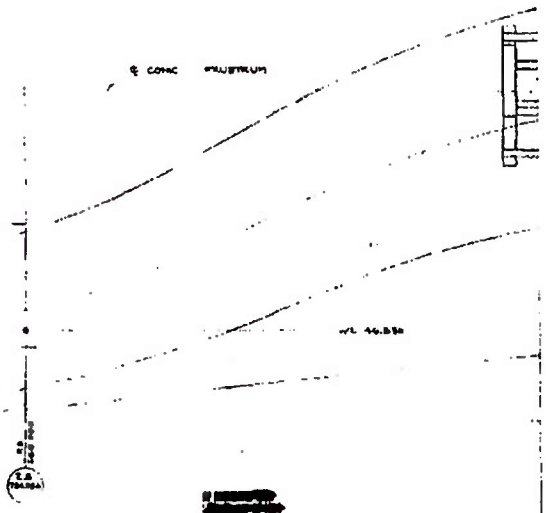

[redacted]

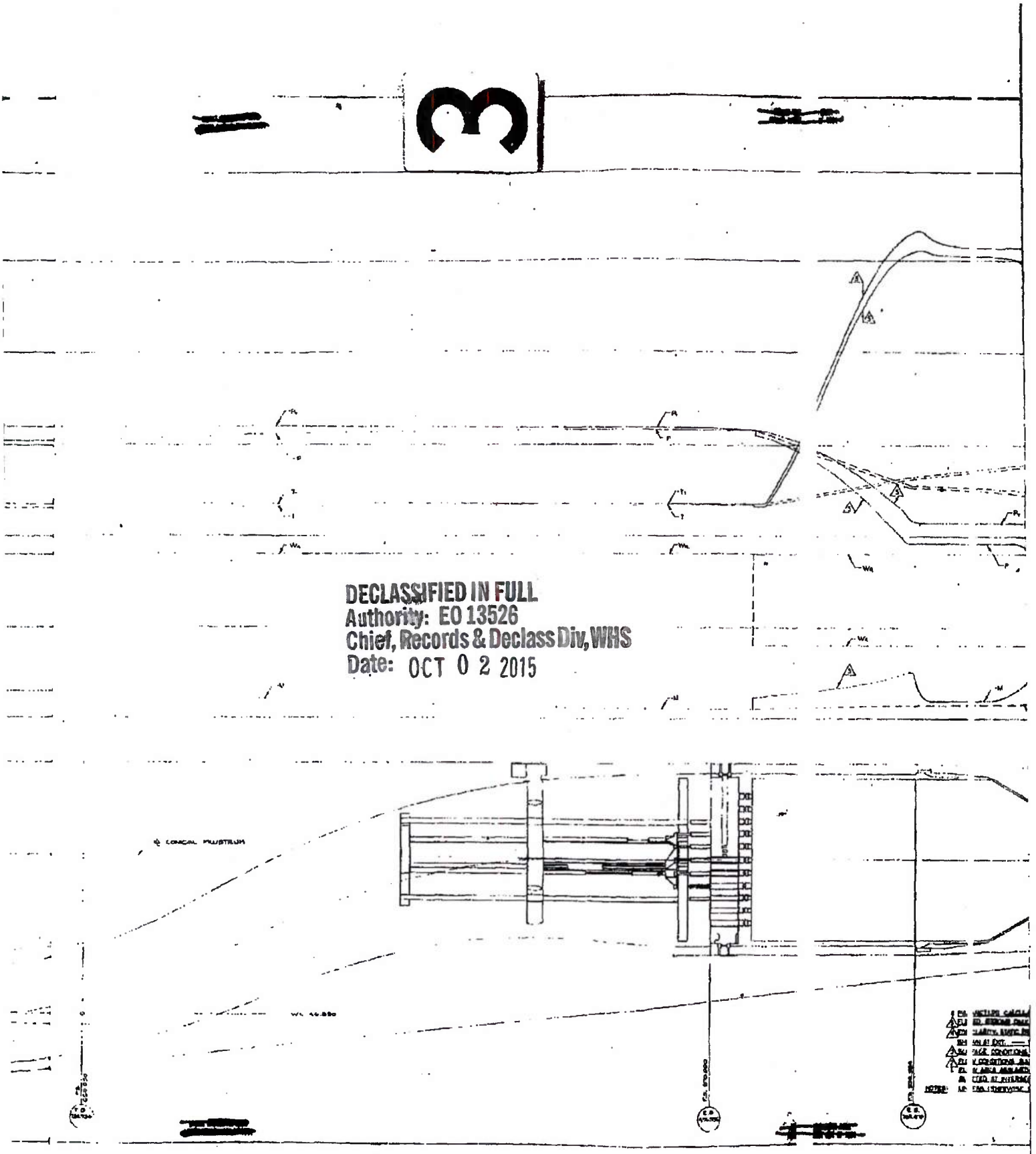

[redacted]

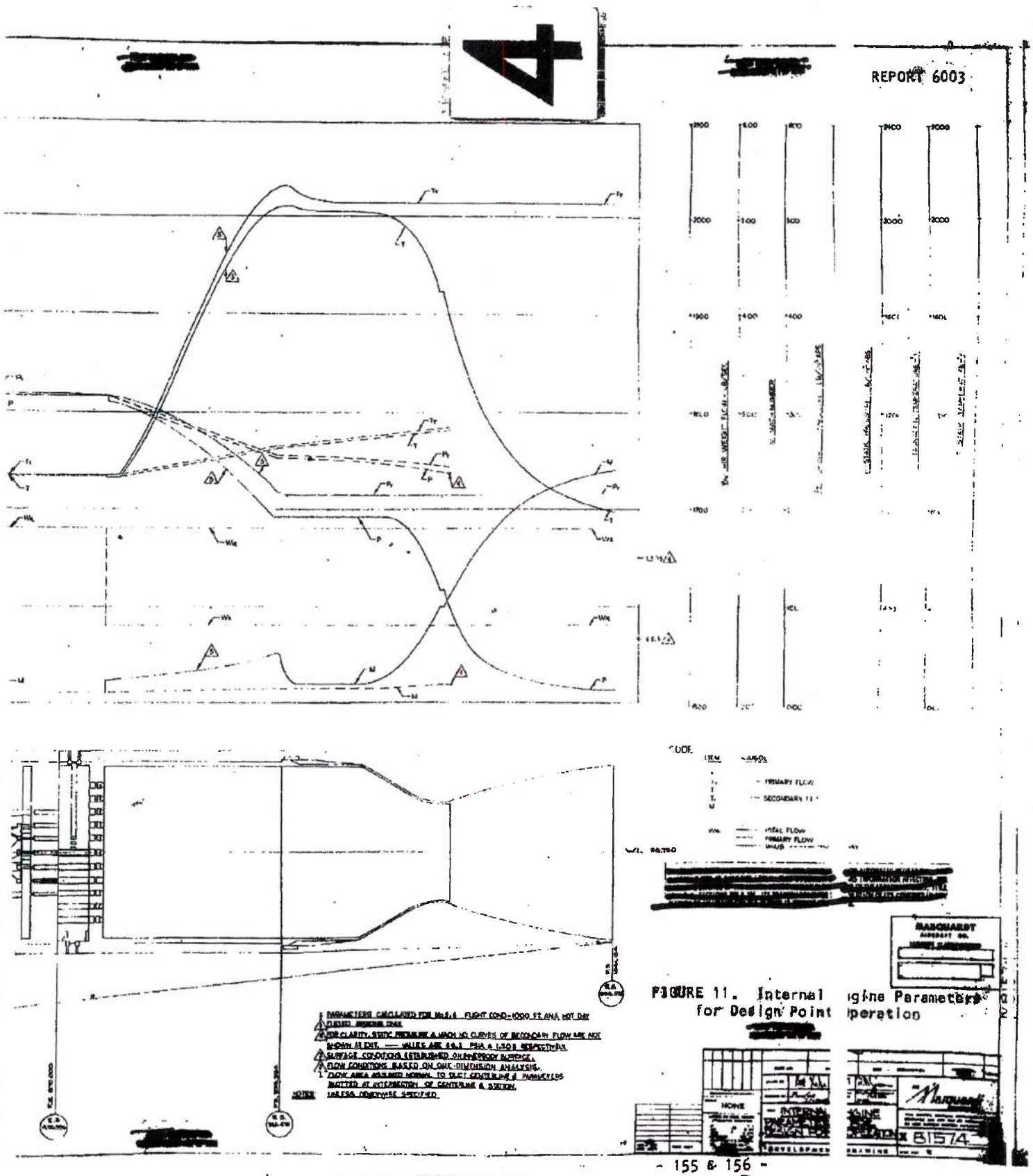

FIGURE 11. Internal [illegible]ngine Parameters for Design Point [illegible]peration

[redacted]

ASD-TDR-63-277, Vol. IV

SECRET ~~RESTRICTED DATA~~

~~ATOMIC ENERGY ACT OF 1954~~

ACTUA AIRFLOW — BY PASS DOORS MOTO
LOCATI OVERBOARD EXHAUST
W_a — MAX.

BOUNDARY-LAYER AIR BLEED
LOCATION: BLEED INLET
W_a — 80
A — 68
T_t 942

COOLING AIRFLOW — INLET INNERBODY
LOCATION: INSIDE INNERBODY STRUTS
W_a — 80
A — 130
T_t — 942

ACTUATING AIRFLOW — BY PASS DOORS MOTOR
LOCATION: AIR INLET FOR MOTOR
W_a — 8 MAX.
T_t — 942
R — 45 TO 350

COOLING AIRFLOW — IRFRAME
LOCATION: BLEED E RANCE FROM
W_a — 41
T_t — 942

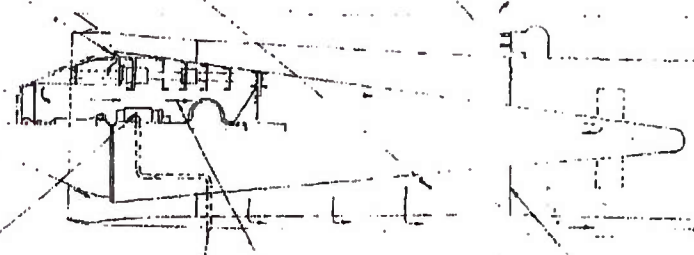

ACTUATING AIRFLOW — NOSE SPIKE MOTOR
LOCATION: AIR INLET FOR MOTOR
W_a — 5 MAX.

COOLING AIRFLOW — INLET NERBODY
LOCATION: INSIDE INNE DY
W_a — 80
T_t — 942

ACTUATING AIRFLOW — NOSE SPIKE MOTOR
LOCATION: OVERBOARD EXHAUST
W_a — 5 MAX.

1

SECRET ~~RESTRICTED DATA~~

~~ATOMIC ENERGY ACT OF 1954~~

[redacted]

8 7 6

[redacted]

2

ACTUATING AIRFLOW — BY PASS DOORS, MOTOR
LOCATION: OVERBOARD EXHAUST
W_a — 5 MAX.

COOLING AIRFLOW — SHADOW SHIELD
LOCATION: AVERAGE SECTION THRU SHIELD
W_a — 5.8
T_r — 94.2
TEMP OF SHIELD — 1200

AIRFLOW — BY PASS DOORS MOTOR
LOCATION: INLET FOR MOTOR
MAX.
TO 350

COOLING AIRFLOW — AIRFRAME
LOCATION: BLEED ENTRANCE FROM MAIN DUCT
W_a — 41
T_r — 94.2

AIR CONDITIONING SYSTEM
LOCATION: EQUIPMENT COMPARTMENT
W_a — 5.5

ACTUATING AIRFLOW — CONTROL ROD MOTOR
LOCATION: AIR FOR MOTOR
W_a — 17 MAX
T_r — 81.2
P — 31.3

EXHAUST AIRFLOW — CONTROL
LOCATION: AIRFLOW EXHAUST
W_a — 17 MAX.

COOLING AIRFLOW — INLET INNERBODY
LOCATION: INSIDE INNERBODY
W_a — 80
T_r — 94.2

COOLING AIRFLOW — INLET INNERBODY
LOCATION: OVERBOARD EXHAUST
W_a — 80
A — 110

COOLING AIRFLOW — AIRFRAME
LOCATION: AROUND ENGINE
W_a — 44
A — VARIABLE
T_r — 94.2
TEMP OF DUCT — 1160
TEMP OF FRAME — 1160
TEMP OF SKIN — 1000

AIRFLOW — NOSE SPIKE MOTOR
OVERBOARD EXHAUST
MAX.

STRUT SHOWN ROTATED TO BOTTOM ℄ FOR DWG CLARITY ONLY
LOWER STRUTS ACTUAL POSITION — 100° AND 210° FROM TOP ℄

[redacted]

[redacted]

X815

6 5 4

3

KING AIRFLOW - SHADOW SHIELD
ATION: AVERAGE SECTION THRU SHIELD
—— 3.6
—— 942
IR OF SHIELD — 1200

ACTUATING AIRFLOW - CONTROL ROD MOTOR
LOCATION: AIR INLET FOR MOTOR
W_a — 117 MAX.
T_t — 842
P — 313

EXHAUST AIRFLOW - CONTROL ROD MOTOR
LOCATION: AIRFLOW EXIT FROM AIRFRAME
W_a — 17 MAX.

COOLING AIRFLOW - REACTOR SUPPORT
LOCATION: AROUND REACTOR
W_a — 100
A — 100
T_t — 942
P_t — 313
TEMP OF SPRINGS — 1400
TEMP OF PRESSURE SHELL — 1200

COOLING AIRFLOW
LOCATION: ENTRA
W_a — 100
A — 72
T_t — 1069
P_t — 270
V — 268
T_w — 1180

UT NOZZLE
TO NOZZLE

COOLING AIRFL W - EXIT N
LOCATION: EXIT FOR EXIT
W_a — 100
A — 42
T_t — 1130
P_t — 55.5
V — 2448
T_w 1210

COOLING AIRFLOW - AIRFRAME
LOCATION: AROUND REACTOR
W_a — 41
A — 600
T_t 942
TEMP OF SUPPORT — 1200

COOLING AIRF
LOCATIONS: Te
W_a — 41
A — 60
T_t — 109
P_t — 45
V — 183
TEMP OF AIRF

AIRFRAME
FUSELAGE FRAME
— 1200

COOLING A FLOW - AIRF
LOCATION: BEHIND EXIT
W_a —
A — 78
T_t — 126
P_t — 3
V — 3

COOLING AIRFLOW - AIRFRAME
LOCATION: AROUND ENGINE DUCT
W_a — 41
A — VARIABLE
T_t 942
TEMP OF DUCT — 1160
TEMP OF FRAME — 1130
TEMP OF SKIN — 1000

NOTES

W_a FLOW — LBS/SEC
A FLOW AREA — IN^2
T_t TEMPERATURE - °F
P_t PRESSURE — LBS/IN^2 ABS.
V VELOCITY — FT/SEC
T_w TEMPERATURE OF AIRFRAME — °F
T_w TEMPERATURE OF NOZZLE — °F

ONLY
E

P. PRELIMINAR
1. ALL DATA F
NOTE:

TA SHOWN, ADDITIONAL DATA WILL BE SHOWN WH
DESIGN POINT OPERATION AT M_0 2.0, 100K FT., AN

[redacted]

X81576 | 1 [redacted]

5 4 3 2

4

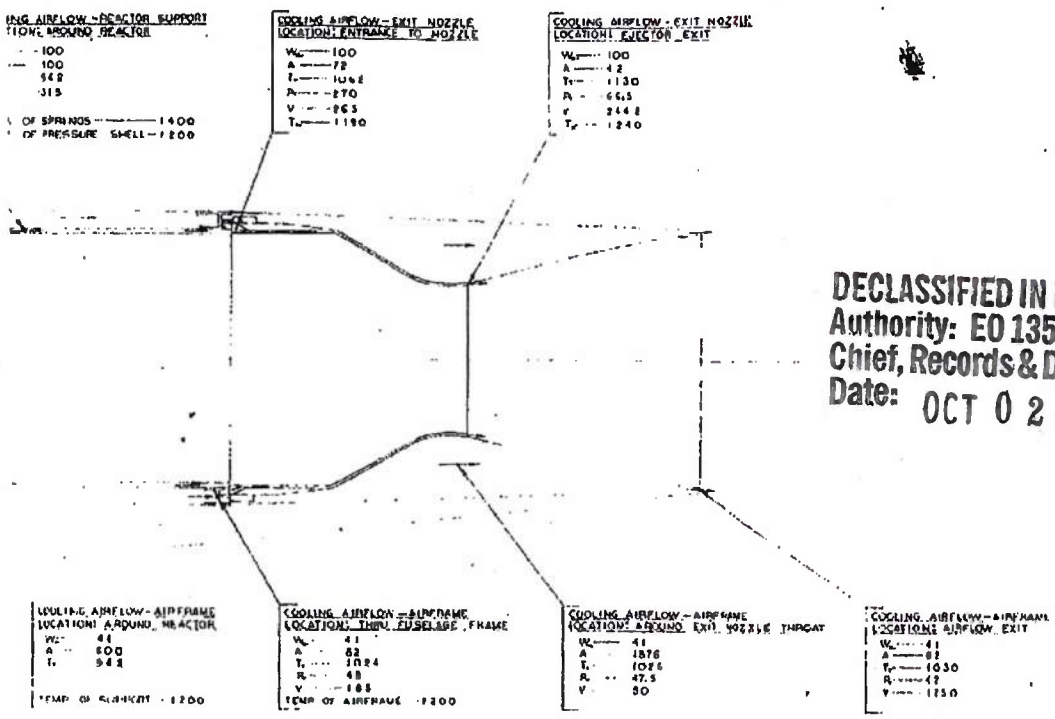

SYMBOLS

W_c AIRFLOW — LBS/SEC
A AIRFLOW AREA — IN^2
T_r AIR TEMPERATURE — °F
P_r AIR PRESSURE — LBS/IN^2 ABS.
V AIR VELOCITY — FT/SEC
T_c TEMPERATURE OF AIRFRAME — °F
T_w TEMPERATURE OF NOZZLE — °F

NOTES:

1. PRELIMINARY DATA SHOWN, ADDITIONAL DATA WILL BE SHOWN WHEN AVAILABLE.
2. ALL DATA FOR DESIGN POINT OPERATION AT M_0 2.8, 1000 FT., ANA 101 DAY.

FIGURE 12. MA50-X6B Propulsion System Auxiliary Air Requirements

[redacted]

Marquardt
MA50-X6
PROPULSION SY
AUXILIARY
REQUIRME
DEVELOPMENT
X81576

X81576A

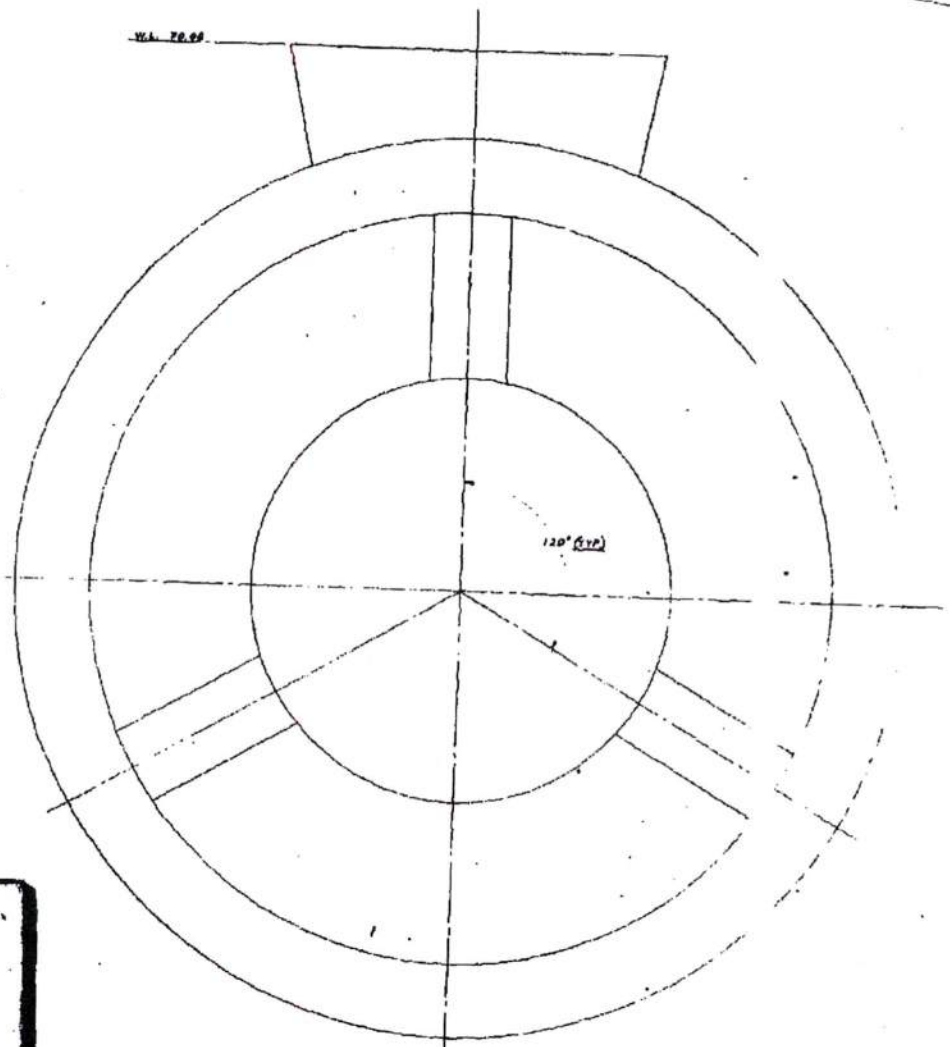

1

C - C

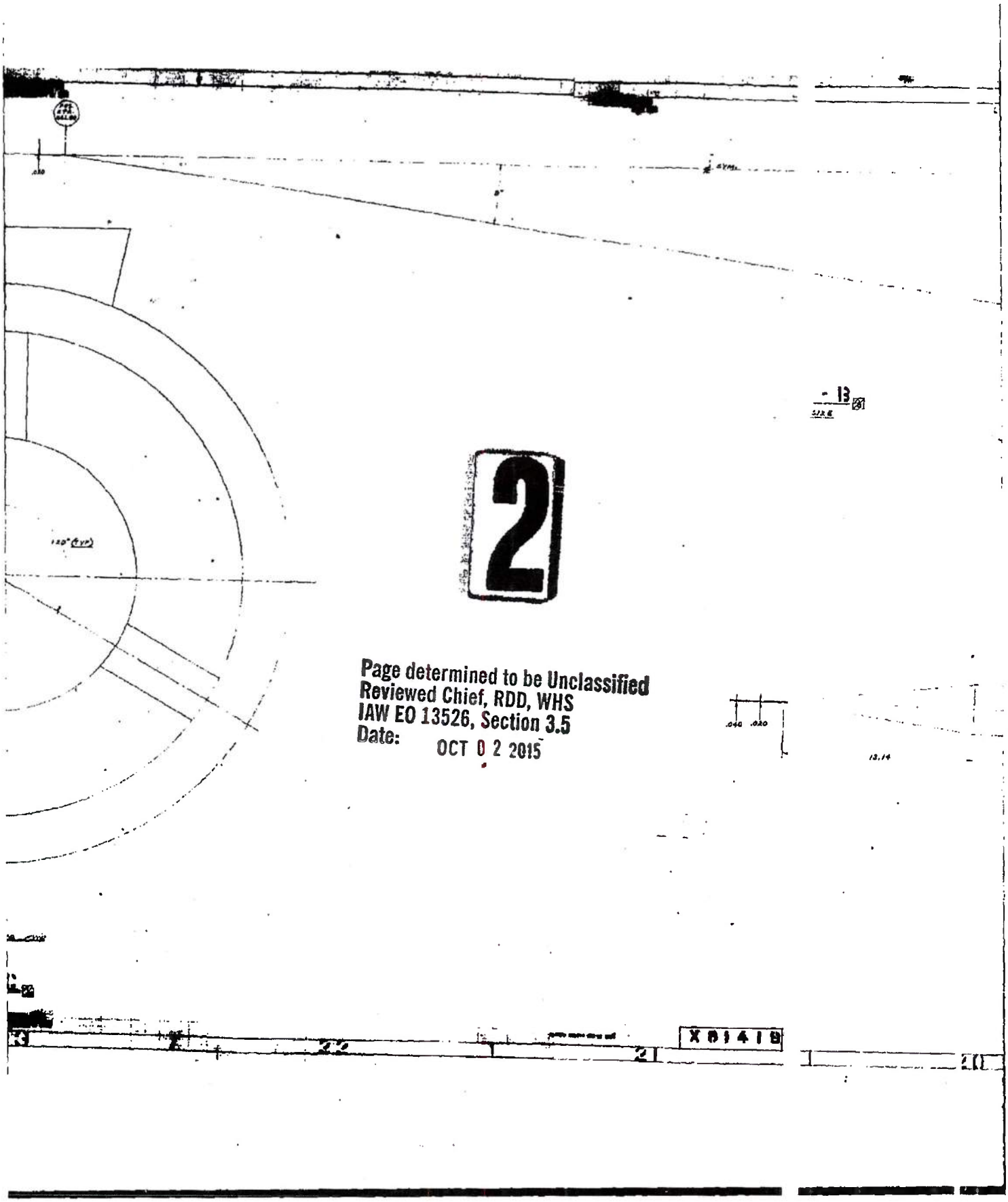
2
Page determined to be Unclassified
Reviewed Chief, RDD, WHS
IAW EO 13526, Section 3.5
Date: OCT 0 2 2015
X 8 1 4 1 8

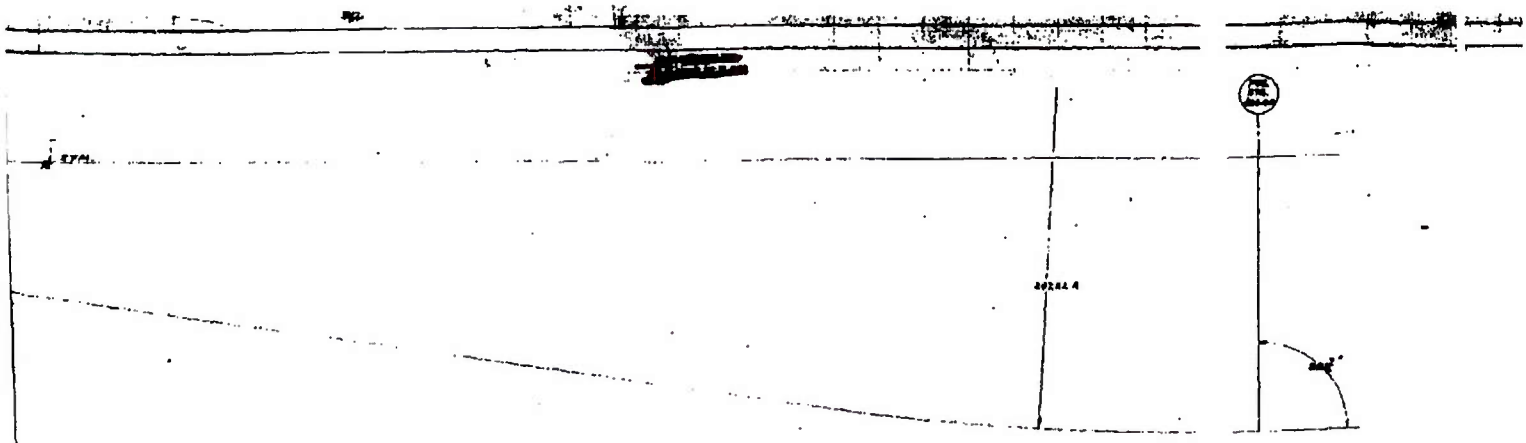

B - B

3

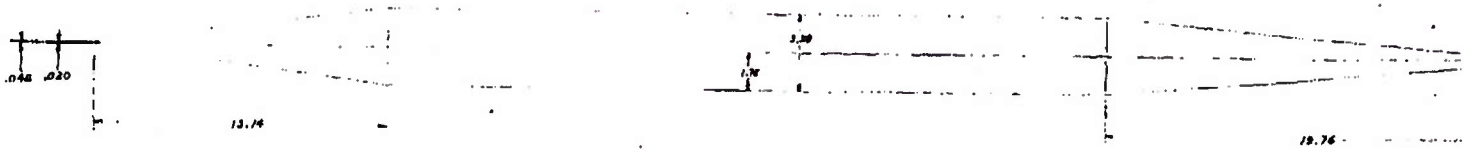

A - A

[redacted]

FUS STA	W.L.	O	R.	R.
[illegible]	[illegible]	[illegible]	[illegible]	[illegible]

AS DETAILED ON REVD. OF DRAWING

4

W.L. 46.85

19.76

DECLASSIFIED IN FULL
Authority: EO 13526
Chief, Records & Declass Div, WHS
Date: OCT 0 2 2015

[redacted]

X 8 1 4 1 9

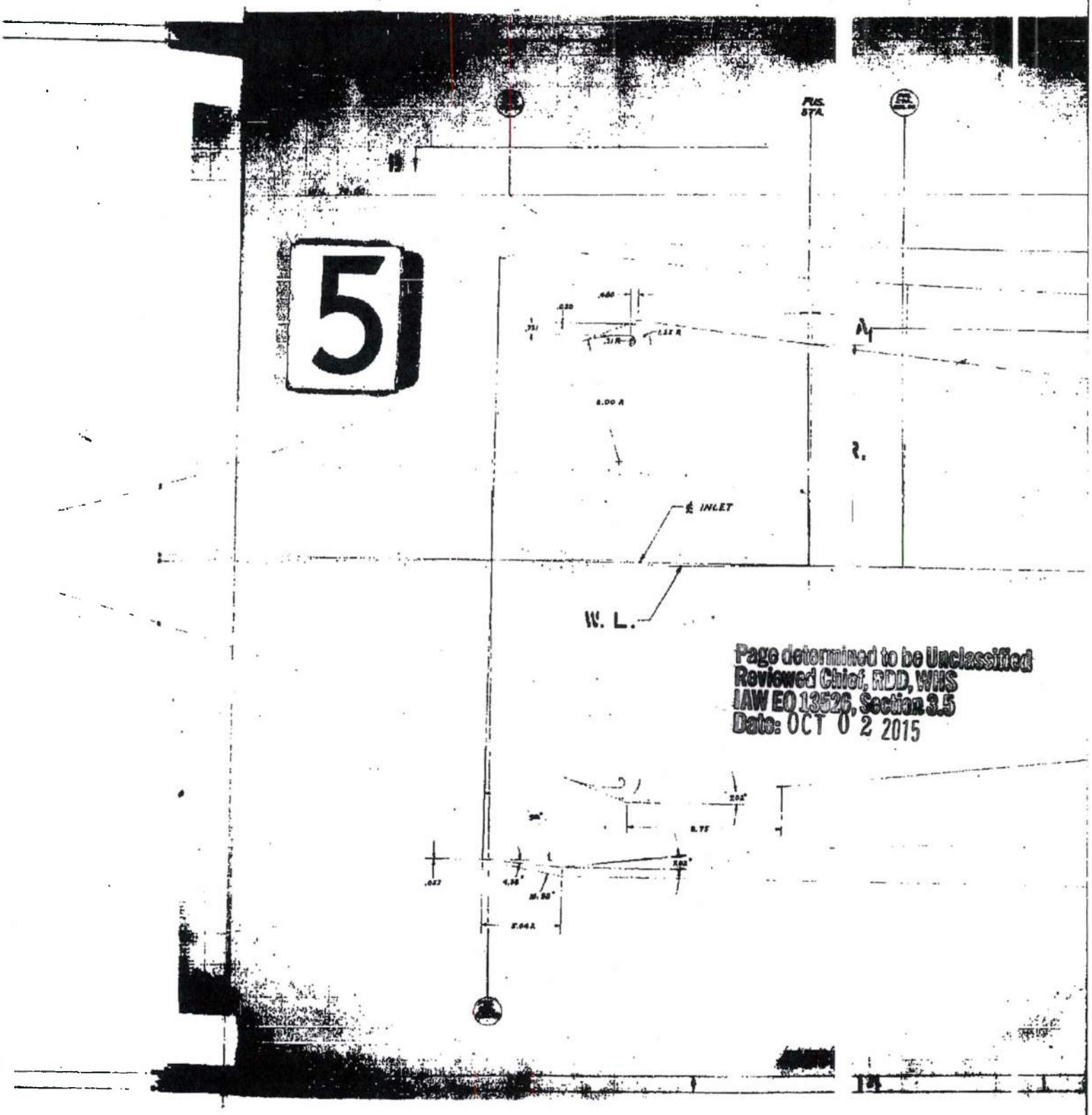

6

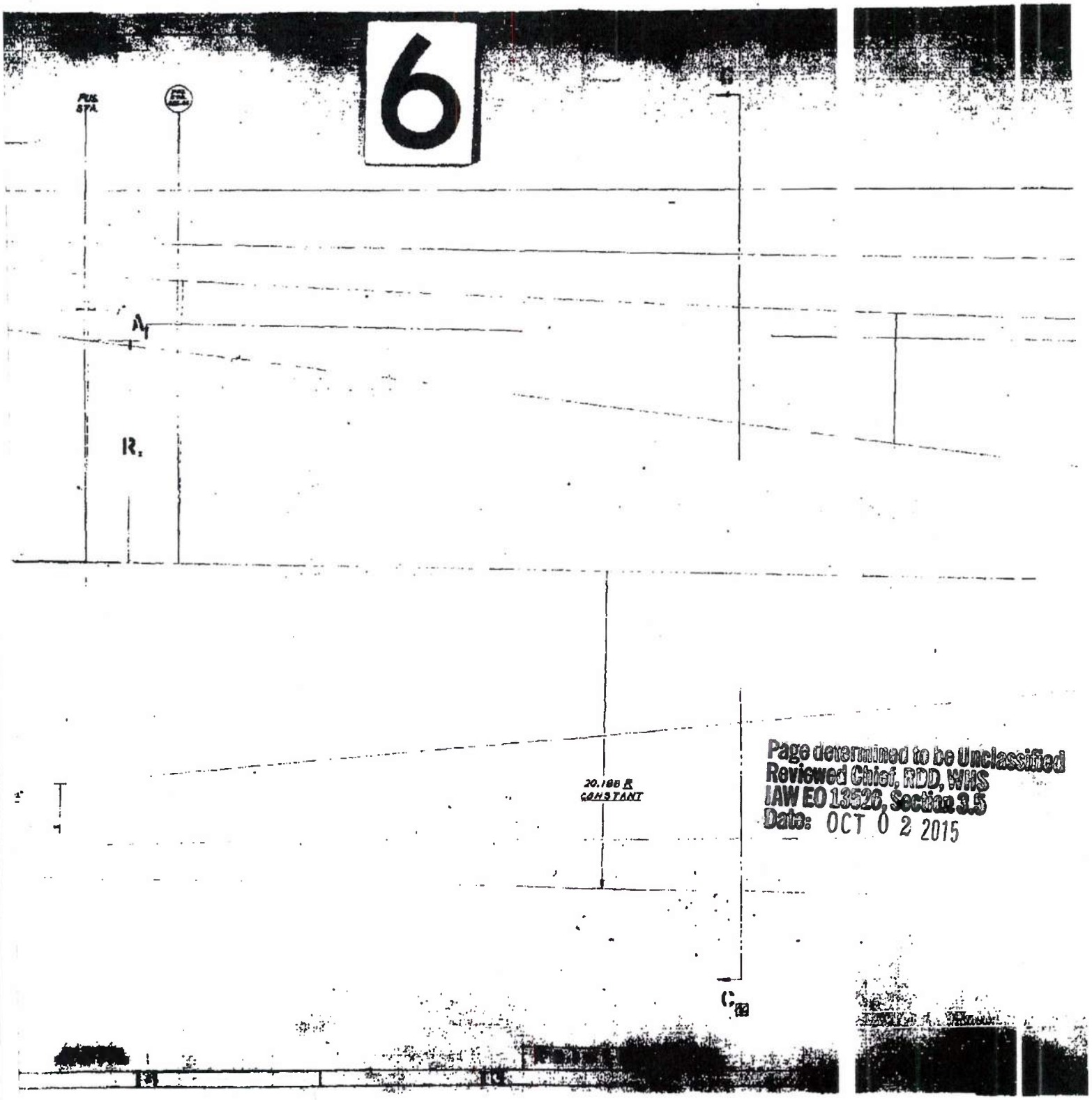

7

7A

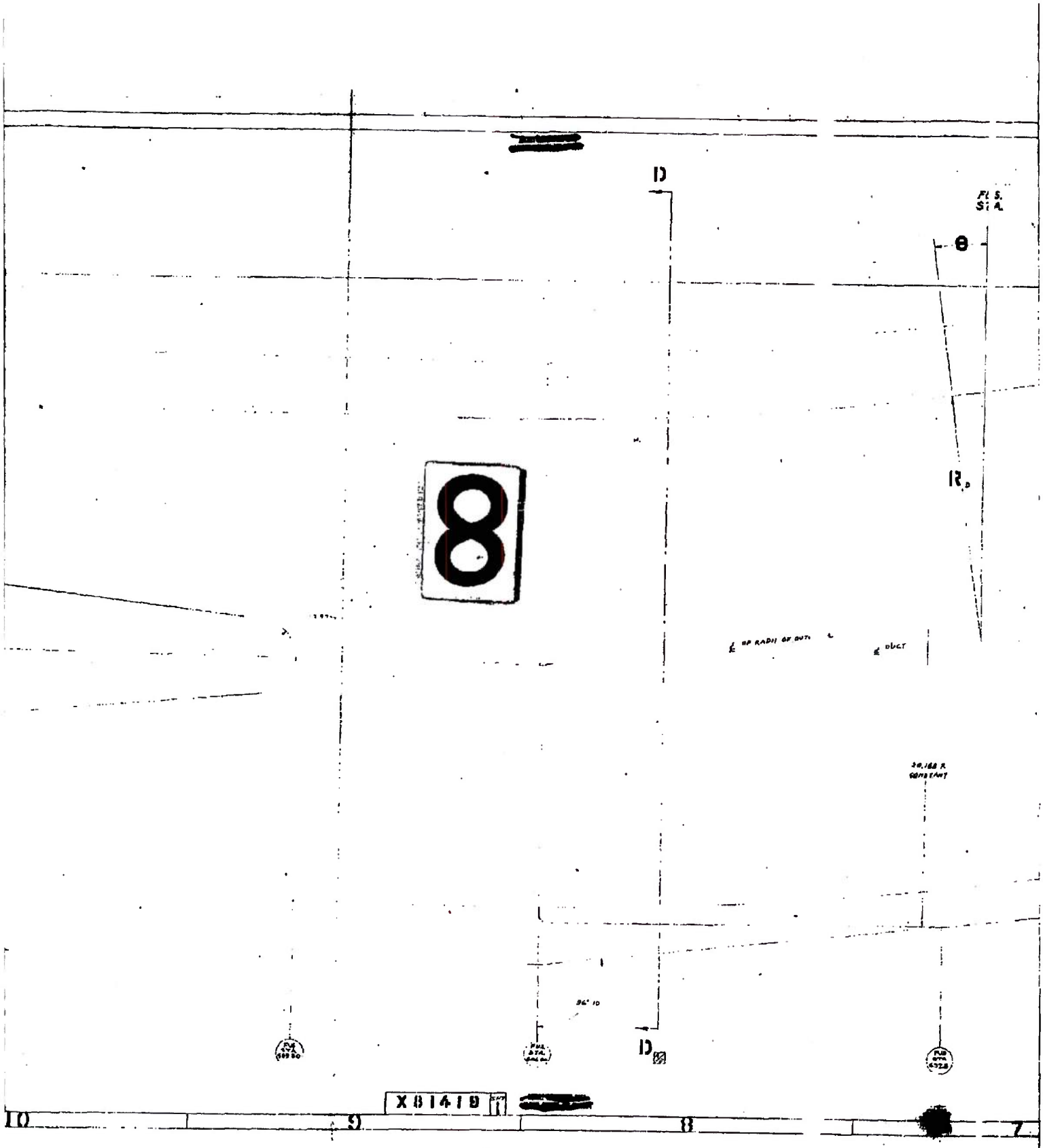

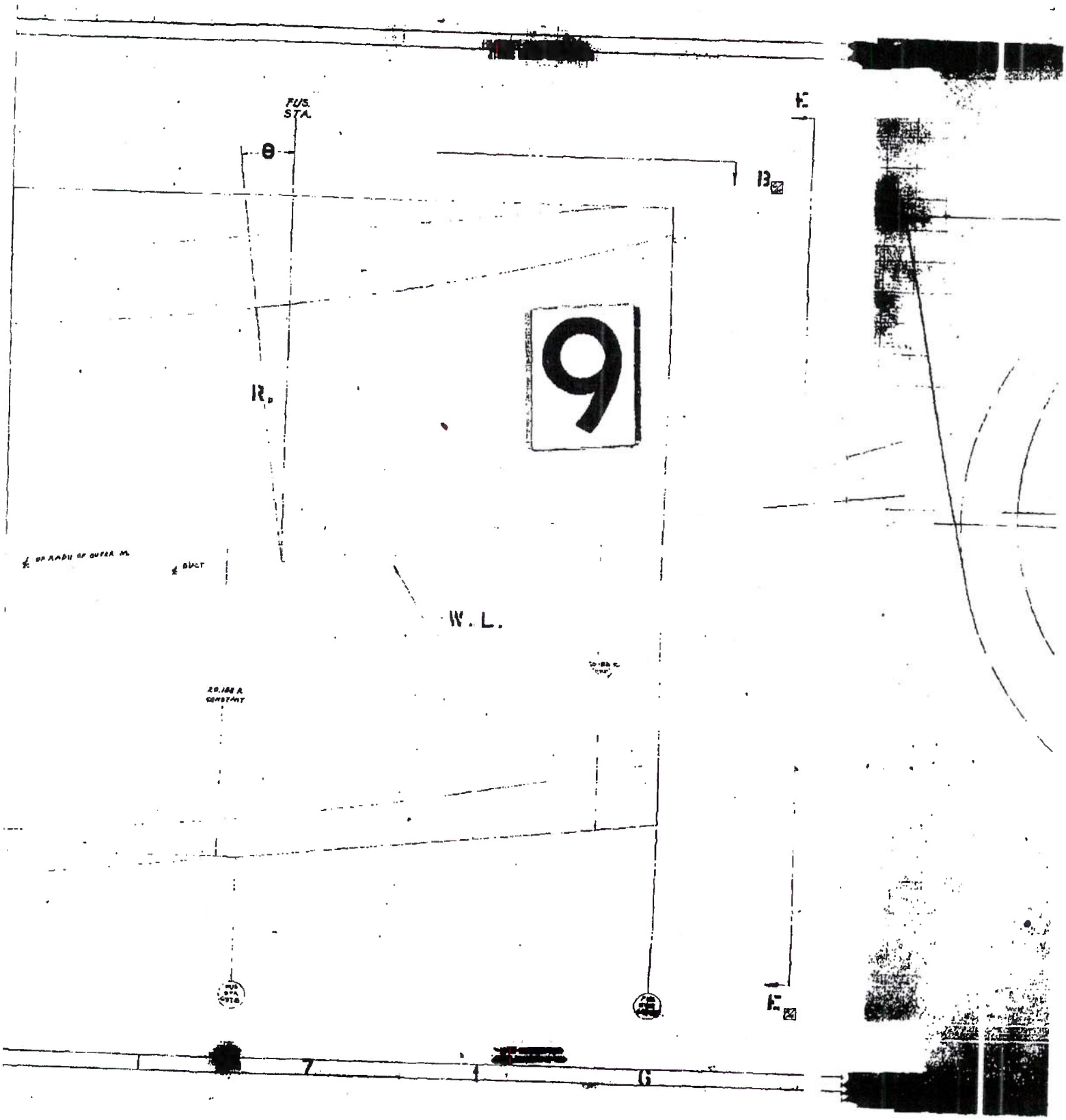

10

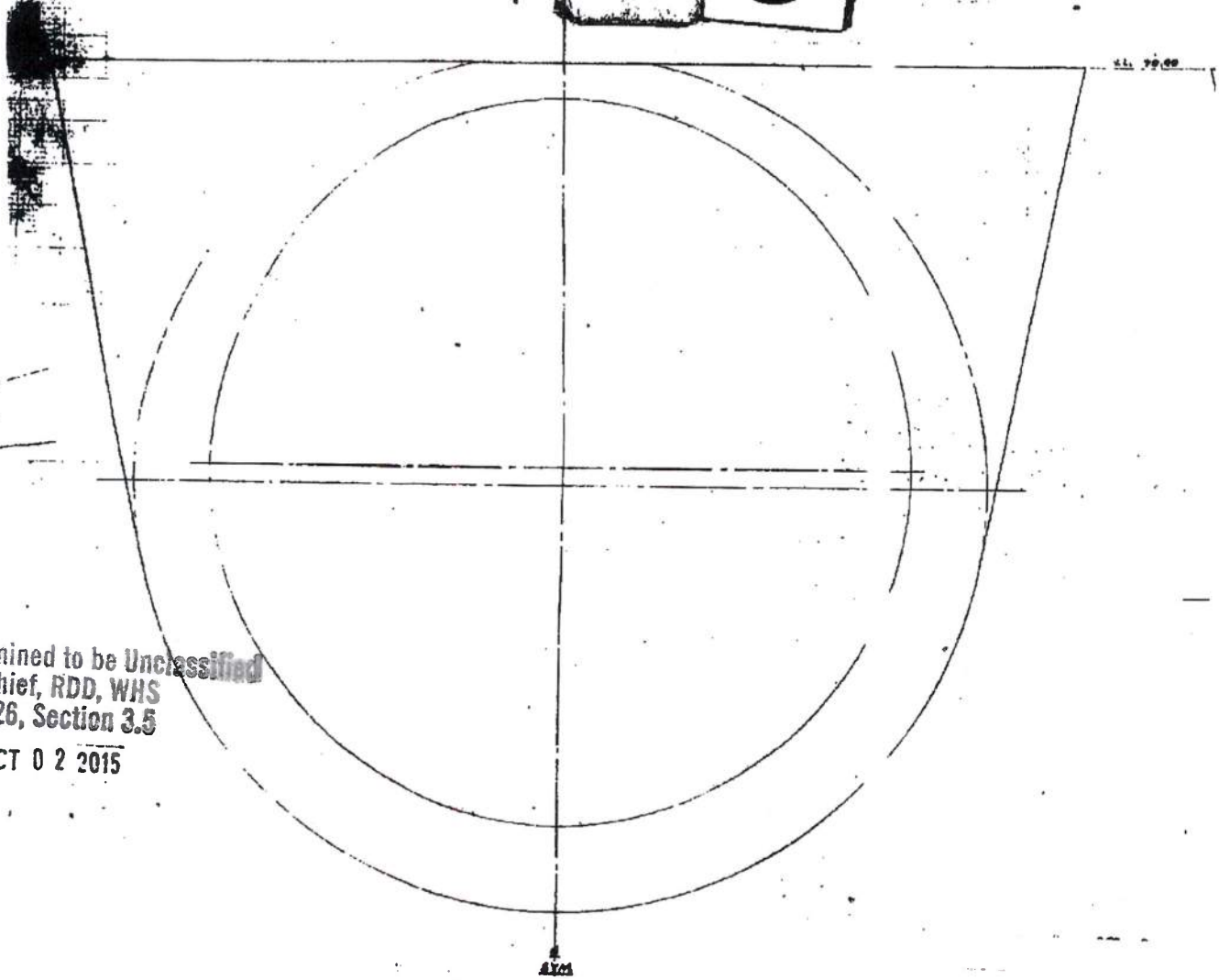

11

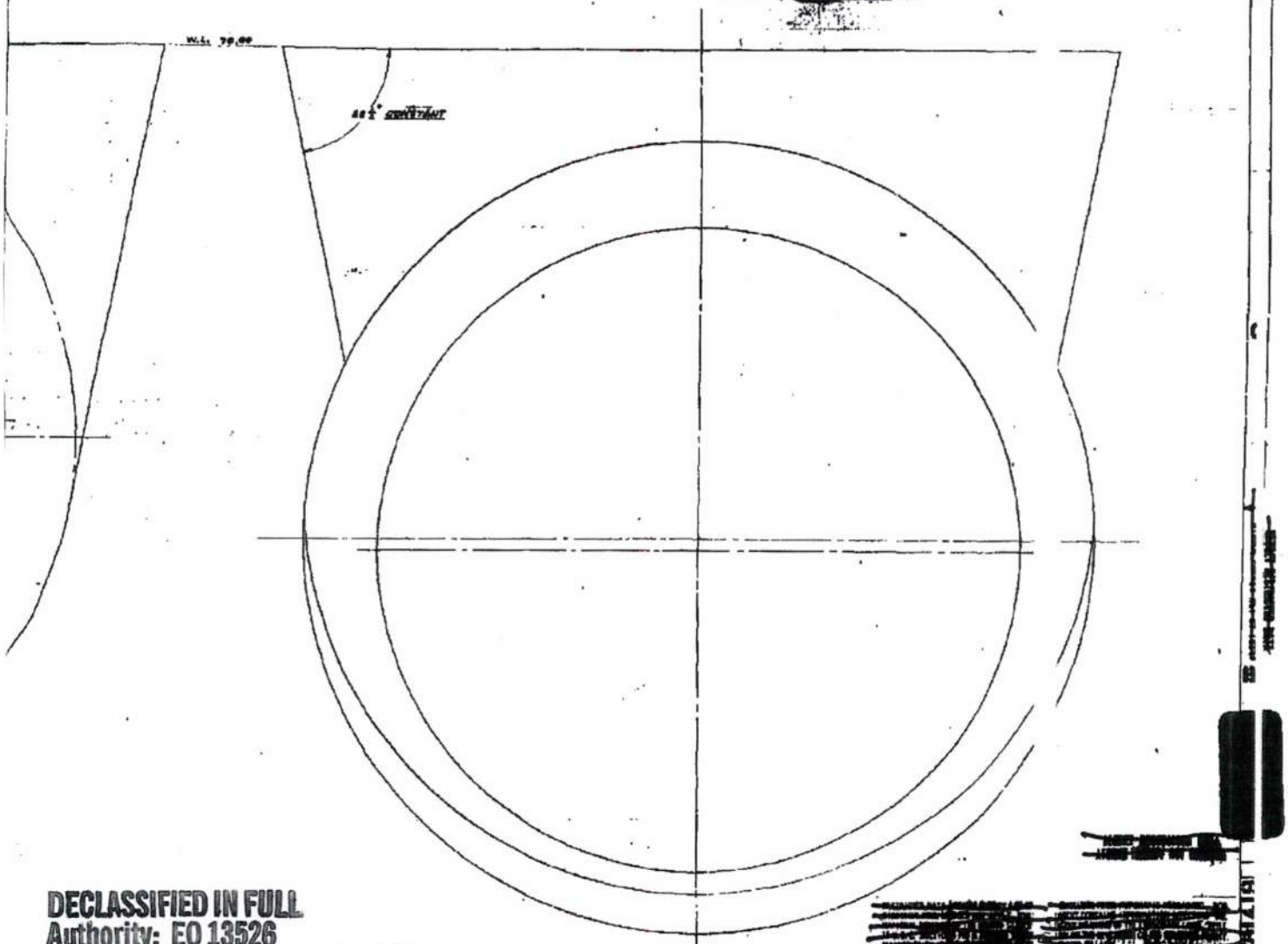

FIGURE 13

12 - 12

SIGN LAYOUT

1

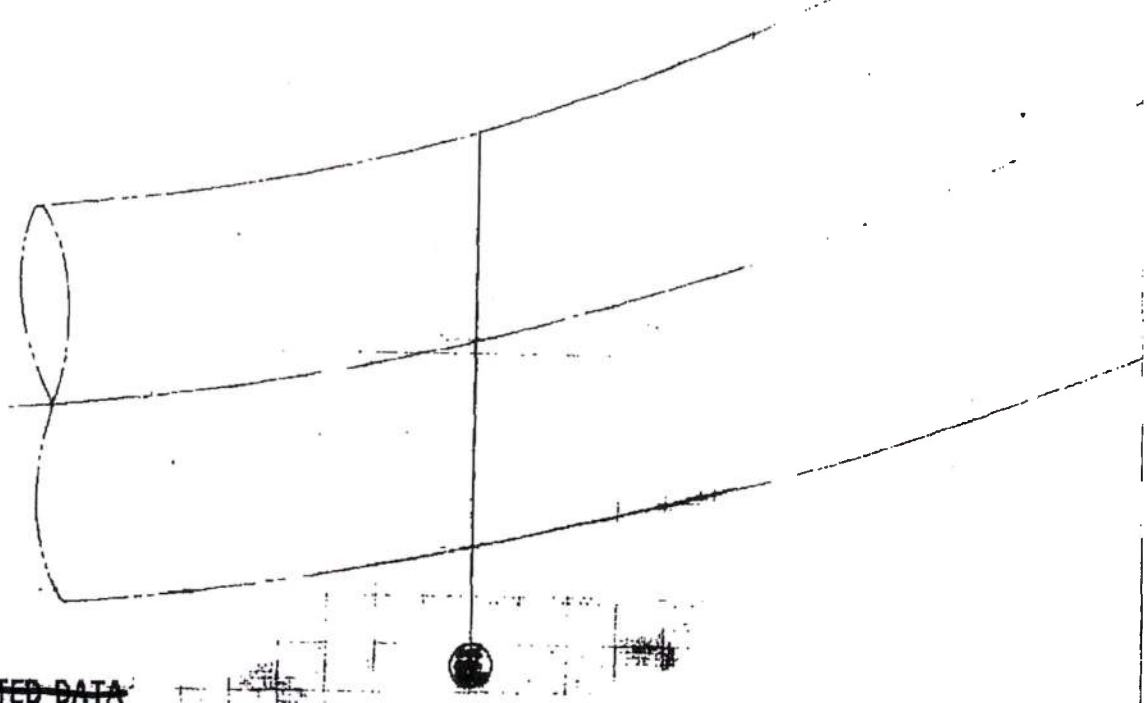

X6

2

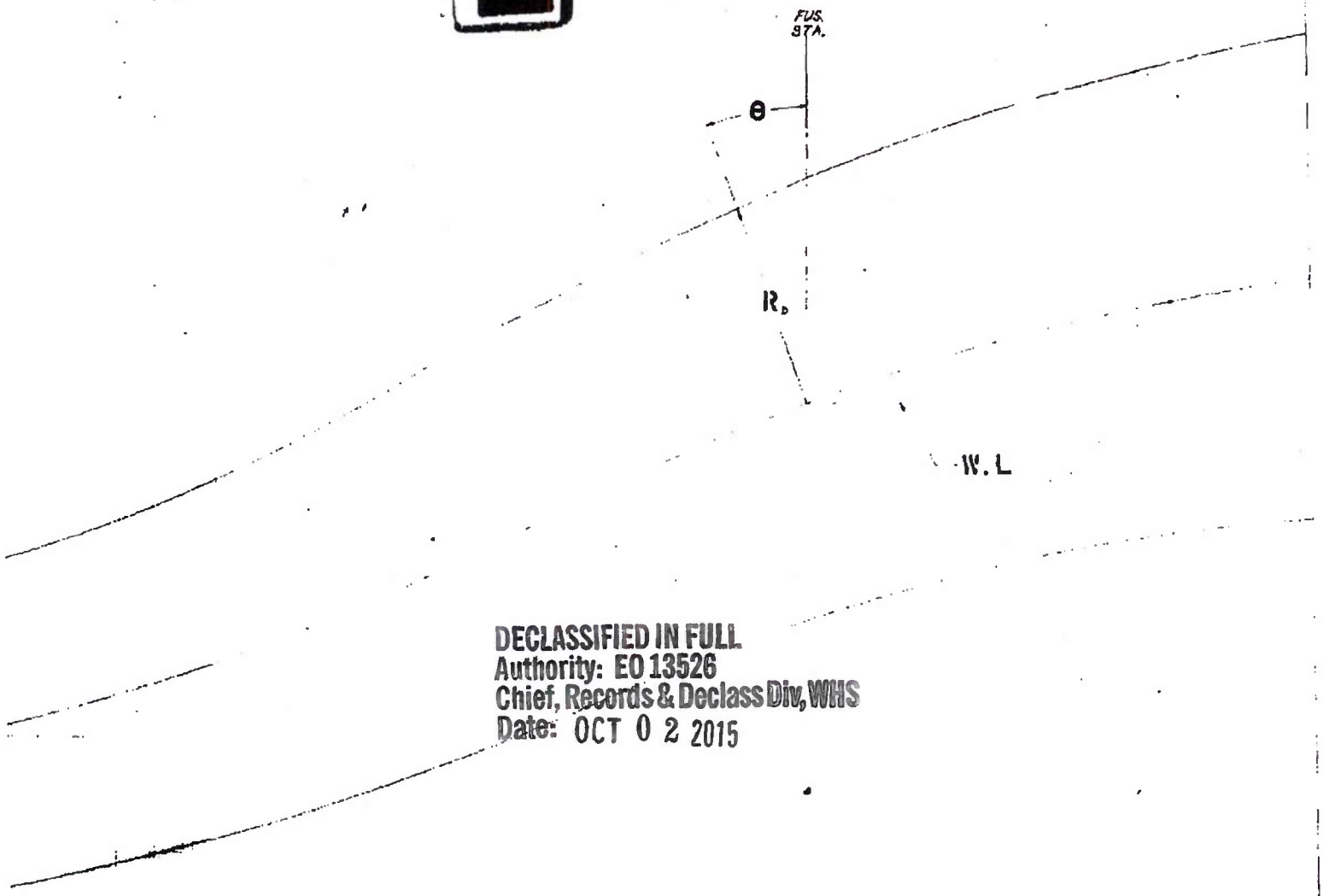

DUCT FROM FU STA. 660.00 TO FUS. STA. 670.00
± SIZE

REFER TO DW 1 FOR TABLE OF DIMENSIONS

X61419 2

5 4 3

[redacted]

3

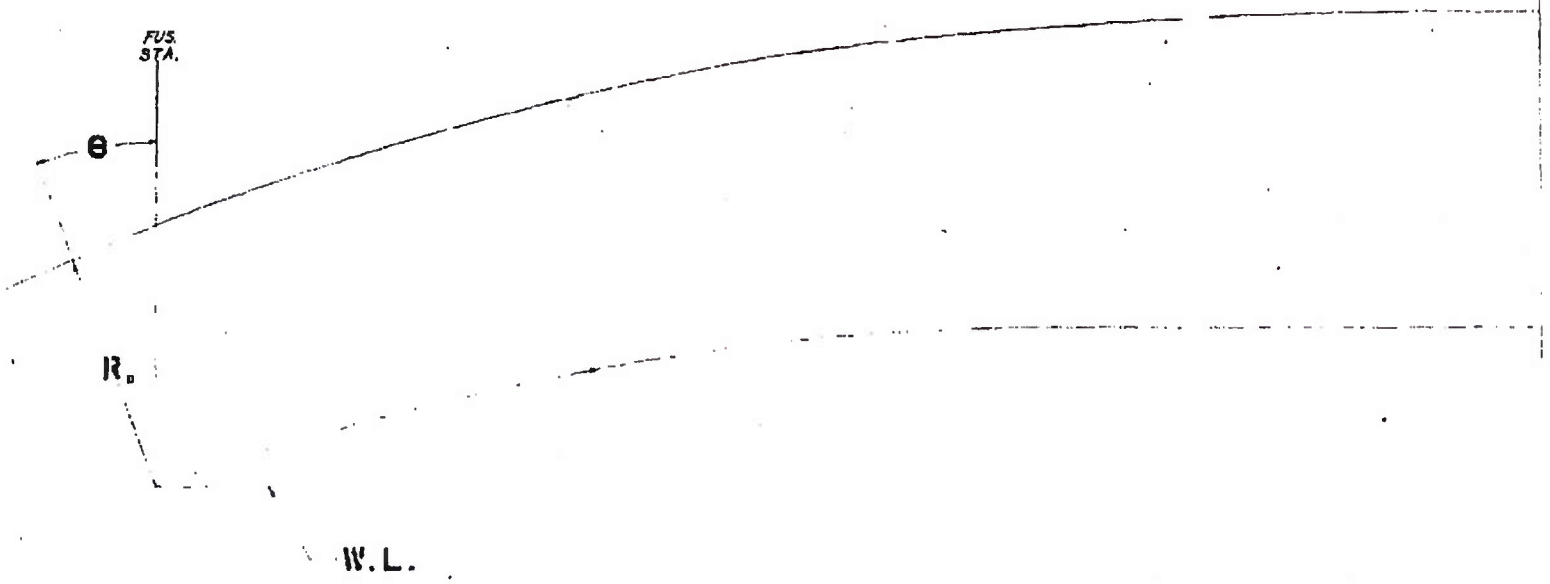

FIGURE 1/. Desig

[redacted]

DUCT FROM FUS. STA. 660.00 TO FUS. STA. 870.00
± SIZE
REFER TO PART I CEB TABLE OF DIMENSIONS

[redacted]

4 3 2

- 161 C

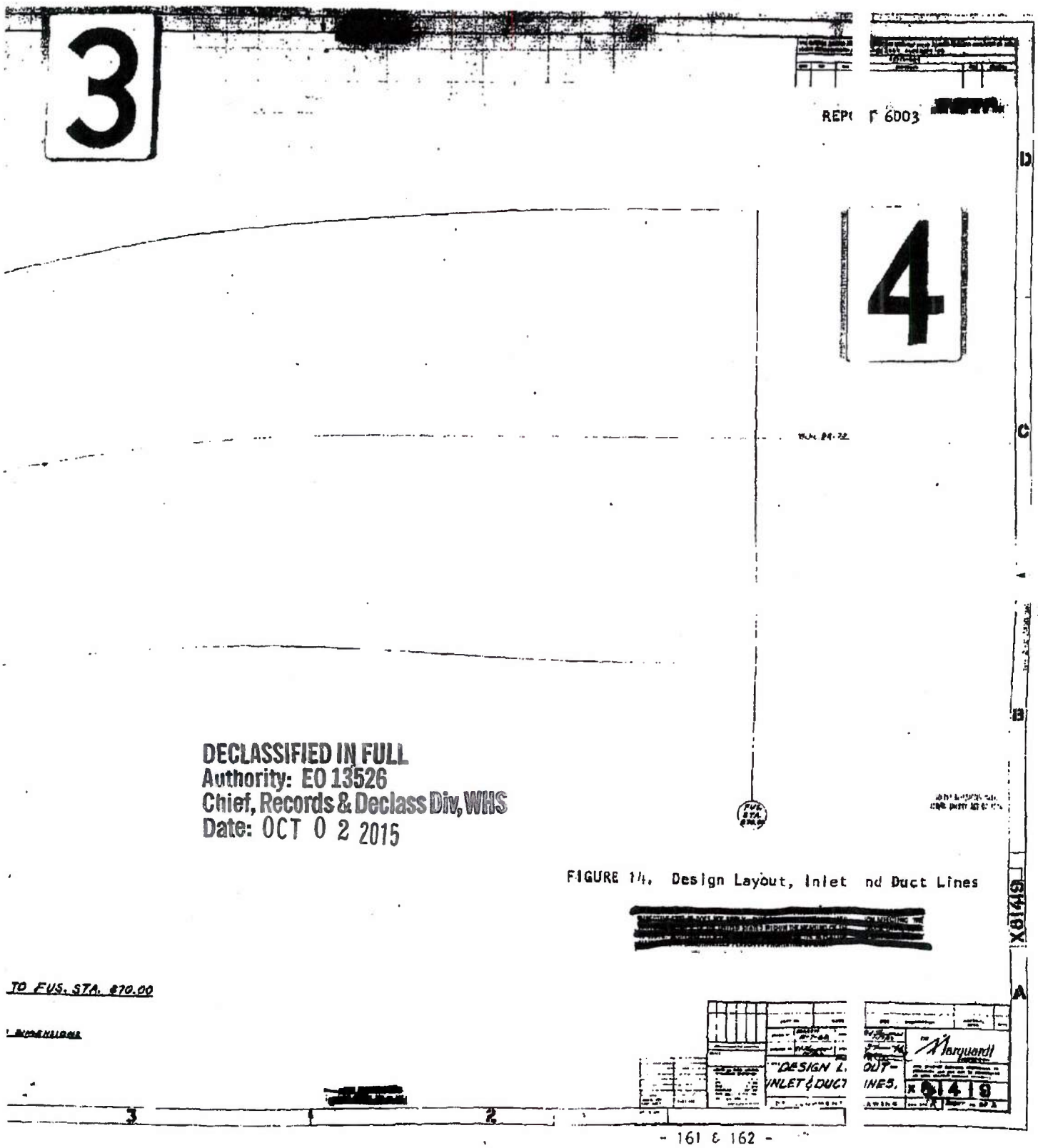

FIGURE 14. Design Layout, Inlet nd Duct Lines

[redacted]

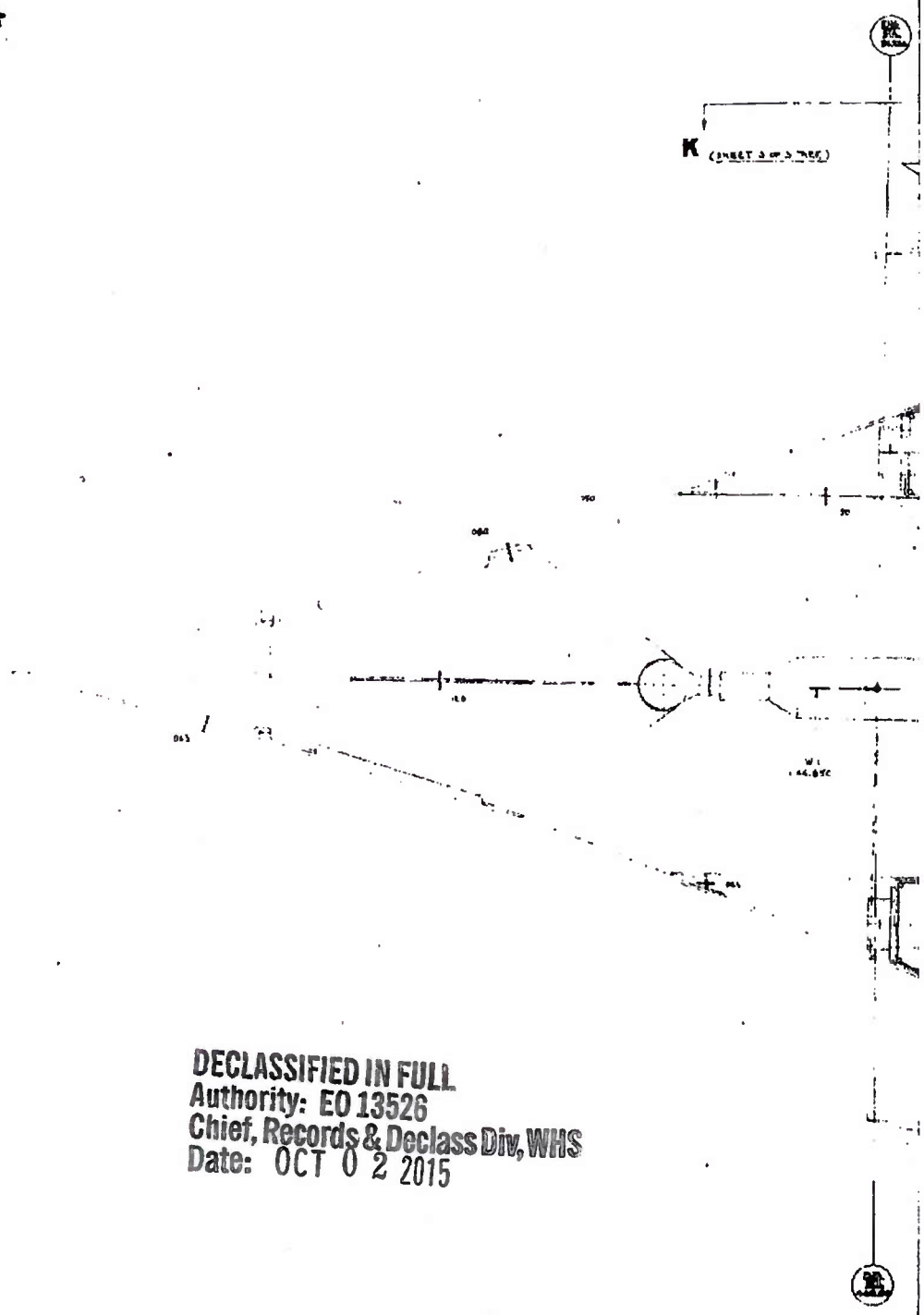

1

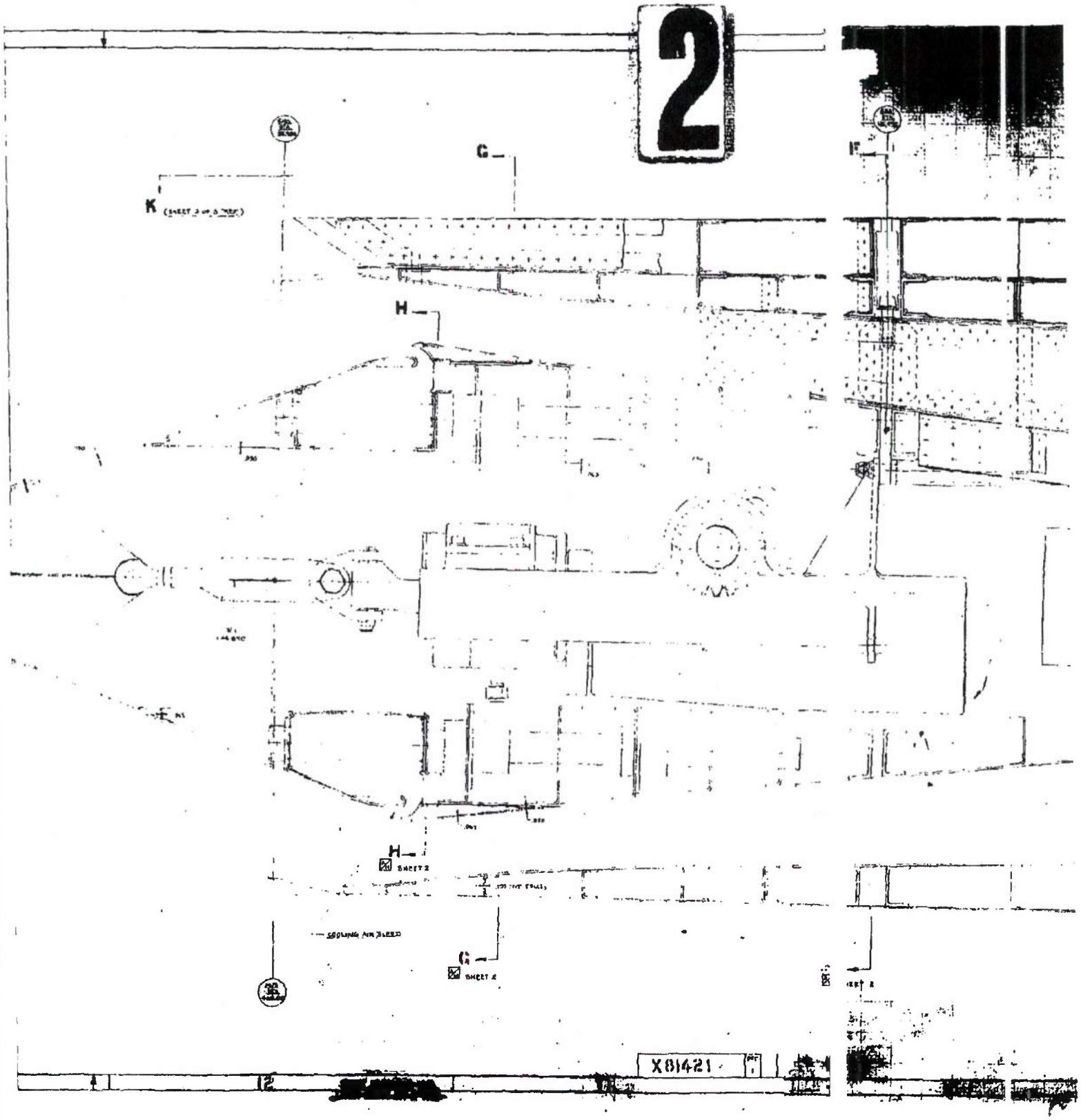

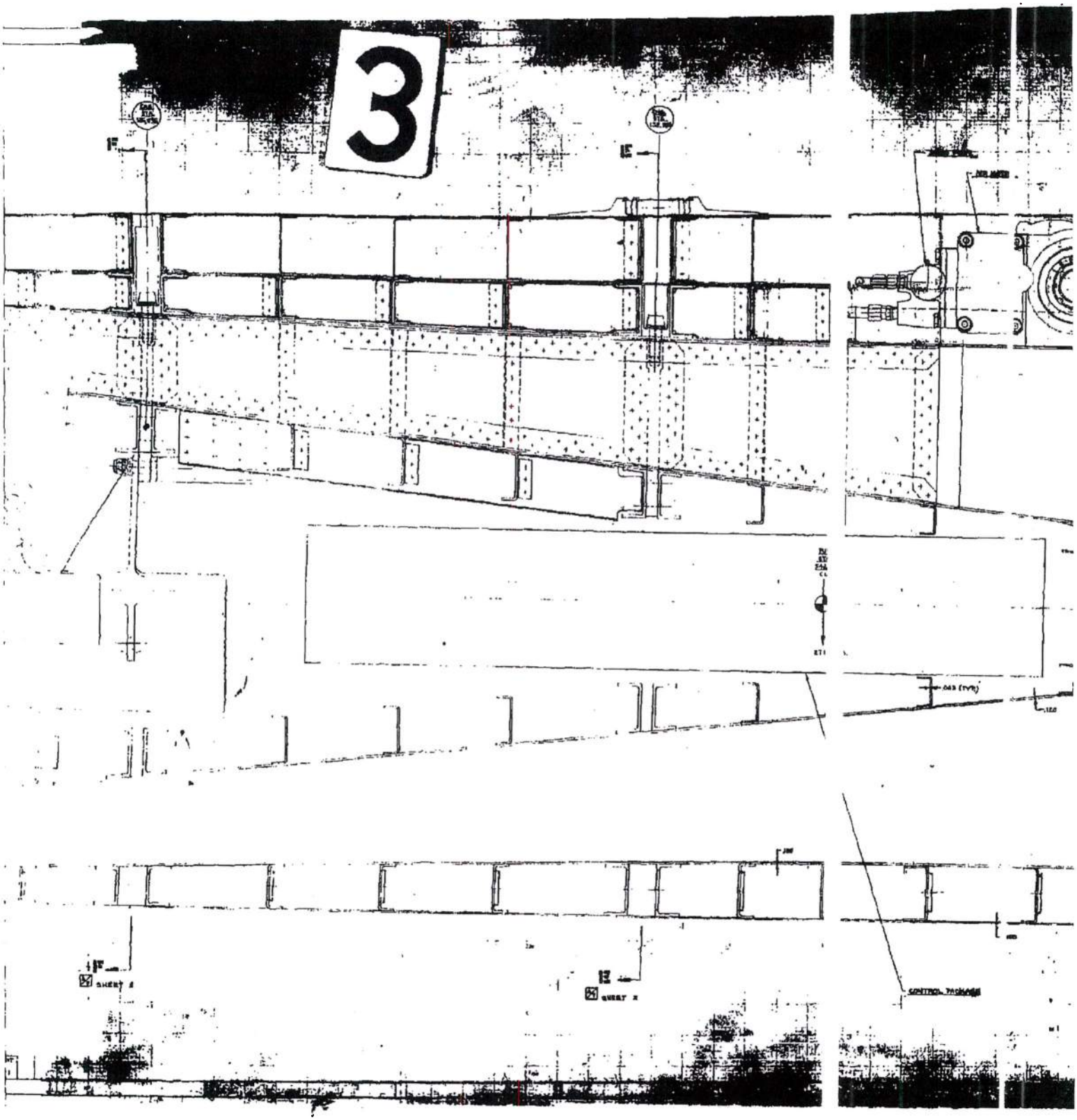

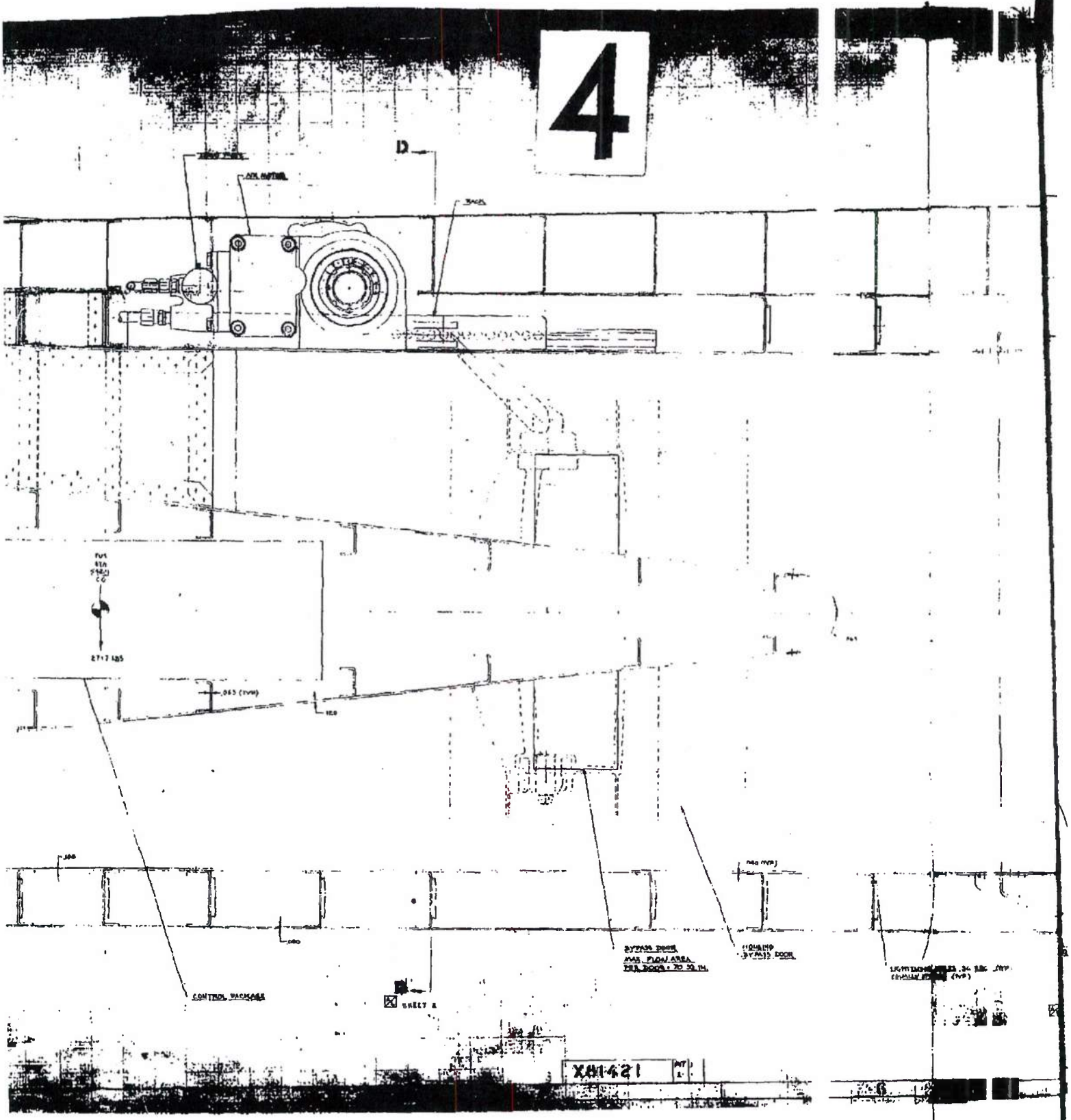

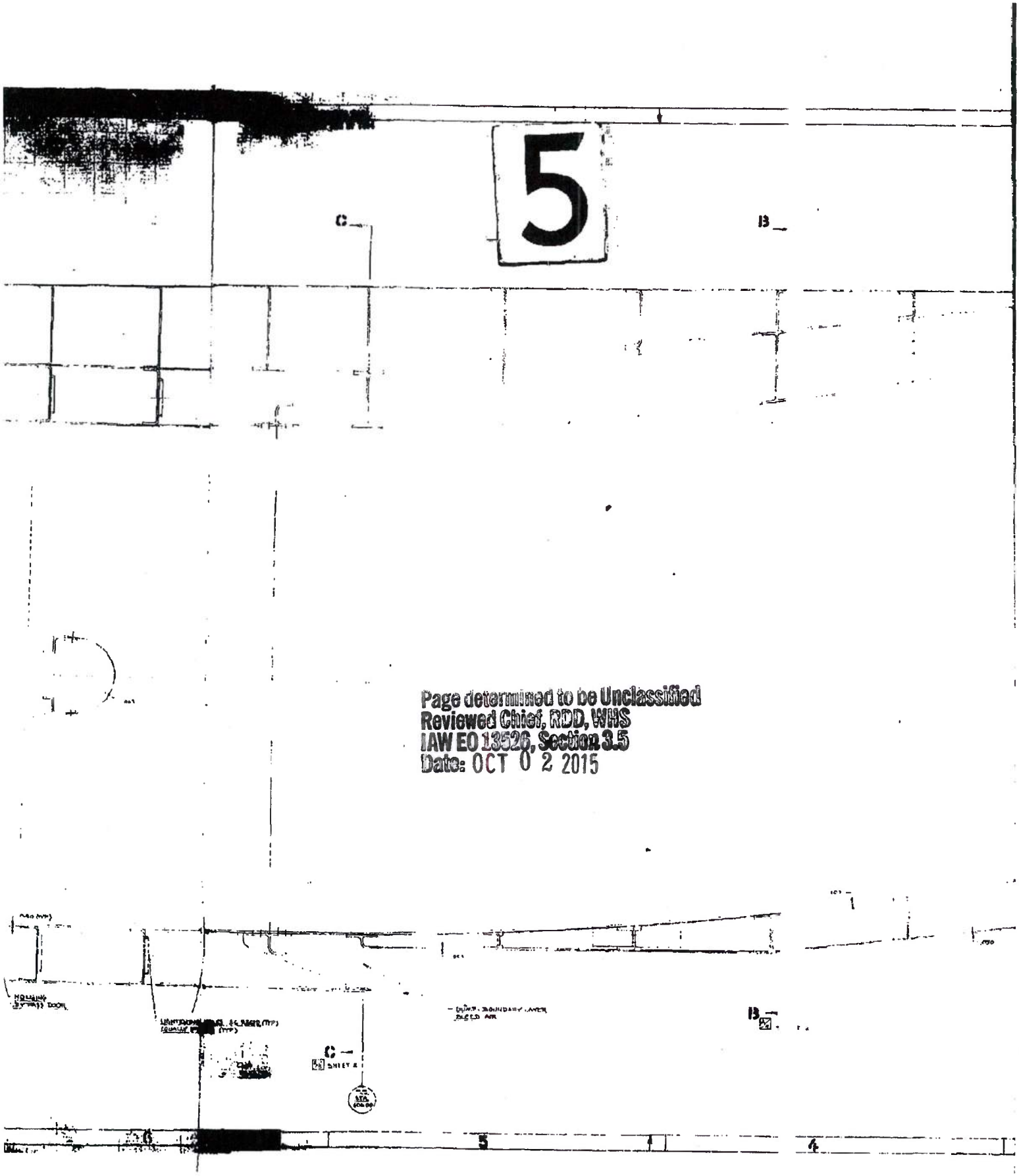

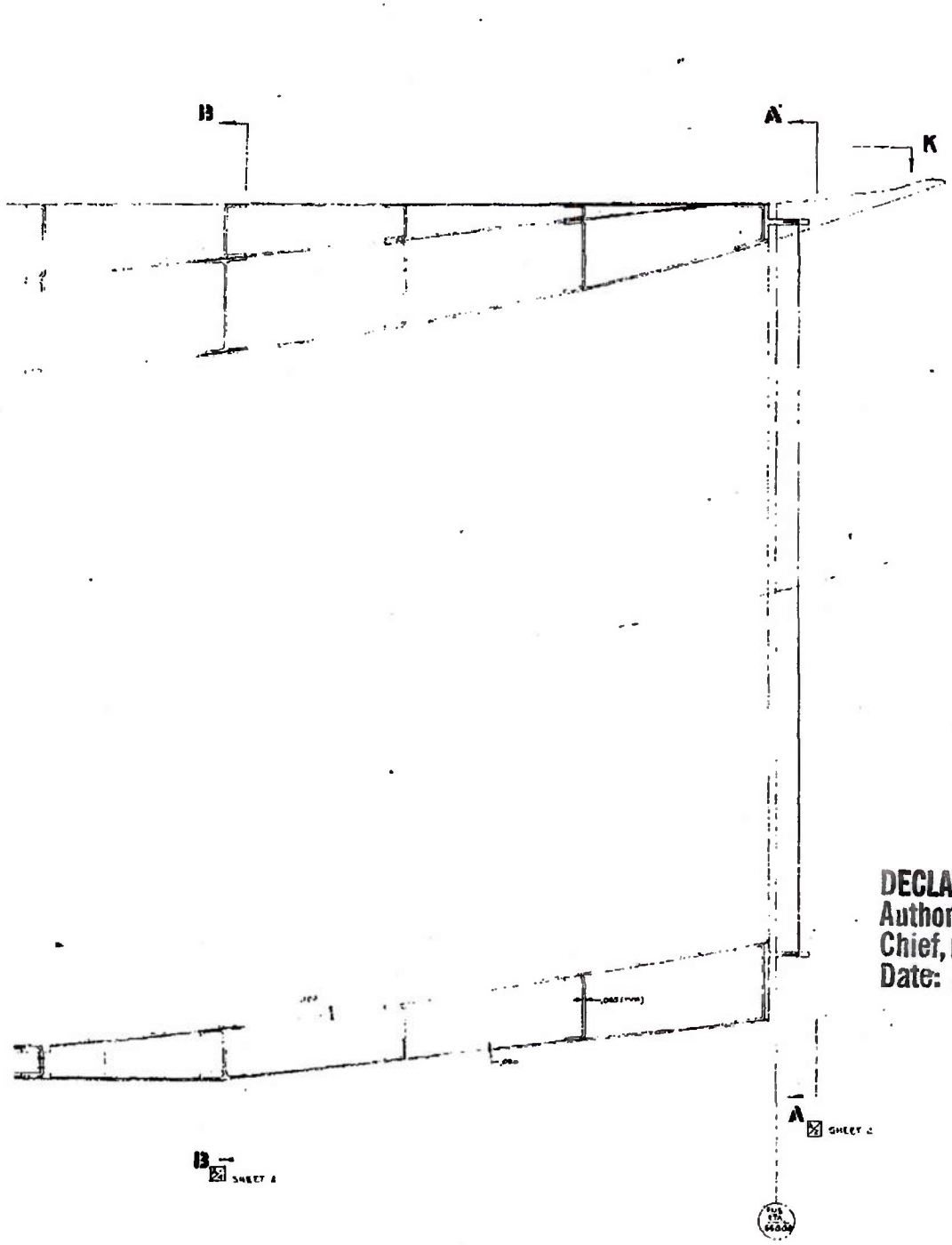

FIGURE

X 81421

[redacted]

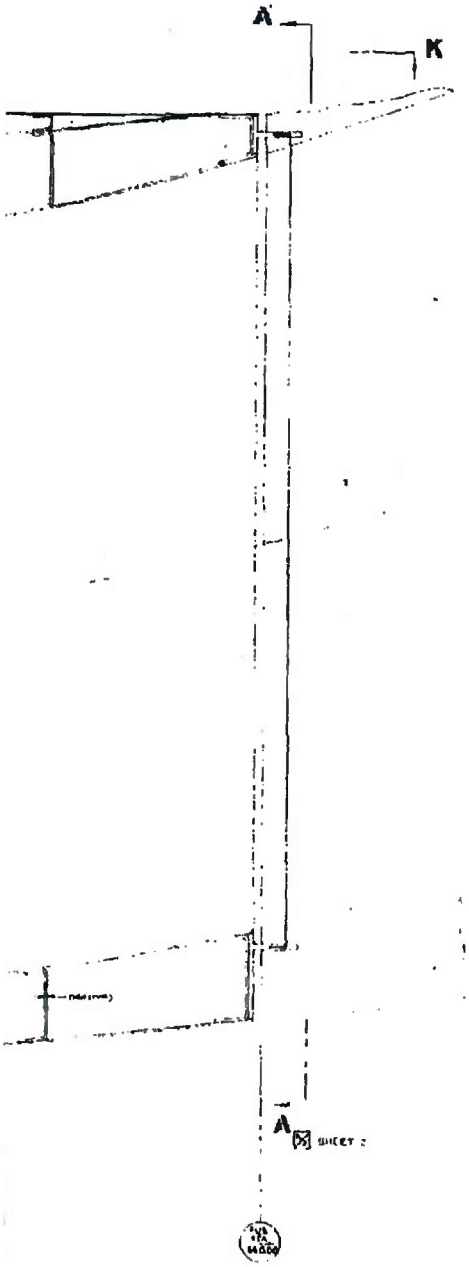

FIGURE 15. Design Layout, Asymmetric Inlet

[redacted]

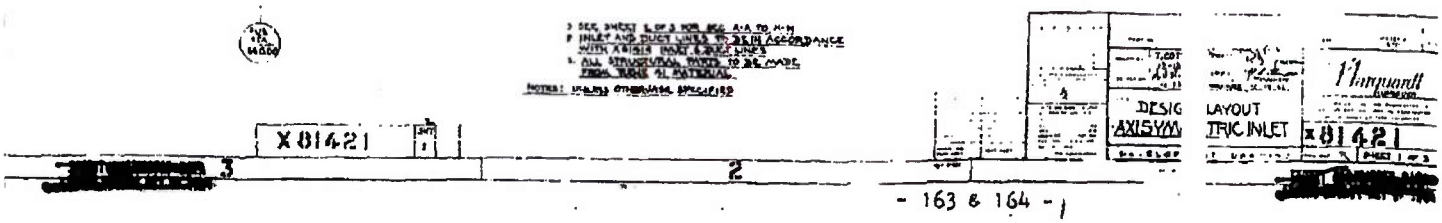

[redacted]

ASD-TDR-63-277, Vol. IV

~~SECRET RESTRICTED DATA~~
~~ATOMIC ENERGY ACT OF 1954~~

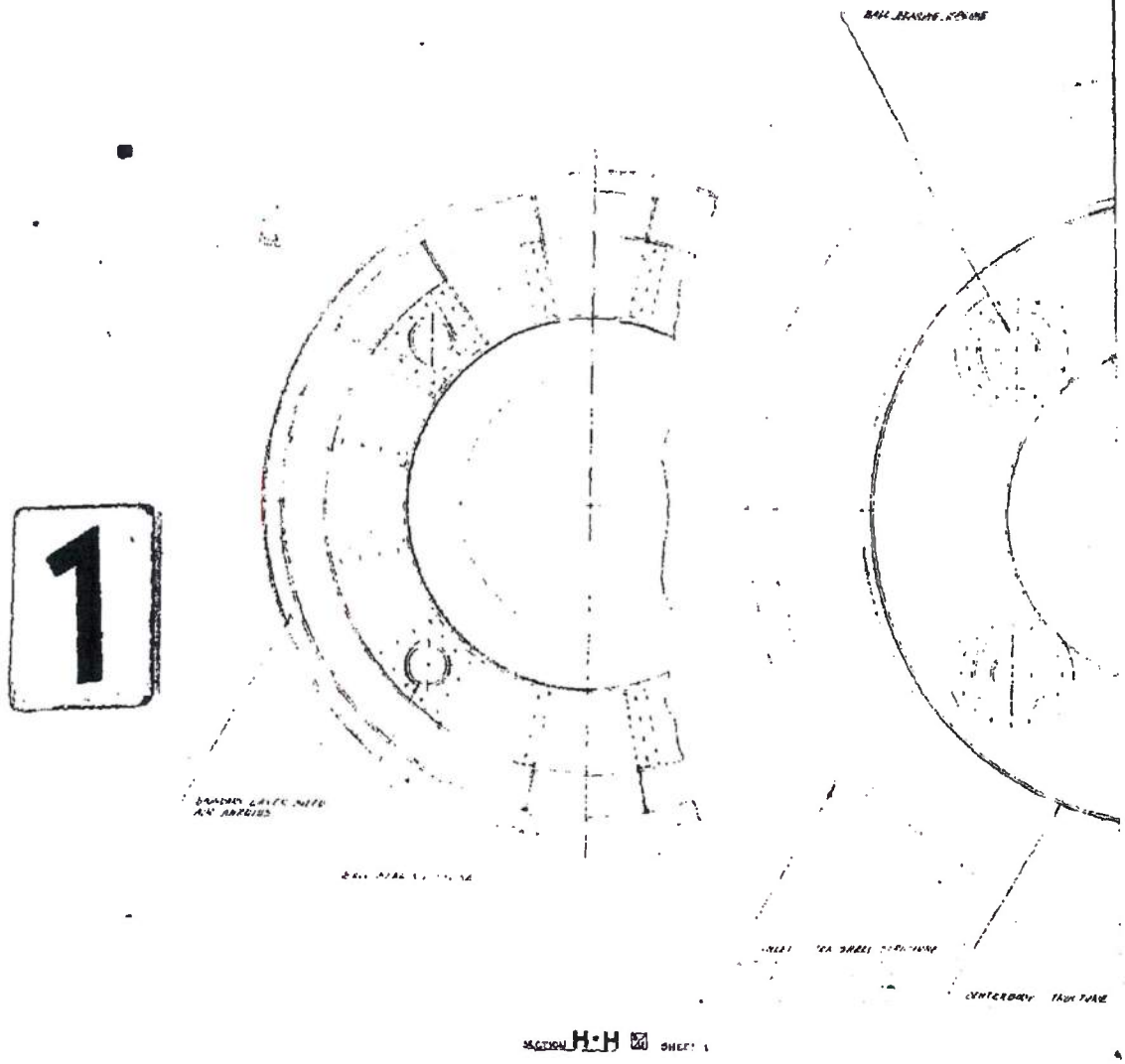

~~SECRET RESTRICTED DATA~~
~~ATOMIC ENERGY ACT OF 1954~~

[redacted]

[redacted]

[redacted]

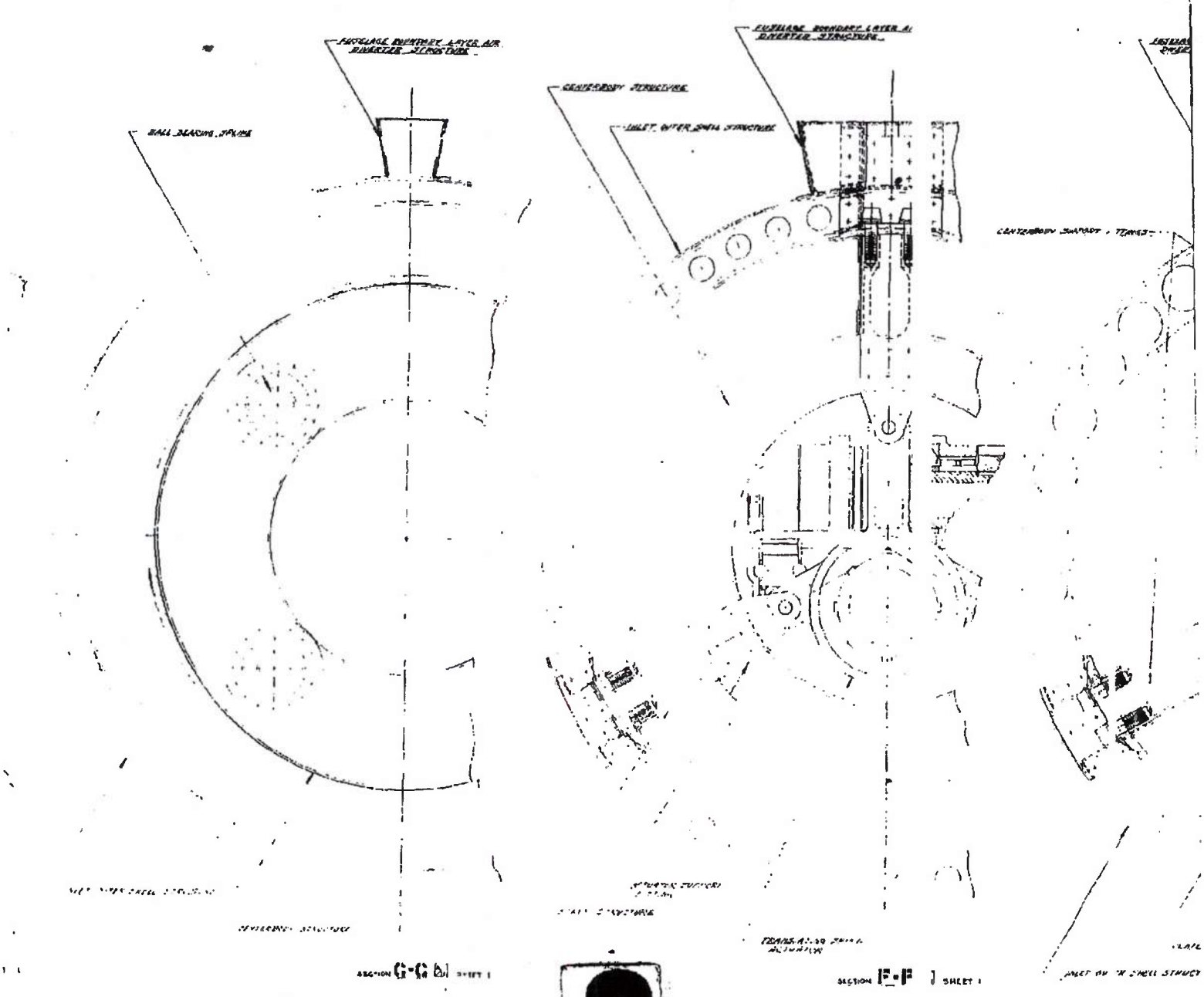

[redacted]

2

X81421

10 9 8

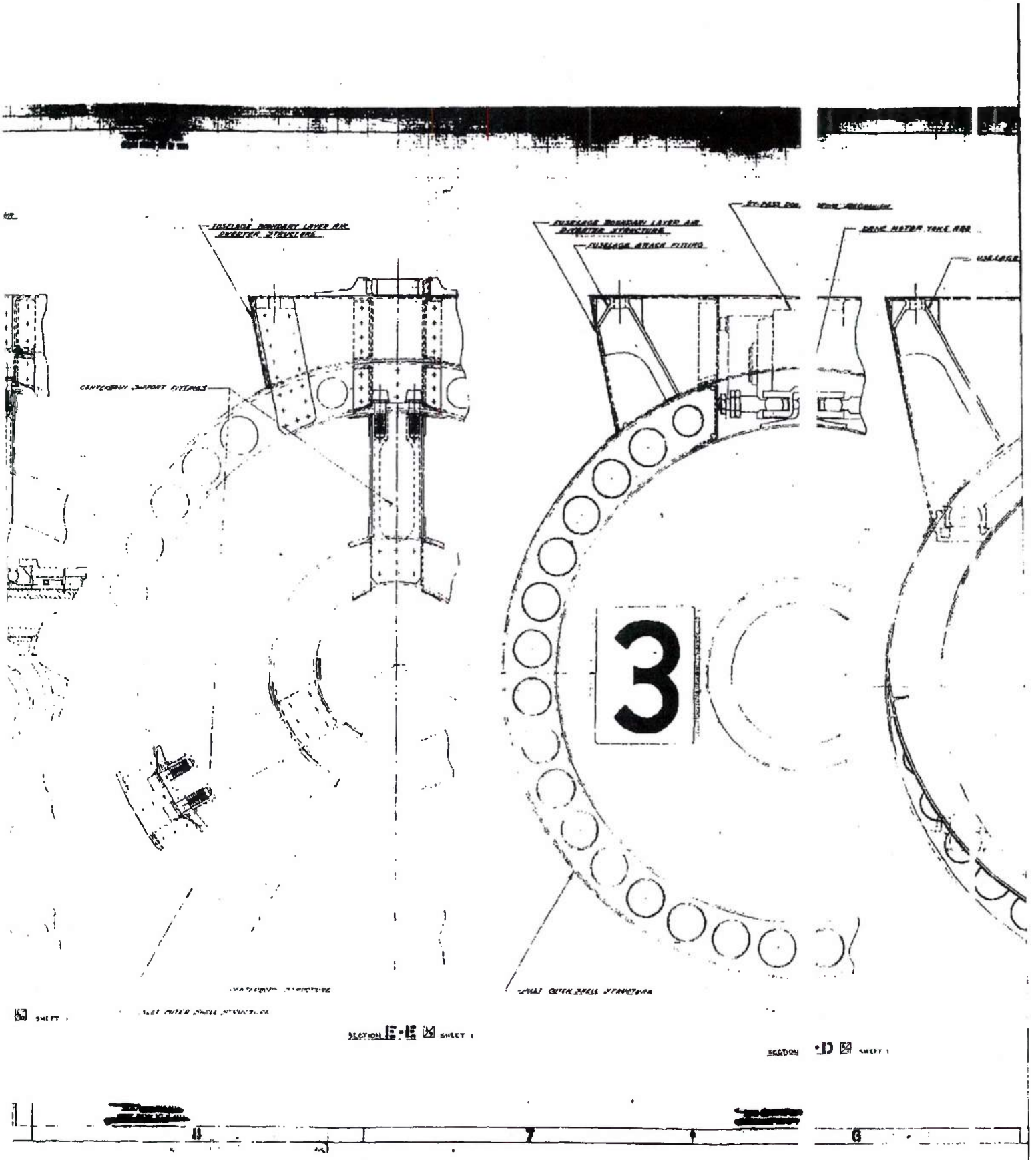

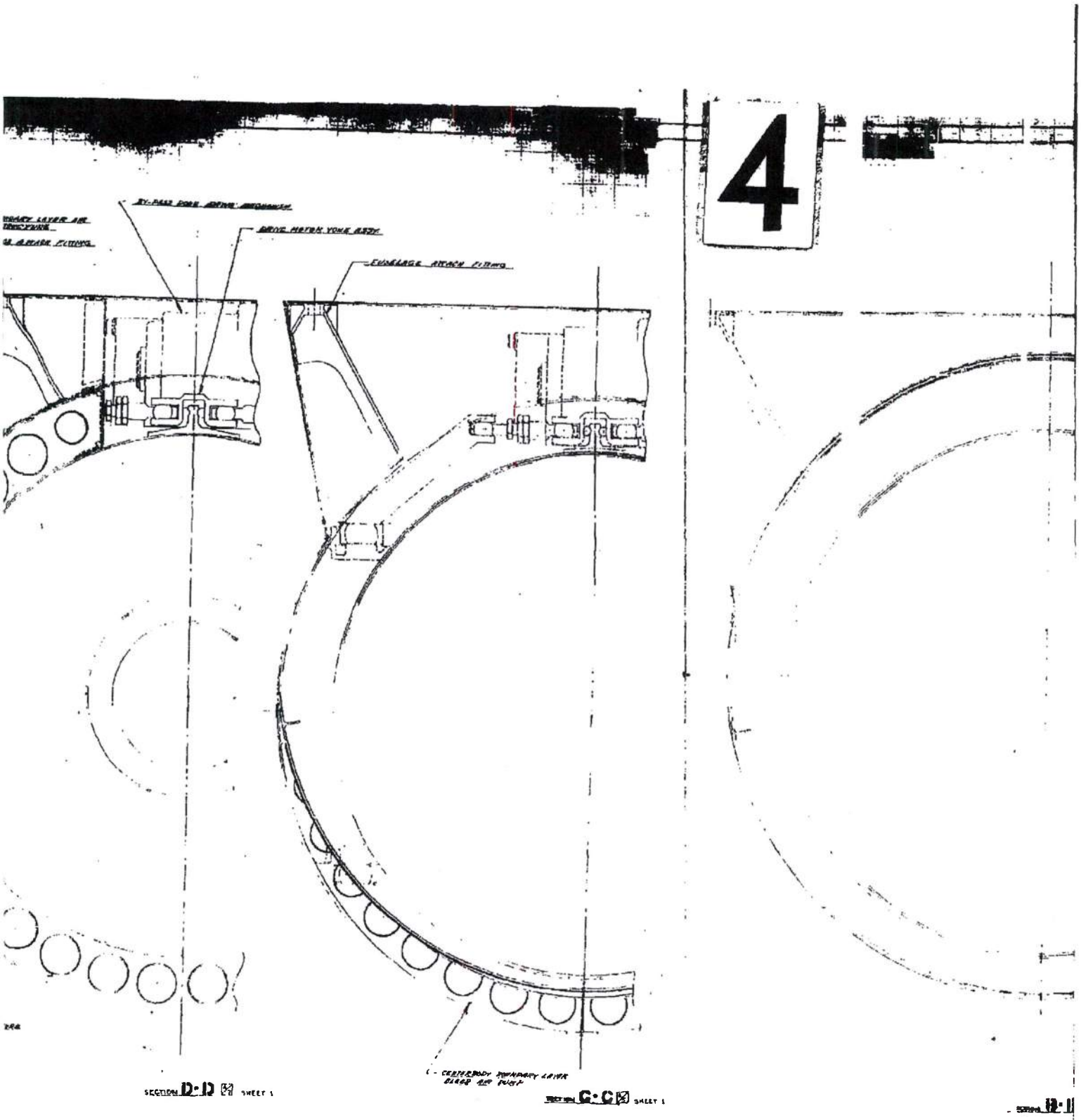

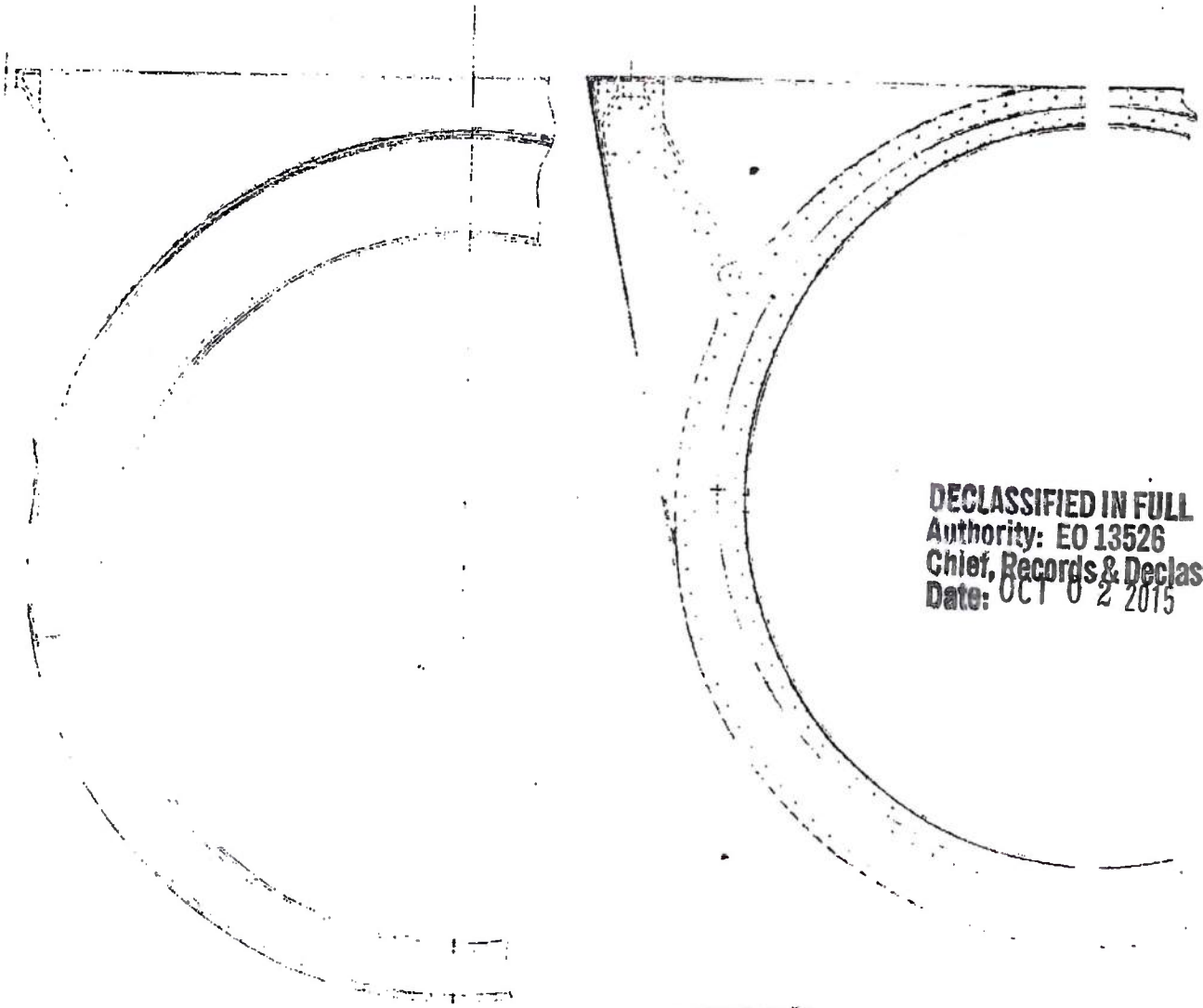

FIGU

5

B-B SHEET 1

A-A SHEET 2

4 3 2

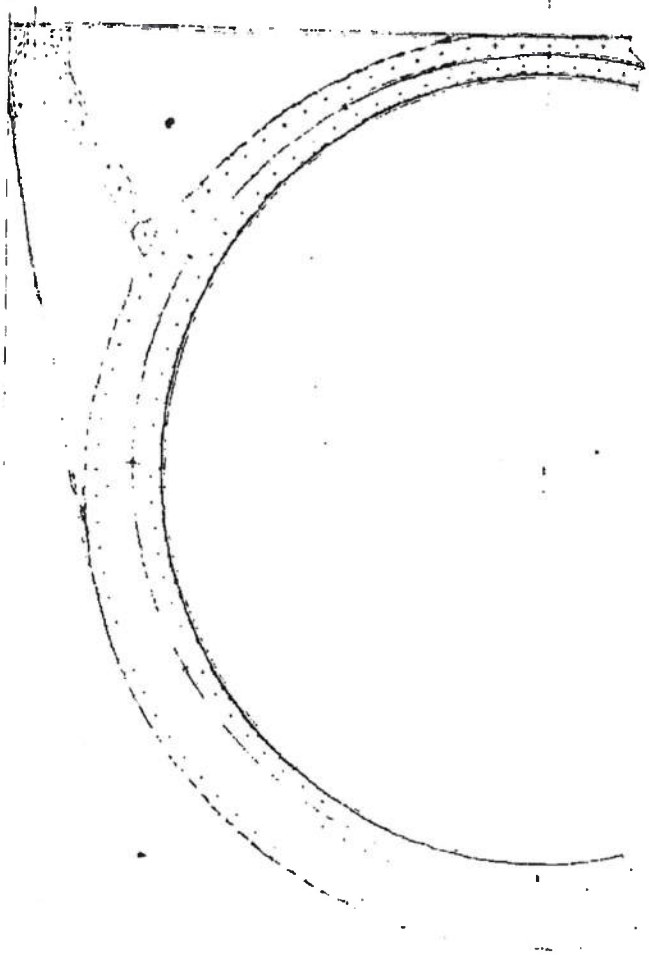

FIGURE 16. Design Layout, Axisymmetric Inlet

[redacted]

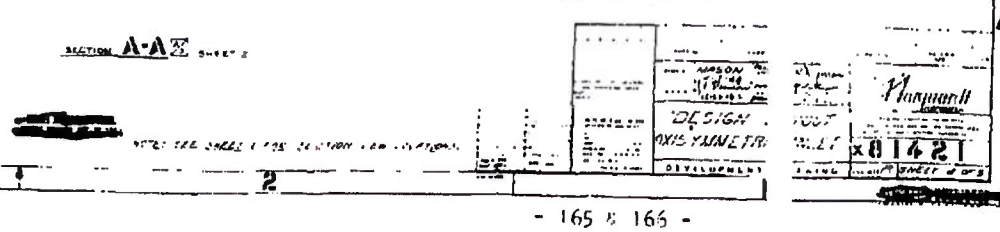

[redacted]

E.O. 10.340

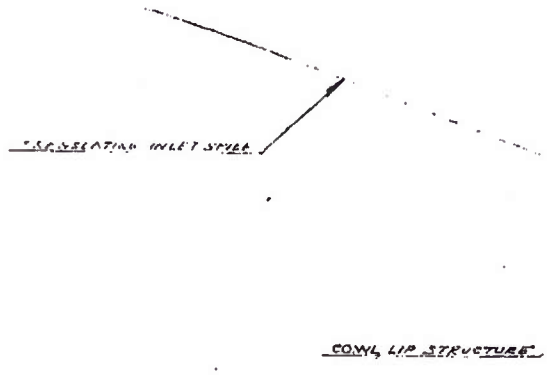

1

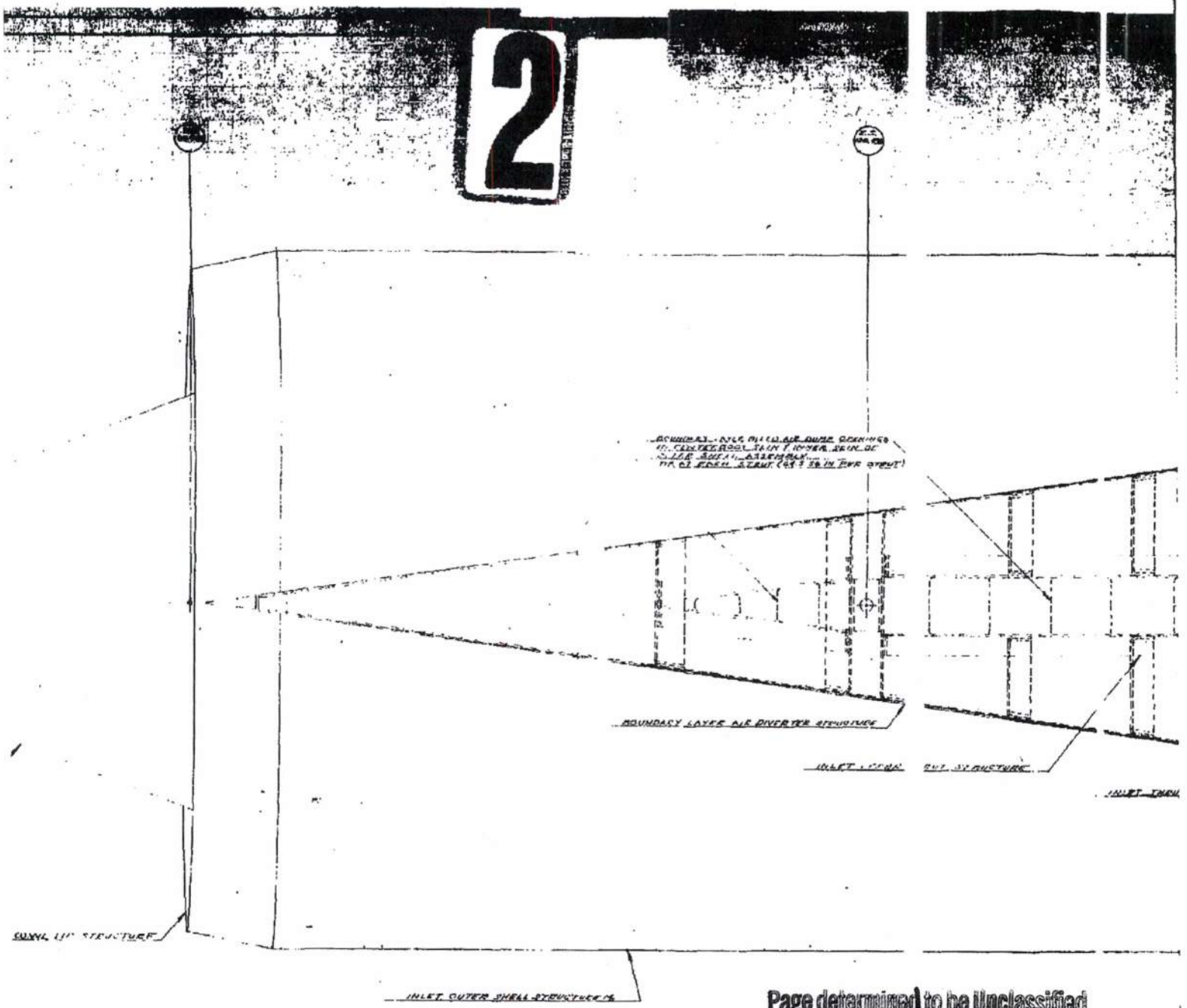

3

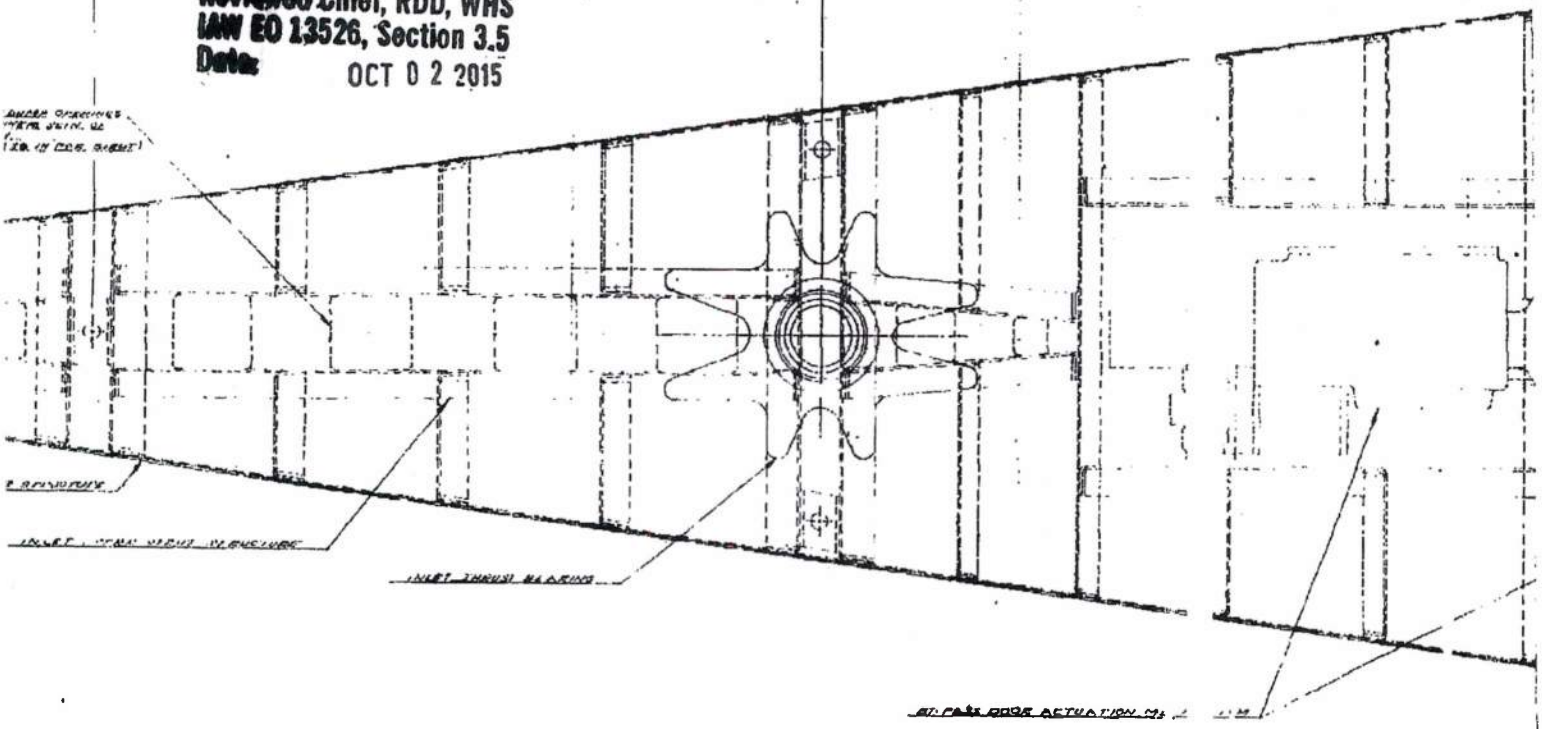

VIEW K-K

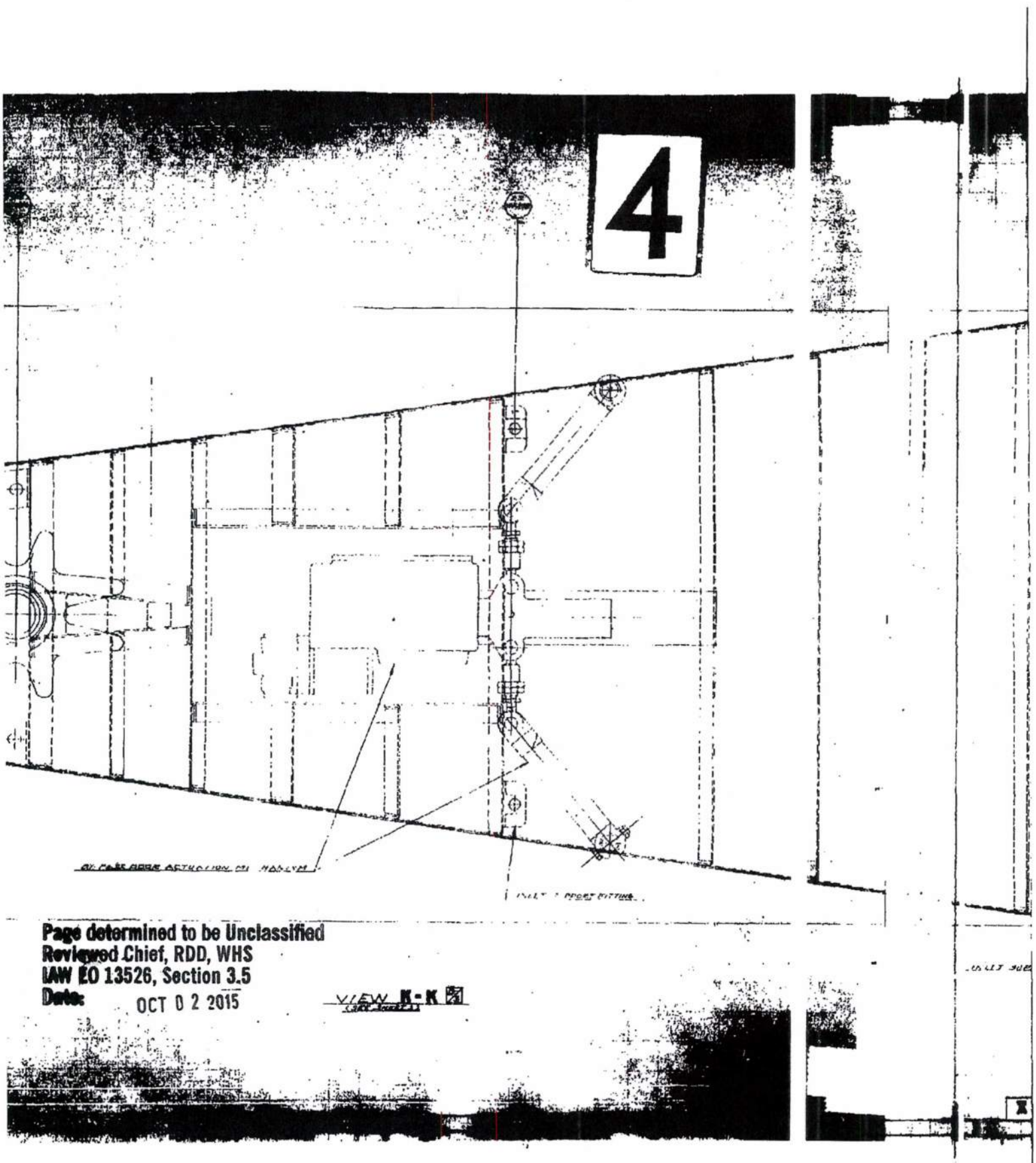

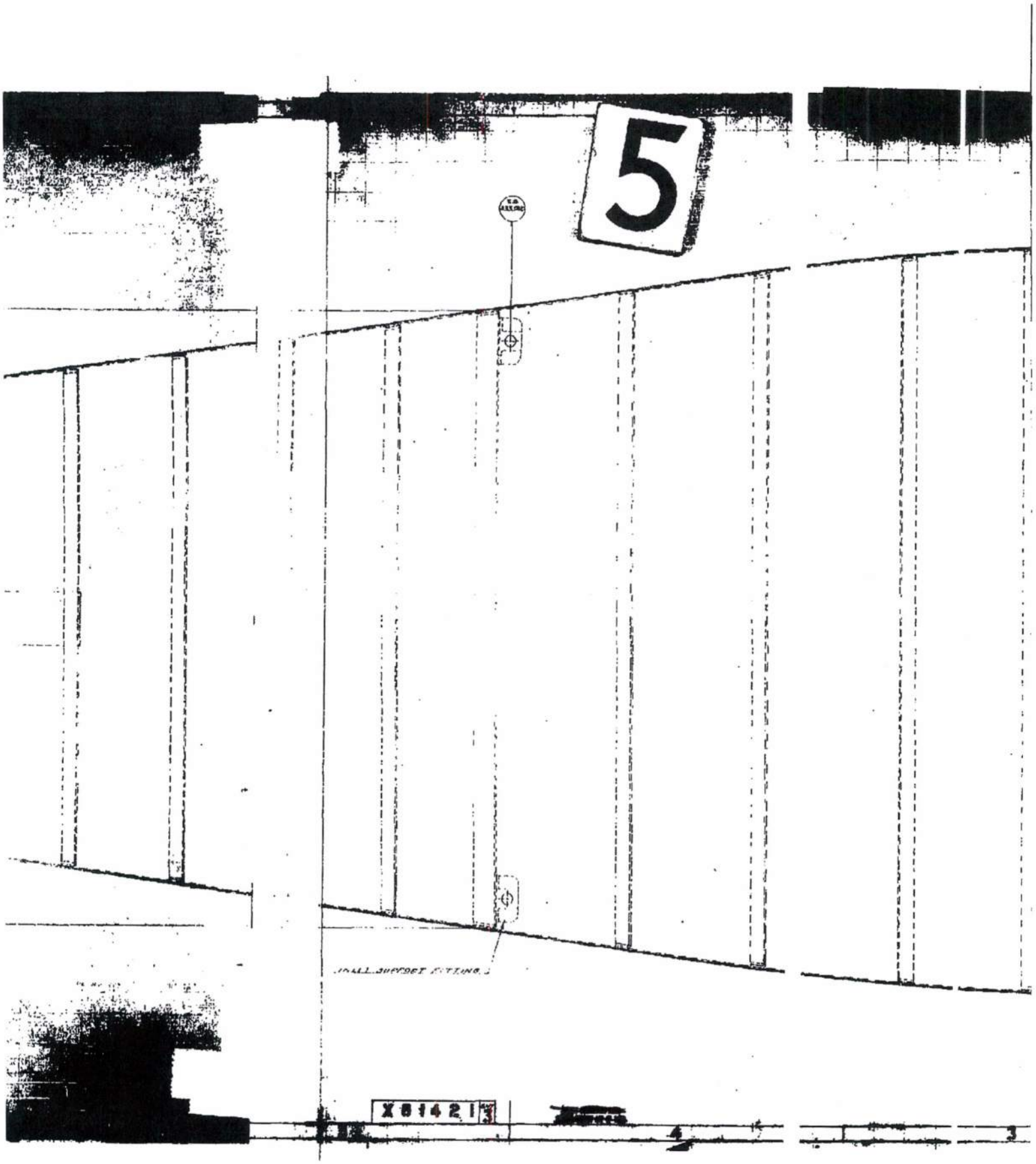

[redacted]

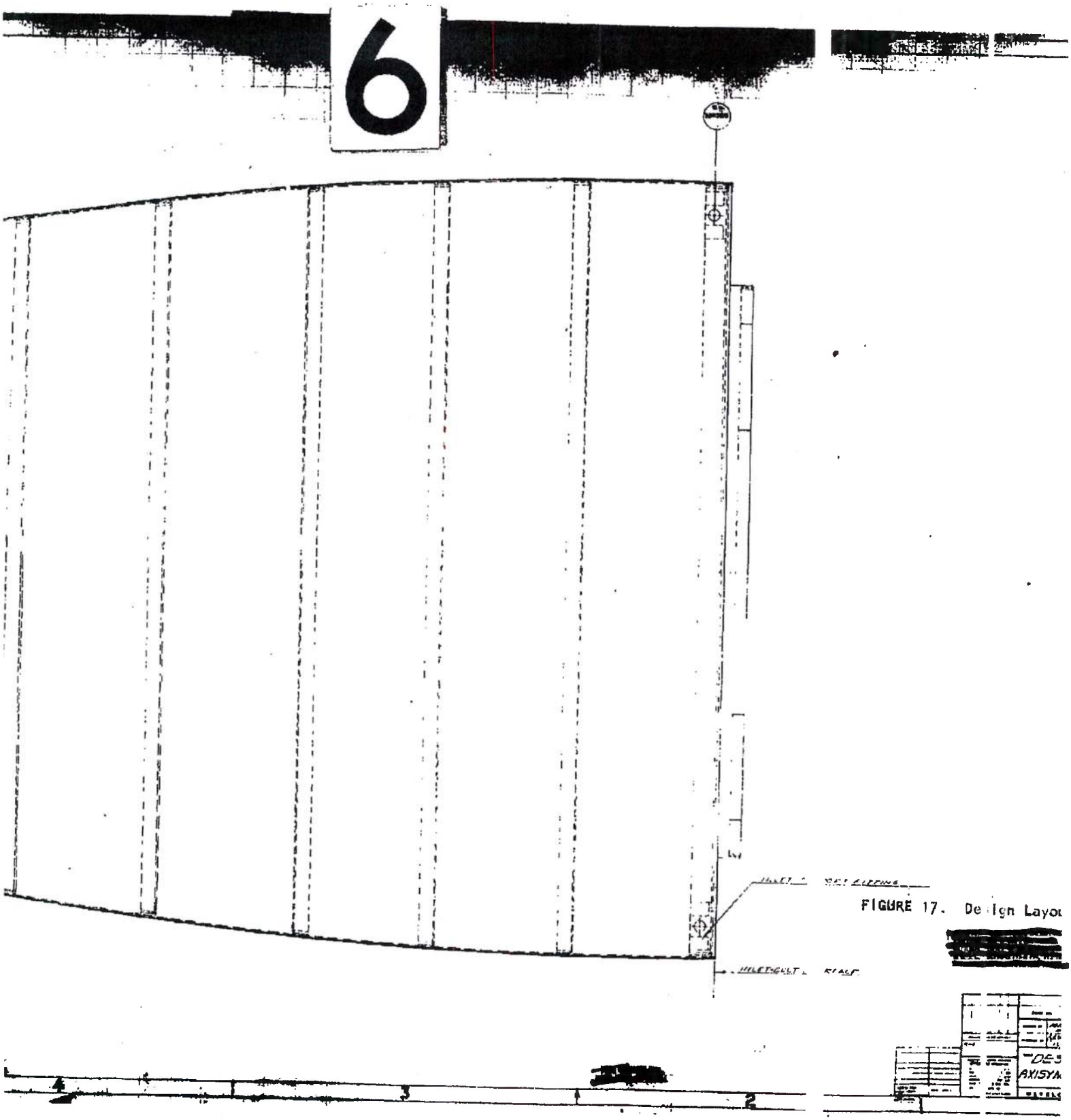

FIGURE 17. Design Layout

[redacted]

7

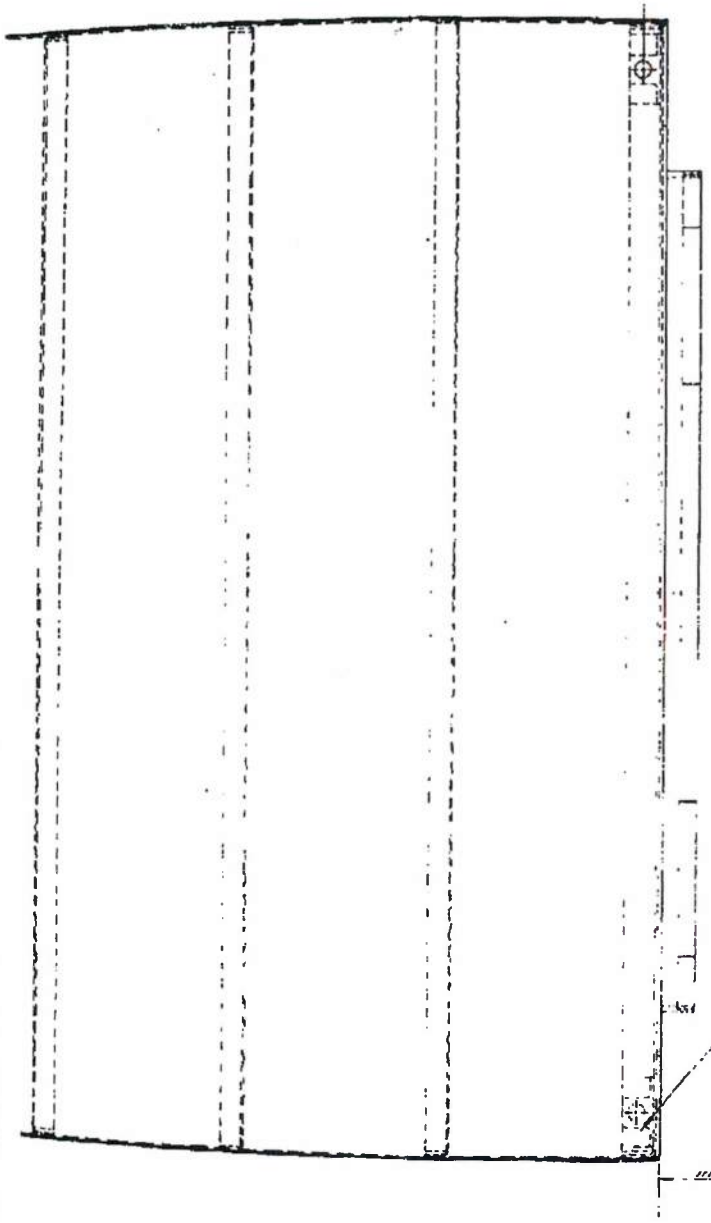

FIGURE 17. Design Layout, xisymmetric Inlet

[redacted]

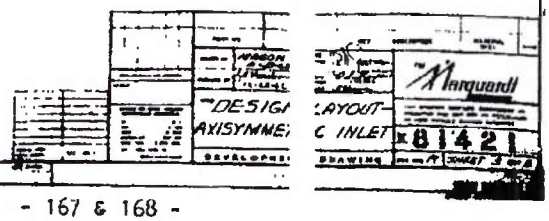

[redacted]

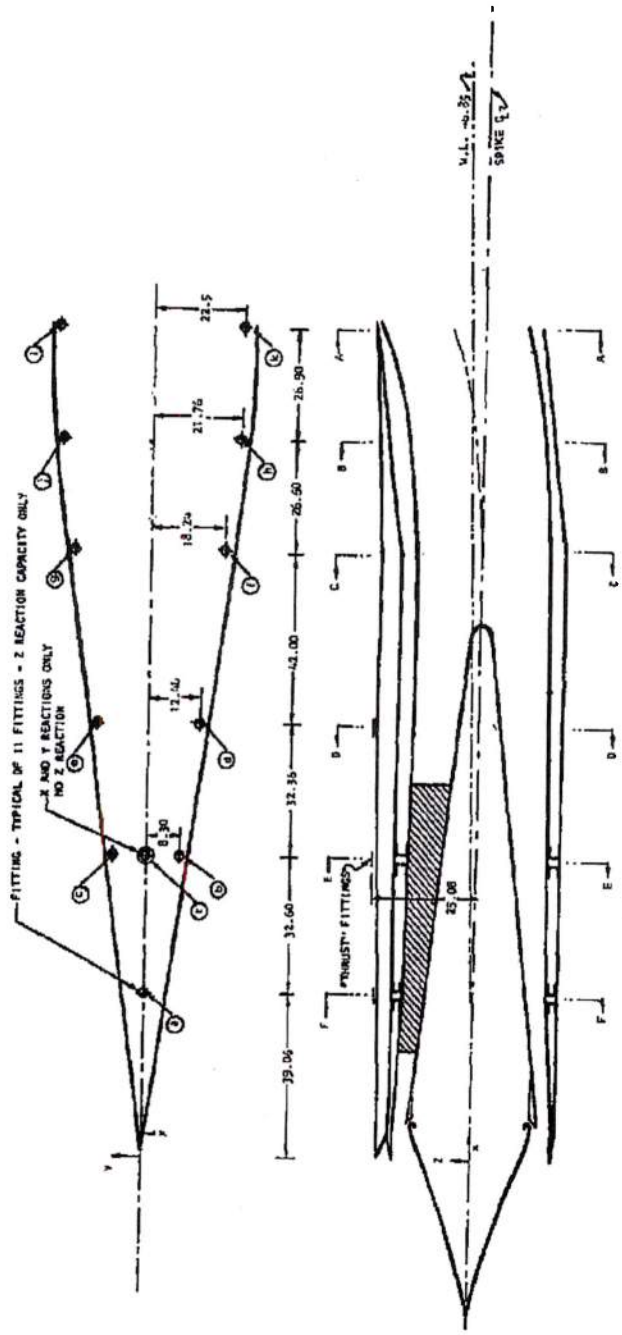

FIGURE 18. Sketch of Inlet Assembly for Inlet Structural Analysis

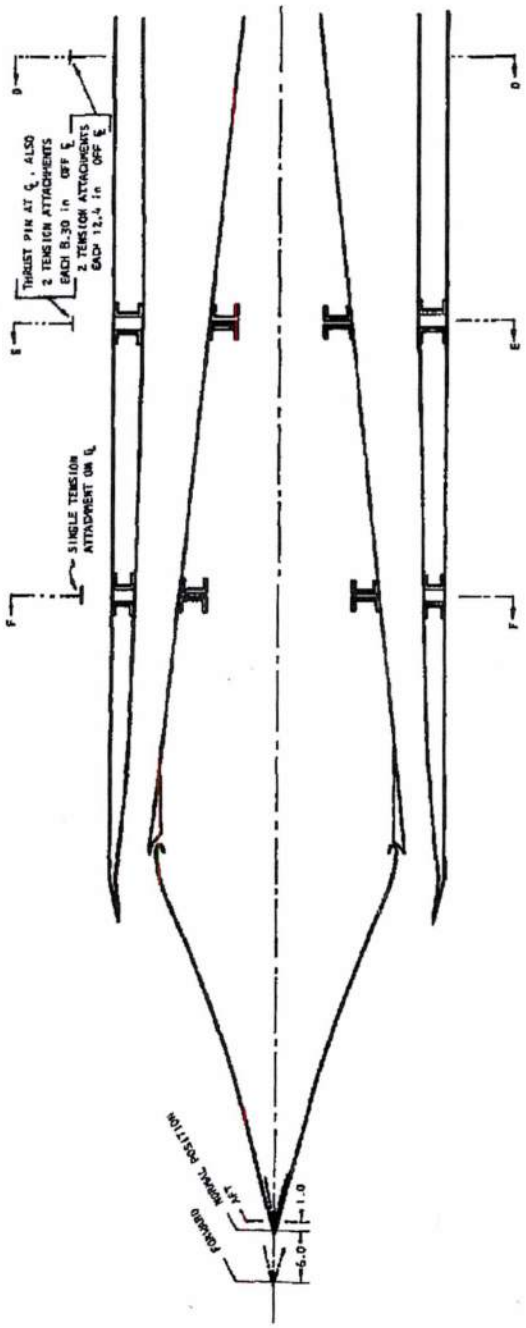

FIGURE 19. Sketch of Spike and Innerbody for Inlet Structural Analysis

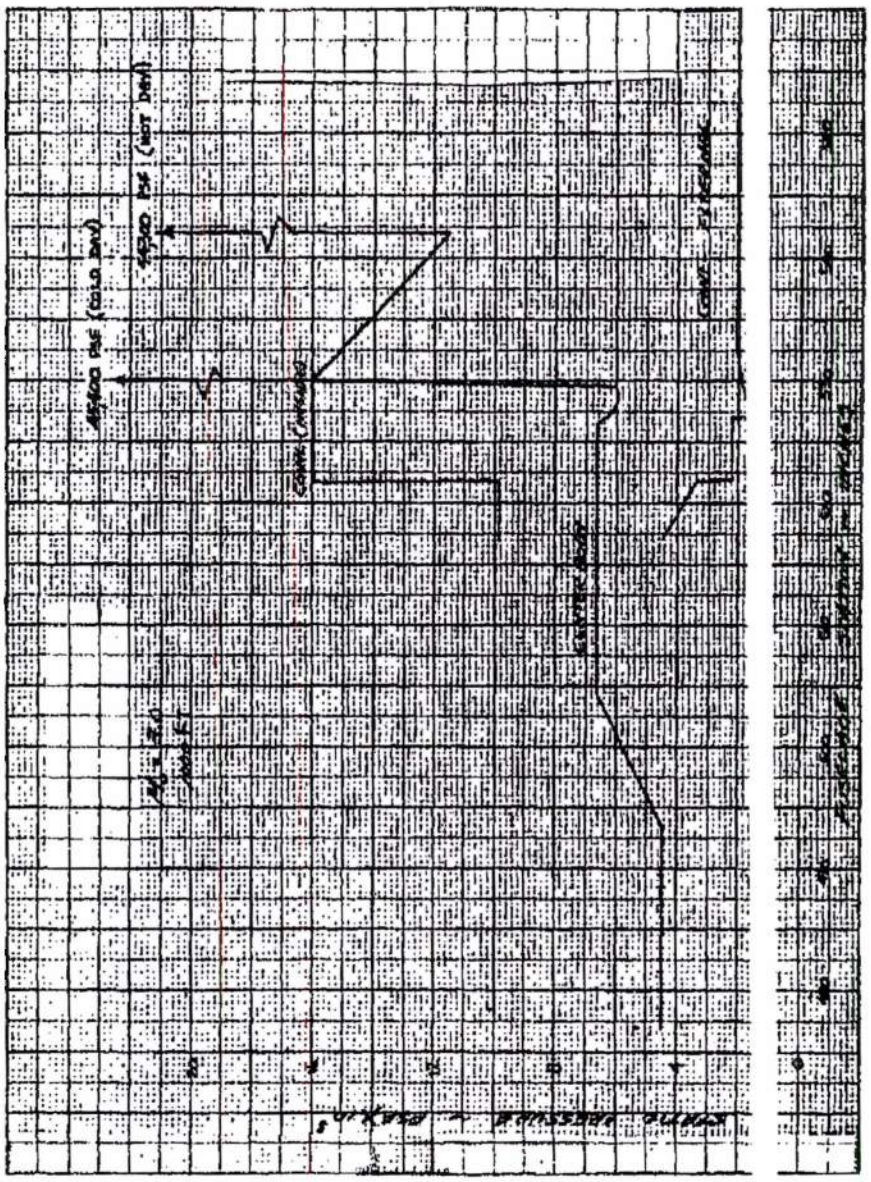

FIGURE 20. MA50-XCA Inlet-Diffuser Static Pressure

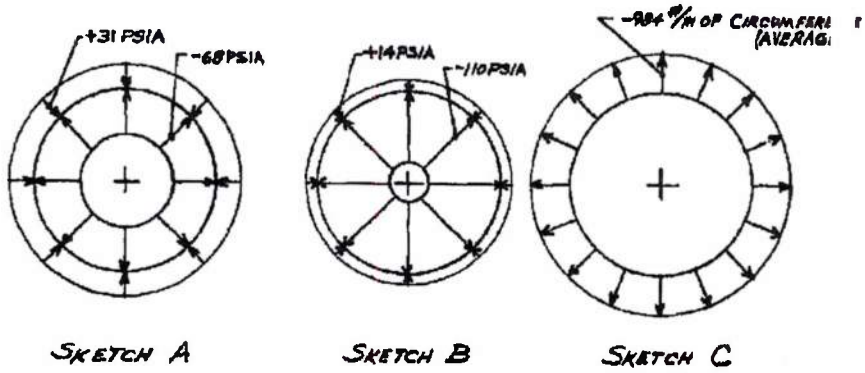

FIGURE 21. Varying Pressures on Inside and Outside Lip and Cowl Surfaces

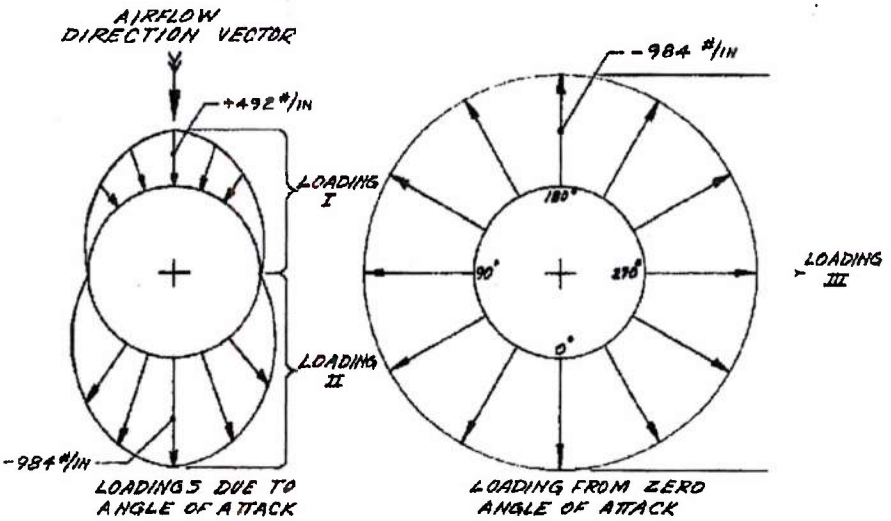

FIGURE 22. Three Loadings for Analysis Structure

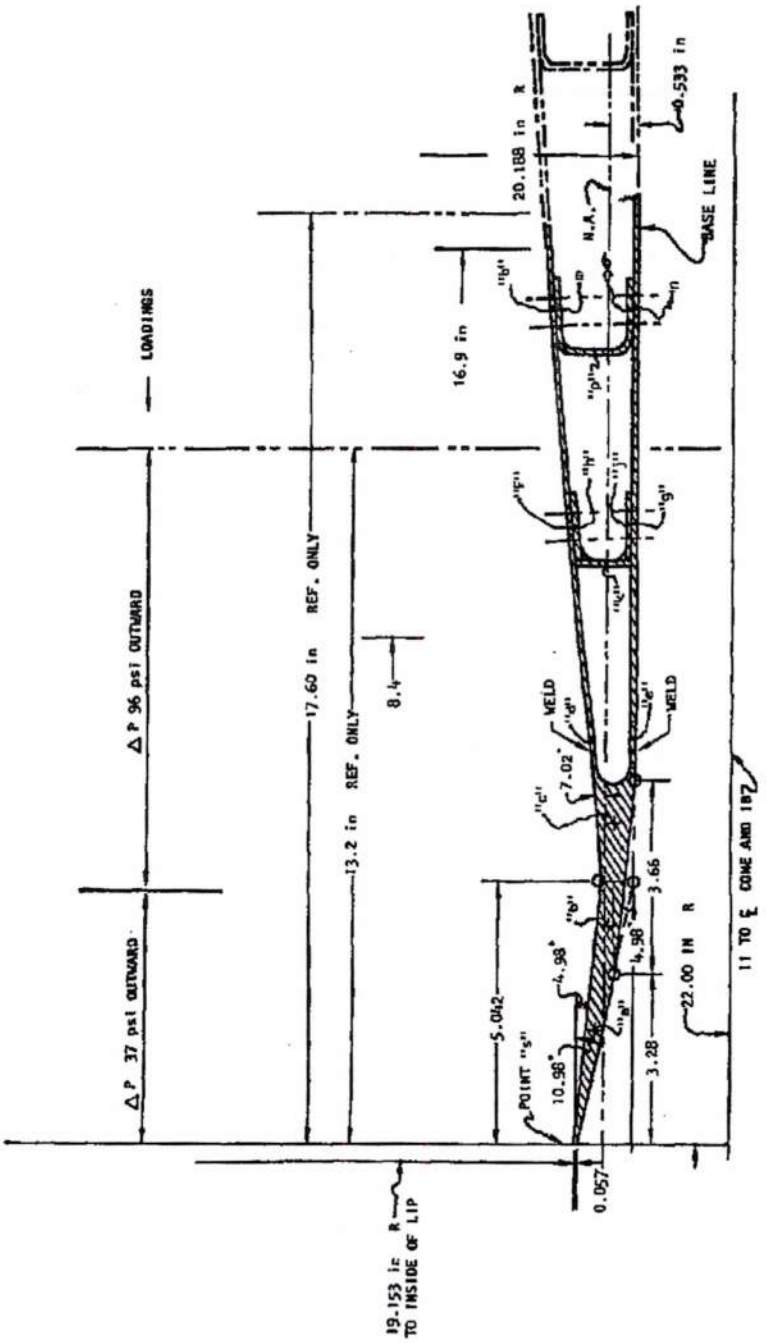

FIGURE 23. Sketch of Cowl Lip for Inlet Structural Analysis

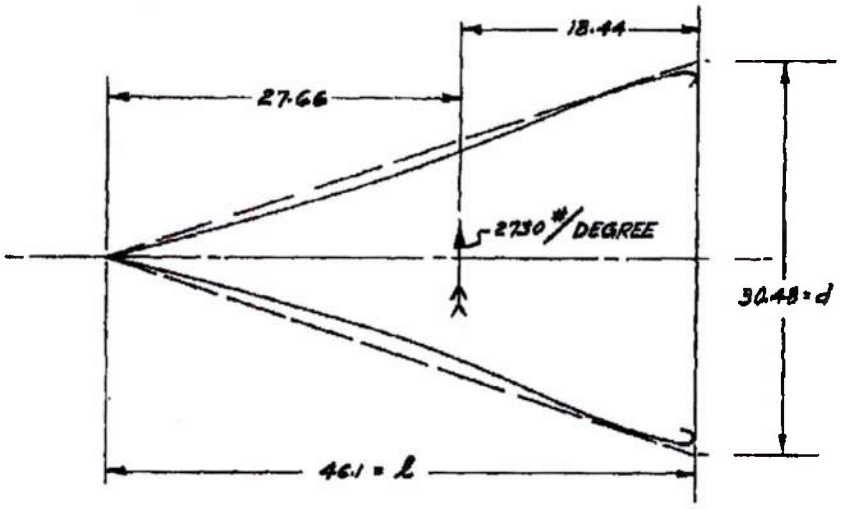

FIGURE 24. Spike Geometry

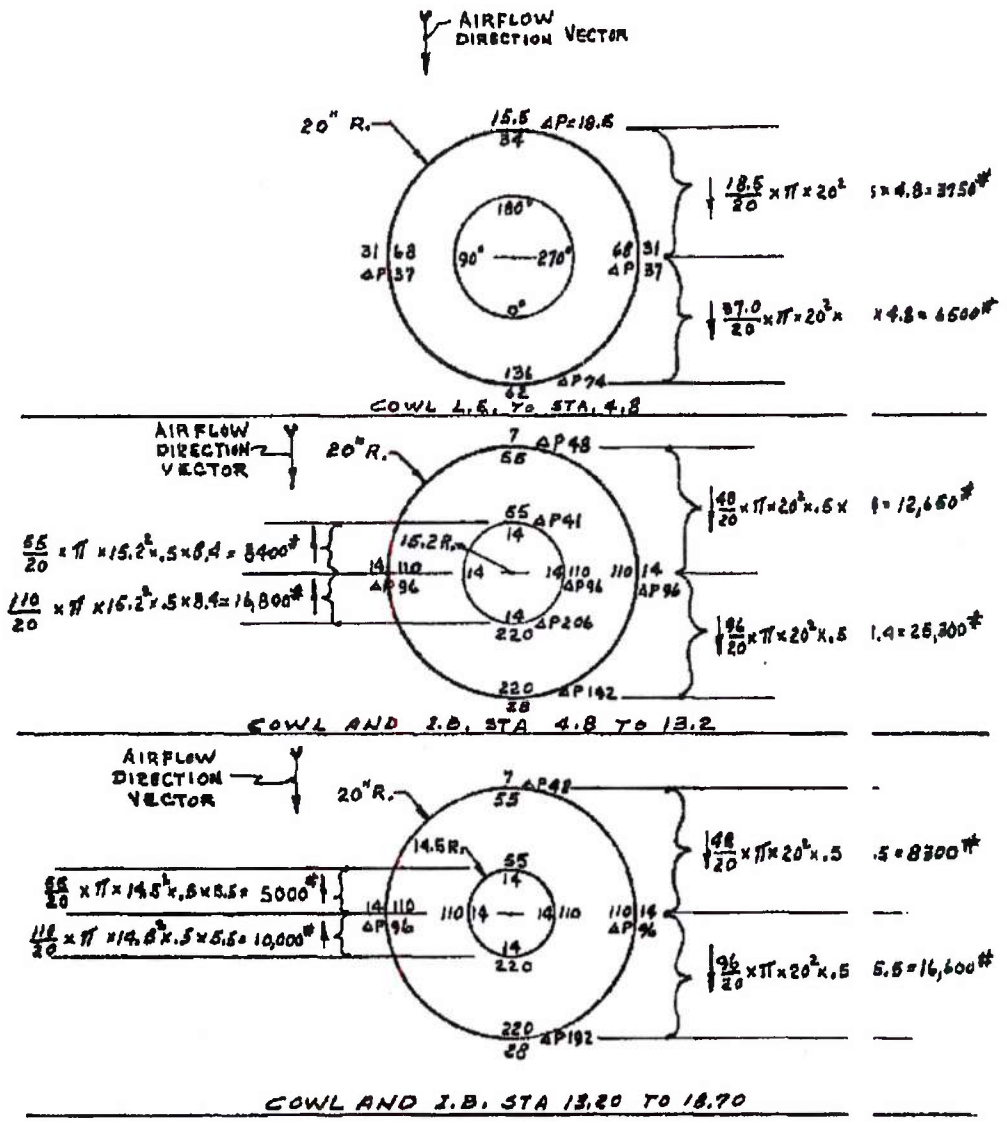

FIGURE 25. Cowl and Innerbody Unsymmetrical Loadings

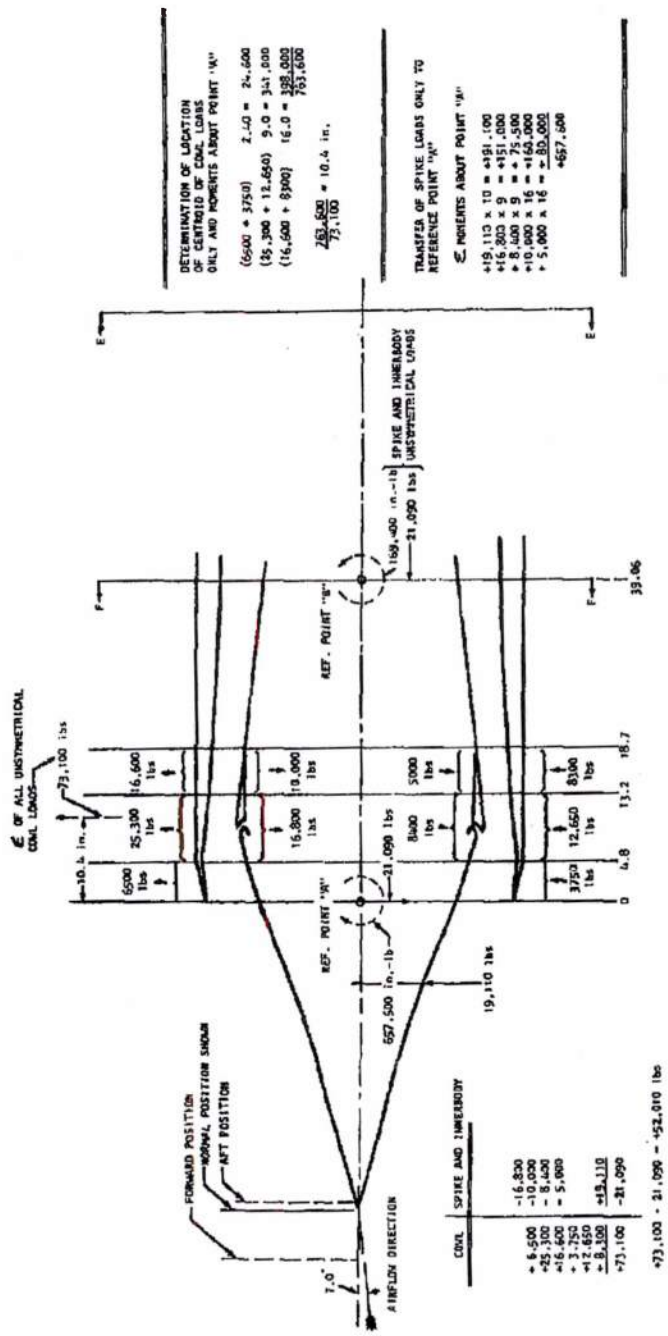

Figure 20. Coal and Innerbody Load Paths (Unsymmetrical Loadings)

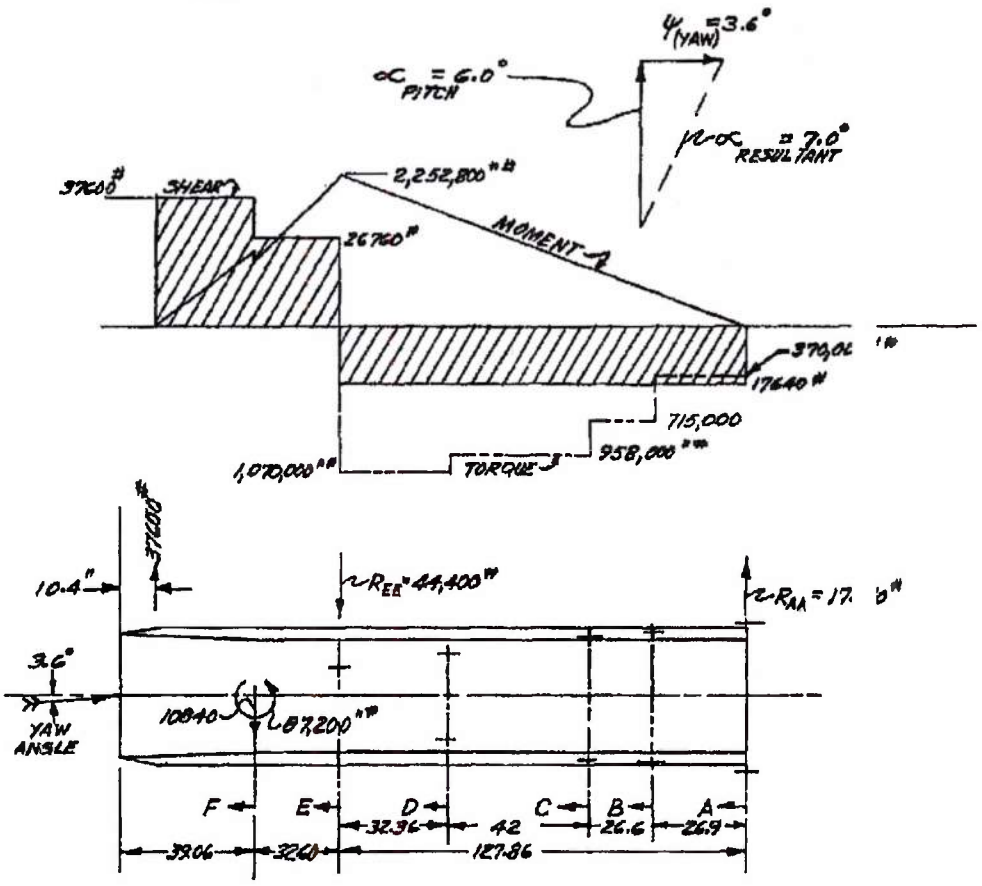

FIGURE 27. Unsymmetrical Air Load Distribution

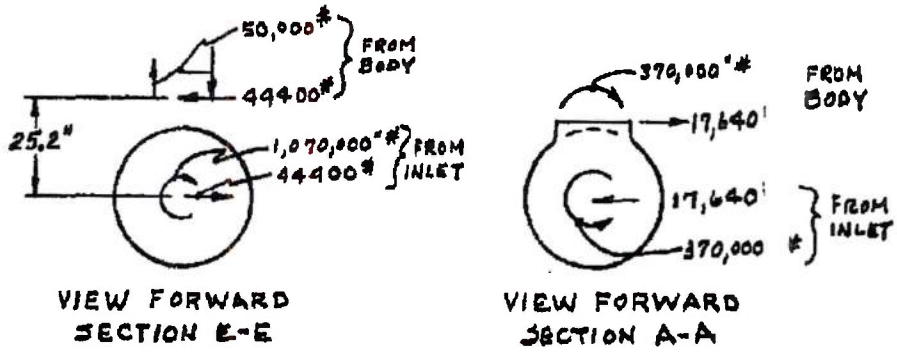

FIGURE 28. Shears, Moments, and Torques from Y Direct on

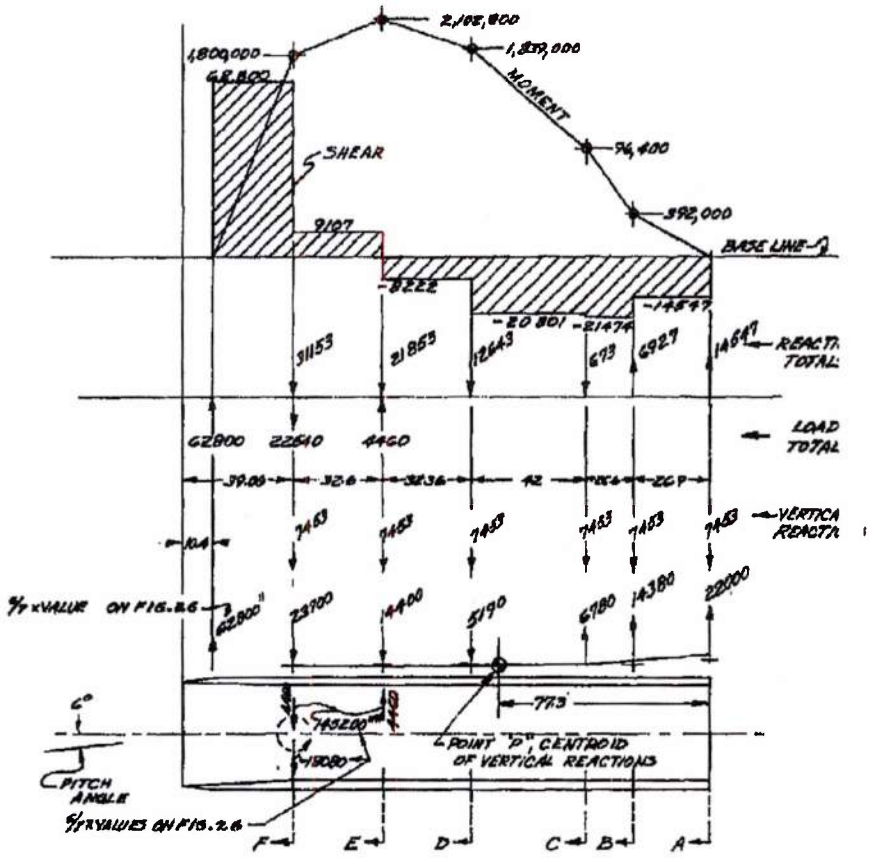

FIGURE 29. Shears and Moments from Z Direction Components

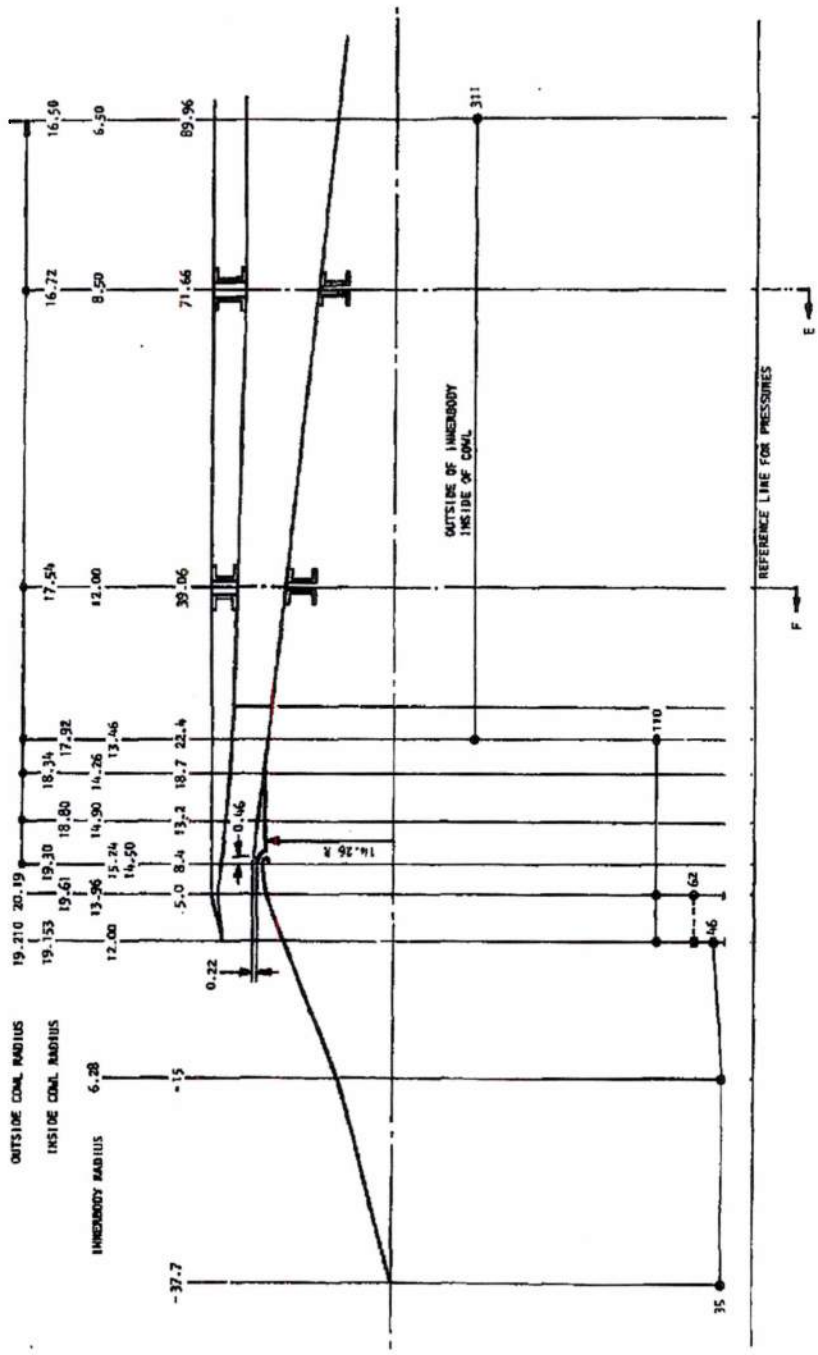

FIGURE 30. Geometry and Pressures for Inlet Structural Analysis

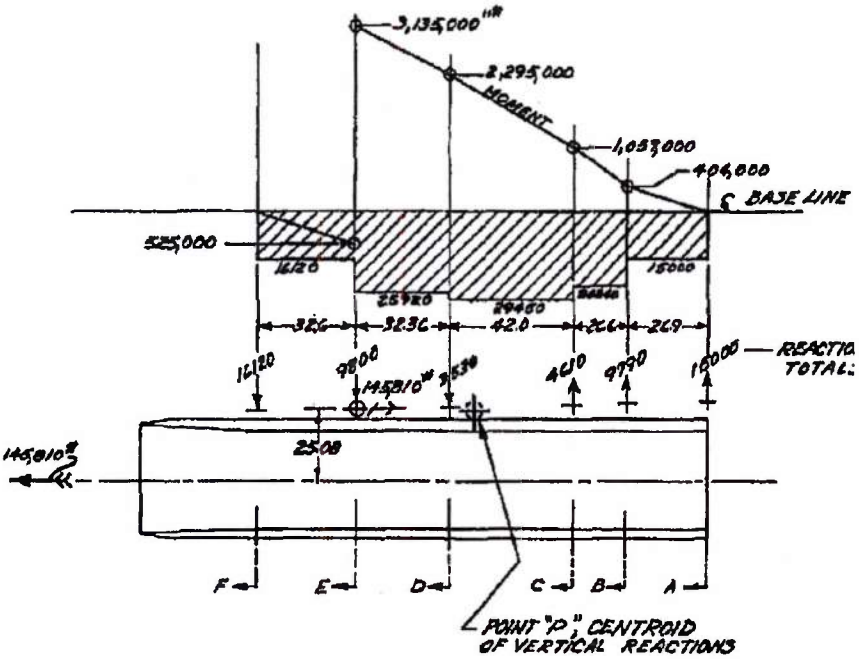

FIGURE 31. Derived Load Distribution on Fittings

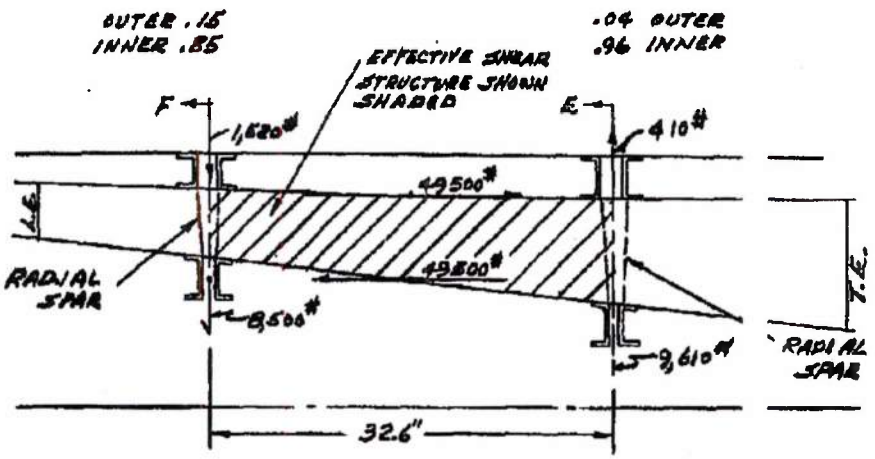

FIGURE 32. Longitudinal Section Through Typical Strut

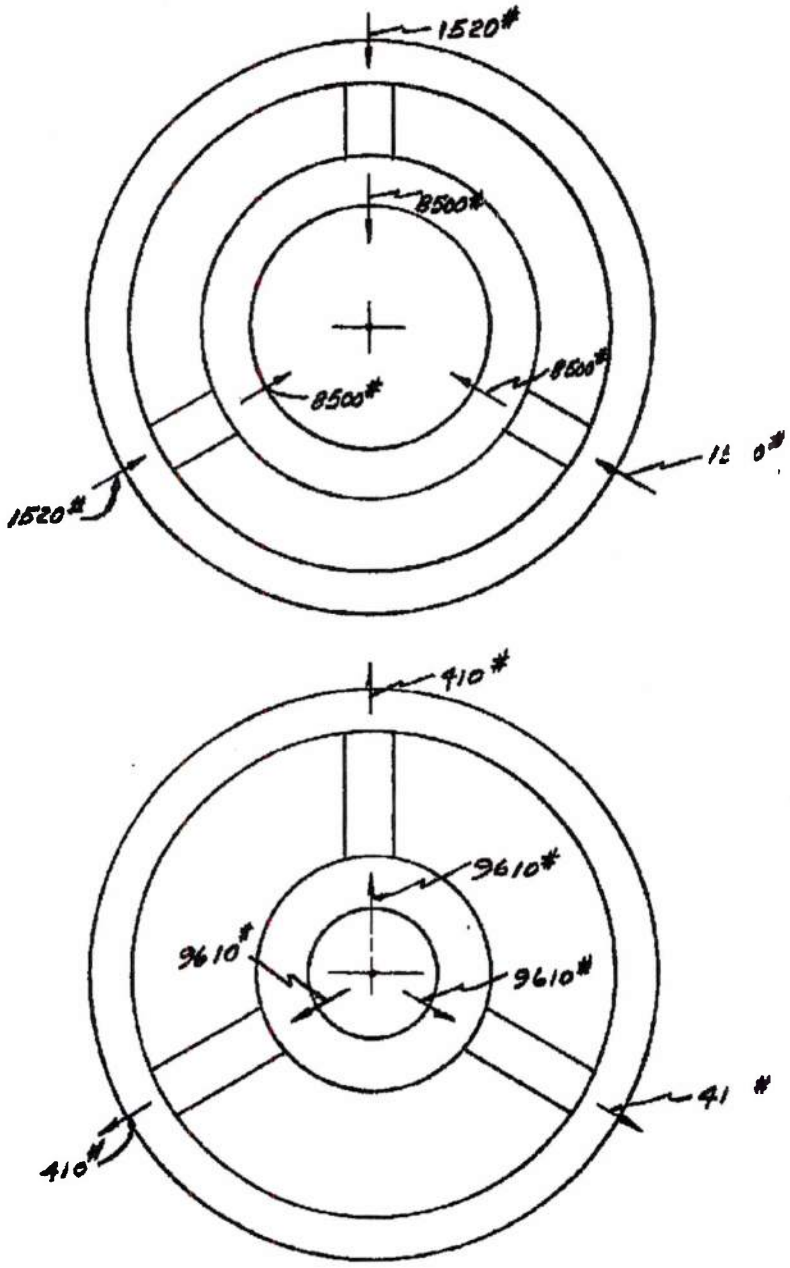

FIGURE 33. Load on Struts from Supporting Rings

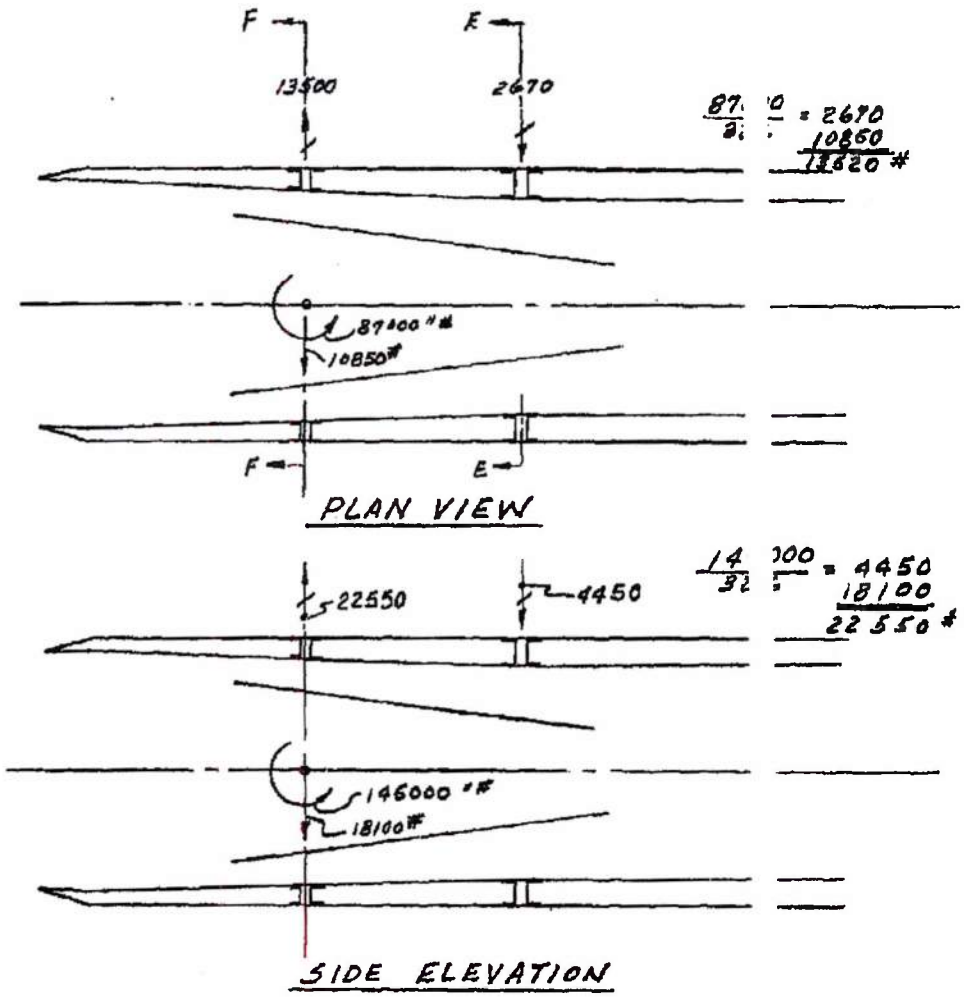

FIGURE 34. Loads on Strut Spars from Unsymmetrical L is

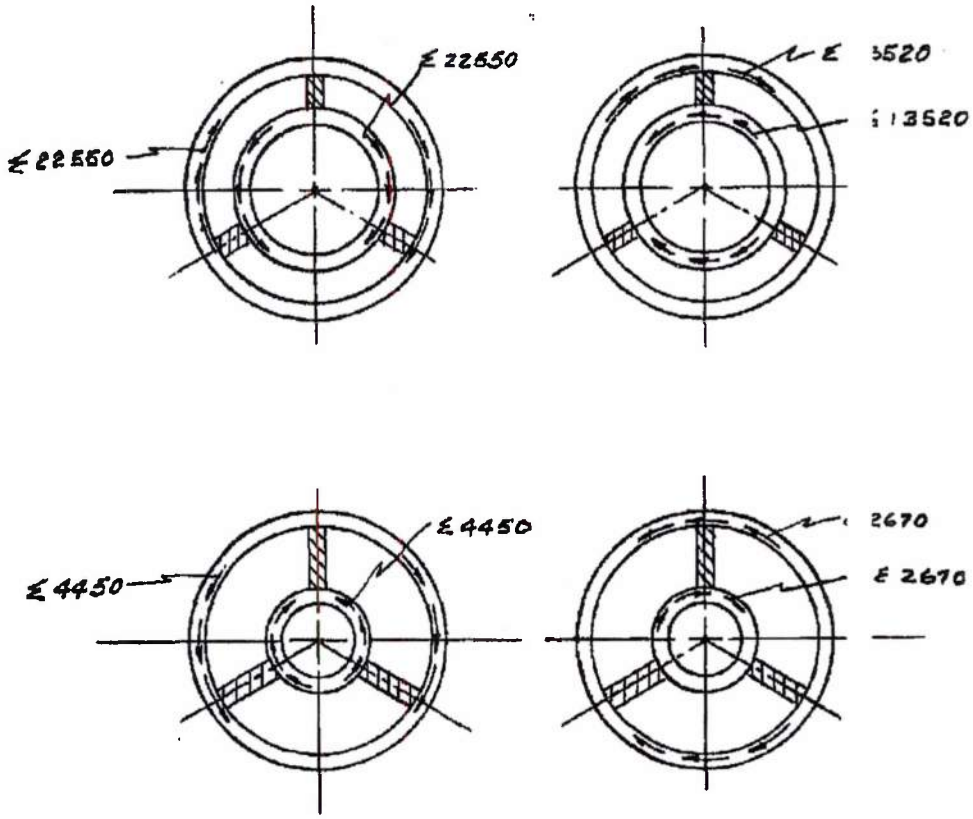

FIGURE 35. Vertical and Horizontal Loads on Strut Spars

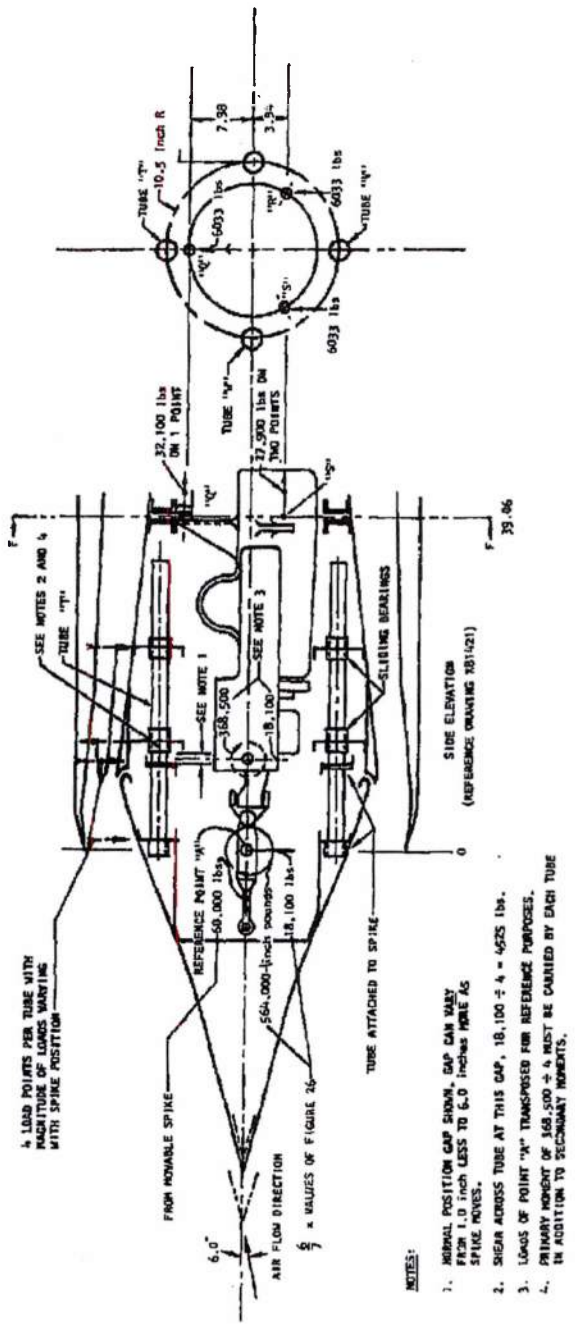

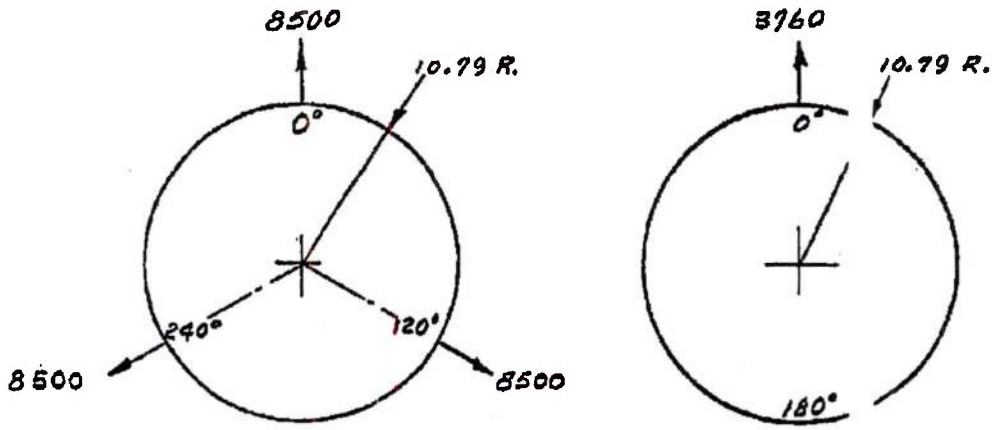

FIGURE 37. Innerbody Ring Loads

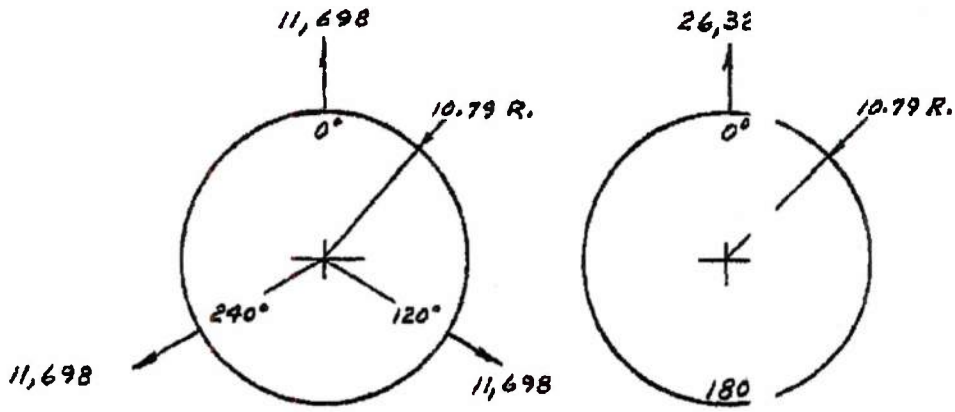

FIGURE 38. Symmetrical and Unsummetrical Loadings

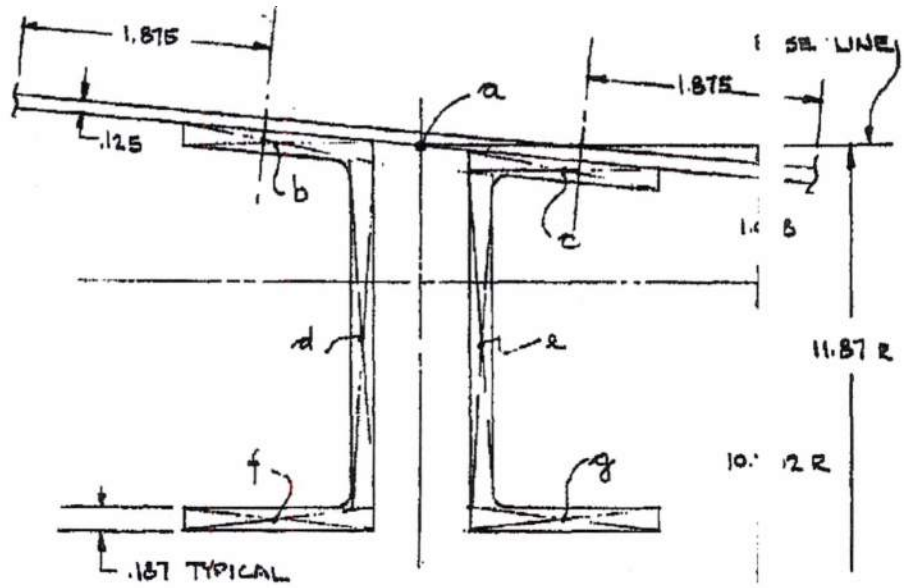

ITEM	SIZE & AREA, A In²	Z	A · Z	$\bar{Z}$	A · $\bar{Z}$	A · $\bar{Z}^2$	I_o
a	.125 x 6.25 = .7810	- .05	-.0390	-1.128	-.8810	.9930	0
b	.18 x 1.50 = .2700	0	0	-1.078	-.2910	.3140	0
c	.18 x 1.50 = .2700	.20	.0540	-.878	-.2370	.2080	0
d	.18 x 2.70 = .4860	1.50	.7290	+.422	+.2050	.0865	.294
e	.18 x 2.60 = .4680	1.51	.7060	+.432	+.2022	.0875	.262
f	.18 x 1.50 = .2700	2.92	.7890	+1.842	+.4975	.9160	0
g	.18 x 1.50 = .2700	2.92	.7890	+1.842	+.4975	.9160	0
	2.8150	1.078	3.0280		-1.4090 +1.4022	3.5230 4.0790 Tot	.5560

I of section with holes is estimated as .80 x 4.079 = 3.27 in.⁴

FIGURE 39. Ring Section Properties

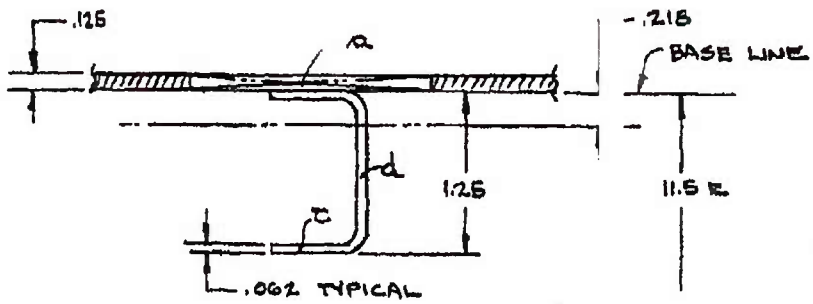

ITEM	SIZE	AREA	ARM Z	A·Z	To $\bar{Z}$ N.A.	A·$\bar{Z}$	A·$\bar{Z}^2$	I_o
a	.125 x 1.86	.2330	- .0625	-.01460	-.2805	-.0653	.01838	0
b	.062 x .75	.0465	+ .0310	+.00144	-.1870	-.0087	.001624	0
c	.062 x .75	.0465	+1.1930	+.05550	+.9750	+.0454	.044206	0
d	.062 x 1.1	.0684	+ .6120	+.04180	+.3940	+.02695	.010600	.00693
		.3944	.218	+.08614			.074804	.00693
							.08	34 in.^{4}

FIGURE 40. Ring Section Properties

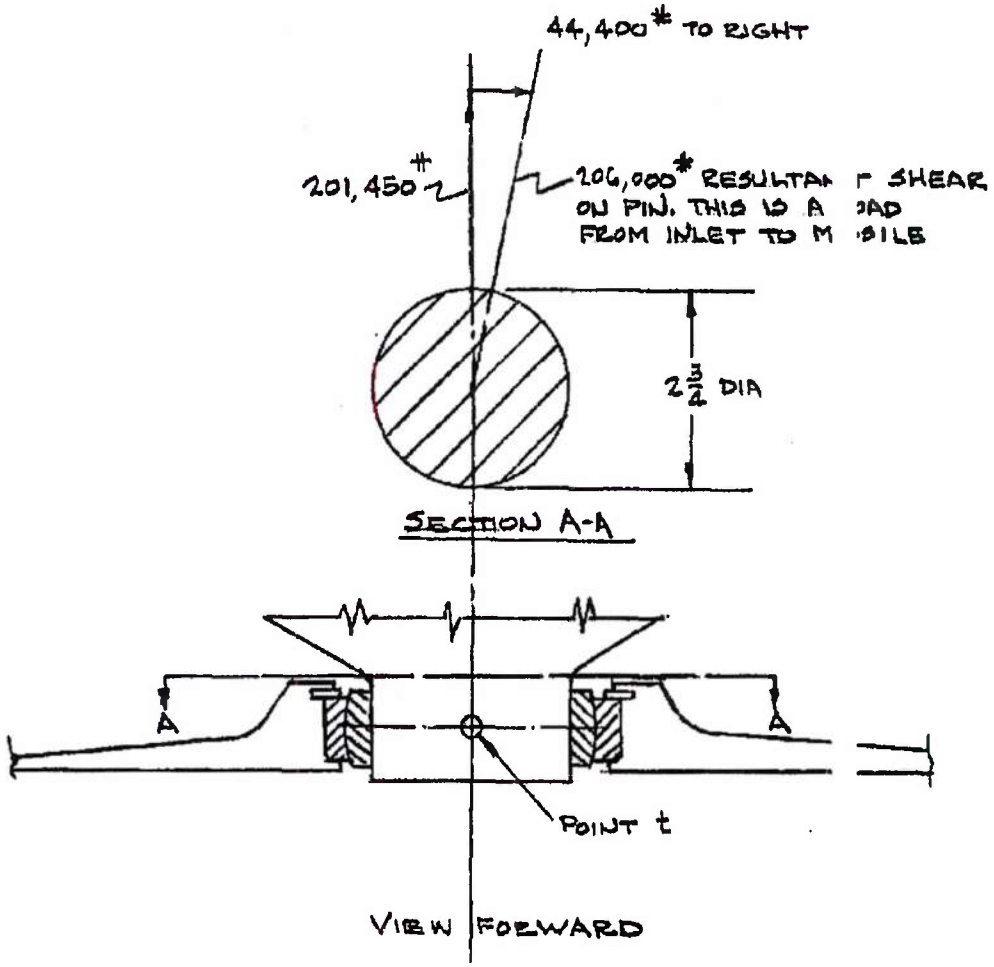

FIGURE 41. Thrust Fitting Loads

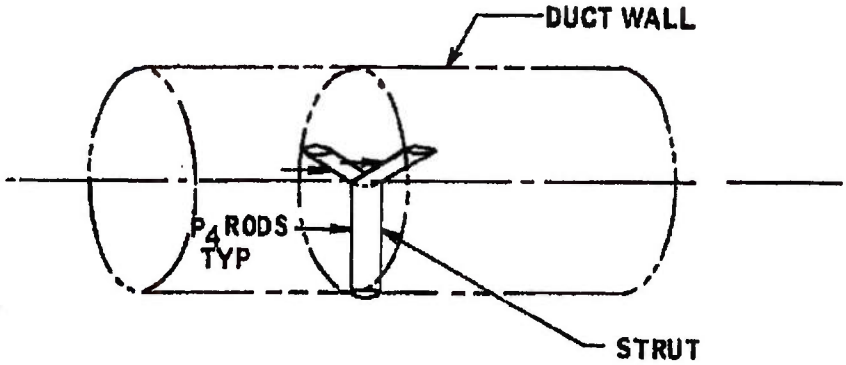

FIGURE 42. Struts

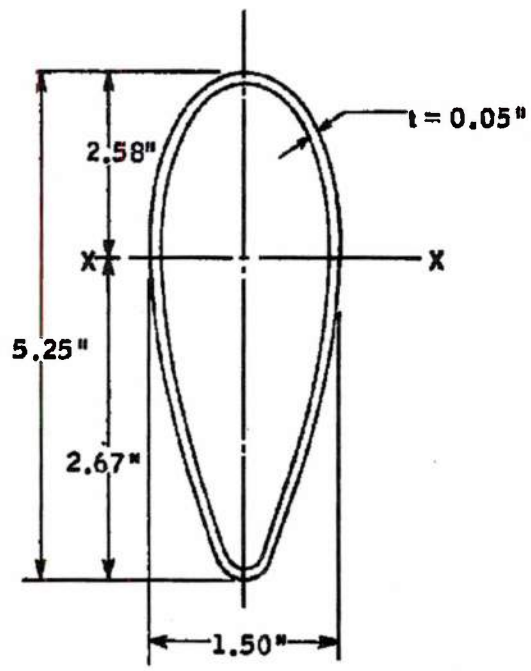

FIGURE 43. Strut Cross Section

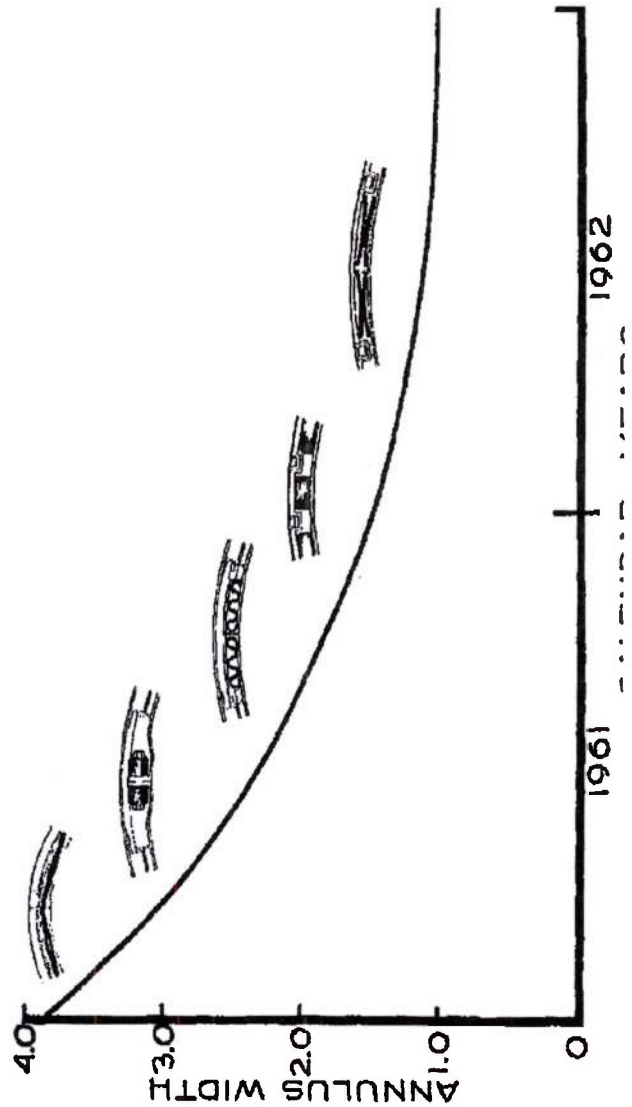

FIGURE 44. Design Progress on Reactor Side Support Structure

~~SECRET RESTRICTED DATA~~
~~ATOMIC ENERGY ACT OF 1954~~

1

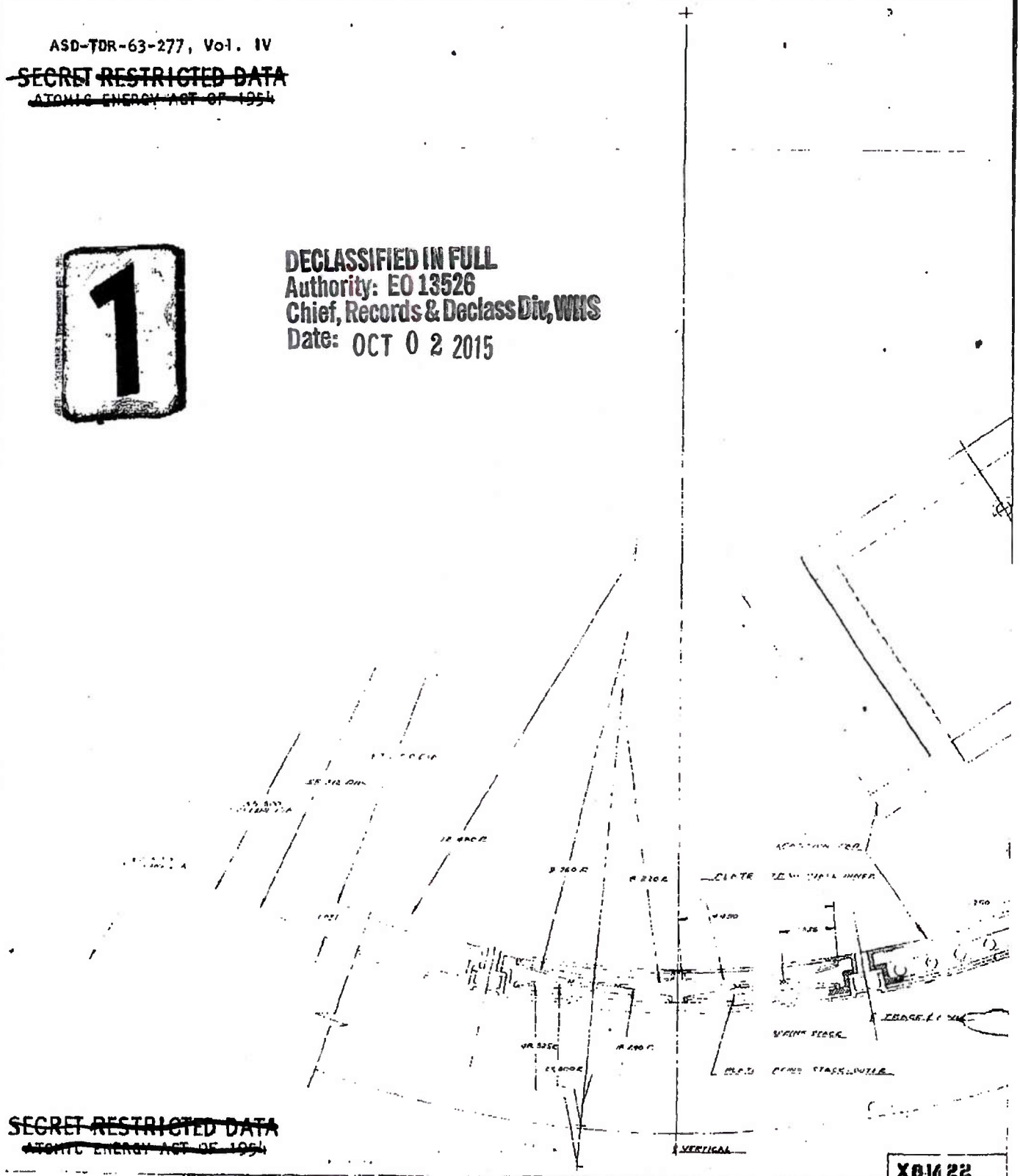

~~SECRET RESTRICTED DATA~~
~~ATOMIC ENERGY ACT OF 1954~~

2

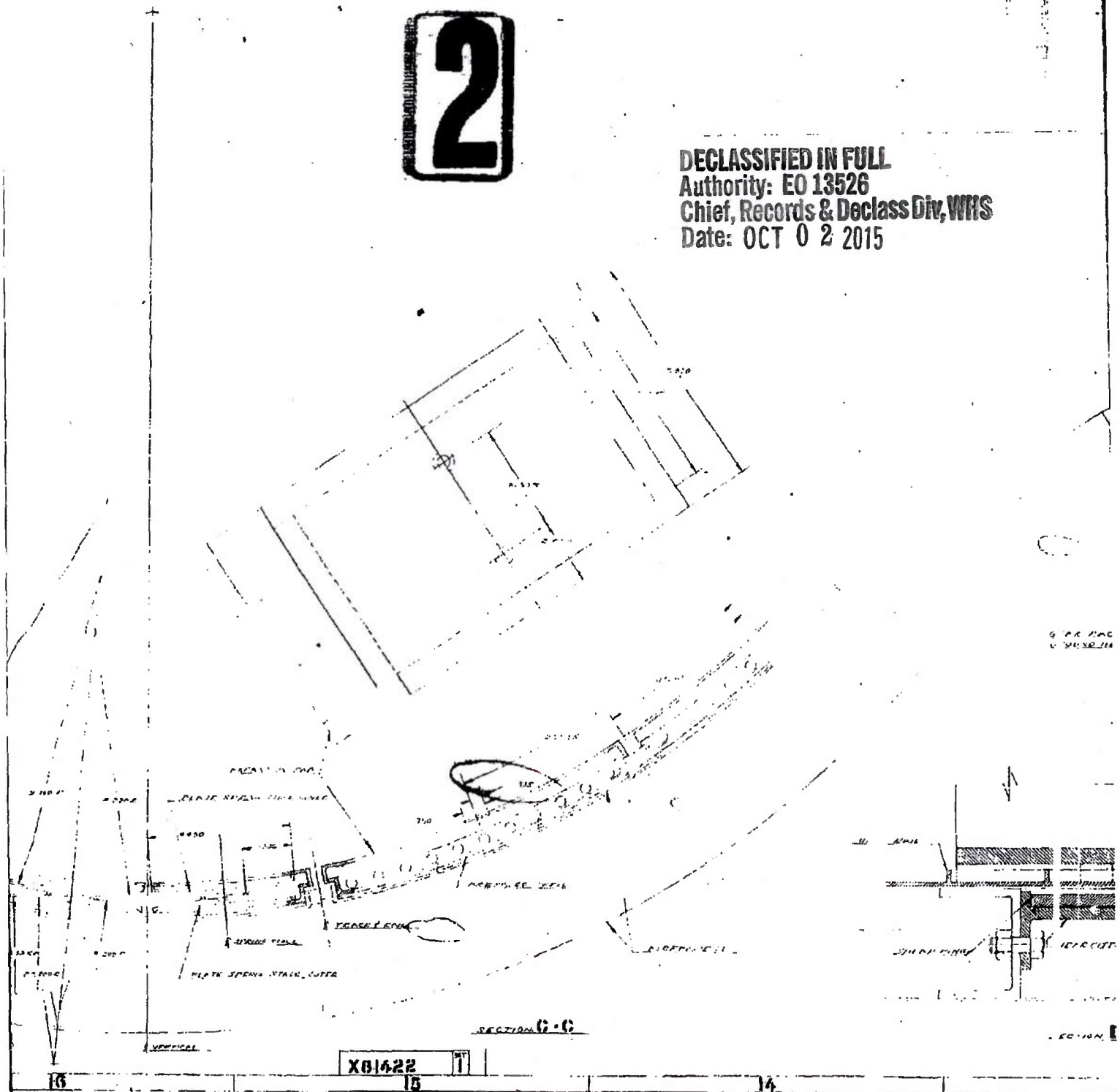

3

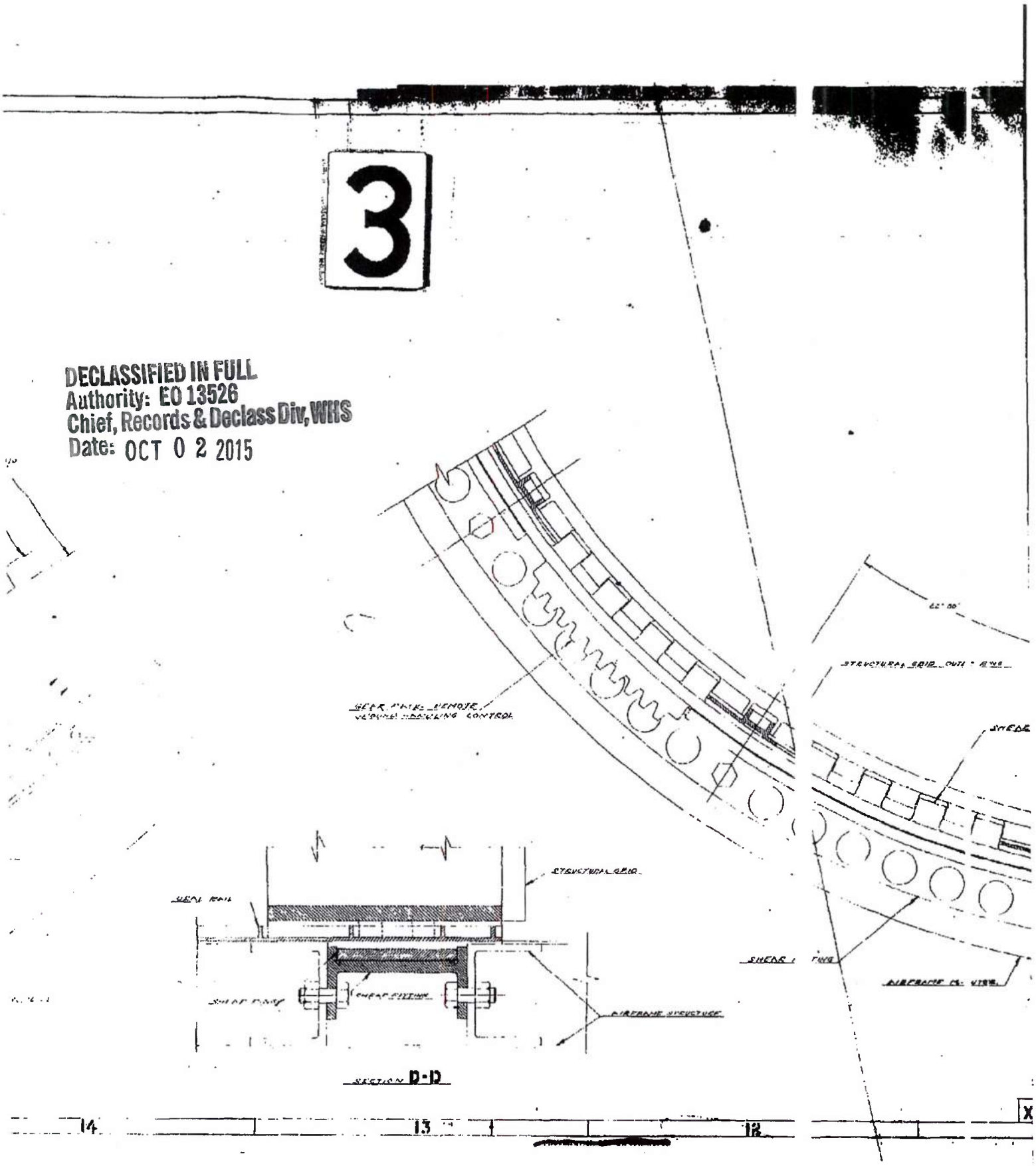

4

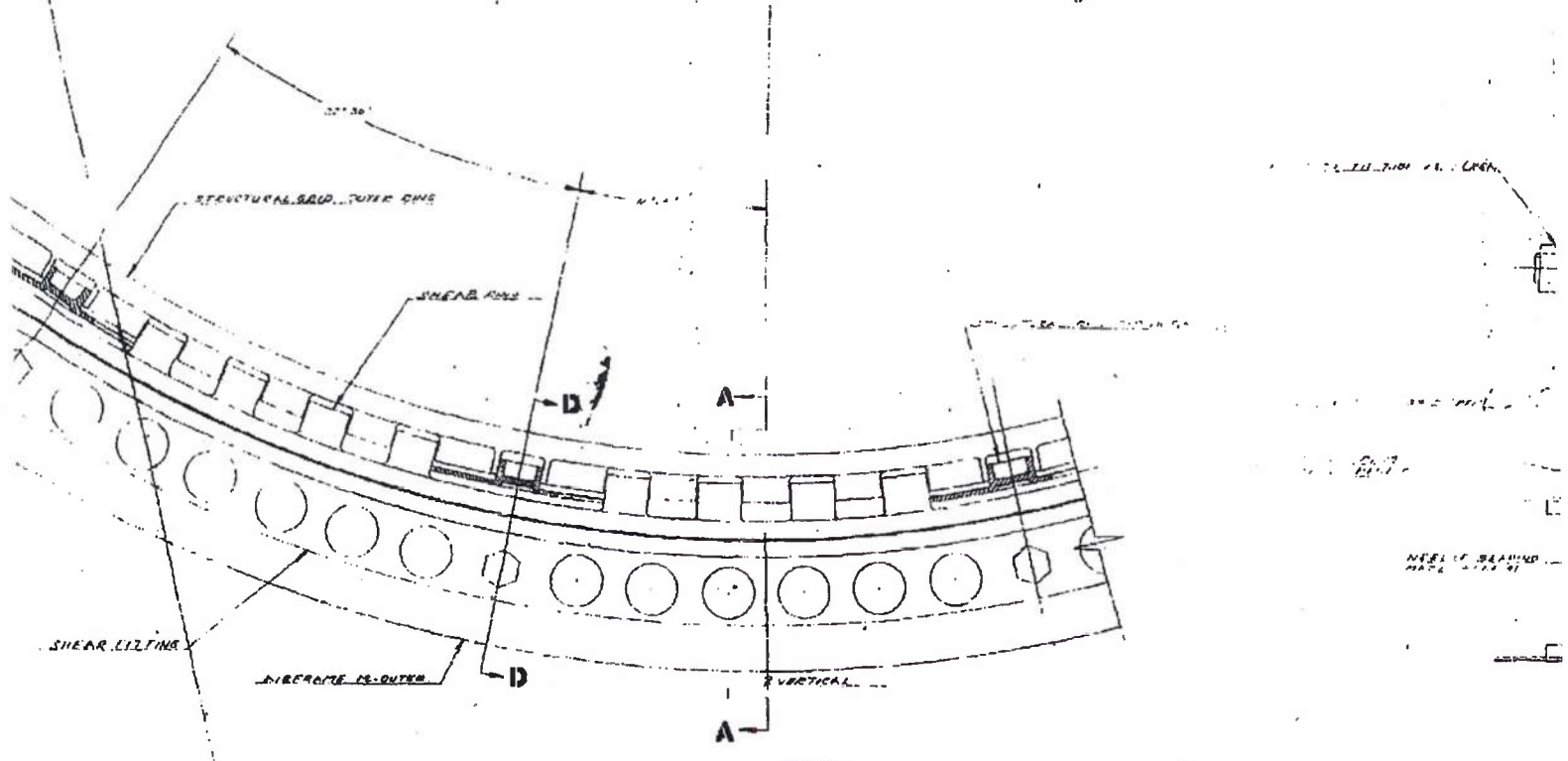

SECTION B-B
SHEAR RING SHOWN IN OPEN POSITION

5

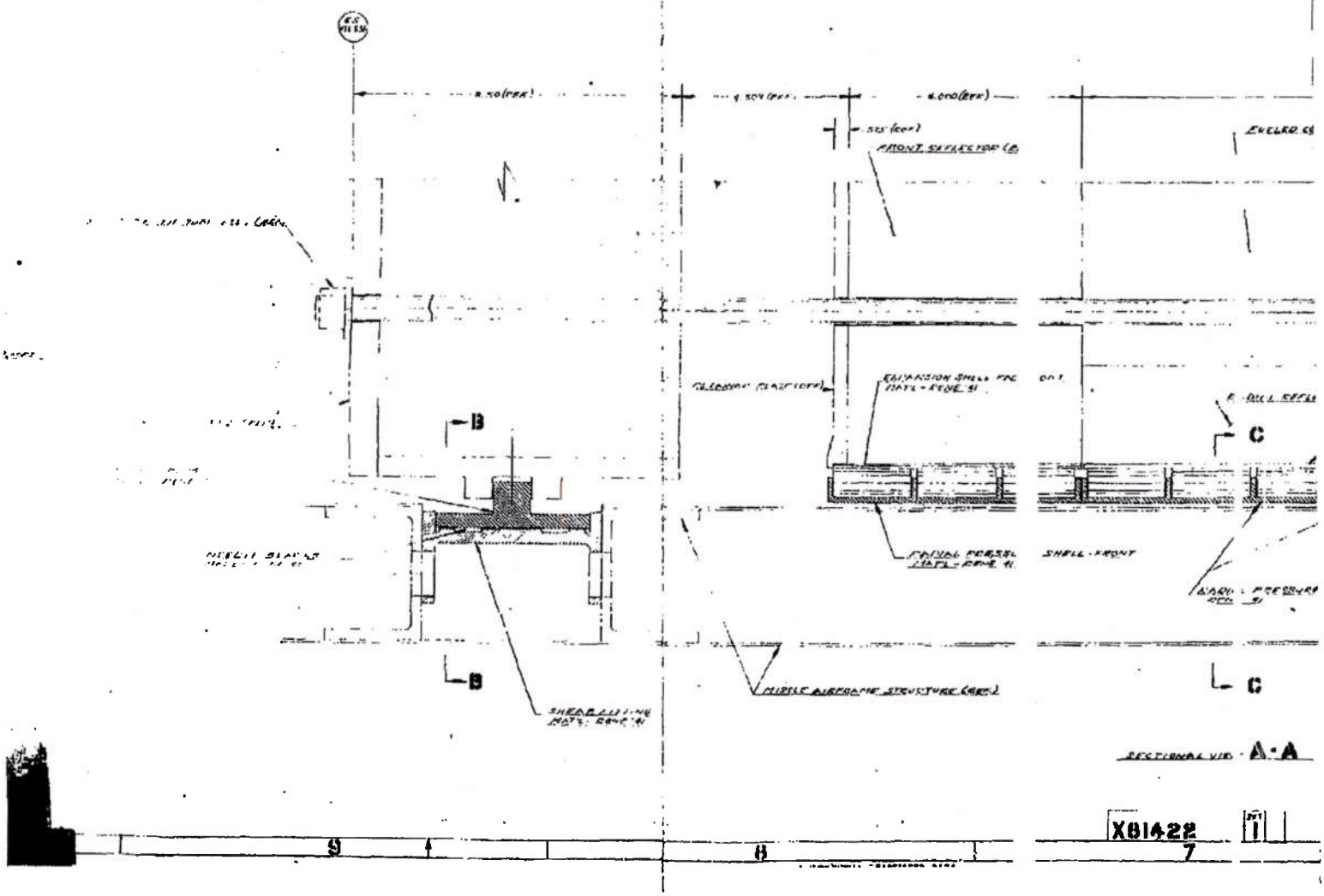

6

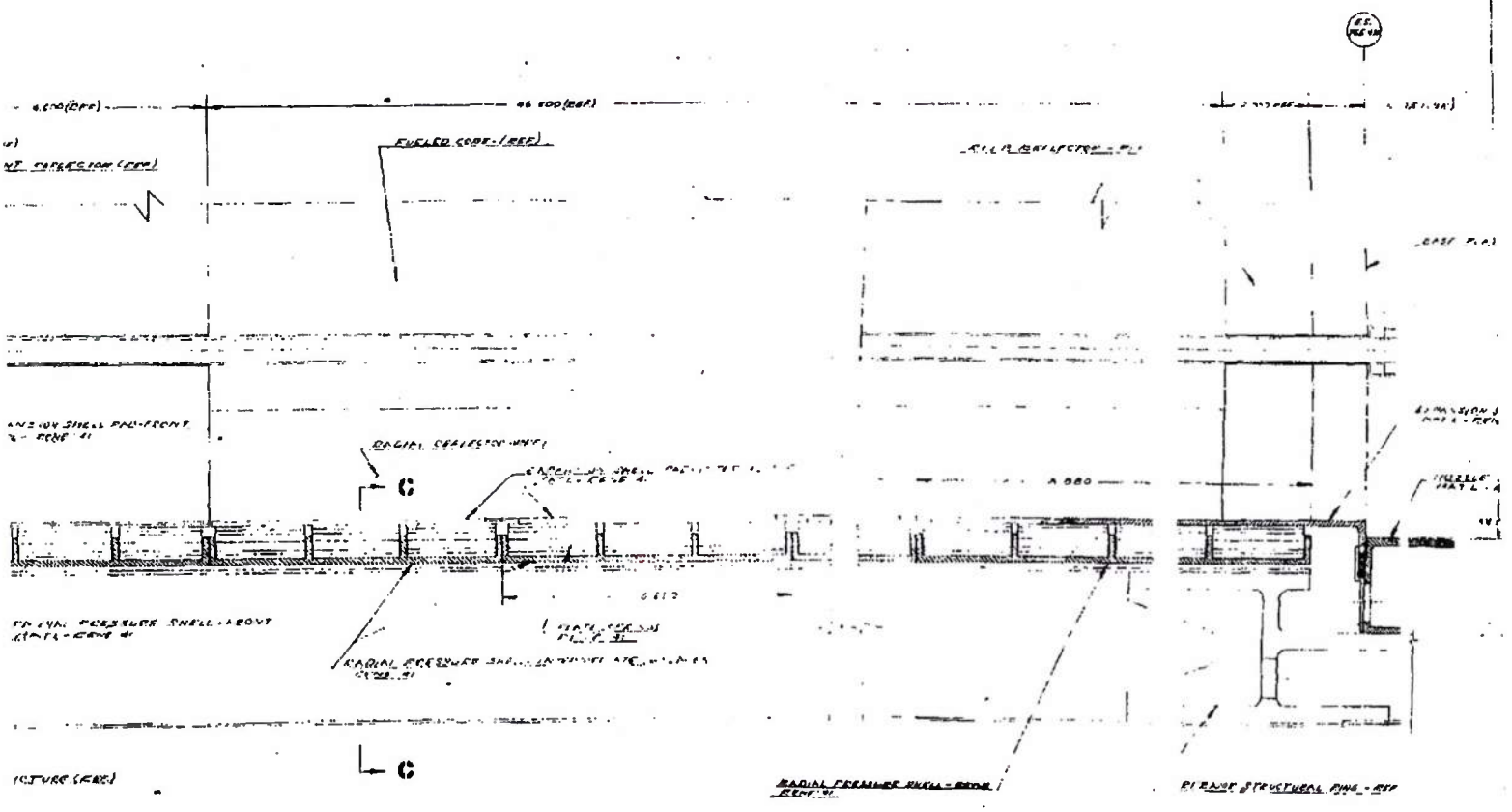

SECTIONAL VIEW A-A

X61422 | 1

7 6 5

7

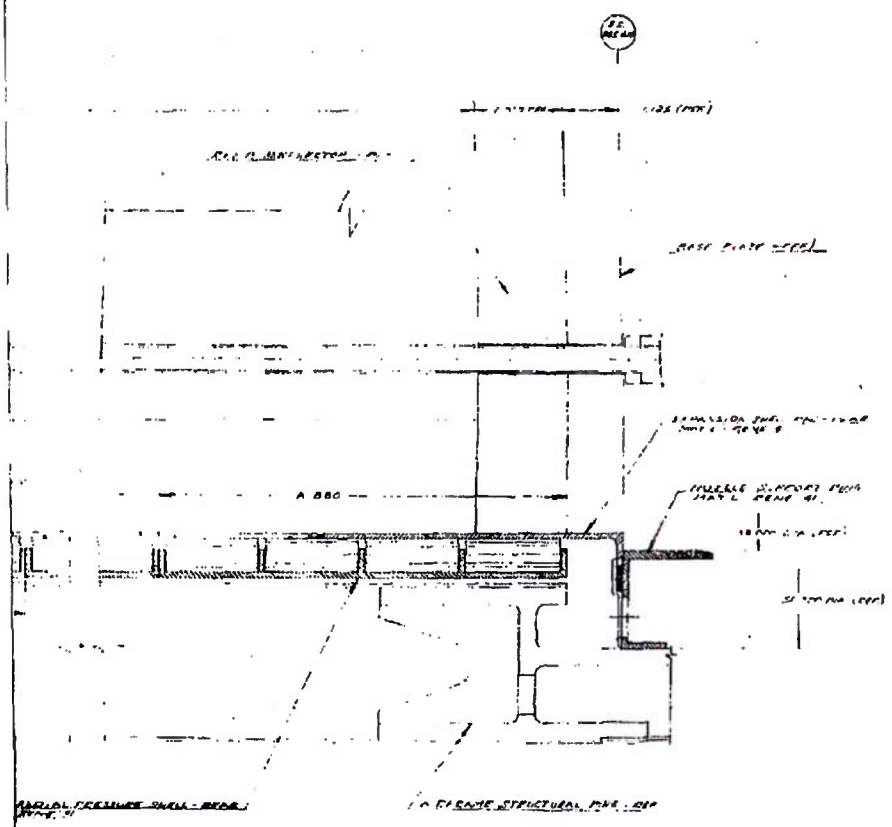

K61422

6 5 4 3

FIGURE 45. Design Layout, Reactor stallation

[redacted]

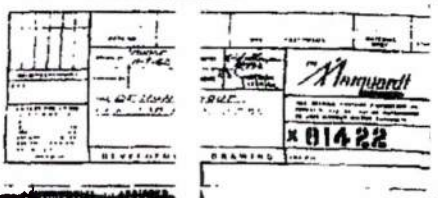

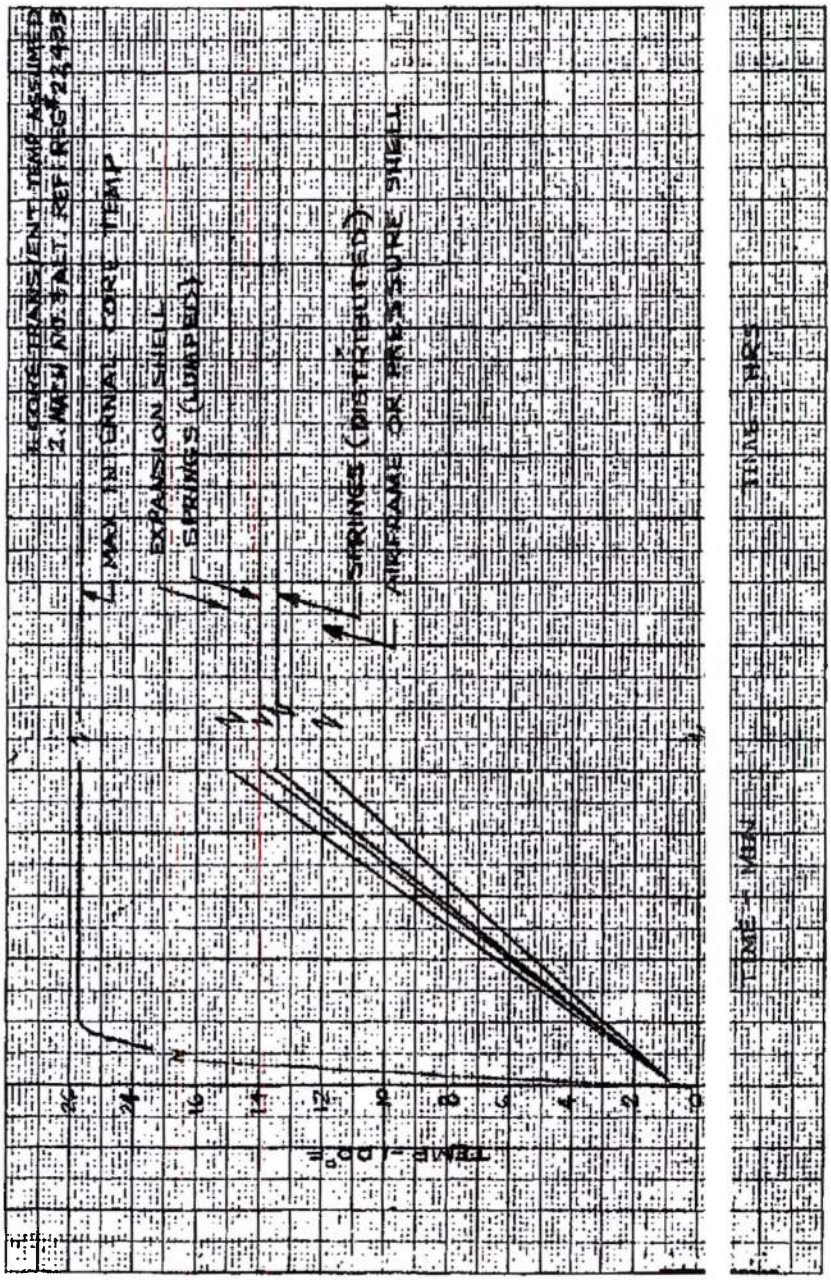

FIGURE 46. Assumed Side Support Temperatures (ANA Hot Day)

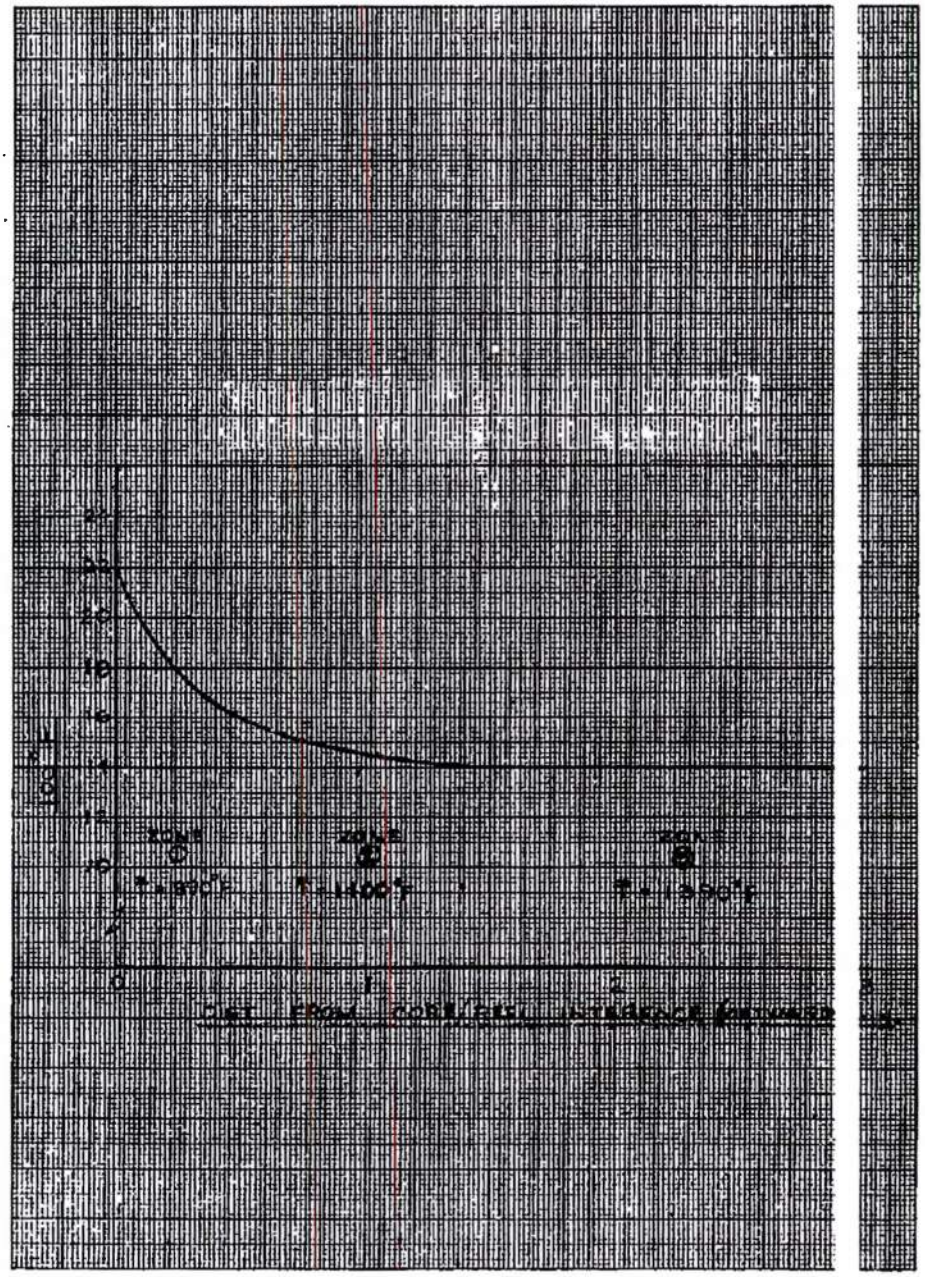

FIGURE 47. Assumed Side Reflector Temperature Distribution

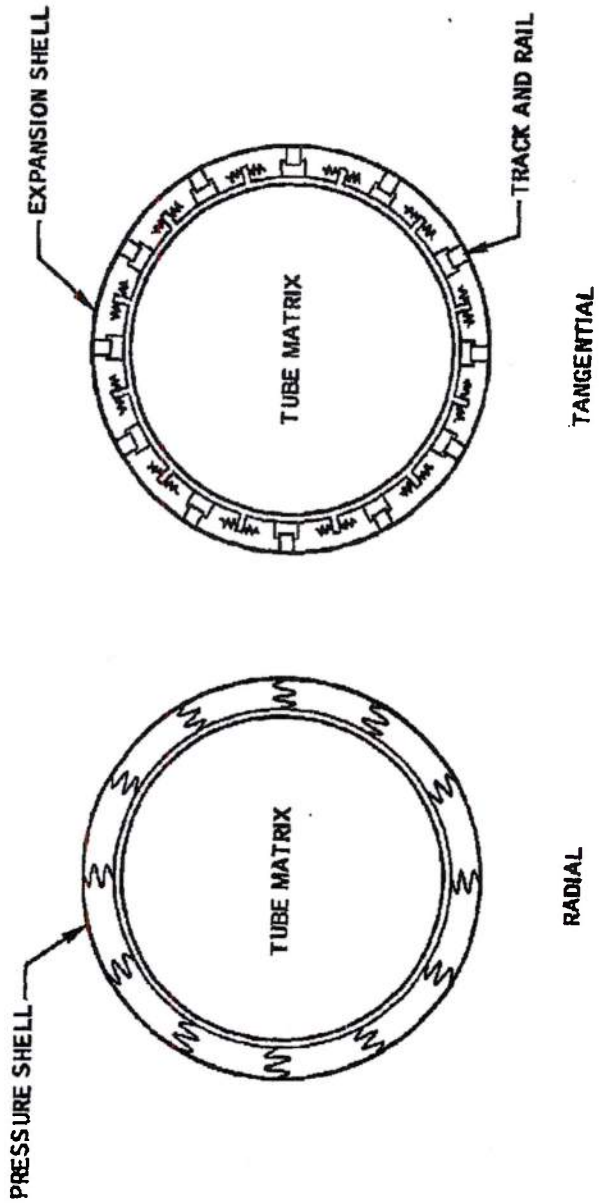

FIGURE 48. Schematic of Radial and Tangential Support Structures

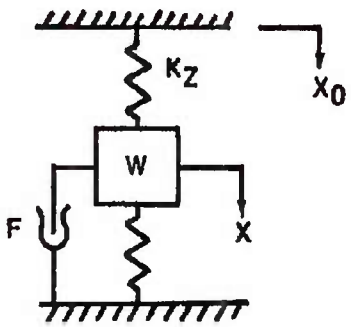

W = WEIGHT OF REACTOR, LBS/AXIAL INCH

K_Z = EFFECTIVE TRANSVERSE SPRING CONSTANT OF LATERAL S PPORT, LBS/AXIAL INCH/TRANSVERSE INCH

F = FRICTION FORCE EXERTED ON PERIPHERY OF REACTOR, LB: AXIAL INCH

X_0 = PRESCRIBED TRANSVERSE DEFLECTION OF VEHICLE, INCHE

X = RESULTING DEFLECTION OF REACTION, INCHES

FIGURE 49. Dynamic System Model

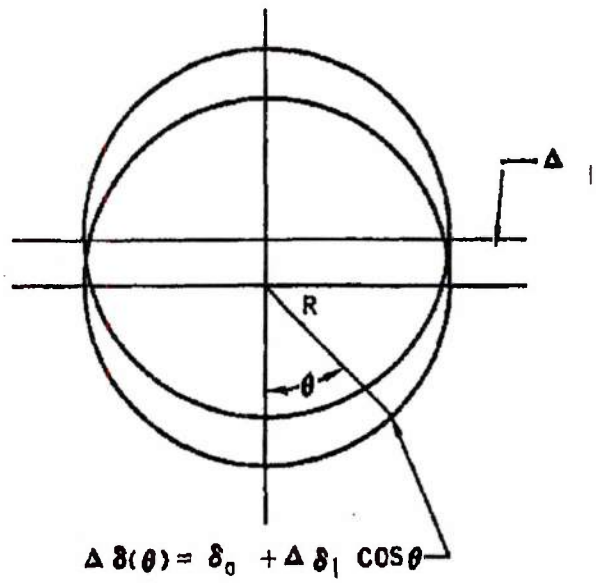

FIGURE 50. Pressure Distribution

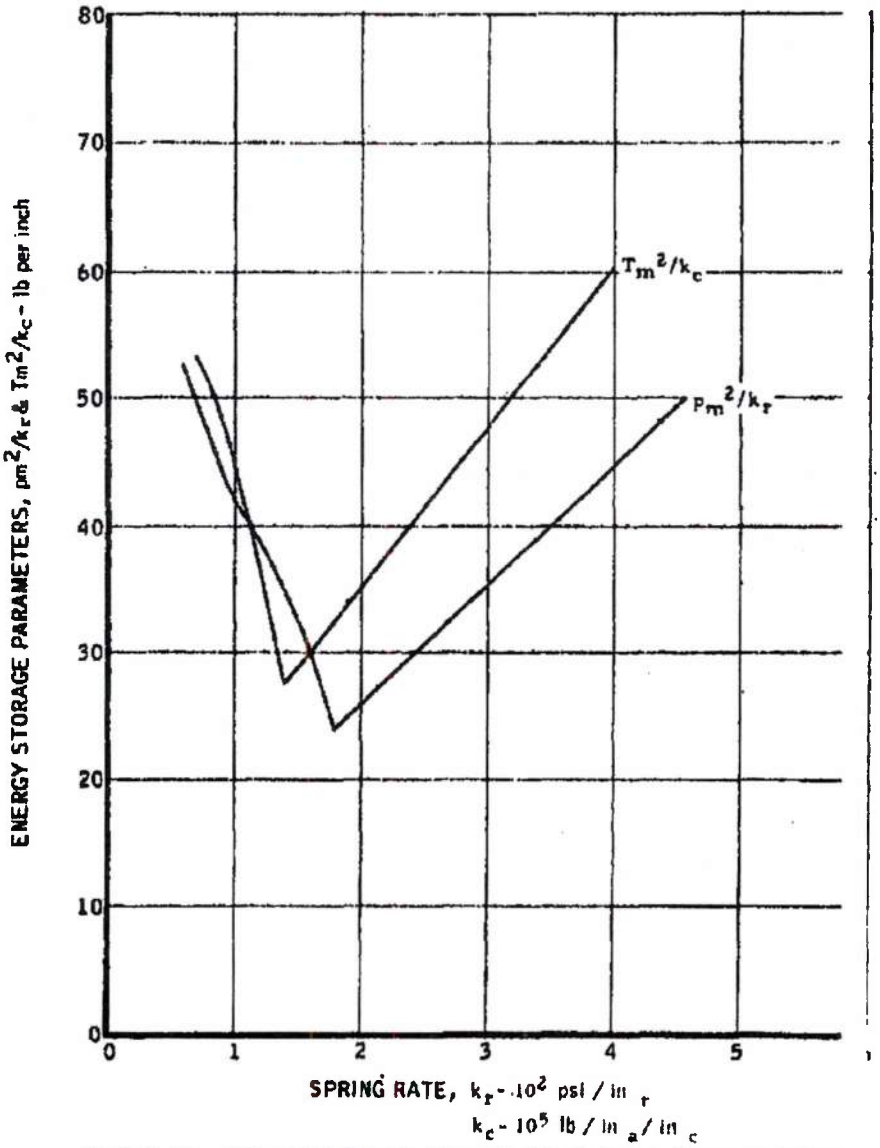

FIGURE 51. Required Energy Storage for Lateral Support System

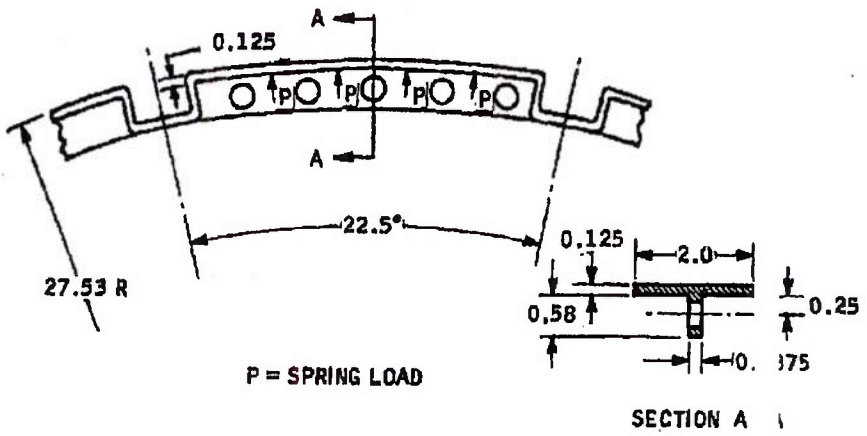

FIGURE 52. Typical Section of Web-Shell Combinatic

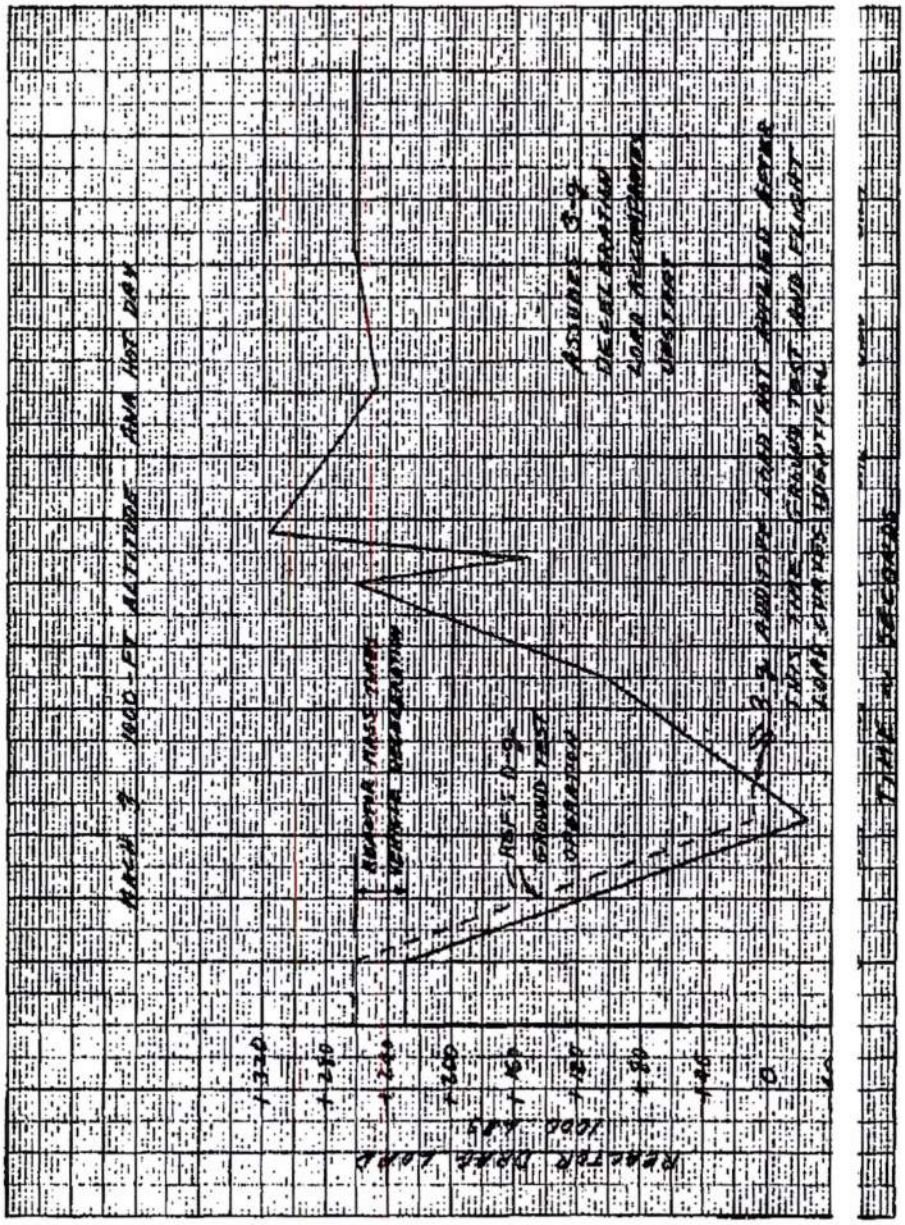

FIGURE 53. Estimated Full Scale Reactor Drag Load Variation During Unstart Transient Flight Operation

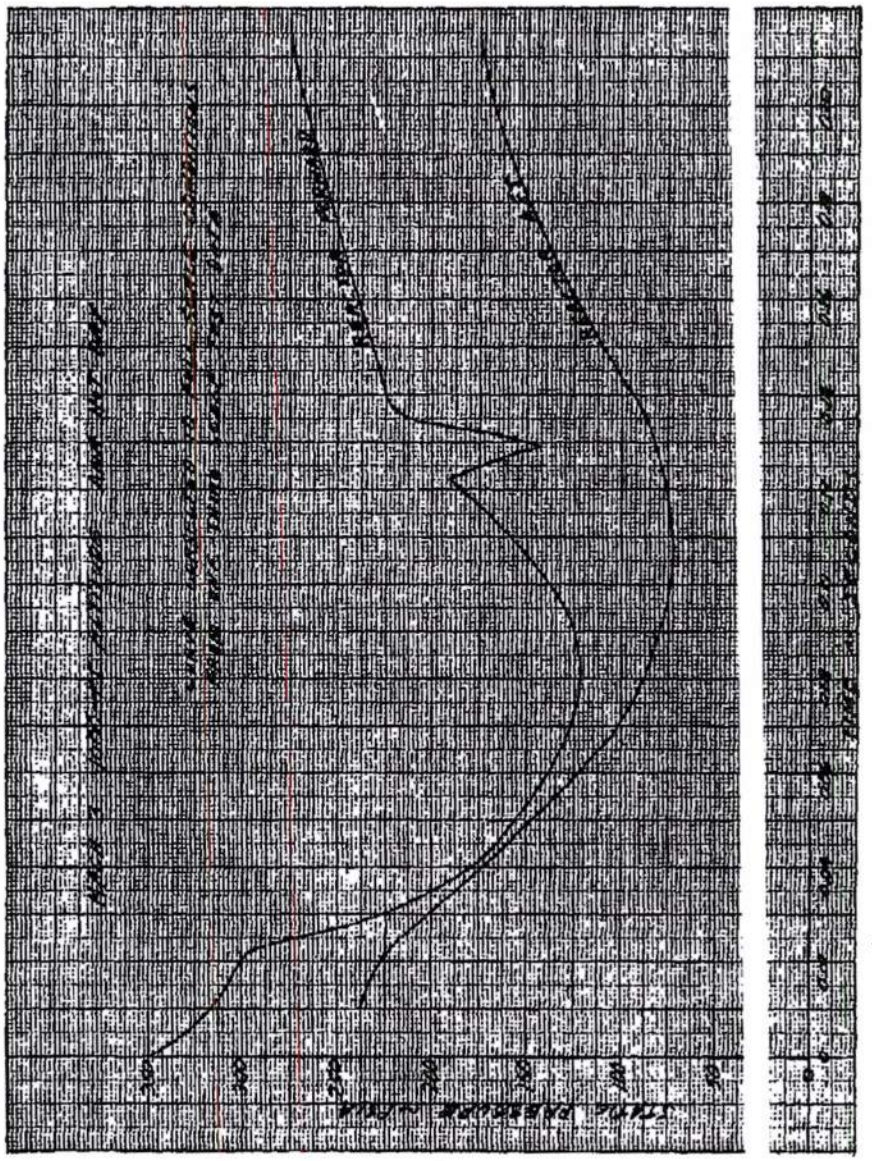

FIGURE 54. Estimated Pressure Transient on Full Scale Reactor During Unstart

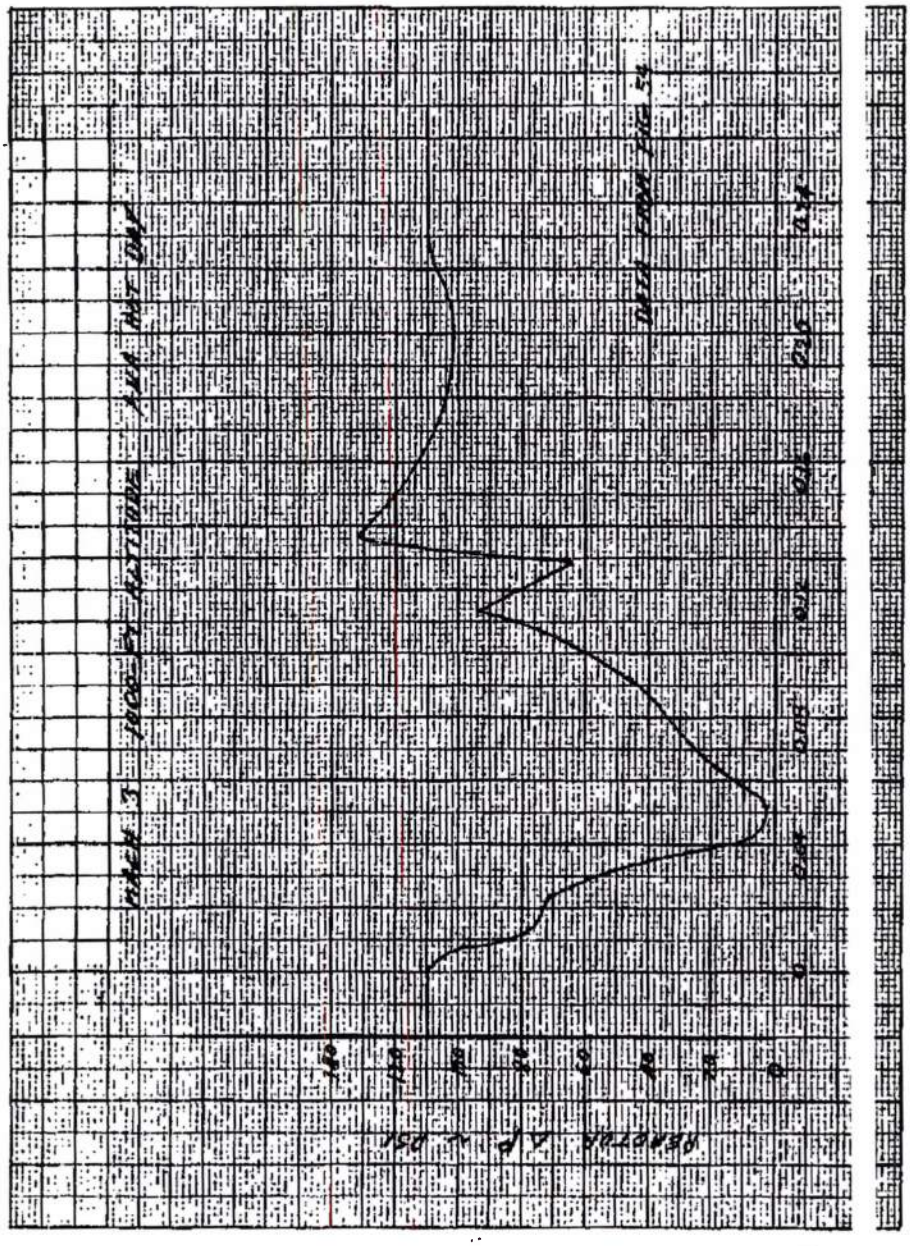

FIGURE 55. Estimated Differential Pressure Variation on Full Scale Reactor During Unstart

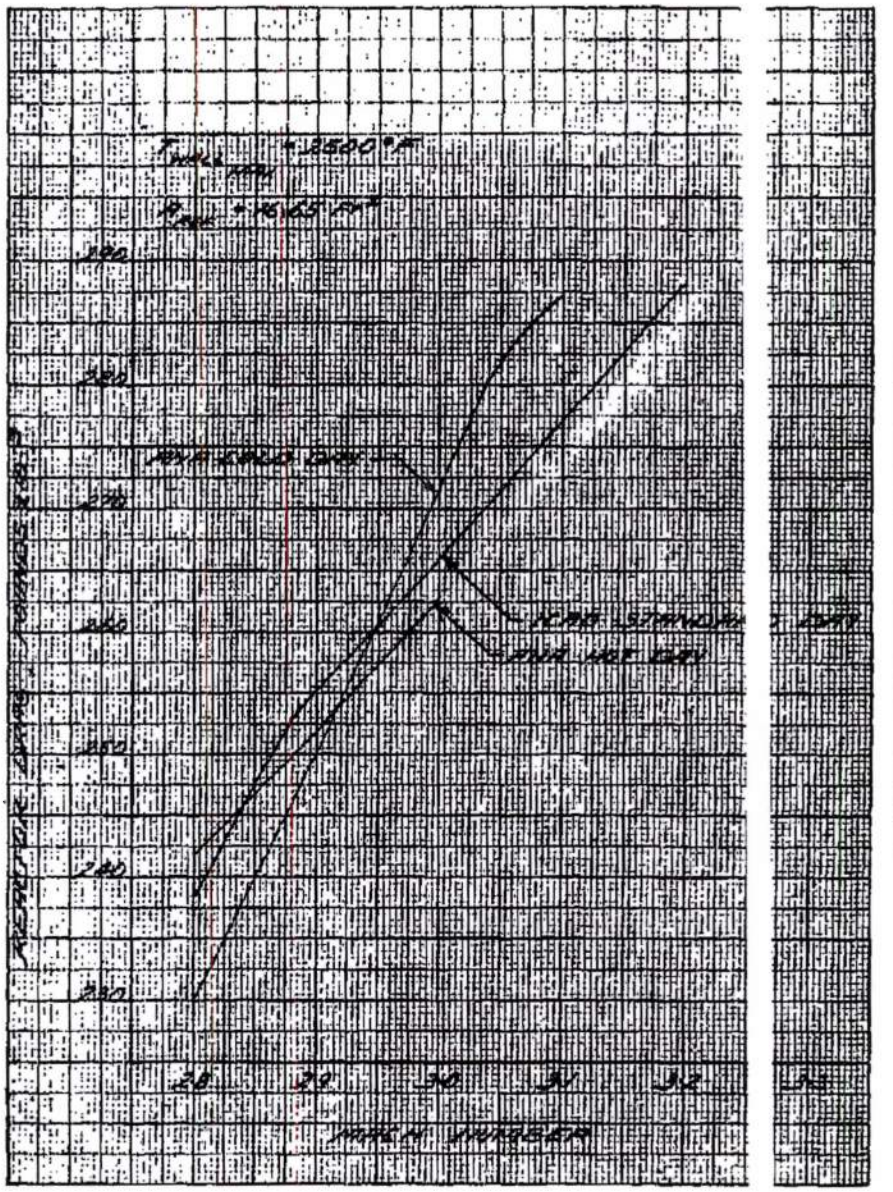

FIGURE 56. Reactor Drag, 1,000-Ft Altitude

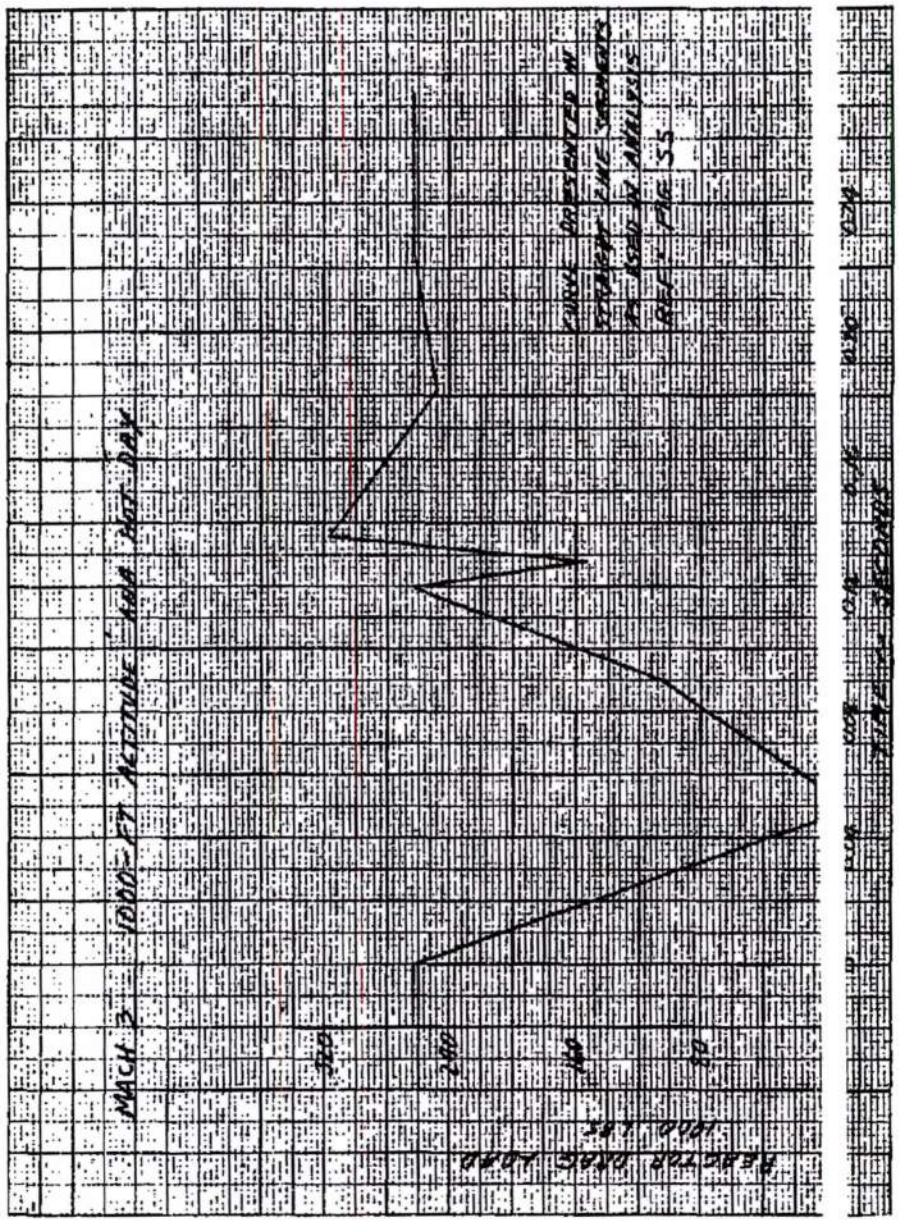

FIGURE 57. Estimated Full Scale Reactor Drag Load Variation During Unstart Transient Ground Test Only

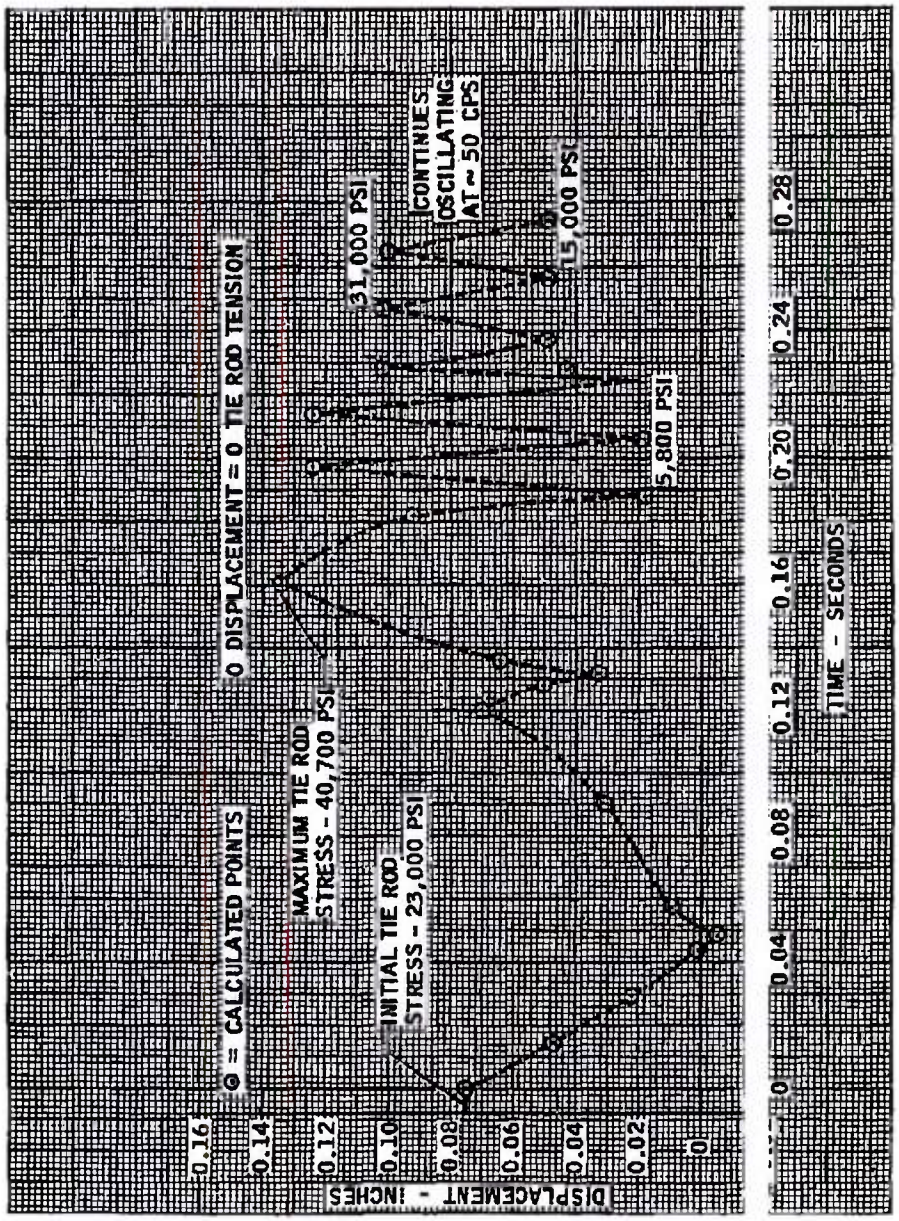

FIGURE 58. Estimated Reactor Displacement During Unstart Transient Ground Test Only--
Mach 3, 1000-Ft Altitude, ANA Hot Day

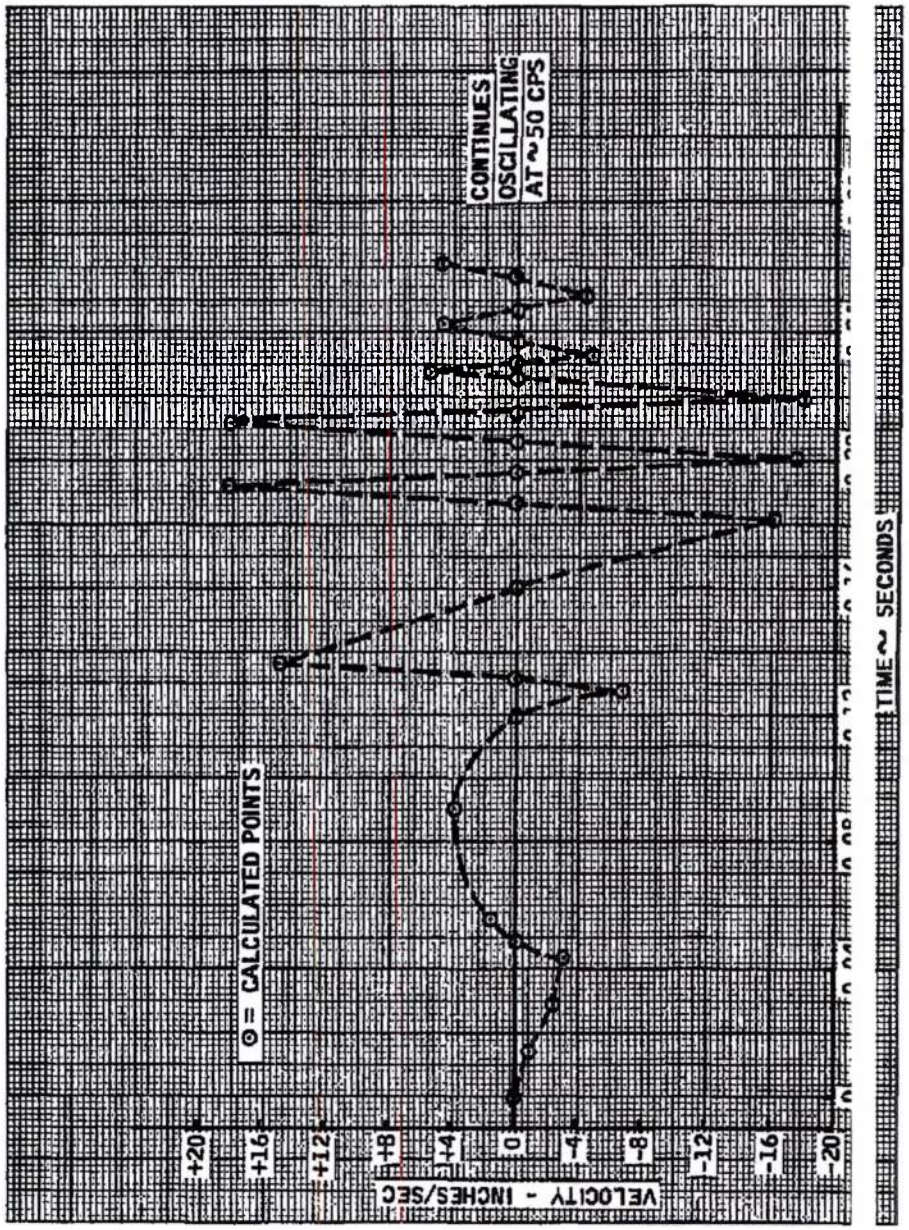

FIGURE 59. Estimated Reactor Velocity During Unstart Transient Ground Test Only--
Mach 3, 1000-Ft Altitude, AMA Hot Day

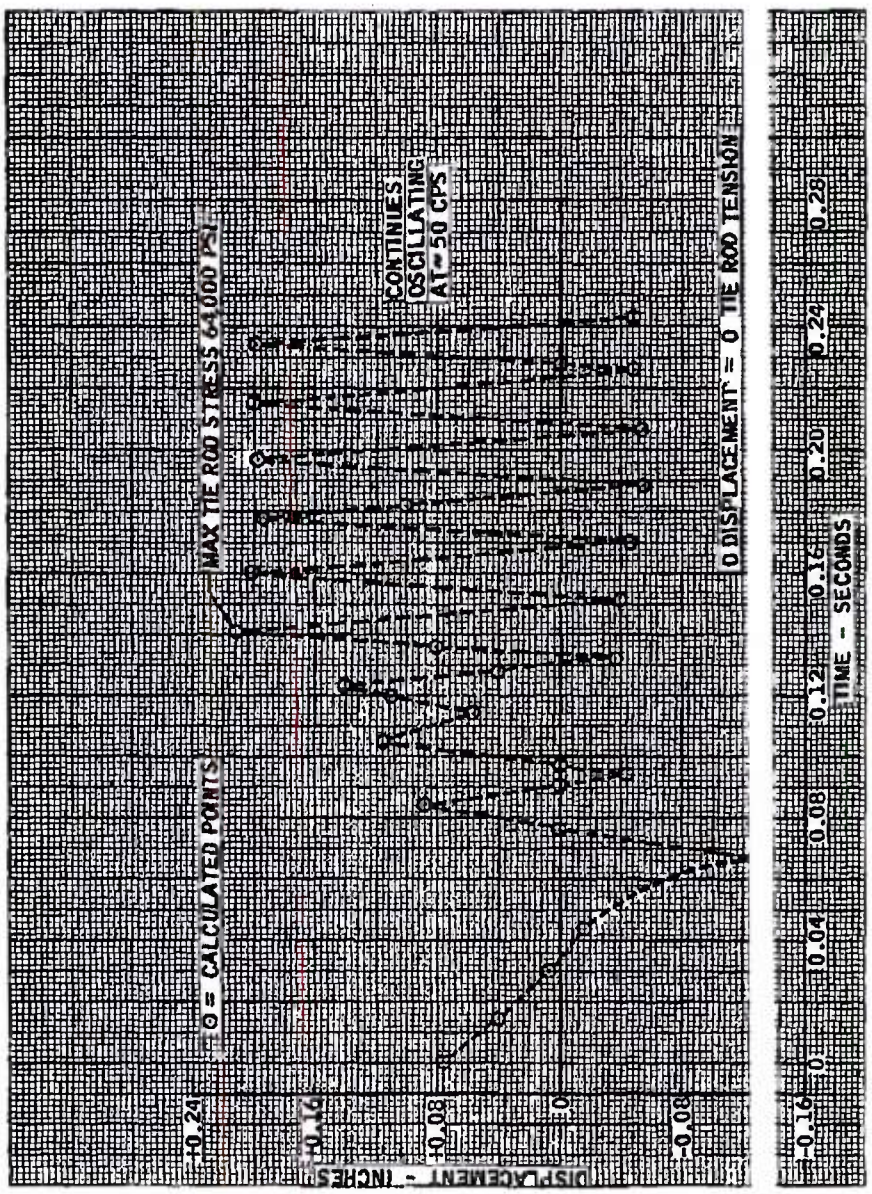

FIGURE 60. Estimated Reactor Displacement During Unstart Transient - Flight Operation With 3 g Vehicle Deceleration--Mach 3, 1000-Ft Altitude, ANA Hot Day

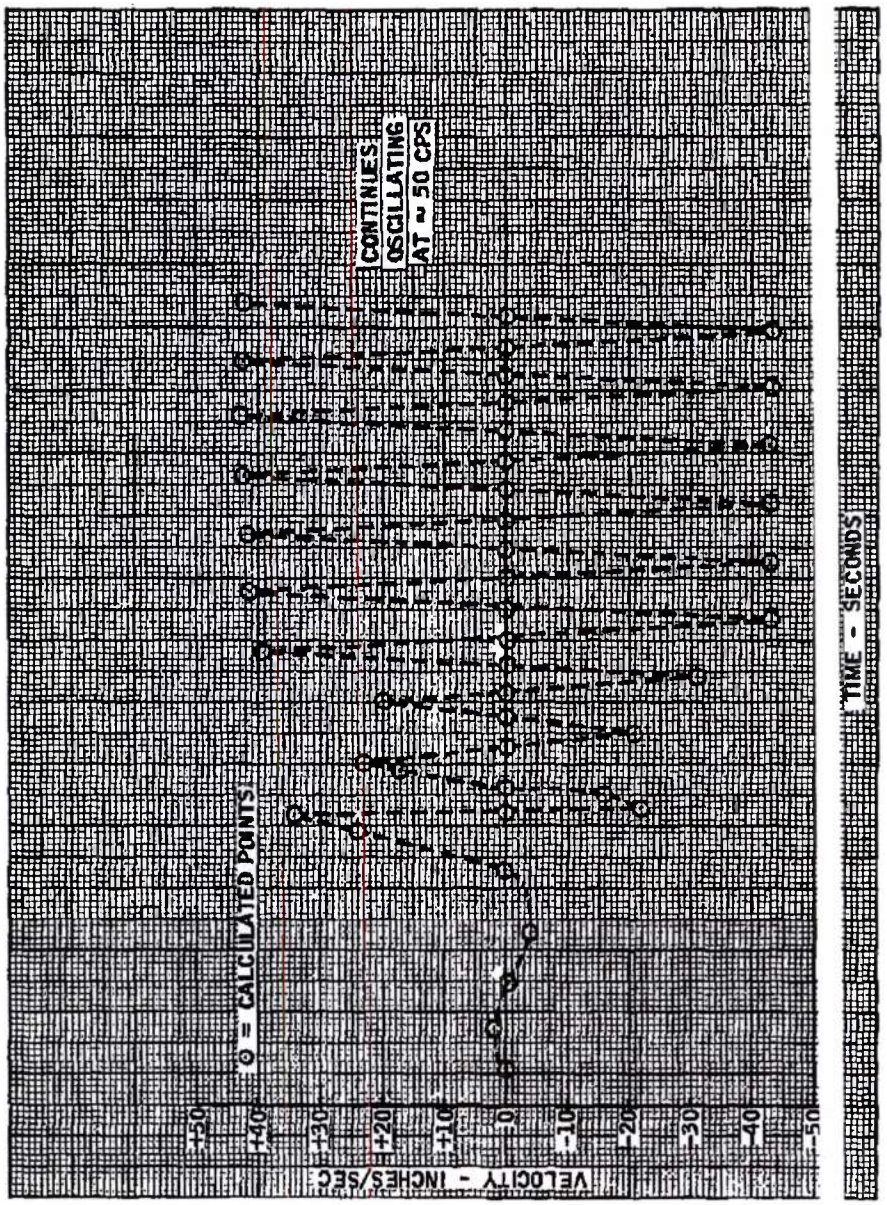

FIGURE 61. Estimated Reactor Velocity During Instart Transient - Flight Operation With 3g Vehicle Deceleration - Mach 3, 1000-Ft Altitude, ANA Hot Day

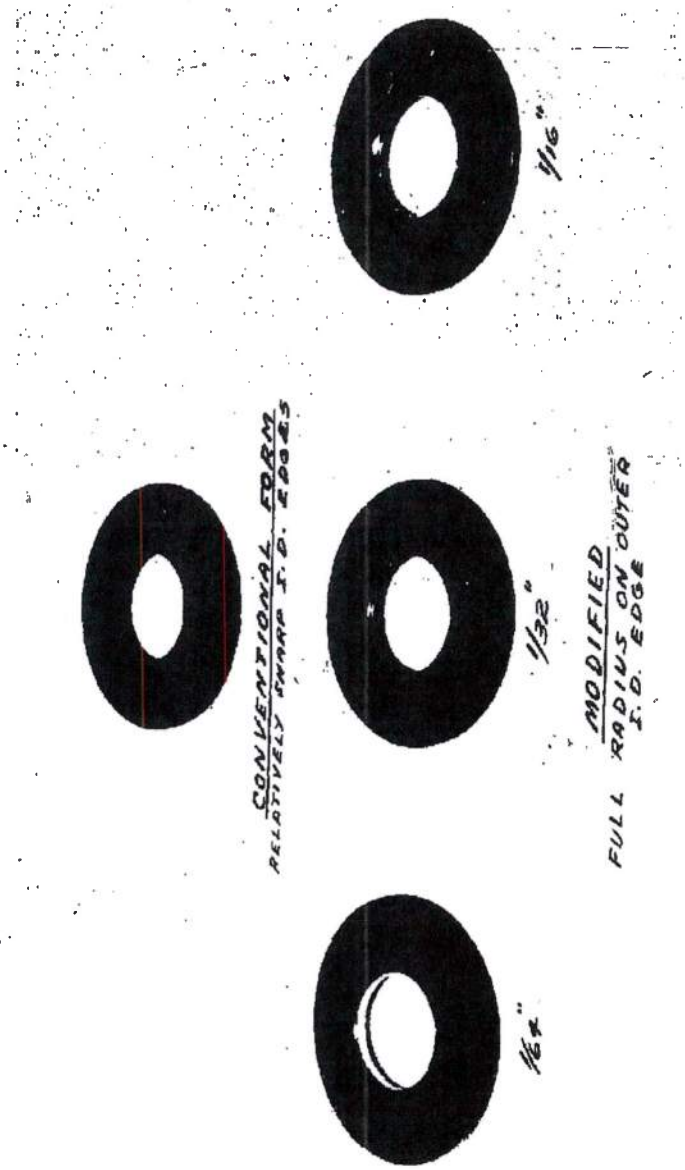

FIGURE 62. Belleville Springs--R-235 Material

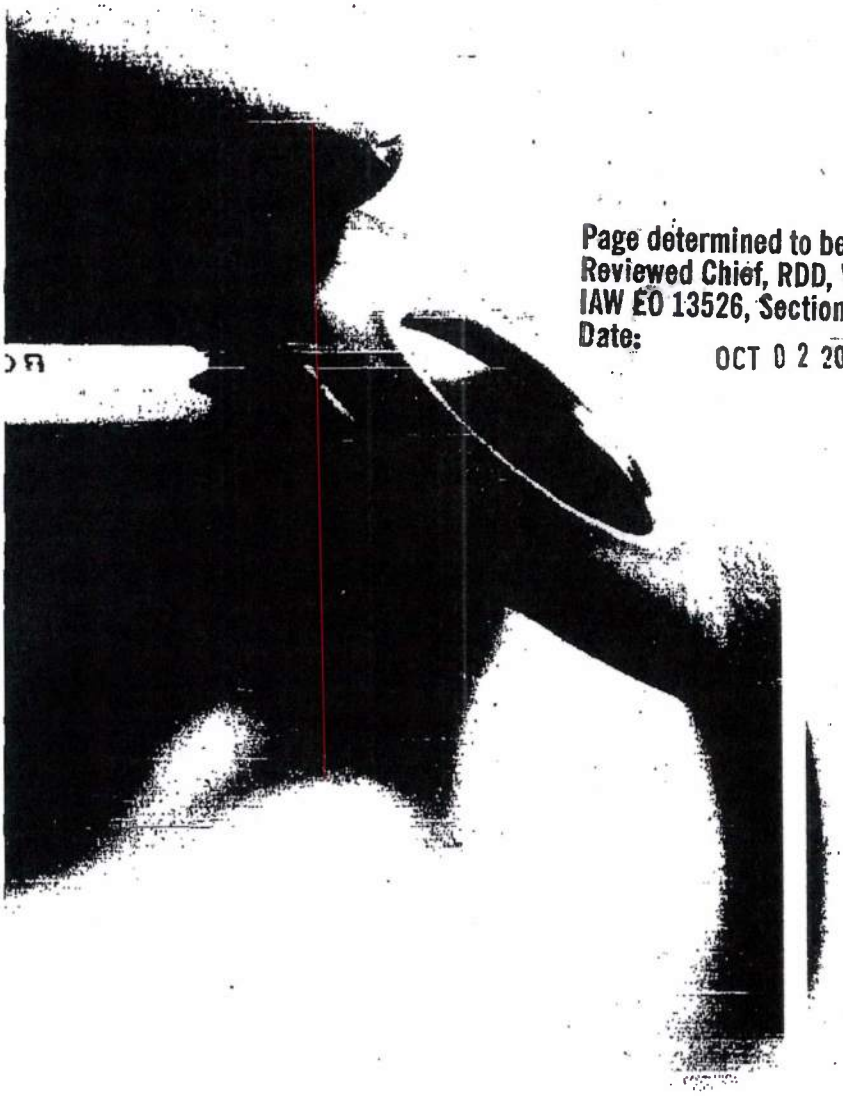

[illegible] 9F 63 Belleville Spring--R-235 Material
[illegible] Both I.D. Edges)

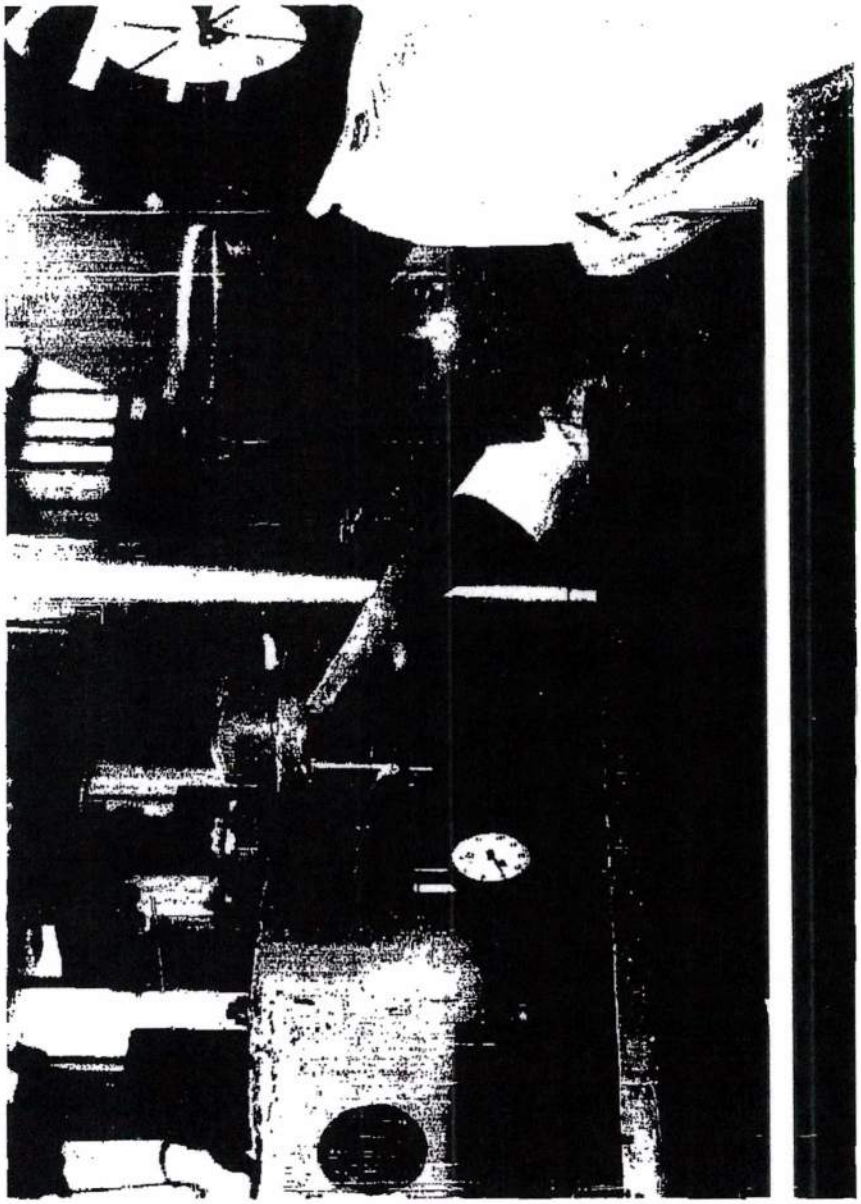

FIGURE 64. Test Setup for Single Belleville Spring--R-235 Material

4155-3

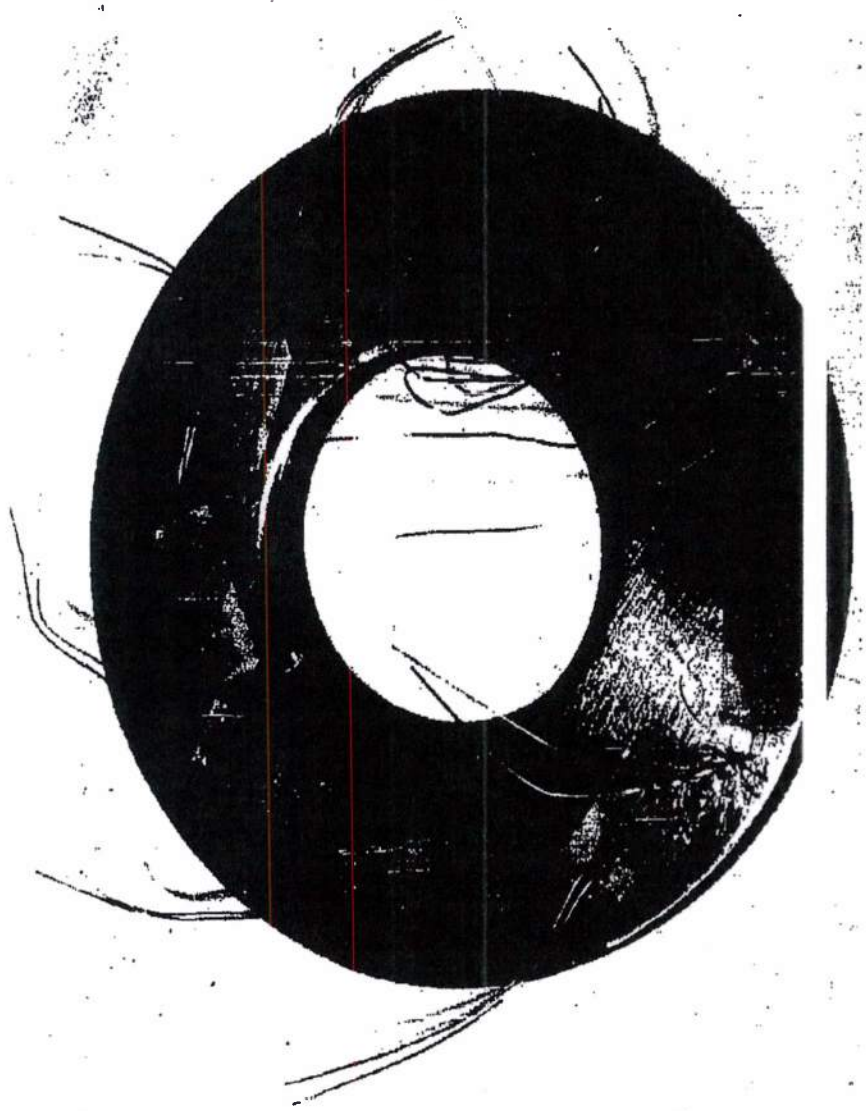

FIGURE 65. Strain Gages Installed on Inner and Outer Surfaces of Modified Belleville Spring (1/16-in. Full Radius Both I.D. Edges)--R-235 Material

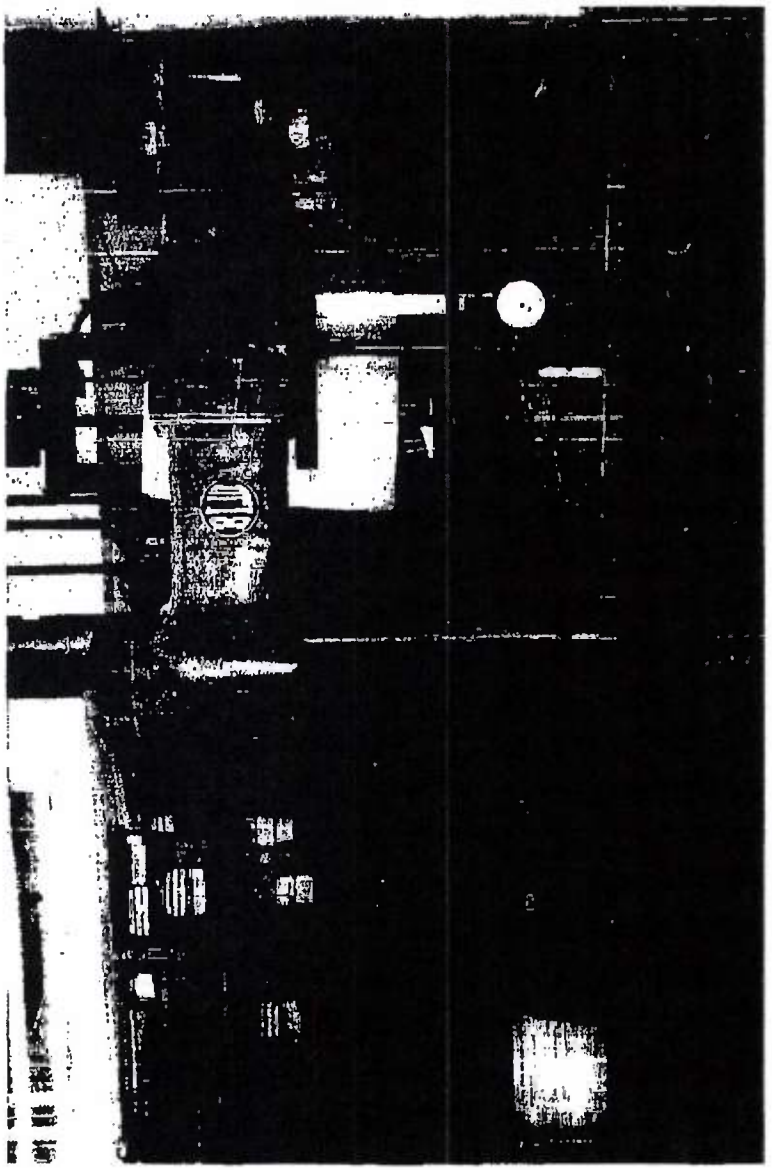

FIGURE 66. Setup for Test of Single Belleville Spring with Strain Gages Installed

(SR-4, A-19 PAPER BACKED, 1/16" x 1/16" STRAIN GAGES)

AMBIENT TEMPERATURE
(EFFECTIVE FLAT PLATE LOADING)

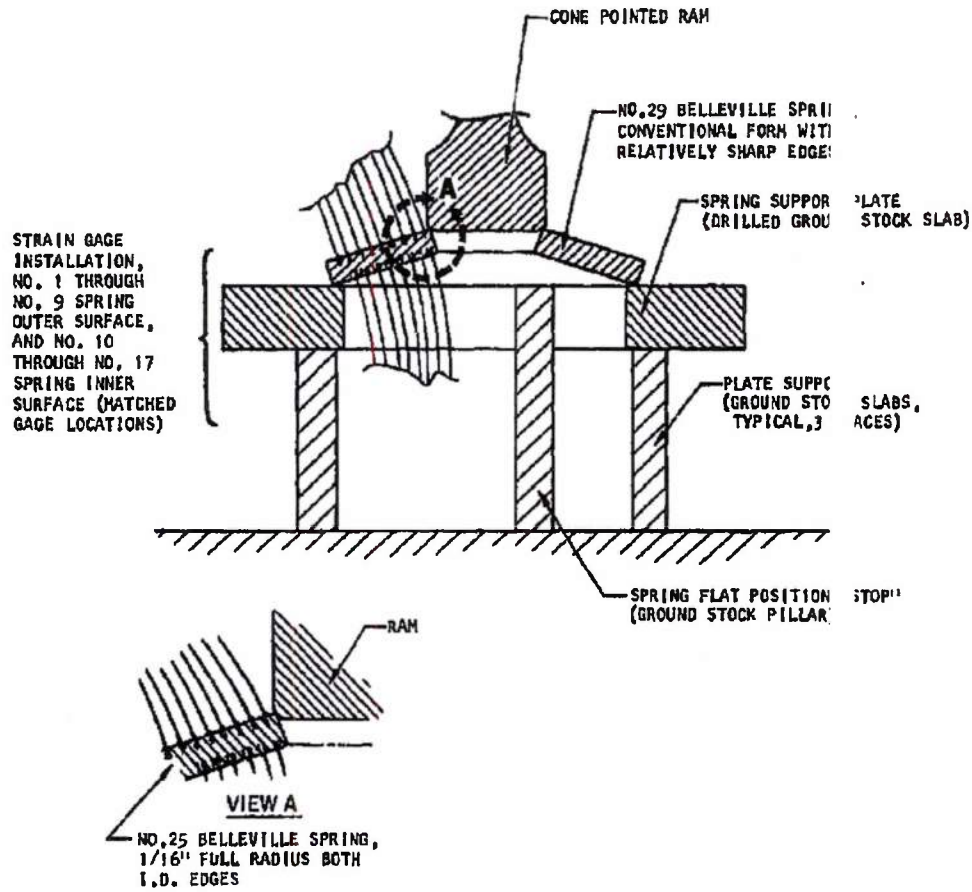

FIGURE 67. Test Setup for Strain Gaged Belleville Springs (R-235 Material)

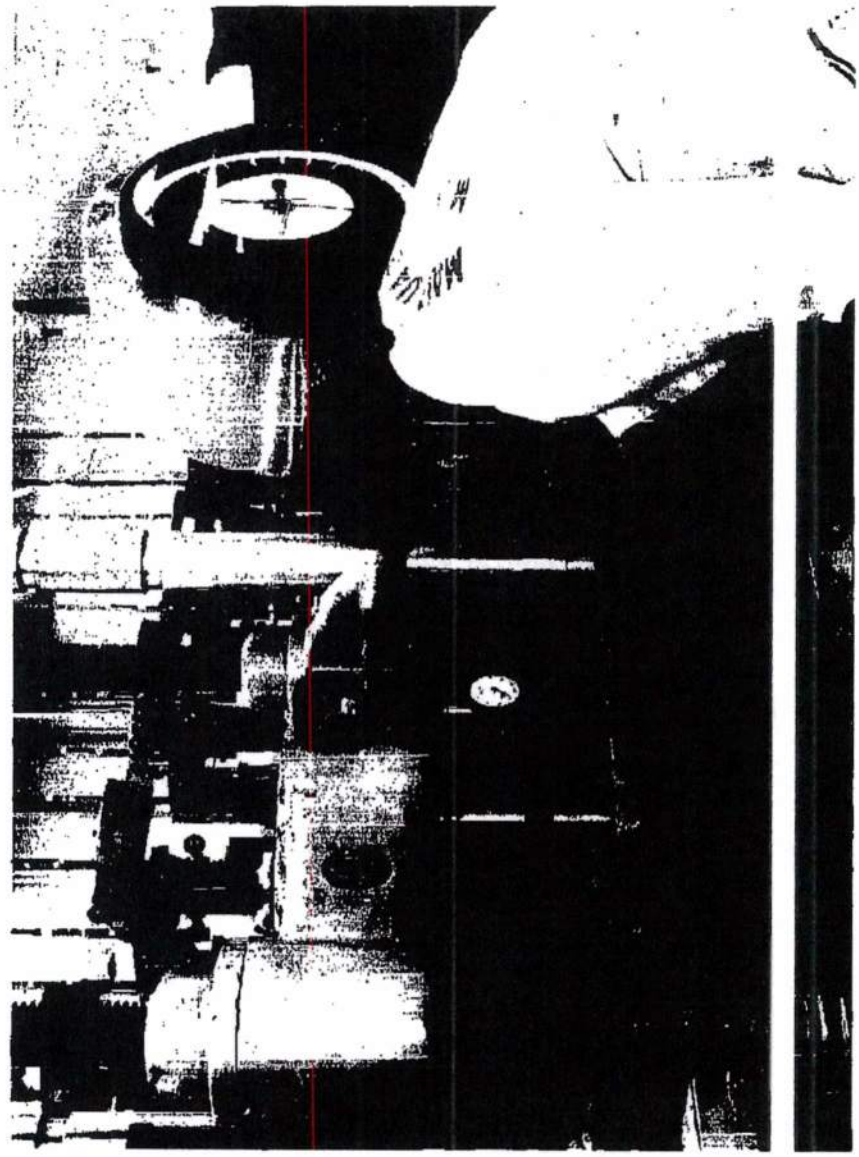

FIGURE 58. Test Setup for 10-Spring Series Stack of Belleville Springs--R-235 Material

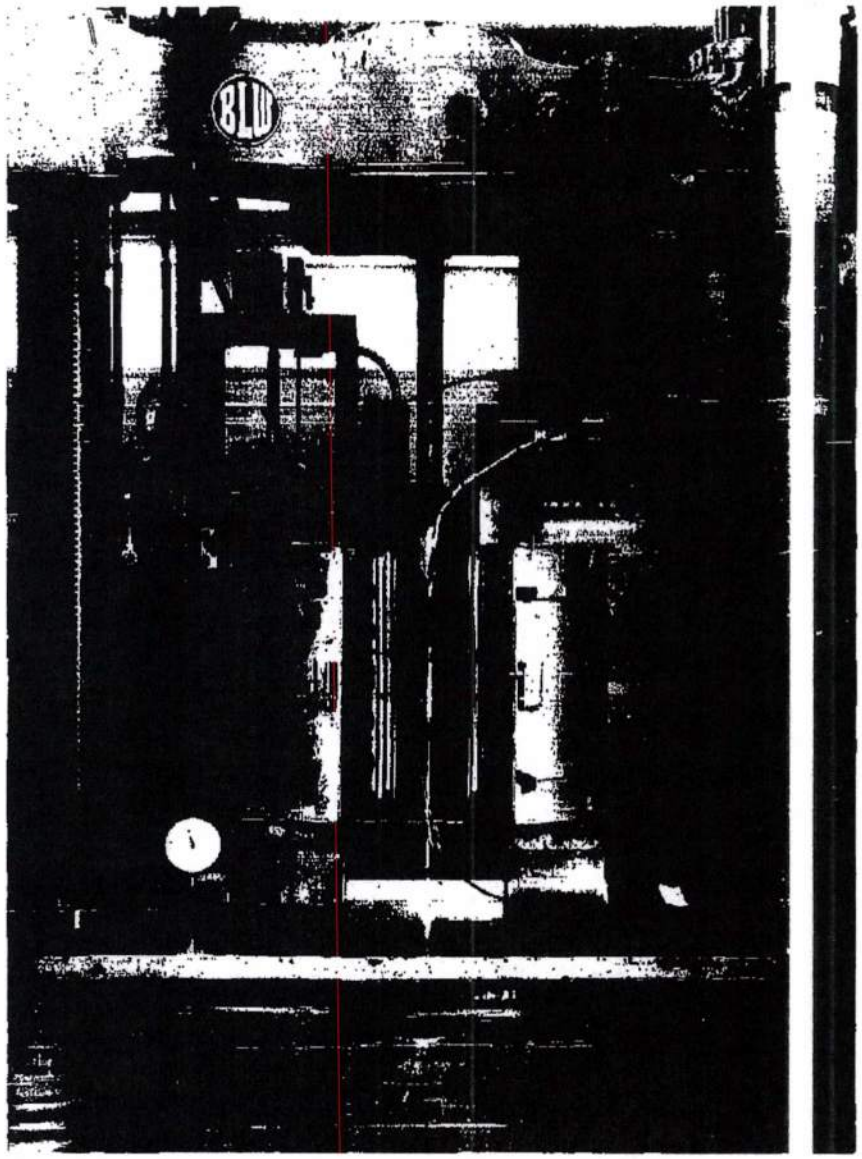

FIGURE 69. Partial Setup for 1400 F Test of 10 Spring Series Stack of Belleville Springs--R-235 Material

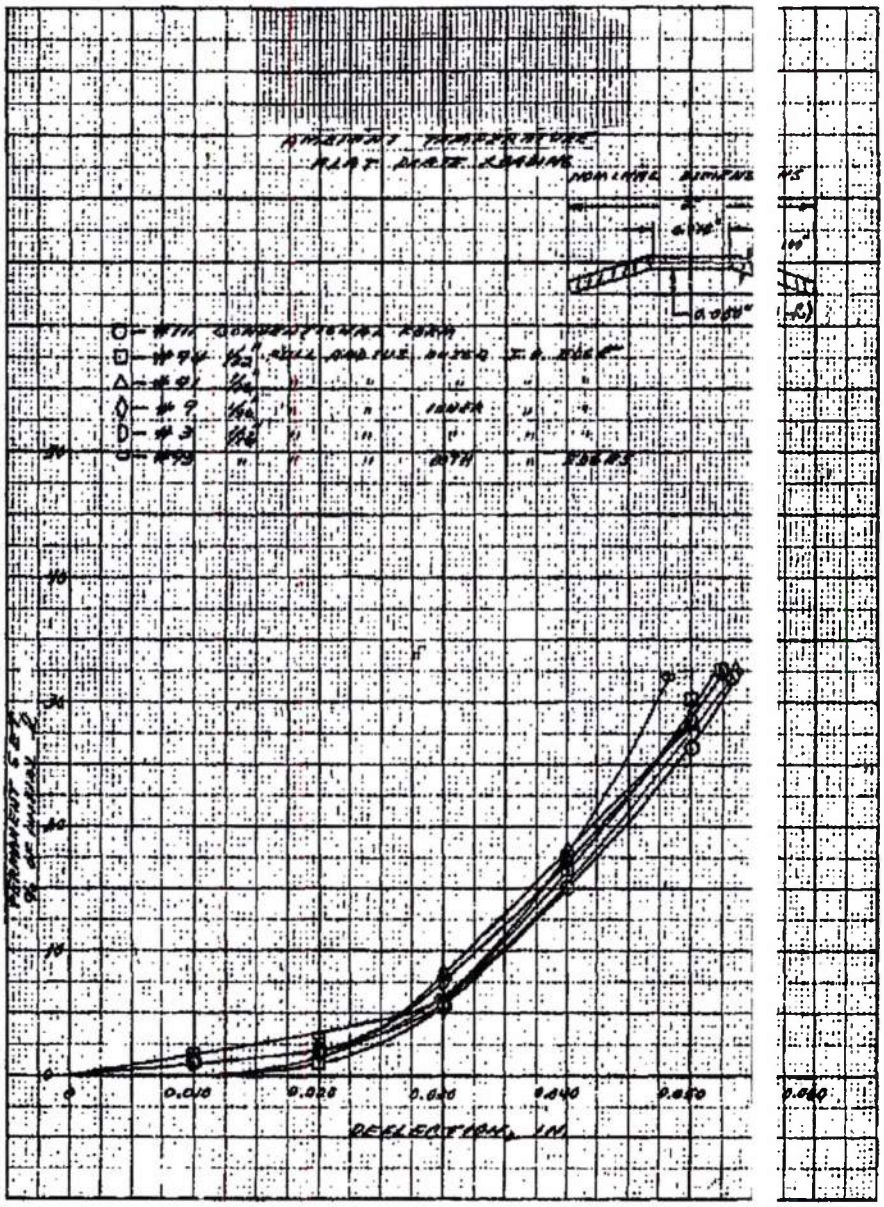

FIGURE 70. Permanent Set vs. Deflection During Presetti of Single Belleville Springs (R-235 Alloy)

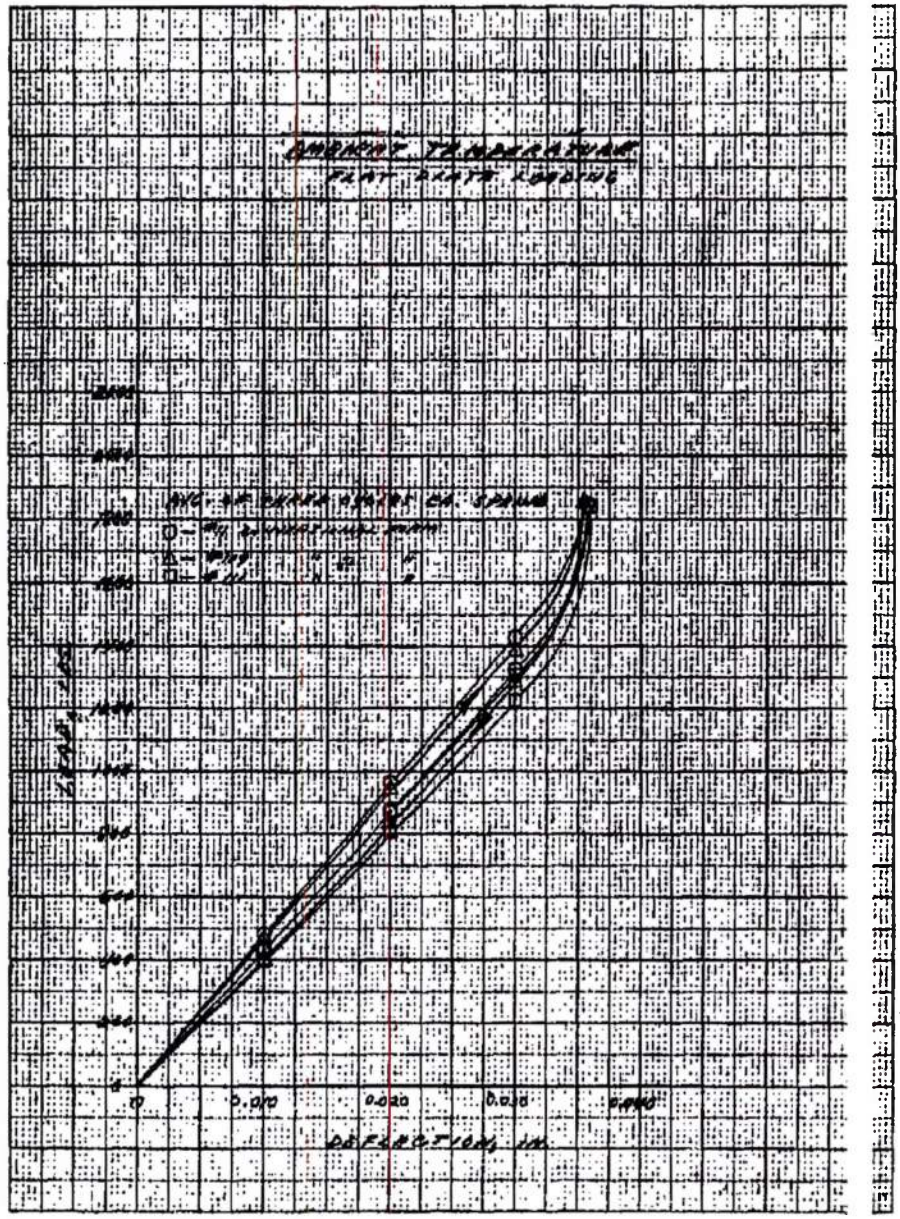

FIGURE 71. Load vs. Deflection: No. 11, No. 109, and No. 111 Single Belleville Springs (R-235 Alloy)

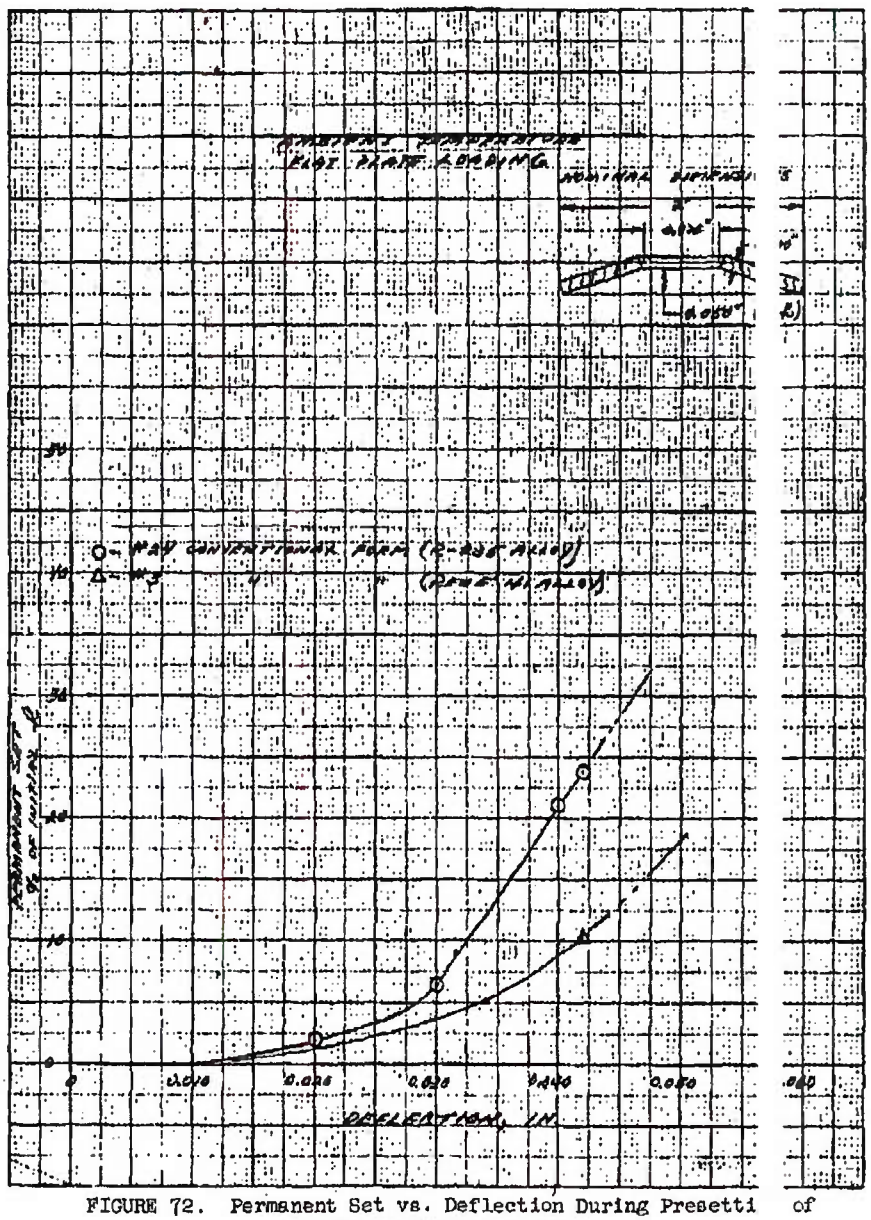

FIGURE 72. Permanent Set vs. Deflection During Presetti of Single Belleville Springs

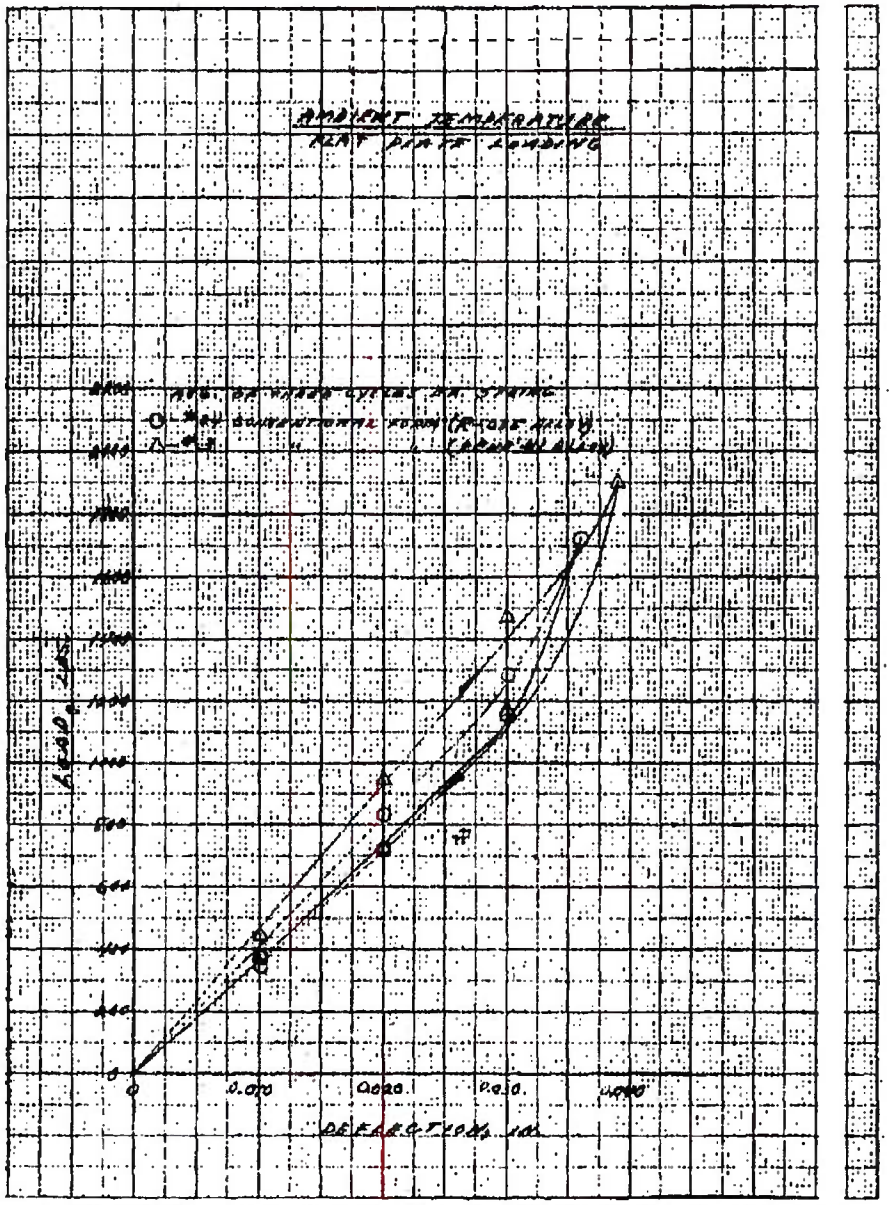

FIGURE 73. Load vs. Deflection for Single Belleville Springs (R-255 Alloy)

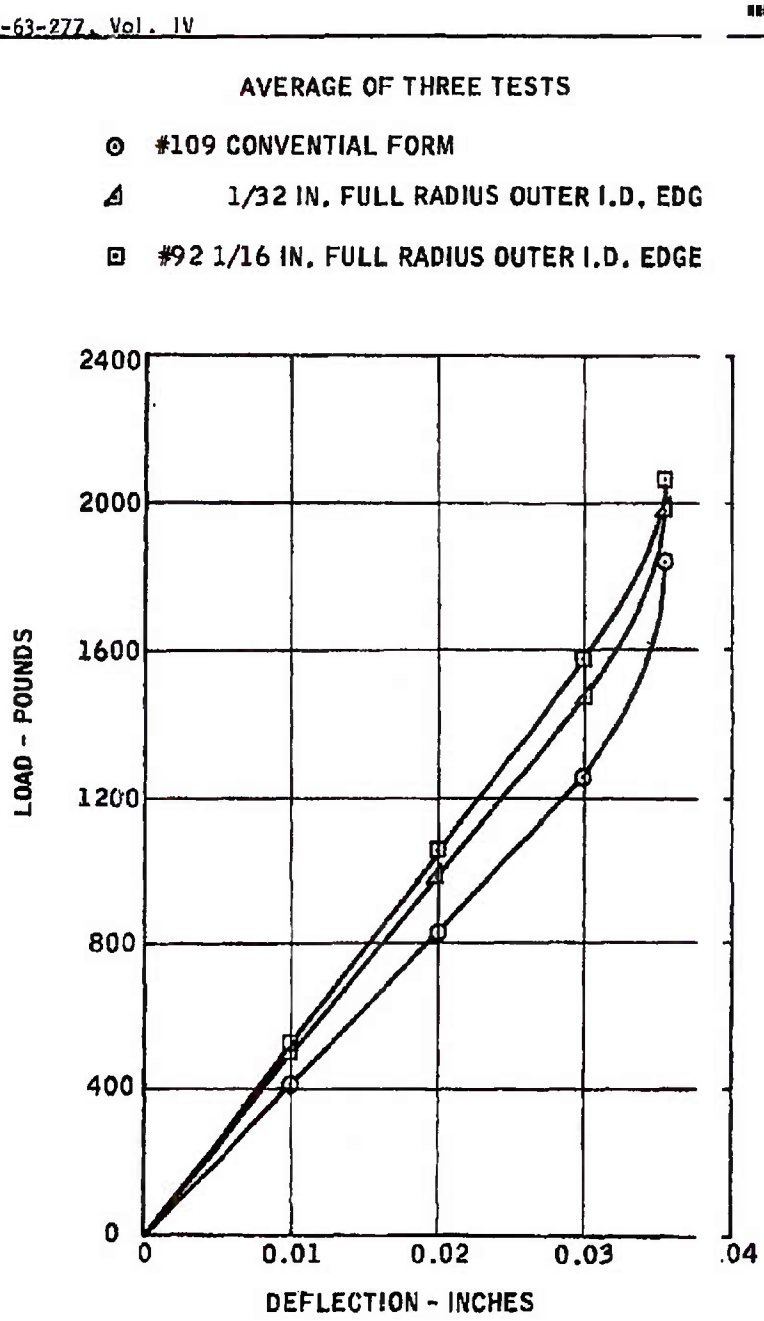

FIGURE 74. Load vs. Deflection for Single Belleville S rings (R-235 Alloy)--Ambient Temperature

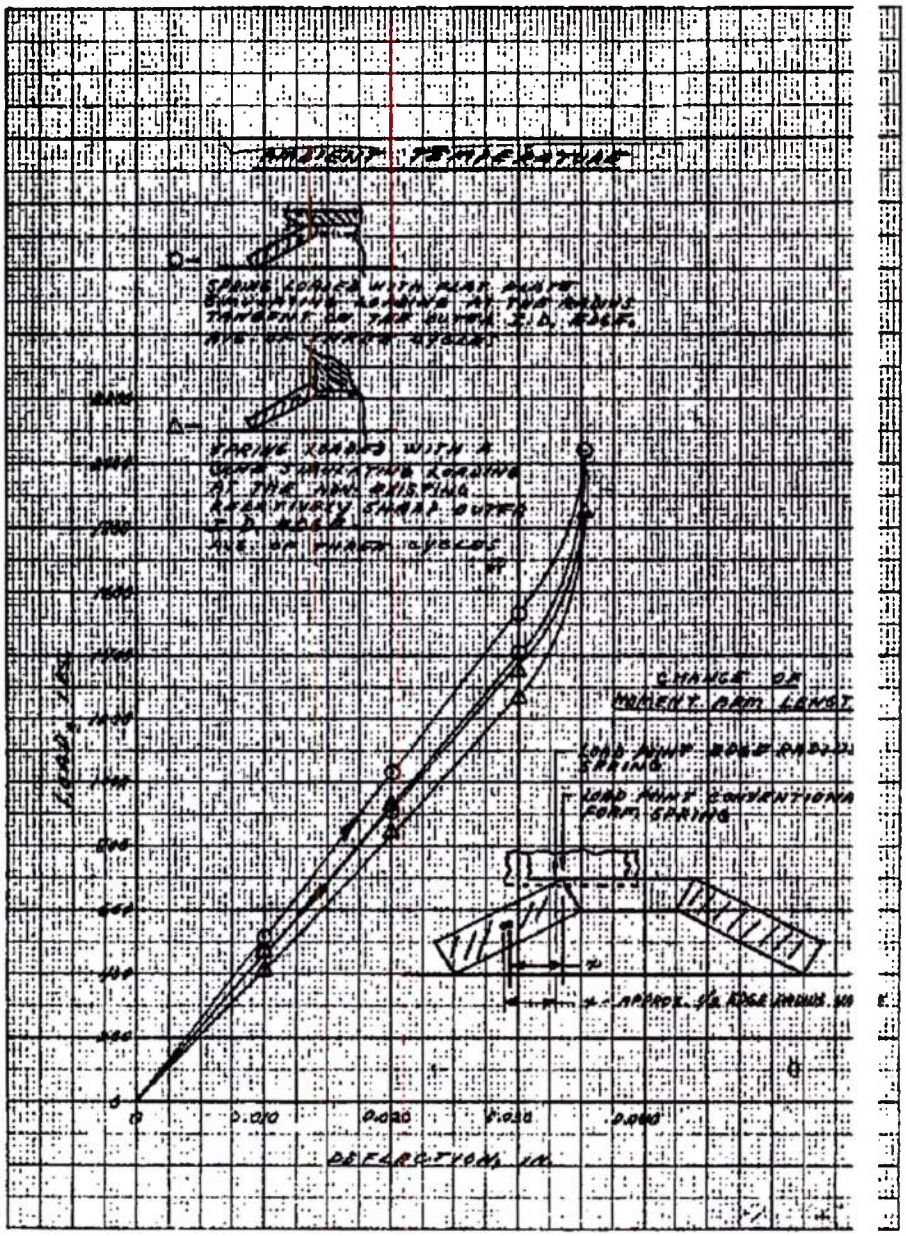

FIGURE 75. Load vs. Deflection: No. 93 Belleville Spring--1/16-in. Full Radius Both I.D. Edges (R-235 Alloy)

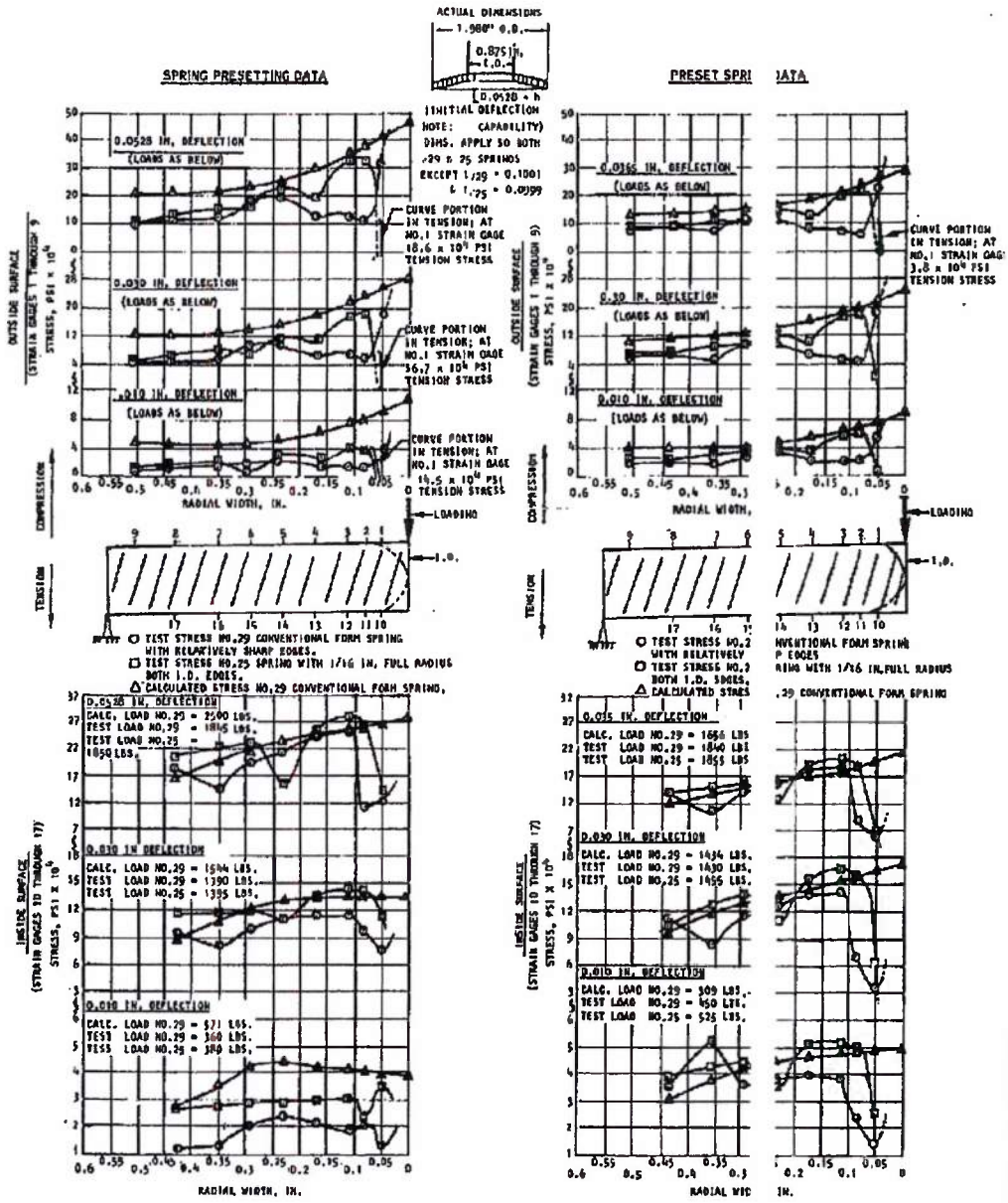

FIGURE 76. Stress vs. Spring Radial Width--Belleville Spring No. 29 and No. 25 (R-235 Material; Ambient Temperature; Flat Plate Loading)

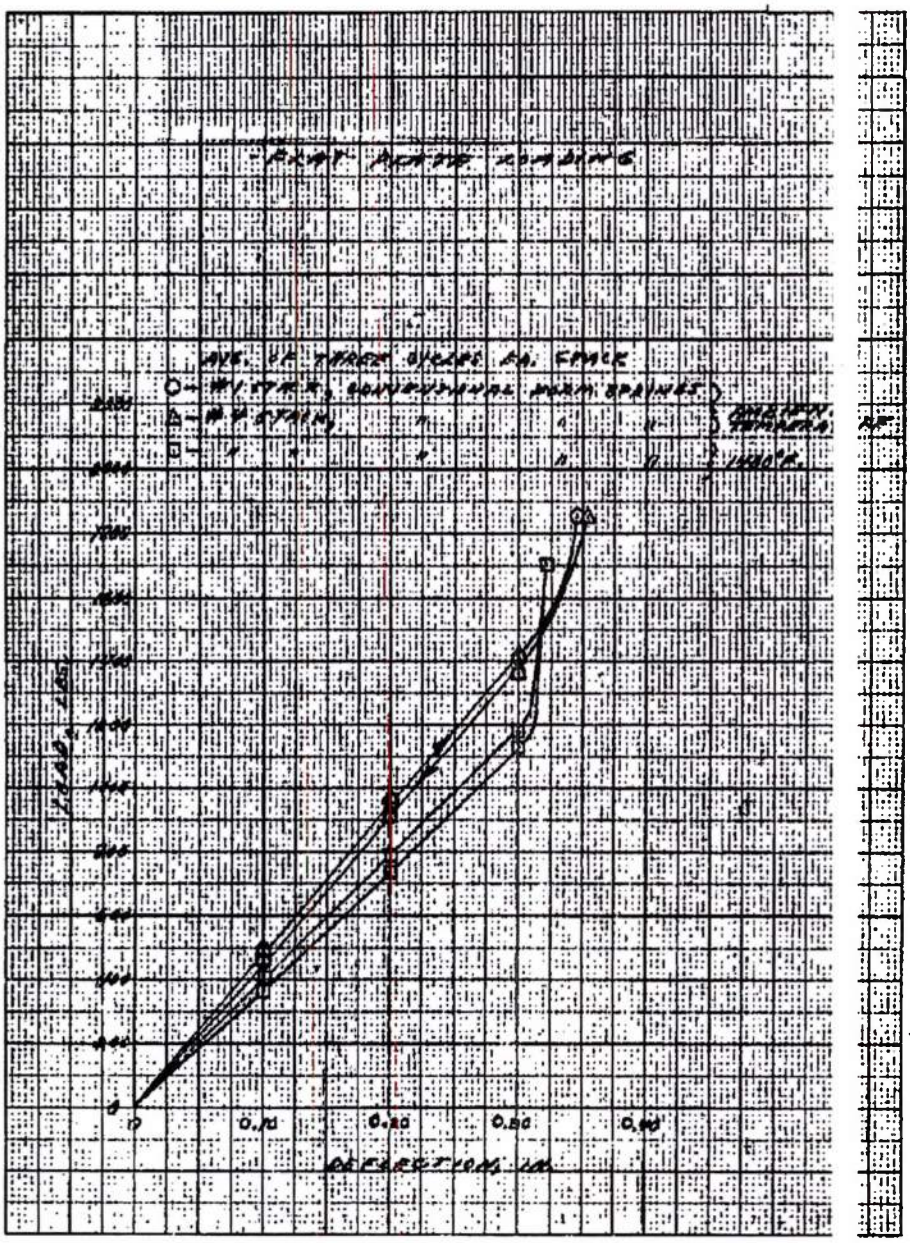

FIGURE 77. Load vs. Deflection: No. 1 and No. 4 10-Spring Serie
Stack of Belleville Springs (R-235 Alloy)

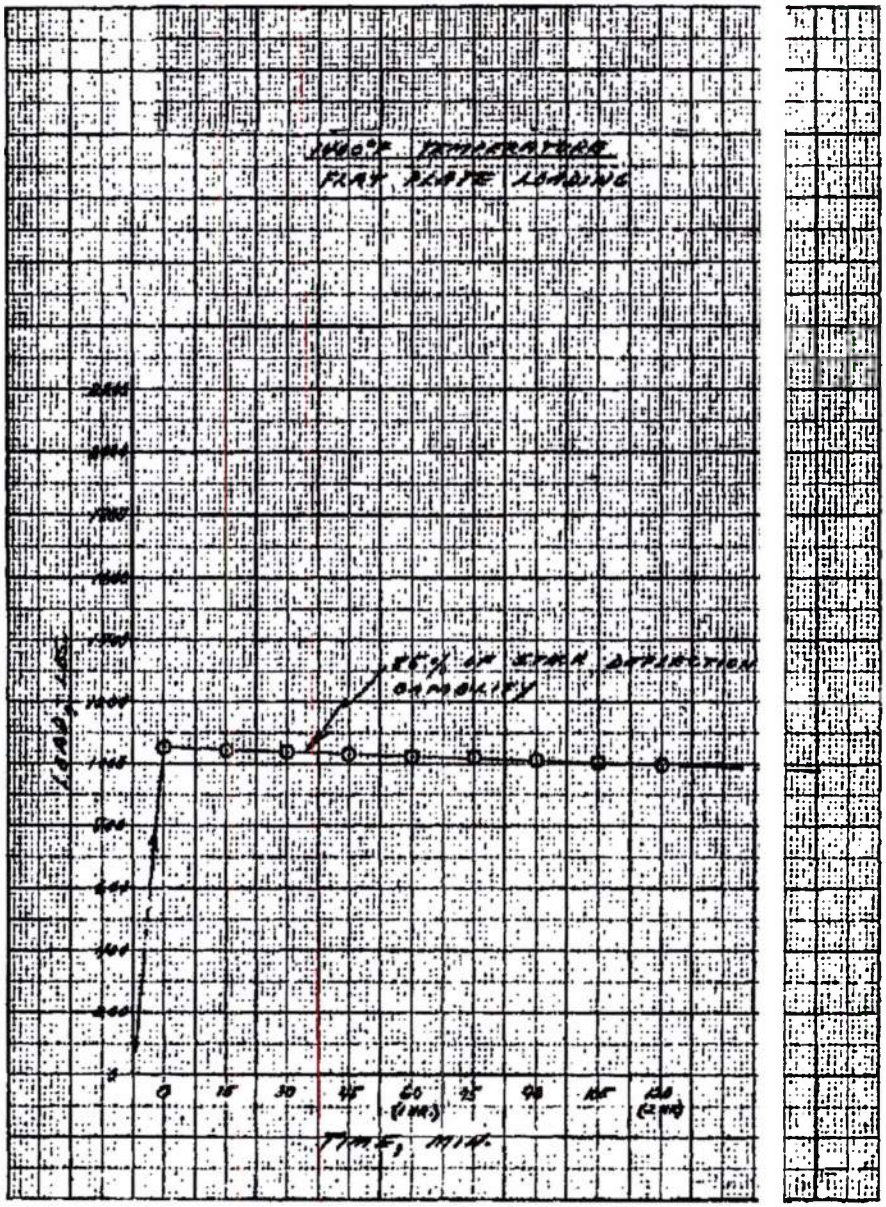

FIGURE 78. Load Loss vs. Time at Constant Spring Deflection: o. 4
10-Spring Series Stack of Belleville Springs (R-235 All)

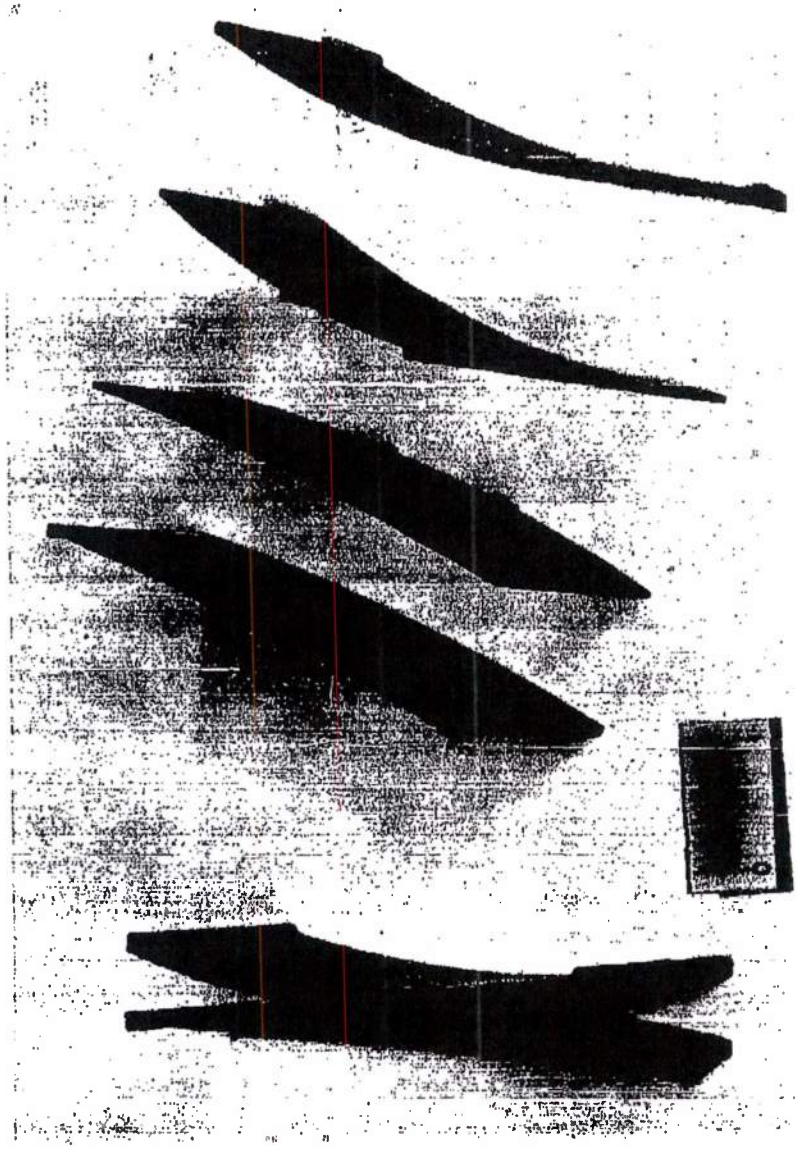

FIGURE 79. Tapered Curved Plate Springs--Rene' 41 Alloy

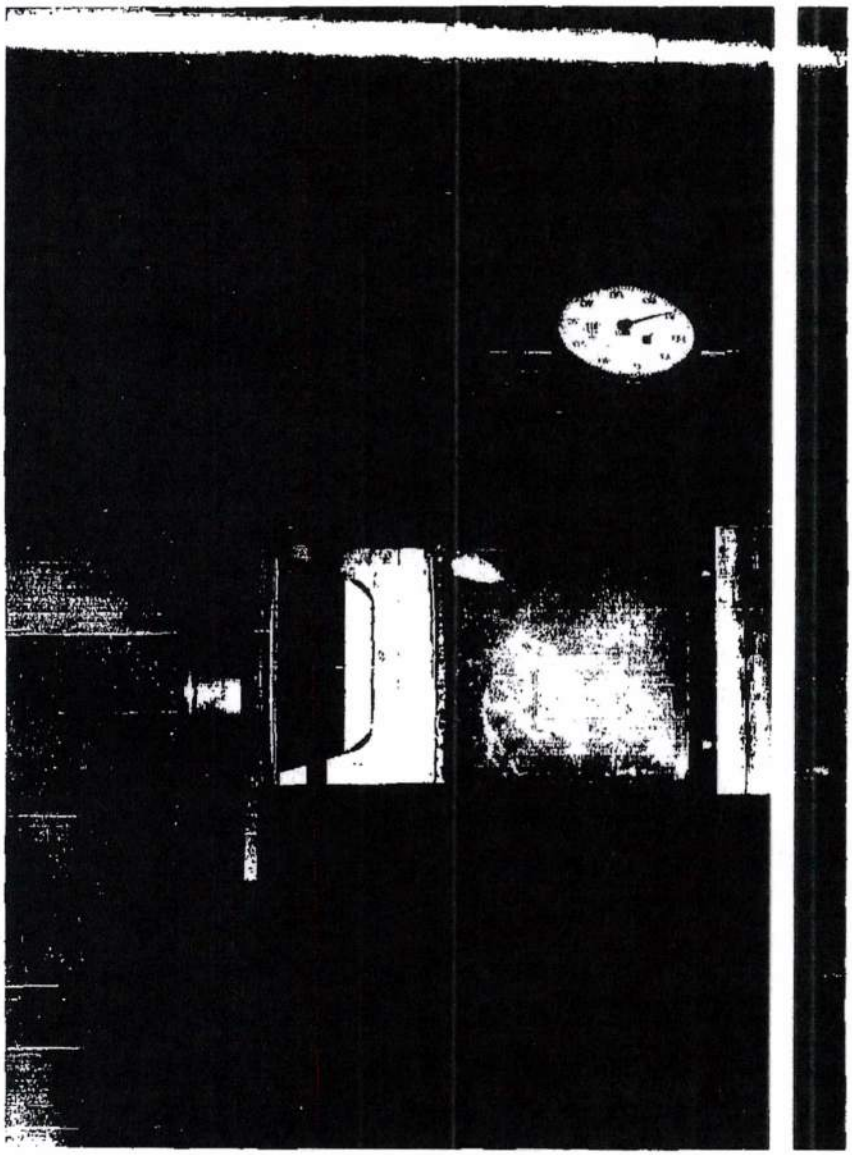

FIGURE 80. Test of Tapered Curved Plate Springs--Spring Stack Profile at 0.370-inch Deflection--Ambient Temperature

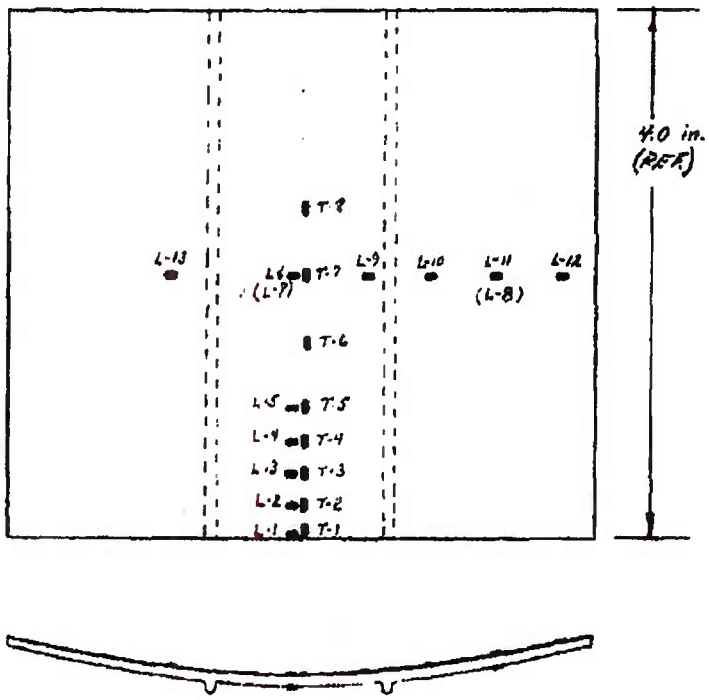

X81415-503

NOTES -

1. Installed SR-4 type A-18 strain gages as sh on on X81415-503, -501 & -1.

2. L-7 & L-8 on opposite side of spring from L-6 & L-11, respectively.

3. T-5, T-6 & L-5 not used on -501. T-3, T- T-5, T-6, T-8, L-3, L-4 & L-5 not used on -1.

4. L— denotes longitudinal orientation
T— " transverse "

FIGURE 81. Strain Gage Layout for Tapered Curved Plate Spring Tes

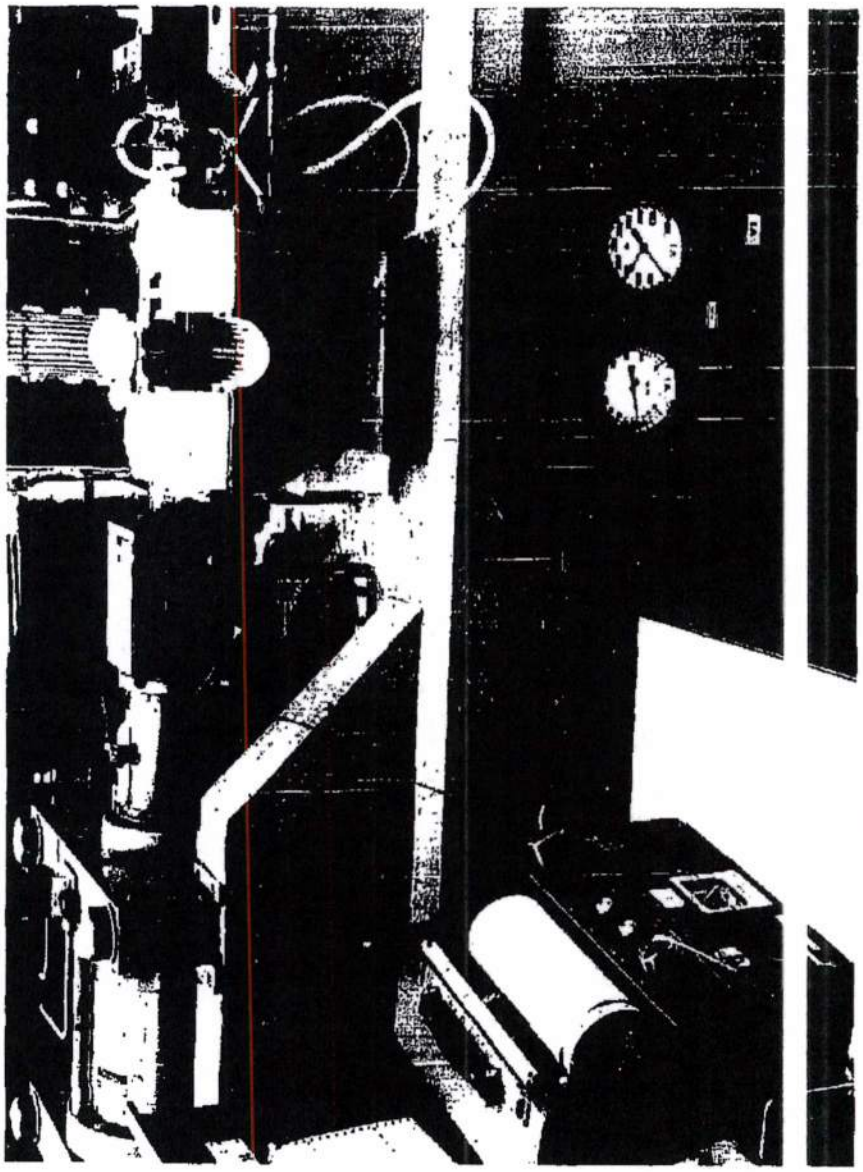

FIGURE 82. Setup for Testing of Tapered Curved Plate Springs (1400°F Cyclic Load-Deflection)

NEG. 4514-7

MAC A673

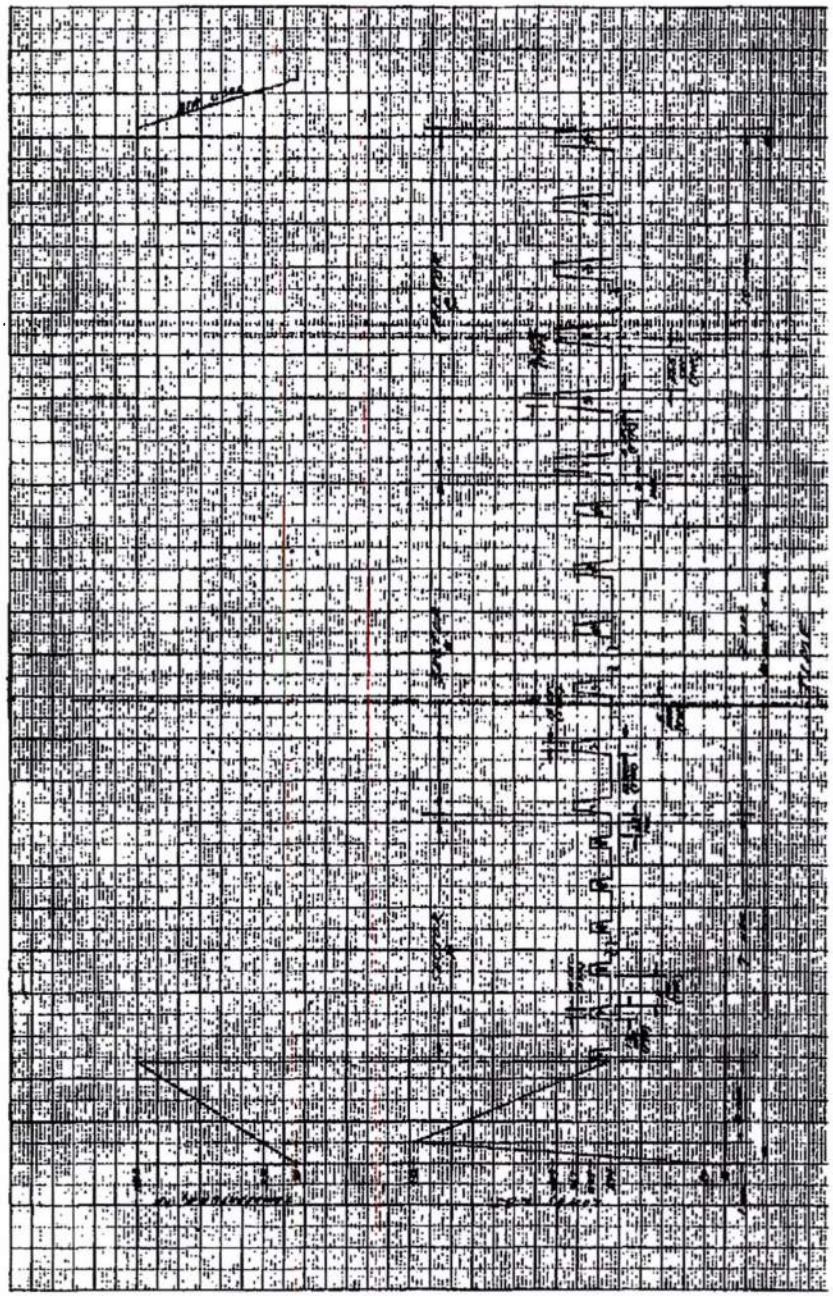

FIGURE 83. Cyclic Load-Deflection for Tapered Curved Plate Springs (2-in. Wide Stacks, S/N 2 and 4)

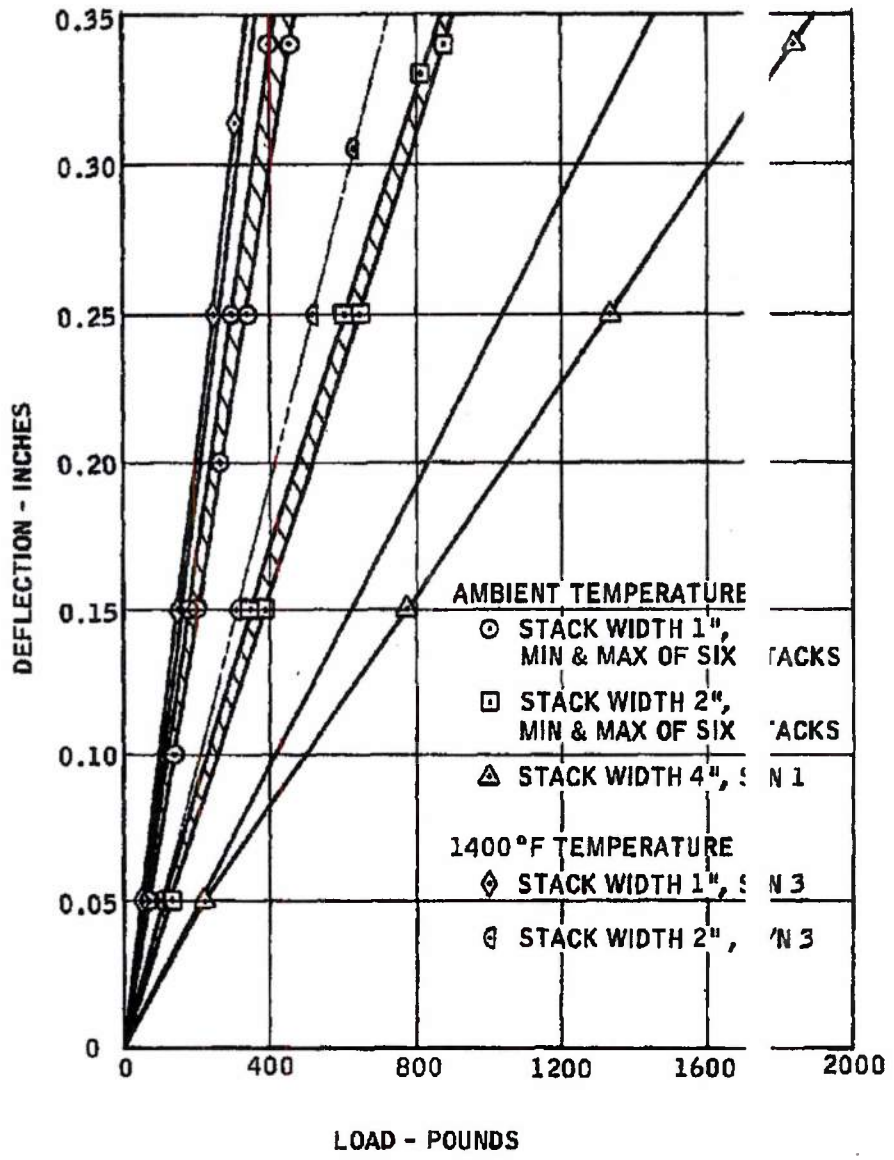

FIGURE 84. Load Deflection Characteristics for Tapered Curved Pla Spring Stack

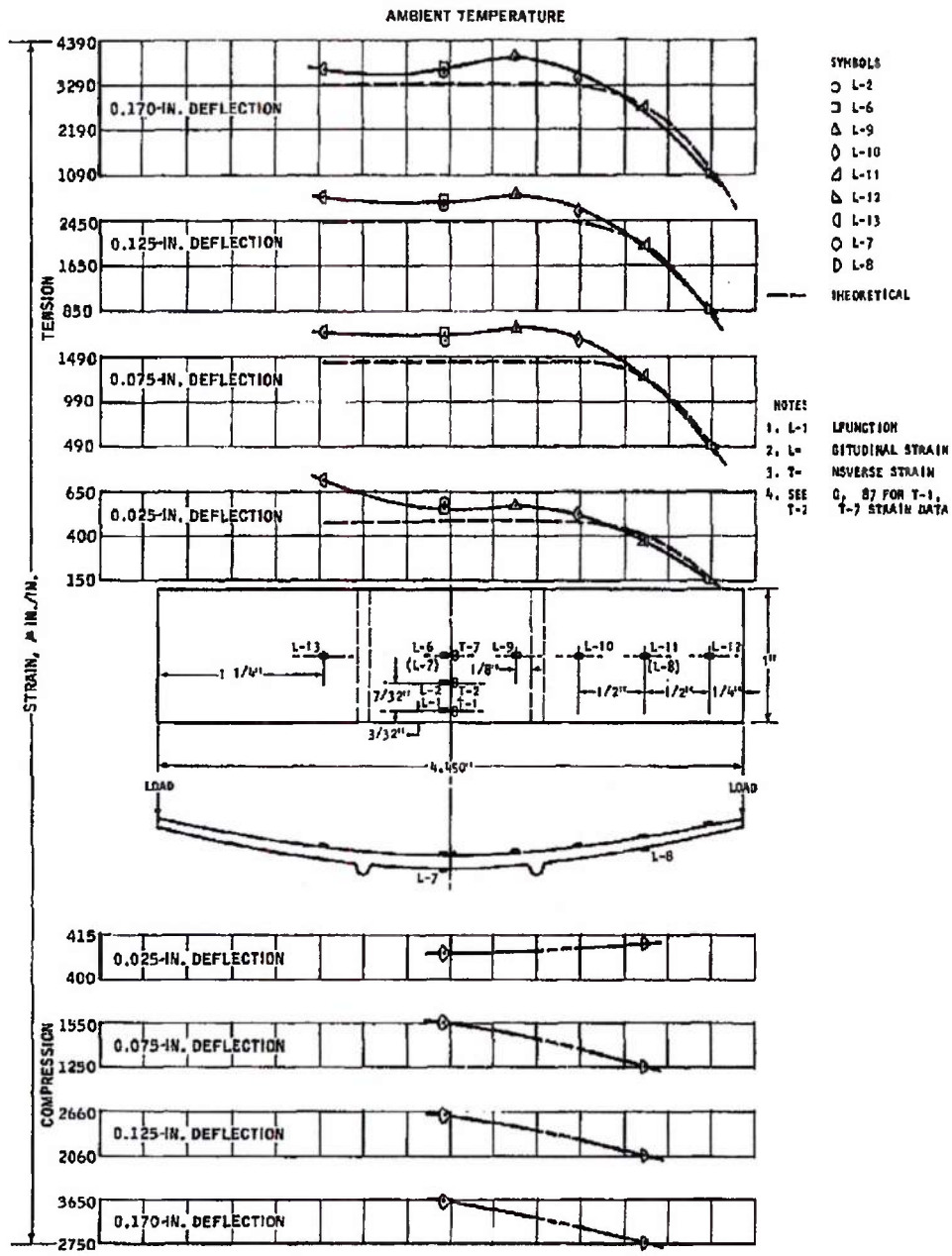

FIGURE 85. Load, Deflection, Strain for Tapered Curved Spring Leaf (From 1-in. Wide Stack, S/N 1) -18415-1

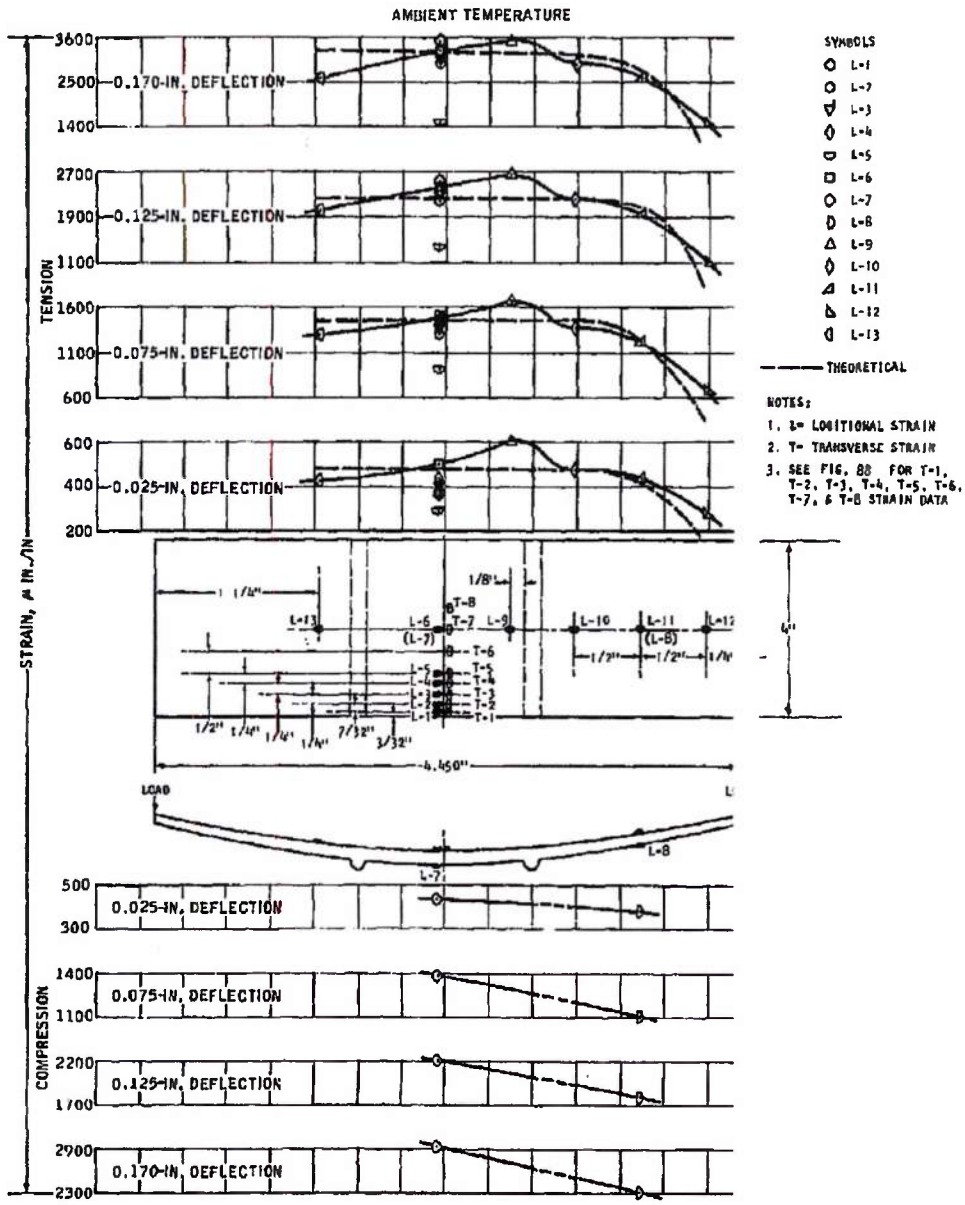

FIGURE 86. Load, Deflection, Strain for Tapered Curved Spring af X-81415-503 (From 4-in. Wide Stack, S/N 1)

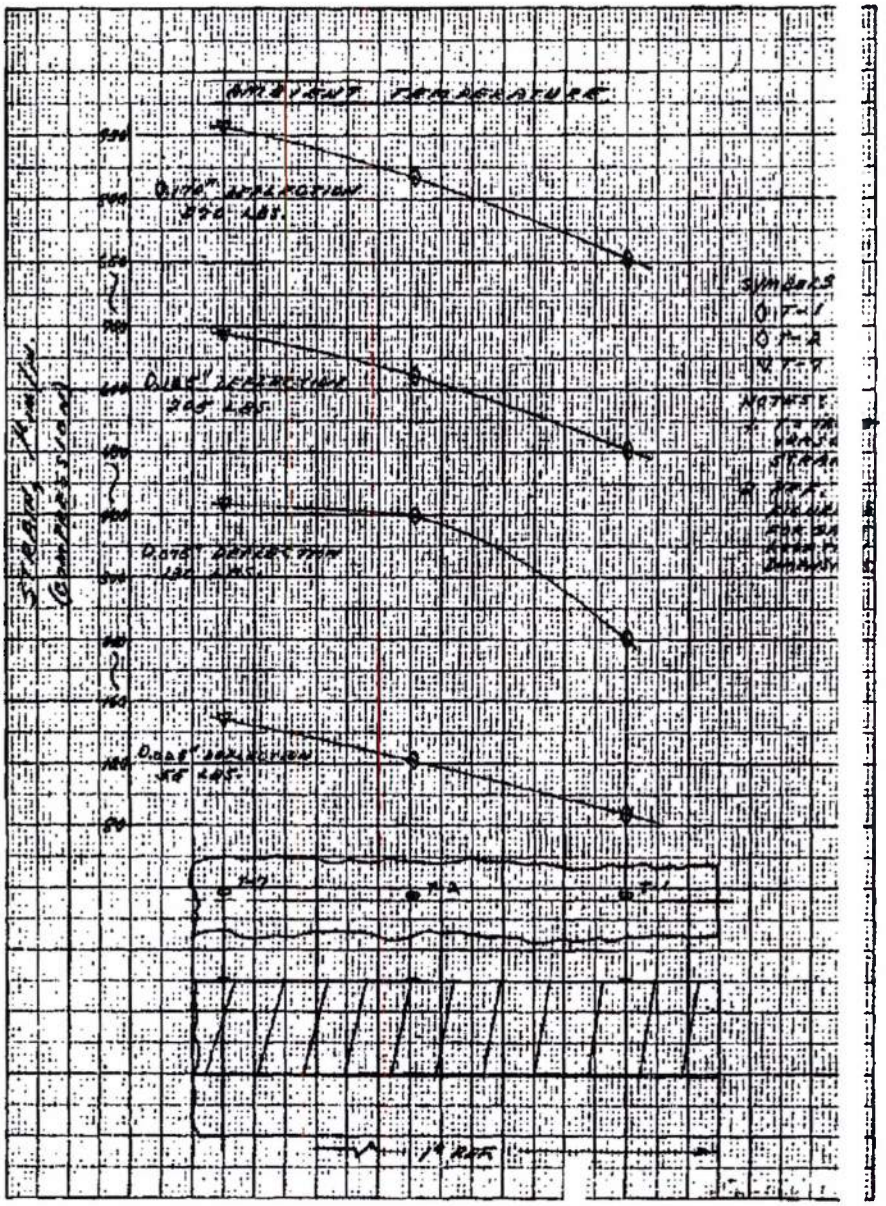

FIGURE 87. Load-Deflection-Strain Data for Tapered Curved Spring Le (X-81415-1) from 1-in. Wide Stack, S/N 1

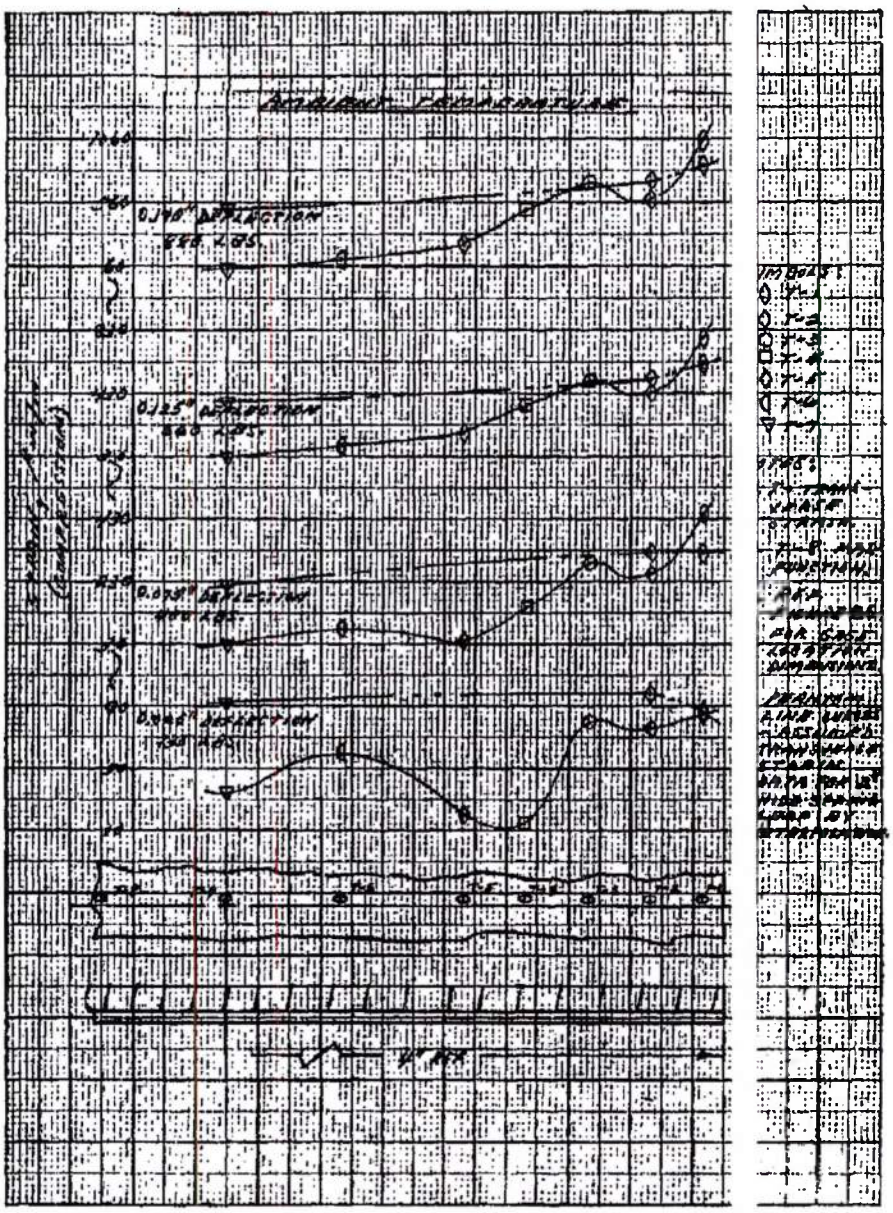

FIGURE 88. Load-Deflection-Strain Data for Tapered Curved ring Leak (X-181415-503) from 4-in. Wide Stack, S/N

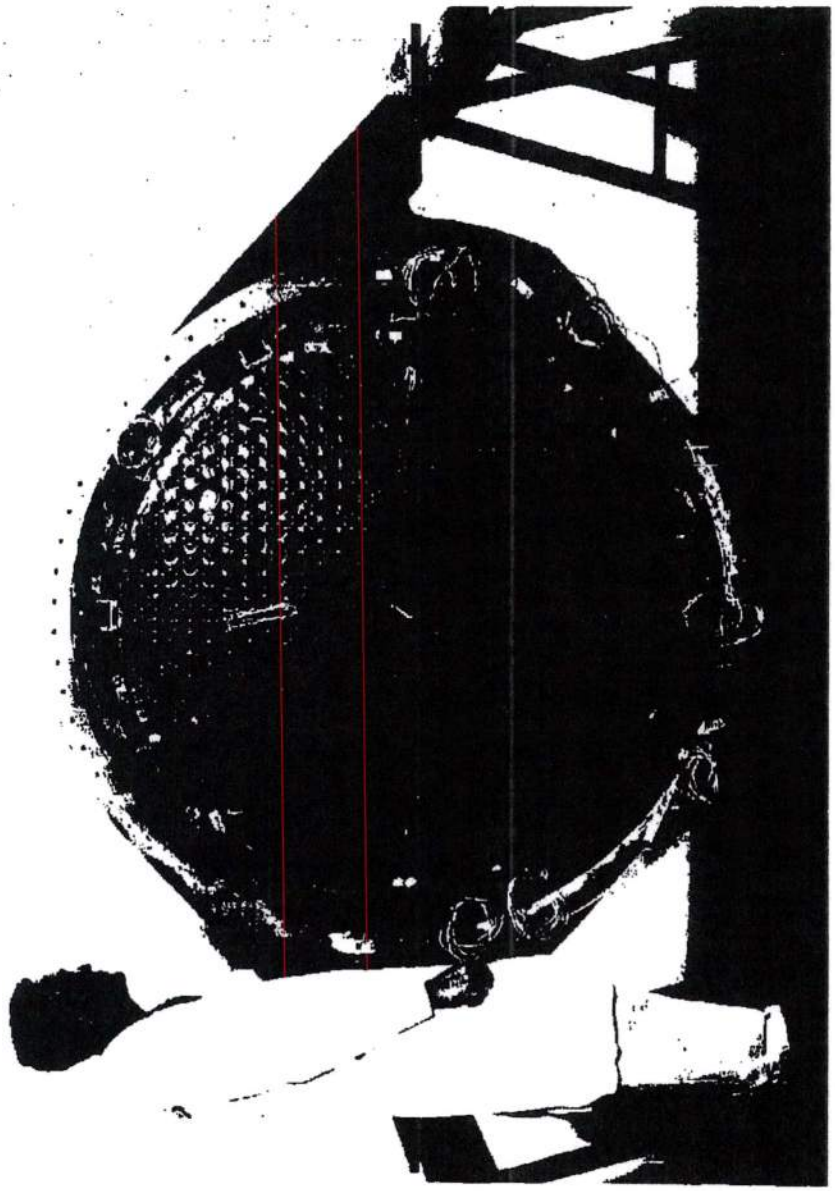

FIGURE 89. Engine-Airframe Lateral Attachment Test Item

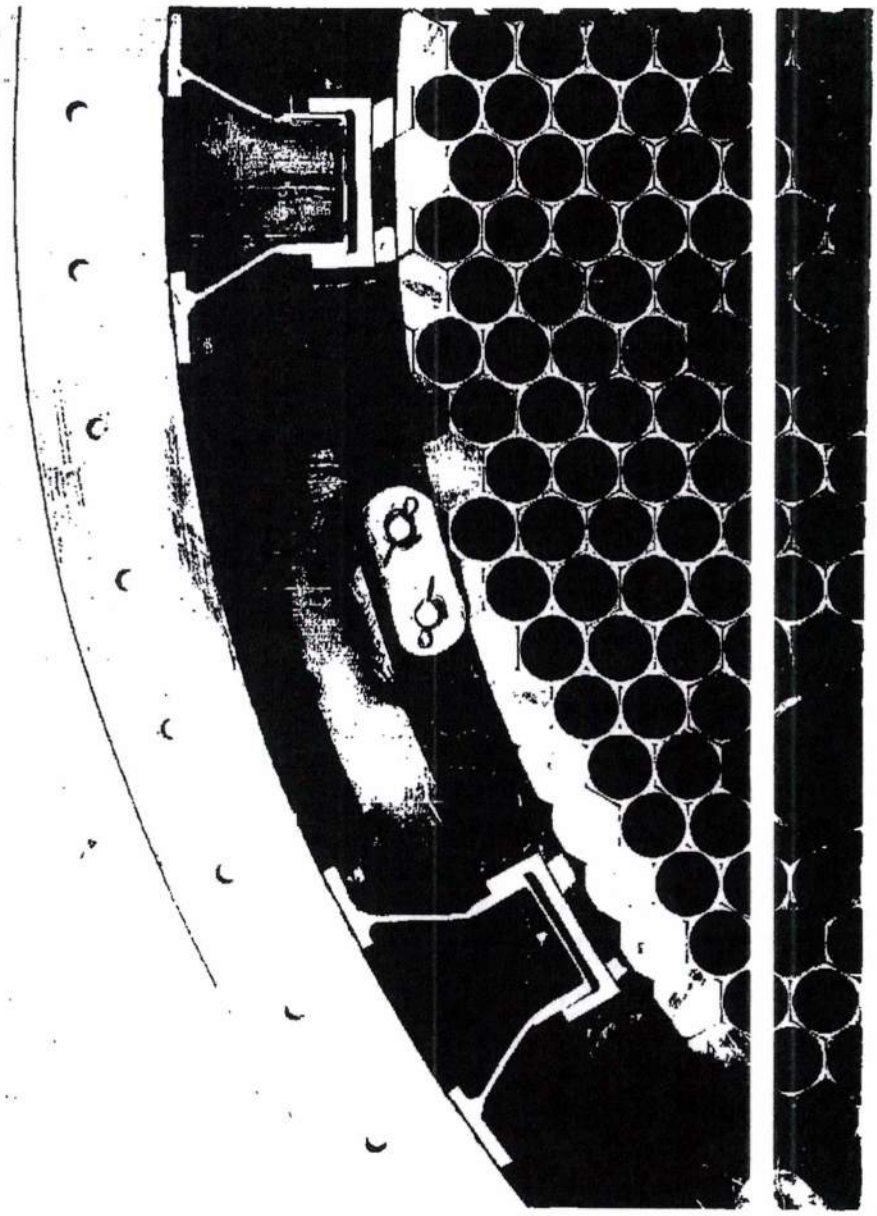

NEG. 4142-14

FIGURE 90. Side Support Detail of Engine-Airframe Lateral Attachment

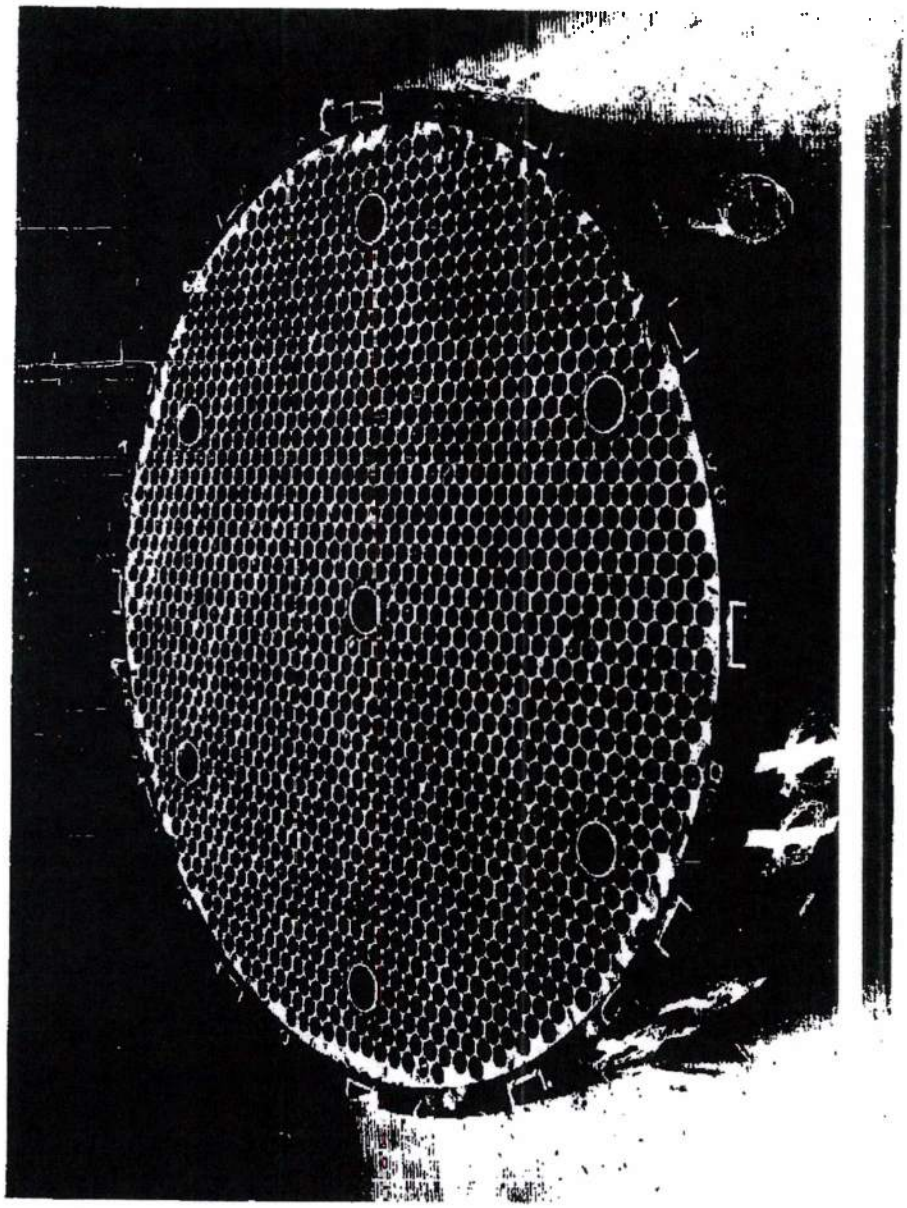

FIGURE 91. Core Matrix and Expansion Shell

4142-9

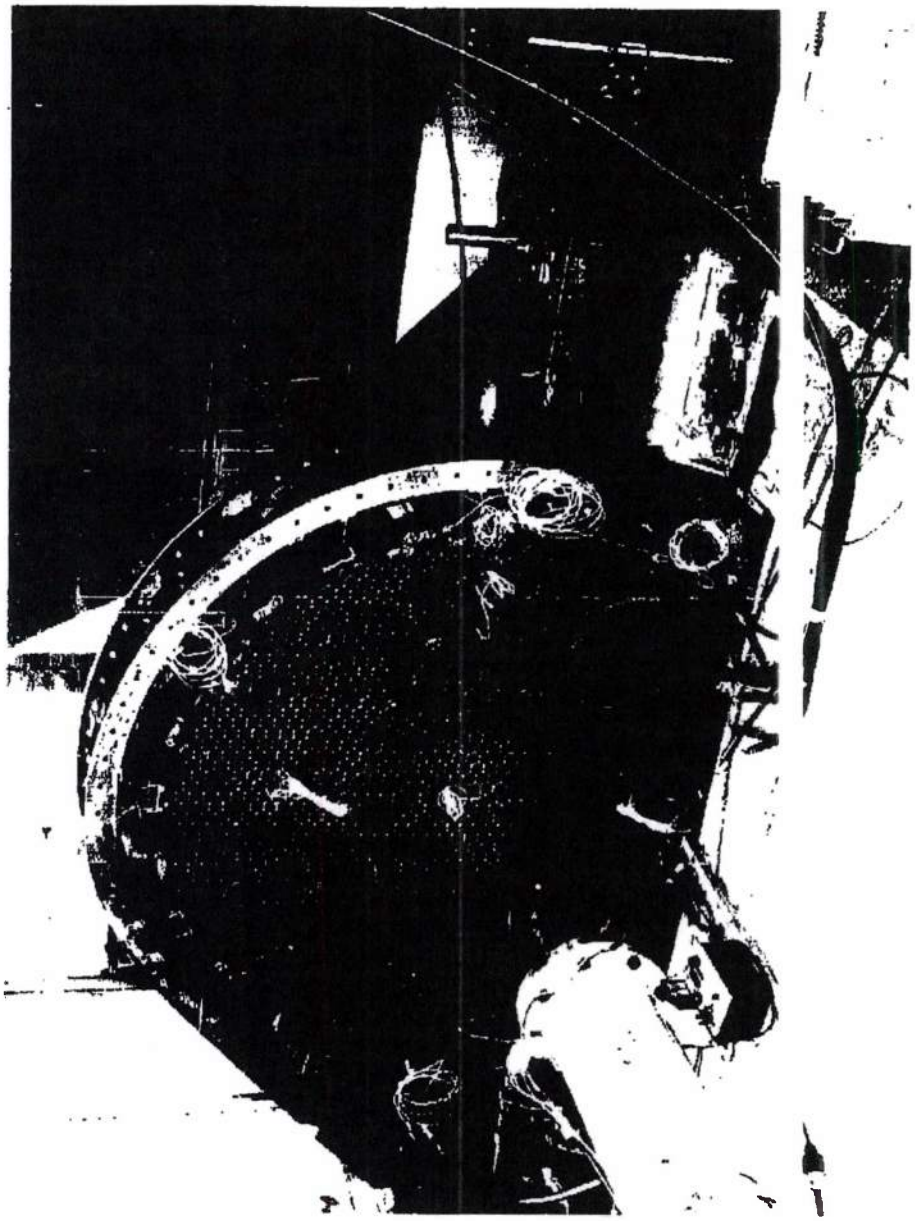

NEG. 4342-17

FIGURE 92. Engine-Airframe Lateral Attachment Test Item in Shaker Facility

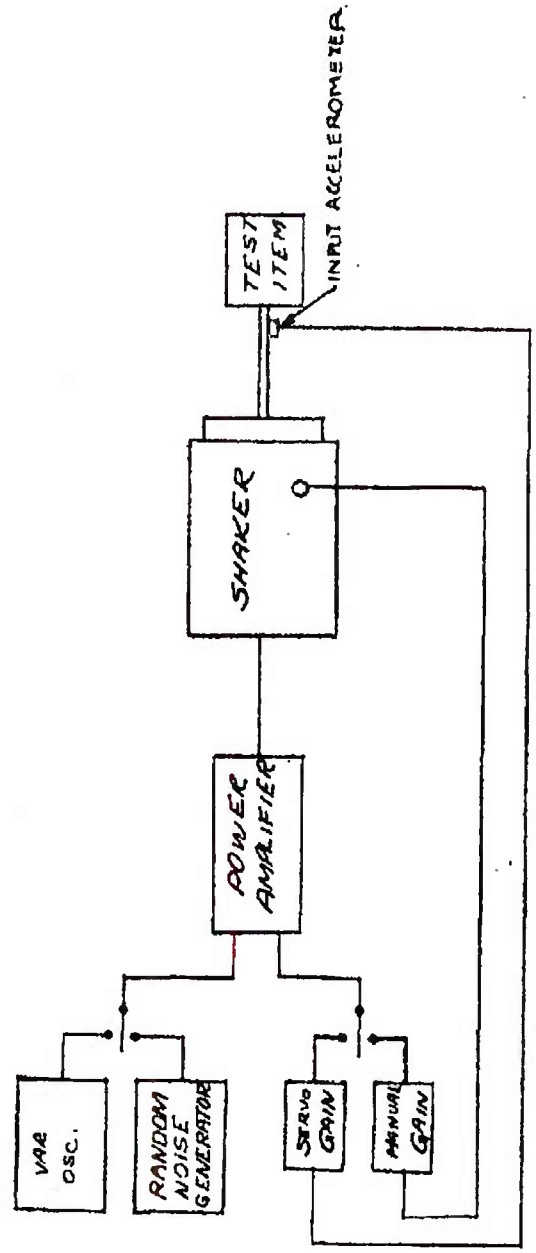

FIGURE 93. Block Diagram of Shaker Control System

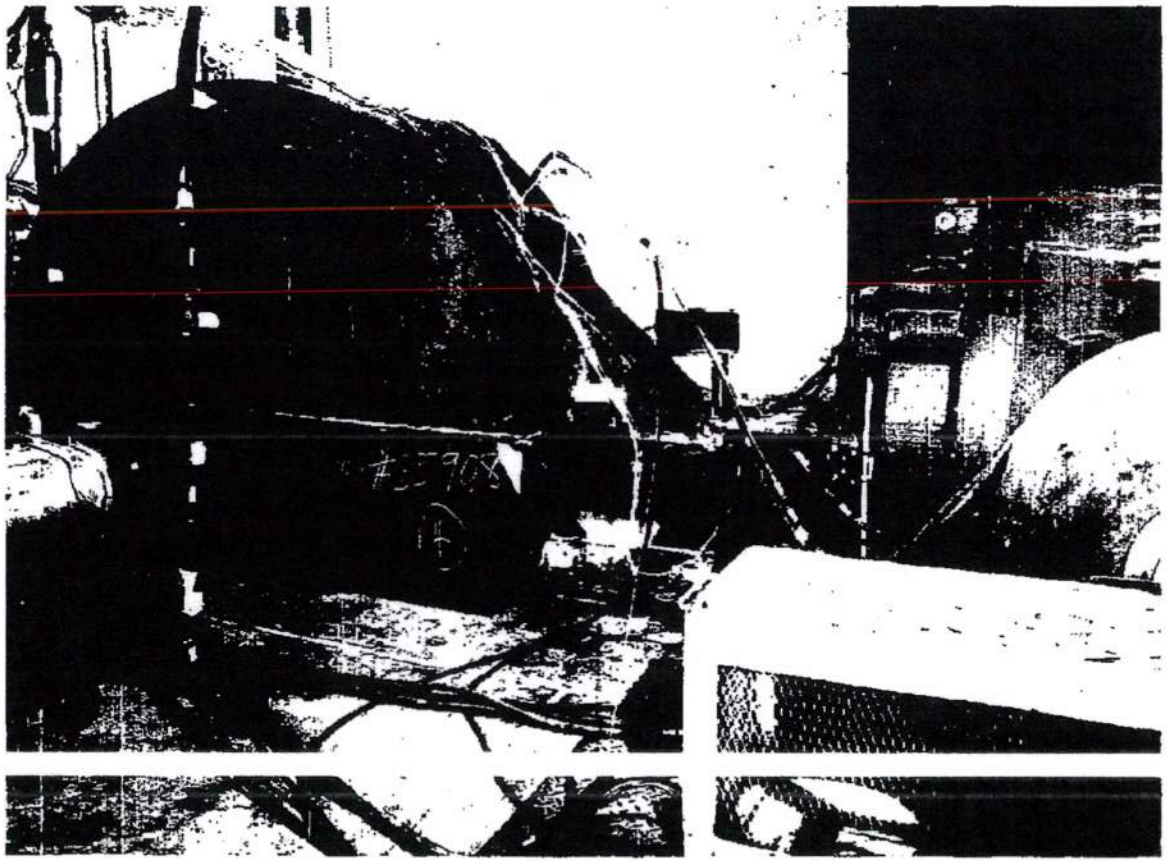

FIGURE 94. Engine-Airframe Lateral Attachment Test Item in Furnace

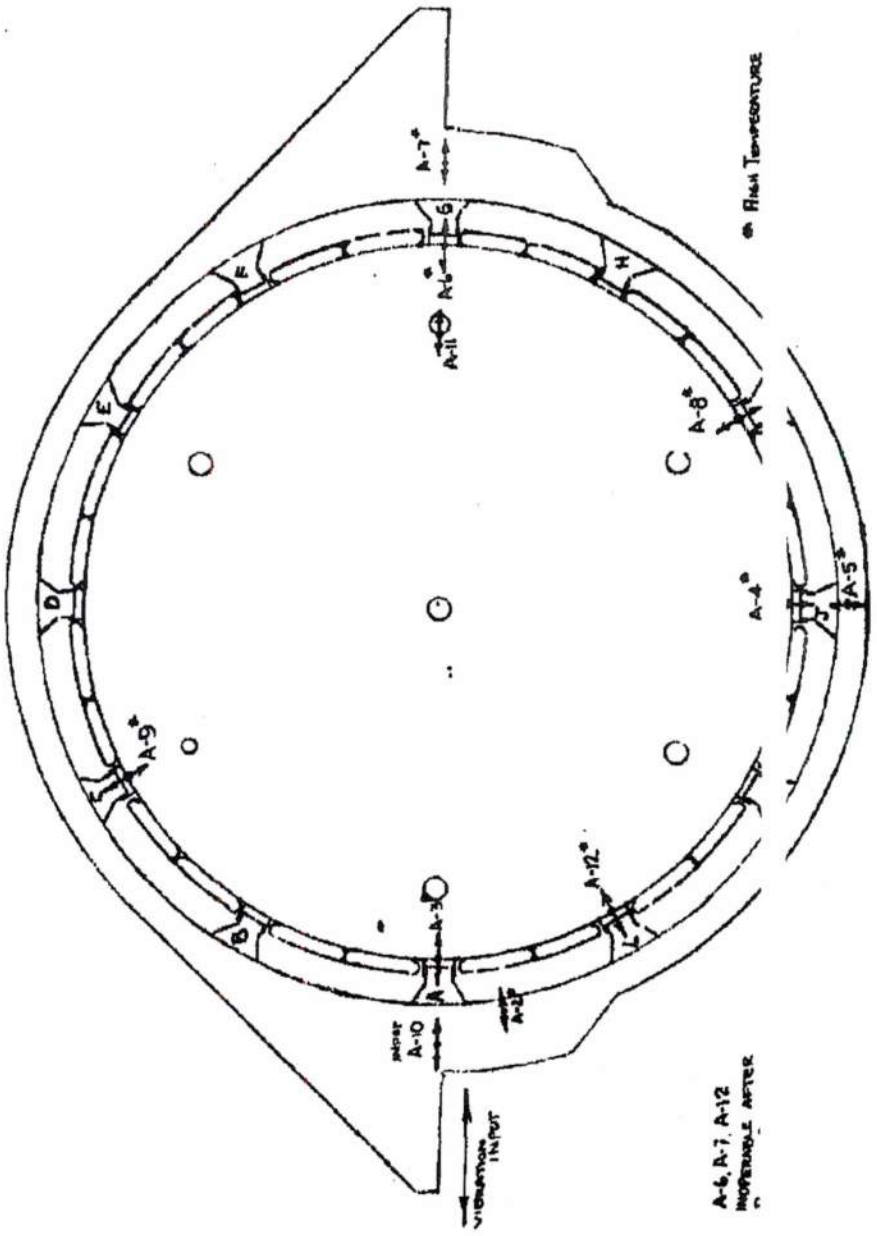

FIGURE 95. Accelerometer Locations

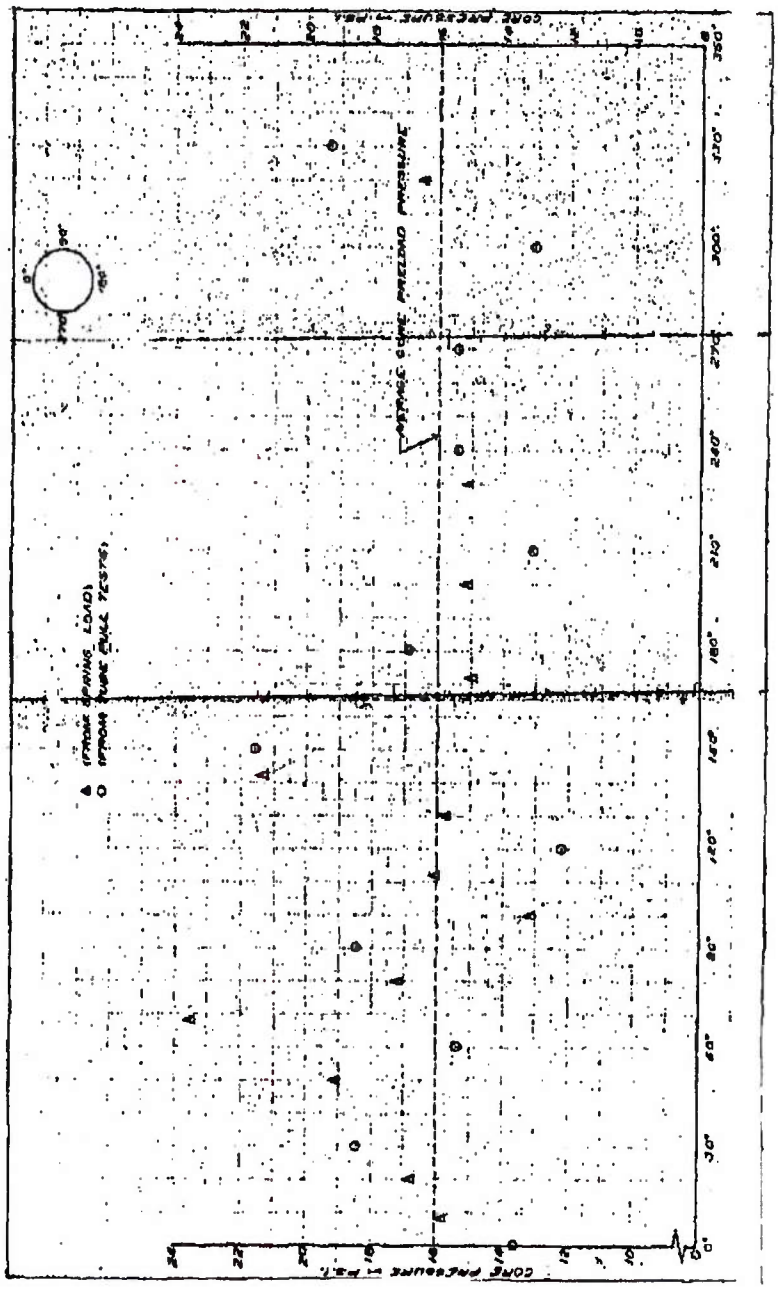

FIGURE 96. Core Preload Pressure

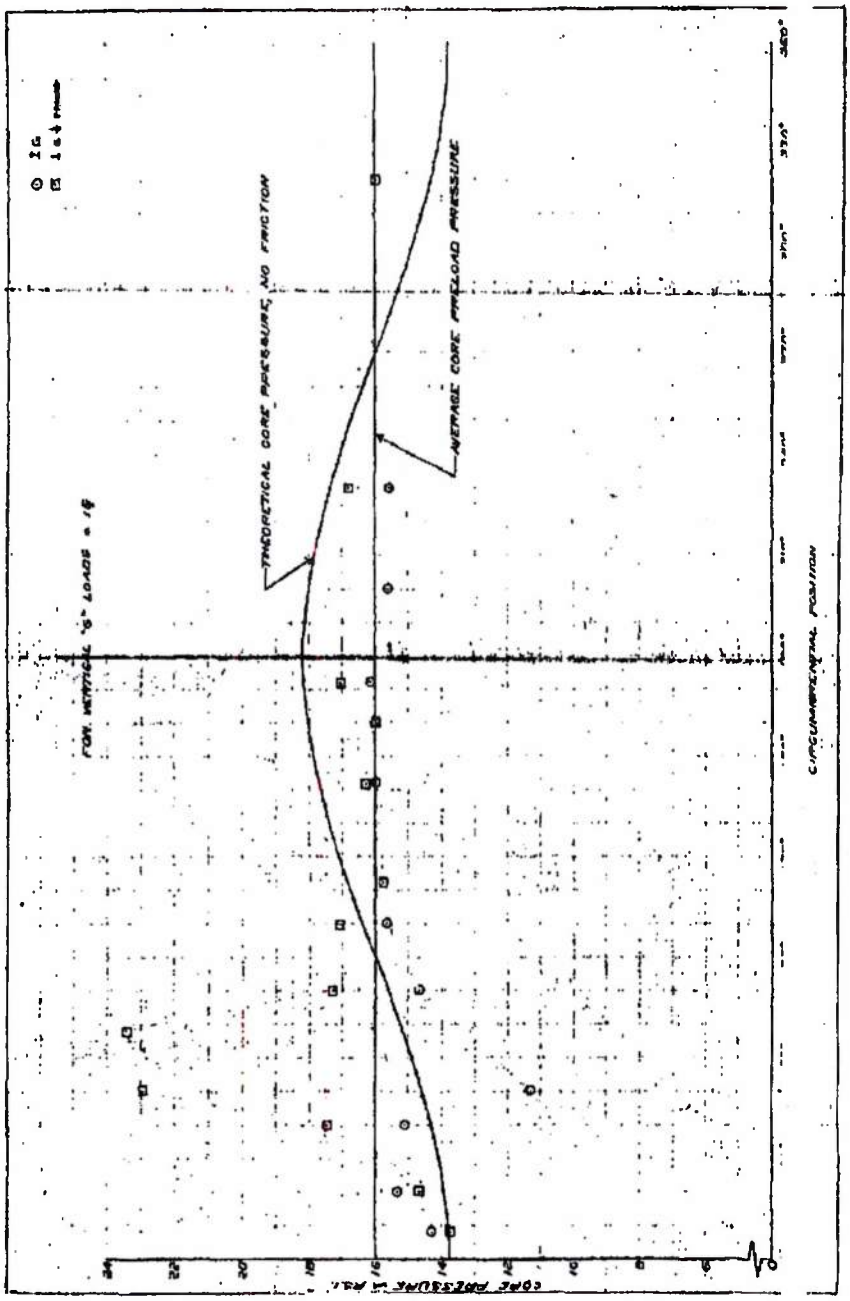

FIGURE 97. Core Pressure (From Spring Loads)

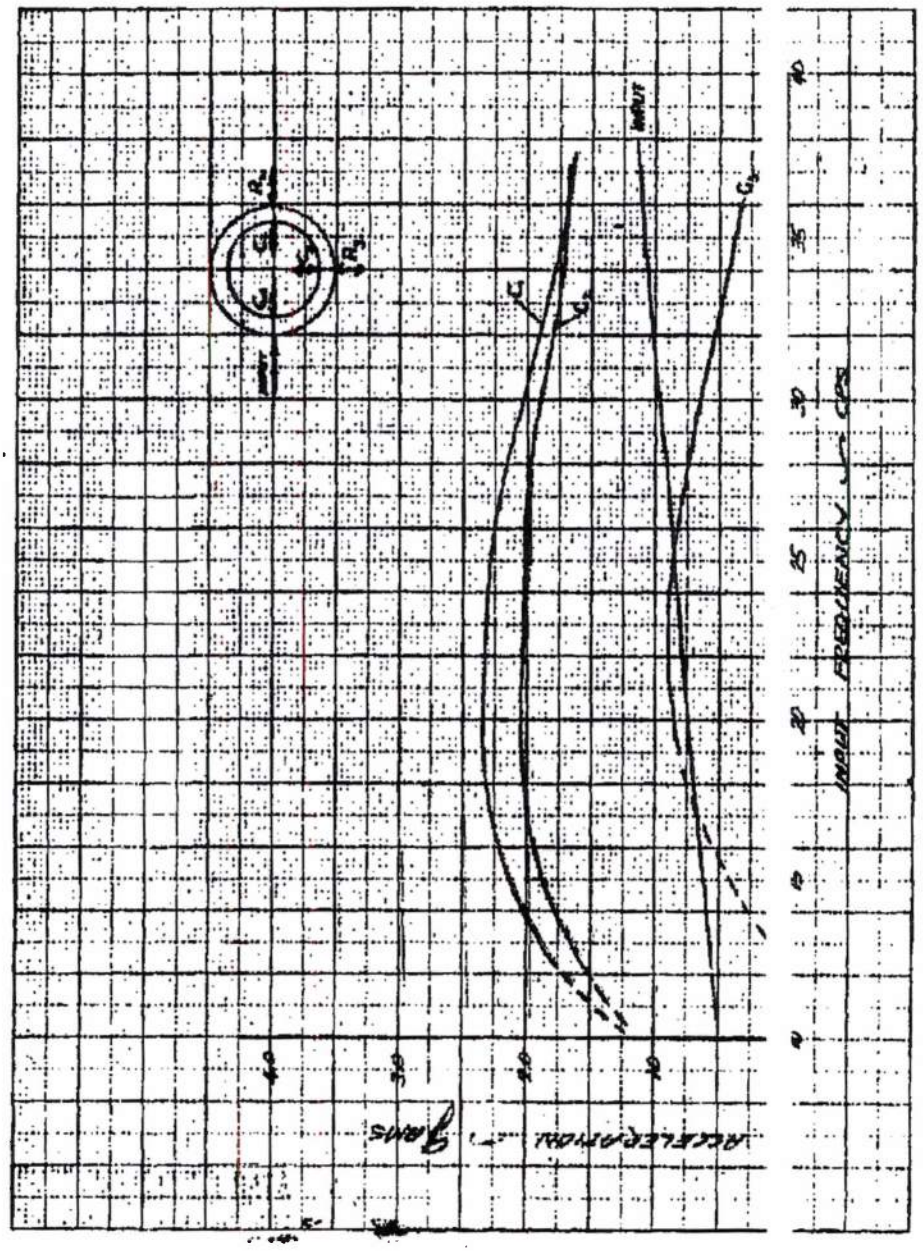

FIGURE 98. Core Dynamic Response (Run No. 4)

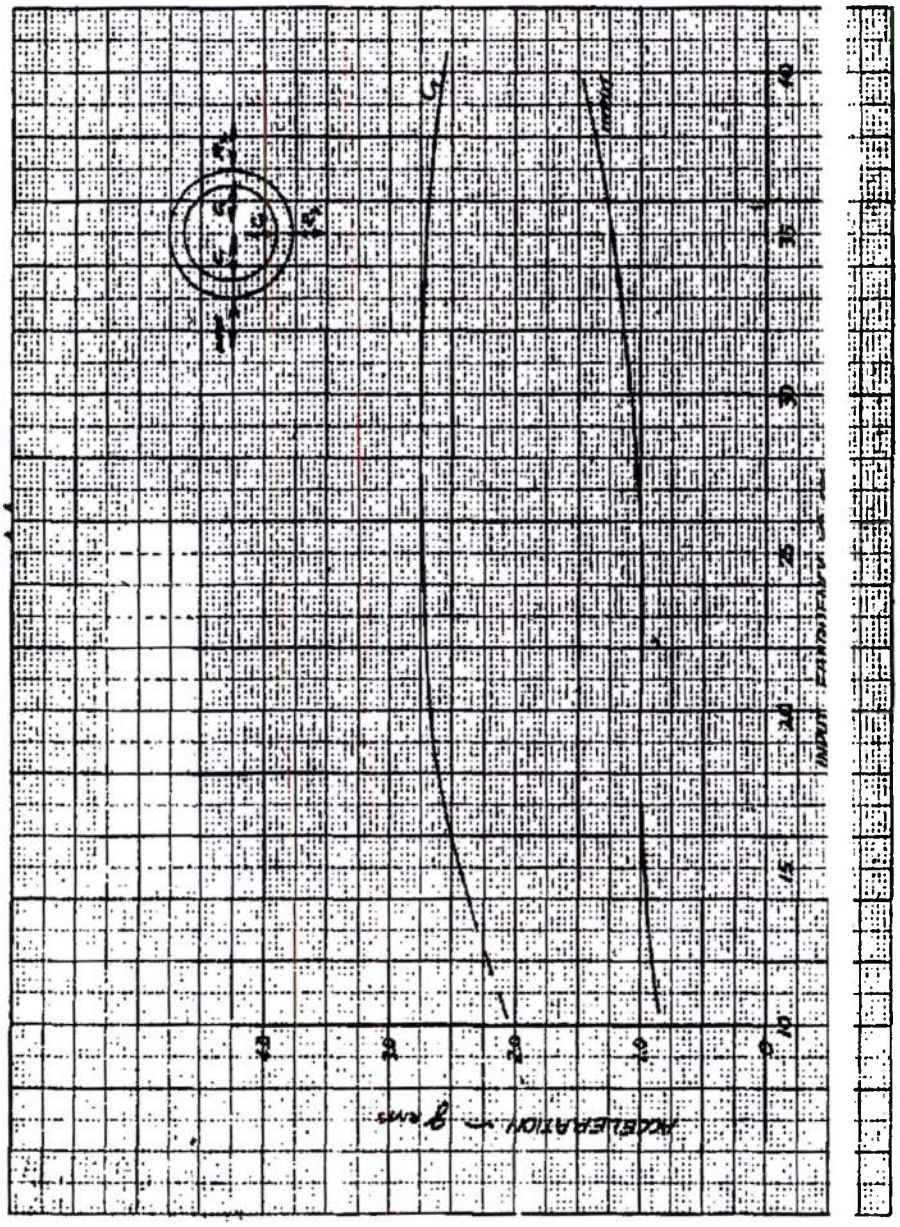

FIGURE 99. Core Dynamic Response (Run No. 10)

~~SECRET RESTRICTED DATA~~
~~ATOMIC ENERGY ACT OF 1954~~

1

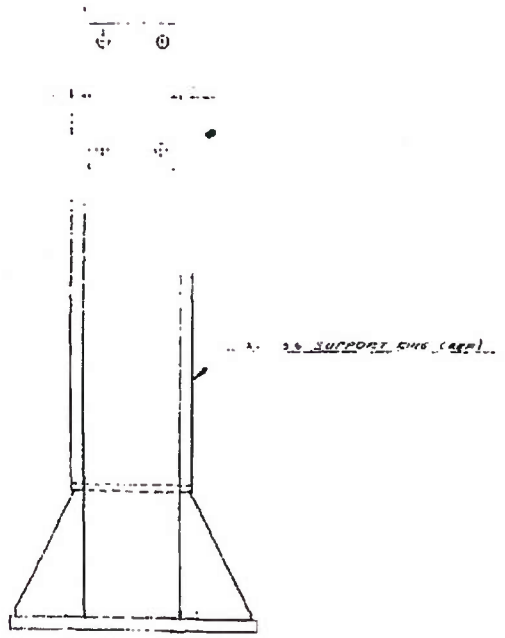

~~SECRET RESTRICTED DATA~~
~~ATOMIC ENERGY ACT OF 1954~~

2

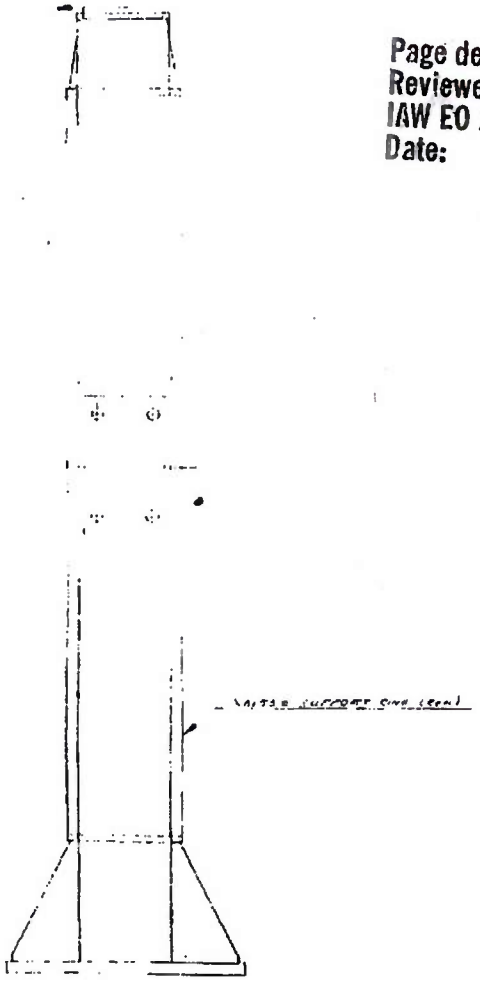

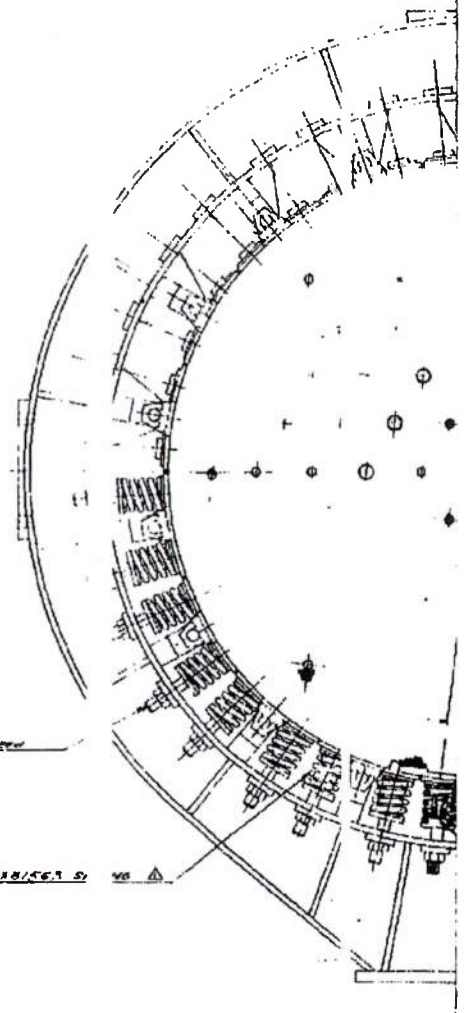

8 7

3

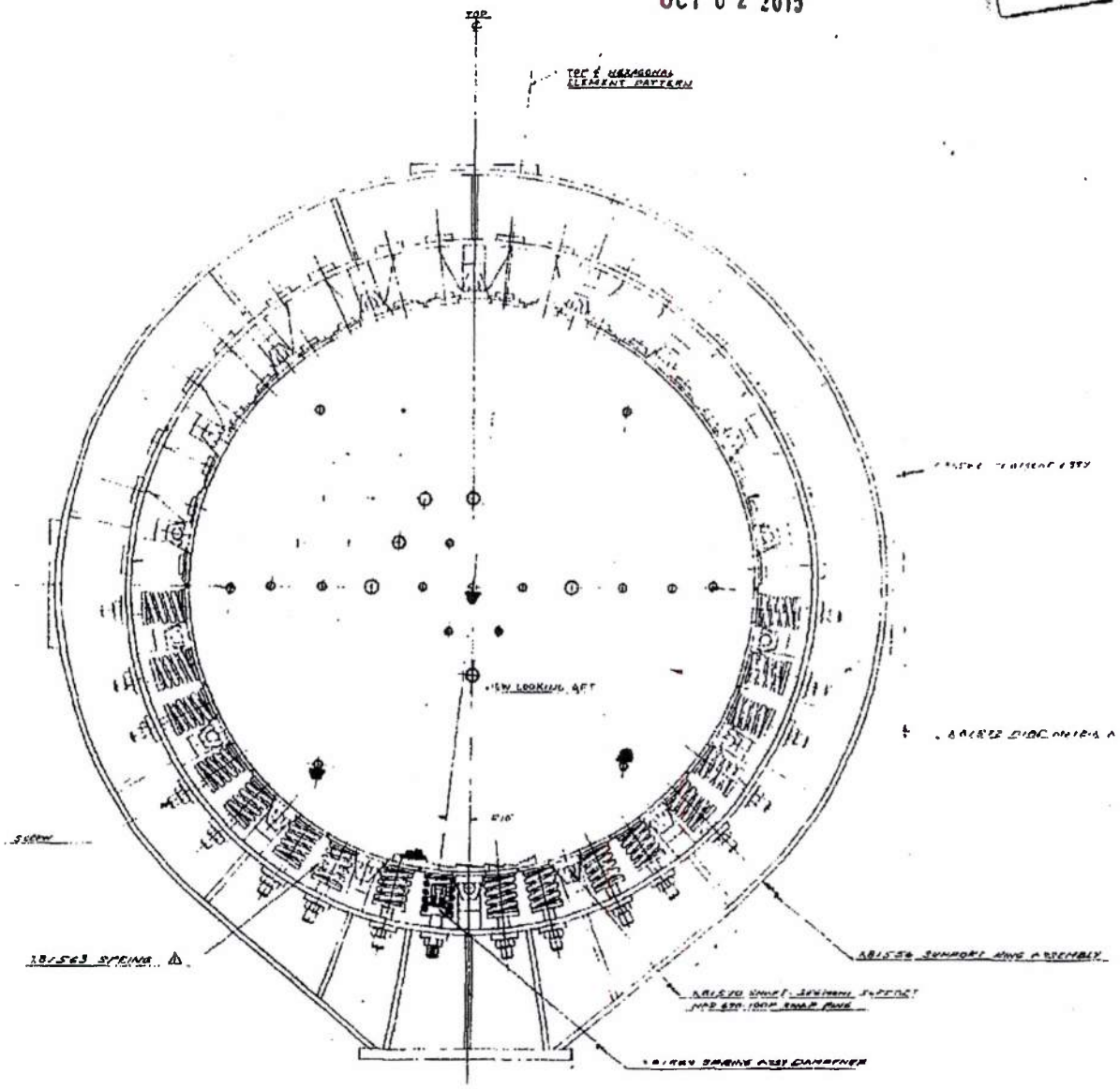

[redacted]

FIGURE 100. La ral Attach Assembly
Engi -Airframe

⚠ SHIMS SPRING MUST BE INDIVIDUALLY CALIBRATED AN
PRE-LOADED IN FINAL ASSEMBLY AT 114 POUNDS.
NOTES: UNLESS OTHERWISE SPECIFIED

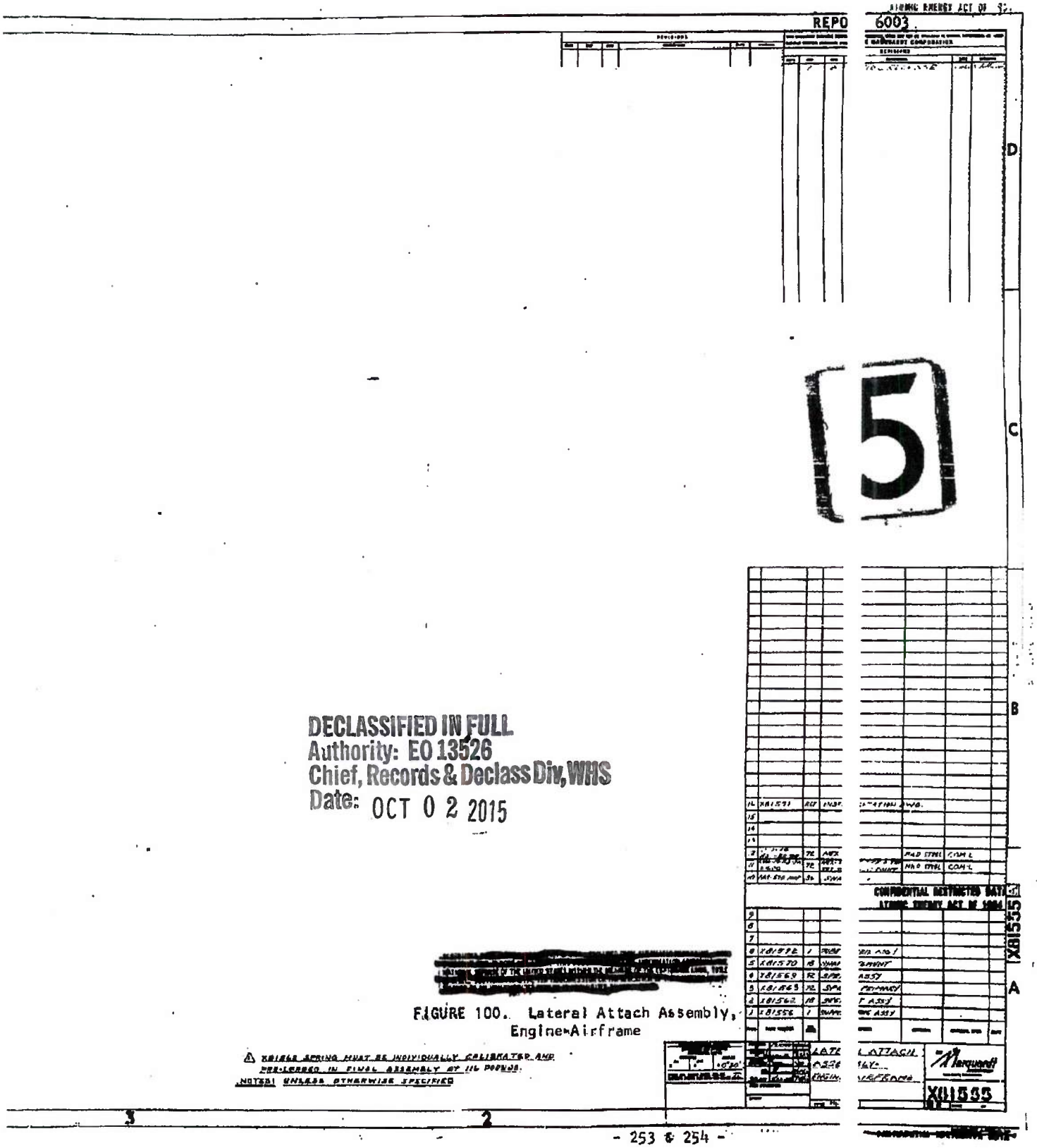

[redacted]

FIGURE 100. Lateral Attach Assembly, Engine-Airframe

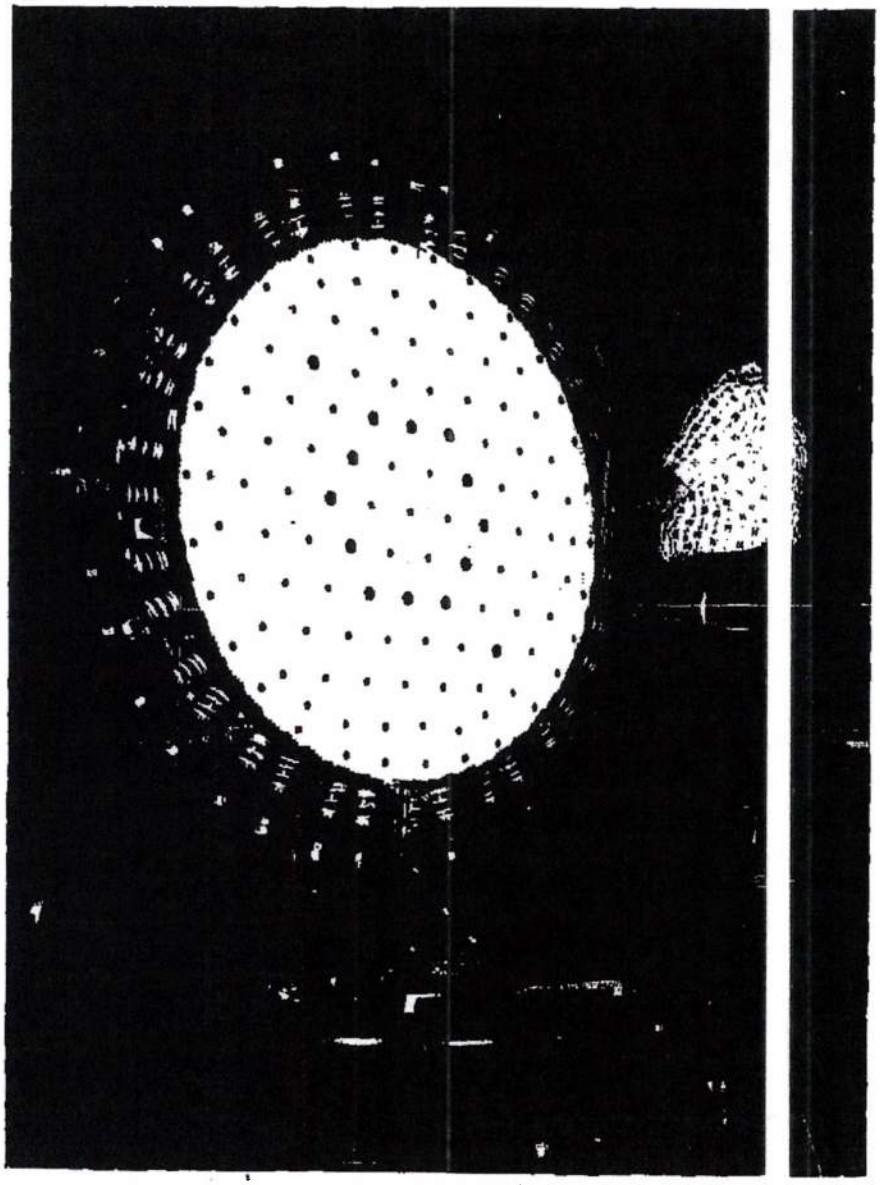

FIGURE 101. Test Item for Engine-Airframe Lateral Attachment Test (Phase II)

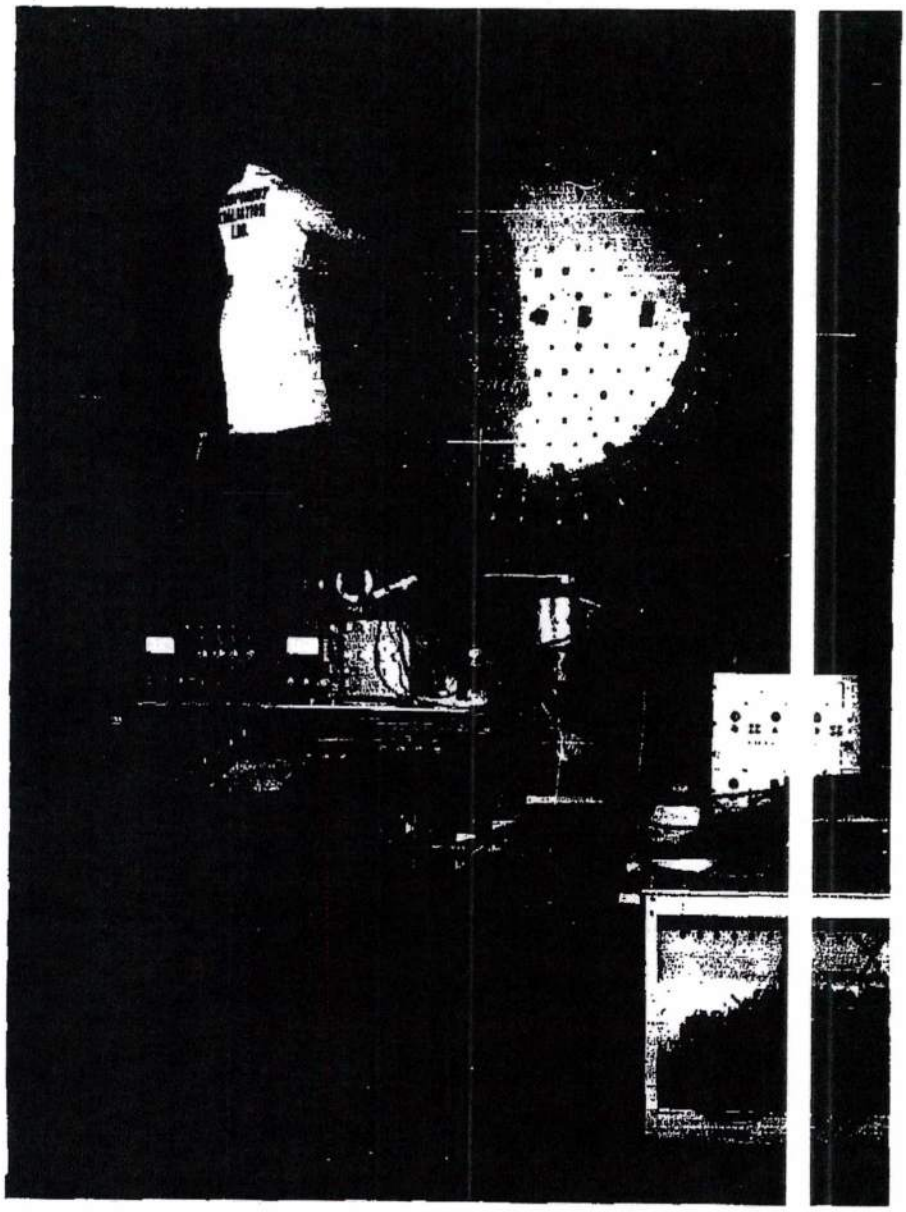

NEG. 4512-7

FIGURE 102. Vibration Test Setup for Engine-Airframe Lateral Attachment Test (Phase I)

MAC A673

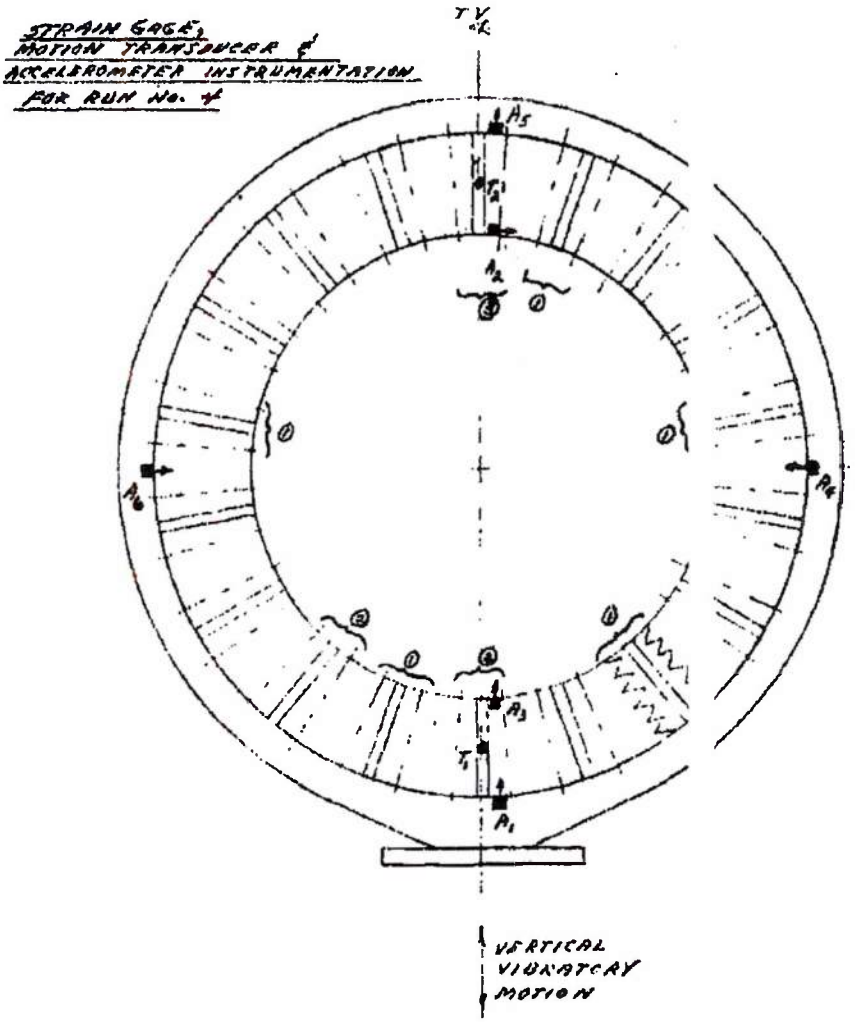

NOTES:

1. ● — MOTION TRANSDUCERS (DISPLACEMENT), T_1 & T_2, ACROSS SPRING BRY.
2. ■ — ACCELEROMETERS, A_1 THROUGH A_6.
3. ⌣ (#a) — LOCATION & NUMBER OF STRAIN GAGED SPRINGS MONITORED.

FIGURE 103. Instrumentation Requirements for Engine-Airfr e Lateral Attachment Test (Phase II)

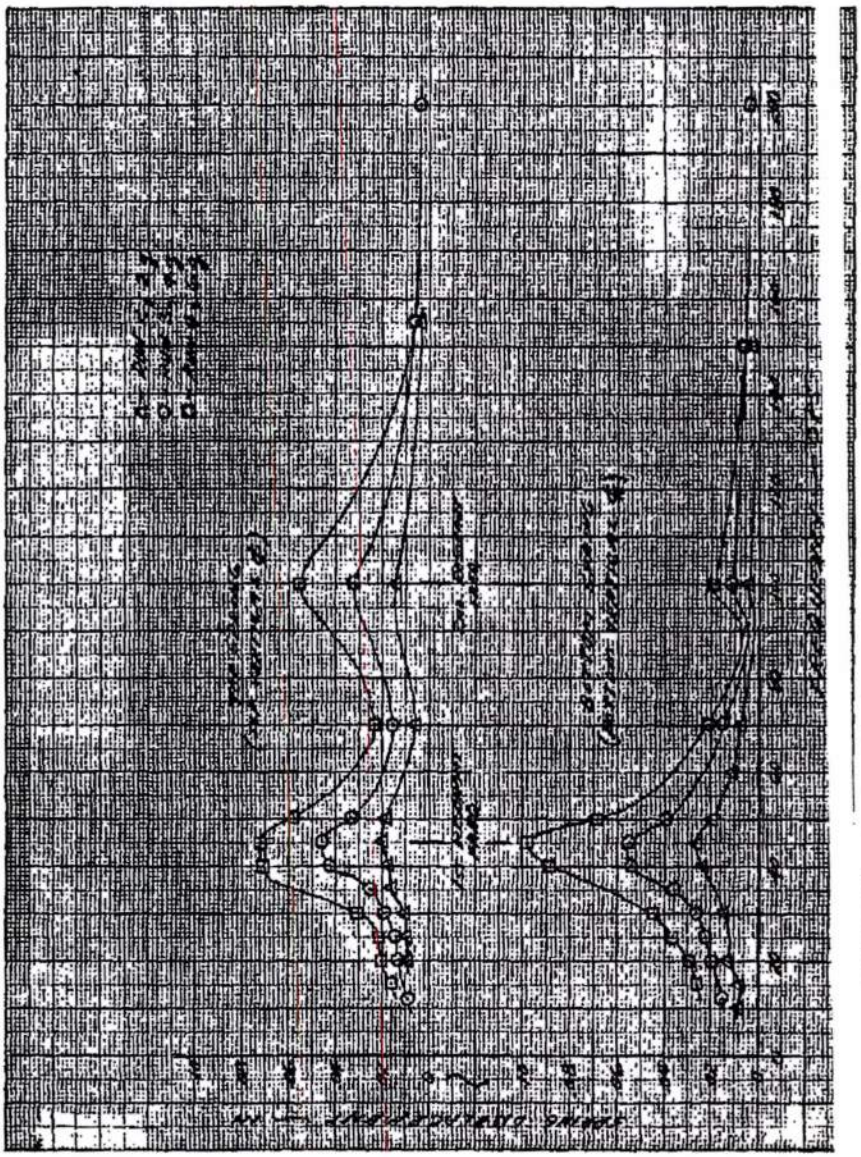

FIGURE 101. Spring Displacement vs. Frequency (15 psi Core Preload)

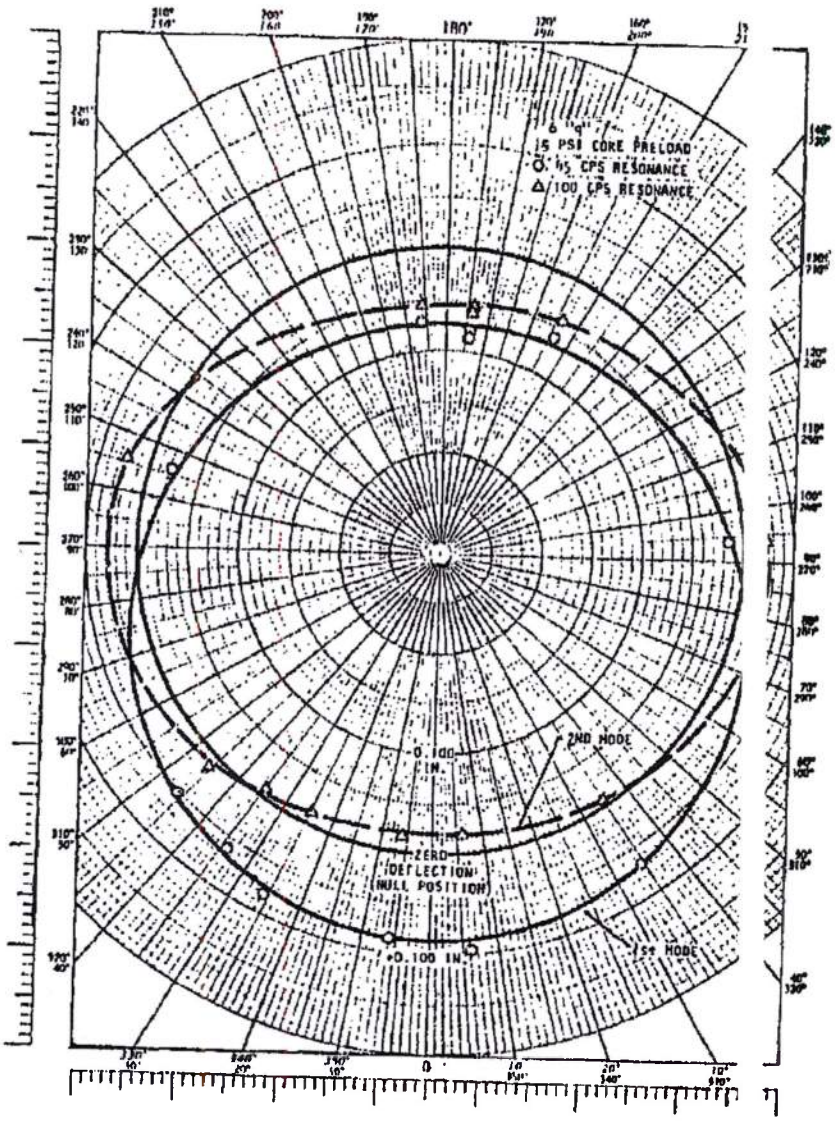

FIGURE 105. Core Deflection Pattern, Run 4

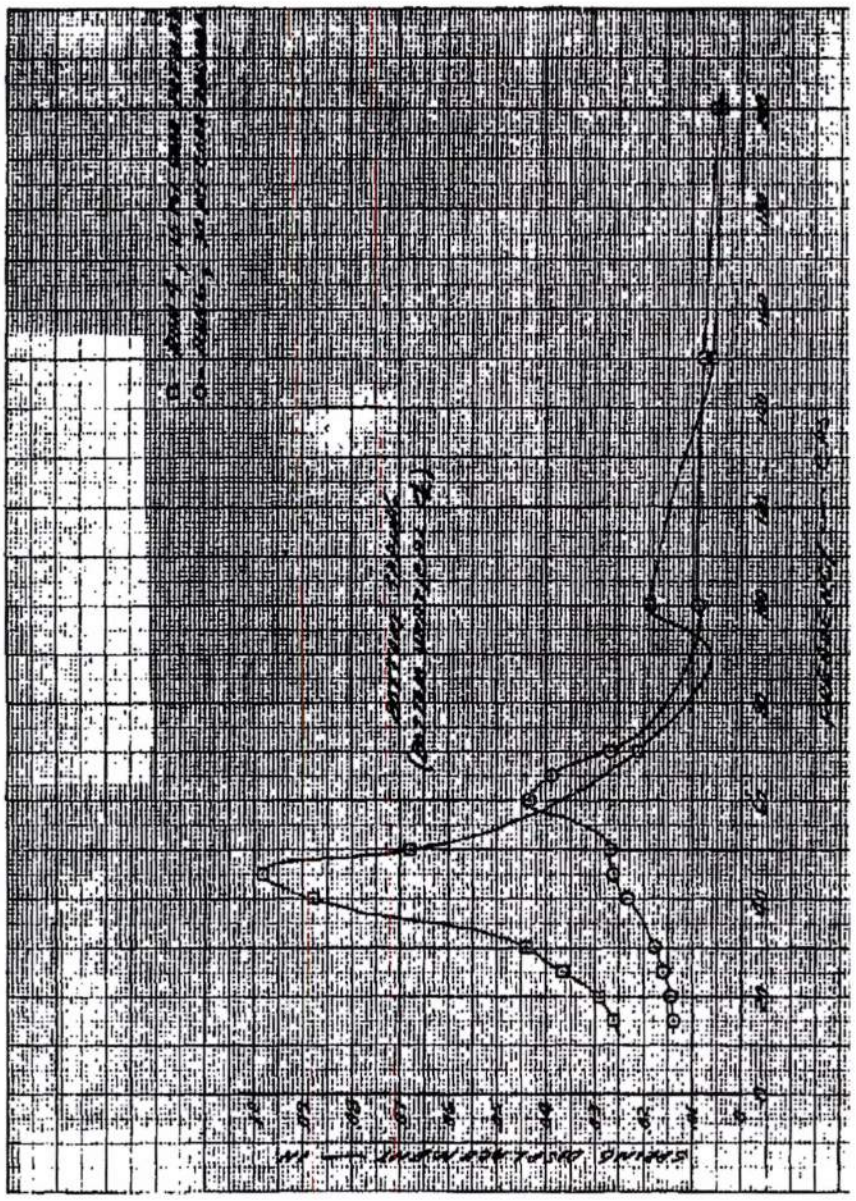

FIGURE 106. Spring Displacement vs. Frequency (6g Force Input)

~~SECRET RESTRICTED DATA~~
~~ATOMIC ENERGY ACT OF 1954~~

1

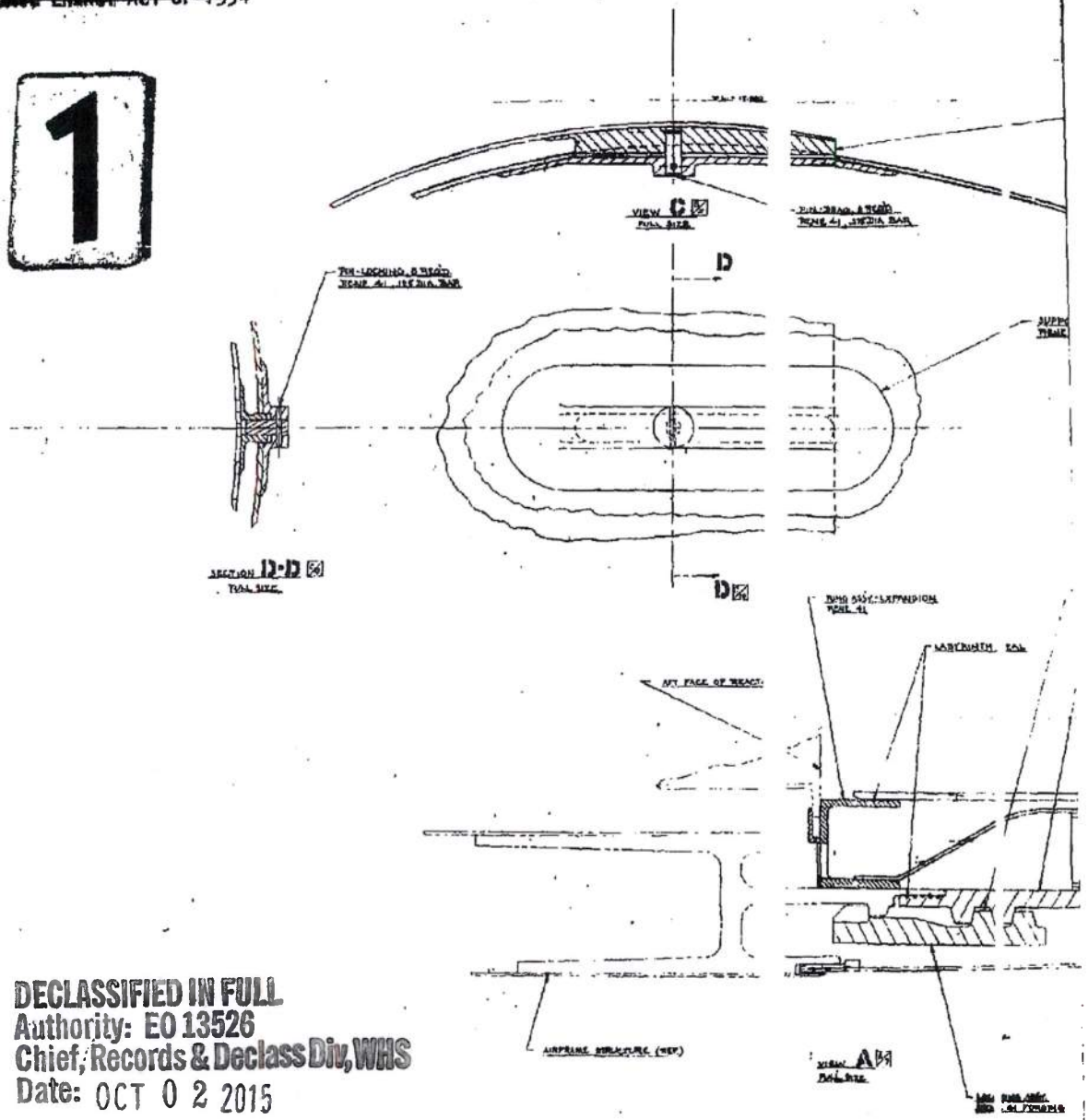

~~SECRET RESTRICTED DATA~~
~~ATOMIC ENERGY ACT OF 1954~~

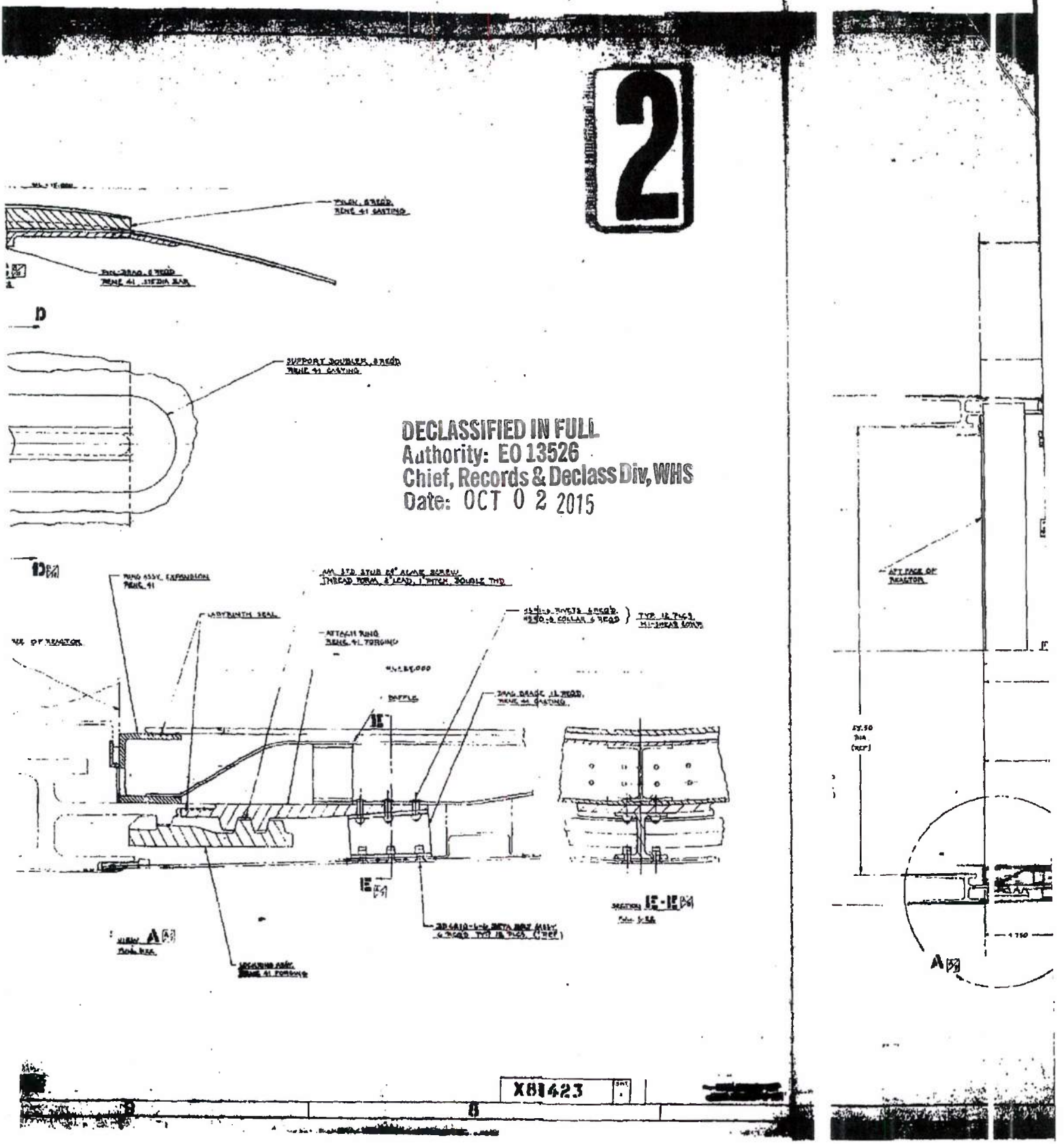

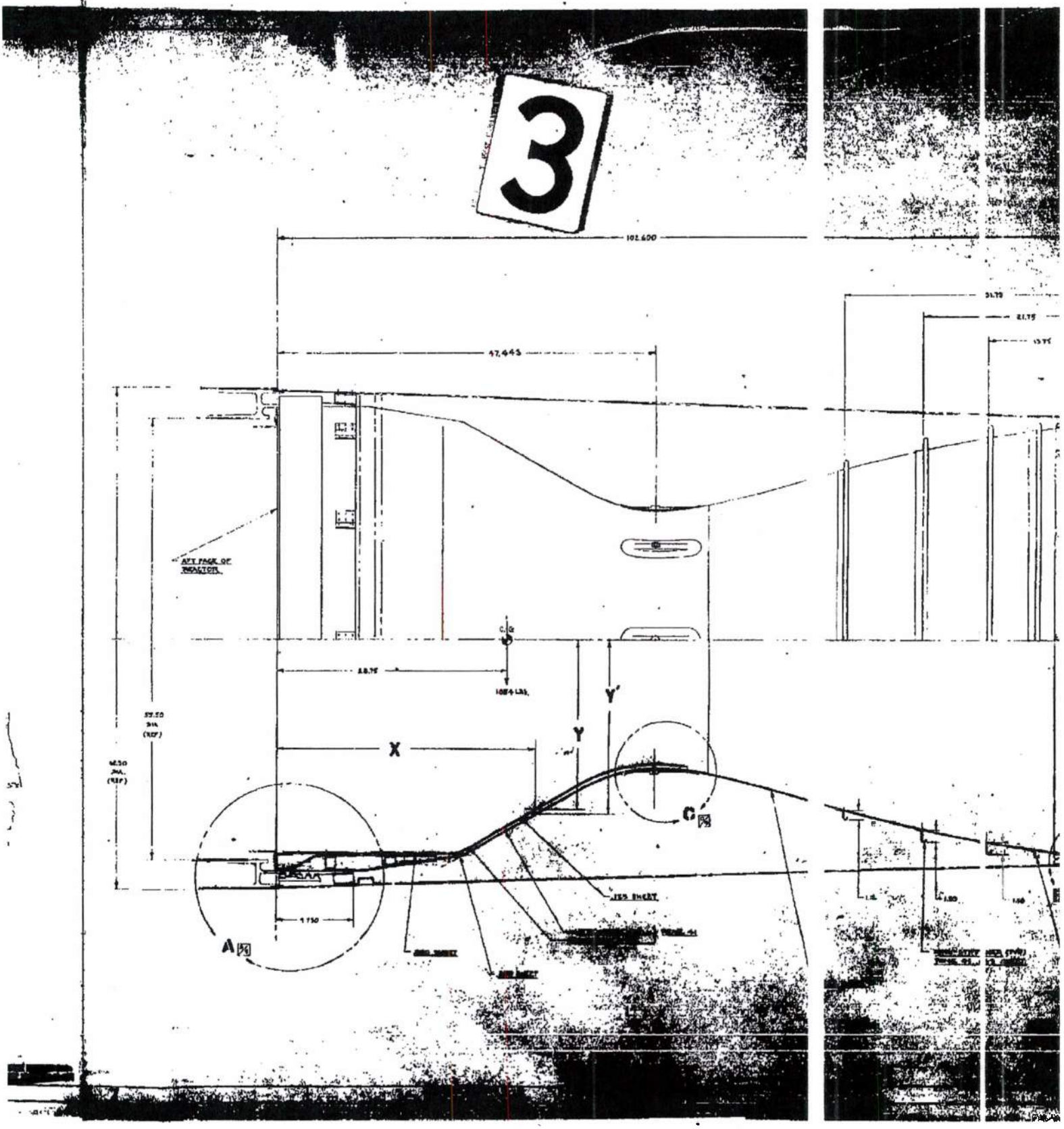

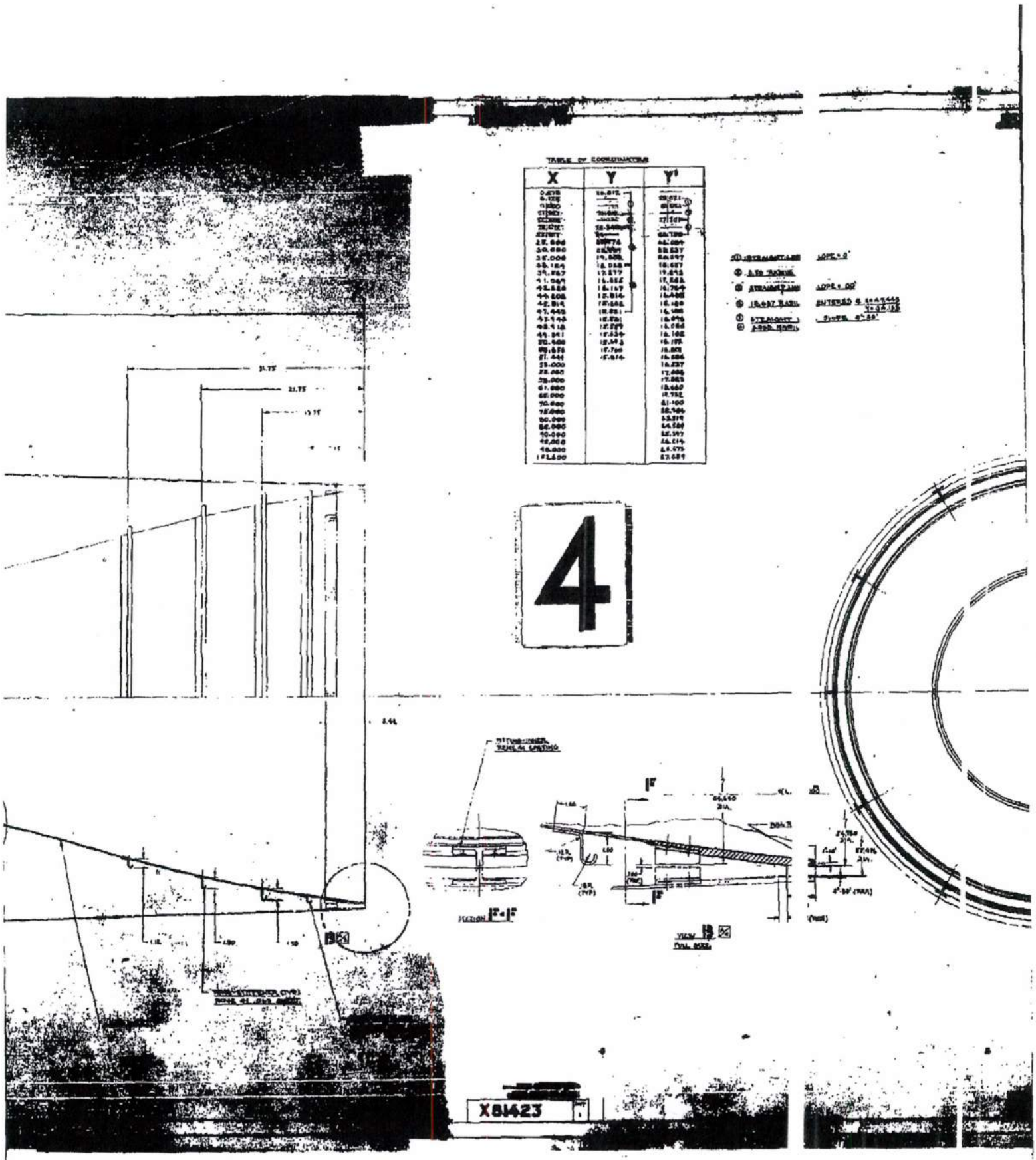

[redacted]

REPORT COPY

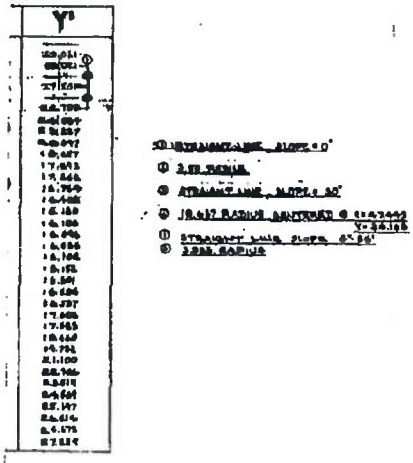

5

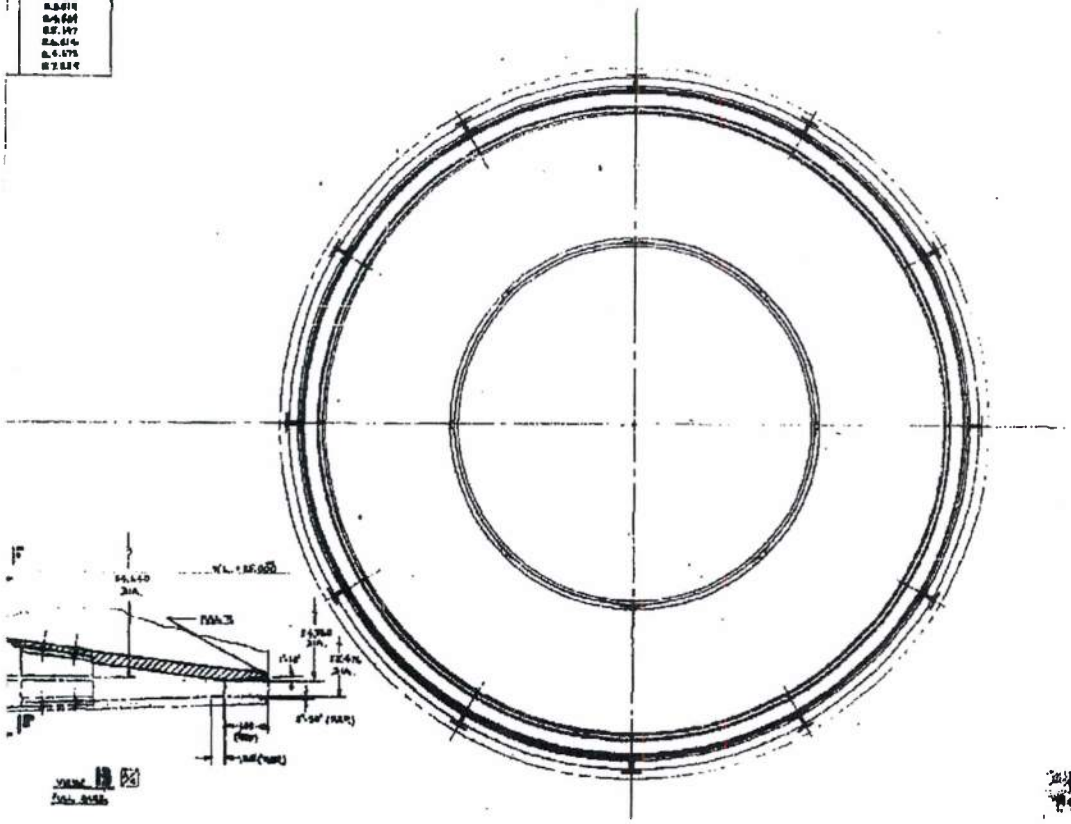

[redacted]

FIGURE 107 Design Layout
Propulsion System Exit Nozzle

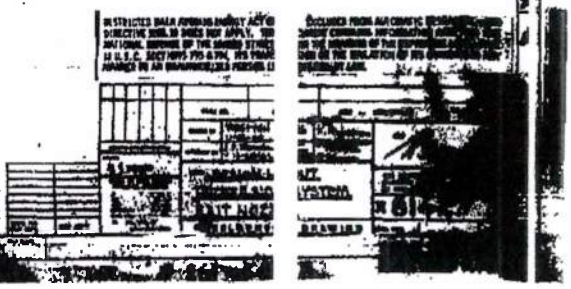

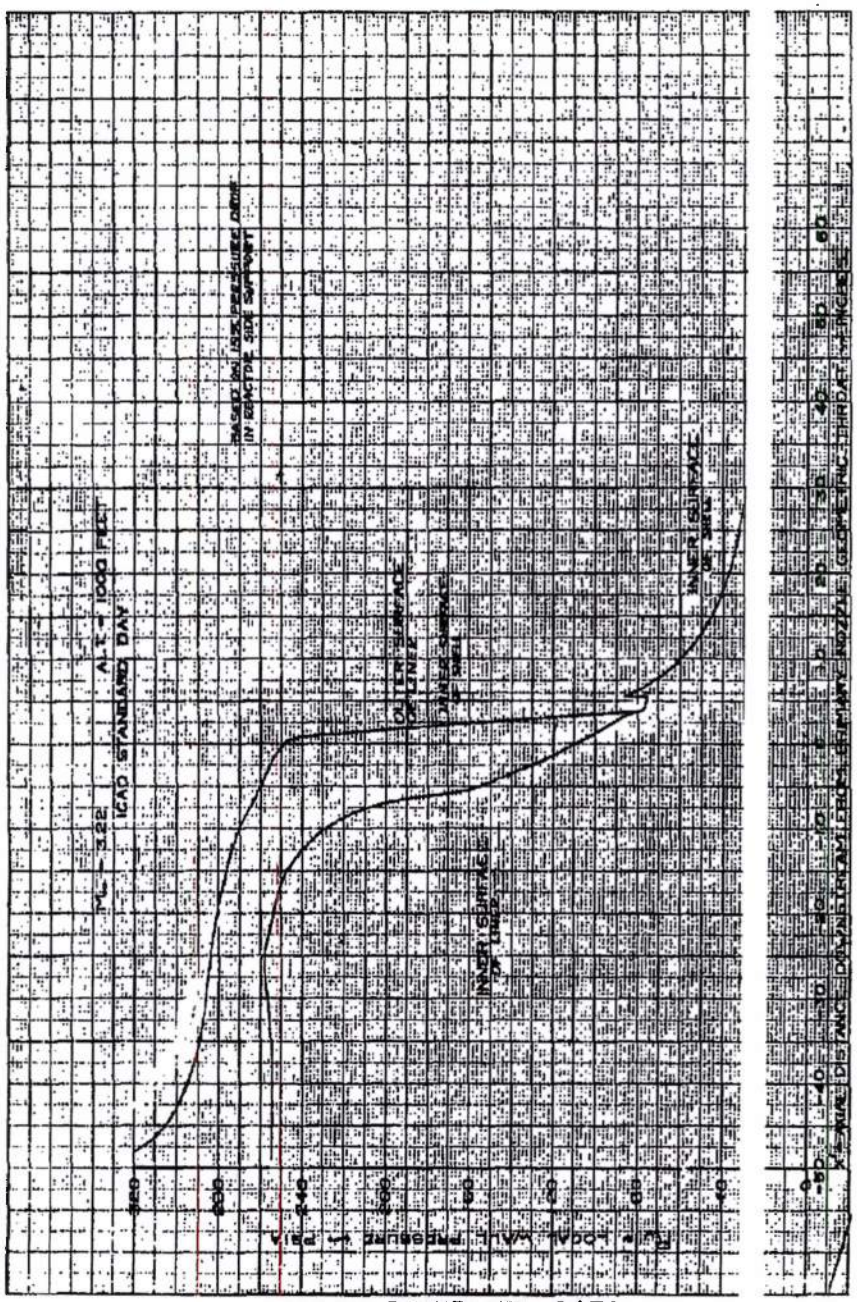

FIGURE 108. Wall Pressure Distribution for MA50-XCB Ejector Nozzle (Altitude = 10,000 Feet)

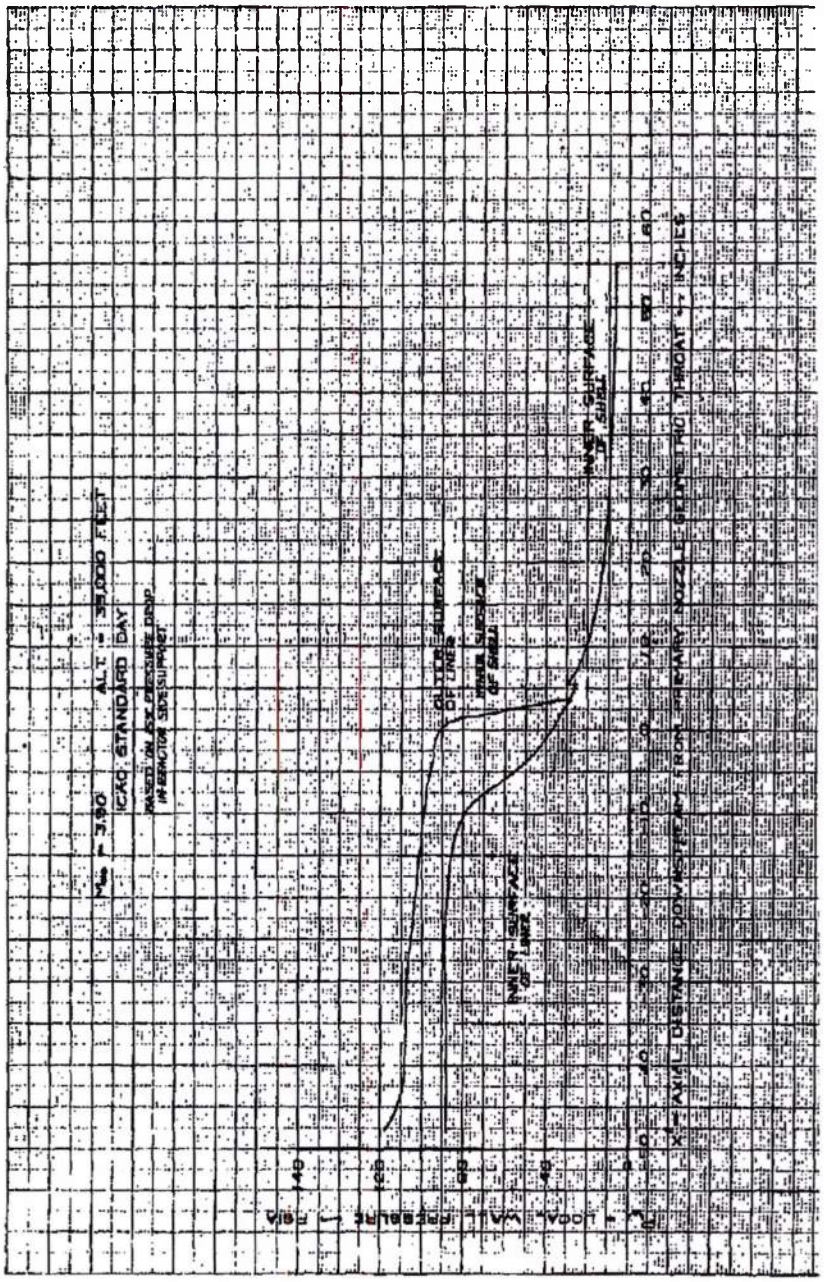

FIGURE 109. Wall Pressure Distribution for MA50-XCB Ejector Nozzle (Altitude = 35,000 Feet)

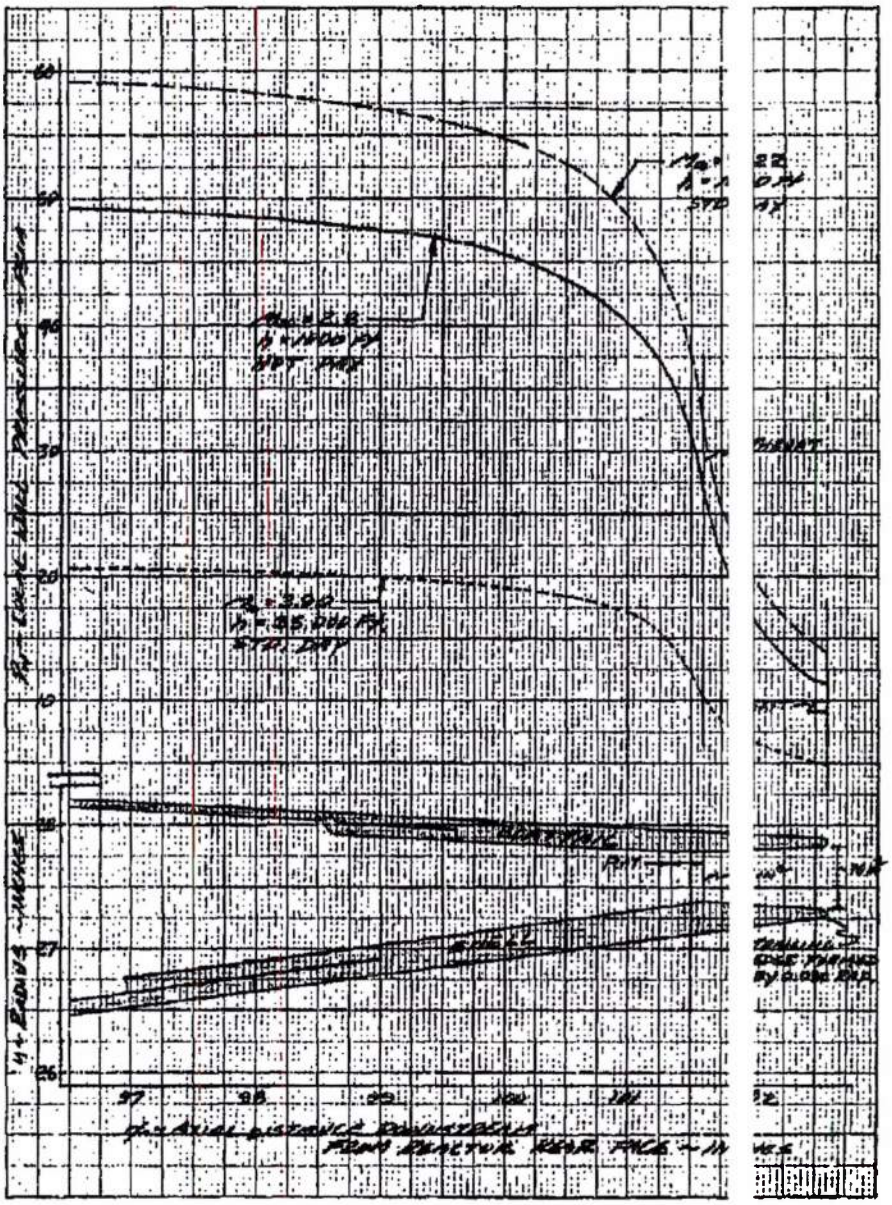

FIGURE 110. Local Wall Pressure Distribution in Exhaust I gion of Airframe Cooling Flow: MA50-XCB Ejector Nozzle

MA50-XCB EJECTOR NOZZLE
AXIAL LOADS (DRAG)

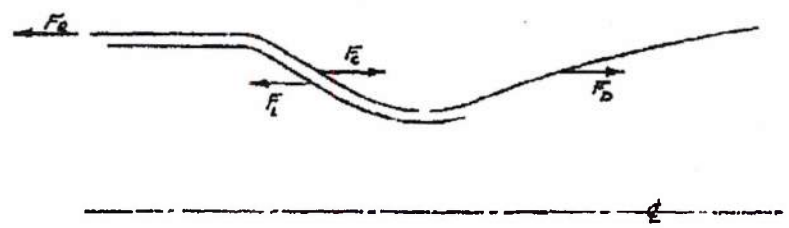

F_L = AXIAL LOAD ON NOZZLE LINER (LB)
F_C = AXIAL LOAD ON SHELL CONVERGENT SECTION (LB)
F_D = AXIAL LOAD ON SHELL DIVERGENT SECTION (LB)
F_R = AXIAL FORCE REQUIRED TO RETAIN NOZZLE ASSEMBLY IN POSITION ON SIDE SUPPORT SHELL (LB)
M_∞ = FLIGHT MACH NUMBER
h = ALTITUDE (FT)

M_∞	h	DAY	F_L	F_C	F_D	F_R
3.22	1000	STD.	59,961	393,749	39,650	367,43
3.90	35,000	STD.	30,931	144,988	13,712	127,76

FIGURE 111. MA50-XCB Ejector Nozzle Axial Loads (Drag)

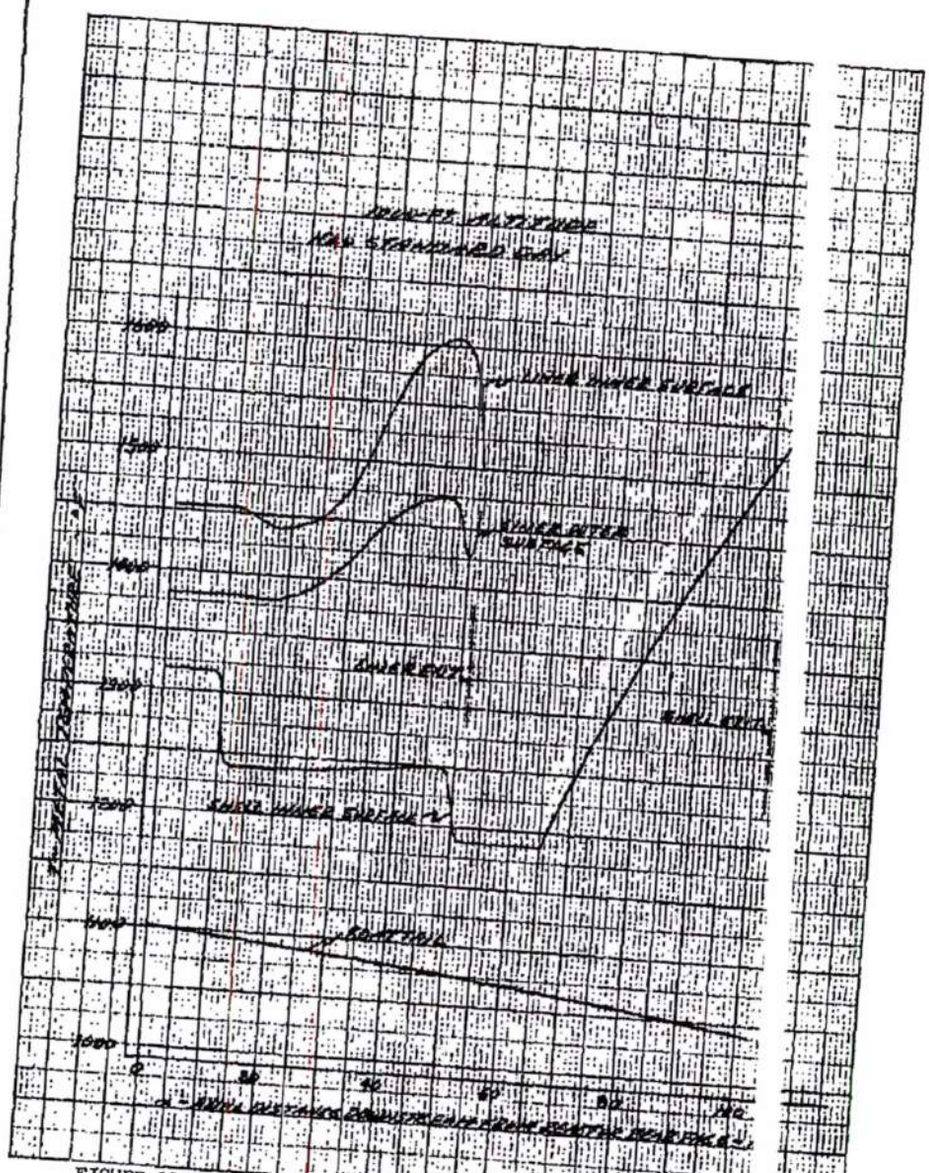

FIGURE 112. Estimated Temperature Distribution for MA50-X
Ejector Nozzle (3.22 M_∞)

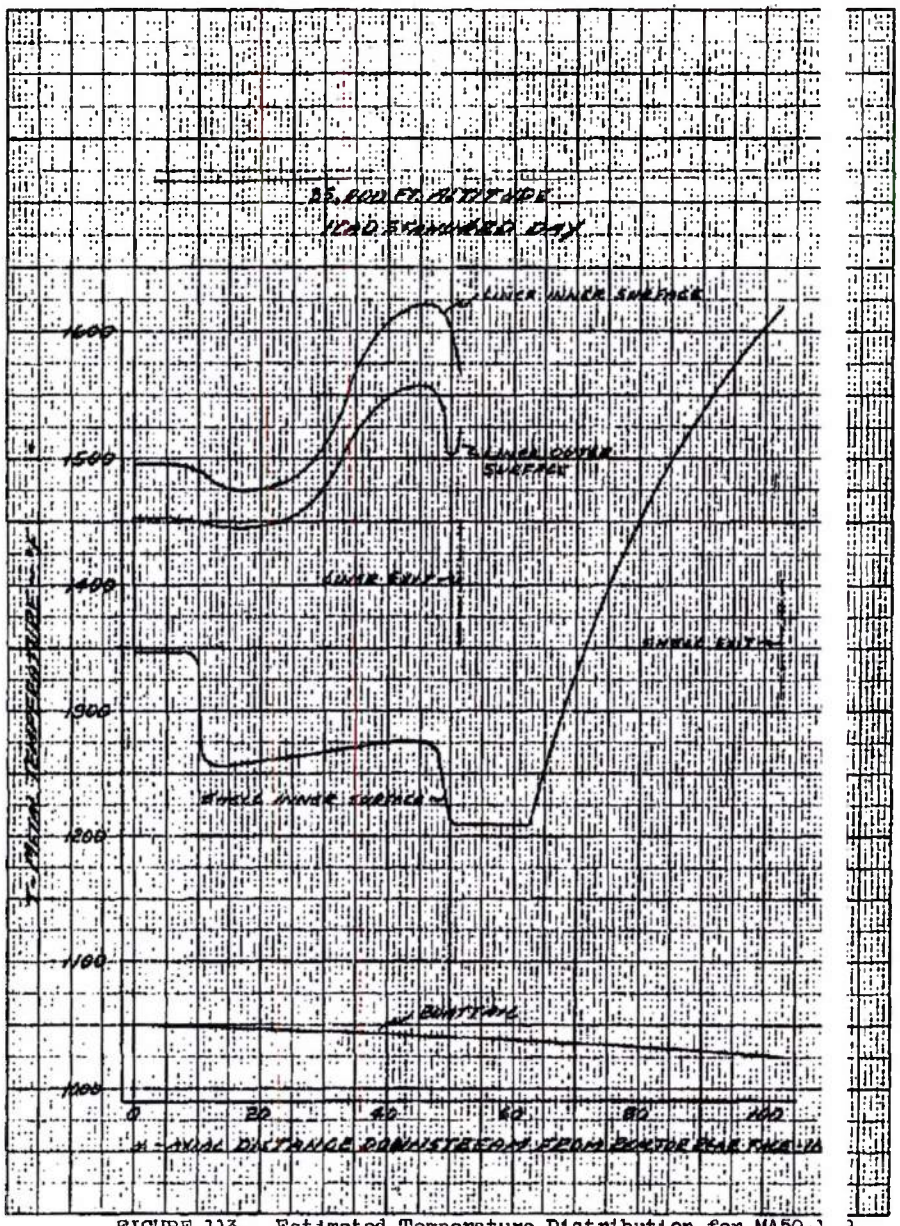

FIGURE 113. Estimated Temperature Distribution for MA50-3
Ejector Nozzle (3.90 M_∞)

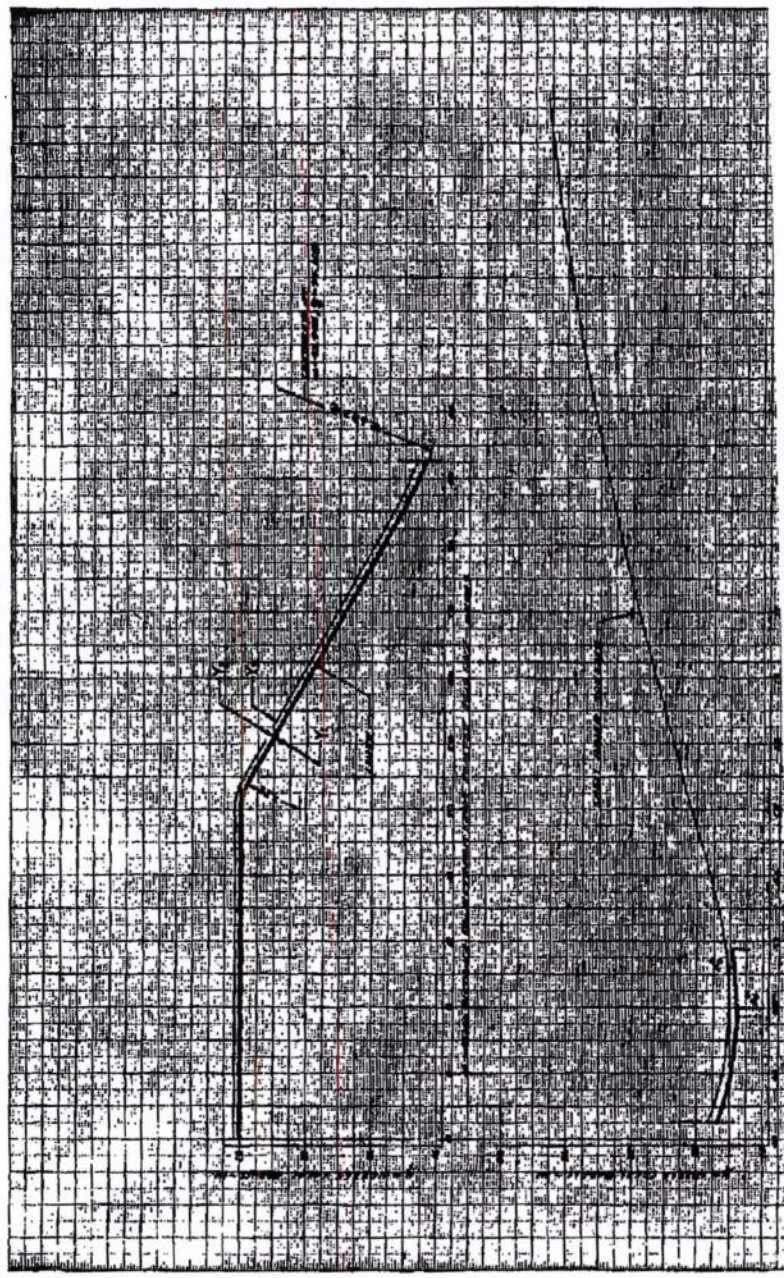

FIGURE 114. MA50-KCB Ejector Nozzle Contours (Based on 0.125 in. Nozzle Liner Thickness)

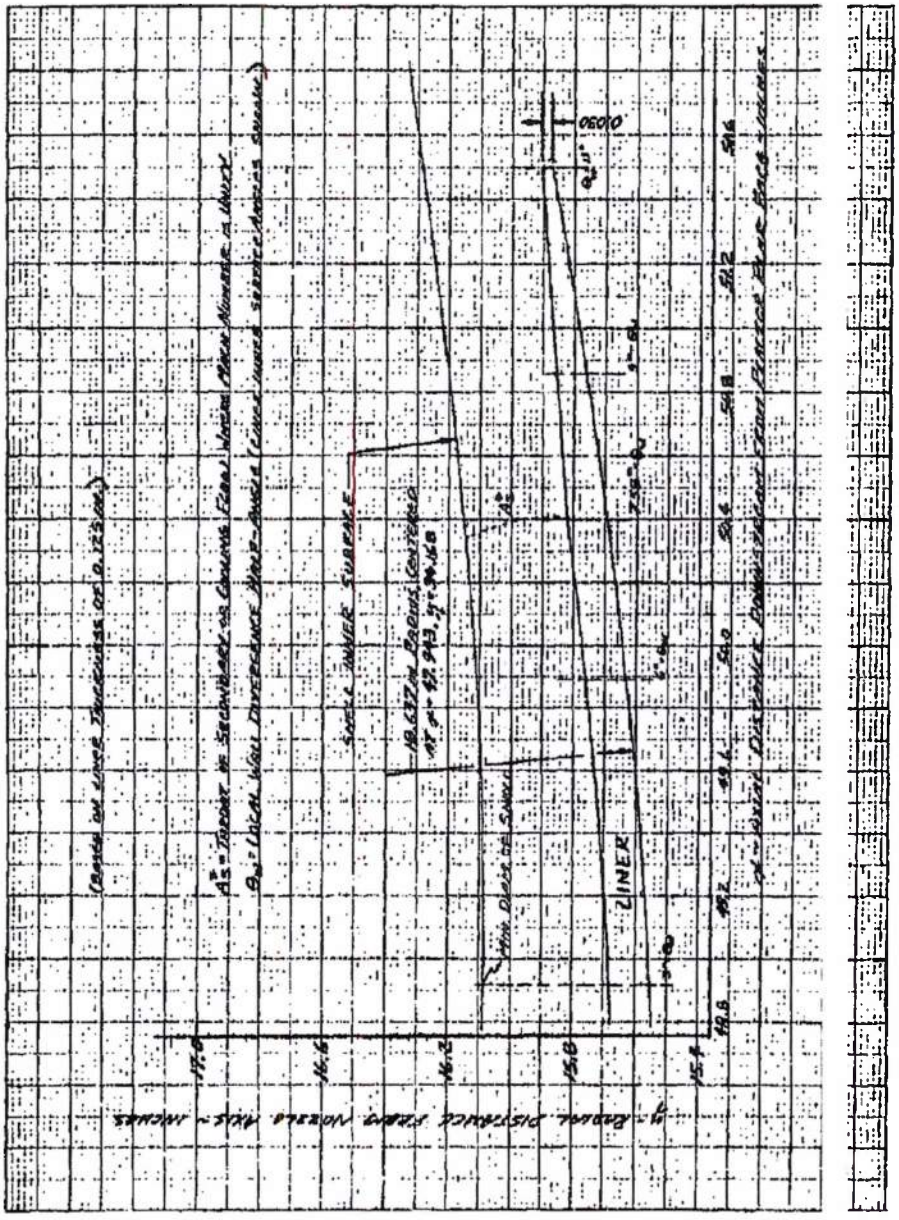

FIGURE 115. MA50-XCB Ejector Nozzle Liner Exit Details

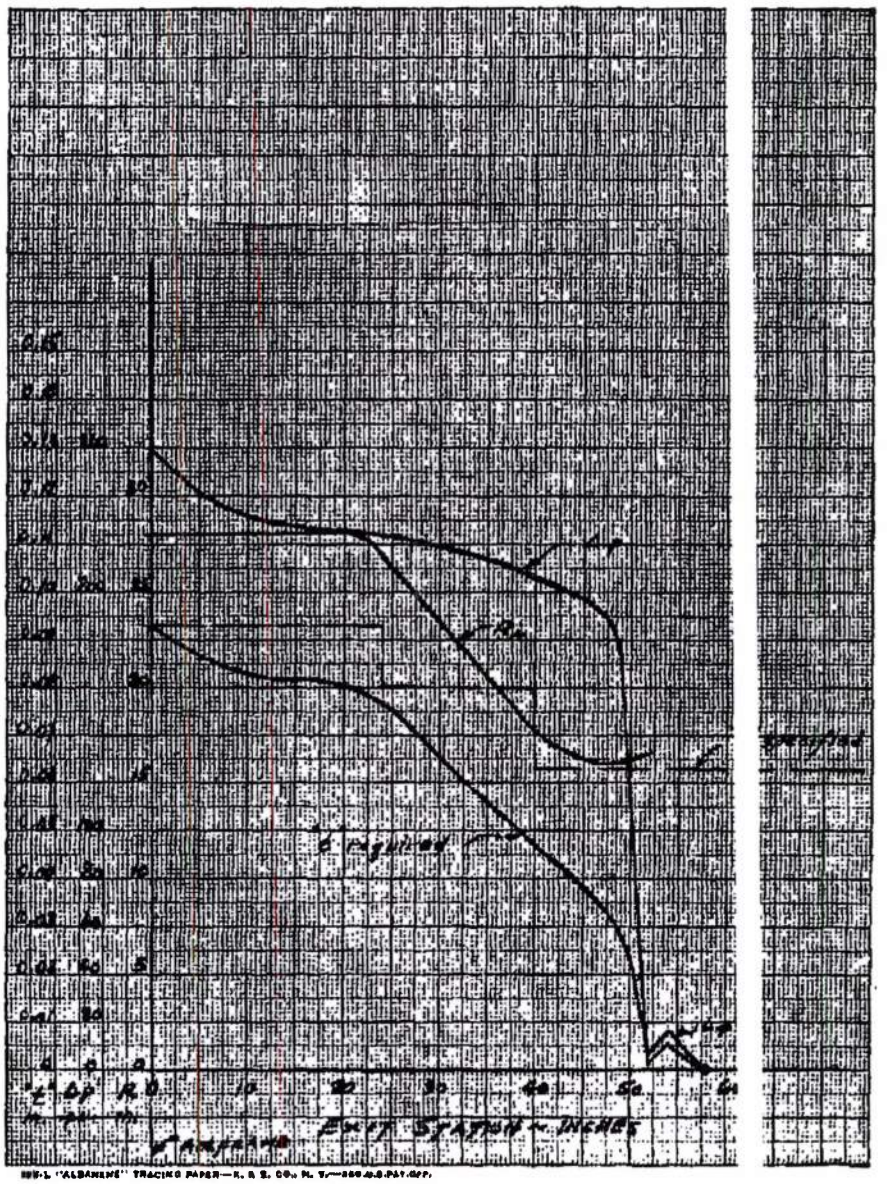

FIGURE 116. Nozzle Load Parameters

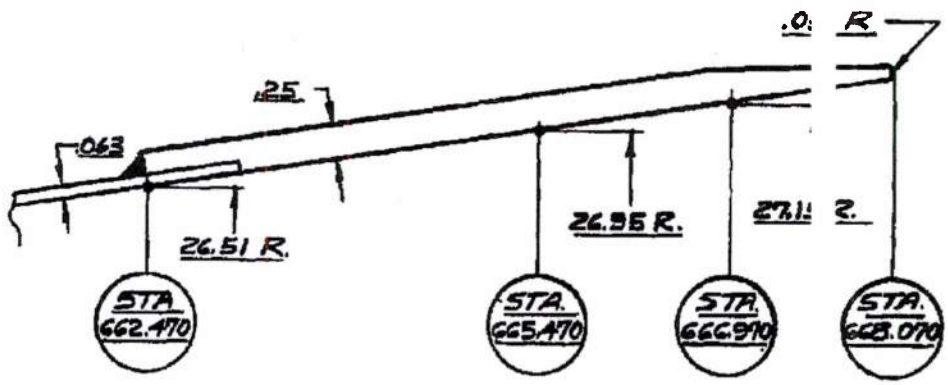

FIGURE 117. Doubler Ring

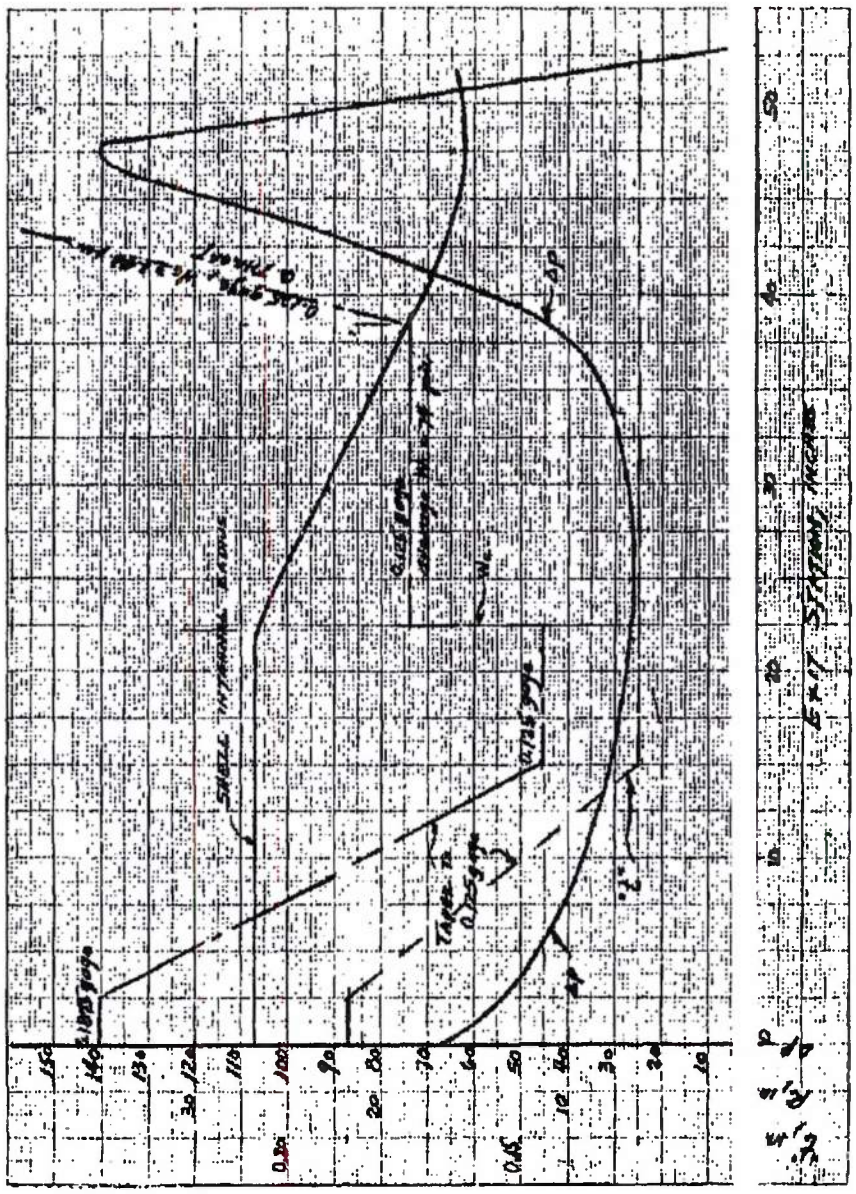

FIGURE 118. Liner Load Parameters

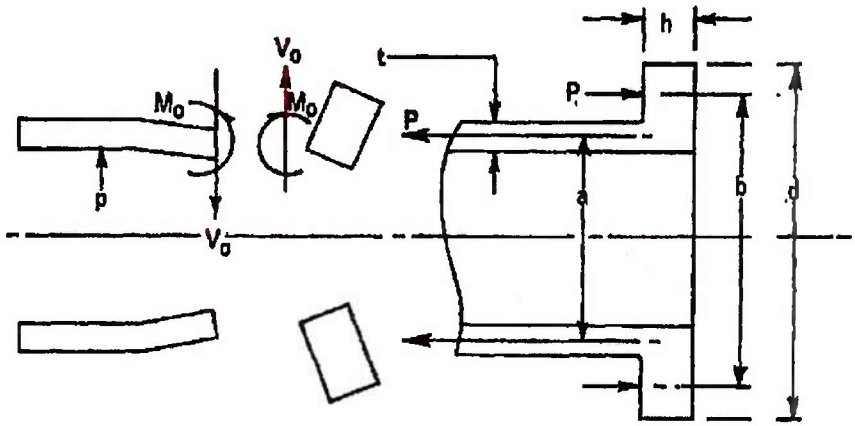

FIGURE 119. Assumed Coupling Geometry

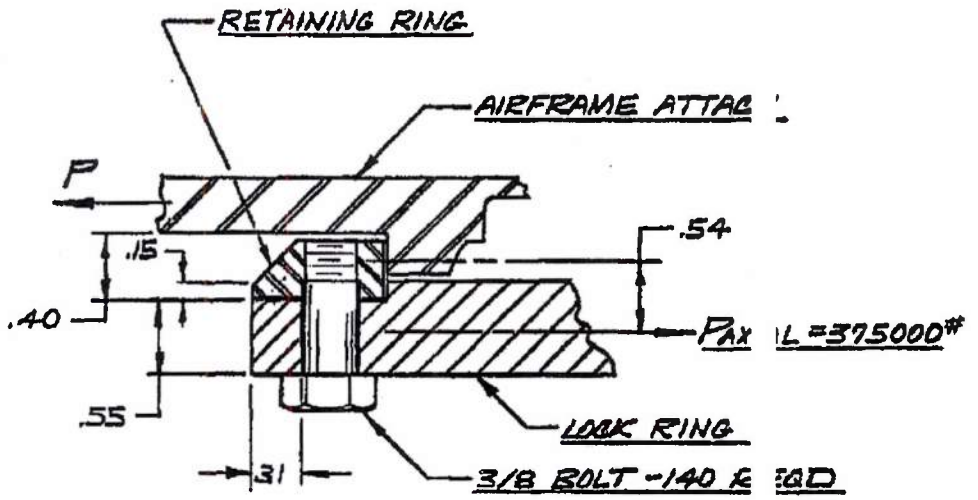

FIGURE 120. Retaining Ring Geometry

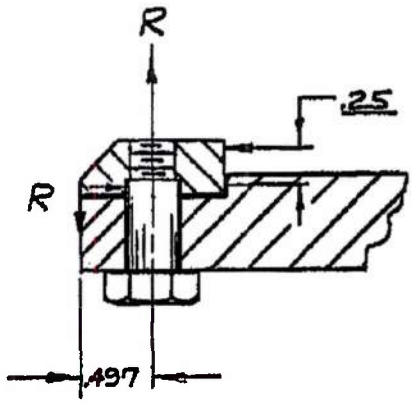

FIGURE 121. Airframe Fitting Shell

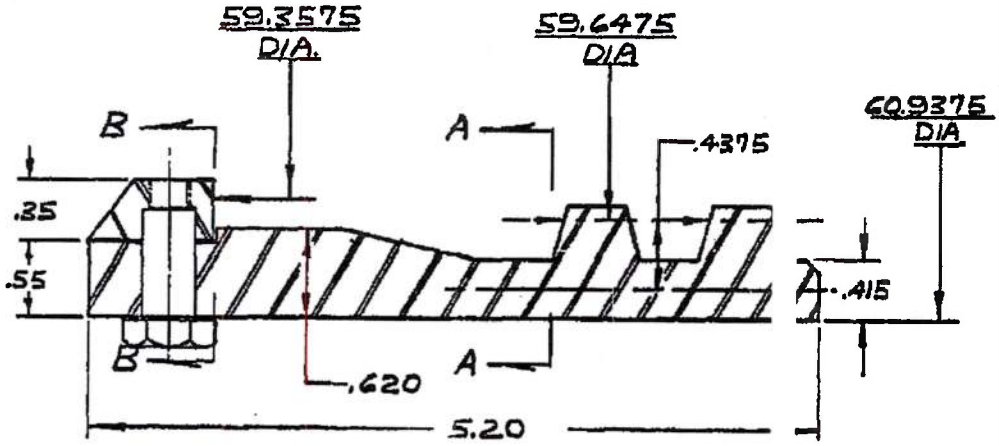

FIGURE 122. Lock Ring

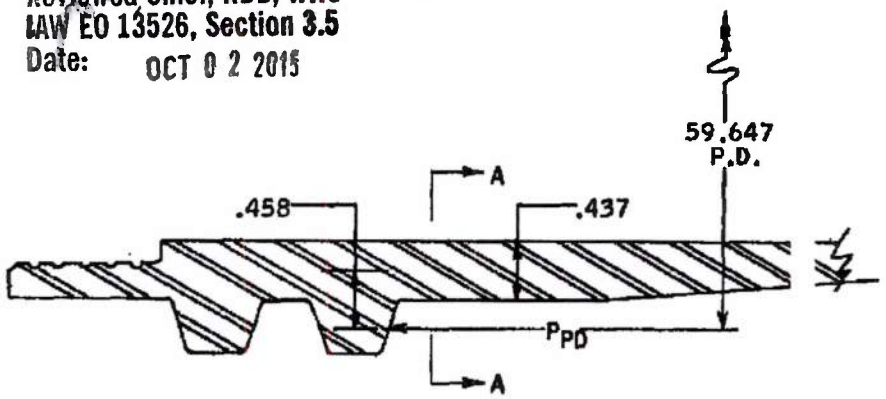

FIGURE 123. Exit Nozzle Attach Ring

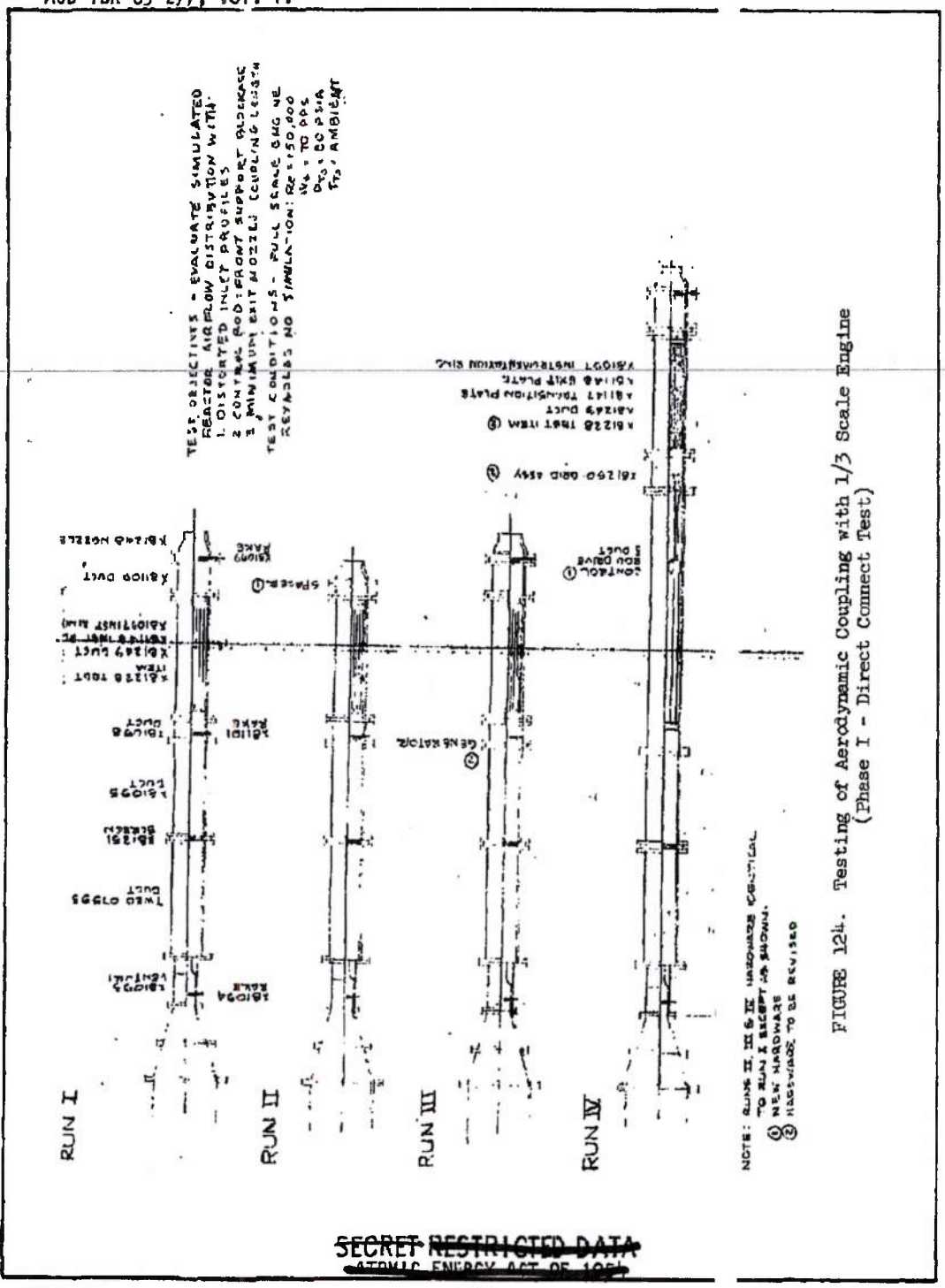

FIGURE 124. Testing of Aerodynamic Coupling with 1/3 Scale Engine (Phase I - Direct Connect Test)

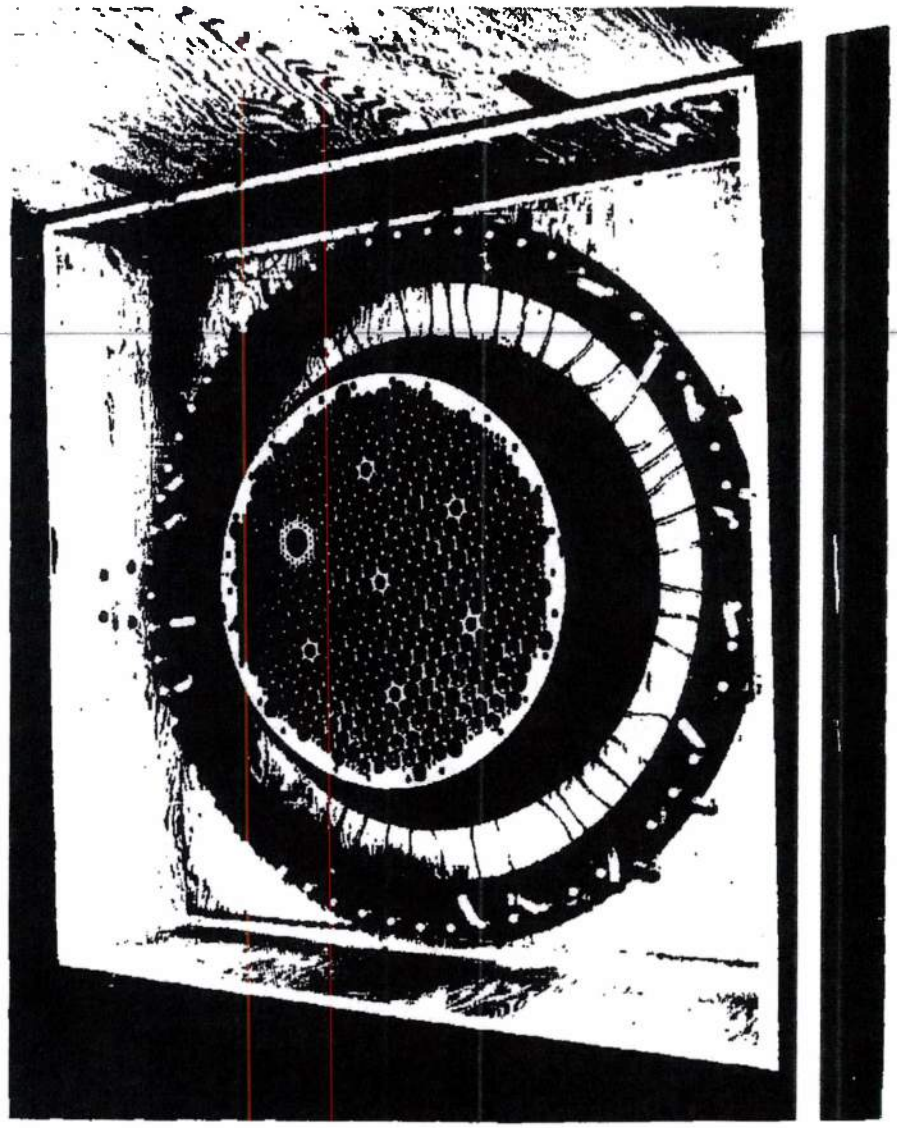

FIGURE 125. Aft Transition Section for Aerodynamic Coupling Test

NEG. C 4267-3

MAC A672

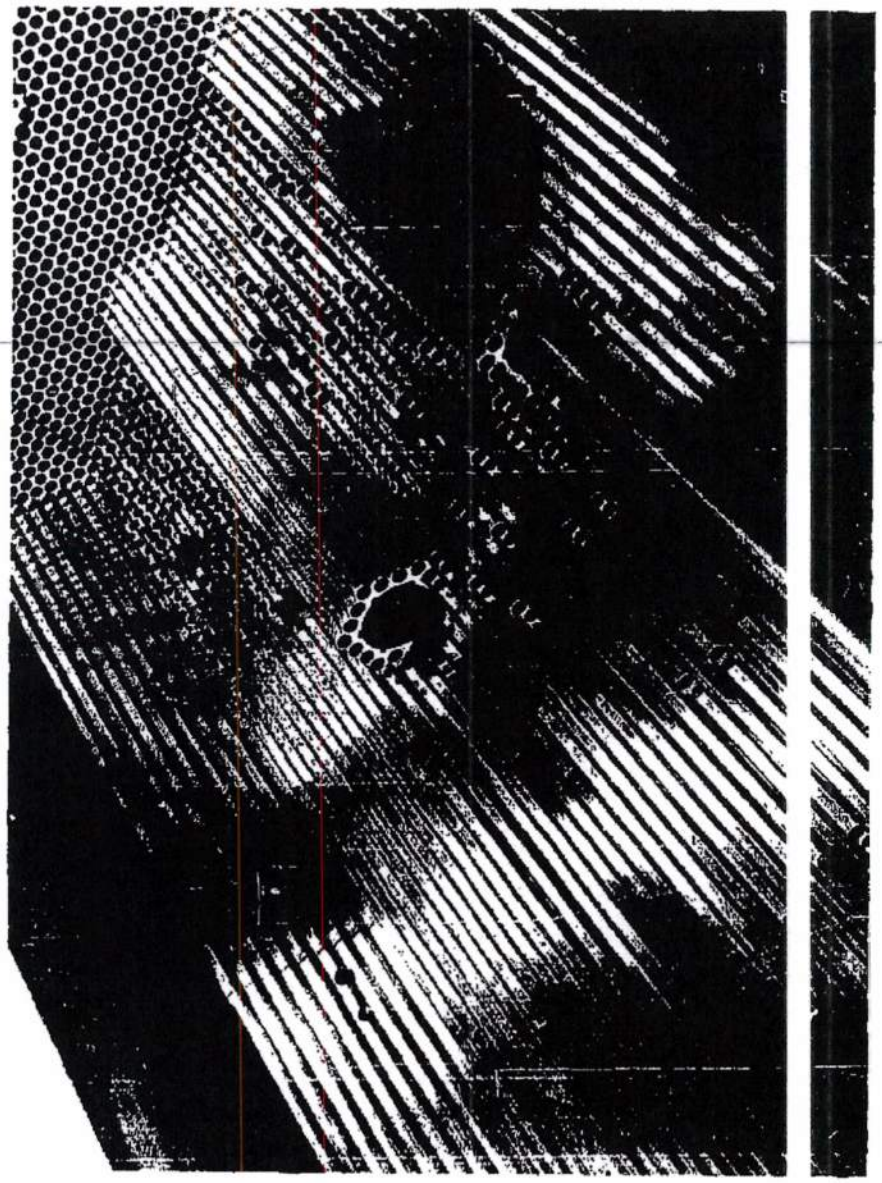

3946-3

FIGURE 126. Buildup of Simulated Reactor Segment for Aerodynamic Coupling Test (Closeup)

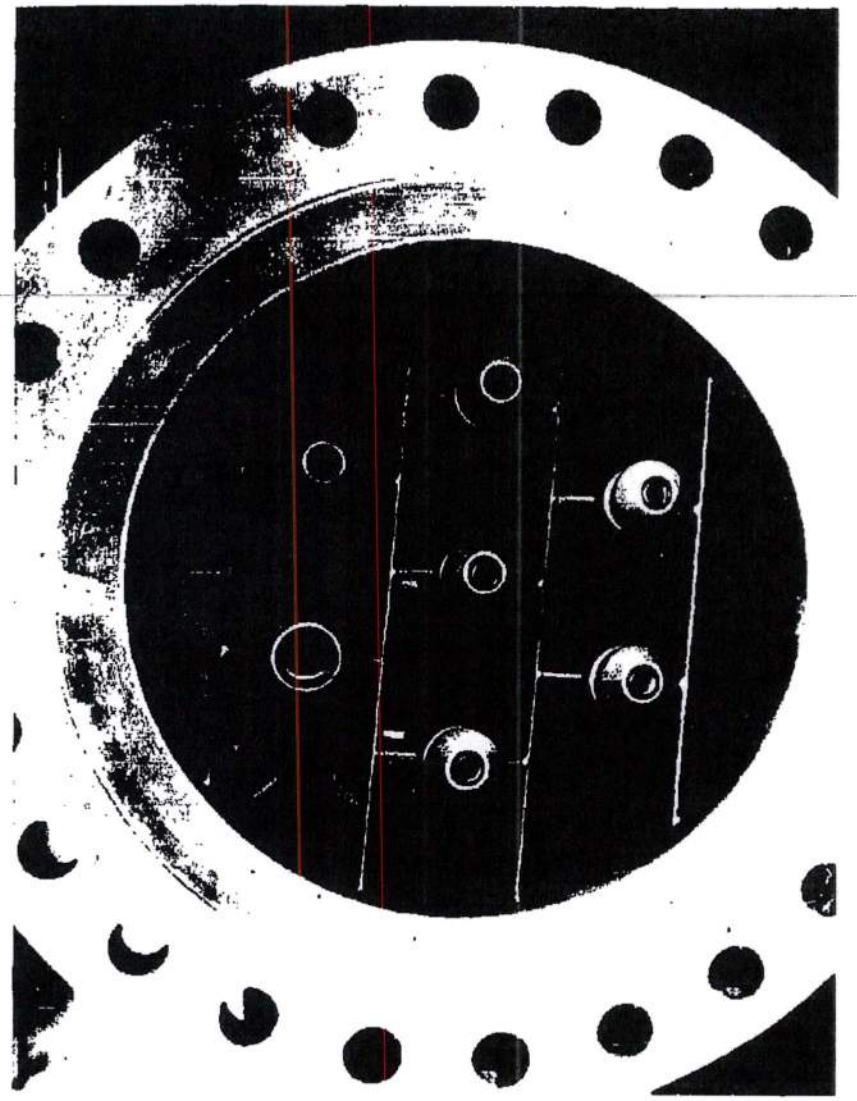

NEG. C 4057-5

FIGURE 127. Front Support Section of Aerodynamic Coupling (Looking Forward)

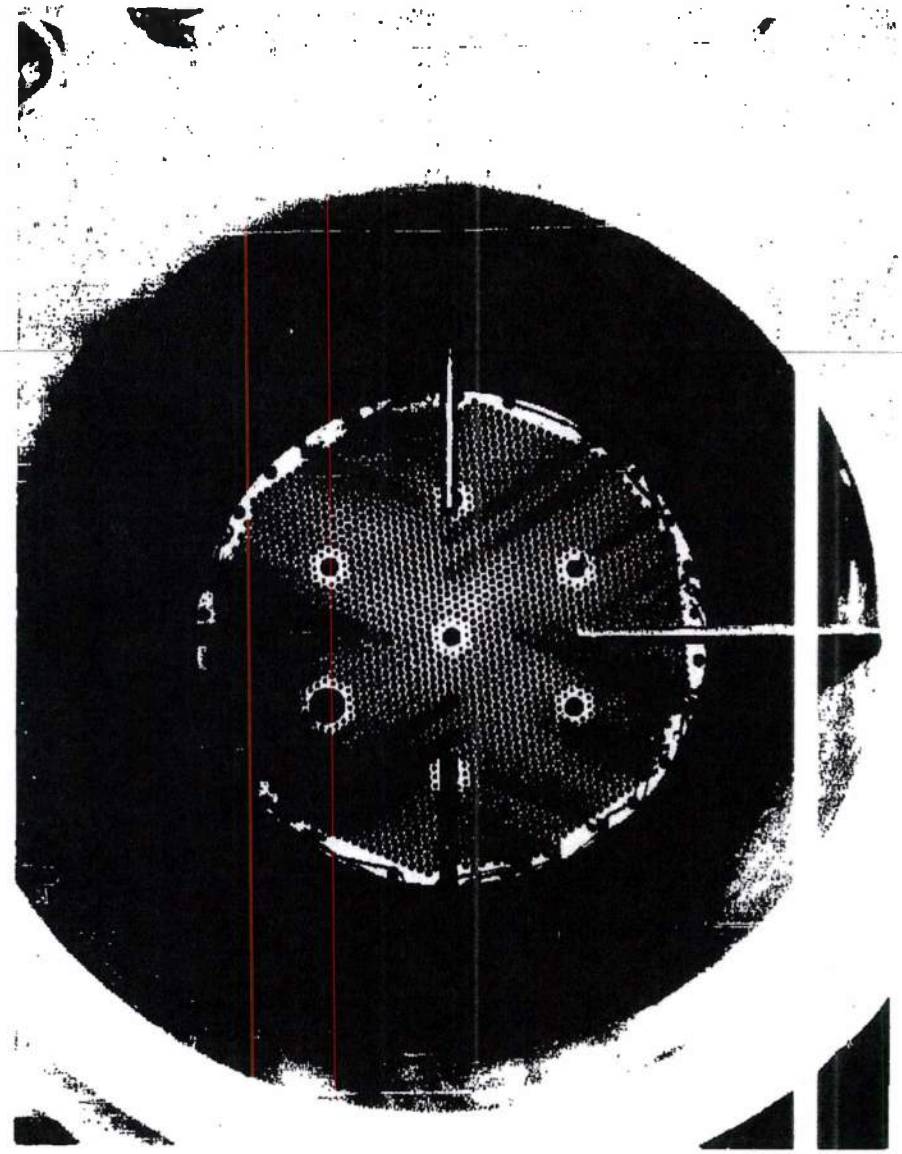

FIGURE 126. Aft End of Simulated Reactor Segment (Viewed Up Exit Nozzle)

~~SECRET RESTRICTED DATA~~
~~ATOMIC ENERGY ACT OF 1954~~

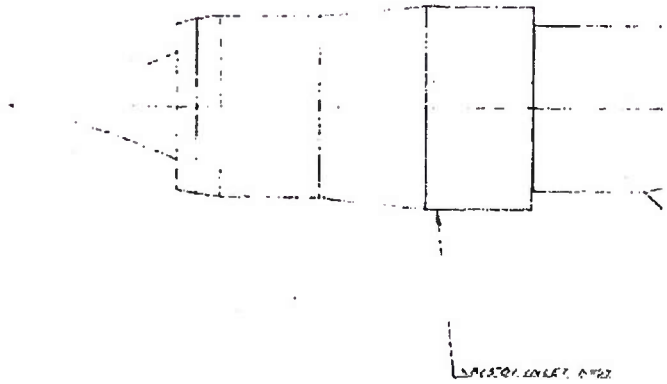

1

2

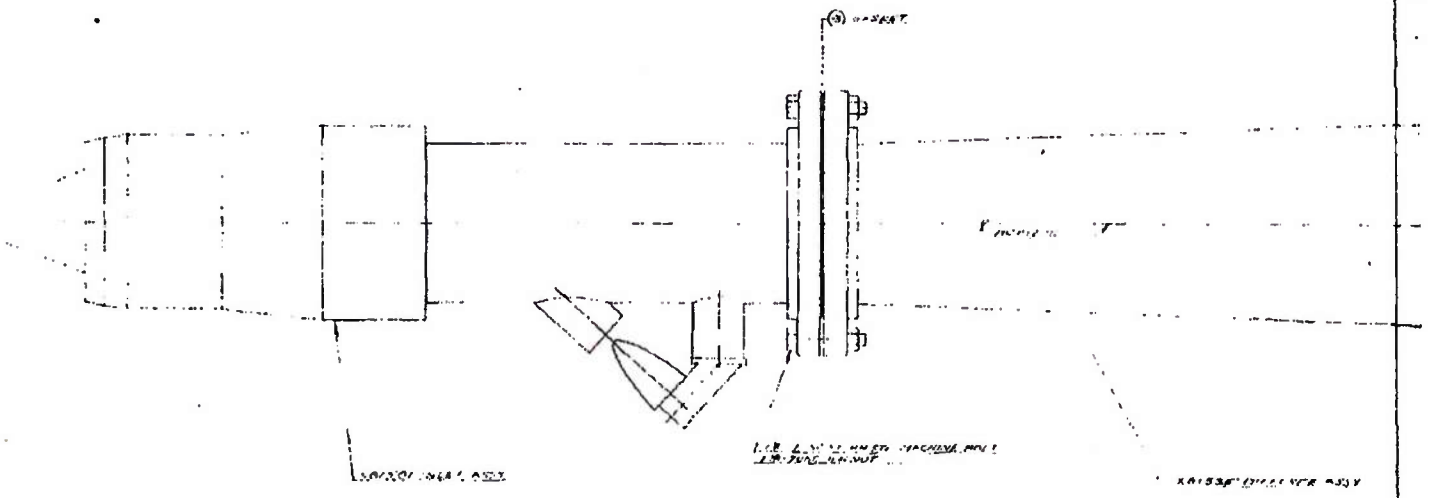

10 9 8

3

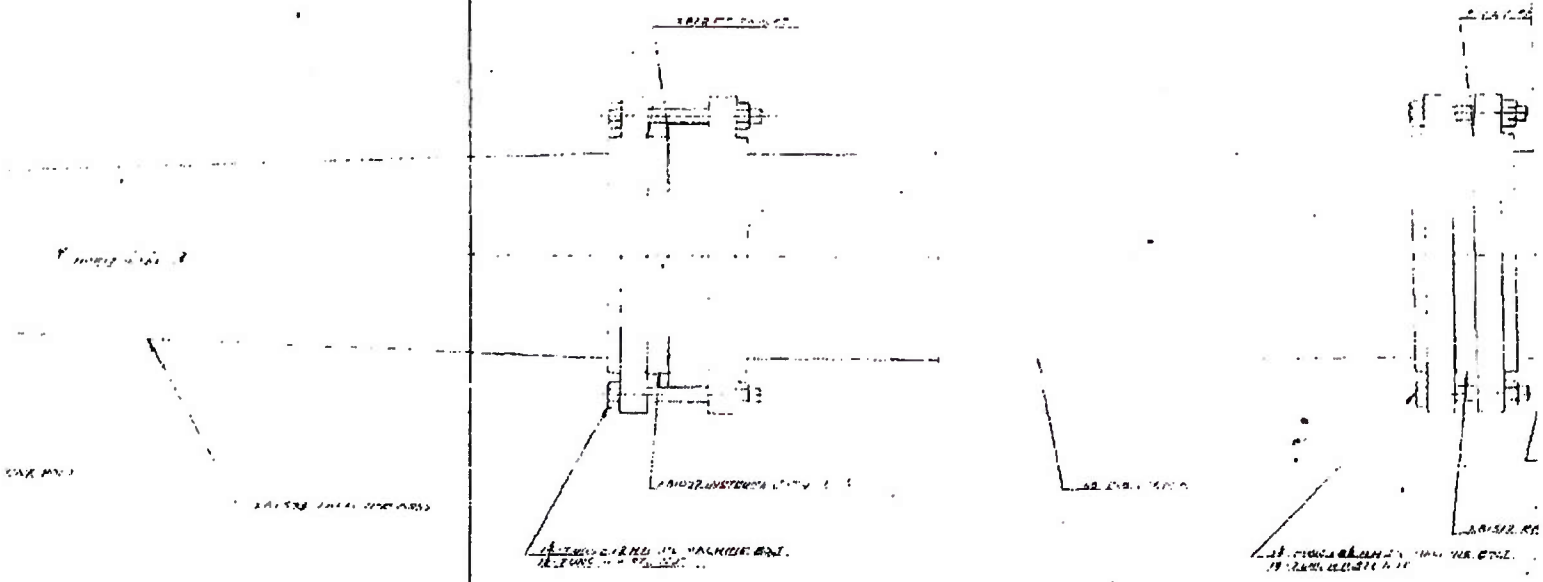

4

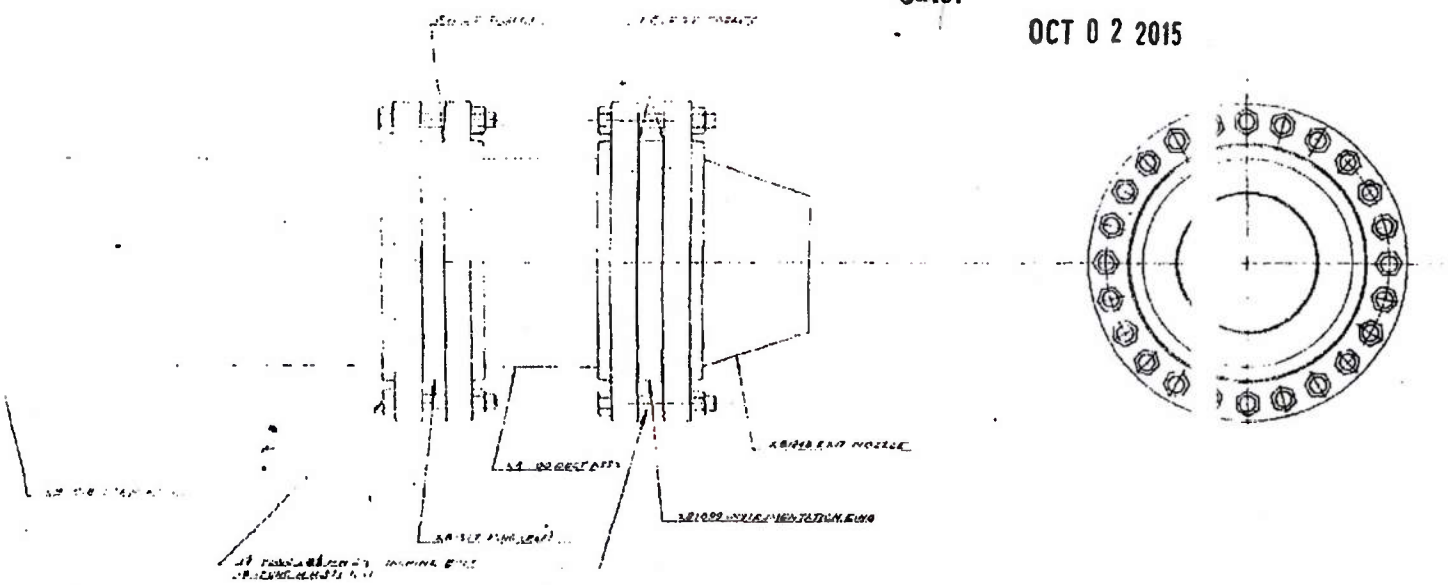

5 4 3

5

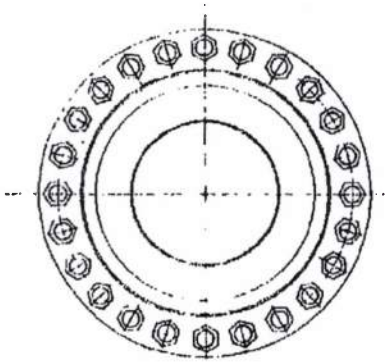

FIGURE 129. Engine Assembly
Aerodynamic Coupling, Free Jet

[redacted]

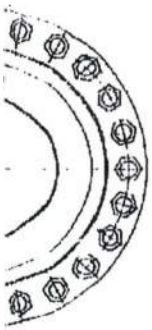

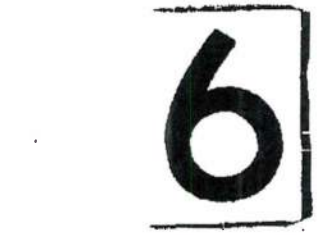

FIGURE 129. Engine Assembly, Aerodynamic Coupling, Free Je

[redacted]

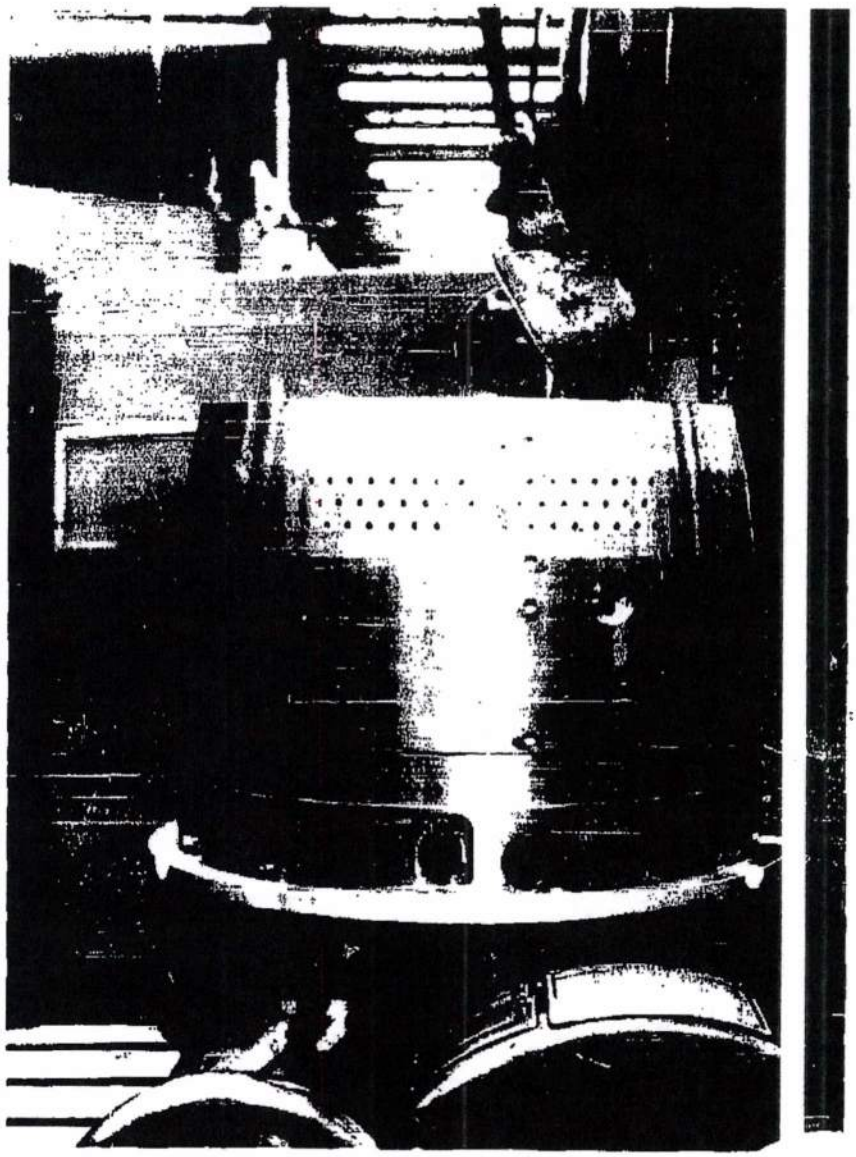

FIGURE 139. Test Assembly for Free Jet Aerodynamic Coupling Test

FIGURE 131. Spike Adapter for Free Jet Aerodynamic Coupling Test

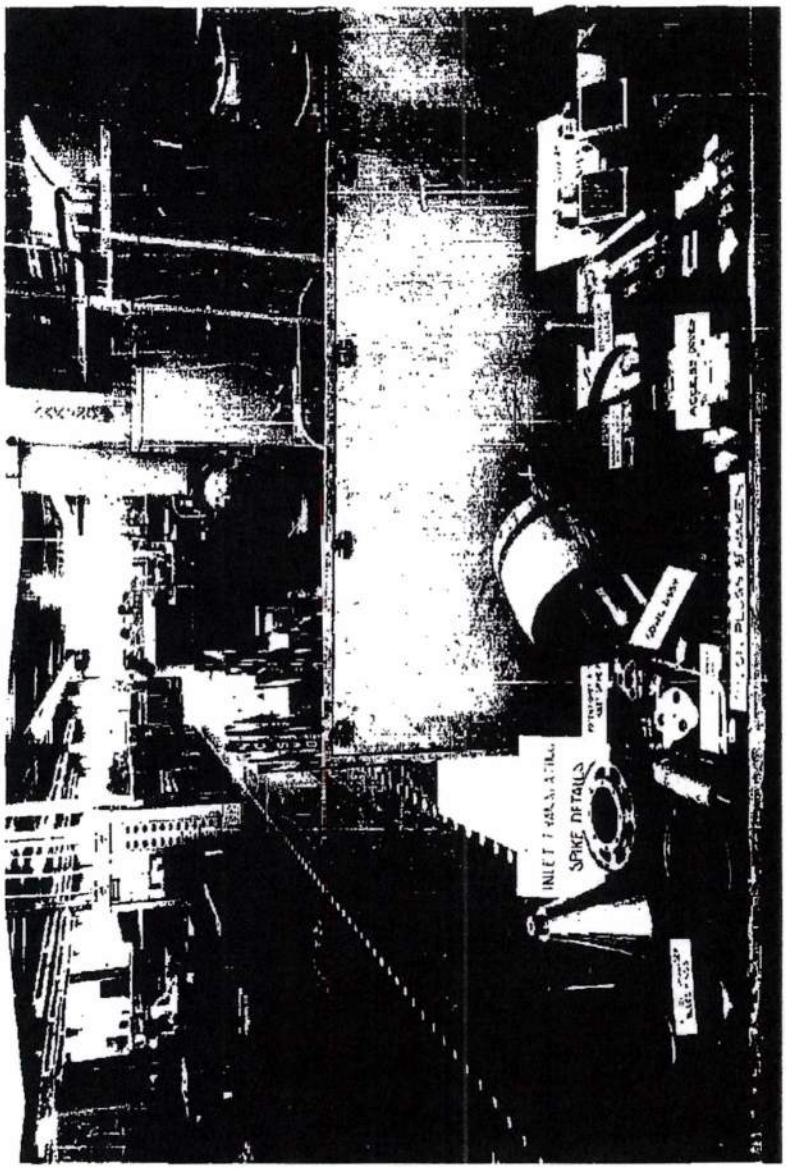

FIGURE 132. Display of Components for Free Jet Aerodynamic Coupling Test

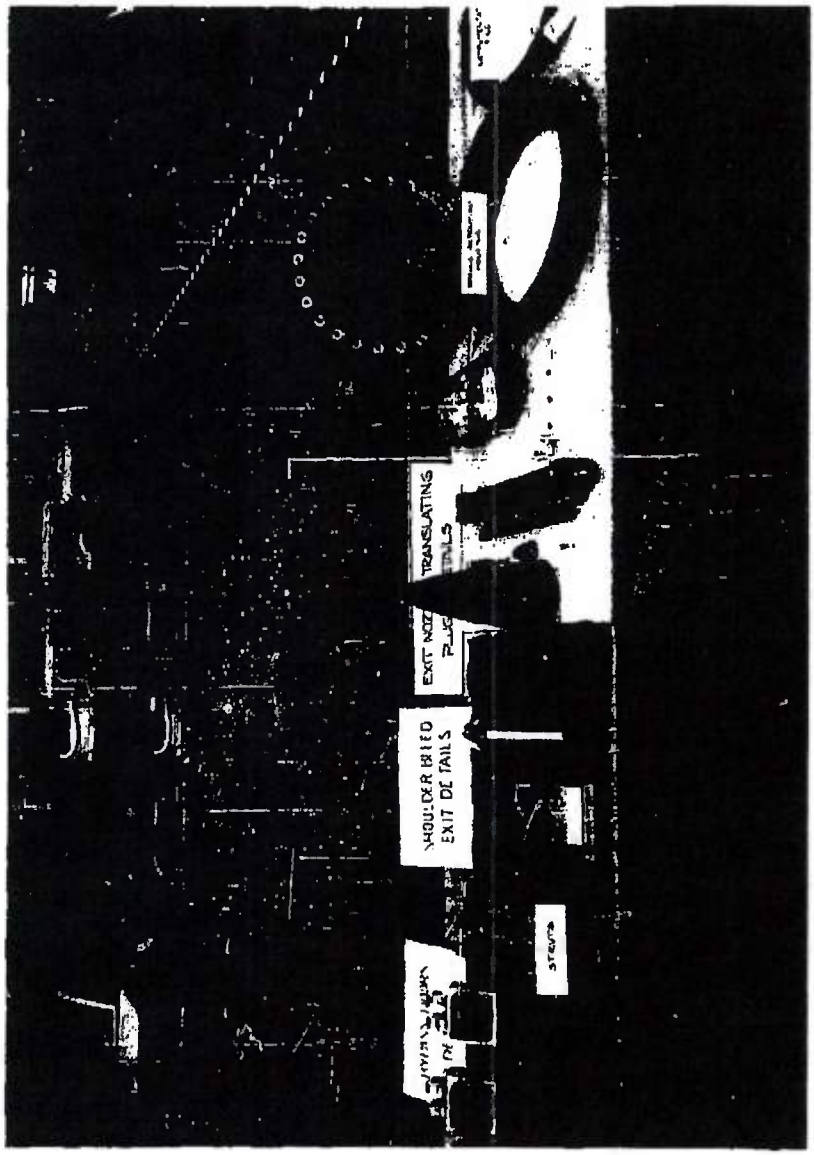

FIGURE 133. Closeup of Components for Free Jet Aerodynamic Coupling Test

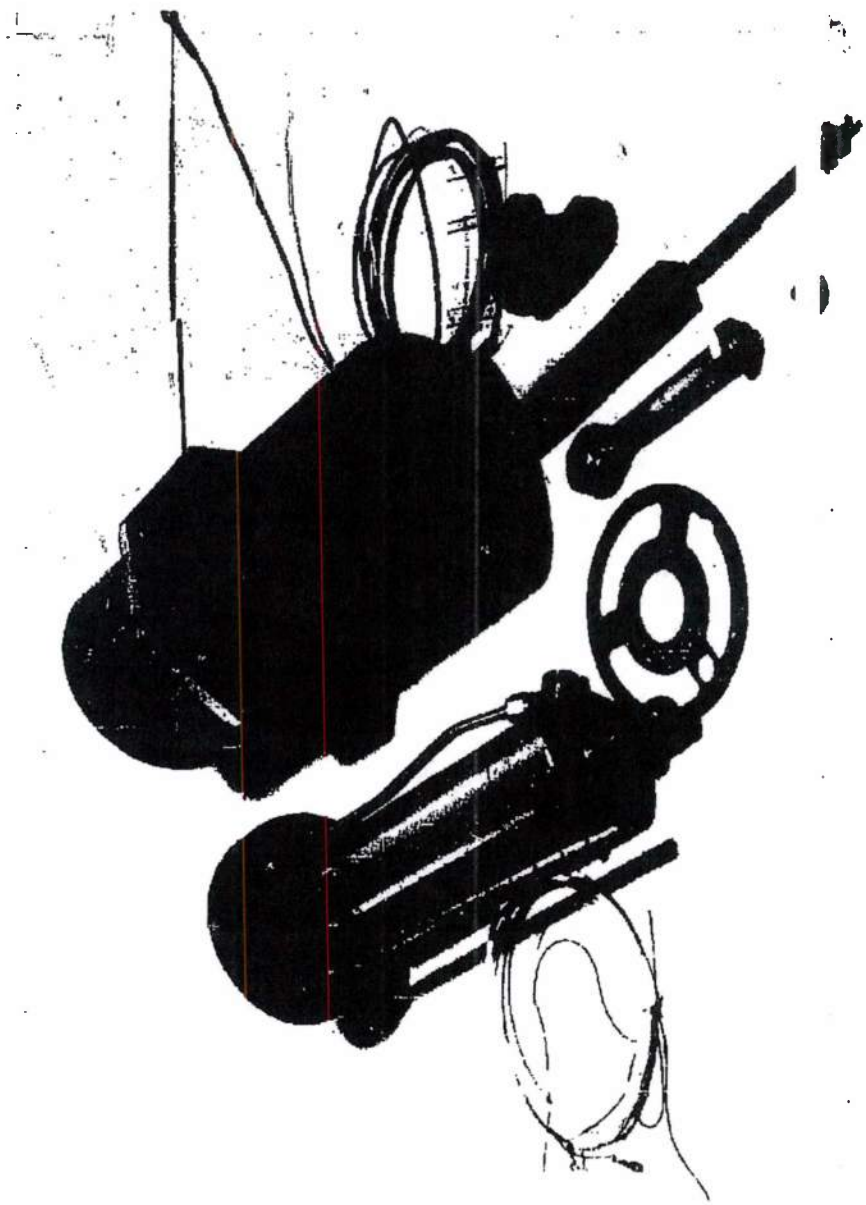

FIGURE 134. Spike Actuator and Housing Details for Free Jet Aerodynamic Coupling Test

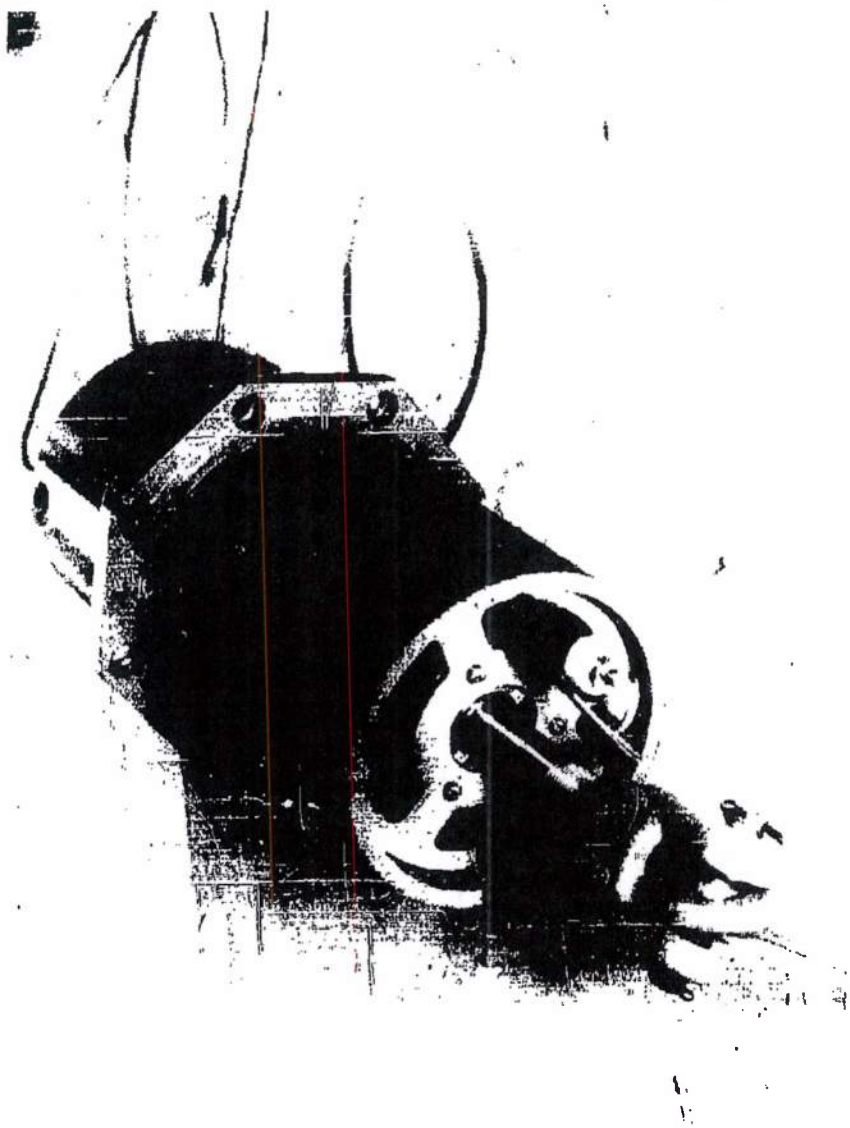

FIGURE 135. Spike Actuator and Housing Assembly for Free Jet Aerodynamic Coupling Test

NEG. 434A-18

MAC A63

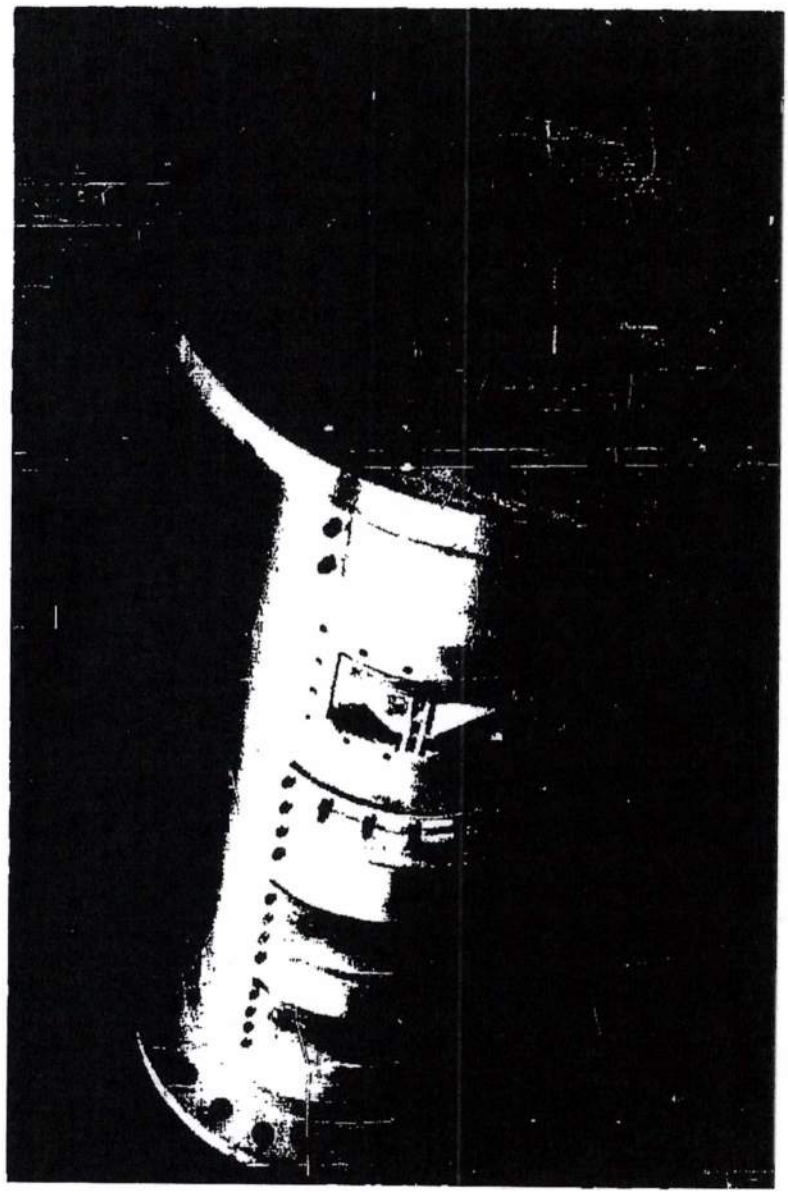

NEG. 4344-19

FIGURE 136. Simulated Reactor and Housing for Free Jet Aerodynamic Coupling Test

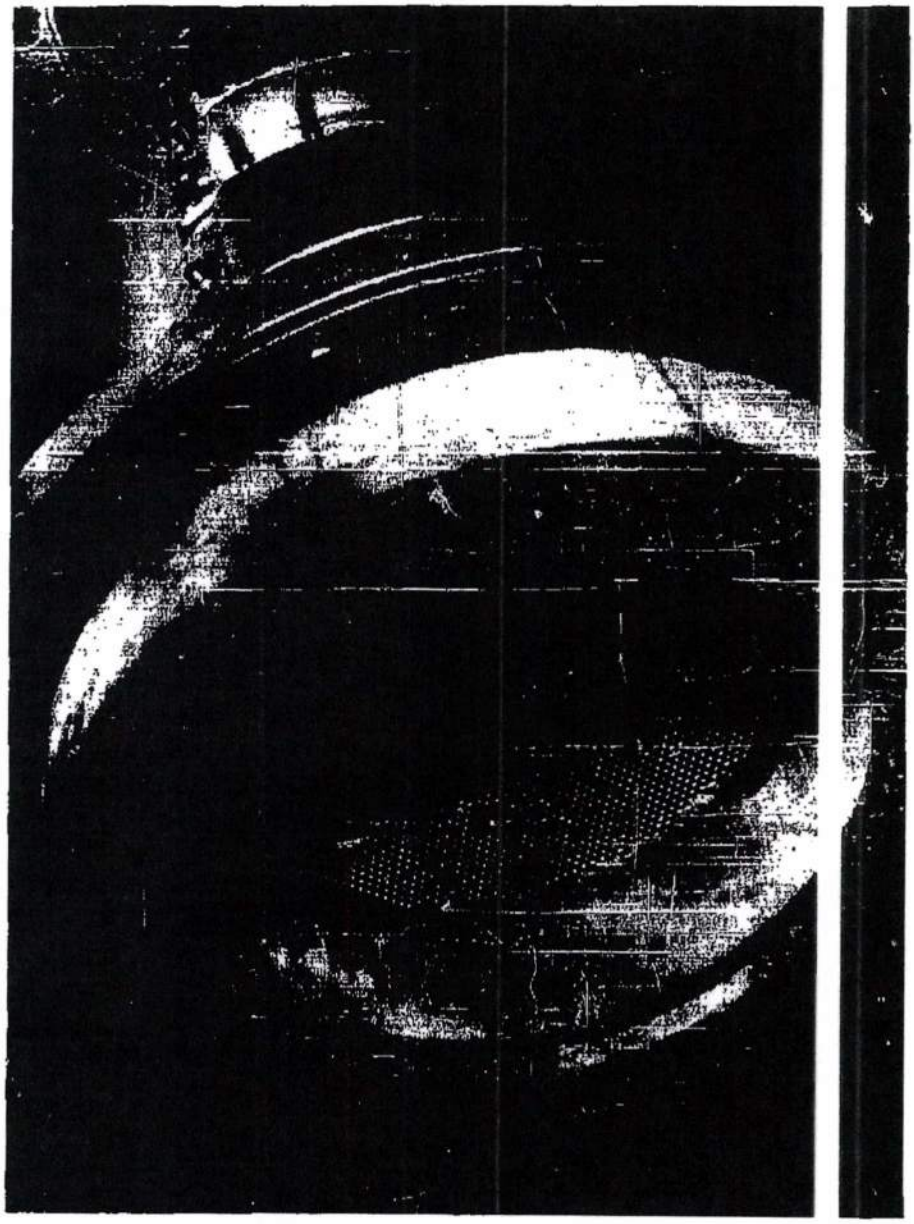

NEG. 4344-21

FIGURE 137. Test Item Assembly (Axial Load Spring Retention) for Free Jet Aerodynamic Coupling Test

FIGURE 138. Centerbody and Inlet Duct for Free Jet Aerodynamic Coupling Test

NEG. 4344-24

NAC A 673

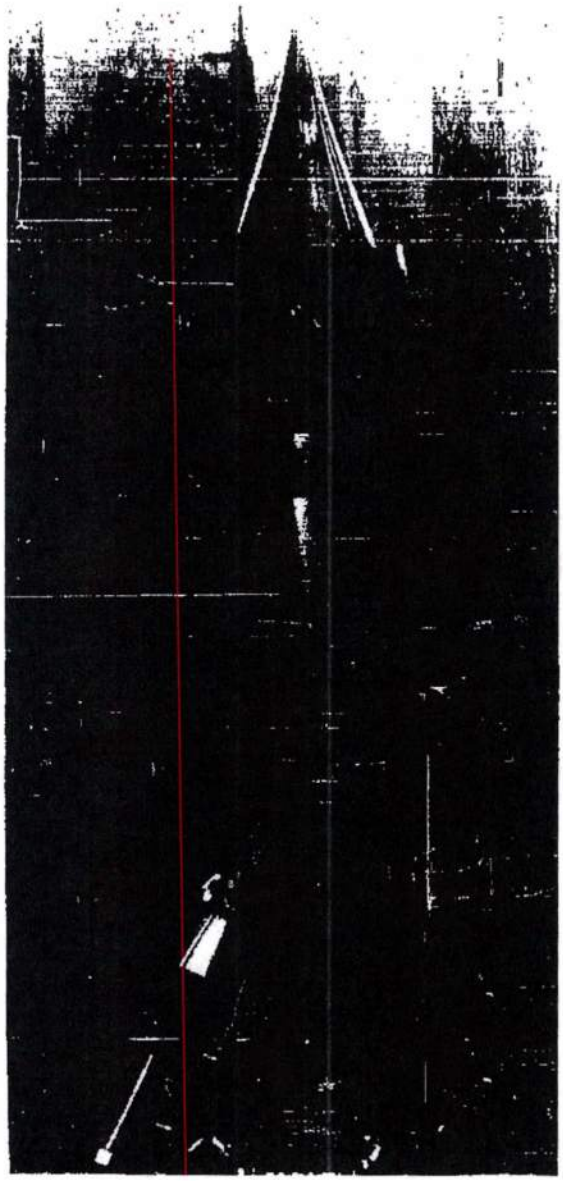

NEG. 4344-26

FIGURE 139. Centerbody and Inlet Duct Assembly for Free Jet Aerodynamic Coupling Test

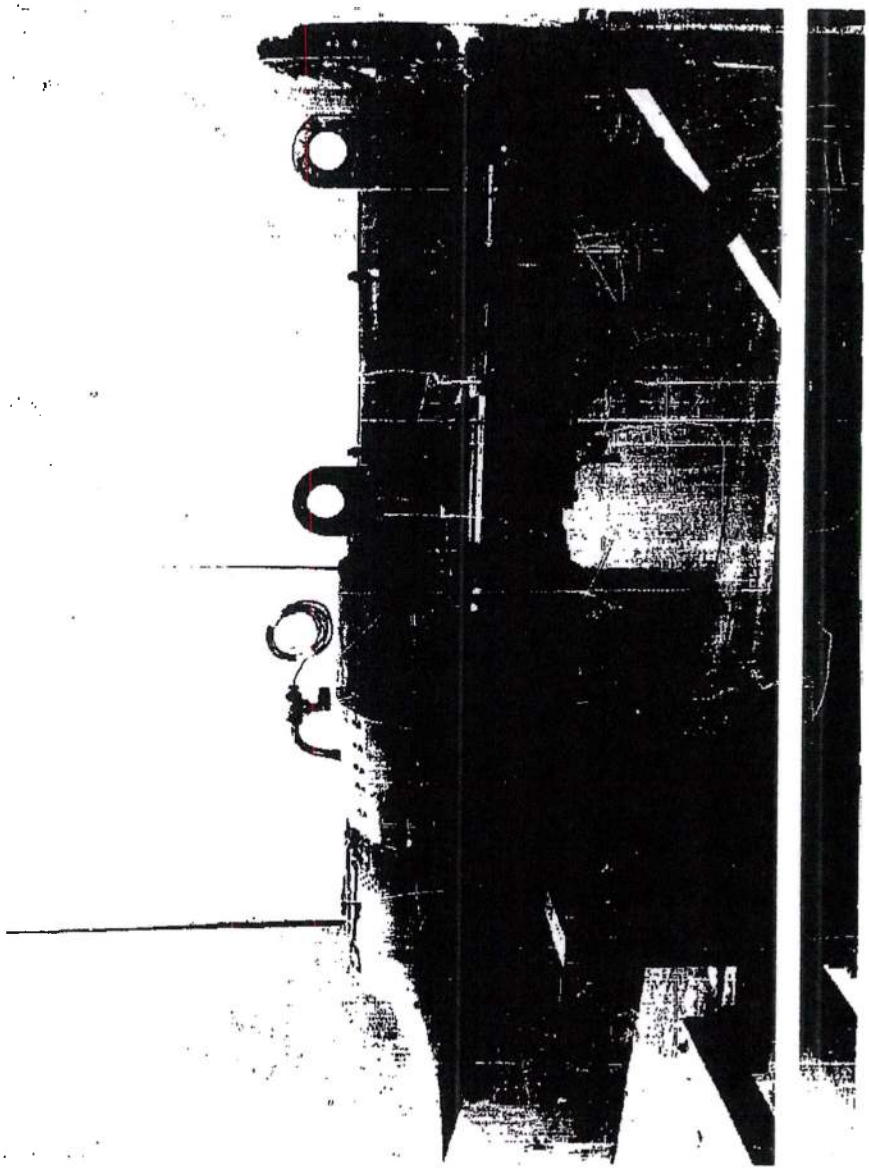

FIGURE 140. Exposed Inlet Assembly for Free Jet Aerodynamic Coupling Test

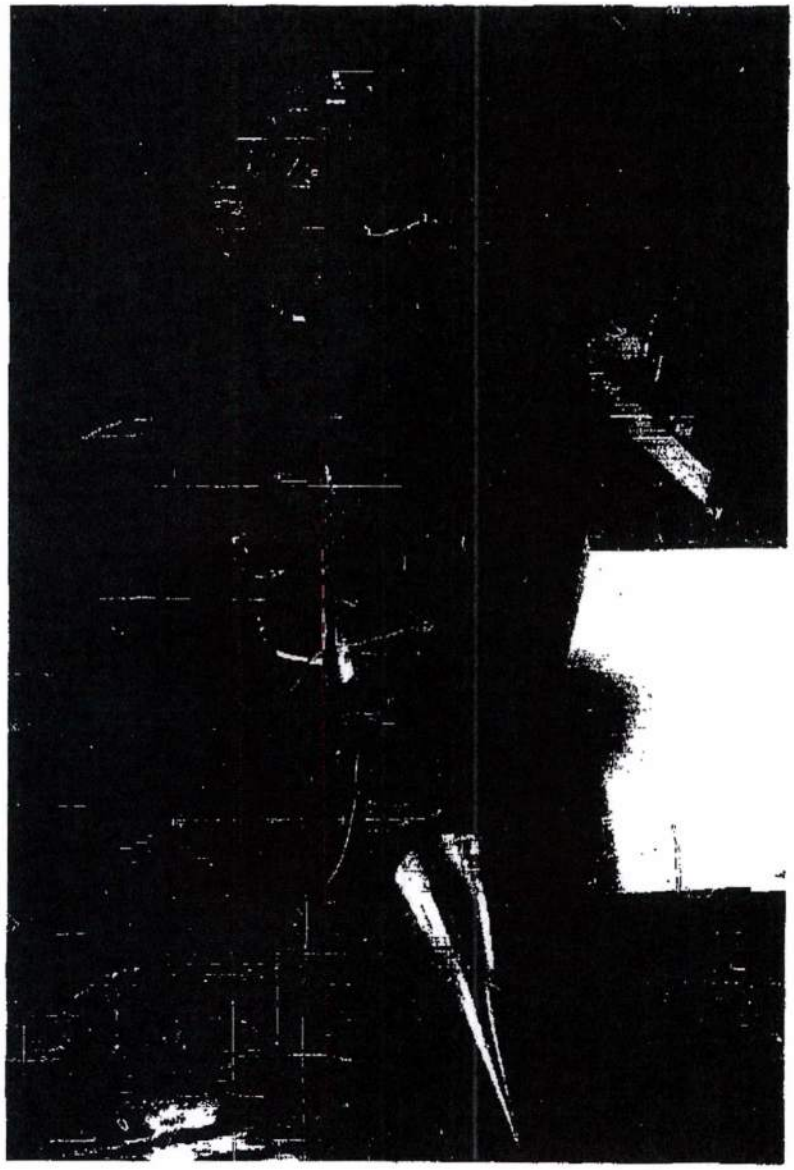

NEG. 4344-31

FIGURE 141. Inlet Assembly for Free Jet Aerodynamic Coupling Test (Three Quarter View)

MAC A673

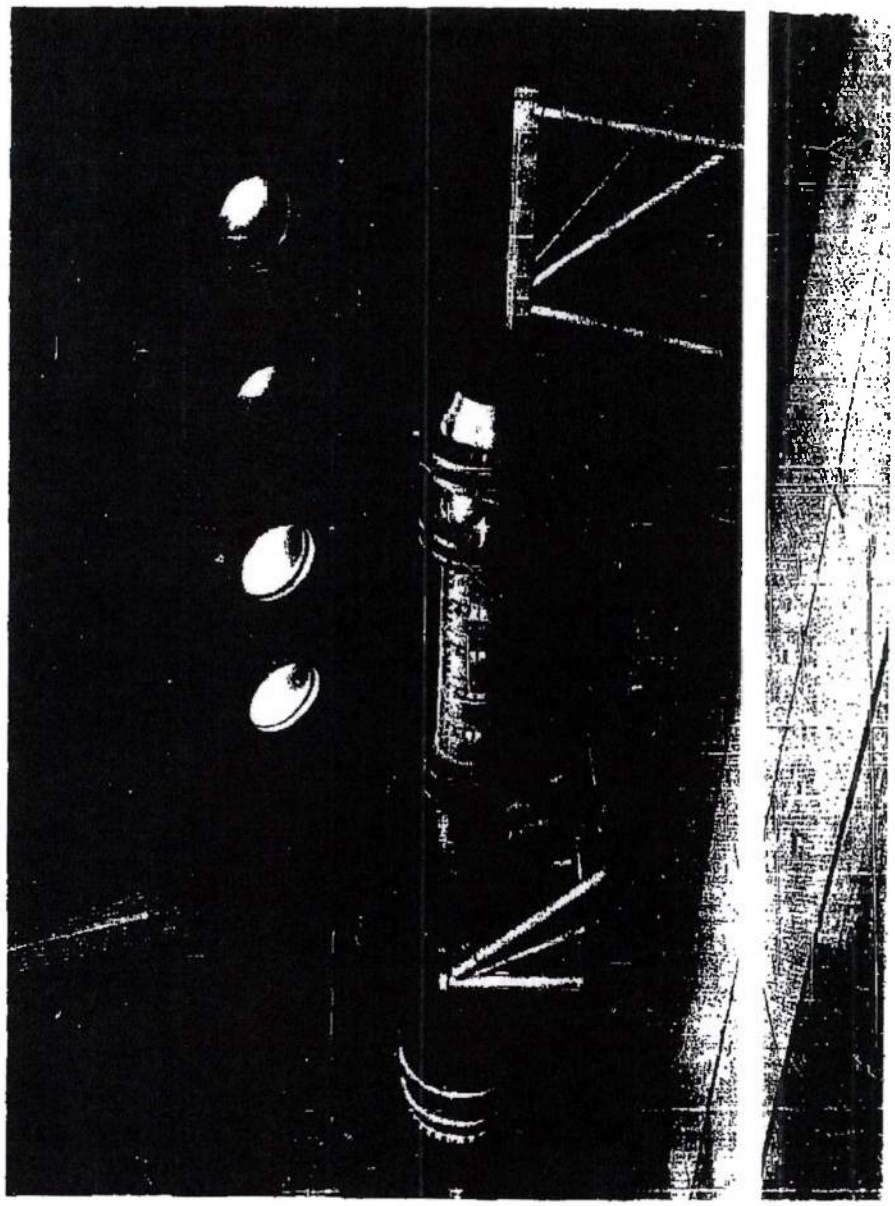

NEG. T-3066-1

FIGURE 142. Setup of Pluto Propulsion System Model for Free Jet Aerodynamic Coupling Test

APPENDIX A

~~CLASSIFIED~~ MATERIALS STUDIES

Cyclic Stress Studies on Rene' 41

To evaluate the behavior of Rene' 41 under conditions cyclic operation, creep specimens of 0.050 in. thick sheet were subjected cyclic tensile stresses at 1400°F in accordance with the stress-time profi shown in Figure A-1. The results of deformations produced by cyclic load g in comparison with deformations produced on control specimens subjected t a standard creep test at the same temperature, subjected to a constant str s of 52 Ksi and for the same total time are presented in Table A-I. A comp ison of results between test and control specimens shows that cycled specim s elongated less by a factor 1/4 to 1/9, indicating strengthening occurred a result of this particular cyclic test. Standard tensile tests were also p formed at a strain rate of 0.001 in./in./sec at 1400°F, the principle strain te of cyclic testing. The results of these tensile tests are compared in Ta e A-II. Cycled specimens show tensile values intermediate to noncycled and eep tested specimens; the creep tested specimens having the highest tensile alues.

Table A-III and Figure A-2 present results of creep-ru ure tests performed on control specimens at 1400°F under a 52 Ksi stress. Th r elongation in 10 hours was approximately 0.2% much higher than the cycled pecimens. Tensile tests were also performed at 1400°F under stress rates whic produced strain rates of 0.001, 0.01, and 0.1 in./in./sec. The results of t se tests are presented in Table A-IV and Figures A-3 and A-4. As expected, e short time tensile properties increased with the strain rate.

The strengthening effect shown by these cyclic tests m be due to a combination of additional precipitation and/or solid solution chanisms stimulated by repeated strains, at the temperature of testing. Cons erable additional testing will be needed to resolve the effects to be expe ed from service cycles. A program of cyclic testing of Rene' 41 and the ot r alloys should be undertaken to study the effects of temperature and stress ycling on precipitation and nonprecipitation hardening alloys.

TABLE A-I

CREEP OF RENE' 41 DURING CYCLIC TESTING

Specimens - Standard, 0.050 in. thick sheet
Creep Measurements - Before and after cyclic testing. Specimens at room temperature. Scribe marks measured with Gaertner toolmaker's microscope
Heating - Resistance

Specimen Number	Length (Inches)		Change in Length In 2 Inches (in.)	Plastic Deformation In 2 Inch Gage Length (%)
	Before Cycling	After Cycling		
G-1	--	1.9978	--	--
G-3	1.9990	2.0008	0.0018	0.09
G-13	1.9988	1.9993	0.0005	0.03
G-14	1.9999	2.0012	0.0013	0.07

CREEP OF RENE' 41 DURING STATIC TESTING

Load, Temperature, and Time - Load - 52,000 psi, constant
- Same temperature as above
- time 5 hours

Specimen Number	Length (Inches)		Change in Length In 2 Inches (in.)	Plastic Deformation In 2 Inch Gage Length (%)
	Before Cycling	After Cycling		
G-10	1.9980	2.0068	0.0088	0.44
G-11	1.9990	2.0079	0.0086	0.43

TABLE A-II

TENSILE PROPERTIES OF RENE' 41 SHEET AFTER CYCLIC TESTING

Heat Treatment - 1950°F, 1/2 hr, rapid air cool, Age at 1400°F, 16 hrs
Heating - Resistance
Hold Time - 5 minutes
Specimens - Standard, 0.050 inch thick sheet

Specimen Number	Strain Rate Start to Rupture (in/in/sec)	Test Temperature (°F)	Proportional Limit (ksi)	0.2% Yield Strength (ksi)	Ultimate Tensile Strength (ksi)	Elongation In 2 Inches (%)	Young's Modulus (x 10^6 psi)
G-1	0.001	1400	97.0	125.0	(127.5)*	(0.9)*	24.0
G-3	0.001	1400	88.0	127.7	141.0	2.4	22.2
G-13	0.001	1400	86.0	126.0	147.0	3.7	23.8
G-14	0.001	1400	90.0	126.0	146.0	3.3	23.1
		Average	90.2	126.2	144.7	3.1	23.3
Average of 3 specimens not cyclic tested.	0.001	1400	77.0	119.7	134.0	2.5	25.3
TENSILE PROPERTIES OF RENE' 41 SHEET AFTER STATIC TESTING SIMULATING CYCLIC TESTING							
G-10	0.001	1400	79.0	133.0	153.8	4.0	24.0
G-11	0.001	1400	81.0	131.8	151.0	4.0	24.0

* Broke at thermocouple weld, not valid.

TABLE A-III

CREEP-RUPTURE OF RENE' 41 SHEET CONTROL SPECIMENS

Test Conditions:

Material - Rene' 41, 0.050 inch thick sheet
Heat Treatment - 1950°F 30 minutes
Age 1400°F, 16 hours
Heating - Resistance
Gage Length - 1.5 inches
Atmosphere - Air
Specimens - Standard

Specimen Number	Test Temperature (°F)	Creep Stress (ksi)	Time to Produce Indicated Plastic Creep (hours)						Time to Rupture (hours)	Elongation In 1.5 Inches (%)
			0.5%	0.1%	0.2%	0.5%	1.0%	2.0%		
G-18	1400	52	0.3	3.6	13.2	30.1	49.1	63.1	73.35	4.0
G-21	1400	52	2.8	8.6	23.3	48.1	64.5	81.0	87.5	2.3

TABLE A-IV

TENSILE PROPERTIES OF RENE' 41 SHEET AT SELECTED STRAIN RATES

Test Conditions:

Heat Treatment - 1950°F, 1/2-hour, rapid air cool
Age at 1400°F, 16 hours
Heating - Resistance
Specimens - 0.050 inch thick sheet, per Dwg. X14281
Hold Time - 5 minutes
Gage Length - 2 Inches

Specimen Number	Strain Rate Start to Rupture (in/in/sec)	Test Temperature (°F)	Proportional Limit (ksi)	0.2% Yield Strength (ksi)	Ultimate Tensile Strength (ksi)	Elongation In 2 Inches (%)	Young's Modulus (x 10^6 psi)
G-2	0.001	1400	78.0	120.0	134.0	2.5	26.3
G-4	0.001	1400	77.0	118.0	134.0	2.5	25.0
G-6	0.001	1400	76.0	121.0	134.0	2.5	25.3
		Average	77.0	119.7	134.0	2.5	25.3
G-7	0.01	1400	80.0	120.0	145.0	4.0	26.6
G-8	0.01	1400	82.0	123.0	148.0	4.0	24.0
G-9	0.01	1400	81.0	123.0	146.0	3.5	22.0
G-28	0.01	1400	78.0	121.0	149.0	4.5	26.7
		Average	80.0	121.8	147.0	4.0	24.8
G-12	0.1	1400	--	--	152.0	8.5	--
G-15	0.1	1400	--	--	160.0	8.5	--
G-5	0.1	1400	--	--	161.0	9.0	--
G-25	0.1	1400	88.0	--	150.0	16.5	24.0
G-33	0.1	1400	98.0	131.5	154.0	7.0	29.0

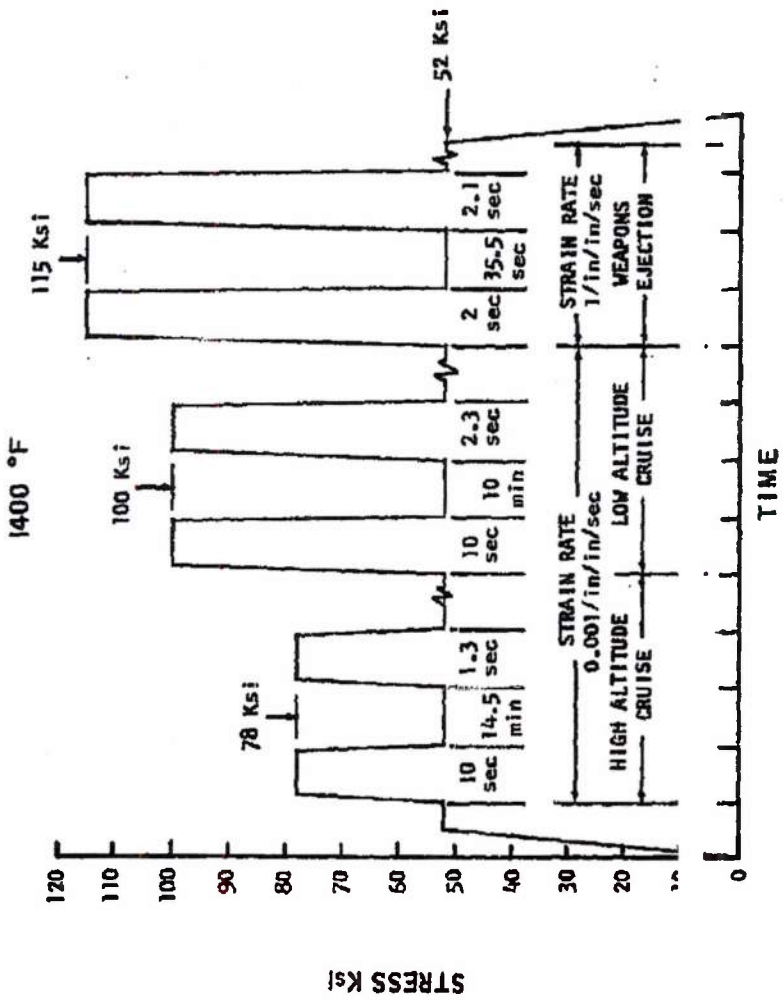

FIGURE A-1. Stress-Time Profile for Rene' 41

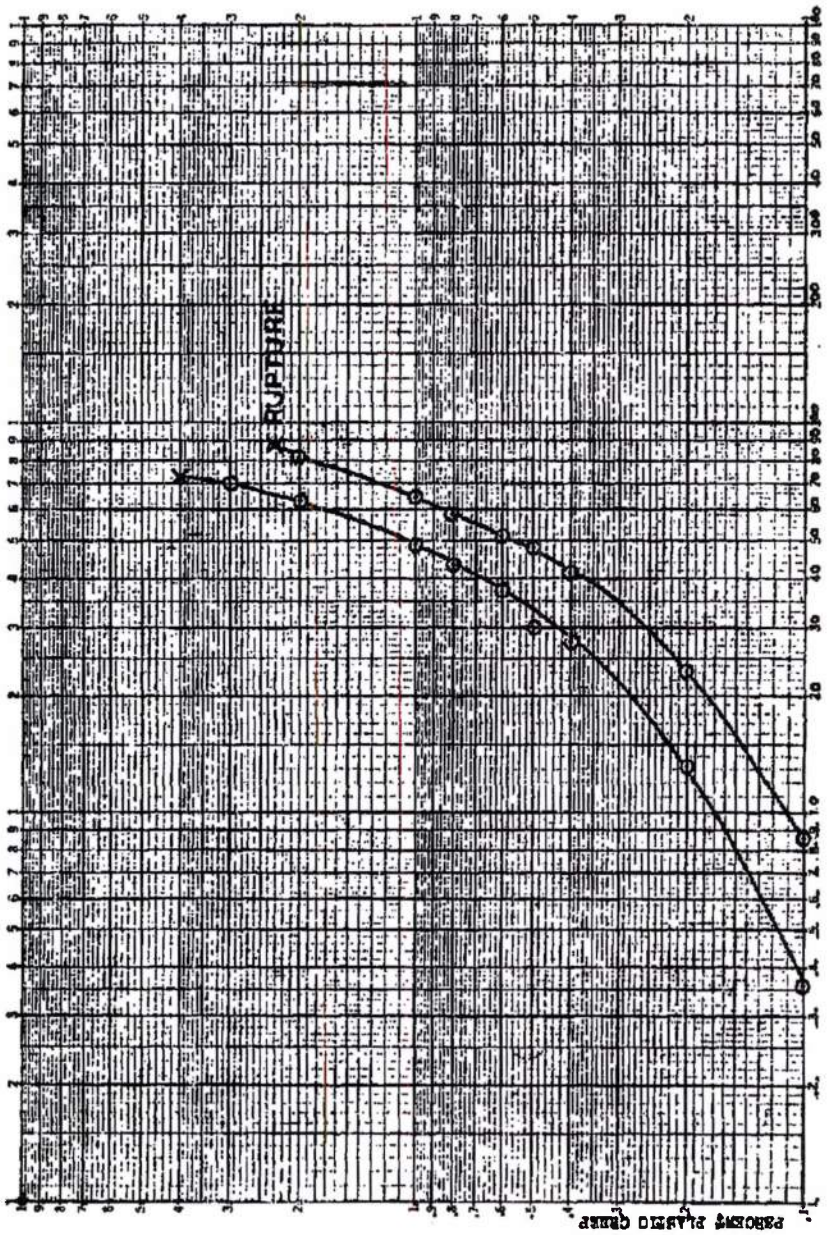

FIGURE A-2. Creep of Rene' 41 Sheet (1400°F; 52 Ksi)

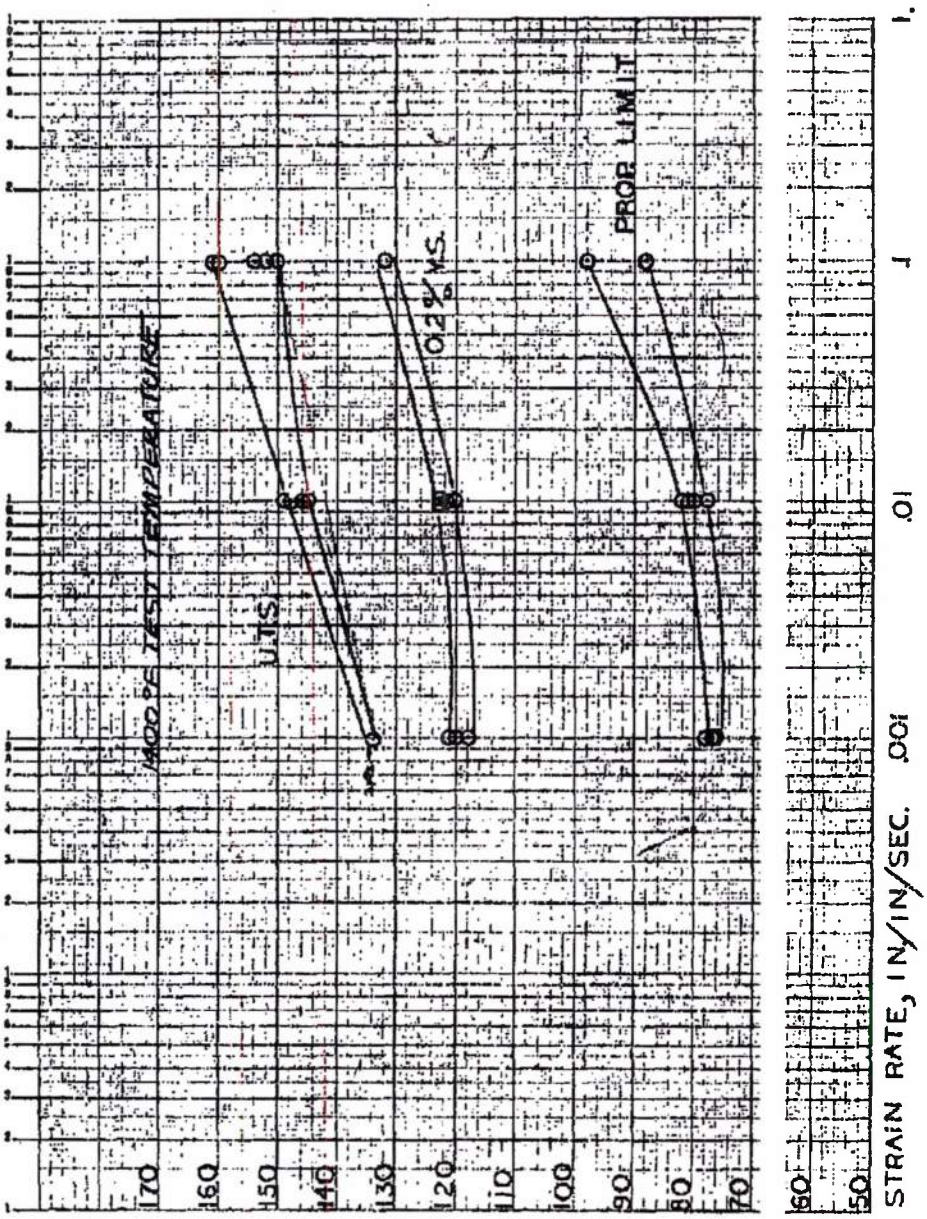

FIGURE A-3. Ultimate Tensile Strength and Yield Strength of Rene' 41 Sheet at Selected Strain Rates

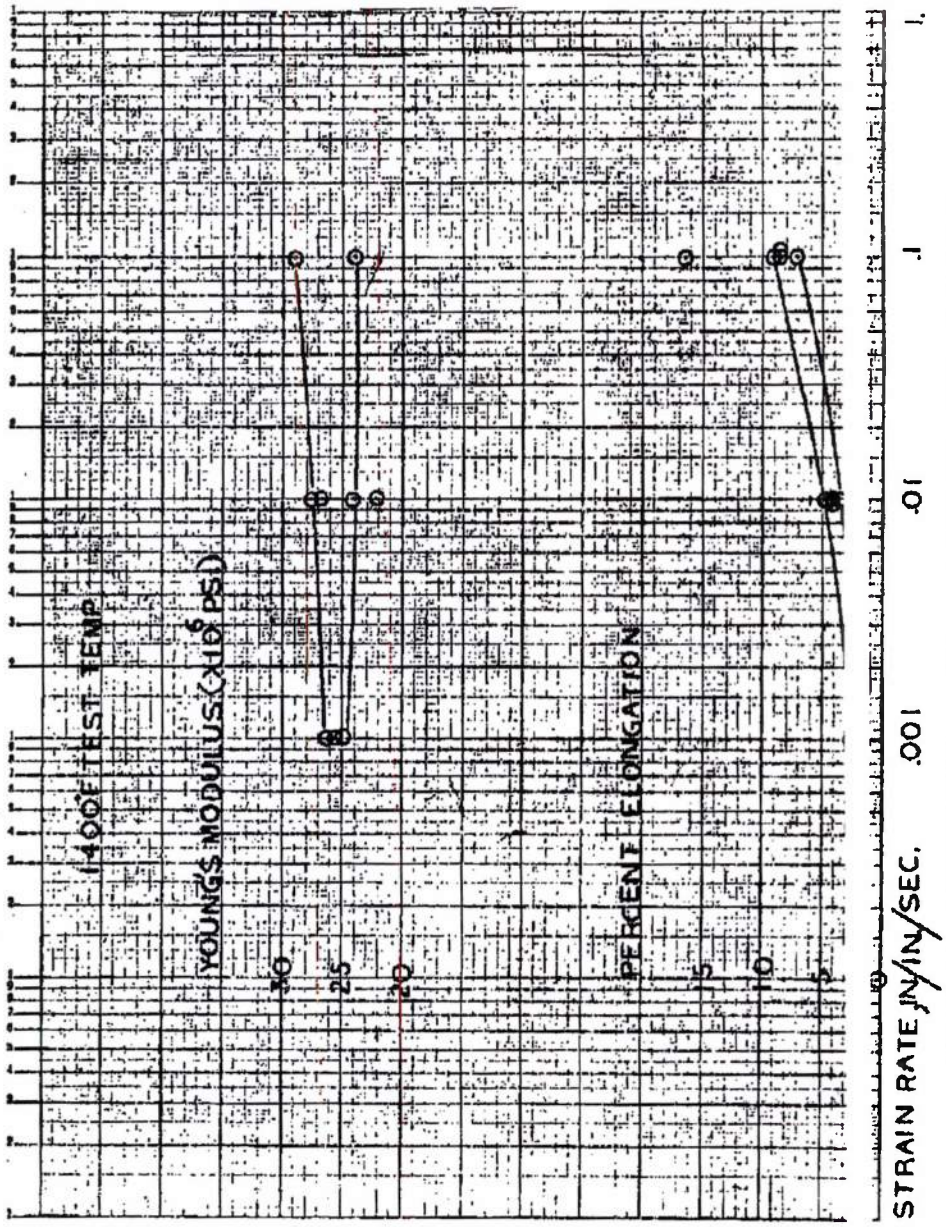

FIGURE A-4. Young's Modulus and Percent Elongation of Rene' 41 Sheet at Selected Strain Rates

Aeronautical Systems Division, Dir/Aeromechanics, Propulsion Lab, Wright-Patterson AFB, Ohio. Rpt Nr ASD-TDR-63-277, vol IV. NUCLEAR RAMJET PROPULSION SYSTEM APPLIED RESEARCH AND TECHNOLOGY (1962 TECHNICAL SUMMARY): VOL. IV. Propulsion System Design and Structural Analysis ~~(U)~~, Annual Summary Report, 15 Feb 63. p incl. illus., tables, 23 refs.

~~Secret Restricted Data~~ Report

Volume contains results of design, material studies, and structures component testing of a nuclear propulsion system for the Pluto reactor program. Design concepts, structural analysis of steady state and dynamic loads, material evaluation, and recommended dynamic and structural test programs are studied. Methods of analysis are outlined.

Unclassified Abstract

UNCLASSIFIED

1. Nuclear ramjet propulsion systems
2. Propulsion systems
3. Aircraft nuclear power propulsion
4. Nuclear powerplants
5. Ramjet engines

I. AFSC Project 655A, Task 1 and 5
II. Contract AF 33(657)-8123
III. The Marquardt Corp., Van Nuys, Calif.
IV. R. D. Grossman
V. TMC Report 6003
VI. Not aval fr OTS

UNCLASSIFIED

Aeronautical Systems Division, Dir/Aeromechanics, Propulsion Lab, Wright-Patterson AFB, Ohio. Rpt Nr ASD-TDR-63-277, vol IV. NUCLEAR RAMJET PROPULSION SYSTEM APPLIED RESEARCH AND TECHNOLOGY (1962 TECHNICAL SUMMARY): VOL. IV. Propulsion System Design and Structural Analysis ~~(U)~~, Annual Summary Report, 15 Feb 63. p incl. illus., tables, 23 refs.

~~Secret Restricted Data~~ Report

Volume contains results of design, material studies, and structures component testing of a nuclear propulsion system for the Pluto reactor program. Design concepts, structural analysis of steady state and dynamic loads, material evaluation, and recommended dynamic and structural test programs are studied. Methods of analysis are outlined.

Unclassified Abstract

UNCLASSIFIED

1. Nuclear ramjet propulsion systems
2. Propulsion systems
3. Aircraft nuclear power propulsion
4. Nuclear powerplants
5. Ramjet engines

I. AFSC Project 655A, Task 1 and 5
II. Contract AF 33(657)-8123
III. The Marquardt Corp., Van Nuys, Calif.
IV. R. D. Grossman
V. TMC Report 6003
VI. Not aval fr OTS

UNCLASSIFIED

Aeronautical Systems Division, Dir/Aeromechanics, Propulsion Lab, Wright-Patterson AFB, Ohio. Rpt Nr ASD-TDR-63-277, vol IV. NUCLEAR RAMJET PROPULSION SYSTEM APPLIED RESEARCH AND TECHNOLOGY (1962 TECHNICAL SUMMARY): VOL. IV. Propulsion System Design and Structural Analysis ~~(U)~~, Annual Summary Report, 15 Feb 63. p incl. illus., tables, 23 refs.

~~Secret Restricted Data~~ Report

Volume contains results of design, material studies, and structures component testing of a nuclear propulsion system for the Pluto reactor program. Design concepts, structural analysis of steady state and dynamic loads, material evaluation, and recommended dynamic and structural test programs are studied.

Unclassified Abstract

UNCLASSIFIED

1. Nuclear ramjet propulsion systems
2. Propulsion systems
3. Aircraft nuclear power propulsion
4. Nuclear powerplants
5. Ramjet engines

I. AFSC Project 655A, Task 1 and 5
II. Contract AF 33(657)-8123
III. The Marquardt Corp., Van Nuys, Calif.
IV. R. D. Grossman
V. TMC Report 6003

UNCLASSIFIED

Aeronautical Systems Division, Dir/Aeromechanics, Propulsion Lab, Wright-Patterson AFB, Ohio. Rpt Nr ASD-TDR-63-277, vol IV. NUCLEAR RAMJET PROPULSION SYSTEM APPLIED RESEARCH AND TECHNOLOGY (1962 TECHNICAL SUMMARY): VOL. IV. Propulsion System Design and Structural Analysis ~~(U)~~, Annual Summary Report, 15 Feb 63. p incl. illus., tables, 23 refs.

~~Secret Restricted Data~~ Report

Volume contains results of design, material studies, and structures component testing of a nuclear propulsion system for the Pluto reactor program. Design concepts, structural analysis of steady state and dynamic loads, material evaluation, and recommended dynamic and structural test programs are studied.

Unclassified Abstract

UNCLASSIFIED

1. Nuclear ramjet propulsion systems
2. Propulsion systems
3. Aircraft nuclear power propulsion
4. Nuclear powerplants
5. Ramjet engines

I. AFSC Project 655A, Task 1 and 5
II. Contract AF 33(657)-8123
III. The Marquardt Corp., Van Nuys, Calif.
IV. R. D. Grossman
V. TMC Report 6003

UNCLASSIFIED

Aeronautical Systems Division, Dir/Aeromechanics, Propulsion Lab, Wright-Patterson AFB, Ohio. Rpt Nr ASD-TDR-63-277, vol IV. NUCLEAR RAMJET PROPULSION SYSTEM APPLIED RESEARCH AND TECHNOLOGY (1962 TECHNICAL SUMMARY): VOL. IV. Propulsion System Design and Structural Analysis ~~(SRD)~~, Annual Summary Report, 15 Feb 63. p incl. illus., tables, 23 refs.

~~Secret Restricted Data~~ Report

Volume contains results of design, material studies, and structures component testing of a nuclear propulsion system for the Pluto reactor program. Design concepts, structural analysis of steady state and dynamic loads, material evaluation, and recommended dynamic and structural test programs are studied. Methods of analysis are outlined.

Unclassified Abstract

UNCLASSIFIED

1. Nuclear ramjet propulsion systems
2. Propulsion systems
3. Aircraft nuclear power propulsion
4. Nuclear powerplants
5. Ramjet engines

I. AFSC Project 655A, Task 1 and 5
II. Contract AF 33(657) -8123
III. The Marquardt Corp., Van Nuys, Calif.
IV. R. D. Grossman
V. TMC Report 6003
VI. Not aval fr OTS

UNCLASSIFIED

Aeronautical Systems Division, Dir/Aeromechanics, Propulsion Lab, Wright-Patterson AFB, Ohio. Rpt Nr ASD-TDR-63-277, vol IV. NUCLEAR RAMJET PROPULSION SYSTEM APPLIED RESEARCH AND TECHNOLOGY (1962 TECHNICAL SUMMARY): VOL. IV. Propulsion System Design and Structural Analysis ~~(SRD)~~, Annual Summary Report, 15 Feb 63. p incl. illus., tables, 23 refs.

Secret Restricted Data Report

Volume contains results of design, material studies, and structures component testing of a nuclear propulsion system for the Pluto reactor program. Design concepts, structural analysis of steady state and dynamic loads, material evaluation, and recommended dynamic and structural test programs are studied. Methods of analysis are outlined.

Unclassified Abstract

UNCLASSIFIED

1. Nuclear ramjet propulsion systems
2. Propulsion systems
3. Aircraft nuclear power propulsion
4. Nuclear powerplants
5. Ramjet engines

I. AFSC Project 655A, Task 1 and 5
II. Contract AF 33(657) -8123
III. The Marquardt Corp., Van Nuys, Calif.
IV. R. D. Grossman
V. TMC Report 6003
VI. Not aval fr OTS

UNCLASSIFIED

Aeronautical Systems Division, Dir/Aeromechanics, Propulsion Lab, Wright-Patterson AFB, Ohio. Rpt Nr ASD-TDR-63-277, vol IV. NUCLEAR RAMJET PROPULSION SYSTEM APPLIED RESEARCH AND TECHNOLOGY (1962 TECHNICAL SUMMARY): VOL. IV. Propulsion System Design and Structural Analysis ~~(SRD)~~, Annual Summary Report, 15 Feb 63. p incl. illus., tables, 23 refs.

~~Secret Restricted Data~~ Report

Volume contains results of design, material studies, and structures component testing of a nuclear propulsion system for the Pluto reactor program. Design concepts, structural analysis of steady state and dynamic loads, material evaluation, and recommended dynamic and structural test programs are studied. Methods of analysis are outlined.

Unclassified Abstract

UNCLASSIFIED

1. Nuclear ramjet propulsion systems
2. Propulsion systems
3. Aircraft nuclear power propulsion
4. Nuclear powerplants
5. Ramjet engines

I. AFSC Project 655A, Task 1 and 5
II. Contract AF 33(657) -8123
III. The Marquardt Corp., Van Nuys, Calif.
IV. R. D. Grossman
V. TMC Report 6003
VI. Not aval fr OTS

UNCLASSIFIED

Aeronautical Systems Division, Dir/Aeromechanics, Propulsion Lab, Wright-Patterson AFB, Ohio. Rpt Nr ASD-TDR-63-277, vol IV. NUCLEAR RAMJET PROPULSION SYSTEM APPLIED RESEARCH AND TECHNOLOGY (1962 TECHNICAL SUMMARY): VOL. IV. Propulsion System Design and Structural Analysis ~~(SRD)~~, Annual Summary Report, 15 Feb 63. p incl. illus., tables, 23 refs.

~~Secret Restricted Data~~ Report

Volume contains results of design, material studies, and structures component testing of a nuclear propulsion system for the Pluto reactor program. Design concepts, structural analysis of steady state and dynamic loads, material evaluation, and recommended dynamic and structural test programs are studied. Methods of analysis are outlined.

Unclassified Abstract

UNCLASSIFIED

1. Nuclear ramjet propulsion systems
2. Propulsion systems
3. Aircraft nuclear power propulsion
4. Nuclear powerplants
5. Ramjet engines

I. AFSC Project 655A, Task 1 and 5
II. Contract AF 33(657) -8123
III. The Marquardt Corp., Van Nuys, Calif.
IV. R. D. Grossman
V. TMC Report 6003
VI. Not aval fr OTS

UNCLASSIFIED